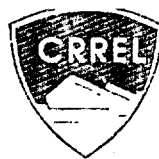


AD-A263 267



DTIC
ELECTE
APR 21 1993
S C D

2

Special Report 92-27

SECOND INTERNATIONAL CONFERENCE ON SNOW ENGINEERING

Santa Barbara, California, June 1992

Wayne Tobiasson and Edmund Wright, Editors



DISTRIBUTION STATEMENT A

Approved for public release
Distribution Unlimited

93 4 20 123

037100 93-08498



Sponsored by

NATIONAL SCIENCE FOUNDATION

Washington, D.C., U.S.A.

ENGINEERING FOUNDATION

New York, N.Y., U.S.A.

JAPAN SOCIETY FOR SNOW ENGINEERING

Sendai, Japan

**U.S. ARMY COLD REGIONS RESEARCH AND
ENGINEERING LABORATORY**

Hanover, N.H., U.S.A.

*Cover: Heavy, uniform snow load on a dwelling near
Donner Summit in the Sierra Nevada of California.
(Photograph by Ian MacKinlay.)*

Second International Conference on Snow Engineering

Santa Barbara, California, June 1992

Wayne Tobiasson and Edmund Wright, Editors

CRREL Special Report 92-27

December 1992

DTIC QUALITY INSPECTED 1

Approved for public release; distribution is unlimited.

Accession For	
NTIS CRA&I	<input checked="checked" type="checkbox"/>
DTIC TAB	<input type="checkbox"/>
Unannounced	<input type="checkbox"/>
Justification	
By	
Distribution /	
Availability Codes	
Dist	Avail and/or Special
A-1	

FOREWORD

We held the Second International Conference on Snow Engineering in Santa Barbara, California, June 21-26, 1992. Scientists, engineers and architects discussed the nature, distribution and behavior of snow as it affects constructed facilities. Participants came from Austria, Canada, Chile, England, France, Japan, Norway, and the United States.

The Engineering Foundation served as conference coordinator, while the National Science Foundation and Japan Society for Snow Engineering provided financial support. The International Standards Organization, American Society of Civil Engineers Technical Council on Codes and Standards, the Japan Society for Snow Engineering and the Japan Society of Snow and Ice contributed technical backing for the conference. The Cold Regions Research and Engineering Laboratory of Hanover, New Hampshire, edited and produced the conference proceedings.

The technical sessions focused on:

1. Ground snow
2. Structural case histories
3. Analytical modeling
4. Experimental modeling
5. Snow control
6. Mechanical properties and behavior
7. Building design
8. Codes and standards.

The final session entitled, "Perspectives," was an open discussion format that summarized the session contents and stimulated participants to discuss past, present and future trends in the field.

At the conclusion of the Conference the Advisory Committee agreed that the Third International Conference on Snow Engineering will be held in Japan, with Dr. Hirozo Mihashi of Tohoku University serving as chair.

RONALD L. SACK
Chairman

**SECOND INTERNATIONAL CONFERENCE
ON SNOW ENGINEERING**

Chairman

Dr. Ronald Sack
School of Civil Engineering and
Environmental Science
University of Oklahoma
Norman, Oklahoma, U.S.A.

Co-Chairman

Dr. Michael O'Rourke
Department of Civil Engineering
Rensselaer Polytechnic Institute
Troy, New York, U.S.A.

Advisory Committee

Dr. Kristoffer Apeland
Oslo School of Architecture
Oslo, Norway

Dr. Peter A. Irwin
Rowan, Williams, Davies and Irwin, Inc.
Guelph, Ontario, Canada

Dr. Shun'ichi Kobayashi
Research Institute for Hazards in Snowy Areas
Niigata University
Niigata, Japan

Dr. Hirozo Mihashi
Department of Architecture
Tohoku University
Sendai, Japan

Dr. Jack Cermak
Cermak/Peterka and Assoc.
Fort Collins, Colorado, U.S.A.

Dr. Nicholas Isyumov
Boundary Layer Wind Tunnel Laboratory
University of Western Ontario
London, Ontario, Canada

Mr. Ian Mackinlay
Ian MacKinlay Architecture, Inc.
San Francisco, California, U.S.A.

Dr. Jiro Suzuya
Tohoku Institute of Technology
Sendai, Japan

Mr. Wayne Tobiasson
Cold Regions Research and Engineering Laboratory
Hanover, New Hampshire, U.S.A.

National Science Foundation

Dr. Ken P. Chong
Director, Structural Systems and Construction
Processes Program

Dr. Eleanora Sabadell
Director, Natural and Man-Made Hazard
Mitigation Program

Engineering Foundation

Mr. Charles V. Freiman, Director
Dr. Gordon Fisher, Secretary, Conference Committee
Mr. Jack Donaldson, Conference Coordinator

To obtain a copy of these proceedings, write to CRREL, 72 Lyme Road,
Hanover, New Hampshire 03755-1290, U.S.A.

ATTENDEES

Prof. Robert G. Albrecht
4501 NE 71st Street
Seattle, Washington 98115
Tel: 206-525-7435

Dr. Kristoffer Apeland
Oslo School of Architecture
Fagerborggt, 12,
0360 Oslo 3, Norway
Tel: 47 2 465080
Fax: 47 2 690319

Mr. Jack V. Donaldson
Engineering Foundation
345 East 47th Street
New York, New York 10017
Tel: 212-705-7835
Fax: 212-705 7441

Mr. Victor Espinosa
Minera Disputada d. Las Condes
P. de Valdivia 291
Santiago, Chile
Tel: 230-6503
Fax: 497-527

Prof. Gordon P. Fisher
Cornell University
309 Hollister Hall
Ithaca, New York 14853
Tel: 607-255-7578

Mr. Richard S. Flood
Ian Mackinlay Architecture
96 Jessie Street
San Francisco, California 94105
Tel: 415-243-4191
Fax: 415-243-9769

Mr. Bill Fyall
Raychem Corporation
300 Constitution Drive
Mail Stop 605/8010
Menlo Park, California 94025-1164
Tel: 415-361-6590
Fax: 415-361-6036

Mr. Dana L. Hart
Raychem Corporation
300 Unicom Park Drive
Woburn, Massachusetts 01930
Tel: 617-933-8001
Fax: 617-932-3341

Mr. Shunichi Hatae
Sumikin Metal Products Co., Ltd.
2-1 Yaesu, 2 Chome, Chuo-ku
Tokyo, 104 Japan
Tel: 813 328 16450
Fax: 813 328 16388

Dr. Yoshio Higashiyama
Department of Electrical and
Information Engineering
Faculty of Engineering
Yamagata University
4-3-16 Jonan, Yonezawa
Yamagata-Pref., 992, Japan

Dr. Peter A. Irwin
Rowan, Williams, Davies & Irwin, Inc.
650 Woodlawn Road, West
Guelph, Ontario N1K 1B8 Canada
Tel: 519 823-1311
Fax: 519 823-1316

Mr. Hideya Ishikawa
Nippon Steel Metal Prod., Co., Ltd.
2-10 Chuo, 2-Chome Aoba-Ku
Sendai, Miyagi 980 Japan
Tel: 022 221-4571
Fax: 022 265 6553

Prof. Nicholas Isyumov
Boundary Layer Wind Tunnel Laboratory
The University of Western Ontario
London, Ontario
N6A 5B9 Canada
Tel: 519 661-3338
Fax: 519 661-3339

Prof. Takeshi Ito
Dept. of Civil Engineering
Akita National College of Technology
1 Bunkyo-cho, Iijima
Akita-shi 011 Japan
Tel: 0188-45-2151, ext. 373
Fax: 0188-57-3191

Dr. Osamu Joh
Department of Architecture
Hokkaido University
Kita-1 3, Mishi-8
Kita-ku, Sapporo, 069 Japan
Tel: 81-11-716-2111, ext. 6235
Fax: 81-11-757-2509

Dr. Seiji Kamimura
Nagaoka University of Technology
1 603-1 Kamitomiokamachi
Nagaoka 940-21 Japan
Tel: 81-258-46-6000, ext. 7346
Fax: 81-258-46-6972

Mr. Katsumi Katakawa
Nakayama Steel Works, Ltd.
1-66, Funamachi 1-Chome
Taisho-ku
Osaka 5 51 Japan
Tel: 81-6-555-3114
Fax: 81-6-555-3181

Dr. Laurie Kennedy
Dept. of Civil Engineering
220 Civil/Electrical Engineering Bldg.
University of Alberta
Edmonton, Alberta
T6G 2G7 Canada
Tel: 403-492-1906
Fax: 403-492-0249

Mr. Randy Kissell
Conservatek
600 Franklin Square
Chapel Hill, North Carolina 27514
Tel: 403-492-1906
Fax: 403-492-0249

Prof. Shunichi Kobayashi
Res. Inst. for Hazards in Snowy Areas
Niigata University, Igarashi
Niigata 950-21
940 Japan
Tel: 81-25-262-7052
Fax: 81-25-262-7050

Dr. Toshiichi Kobayashi
Nagaoka Institute of Snow and Ice Studies
187-16 Suyoshi-Machi
Nagaoka-Shi, 9 4 0 Japan
Tel: 81-258-35-7522
Fax: 81-258-35-0020

Mr. Ian Mackinlay
Ian Mackinlay Architecture
96 Jessie Street
San Francisco, California 94105
Tel: 415-243-4191
Fax: 415-243-9769

Mr. Hiroshi Matsuda
Shinko Kenzai, Ltd.
46 Marushima-Cho
Amagasaki, Hyogo 660 Japan
Tel: 81-6-413-0198
Fax: 81-6-41 9-8776

Dr. Hirozo Mihashi
Tohoku University
Department of Architecture
Aramaki Aoba
Sendai 980, Japan
Tel: 81-22-222-1 800, ext. 4628
Fax: 81-22-268-3690

Prof. Ichiro Mizuno
Department of Architecture
Kanazawa Institute of Technology
7-1 Ohgigaoka, Nonoichi, Kanazawa
Ishikawa 921 Japan
Tel: 81-762-94-6714
Fax: 81-762-94-671 5

Dr. Tsutomu Nakamura, Director
Nagaoka Institute of Snow & Ice Studies
187-16 Suyoshi
Nagaoka 940 Japan
Tel: 81 25 835-7522
Fax: 81 25 835-0020

Mr. Toshikazu Nozawa
Tohoku Institute of Technology
35-1 Kasumicho Yagiyama
Taihakuku, Sendai 982 Japan

Prof. Michael O'Rourke
Rensselaer Polytechnic Institute
Civil & Environmental Department
Troy, New York 12180-3590
Tel: 518-276-6933
Fax: 518-276-4833

Mr. Stewart G. Osgood
Metcalf & Eddy
P.O. Box 4043
Woburn, Massachusetts 01888-404
Tel: 617-246-5200
Fax: 617-245-0823

Mr. Kiyotoshi Otsuka
Obayashi Corporation
Technical Research Institute
4-640, Shimokiyoto, Kiyose-Shi
Tokyo 204 Japan
Tel: 81-0424-95-0990
Fax: 81-0424-95-0904

Mr. Jonathan C. Paine
Snow Country Consultants, Ltd.
1080 Millar Creed Road, #202
Whistler, British Columbia
V0N 1B1 Canada
Tel: 604 932-3874
Fax: 604 932-3764

Prof. Douglas R. Powell
Sonoma State University
2418 Acton Street
P.O. Box 2654
Berkeley, California 94928
Tel: 510 843-6879

Dr. Ronald L. Sack
University of Oklahoma
School of Civil Engr. & Env. Science
202 West Boyd Street, Rm. 334
Norman, Oklahoma 73019-0631
Tel: 405-325-5911
Fax: 405-325-7508

Prof. Shuji Sakurai
Dept. of Bldg. Engineering
Hokkaigakuen University
W-11, S-26, Chuouku
Sapporo, 064 Japan
Tel: 011 841 1161, ext.731
Fax: 011 561 2951

Mr. Rune Sandvik
Norwegian Council for
Build. Standardization
Postbox 129, Blindern, 0314
Oslo Norway
Tel: 47 2 96 59 50
Fax: 47 2 60 85 70

Prof. Mikio Sasaki
Hachinohe Inst. of Technology
Department of Civil Engineering
Myo Ohbiraki 88-1
Hachinohe, Aomori 031 Japan
Tel: 01 78-25-3111
Fax: 01 78-25-0722

Dr. Horst Schaffhauser
Inst. of Avalanche Research
Austrian Federal Forestry Research
Hofburg Rennweg 1
Innsbruck, A-6010, Austria
Tel: 0043 512 57 3933
Fax: 0043 512 672820

Mr. Ashvin A. Shah
ASCE
345 East 47th Street
New York, New York 10017
Tel: 212-705-7362
Fax: 212-980-4681

Mr. Chuichi Shimomura
Snow Research Center
1-5-1 2 Moto-Akasaka
Minato-Ku
Tokyo, 107 Japan
Tel: 03-3497-1 320

Prof. Tetsu Suzuki
Faculty of Engineering
Niigata University
Ikarashi 2-nocho
Niigata City, 950-21, Japan
Tel: 81-25-262-721 1
Fax: 81-25-263-31 74

Prof. Jiro Suzuya
Tohoku Institute of Tech.
35-1 Kasumicho Yagiyama
Taihakuku,
Sendai, 982, Japan
Tel: 022-229-1151
Fax: 022-229-8279

Dr. Toru Takahashi
Faculty of Engineering
Chiba University
1-33, Yayoi-cho, Inage-ku
Chiba, 263 Japan
Tel: 81-43-251-1111, ext. 2955
Fax: 81-43-251-7337

Dr. Moriaki Tamura
Oji-ya High School
Hiyu 1111,
Ojiya-ya City 947 Japan
Tel: 81 258 83 2262
Fax: 81 258 82 0646

Mr. Wayne Tobiasson
USACRREL
72 Lyme Road
Hanover, New Hampshire 03755-1290
Tel: 603-646-4223
Fax: 603-646-4640

Mr. John R. Tory
Building Research Establishment
Structural Design Division
Garston, Watford
WD2 7JR United Kingdom
Tel: 44 92 366 4388
Fax: 44 92 366 4096

Prof. Kuniaki Toyoda
Hokkaido Inst. of Technology
419-2 Teine-Maeda
Nishi-ku
Sapporo, Hokkaido, 061-24 Japan
Tel: 011 681-2161
Fax: 011 685-1030

Dr. Yasushi Uematsu
Dept. of Architecture
Tohoku University
Aoba, Aramaki
Sendai, Miyagi, 980, Japan
Tel: 22-222-1800, ext. 4642
Fax: 22-268-3690

Prof. Teruyosi Umemura
Dept. of Mechanical Engr.
Nagaoka University of Technology
1603-1 Kamitomioka
Nagaoka, 940 - 21 Japan
Tel: 011 258 6000
Fax: 011 258 6972

Dr. Masatomo Watanabe
Department of Architectural Engineering
Hachinohe Institute of Technology
88-1 Obiraki Myo,
Hachinohe, 031 Japan
Tel: 0178 25 3111
Fax: 0178 25 5018

Dr. Jerzy Wiancki
Centre Experimental de Recherches
et d'Etudes du Batiment et des
Travaux Publics
Saint-Paul, BP 37
78470 St.-Remy-les-Chevreuse, France
Tel: 1 30-85-23-04
Fax: 1 30-85-23-14

Mr. Karl Wieser
Fluid Dynamics Res. Dept.
AVL-List GmbH,
Kleiststrasse 48
A-8020 Graz Austria
Tel: 43 316 987746
Fax: 43 316 987777

Dr. Colin John Williams
RWDI, Inc.
650 Woodlawn Road, West
Guelph, Ontario
N1K 1B8 Canada
Tel: 519 823-1311
Fax: 519 823-1316

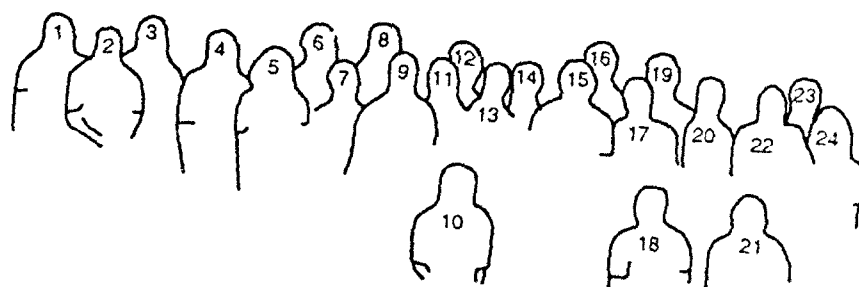
Mr. Edmund Wright
USACRREL
72 Lyme Road
Hanover, New Hampshire 03755-1290
Tel: 603-646-4314

Dr. Yutaka Yamada
Nagaoka Inst. of Snow and Ice Studies
187-16 Suyoski-nochi, Nagaoka-shi
Suyoshi, Nagaoka
Niigata 940 Japan
Tel: 0258 35 7522
Fax: 0258 35 0020

Mr. Hideharu Yamaguchi
Hokkaido Inst. of Technology
1 5-Chome, 7-Jo
Maeda, Teine-Ku
Sapporo 006 Japan
Tel: 011 681 2161
Fax: 011 681 3622



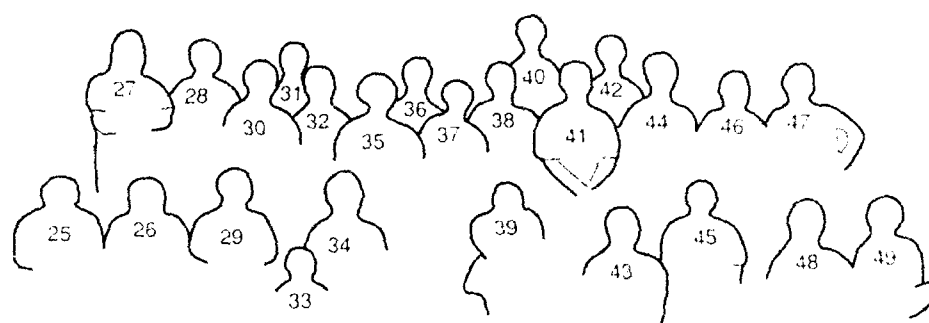
Special Attendee: Midori Nakamura—representing the next generation of snow specialists.



1. Stewart Osgood
2. Nicholas Isyumov
3. Kristoffer Apeland
4. Jerzy Wiannecki
5. Yoko Otsuka
6. Kiuotoshi Otsuka
7. Shun'ichi Kobayashi
8. Randy Kissell

9. Horst Schaffhauser
10. Victor Espinosa
11. Ashvin Shah
12. Jiro Suzyua
13. Toshikazu Nozawa
14. Yoshio Higashiyama
15. Yutaka Yamada
16. Bill Fyall

17. Kuniaki Toyoda
18. Teruyosi Umemura
19. Douglas Powell
20. Toru Takahashi
21. Ichiro Mizuno
22. Jack Donaldson
23. Lauri Kennedy
24. Takako Mizuno



25. Robert Albrecht
 26. Tetsu Suzuko
 27. Michael O'Rourke
 28. Rune Sandvik
 29. Tsutomu Nakamura
 30. Yasushi Uematsu
 31. Peter Irwin
 32. Colin Williams

33. Mideri Nakamura
 34. Hisako Nakamura
 35. Mikio Sasaki
 36. Richard Flood
 37. Toshiichi Kobayashi
 38. Masatomo Watanabe
 39. Ronald Sack
 40. Wayne Tobiasson
 41. Jonathan Paine

42. Ian Mackinlay
 43. Peg Sack
 44. Seiji Kamimura
 45. Moriaki Tamura
 46. Hirozo Mihashi
 47. John Tory
 48. Shuji Sakurai
 49. Osamu Joh

CONTENTS

	Page
Foreword	iii
Attendees	iv
 1. Ground Snow	
Statistical Analysis of Annual Extreme Ground Snow Weights for Structural Design, <i>O. Joh, S. Sakurain and T. Shibata</i>	3
Snow Load Variation with Altitude in Norway, <i>R. Sandvik</i>	15
Estimation of Ground Snow Depth Based on Topographic Factors, <i>T. Takahashi, H. Mihashi and M. Izumi</i>	21
Continuous Measurement of Snowfall Intensity per Short Time Interval, <i>M. Tamura</i>	33
The Use of Snow Survey Data in Determination of Ground Snow Loads, <i>D.R. Powell</i>	45
 2. Structural Case Histories	
Effects of Roof Size and Heat Transfer on Snow Loads on Flat Roofs, <i>P.A. Irwin, S.L. Gamble, W.H. Smeaton and D.A. Taylor</i>	59
Field Measurement and Characteristic Analyses of Snow Loads on Flat Roofs, <i>H. Mihashi, T. Takahashi and M. Izumi</i>	69
Roof Snow Observation and Application to House Construction, <i>T. Nakamura, O. Abe and S. Takada</i>	81
Survey of Roof Snow Depths by Aerial Photogrammetry, <i>S. Sakurai, O. Joh and T. Shibata</i> ..	93
Wind Effects on Snow Accumulation on a Flat Roof, <i>J. Suzuya, Y. Uematsu and T. Nozawa</i> ..	105
 3. Analytical Modeling	
Three-Dimensional Simulation of Powder Avalanches, <i>W. Brandstatter, K. Wieser and H. Schaffhauser</i>	119
Snow Load Prediction in the Andes Mountains and Downtown Toronto—FAE Simulation Capabilities, <i>P.A. Irwin, C.J. Williams, S.L. Gamble and R. Retziuff</i>	135
Investigations on Snow Disasters and Development of a Disaster Potential Index, <i>T. Ito</i>	147
Estimation of Daily Snow Mass on the Ground Using Air Temperature and Precipitation Data, <i>S. Kamimura and T. Umemura</i>	157
Simulation of Depth of Newly Fallen Snow Based on AMeDAS Data, <i>Y. Yamada and T. Ikarashi</i>	169
 4. Experimental Modeling	
Wind Tunnel Modeling of Snow Accumulations on Large-Area Roofs, <i>N. Isyumov and M. Mikitiuk</i>	181
Laboratory Studies of Snow Drifts on Multilevel Roofs, <i>M. O'Rourke and N. Weitman</i>	195
Development of a Wind Tunnel for the Study of Snowdrifting, <i>K. Toyoda and T. Tomabechi</i>	207
Excess Loads on Flat Roofs of Buildings With and Without Parapets Under the Action of Wind and Snow, <i>J. Wiancki and A. Chevallier</i>	215

5. Snow Control	Page
Static Friction of Roofing Materials Against an Ice Mass, <i>M. Watanabe and K. Hirai</i>	231
Specifying Snow Melting System Performance, <i>B. Fyall and D. Hart</i>	241
Snow Removal from a Pantiled Roof Using Electrically Heated Roof Tiles, <i>Y. Higashiyama, K. Asano, A. Miyano and Y. Murata</i>	253
Removal of Snow from Membrane Structures, <i>K. Otsuka and Y. Homma</i>	263
Engineering Studies on Pneumatic Conveying Systems of Snow, <i>T. Kobayashi and M. Kumagai</i>	275
Hydraulic Transportation Machine Development for Snow Removal from Urban Areas, <i>T. Umemura</i>	287
6. Mechanical Properties and Behavior	
Flow Characteristics of Snow-Water Mixtures in Horizontal Pipes, <i>T. Kawashima, M. Sasaki and H. Takahashi</i>	301
Mechanical Properties of High Water Content Snow, <i>S. Kobayashi</i>	313
Characteristics of Snow Pressure Acting on Avalanche-Preventive Fences, <i>K. Katakawa, C. Shimomura, H. Ishikawa, S. Hatae and H. Matsuda</i>	323
Use of a Cold Energy Element in a Low-Temperature Storage System, <i>T. Suzuki</i>	333
7. Building Design	
Design of North Cascade Visitor Center Located in Deep Snow Country, <i>R.G. Albrecht</i> ...	343
Roof Snow/Ice Loads at North-Facing Roof Eaves Compared to Ground Snow Load: Proposed Testing, <i>I. Mackinlay and R. Flood</i>	353
Reapplication of Traditional Architectural Schemes in Snow Country, <i>I. Mizuno</i>	365
Design Review for Snow Country, <i>J. Paine</i>	373
ASCE Standard 7 Snow Loads, <i>R.L. Sack and A. Shah</i>	381
An Overview of Snow Loads for Fairbanks, Alaska, <i>W. Tobiasson and A. Grestorex</i>	393
Snow Recycling House in a Heavy Snowfall District, <i>T. Higuchi</i>	405
8. Codes and Standards	
Standardization of Snow Loads on Roofs—DIS 4355: Revision of ISO Standard 4355, <i>K. Apeland</i>	411
The Effectiveness of Code Provisions for Snow Accumulations on Stepped Roofs, <i>D.J.L. Kennedy, N. Isyumov and M. Mikitiuk</i>	439
The Codification of European Snow Loading, <i>J.R. Tory</i>	453
9. Perspectives	
Ground Snow, <i>H. Mihashi</i>	467
Structural Case Histories, <i>M.J. O'Rourke</i>	469
Analytical Modeling, <i>P.A. Irwin</i>	471
Experimental Modeling, <i>N. Isyumov</i>	473
Snow Control, <i>C. Williams</i>	477
Mechanical Properties and Behavior, <i>W. Tobiasson</i>	479
Building Design, <i>I. Mackinlay and R.S. Flood</i>	481
Codes and Standards, <i>K. Apeland</i>	485

1

Ground Snow

Hirozo Mihashi, Chairman



Measuring the depth and density of snow on the ground in central Afghanistan. (Photograph by Douglas Powell.)

Statistical Analysis of Annual Extreme Ground Snow Weights for Structural Design

Osamu Joh,* Shuji Sakurai,[†] and Takuji Shibata**

*Department of Architecture, Hokkaido University, Sapporo, Japan

[†]Department of Architecture, Hokkai-Gakuen University, Sapporo, Japan

**Department of Architecture, Hokkaido University, Sapporo, Japan

ABSTRACT

Extreme snow load may not be represented by the product of the extreme snow depth and its average snow density. This is because the extreme snow load generally appears later in the season than the extreme snow depth and is larger than the snow load at the time of the extreme snow depth.

This paper presents a statistical analysis of the annual extreme ground snow loads and depths measured at 12 sites located in a heavy snow district of Japan. The analysis shows that there exists a linear relation between the mean recurrence interval (MRI) values of the extreme snow depth and the extreme snow load for 10, 30, 50 and 100 years in MRI. It is a peculiarity that the above relation is acceptable to all the observation sites regardless of the differences of the latitude or the weather conditions such as temperature, humidity, magnitude of snowfall and geographical features. The assessment of design snow load may be improved by using the statistical treatment of the annual extreme snow depth and the proposed equation.

INTRODUCTION

Snow loads specified for structural design in the Building Standard Law Enforcement Order of the Japanese Government are calculated as the products of the maximum values of snow depth recorded at construction sites and the specified values of snow density. The maximum value of snow depth for structural design purposes in each district is recommended by the administrative agency concerned. Although a rational method for assessment of the design snow depth is introduced in the Structural Standard of the Architectural Institute of Japan, the values recommended by administrative agencies concerned are certainly not based on rational methods. The specified values of snow density are regulated simply as 0.3 gf/cm^3 (about 300 N/m^3) for heavy snow districts and 0.2 gf/cm^3 for the other districts. The heavy snow district is defined as the district where the maximum snow depth equals or

exceeds one meter. From investigation reports on building structures collapsed due to heavy snow, it is obvious that the excess of actual snow loads over the design snow loads was often the principal cause of the structural damages.

The data of measurement of snow depth for many years are available at over 300 meteorological stations on the Japan Islands. Therefore, the rational value of snow depth for design purposes can be obtained from the statistical analysis of the annual extreme snow data in each district. On the other hand, the data of continuous measurement of average snow density throughout many seasons are not generally obtained from the meteorological stations. Moreover, there is the difficulty that the extreme snow load appears generally later than the extreme snow depth occurs within one season. Consequently, even if the extreme snow depth and the average snow density are simultaneously measured, their product may not represent the extreme snow load. If the coupled data of snow depth and snow density measured continuously throughout many years are obtained, the rational estimation of design snow loads may be proposed by using the extreme snow load vs. the extreme snow depth relationship from the data analysis.

DATA OF ANNUAL EXTREME GROUND SNOW WEIGHTS IN JAPAN

Fortunately, we have obtained the data of snow depth and snow weight measured continuously on the ground for many years at 12 observation sites, which are distributed from 43 degree north latitude (Sapporo, Hokkaido Prefecture) to 37 degree north latitude (Shiozawa, Niigata Prefecture) in heavy snow districts of northern Japan as shown in Figure 1. The measurements were carried out in almost every days at Tokamachi, Joetsu and Shiozawa, and in about every five days to ten days at the others. A summary of the annual extreme ground snow weights and snow depths of each site is shown in Table 1. Though the periods of observation are different from each other, all data were used in the analysis because the number of reported data of snow weight is very low. The average monthly temperatures of January and February at Sapporo are -4.9 and -4.2 centigrade respectively and are the lowest among 12 sites. Those at Joetsu are +1.9 centigrade both and are the warmest. It is a peculiarity that the meteorological conditions of 12 sites are over a wide range.

At Sapporo, the maximum recorded value of the snow depth is 128 cm and the maximum recorded snow weight is 418 kgf/m² for 17 years (1963-1981). At Shiozawa, the maximum recorded value of the snow depth is 297 cm and the maximum recorded value of the snow weight is 1019 kgf/m² for 18 years (1952-1970). Tokamachi shows the largest values in the maximum recorded values of the snow depth and the snow weight among the 12 sites, which are 385 cm and 1571 kgf/m² respectively.

Samples of changes in the snow depth and snow weight during a winter are shown in Figure 2. The time lag between occurrences of the annual extreme snow depth and snow weight is obvious. The number of years in which the annual extreme snow weight appeared later than the annual extreme snow depth is greater than that in which both the values occur in a same day, in all sites as shown in Table 2. The average time lags at each site range from 10.5 days at Joetsu to 22.5 days at Shiozawa and the maximum time lag among the whole data is 68 days at Yonezawa. The maximum ratio of the annual extreme snow weight to the weight at the annual extreme snow depth among the whole data is 2.33 at Tokamachi, and their average ratios at each site range from 1.10 at Shinjo to 1.24 at Yuda.

SELECTION OF PROBABILISTIC MODELS

Extension of PPCC Criterion

The probability plot correlation coefficient (PPCC) test proposed by Filliben(1975) is used for testing five types of probability distribution functions for their goodness of fit to the data samples. The five types chose are the Type I, Type II and Type III distributions of extreme values, and the normal and lognormal distributions. These probability distribution functions $F(x)$ are described as follows:

$$\begin{array}{lll} \text{Type I} & F(x) = \exp\{-\exp[-\alpha(x-u)]\} & -\infty < x < +\infty \\ \text{Type II} & F(x) = \exp[-(v/x)^k] & 0 \leq x < +\infty \\ \text{Type III} & F(x) = \exp\{-[(\epsilon-x)/(\epsilon-w)]^k\} & -\infty < x \leq \epsilon \\ \text{Lognormal} & F(x) = \phi[(\ln x - \lambda)/\zeta] & \end{array}$$

where ϕ : Standard normal distribution function
 $k, u, v, w, \alpha, \epsilon, \zeta, \lambda$: Parameters of $F(x)$

Estimates of the distribution parameters are obtained by the regression analysis of the plots on probability papers for normal distribution of extreme values. The upper limit value ϵ of the Type III distribution was obtained by convergence calculations as the value when the correlation coefficient reached the maximum value.

The PPCC is calculated by using the following equation:

$$r = \sum (X_i - \bar{X})(M_i - \bar{M}) / \sqrt{\sum (X_i - \bar{X})^2 \sum (M_i - \bar{M})^2}$$

where X_i : Ordered observations

$M_i = \Phi^{-1}(m_i)$: Order statistic medians

Φ : Probability distribution function

m_i : Uniform order statistic medians

$$m_i = 1 - m_n \quad i=1$$

$$m_i = (i - 0.3175) / (n + 0.365) \quad i=2, 3, \dots, n-1$$

$$m_i = 0.5 \quad i=n \quad (n: \text{No. of Samples})$$

Filliben employed empirical sampling to obtain an approximation to the distribution of r under normality. For each sample size n (n equals from 3 to 100) normal random samples were generated on a computer. $N = 10^5$ samples were generated for $n \leq 10$, and $N = [10^5/n]$ samples were generated for the specified sample sizes $n > 10$. The smoothed percentage points p are given in a table resulting from the empirical sampling.

The authors carried out the empirical sampling to r under the Type I distribution of extreme values by using the Filliben's method and obtained a table showing the relationship among three valuables of the PPCC r , the percent point p (it is called a level) = 0.005, 0.01, 0.025, 0.05, 0.10, 0.25, 0.5, 0.75, 0.90, 0.95, 0.975, 0.99 and 0.995, and the sample size $n = 10 - 100$. The percentage points for the Type II and Type III distributions of extreme values can be calculated by using the above table after transforming the valuables of the Type II and Type III into logarithms.

Test of Five Probability Distribution Functions for Goodness of Fit

The level p and the PPCC r of the annual extreme ground snow weight and depth in each probability distribution function are shown in Table 3. The symbols of \odot for the level of more than 50%, \circ for the level of 5% to 50%, \triangle for the level of 1% to 5%, and \times for the level less than 1% are used to simplify the Table. The Type III and normal distributions provide a better fit on the result that the levels of the snow weights and snow depths in all observation sites exceed 5% as shown in Tables 3(c) and 3(d) respectively. The Type I distribution also provides a better fit excepting the snow weight of Yoroihata and the snow depth of Tokamachi.

Figure 3 shows the numbers of observation sites fitting to each level in five probability distribution functions. The Type III distribution provides the best fit among the five types for the snow weight and snow depth, and most of the numbers are the level of more than 50%. Figure 4 shows the five probability distributions of annual extreme weights for each observation site. The figure also shows that the Type III distribution is the best fit and the Type I and normal distribution are better. All the annual extreme snow weights were plotted on the probability papers for normal distribution and extreme value in every site as shown in Figure 4.

Judging from the above-mentioned results, the probability distribution functions for the annual extreme snow weight must be same to that for the annual extreme snow depth at each site, and the Type III and normal distribution functions show the best and better fit respectively for both the annual extreme snow weight and depth at all the sites.

MEAN RECURRENCE INTERVAL VALUE

Table 4 is the comparison of each probability distribution to the optimum distribution for mean recurrence interval values of snow weights. The optimum distribution was determined in each observation site by using the MPPCC. Figure 5 interprets graphically the relationship between the ratio of MRI values and recurrence interval. The ratio of MRI values is the amount of MRI value calculated using the provided distribution divided by the MRI value calculated using the optimum distribution for each observation site. The averages of the ratios of MRI values calculated using the Type III and normal distributions provided are plotted on the neighborhood of 1.0 in every interval. Those using the Type I distribution become slightly larger than 1.0 as the interval increases. Those using the other distributions are remarkably larger than 1.0 as the interval increases. The average and standard deviation of the ratios of each probability distribution to optimum distribution for 50-year MRI values of snow weights at twelve observation sites are shown in Figure 6. The standard deviations calculated using the Type III, Type I and normal distribution are 0.041, 0.092 and 0.095 respectively, and the scattering is very narrow.

These behaviors appear also on the ratios of MRI values of snow depths calculated using five probability distributions to those calculated using optimum distribution for each observation site as shown in Figure 7.

RELATIONSHIP BETWEEN MEAN RECURRENCE INTERVAL VALUES OF SNOW WEIGHTS AND THOSE OF SNOW DEPTHS

The relationship between the annual extreme snow weights W_{\max} and snow depths H_{\max} has to be obtained in order to evaluate the snow load calculating

from many data of snow depths measured by the more than 300 meteorological stations in Japan. Figure 8 shows the relationship between W_{\max} and H_{\max} of every year for the observation sites. The relationship is expressed by using the function $W_{\max} = 3.2 H_{\max}$.

Since only the mean recurrence interval values of snow depths can be calculated from the data mentioned above, it is more useful that the relationship between mean recurrence interval values of snow weights and those of snow depths is obtained. It was proved in the foregoing section that the probability distributions of the annual extreme snow weights and snow depths can be seen to be very close to each other and the Type III, Type I and normal distributions are adequate to describe the annual extreme snow weights and depths. Therefore, ratios of MRI values of extreme snow weights to those of extreme snow depths were calculated using the three kinds of distributions for the recurrence intervals of 10, 30, 50 and 100 years. The ratios are correspond to conversion coefficients from snow depths to snow weights.

The averages and deviations of the ratios for the 12 observation sites are shown in Table 5 and plotted in Figure 9. The results of calculations suggest adequate correlations between RMI values of snow weights and depths, and the coefficients of correlation are 0.970, 0.964 and 0.971 for the Type I, Type III and normal distributions respectively. The conversion coefficients increases slightly as the MRI value increases. From the results shown in Table 5, however, it may be proposed that the conversion coefficient is 3.5 as a practical value for every recurrence interval not more than 100 years.

$$W_{MRI} = 3.5 H_{MRI}$$

where W_{MRI} is MRI value of annual extreme snow weight (kgf/m^2)

H_{MRI} is MRI value of annual extreme snow depth (cm)

It is noteworthy that this equation is adapted to all the sites which are located widely from the cold district to the relatively warm district. This means that the snow densities which were different remarkably to each other site at the annual extreme snow depth increase after the time as shown in Fig. 2, and approach closely at the annual extreme snow weight as shown by Nakamura(1992).

CONCLUSIONS

This paper presents a statistical analysis of the extreme ground snow weights and depths measured at twelve sites located in heavy snow district of Japan. From the analytical results, the following conclusions can be drawn:

(1)The analysis shows that the Type III distribution is the best adequate to describe the annual extreme ground snow weights and depths at all the sites, the Type I and normal distributions are better adequate, but the Type II and lognormal distributions are not adequate.

(2)There exists an obvious linear relation between the mean recurrence interval values of the extreme snow depths (H_{MRI} (cm)) and the extreme snow weights (W_{MRI} (kgf/m^2)) for the mean recurrence interval, MRI = 10, 30, 50 and 100 years in the heavy snow districts of Japan. The relationship can be seen that $W_{MRI} = 3.5 H_{MRI}$ for three above mentioned distributions.

(3)The assessment of design snow load may be improved by using the statistical treatment of the annual extreme snow depths and the equation proposed in this paper.

ACKNOWLEDGMENTS

The authors are also grateful to the snow researchers for providing their essential observed data and their useful comments.

REFERENCES

Filliben, J.J., "The Probability Plot Correlation Coefficient Test for Normality," *Technometrics*, Vol.17, No.1, Feb.1975, pp.111-117

Nakamura, T.(1992) "Roof-Snow Observations and the Applicant to House Construction," *Proceeding of the Second International Conference on Snow Engineering* (this proceeding).

Table 1. Summary of Annual Extreme Ground Snow Weights

Observation sites	Sap-poro	Hiro-saki	Yoro-ihata	Yuda	Kama-buchi	Shin-jo	Obana-zawa	Yone-zawa	Tada-mi	Toka-machi	Jo-etsu	Shino-zawa
Observation years	1964-'86	1965-'86	1961-'72	1961-'75	1941-'87	1974-'88	1958-'75	1958-'75	1962-'76	1940-'85	1962-'80	1953-'70
No. of years	21	16	11	12	43	15	17	13	12	46	19	18
Maximum	W	418	362	400	1148	1071	710	892	760	1221	1571	721
	H	128	120	171	296	292	214	225	170	339	385	220
Minimum	W	189	61	187	306	147	126	223	222	267	233	27
	H	64	21	71	94	48	54	80	77	110	97	19
Mean	W	306	217	333	644	541	420	575	424	803	816	390
	H	100	69	129	187	157	129	147	124	223	237	131
Standard deviation	W	70	82	67	251	209	160	200	143	286	319	211
	H	19	25	35	61	53	43	45	26	65	74	57
Average temp.	Jan	-4.9	-2.0		-3.3		-1.6	-1.8	-1.3	-1.9	-0.4	+1.9
	Feb	-4.2	-1.8		-3.1		-1.4	-1.7	-1.3	-1.7	-0.1	+1.9

W : Annual extreme ground snow weights (kgf/m²)

Average temperature : (°C)

H : Annual extreme ground snow depths (cm)

Table 2. Time Lag of Annual Extreme Ground Snow Weights

Observation sites	Sap-poro	Hiro-saki	Yoro-ihata	Yuda	Kama-buchi	Shin-jo	Obana-zawa	Yone-zawa	Tada-mi	Toka-machi	Jo-etsu	Shino-zawa
Number of years ※	17 (21)	9 (16)	7 (11)	10 (12)	33 (43)	12 (15)	14 (17)	10 (13)	10 (12)	43 (46)	17 (19)	16 (18)
Time lag (days)	Max.	38	18	37	57	43	37	63	68	57	62	25
	Mean	18.6	11.7	18.6	22.0	18.4	15.2	17.4	20.8	19.7	20.1	10.5
	σ_D	11.1	3.8	9.8	15.2	12.3	9.1	16.6	19.7	17.0	13.9	7.7
$\frac{W_{max}}{H_{max}}$	Max.	1.72	1.37	1.46	1.48	1.83	1.16	1.55	1.52	1.50	2.33	1.68
	Mean	1.19	1.19	1.16	1.24	1.17	1.10	1.20	1.21	1.21	1.19	1.23
	σ_D	0.22	0.12	0.14	0.14	0.15	0.04	0.15	0.18	0.15	0.22	0.21

[Notes] ※ Number of years in which W_{max} delayed H_{max}

σ_D : Standard deviation

() indicates total number of observed years

W_{max} : Annual extreme ground snow weight (kgf/m²)

H_{max} : Snow weight at annual extreme ground snow depth H_{max} (kgf/m²)

Table 3. Modified Probability Plot
Correlation Coefficient Test

W : Annual extreme ground
snow weights (kgf/m²)

H : Annual extreme ground
snow depths (cm)

n : Number of observed
years

⊙ : Level > 50%

○ : 5% < Level ≤ 50%

△ : 1% < Level ≤ 5%

× : Level ≤ 1%

(a) Type I Distribution

Observ. Spots	n		Level:															r value in ()		
			0.5	1	2.5	5	10	25	50	75	90	95	97.5	99	99.5					
Sapporo	21	W								○							10~25 (0.985) 5~10 (0.947)			
Hiroaki	16	W								○							25~50 (0.986) 25~50 (0.975)			
Yorihata	11	W			△					○							1~2.5 (0.983) 5~10 (0.923)			
Toda	12	W												⊙			97.5 (0.983) 75~90 (0.985)			
Kamibuchi	43	W								○							25~50 (0.984) 50 (0.987)			
Shirao	15	W								○							25~50 (0.973) 25~50 (0.972)			
Obanazawa	17	W							○								5~10 (0.945) 25~50 (0.978)			
Yonematsu	13	W												⊙			90 (0.989) 25~50 (0.985)			
Tadami	12	W								○							10~25 (0.944) 50~75 (0.979)			
Tokamachi	46	W								○							5~10 (0.989) 2.5~5 (0.969)			
Joetsu	19	W								○							5~10 (0.940) 5~10 (0.940)			
Shiozawa	18	W								○							10 (0.949) 10~25 (0.954)			

(b) Type II Distribution

Observ. Spots	n		Level															r value in ()		
			0.5	1	2.5	5	10	25	50	75	90	95	97.5	99	99.5					
Sapporo	21	W H			Δ			○									5~10 (0.943) 1~2.5 (0.920)			
Hiroaki	16	W H			x Δ												0.5~1 (0.877) 1~2.5 (0.893)			
Yorihata	11	W H			x Δ												~0.5 (0.838) 1~2.5 (0.889)			
Toda	12	W H											⊙				50~75 (0.979) 25~50 (0.964)			
Kamibuchi	43	W H	x x														~0.5 (0.905) ~0.5 (0.917)			
Shirao	15	W H			Δ Δ												1~2.5 (0.890) 1~2.5 (0.904)			
Obanazawa	17	W H			x												0.5~1 (0.889) 10~25 (0.949)			
Yonematsu	13	W H															75~90 (0.984) 5~10 (0.935)			
Tadami	12	W H				Δ											1~2.5 (0.874) 10~25 (0.942)			
Tokamachi	46	W H	x x														~0.5 (0.892) ~0.5 (0.901)			
Joetsu	19	W H	x x														~0.5 (0.812) ~0.5 (0.824)			
Shiozawa	18	W H			x Δ												1 (0.897) 2.5~5 (0.933)			

(c) Type III Distribution

Observ. Spots	n		Level															r value in ()		
			0.5	1	2.5	5	10	25	50	75	90	95	97.5	99	99.5					
Sapporo	21	W															50~75 (0.985) 75~90 (0.989)			
Hiroaki	16	W															75~90 (0.989) 75~90 (0.987)			
Yorihata	11	W															50~75 (0.974) 95~97.5 (0.981)			
Toda	12	W															95~97.5 (0.982) 75~90 (0.987)			
Kamibuchi	43	W															50~75 (0.988) 90 (0.984)			
Shirao	15	W															75~90 (0.988) 75~90 (0.986)			
Obanazawa	17	W															50~75 (0.984) 97.5 (0.983)			
Yonematsu	13	W															90 (0.989) 90 (0.989)			
Tadami	12	W															10~25 (0.954) 75~90 (0.987)			
Tokamachi	46	W															25~50 (0.985) 50 (0.988)			
Joetsu	19	W															75~90 (0.989) 75~90 (0.985)			
Shiozawa	18	W															50~75 (0.983) 75~90 (0.987)			

(d) Normal Distribution

Observ. Spots	n		Level															r value in ()		
			0.5	1	2.5	5	10	25	50	75	90	95	97.5	99	99.5					
Sapporo	21	W H															50-75 (0.985) 50-75 (0.983)			
Hiroaki	16	W H															90 (0.989) 90-95 (0.990)			
Yorihata	11	W H															10-25 (0.948) 25-50 (0.965)			
Toda	12	W H															50 (0.973) 50-75 (0.981)			
Kamibuchi	43	W H															10-25 (0.983) 50-75 (0.990)			
Shirao	15	W H															75-90 (0.987) 75 (0.984)			
Obanazawa	17	W H															25-50 (0.975) 75-90 (0.988)			
Yonematsu	13	W H															10-25 (0.981) 90-95 (0.990)			
Tadami	12	W H															10-25 (0.956) 75-90 (0.986)			
Tokamachi	46	W H															25-50 (0.988) 50 (0.990)			
Joetsu	19	W H															25-50 (0.975) 50 (0.986)			
Shiozawa	18	W H															50-75 (0.983) 75-90 (0.987)			

(e) Lognormal Distribution

Observ. Spots	n		Level															r value in ()
			0.5	1	2.5	5	10	25	50	75	90	95	97.5	99	99.5			
Sapporo	21	W H														50-75 (0.982) 10-25 (0.972)		
Hiroaki	16	W H														5-10 (0.941) 10 (0.952)		
Yorihata	11	W H														2.5-5 (0.914) 10-25 (0.948)		
Toda	12	W H														97.5-99 (0.983) 75-90 (0.987)		
Kamibuchi	43	W H														1-2.5 (0.982) 2.5-5 (0.971)		
Shirao	15	W H														5-10 (0.947) 10-25 (0.952)		
Obanazawa	17	W H														5-10 (0.948) 50-75 (0.984)		
Yonematsu	13	W H														90-95 (0.989) 50-75 (0.978)		
Tadami	12	W H														2.5-5 (0.920) 50-75 (0.978)		
Tokamachi	46	W H														0.5-1 (0.980) 1-2.5 (0.987)		
Joetsu	19	W H														~0.5 (0.980) ~0.5 (0.986)		
Shiozawa	18	W H														10-25 (0.981) 25-50 (0.978)		

Table 4. Comparison of each Probability Distribution to Optimum Distribution for MRI Values of Snow Weights

MRI		Type I	Type II	Type III	Normal	Log.
10-yr	x	1.02	1.10	1.00	1.00	1.09
	σ	0.018	0.079	0.008	0.024	0.096
30-yr	x	1.10	1.42	0.99	1.00	1.23
	σ	0.067	0.336	0.031	0.074	0.257
50-yr	x	1.13	1.63	0.98	1.00	1.30
	σ	0.092	0.540	0.041	0.095	0.346
100-yr	x	1.18	2.00	0.98	1.01	1.41
	σ	0.129	0.952	0.053	0.125	0.486

[Note] The values show the ratio of the MRI values of snow weights calculated from five probability distributions to those calculated from optimum distribution for each observation site.

Table 5. Conversion Coefficients from Snow Depths to Snow Weights

MRI		Type I	Type III	Normal
10-yr	x	3.47	3.47	3.46
	σ	0.142	0.446	0.427
30-yr	x	3.54	3.53	3.50
	σ	0.496	0.512	0.461
50-yr	x	3.57	3.56	3.52
	σ	0.516	0.594	0.472
100-yr	x	3.60	3.59	3.54
	σ	0.540	0.669	0.486
10~100-yr	x	3.51	3.54	3.51
	σ	0.186	0.552	0.418
	v	0.137	0.156	0.128

[Note] x is the ratio of MRI value of extreme snow weight to that of extreme snow depth.

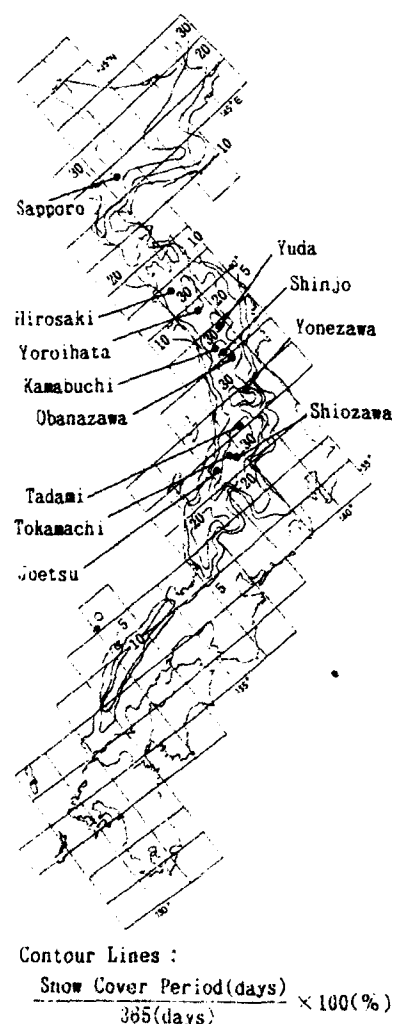


Fig. 1 Observation Sites

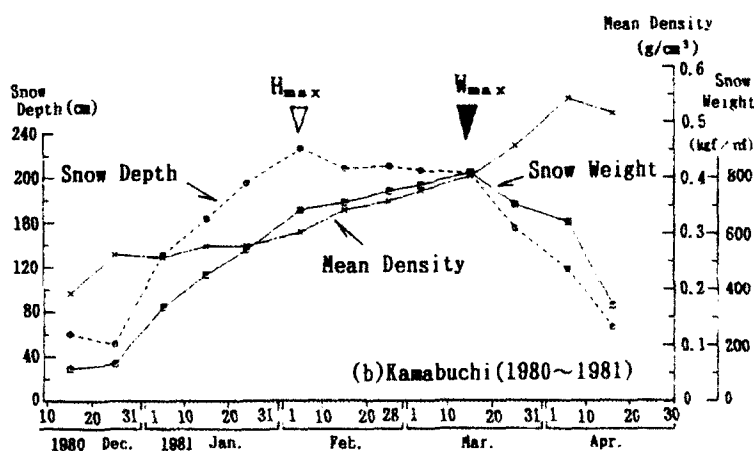
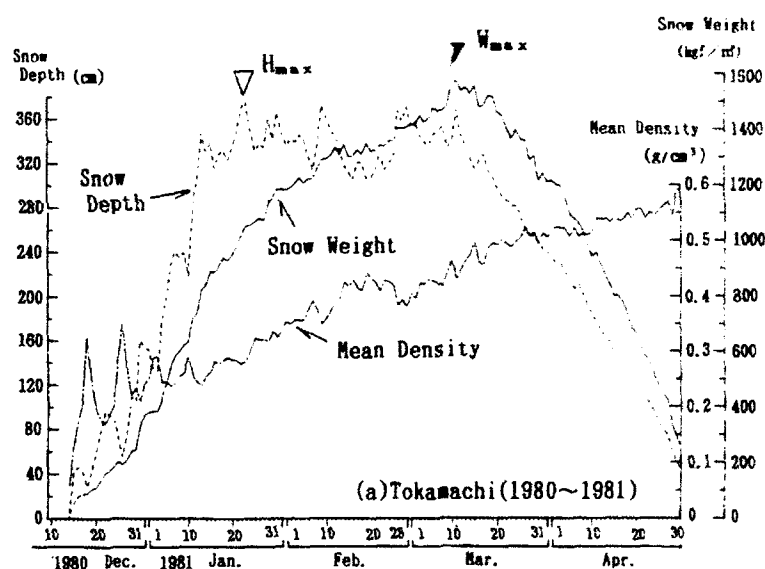


Fig. 2 Change of Snow Data during the Winter

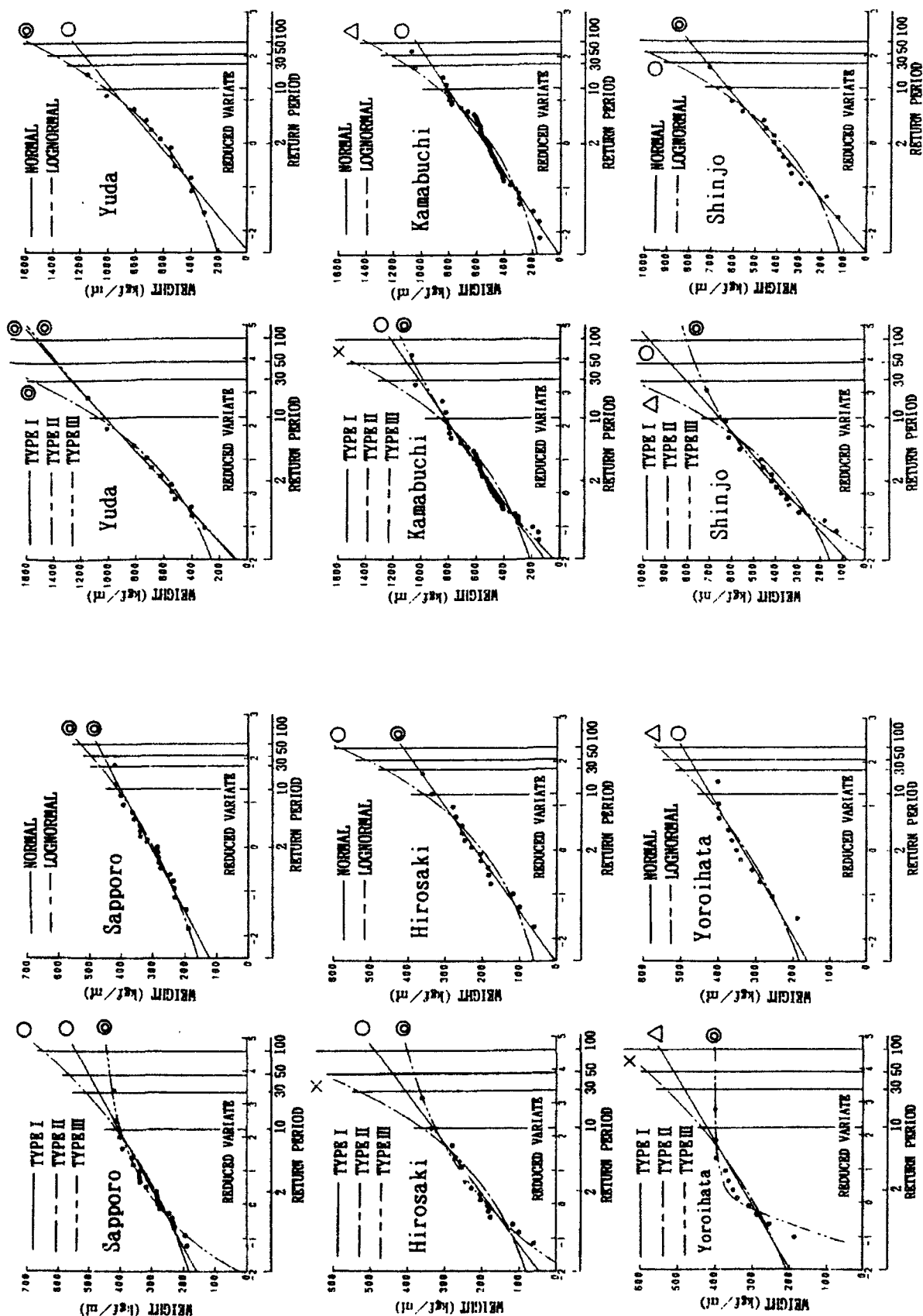


Fig. 4(a) Five Probability Distributions of Annual Extreme Weights for Each Observation Site

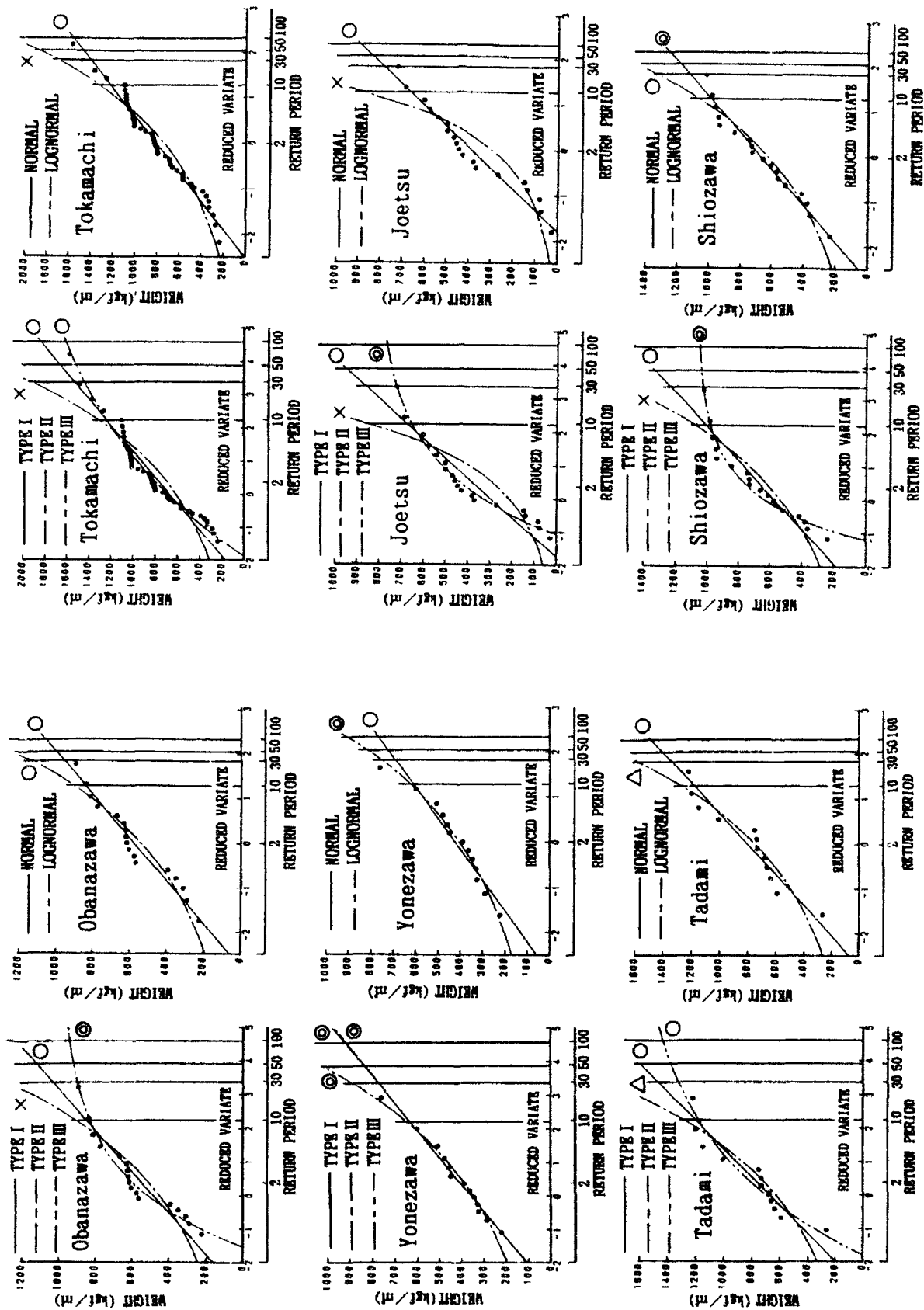


Fig. 4(b) Five Probability Distributions of Annual Extreme Weights for Each Observation Site

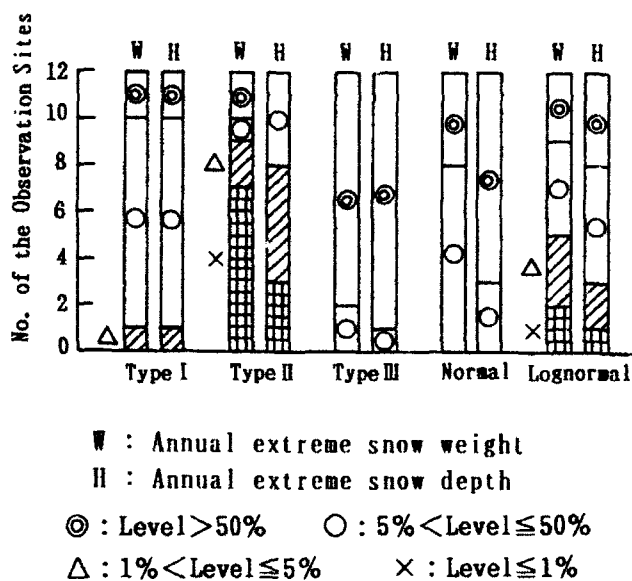


Fig. 3 Number of the Observation Sites for Significant Levels

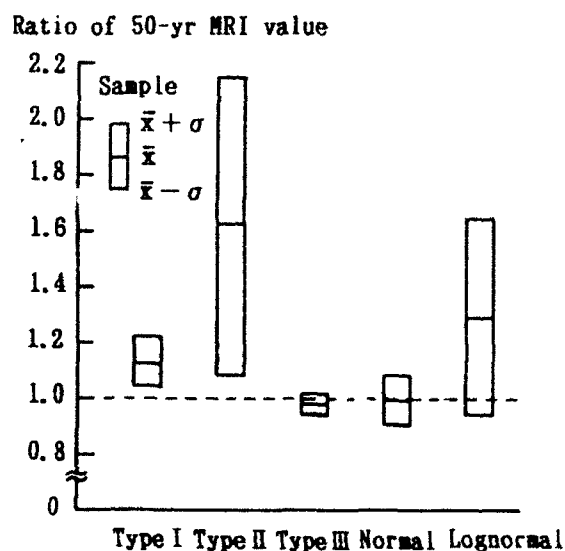


Fig. 6 Comparison of Each Probability Distribution to Optimum Distribution for 50-year MRI Values of Snow Weights

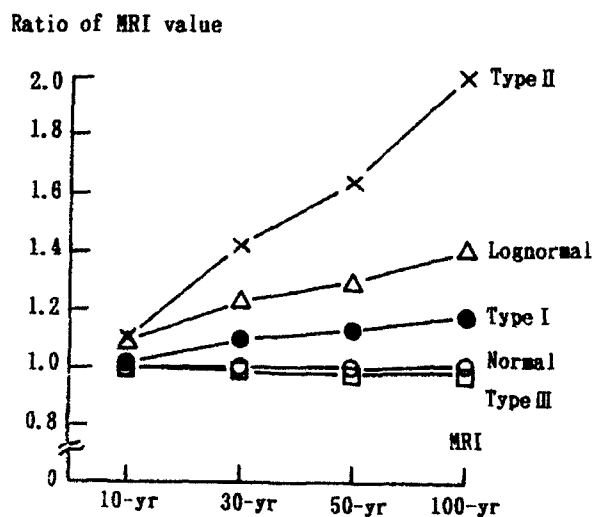


Fig. 5 Comparison of Each Probability Distribution to Optimum Distribution for MRI Values of Snow Weights

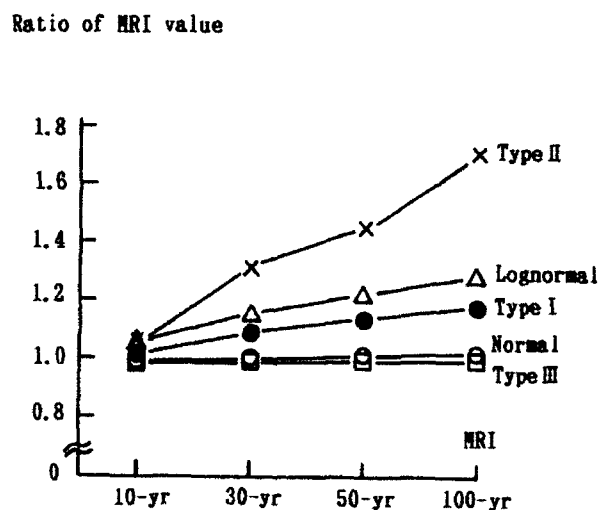


Fig. 7 Comparison of Each Probability Distribution to Optimum Distribution for MRI Values of Snow Depths

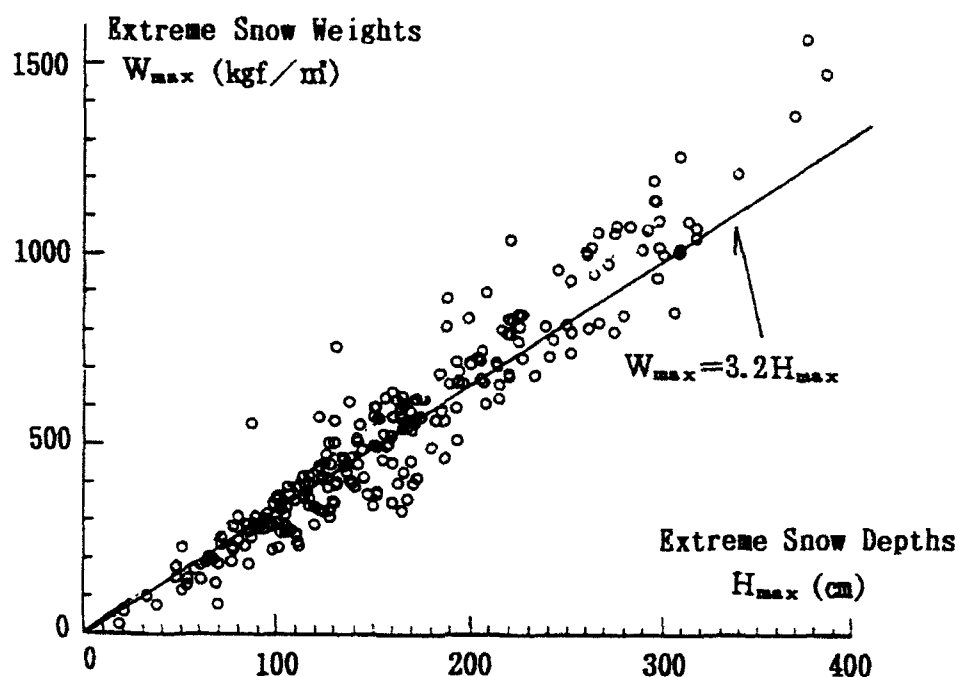
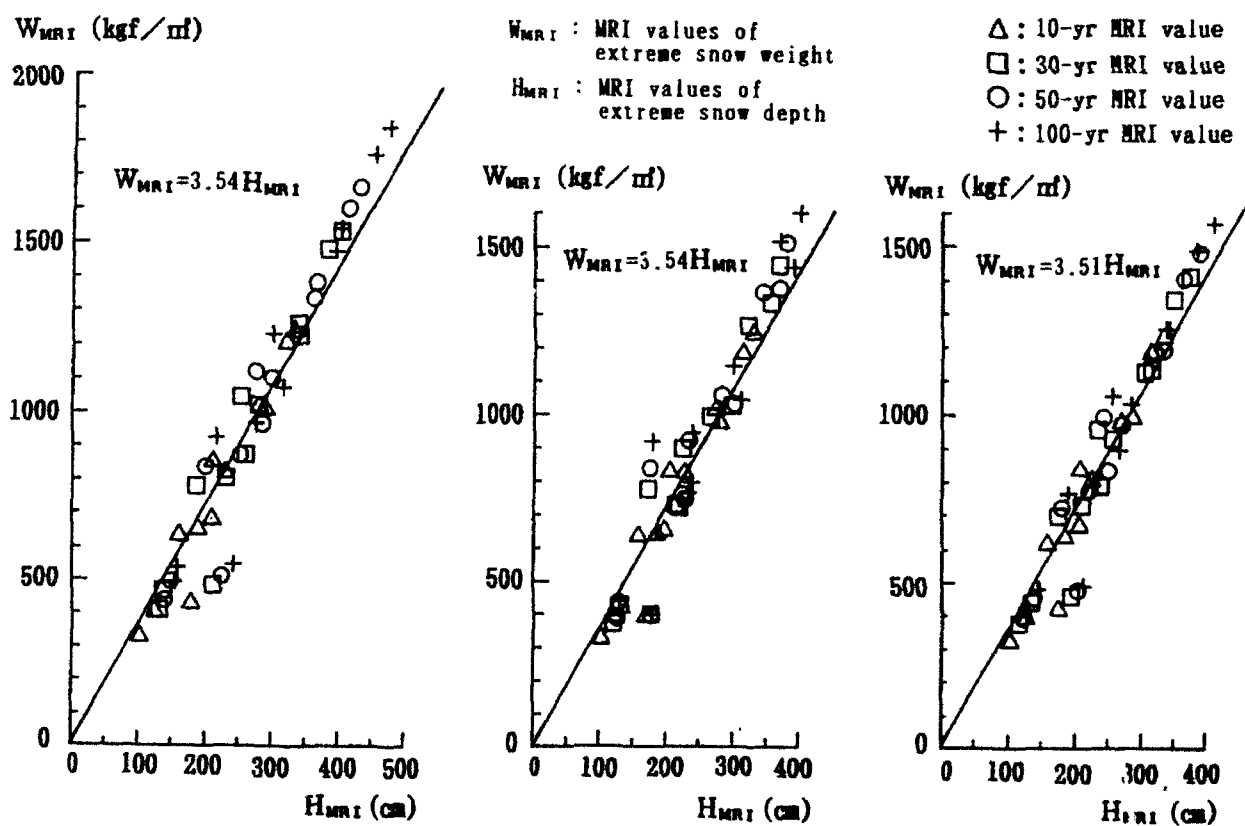


Fig.8. Relationship between W_{max} and H_{max}



(a) Type I Distribution

(b) Type III Distribution

(c) Normal Distribution

Fig.9. Relationship between W_{MRI} and H_{MRI}

Snow Load Variation with Altitude in Norway

Rune Sandvik
Norwegian Council for Building Standardization
Oslo, Norway

ABSTRACT

Snow load variation with altitude is important to consider in load standards for design of structures and is commonly given by mathematical functions, the validity of which are usually limited to defined geographical subareas in many national standards. In this paper the variation of characteristic snow load on the ground in different parts of Norway has been analyzed on the basis of calculated snow load on the ground with a return period of 50 years for approximately 200 meteorological stations. So far, no general climatical criteria have been derived on how to divide a geographical area into subareas with specific functions for the variation of snow load with altitude. The selection of subareas for the present analyses was made in order to deduce whether a specific function derived for a very small area can be relied upon when the area is enlarged without any considerable change in the climatic conditions. Another area with much the same amount of precipitation, but with lower winter temperature was analyzed, and also some areas with great differences in precipitation quantity, e.g., areas located close to the west-coast of Norway and areas shaded from heavy precipitation by mountains, are considered.

INTRODUCTION

At the end of the seventies several collapses of buildings due to snow overloading initiated an important study on snow load on the ground in Norway. As a result of a study done by Norwegian meteorological staff, many regions experienced a considerable increase in the characteristic snow load based on calculated values for a return period of 5 years. It was decided, with some exceptions, to fix an average value of the characteristic snow load for each of more than 400 municipalities. No standardized values were generally given for altitudes above 600 meters. It was of course realized that the snow load in many regions had a strong variation with altitude, also below 600 meters above sea level. However, due to the climatological complexity of mapping such subareas in Norway, and the lack of economical support, further investigations in the field were prevented.

During the last few years work was done in Germany by Gränzer (1989) resulting in a set of functions for variation of ground snow load with altitude applied by Draft Eurocode 1,

"Eurocode for the actions on structures" (1990). In Canada considerable work reported by Newark (1989) has been done to revise the ground snow load map for the National Building Code of Canada with consideration of snow load variation with altitude. In Austria, a definition of zones for snow load variation with altitude is reported by Gabl (1989).

Since 1990 the work on Eurocode 1 is also including Norway as a CEN member, and it is necessary to make further studies on the validity of the formulas proposed in Draft Eurocode 1 for the different parts of Norway.

CLIMATIC CONDITIONS OF THE REGIONS ANALYZED

Norway has a long coastline facing the North Sea and the Atlantic Ocean with heaviest precipitation, from about 1200 mm to approximately 2500 mm a year combined with relatively high winter temperatures, close to 0 degrees Celsius, at the coast. Eastern parts of central and southern Norway experience less than half this amount of precipitation and has a considerably colder winter climate.



It is important to find out whether areas can be mapped for the use of a specific formula according to some recognizable climatic parameters, as for example the normal precipitation and the winter temperature. If so, for selected areas with small variation in climate, the behavior of the characteristic snow load with altitude should be systematic.

Three dry regions were selected at the central eastern part of Norway. The first, A, is the county of Oslo, 450 sq. kilometers, and the second is Oslo and the county Akershus, B, which surrounds Oslo and covers more than 10 times its area. The third region is the county of Hedmark, C, 27.000 sq. kilometers with much the same precipitation, but a generally colder winter climate. The locations of the areas are shown on the map in Fig. 1.

On the western coast, two neighbouring coastal regions, D and E, were selected, covering a distance up to 50 kilometers from the coast. Both of these regions have a rather warm winter climate, but the northernmost region, covering the counties of Møre og Romsdal, Trøndelag and Nordland, has less precipitation.

Figure 1. Regions analyzed. See text.

In addition, a region covering eastern parts of the counties of Hordaland and Sogn og Fjordane, F, was selected to distinguish the drier parts of these counties from the wet western parts. Both regions are, however, located to the west of the main mountain ridge with a south - north direction.

All three regions at the western part of Norway are mountainous with precipitation advection by westerly winds, while precipitation from southern and eastern winds are dominant for the three eastern areas selected in this study which includes calculated values of snow load with 50-year return period for approximately 200 meteorological stations.

DISCUSSION OF RESULTS

As shown in Fig. 2, a linear function of the altitude fits the data quite well for the small area of Oslo. However, a linear function of the logarithm of the altitude has a higher correlation coefficient, 0.88 as compared to 0.85. The altitude of the region is limited to about 600 meters, and the logarithmic function seems to be preferable at an interval to 100 - 600 meters.

Figure 3 shows that the enlarged area makes the functions less reliable; however, this may still be a reasonable approach, adjusting the coefficients toward lower values and increasing the constants of both equations.

The county of Hedmark, region C, shown in Fig. 4, does not climatically differ much from the conditions typically for regions A and B, although it has slightly colder winter temperature. All three regions have maximum snow loads accumulated from several snowfalls during the winter. In spite of this, region C has no regular snow load variation with altitude, even for an interval from 100 - 800 meters. Looking at the results from all three regions it is noted that the regularity of snow load variation with altitude for dry regions located at eastern central Norway is decreasing and disappears as the area covered gradually increases.

Region F, represented in Fig. 5, the dry part of western Norway, shaded by mountains from heavy precipitation in all directions, has low values close to the sea level that increase very fast with altitude up to approximately 400 meters, and then decrease to moderate values further up to 1000 meters. The spreading of the data is very strong, which indicates that the snow load depends very much on other factors not taken into account in the selection of the climatological homogeneous area.

The area at the southern part of the west coast is represented in Fig. 6. No data are available above 400 meters. A linear function is reasonable from sea level up to 400 meters. The spreading of data is much less than for the area located more to the east. However, the coefficient is high for the equation and an extrapolation exceeding approximately 600 meters is not possible.

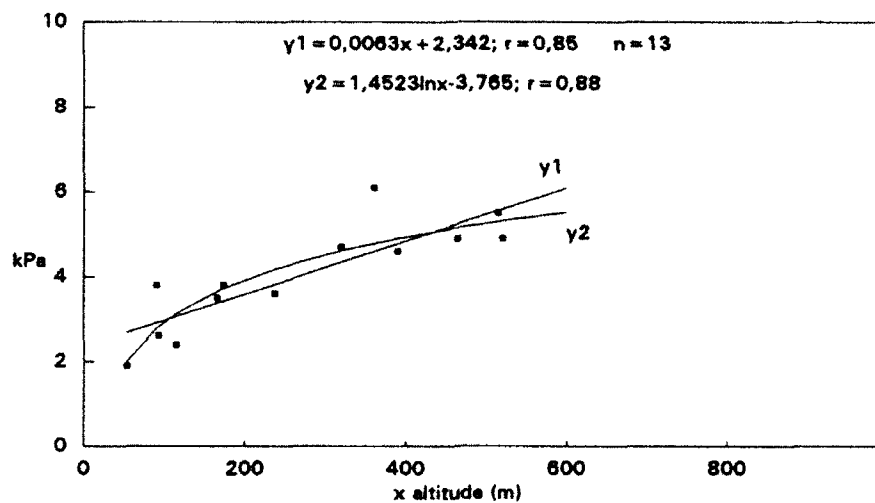


Figure 2 Snow load; 50-year return period. County: Oslo (A).

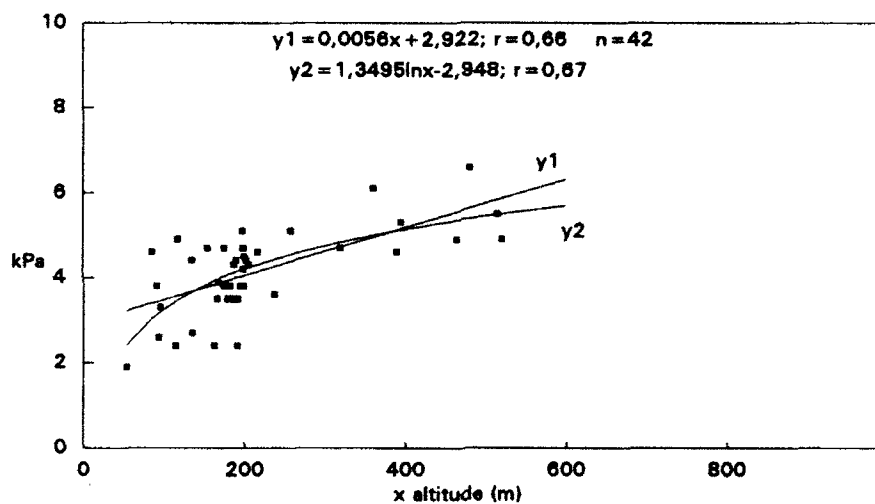


Figure 3 Snow load; 50-year return period. Counties: Oslo and Akershus (B).

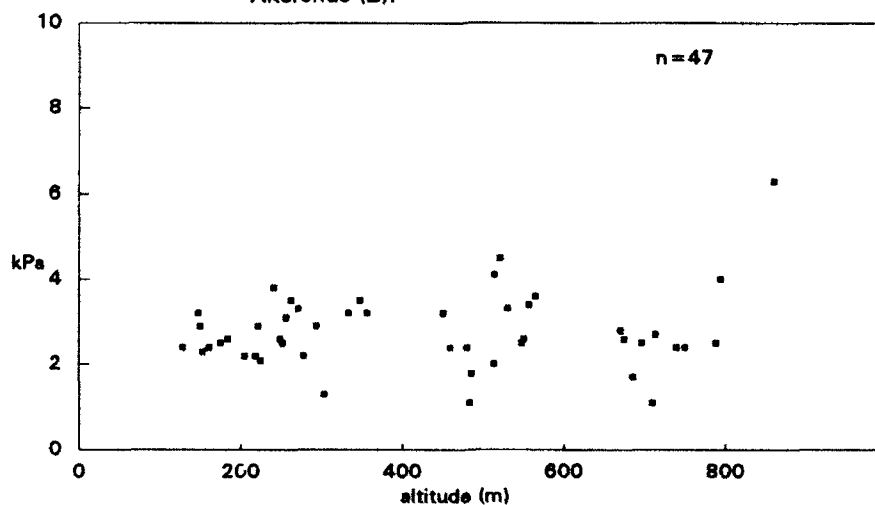


Figure 4 Snow load; 50-year return period. County: Hedmark (C).

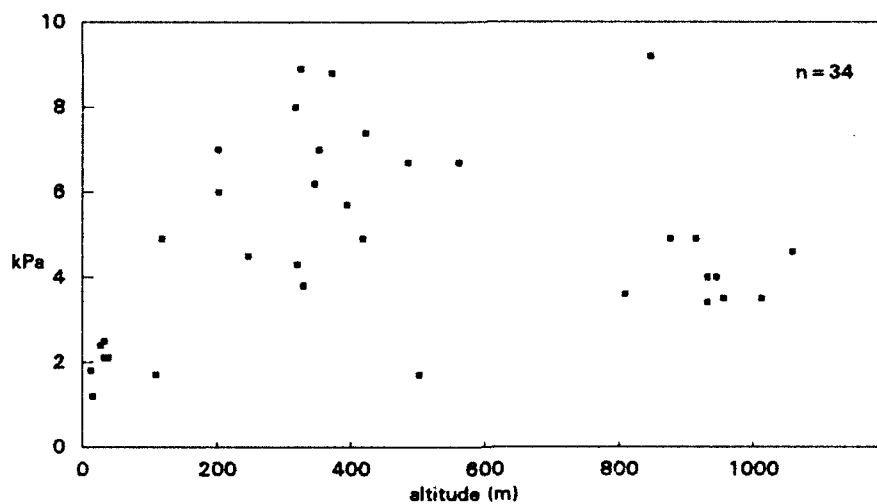


Figure 5 Snow load; 50-year return period. Counties: Hordaland and Sogn og Fjordane. Eastern parts. (F)

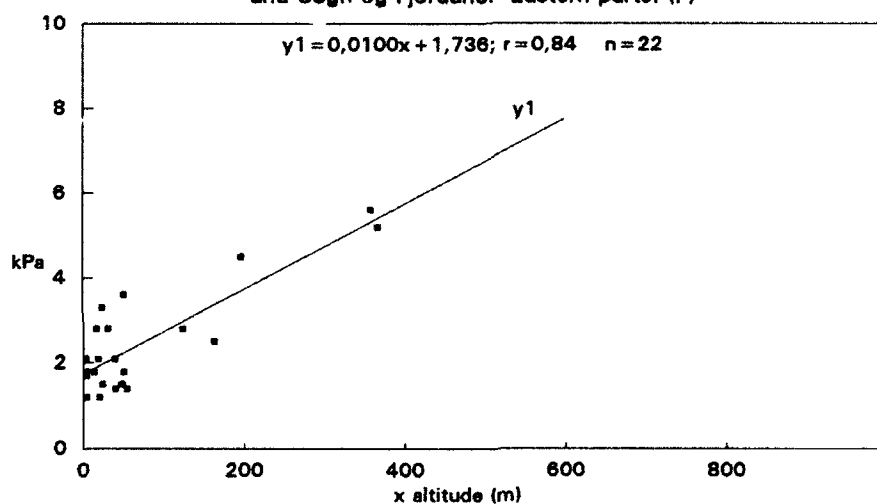


Figure 6 Snow load; 50-year return period. Counties: Hordaland and Sogn og Fjordane. Western parts. (D)

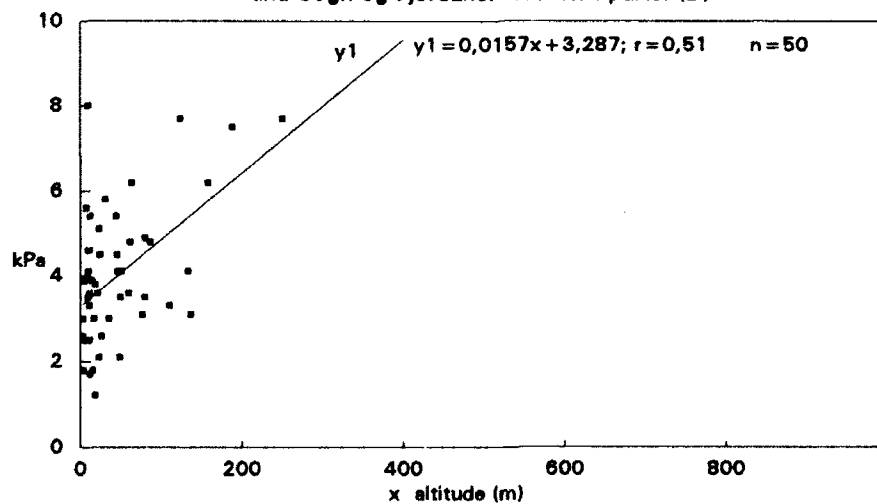


Figure 7 Snow load; 50-year return period. Counties: Møre og Romsdal, Trøndelag and Nordland. Western parts. (E)

The costal area, farther north, Fig. 7, shows very great spreading of the data, and the coefficient for the linear equation is also very high, which causes unrealistic values when extrapolating beyond 300 meters altitude.

Generally concerning both area E and F, no conclusions on the behavior of snow load with altitude can be stated.

Comparing the linear functions for the two areas, A and D, which had the highest correlation coefficient among all areas included in this study, it is notable that the snow load increase with altitude is much stronger for the area located at the west coast as compared to the Oslo area. Special care must be taken if extrapolation of the functions is considered.

The preliminary analysis on which this paper is based, demonstrates the complexity of regionalizing the behavior of snow load variation with altitude from a small area to a larger area, even when the small area remains as a central part of the larger area. It also clearly states that the climatic conditions that normally are expected to govern snowload, e.g., precipitation and temperature, are not solely reliable for the geographical mapping of formulas to determine the snow load variation with altitude.

CONCLUSION

Regionalizing snow load variation with altitude is very complex. Unexpected major irregularities occur, even for regions with closely related winter climate. In some regions the snow load variation with altitude can be represented by a linear function up to a certain level, and for a limited interval of altitude, in some cases, it is better fitted by a logarithmic function.

REFERENCES

British Research Establishment (1990), "Eurocode for actions on structures," draft, June 1990, Watford, UK.

Gabl, K. (1989), "Snow load in mountainous terrain," USA Cold Regions Research and Engineering Laboratory, Special Report 89-6. First International Conference on Snow Engineering, Santa Barbara, California, July 1988.

Gränzer, M. (1989) "Angabe von schneelasten, geografisch nach Zonen gegliedert, für den Eurocode Lasten Teil 7," Landstelle für Baustatik Baden-Württemberg, Tübingen.

Newark, M. J., Welsh, L. E., Morris, R. J. and Dnes, W. V (1989) "Revised ground snow loads for the 1990 National Building Code of Canada," Canadian Journal of Civil Engineers, Vol 16, page 267-278.

Estimation of Ground Snow Depth Based on Topographic Factors

Toru Takahashi,* Hirozo Mihashi[†] and Masanori Izumi[†]

*Department of Architecture, Chiba University, Chiba, Japan

[†]Department of Architecture, Tohoku University, Sendai, Japan

ABSTRACT

Multiple regression analyses were carried out for estimating values of AMD (Annual Maximum Snow Depth) and AMI7 (Annual Maximum Increasing Intensity of Snow Depth in 7 days) for areas without observatories. The data were those observed at 423 observation points of the Japan Meteorological Agency and several topographic factors calculated from the digital national land information of Japan. The mechanism of snowfall and actual state of structural damage were adequately related by comparing these maps with the data of heavy snow disasters.

INTRODUCTION

In Japan there are about one thousand meteorological observation points, which belong to the Japan Meteorological Agency, for daily snow depth observation. The reality is, though, that only 423 stations can be used for estimating extreme values for long return periods. Therefore, it is problem to estimate extreme values on areas without observatories. Sack and Sheikh-Taheri (1986) estimated ground snow load as related to altitude. In Europe, each country suggests estimating snow load according to altitude (Judge, 1988 and Zuranski, 1988).

On the other hand, there are several studies estimating snow depth using topographic factors (for example, Ishihara et al., 1967-75). The authors sorted out these studies (Izumi et al., 1987) and pointed out some problems. These are mainly the limitation of estimation area, and imbalance of the number of observation points and topographic factors.

In this paper, multiple regression analyses are carried out. Then the reliability of the analysis was verified, using estimated mesh maps and examining the case of heavy snow disaster in the year of 1963 and 1981.

ESTIMATION OF SNOW DEPTH

Figure 1 shows relation between snow depth and altitude. Extreme values of mean recurrence interval of 50 years are estimated by the method of the authors (Izumi et al., 1988). There does not seem to be a simple relation. The special feature is heavy snow at low altitude points. For snow depth estimation, area divisions are needed.

With consideration of snowfall characteristics, we have divided the Japanese mainland into 16 blocks as shown in Figure 2 excepting Hokkaido and Okinawa prefecture. The flowchart of producing the mesh map is shown in Figure 3. The area division was done by trial and error.

We do not adopt minute topographic factors due to the lack of observation points compared to the number of meshes. This is different from the method of Shibata et al. (1980). Topographic factors used in the analyses are shown in Table 1. Figure 4.1, 4.2 and 4.3 shows the illustrations of sea / area ratio, inclination of the land and land closing ratio, respectively. Topographic factors of each one-square-kilometer mesh have been calculated with a supercomputer because of the large number of meshes. (There are 367,811 meshes to cover the whole Japan.)

Using a supercomputer, the problem of limited geographic area was solved. After the multiple regression analysis, we got the following formula.

$$d = \sum_i a_i x_i + b - q \quad (1)$$

where, d : snow depth (dependent variable)

a_i : partial regression coefficient (independent coefficient)

b : intercept

q : variable for residual adjustment, expressed by following equation

$$q = \left(\sum_{j=1}^4 q_j / r_j \right) / \left(\sum_{j=1}^4 1 / r_j \right) \quad (2)$$

where, q_j : residual at j -th near observation point

r_j : distance from the object mesh

Tables 2.1 and 2.2 show standardized partial regression coefficients for each divided area of AMD and AMI7 for a mean recurrence interval of 50 years. The values of contribution rate with F-test and multiple correlation coefficients are also shown in Table 2.1 and 2.2. The value of contribution rate was proven to be significant by F-test for almost all districts. Topographic factors and snow depth of each point are standardized beforehand, so the values of coefficients are directly related to efficiency for the analysis. The effect of altitude is generally great, especially in AMD, and the sea / area ratio is influential in some districts. Information of latitude and longitude is also effective in several districts where the ground snow depth varies as a linear function of the geographical location.

Substituting the topographic factors of each one-square-kilometer mesh into Eq.1 with non-standardized coefficients, we get the mesh maps for snow depth. Actual partial regression coefficients for Niigata prefecture are shown in Tables 3 and 4 for AMD and AMI7, respectively. Corresponding mesh-maps are shown in Figures 5.1, 5.2, 6.1 and 6.2, respectively. On the map, the value should be neglected for areas with altitudes of 1000 m or more, because of the lack of observed data of snow depth. The special feature in these figures is that the partial regression coefficient of altitude in AMI7 is smaller than that of AMD. As you see in Figure 6.2, AMI7 values of mean recurrence interval of 50 years are uniformly accumulated. This is caused by the snowfall mechanism in this district. They sometimes have short-term heavy snowfall even in a seashore area. On the other hand, the annual maximum snow depth is the value accumulated through the winter season. Snow in the seashore area is apt to melt, and the value of AMD is smaller than that on mountainsides. The difference between AMD and AMI7 should be considered in snow load for building design, and it is verified in the following section. Additional information, colored maps for areas A to H, are illustrated in another report presented by the authors (Izumi et al., 1987, 1989).

The other feature of this analysis is that a hearing was carried out with each prefectural government. Because of the necessity of supervising building design, they have other information for snow depth. The data they have are not specified as the statistical data, but an outline of the comparison could be adopted. It is hard to estimate the values, such as area I and J shown in Figure 2. This might be because an observation point is lacking on the ridge of the mountains in those areas, and the information for ridge area is lacking. Furthermore, factor such as sea / area ratio would not be effective there. Therefore, further consideration is needed for such an area.

VERIFICATION OF ESTIMATED MESH MAP

To verify the reliability of the estimated maps, we compare them with actual snow depth for the heavy snow disasters in 1963 and 1981. We consider four prefectures damaged by heavy snow disasters in 1963 and 1981, i.e., Yamagata, Niigata, Toyama and Ishikawa prefectures. Tables 5.1 and 5.2 show correlation matrices of estimated snow depth based on the estimated maps and collapsed or damaged residential buildings' ratio (the ratio of collapsed or damaged

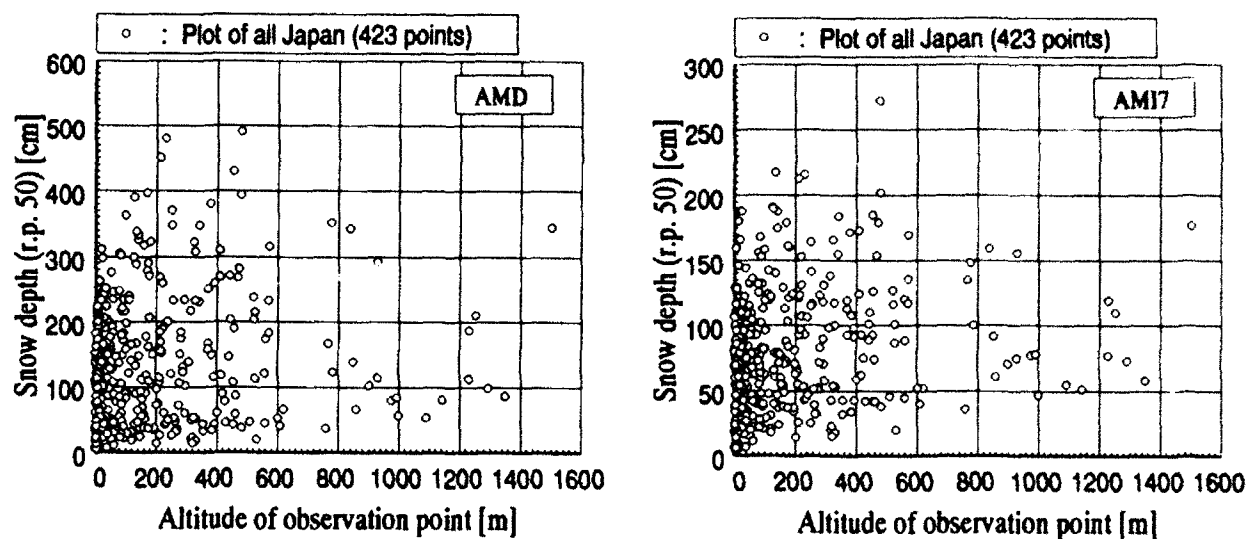


Figure 1. Relation between snow depth and altitude.

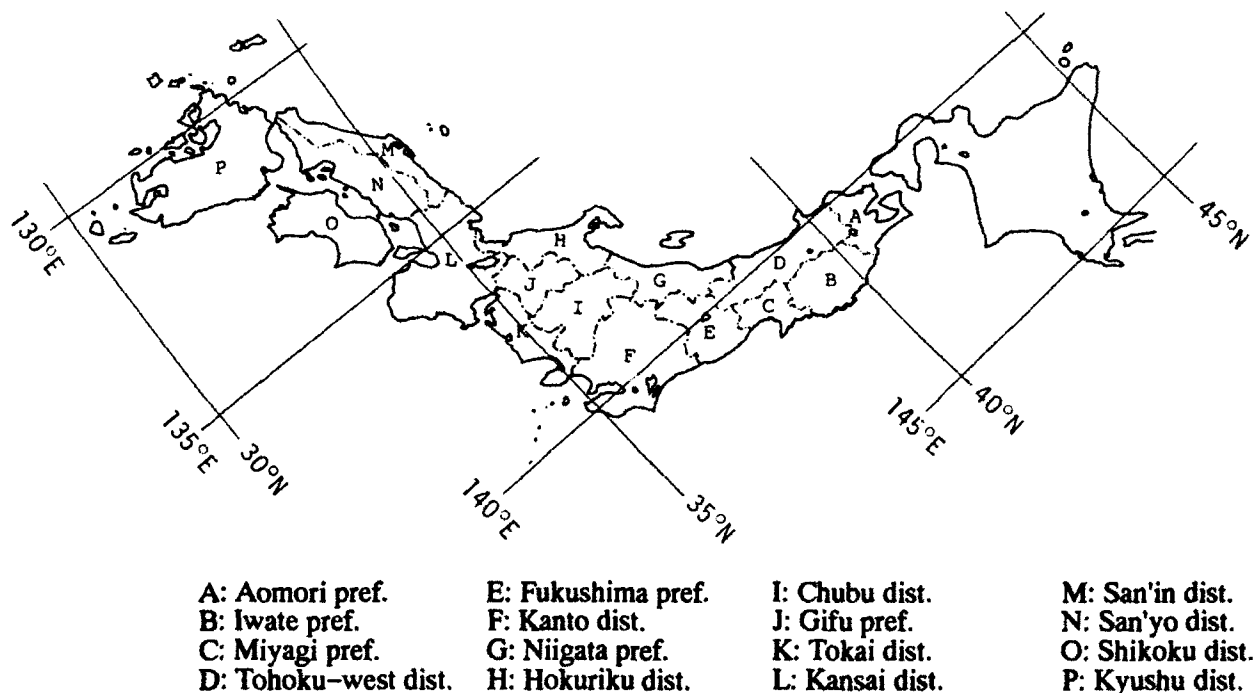


Figure 2. Area division used in multiple regression analyses.

Table 1. Topographic factors used in a multiple regression analysis.

1. Latitude
2. Longitude
3. Altitude
4. Sea / area ratio with radius of 40 km and 20 km [See Figure 4.1. (radius: 10 km)]
5. Inclination of the land in four directions with radius of 10 km (See Figure 4.2.)
6. Land closing ratio with radius of 10 km [See Figure 4.3. (radius: 5 km)]

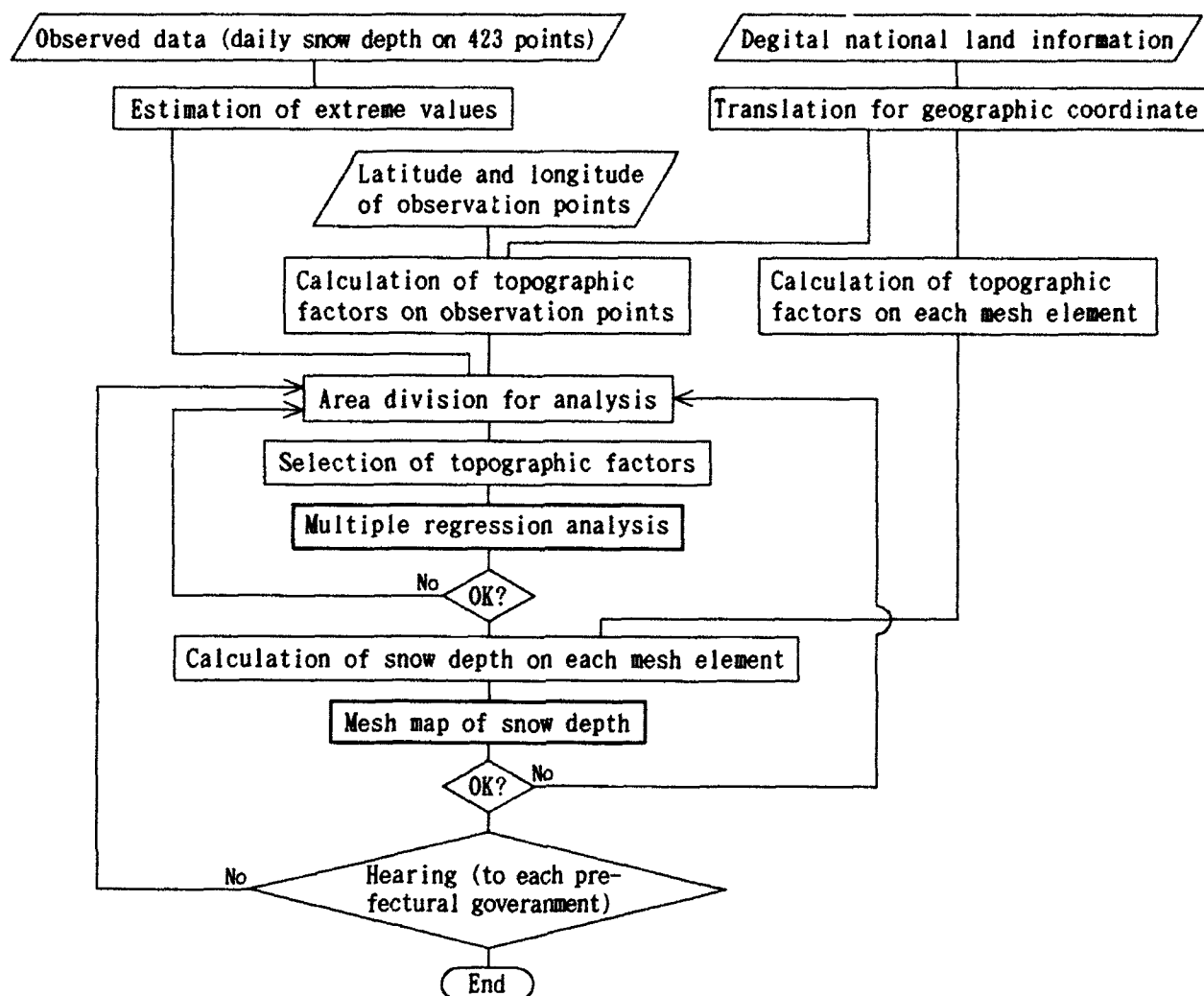
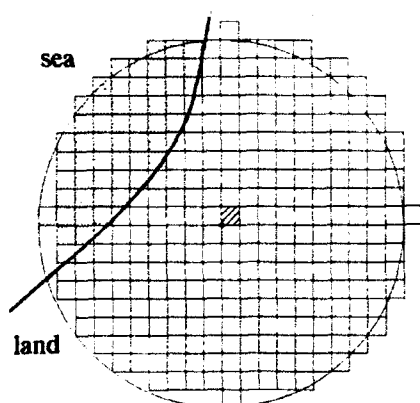
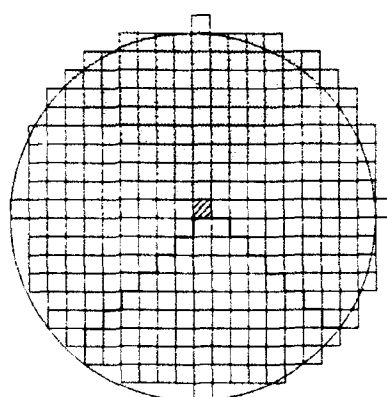


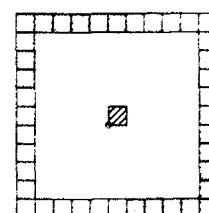
Figure 3. Flowchart for producing a mesh map of snow depth.



$$\begin{aligned} \text{SEARAT} &= \text{sea area} / \text{whole area} \\ &= 54 / 317 \\ &= 0.17 \end{aligned}$$



$$\begin{aligned} \text{INCL-N} &= \text{mean altitude of dotted area} \\ &\quad - \text{altitude of object area} \\ &\quad (\text{in this case, 'N' means north}) \end{aligned}$$



$$\begin{aligned} \text{LANDCL} &= \text{ratio of surrounding mesh} \\ &\quad \text{altitude of which is at least} \\ &\quad \text{100m higher than that of} \\ &\quad \text{object mesh.} \\ &\quad (\text{in this case,} \\ &\quad \text{LANDCL} = 18 / 40 = 0.45) \end{aligned}$$

Figure 4.1. Concept of sea / area ratio.

Figure 4.2. Concept of inclination of the land.

Figure 4.3. Concept of land closing ratio.

Table 2.1. Result of multiple regression analysis of AMD (standardized partial regression coefficients)

AMD-50	A (24)	B (52)	C (31)	D (29)	E (23)	F (31)	G (25)	H (27)
Contribution rate (F-test)	0.6850*	0.6181**	0.8722**	0.5914*	0.9360**	0.7171**	0.9548**	0.8338**
Multiple correlation coefficient R	0.8276	0.7862	0.9339	0.7690	0.9675	0.8468	0.9771	0.9131
R adjusted by degree of freedom	0.6653	0.7323	0.9041	0.6037	0.9443	0.7587	0.9605	0.8544
Latitude	0.6077*	0.5920**	0.9535**	0.0945	0.2808**	0.3418	0.2022	-0.5246
Longitude	-0.4764*	-0.9176**	-1.2495**	-0.2588	-0.7876**	-0.1168	-0.5674	0.5634
Average altitude	0.6131*	0.3847**	0.5050**	0.4659	0.3835*	0.4907	0.3502**	0.5227*
Sea area ratio (radius: 40km)	0.0327	0.1462	0.3697*	0.2726	0.3772*	-0.2963	-0.6279	0.3203
Sea area ratio (radius: 20km)	-0.3573	-	-	-0.8402	-	0.1962	-0.3474	-0.5842
Land inclination - south	-0.3746	0.0284	-0.0434	0.0707	-0.1831	0.0336	-0.4093*	-0.0062
Land inclination - west	0.0903	0.0988	-0.0368	-0.0254	0.0911	0.4227*	-0.0212	-0.1840
Land inclination - north	-0.2223	0.1009	0.0254	-0.0355	-0.2913	0.0140	-0.1055	0.0717
Land inclination - east	-0.0818	0.0297	0.0284	-0.1699	0.3636*	0.2165	0.1791	0.2245
Land closing ratio (radius: 10km)	0.1680	-0.1233	0.0435	0.0004	0.1874	-0.2730	0.2488	-0.0903
Residual	-1.084 ~ 1.151	-1.374 ~ 1.903	-0.715 ~ 1.052	-1.257 ~ 0.938	-0.713 ~ 0.466	-0.884 ~ 1.645	-0.416 ~ 0.552	-0.863 ~ 1.289

AMD-50	I (25)	J (35)	K (20)	L (23)	M (34)	N (33)	O (34)	P (32)
Contribution rate (F-test)	0.8224**	0.8396**	0.9218**	0.8268**	0.9128**	0.8159**	0.4326	0.7969**
Multiple correlation coefficient R	0.9069	0.9163	0.9601	0.9093	0.9554	0.9033	0.6577	0.8927
R adjusted by degree of freedom	0.8340	0.8791	0.9138	0.8261	0.9353	0.8557	0.4312	0.8368
Latitude	0.7079**	1.0728**	1.2473**	1.2856**	0.4828*	0.3728	-0.1353	-0.1744
Longitude	-0.0075	-0.7934**	-1.3402**	-0.0440	-0.0869	-0.1968	-0.2234	0.2065
Average altitude	-0.0160	0.2003	0.9818**	0.2151	0.6595**	1.1393**	0.2659	0.4072**
Sea area ratio (radius: 40km)	0.2562	0.0464	0.4877*	-0.0392	0.0063	0.6184*	0.0714	0.5009
Sea area ratio (radius: 20km)	-0.2611	-0.0713	-0.2222	-0.3000	-0.4364*	0.0319	-0.6618	-0.4374
Land inclination - south	0.2088	0.3562*	-0.0730	-0.0369	0.2701*	0.2937	0.1616	-0.2064
Land inclination - west	0.0862	0.1783	0.0406	0.1770	0.0124	-0.2609	0.0837	-0.4054
Land inclination - north	-0.0819	-0.0756	0.3330	0.4472	0.0358	0.1843	-0.2551	-0.2802
Land inclination - east	0.1103	-0.0794	0.0683	-0.1183	0.0305	-0.1164	-0.0251	0.3323
Land closing ratio (radius: 10km)	-0.3253	0.0374	-0.3471	-0.6538	-0.5772**	0.3085	-0.1330	0.4849*
Residual	-0.651 ~ 0.769	-0.848 ~ 1.077	-0.610 ~ 0.405	-0.741 ~ 0.785	-0.724 ~ 0.755	-0.690 ~ 0.826	-1.140 ~ 3.024	1.417 ~ 0.914

Table 2.2. Result of multiple regression analysis of AMI7 (standardized partial regression coefficients)

AMI7-50	A (24)	B (52)	C (31)	D (29)	E (23)	F (31)	G (25)	H (27)
Contribution rate (F-test)	0.5517	0.5566**	0.7232**	0.6663**	0.9180**	0.7704**	0.8785**	0.6528*
Multiple correlation coefficient R	0.7427	0.7460	0.8504	0.8163	0.9581	0.8777	0.9373	0.8080
R adjusted by degree of freedom	0.4547	0.6794	0.7776	0.6935	0.9280	0.8097	0.8898	0.6602
Latitude	0.5262	0.6154**	0.8694**	0.2586	0.4038**	0.2140	-0.7728	-0.5417
Longitude	-0.2206	-0.7897**	-0.9236*	-0.6562	-0.8784**	-0.0744	0.2698	0.7156
Average altitude	0.7035*	0.5289**	0.6552**	0.3125	0.4416	0.5845*	-0.0148	0.3890
Sea area ratio (radius: 40km)	0.1345	0.2423	0.2679	-0.1480	0.4423*	-0.2658	0.6874	0.0606
Sea area ratio (radius: 20km)	-0.4680	-	-	-0.6290	-	0.1508	-0.8768	-0.2700
Land inclination - south	-0.0518	0.0829	-0.0669	-0.1664	-0.0578	0.0227	-0.1290	-0.1692
Land inclination - west	-0.1608	0.0550	0.0561	-0.0178	-0.0678	0.4064*	-0.1022	-0.3670
Land inclination - north	0.0232	-0.1089	-0.0591	-0.1292	0.0308	-0.0801	-0.1895	0.1363
Land inclination - east	-0.3131	0.0103	-0.0282	-0.1596	0.0527	0.1700	0.2400	0.2132
Land closing ratio (radius: 10km)	0.2010	-0.1285	0.0467	0.3318	0.1719	-0.1404	0.2436	0.1075
Residual	-1.676 ~ 1.040	-1.425 ~ 1.685	-0.819 ~ 1.215	-1.148 ~ 1.003	-0.503 ~ 0.616	-0.901 ~ 1.307	-0.895 ~ 0.655	-1.294 ~ 1.528

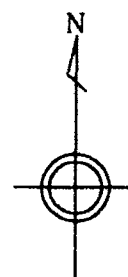
AMI7-50	I (25)	J (35)	K (20)	L (23)	M (34)	N (33)	O (34)	P (32)
Contribution rate (F-test)	0.8859**	0.8606**	0.9185**	0.8351**	0.8774**	0.8402**	0.4880	0.6988**
Multiple correlation coefficient R	0.9412	0.9277	0.9584	0.9138	0.9367	0.9166	0.6986	0.8360
R adjusted by degree of freedom	0.8969	0.8958	0.9099	0.8353	0.9078	0.8761	0.5152	0.7453
Latitude	0.6610**	0.9990**	1.2035**	1.2621**	0.4693*	0.4069	-0.0546	-0.2746*
Longitude	0.0365	-0.7692**	-0.9196*	-0.1280	0.2280	-0.2300	-0.2407	-0.2209
Average altitude	0.0752	0.1116	0.7127*	0.3800	0.5876**	1.0032**	0.2926	0.2897
Sea area ratio (radius: 40km)	0.4741*	-0.1535	0.5486*	-0.1051	0.0924	0.3614	0.2385	0.5922
Sea area ratio (radius: 20km)	-0.2796	0.2433	-0.1099	0.0038	-0.2760	0.0274	-0.8055	-0.6008
Land inclination - south	0.2434	0.3677*	0.0260	-0.0907	0.1203	0.2403	0.2005	-0.0613
Land inclination - west	0.1243	0.2022	0.0445	-0.0479	-0.0760	-0.0941	0.1159	-0.4851
Land inclination - north	-0.0536	0.0959	0.4467*	0.3946	0.0327	0.1053	-0.2843	-0.1476
Land inclination - east	0.0967	-0.1091	-0.0828	-0.2536	-0.0199	-0.0309	-0.0201	0.3775
Land closing ratio (radius: 10km)	-0.2749	0.0326	-0.4242	-0.3345	-0.1432	0.1780	-0.1356	0.4027
Residual	-0.552 ~ 0.591	-0.813 ~ 0.921	-0.458 ~ 0.611	-0.819 ~ 0.926	-0.729 ~ 0.737	-0.702 ~ 0.949	-1.245 ~ 2.478	-1.659 ~ 0.981

rejective probability **: 1%, *: 5%

Table 3. Result of multiple regression analysis of AMD
(nonstandardized partial regression coefficients)

Niigata Pref. (25 points)	AMD02	AMD50
Contribution rate (F-test)	0.968**	0.955**
Multiple correlation coefficient R	0.984	0.977
R adjusted by degree of freedom	0.972	0.960
Intercept	5664.83	18931.9
Latitude	-22.002	58.036
Longitude	-34.001	-149.668
Average altitude	0.422**	0.365**
Sea area ratio (radius: 40km)	-87.112	-305.863
Sea area ratio (radius: 20km)	-74.872	-185.615
Land inclination - south	-0.267**	-0.417*
Land inclination - west	-0.021	-0.020
Land inclination - north	-0.050	-0.117
Land inclination - east	0.007	0.167
Land closing ratio (radius: 10km)	136.457**	130.263
Residual (cm)	-34.9 ~ 37.9	-51.0 ~ 67.7

rejective probability **: 1%, *: 5%



Niigata prefecture

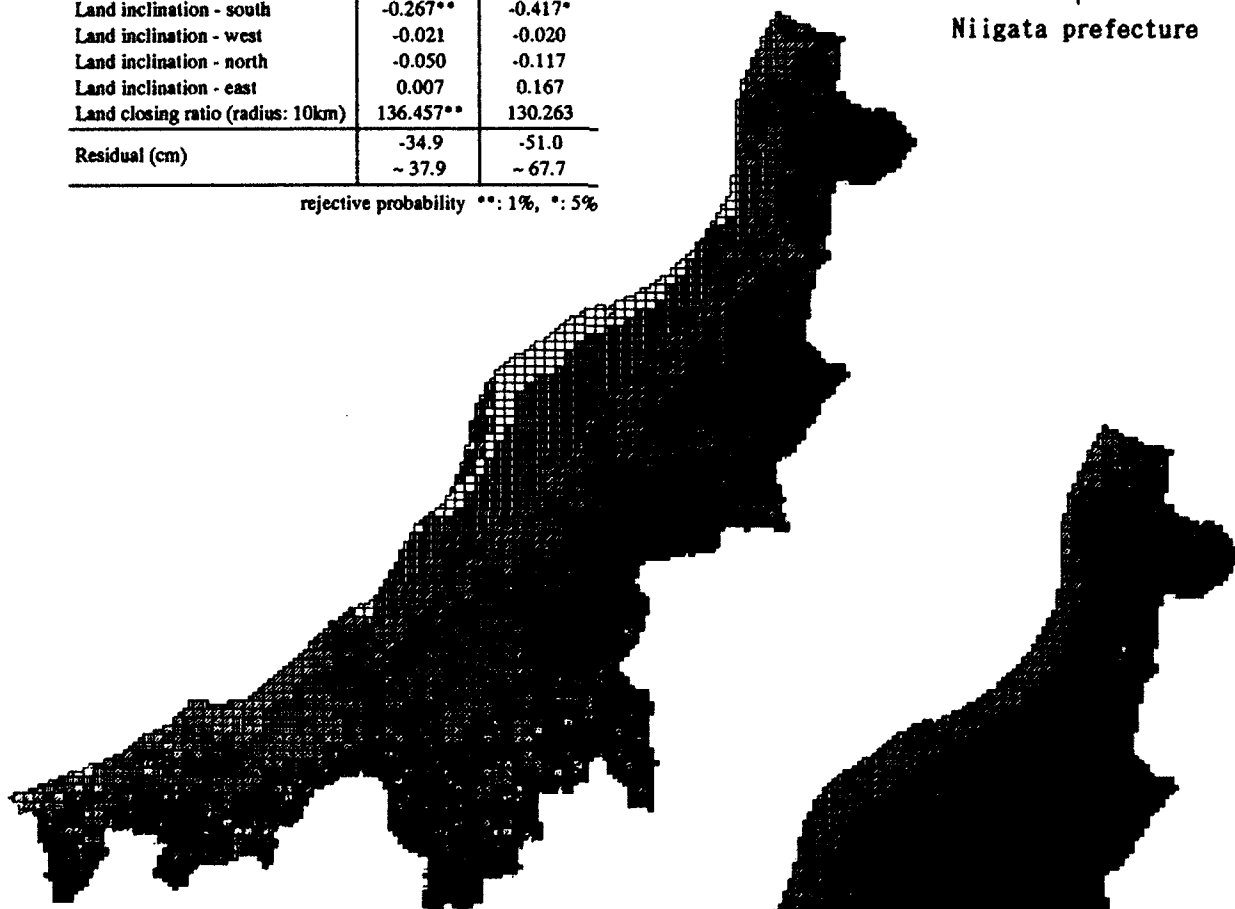


Figure 5.1. Estimated mesh map of AMD
(average year)

0 50km

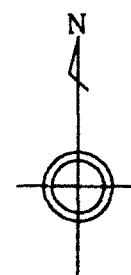


Figure 5.2. Estimated mesh map of AMD (mean recurrence interval 50 years)

Table 4. Result of multiple regression analysis of AMI7
(nonstandardized partial regression coefficients)

Niigata Pref. (25 points)	AMI702	AMI750
Contribution rate (F-test)	0.976**	0.879**
Multiple correlation coefficient R	0.988	0.937
R adjusted by degree of freedom	0.979	0.890
Intercept	2081.74	-430.04
Latitude	-23.219	-82.491
Longitude	-8.173	-26.355
Average altitude	0.104**	-0.006
Sea area ratio (radius: 40km)	-23.707	123.263
Sea area ratio (radius: 20km)	-44.097	-174.101
Land inclination - south	-0.077*	-0.049
Land inclination - west	0.000	-0.037
Land inclination - north	-0.028	-0.077
Land inclination - east	0.013	0.082
Land closing ratio (radius: 10km)	45.826**	48.119
Residual (cm)	-10.3	-40.7
	~ 15.1	~ 29.8

rejective probability **: 1%, *: 5%



Niigata prefecture

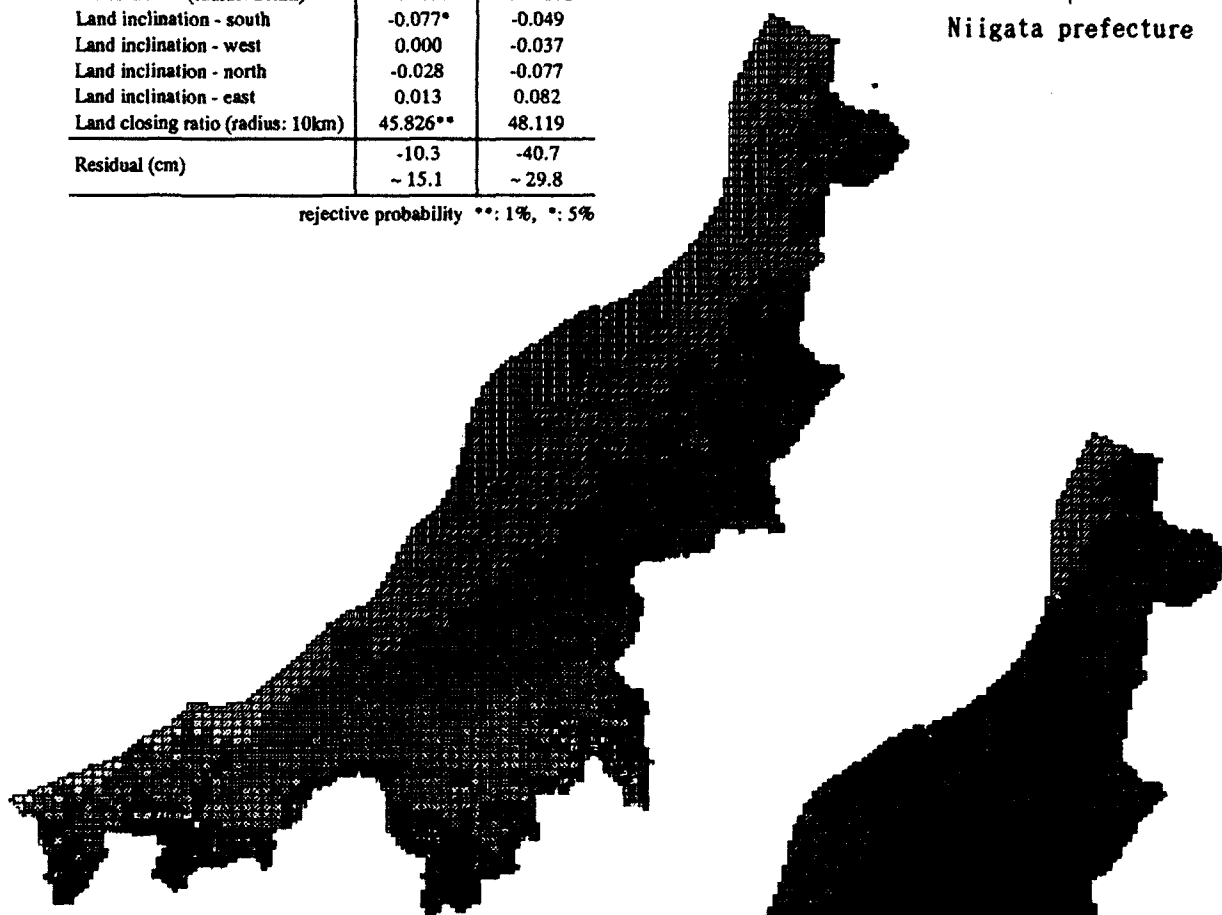
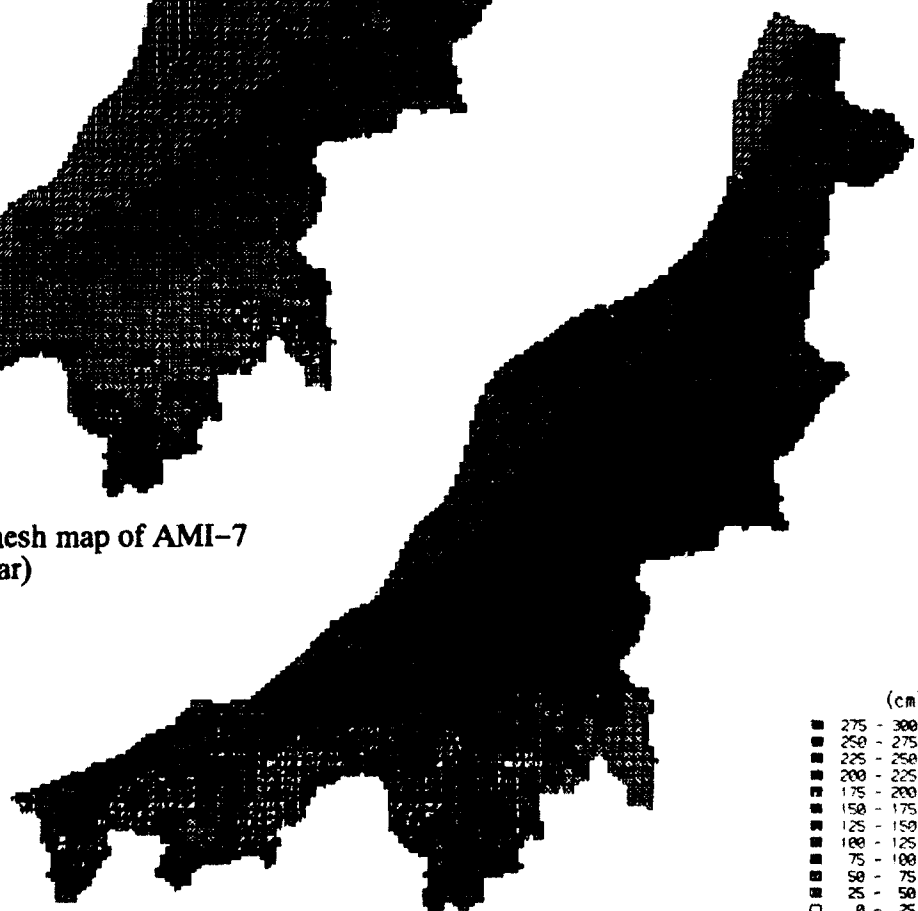


Figure 6.1. Estimated mesh map of AMI-7
(average year)

0 50km



(cm)

- 275 - 300
- 250 - 275
- 225 - 250
- 200 - 225
- 175 - 200
- 150 - 175
- 125 - 150
- 100 - 125
- 75 - 100
- 50 - 75
- 25 - 50
- 0 - 25

Figure 6.2. Estimated mesh map of AMI-7 (mean recurrence interval 50 years)

buildings to all buildings). The number of damaged and collapsed houses is based on the published reports (Dept. of Architecture, 1963, National Research Center for Disaster Prevention, 1982, 1983). Total number of residential houses in each town is based on the national census (Statistical Bureau, 1960, 1965, 1980). Notable relations are correlation coefficients between the damaged buildings' ratio and snow depth. They are negative in Yamagata and Ishikawa prefecture in 1963. On the other hand, in 1981, they have adequate correlation especially in Niigata and Ishikawa prefecture. Figure 7 shows the relation between damaged buildings' ratio (including collapsed buildings) of each town and its altitude. Each altitude is represented as that of each town hall. Table 5.1 and Figure 7 (a) show that the heavy snow disaster in 1963 occurred mainly in the plain areas and not much snow had been expected there. Figure 8 shows the relation between damaged buildings' ratio and estimated AMD. Characteristic of Figure 8 (a) is that the seriously damaged towns are concentrated in the range from 100 cm to 200 cm especially in Ishikawa prefecture. Such a characteristic does not appear in the figure of 1981. On the other hand, according to AMI7, characteristics in Figure 8 (a) do not appear in Figure 9 (a). In other words, the larger the AMI7, the more serious the damage. This result of estimation might mean that short-term heavy snowfall is the main cause of damage of buildings.

Let us consider the data from the other point of view. In Figure 10, the ratio of actual AMD of that year to estimated AMD-T50 (AMD of mean recurrence interval of 50 years), should be read along the horizontal axis. Actual AMDs in seriously damaged towns are about 1.0. After that, it can be said that the design load of these buildings may be about the value of mean recurrence interval of 50 years or a little less than that. There are a few towns that have more snow than the value of the mean recurrence interval of 50 years and are little damaged, especially in 1963. We checked the towns and the following were pointed out; they are towns mountainsides and they regularly have heavy snow. So, they probably have a custom of roof snow removal. To verify this hypothesis, Figure 12 shows the damaged buildings' ratio versus ratio of actual AMI7 of that year to estimated AMI7-T50 (AMI7 of mean recurrence interval 50 years). Unfortunately, daily snow depth is not observed in every town, and data are limited to those of the Japan Meteorological Agency (JMA). For strict comparison, the same data of Figure 12 are taken up from Figure 10 and shown in Figure 11. Comparing Figure 12 with Figure 11, such towns disappear, actual AMI7 of which is larger than the value of mean recurrence interval of 50 years and has no damage. This result means that removal of roof snow requires an interval of unit of snowfall. Then, it can be said that it is dangerous when the unit of snowfall is heavy and the value is larger than the value of mean recurrence interval of 50 years. In other words, the short-term snowfall should be considered so that buildings, especially residential houses, can be protected against heavy snow disaster.

CONCLUSIONS

Substituting the topographic factors of each one-square-kilometer mesh into the formula given by the multiple regression analyses, we obtained the mesh maps for AMD and AMI7 of mean value and the value of mean recurrence interval of 50 years. By using this formula and maps, we can estimate the value of snow depth of the areas without observatories.

Furthermore, the relation between the mechanism of snowfall and the actual state of structural damage is explained, by comparing these maps with the data of heavy snow disasters. This verification also explains the importance of snowfall in short term, for the safety of residential buildings. It is also can be said that the AMI7 might be useful for the safety of building that use snow melting or snow removal systems.

ACKNOWLEDGMENTS

Data of daily snow depth and digital national land information used in this paper were provided for "Development of Comprehensive Technology on the Construction of the Cities Preventing Snow Disaster," supported by the Japanese Ministry of Construction. The authors wish to acknowledge Mr. T. Murota who made it possible to be used. The authors should also thank officers in charge of hearing and Mr. H. Okada who gathered the report of the hearing.

Table 5.1. Correlation matrix of estimated snow depth and collapsed or damaged ratio (caused by heavy snow in 1963).

(a) Yamagata pref. (1963)

	AMD-02	AMD-50	AMI302	AMI350	AMI702	AMI750	COLLAP	DAMAGE
AMD-02	1.00**							
AMD-50	.977**	1.00**						
AMI302	.978**	.942**	1.00**					
AMI350	.910**	.879**	.964**	1.00**				
AMI702	.978**	.956**	.995**	.954**	1.00**			
AMI750	.810**	.860**	.853**	.867**	.876**	1.00**		
COLLAP	.280	.262	.357	.366	.338	.334	1.00**	
DAMAGE	.344	.322	.406	.466*	.384	.382	.496*	1.00**

(b) Niigata pref. (1963)

	AMD-02	AMD-50	AMI302	AMI350	AMI702	AMI750	COLLAP	DAMAGE
AMD-02	1.00**							
AMD-50	.962**	1.00**						
AMI302	.973**	.979**	1.00**					
AMI350	.748**	.868**	.873**	1.00**				
AMI702	.981**	.977**	.996**	.845**	1.00**			
AMI750	.740**	.852**	.845**	.935**	.842**	1.00**		
COLLAP	.219	.212	.203	.184	.194	.142	1.00**	
DAMAGE	.217	.220	.184	.117	.177	.082	.127	1.00**

(c) Toyama pref. (1963)

	AMD-02	AMD-50	AMI302	AMI350	AMI702	AMI750	COLLAP	DAMAGE
AMD-02	1.00**							
AMD-50	.987**	1.00**						
AMI302	.971**	.957**	1.00**					
AMI350	.514**	.487**	.651**	1.00**				
AMI702	.994**	.987**	.989**	.571**	1.00**			
AMI750	.866**	.880**	.904**	.802**	.898**	1.00**		
COLLAP	.120	.046	.170	.277	.123	.123	1.00**	
DAMAGE	.199	.198	.264	.435*	.227	.374	.090	1.00**

(d) Ishikawa pref. (1963)

	AMD-02	AMD-50	AMI302	AMI350	AMI702	AMI750	COLLAP	DAMAGE
AMD-02	1.00**							
AMD-50	.997**	1.00**						
AMI302	.989**	.985**	1.00**					
AMI350	.962**	.964**	.945**	1.00**				
AMI702	.995**	.993**	.998**	.953**	1.00**			
AMI750	.984**	.984**	.988**	.969**	.991**	1.00**		
COLLAP	.792**	.780**	.764**	.796**	.768**	.764**	1.00**	
DAMAGE	.206	.227	.232	.212	.228	.229	.088	1.00**

Table 5.2. Correlation matrix of estimated snow depth and collapsed or damaged ratio (caused by heavy snow in 1981).

(a) Yamagata pref. (1981)

	AMD-02	AMD-50	AMI302	AMI350	AMI702	AMI750	COLLAP	DAMAGE
AMD-02	1.00**							
AMD-50	.953**	1.00**						
AMI302	.986**	.920**	1.00**					
AMI350	.946**	.890**	.977**	1.00**				
AMI702	.990**	.949**	.992**	.968**	1.00**			
AMI750	.910**	.965**	.890**	.885**	.922**	1.00**		
COLLAP	.313	.311	.277	.287	.306	.337	1.00**	
DAMAGE	.328	.355	.316	.344	.346	.311	.008	1.00**

(b) Niigata pref. (1981)

	AMD-02	AMD-50	AMI302	AMI350	AMI702	AMI750	COLLAP	DAMAGE
AMD-02	1.00**							
AMD-50	.974**	1.00**						
AMI302	.977**	.991**	1.00**					
AMI350	.825**	.915**	.922**	1.00**				
AMI702	.985**	.990**	.997**	.902**	1.00**			
AMI750	.816**	.906**	.901**	.959**	.896**	1.00**		
COLLAP	.382**	.378**	.389**	.369**	.401**	.432**	1.00**	
DAMAGE	.386**	.349**	.374**	.324**	.383**	.351**	.866**	1.00**

(c) Toyama pref. (1981)

	AMD-02	AMD-50	AMI302	AMI350	AMI702	AMI750	COLLAP	DAMAGE
AMD-02	1.00**							
AMD-50	.995**	1.00**						
AMI302	.979**	.976**	1.00**					
AMI350	.531**	.565**	.611**	1.00**				
AMI702	.996**	.994**	.992**	.572**	1.00**			
AMI750	.879**	.903**	.888**	.834**	.895**	1.00**		
COLLAP	.466*	.436*	.430*	.043	.446*	.273	1.00**	
DAMAGE	.548**	.547**	.565**	.265	.554**	.499*	.215	1.00**

(d) Ishikawa pref. (1981)

	AMD-02	AMD-50	AMI302	AMI350	AMI702	AMI750	COLLAP	DAMAGE
AMD-02	1.00**							
AMD-50	.996**	1.00**						
AMI302	.989**	.985**	1.00**					
AMI350	.956**	.956**	.933**	1.00**				
AMI702	.995**	.993**	.998**	.952**	1.00**			
AMI750	.984**	.986**	.987**	.952**	.992**	1.00**		
COLLAP	.826**	.810**	.798**	.836**	.804**	.792**	1.00**	
DAMAGE	.872**	.870**	.865**	.854**	.864**	.841**	.820**	1.00**

rejective probability **: 1%, *: 5%

AMD-02: Annual maximum snow depth of average year.
AMD-50: Annual maximum snow depth of return period 50 years.
AMI302: Annual maximum increasing intensity of snow depth in 3 days of average year.
AMI350: Annual maximum increasing intensity of snow depth in 3 days of mean recurrence interval 50 years.
AMI702: Annual maximum increasing intensity of snow depth in 7 days of average year.
AMI750: Annual maximum increasing intensity of snow depth in 7 days of mean recurrence interval 50 years.
COLLAP: Collapsed buildings' ratio of residential houses.
DAMAGE: Damaged buildings' ratio of residential houses.

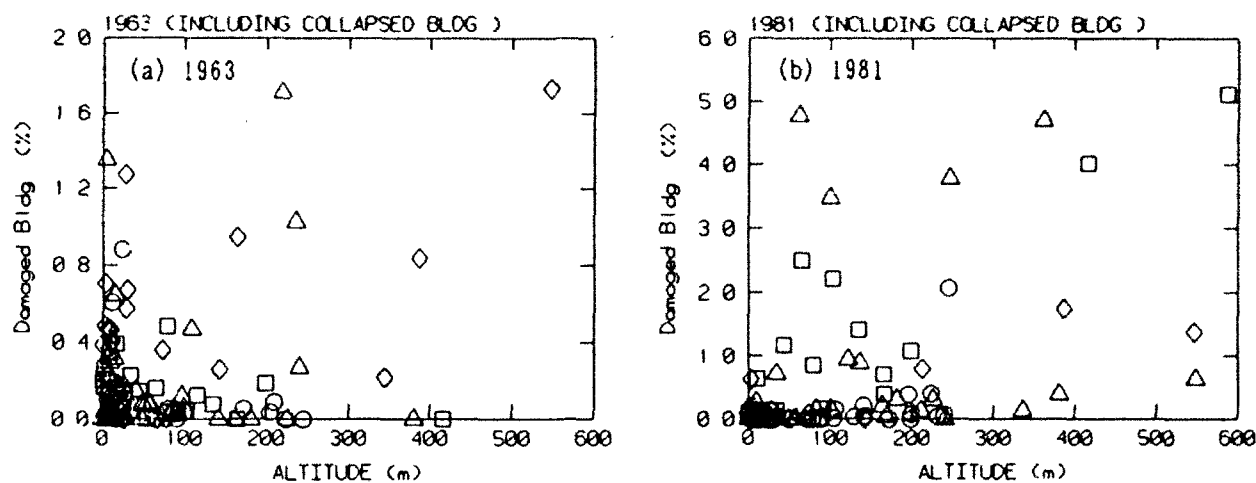


Figure 7. Damaged residential house ratio of each town vs. altitude.

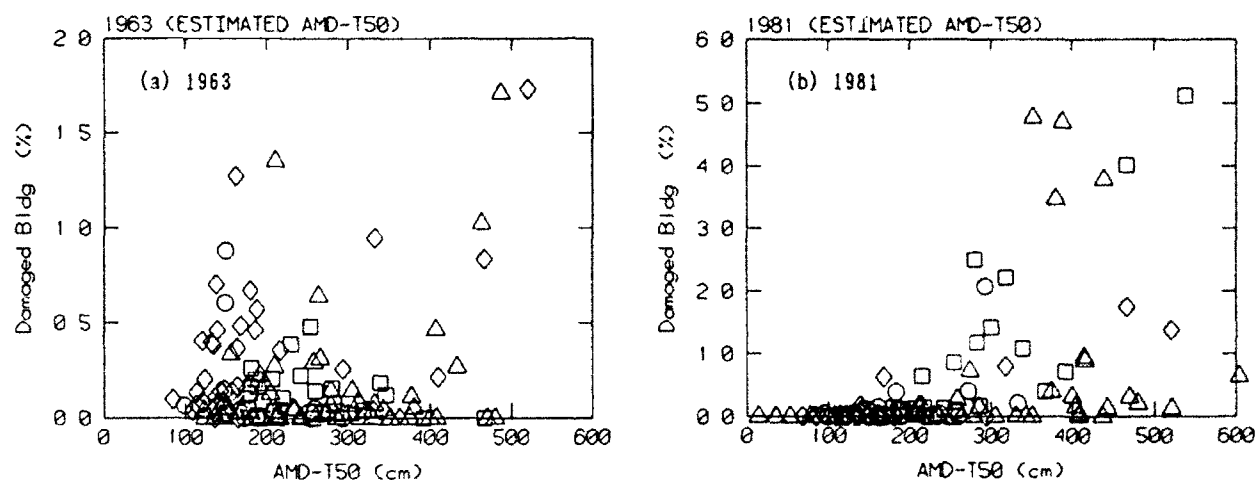


Figure 8. Damaged residential house ratio of each town vs. estimated AMD (mean recurrence interval: 50 years).

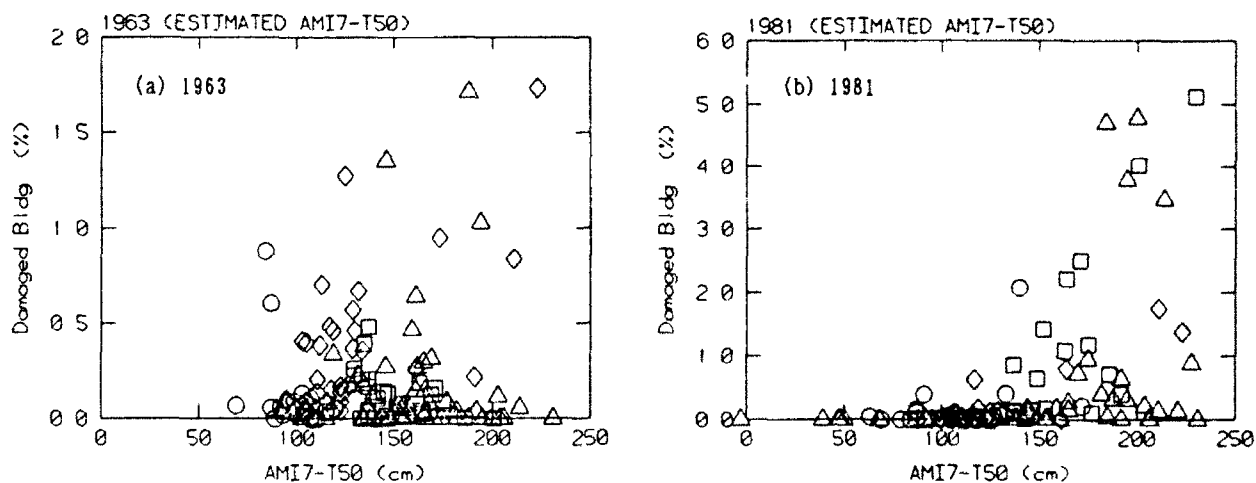


Figure 9. Damaged residential house ratio of each town vs. estimated AMI7 (mean recurrence interval: 50 years).

(○: Yamagata pref., △: Niigata pref., □: Toyama pref., ◇: Ishikawa pref.)

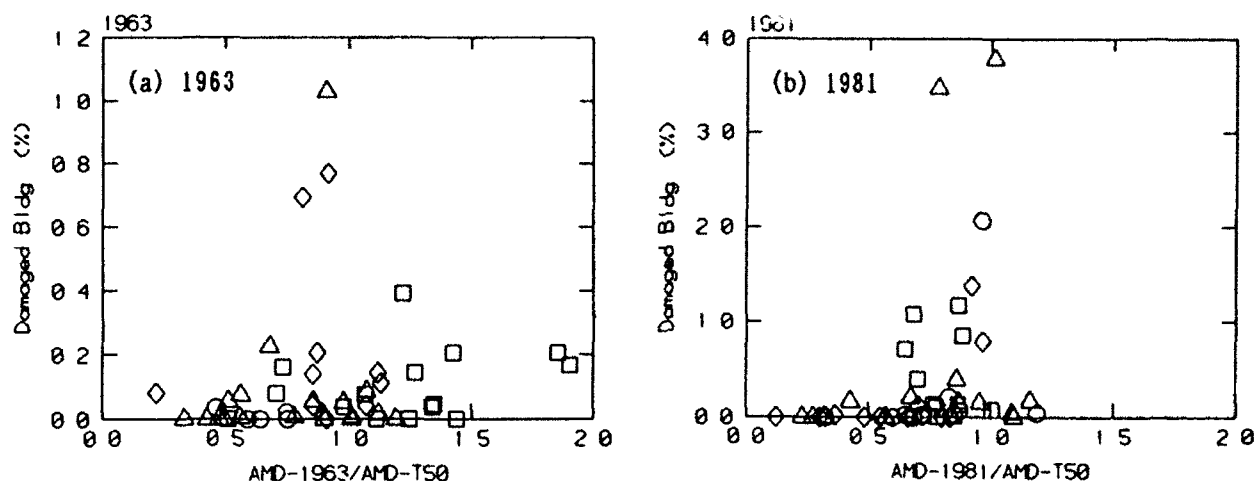


Figure 10. Damaged residential house ratio of each town v's.
ratio of actual AMD to estimated AMD of mean recurrence interval 50 years.

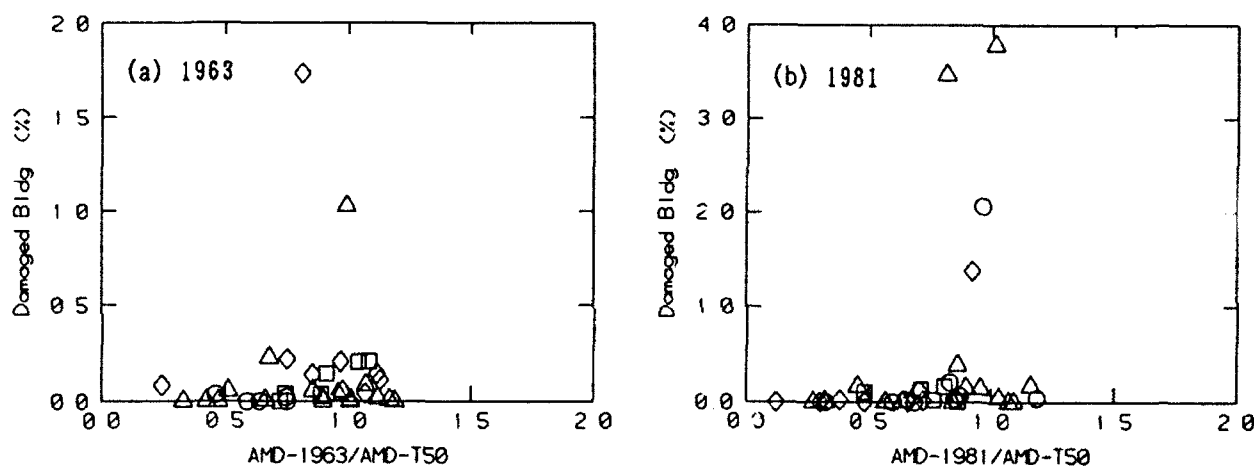


Figure 11. Damaged residential house ratio of each town vs. ratio of actual AMD to estimated
AMD of mean recurrence interval 50 years (only the observation points of JMA).

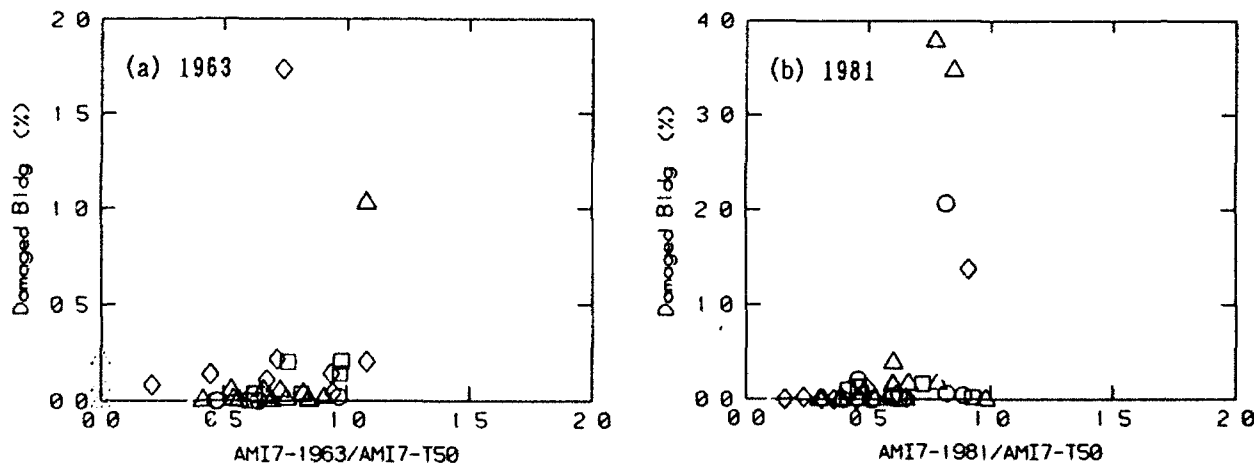


Figure 12. Damaged residential house ratio of each town vs. ratio of actual AMI7 to estimated
AMI7 of mean recurrence interval 50 years (same observation points as Figure 11).
(○: Yamagata pref., △: Niigata pref., □: Toyama pref., ◇: Ishikawa pref.)

Mr. M. Yamamoto entered the large number of data of snow disasters into the computer.

REFERENCES

Dept. of Architecture, Tohoku University (1963) *Report on Heavy Snow Disaster in January 1963*, Tohoku University, Sendai (in Japanese).

Ishihara, K. et al. (1972) "Study on Making 4km Mesh Maps for Annual Maximum Snow Depth and Mean Temperature in Winter - for Niigata Prefecture," Report of Japan Snow Union No.120, March 1972 (in Japanese).

Izumi, M., Mihashi, H. and Takahashi, T. (1988) "Statistical Properties of the Annual Maximum Series and a New Approach to Estimate the Extreme Values for Long Return Periods," *First International Conference on Snow Engineering*, CRREL Special Report 89-6, 25-34, July 1988.

Izumi, M., Mihashi, H., Takahashi, T. and Ono, M. (1987) "An Estimation of Geographical Distribution of Annual Maximum Snow Depth Based on Topographic Factors" *The Architectural Reports of The Tohoku University*, No.26, 75-83, March 1987 (in Japanese with English abstract).

Izumi, M., Mihashi, H., Takahashi, T. and Yamamoto, M. (1989) "Estimation of Geographical Distribution of Annual Maximum Increasing Intensity of Snow Depth and its Relation with Heavy Snowfall Damage" *The Architectural Reports of The Tohoku University*, No.28, 29-40, March 1989 (in Japanese with English abstract).

Judge, C.J. (1988) "Developing the Eurocode," *First International Conference on Snow Engineering*, CRREL Special Report 89-6, 403-412, July 1988.

National Research Center for Disaster Prevention, Science and Technology Agency (1982) "Report on Heavy Snow Disaster in Hokuriku District in 1981," Report on Major Disaster No.17, February 1982, Tsukuba (in Japanese).

National Research Center for Disaster Prevention, Science and Technology Agency (1983) "Report on Snow Disaster and the Existing State of Countermeasure for Snow in Heavy Snow Area 1980 - 1981," February 1983, Tsukuba (in Japanese).

Sack, R.L. and Sheikh-Taheri, A. (1986) *Ground and Roof Snow Loads for Idaho*, Univ. of Idaho, Moscow.

Shibata, H. and Tanaka, A. (1980) "Estimation of the Distribution of the Depth of Snow Cover," *Journal of Meteorological Research*, Vol.32, Nos.1-2, 51-57, Japan Meteorological Agency (in Japanese).

Statistical Bureau, Prime Minister's Office (1960,1965,1980) *Report of National Census*, Prime Minister's Office, Tokyo (in Japanese).

Zuranski, J.A. (1988) "Snow Loads on Roofs in East European Standards and Codes of Practice," *First International Conference on Snow Engineering*, CRREL Special Report 89-6, 419-428, July 1988.

Continuous Measurement of Snowfall Intensity per Short Time Interval

Moriaki Tamura
Nagaoka Technical High School
Saiwaicho 2-7-70, Nagaoka, Niigata Pref., 940 Japan

ABSTRACT

Snowfall intensity was measured per minute for 3 months during the wintertime from 1990 to 1991 in Nagaoka, Japan for the purpose of obtaining basic data for controlling an automatic snow-melting system. The measuring was carried out using a funnel-shaped receptacle with a heater. This instrument was used to catch and melt snowflakes so that the water drops to be counted by the light beam sensor could be recorded. For the purpose of differentiating the two types of precipitation, snow and rain, a temperature sensor was employed. The critical temperature of the air or the snow was established at 0.7°C . It was considered that at temperatures equal to and below 0.7°C there was snowfall, and at temperatures above 0.7°C there was rain.

The results of this measurement are (1) the maximum intensity was 0.35 mm/min in precipitation, (2) an exponential curve was derived relating snowfall intensity and frequency, and (3) 90 % of the total frequencies were in the 0.070 mm/min range.

INTRODUCTION

The Hokuriku district of the Main Island of the Japanese Islands, facing the Sea of Japan, has heavy snow in the winter due to the seasonal wind flowing from the continent and water vapor coming from the sea. There have been cases of 80 cm of snowfall in one day. The concentrated and continuous snowfalls of high accumulation are a bother for the people living in this district.

The snowfall has obstructed the narrow roads in the urban district. To remove these, there are methods by which snow can be melted instantaneously and continuously by sprinkling warm underground water on the roads. Figure 1 shows a snow melting system using underground water for roads.

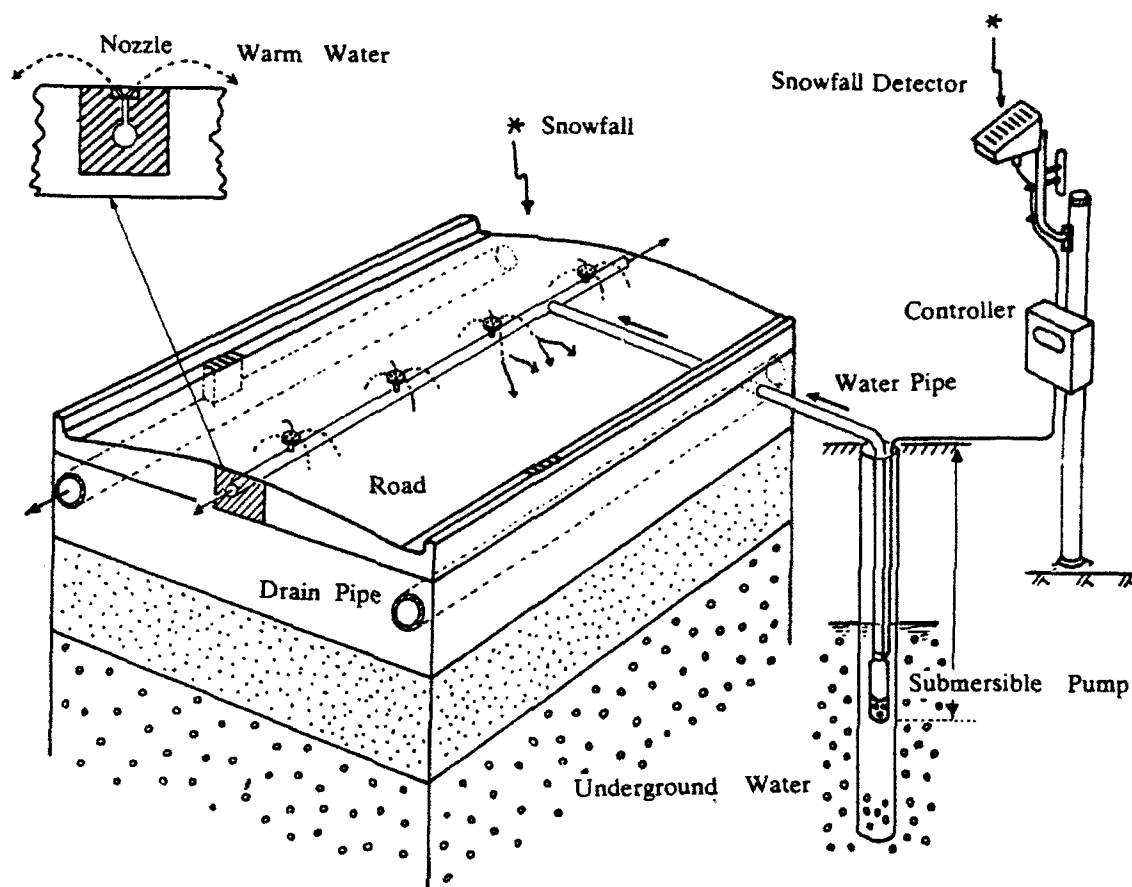


Figure 1. A snow melting system using underground water for roads.

At present, the amount of the water sprinkled on the road, per units of time and area, can be determined by considering snowfall intensity, air temperature, wind velocity and solar radiation. Now, the actual method of control generally used is to sprinkle a constant amount of the water during the time continuous snowfall.

A problem with this treatment is that a 1-hour snowfall intensity is used to determine the amount of water sprinkling. But, variations in the actual snowfall intensity by some minutes and seconds come to unbalance heat supplied by the method of constantly sprinkling the water. To use effectively the heat of the water, the amount of water sprinkling and a control method of snow melting system should be determined on the basis of the frequency distribution of the actual snowfall intensity.

Results of the snowfall intensities measured with a snowfall detector of the water drop counting type, given for a 1-minute interval continuously during 3 months, are presented.

INSTRUMENTS

The precipitation meter of a water drop counting type used at weather stations to measure the precipitation per short time has not been widely used because of its complex structure, heavy weight and high expense. Thus, a snowfall detector of a water drop counting type has been developed to be compact, lightweight and of a simple structure. The equipment consists of water drop and snow temperature detecting parts, the structures of which are shown in Fig. 2. A receptacle in the water drop detecting part has an opening aperture of 117 cm^2 , and is funnel shaped to catch raindrops and snowflakes. Caught snowflakes can be melted with the 10-W heater setting behind the receptacle. At the tip nozzle of the water duct the water can be transformed to water drops, which are precipitated. The precipitated water drop crosses the light beam to be counted one by one with the counting device of the equipment. Therefore the smallest measuring unit is 0.0070 mm in precipitation, which should be given by the mass of one water drop divided by the cross sectional area of receptacle.

Figure 3 shows the structure of the funnel-shaped receptacle. Using a ring-shaped small wire at the upper entrance of the receptacle, the water can flow smoothly from the receptacle. The inner part of the nozzle is cut to 1-mm width and 20-mm length from the tip nozzle of the water duct, so that the precipitated water from the duct can be separated to water drops with a constant mass.

A characteristic curve relating to the mass and the dropping frequency per minute for precipitated water drops is obtained by laboratory experiments (Fig. 4). This figure indicates that the mass of the water drop seems to be almost constant under stable separations until a dropping frequency of 300 drops 1 minute is reached. Then it becomes unstable and varies widely above 300 drops. Then, the drops can not be separated and they continuously exit by water flow.

A qualitative discrimination between snowfall (containing sleet and hail) or rain can be performed with a device detecting snow temperature (Fig. 2, Photo 1). The structure consists of an element detecting the temperature setting in the central part of a cup-shaped snow receptacle. When the element temperature has been less than the discrimination temperature, the temperature circumstance of snowfall (containing sleet and hail) can be estimated. Under this condition, all precipitation should be discriminated as the snowfall. When the element temperature is greater than the discrimination temperature,

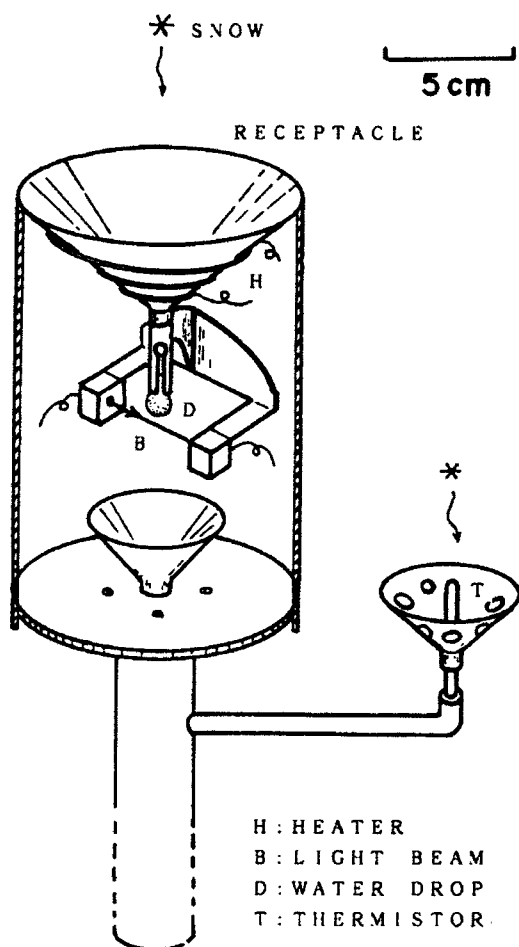


Figure 2. Snowfall detector.

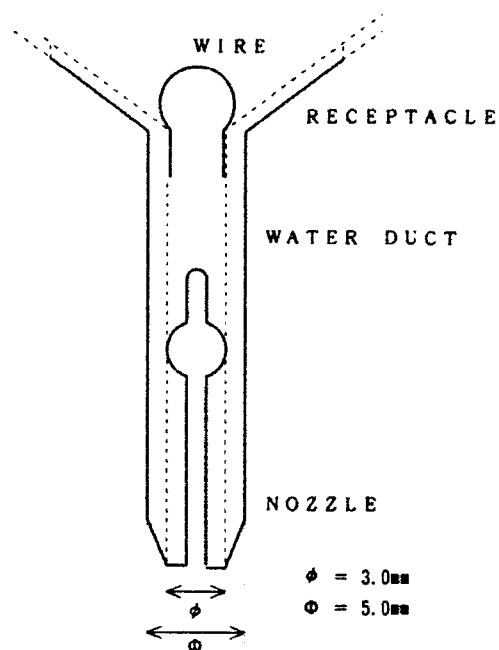


Figure 3. Structure of funnel-shaped receptacle.

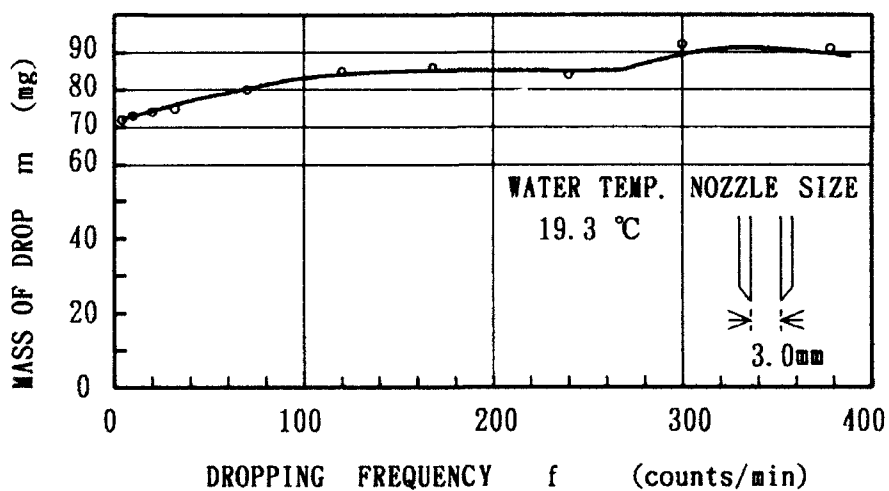


Figure 4. Mass of water drop to dropping frequency.

all precipitation should be identified as the rain.

The discrimination temperature could be set to be 0.7°C . The characteristics of this discriminative structure for rain and snowfall show that, even in the case of snowfall at an air temperature greater than the discrimination temperature, the presence of snowfall could be found with the element detecting the temperature. The temperature should be dropped below the discrimination temperature if snowfall lying on the snow receptacle. It could be estimated to be several percent of the discriminative erroneous rate for rain and snow, which has been expected with this discriminative equipment.



Figure 5 was obtained from results

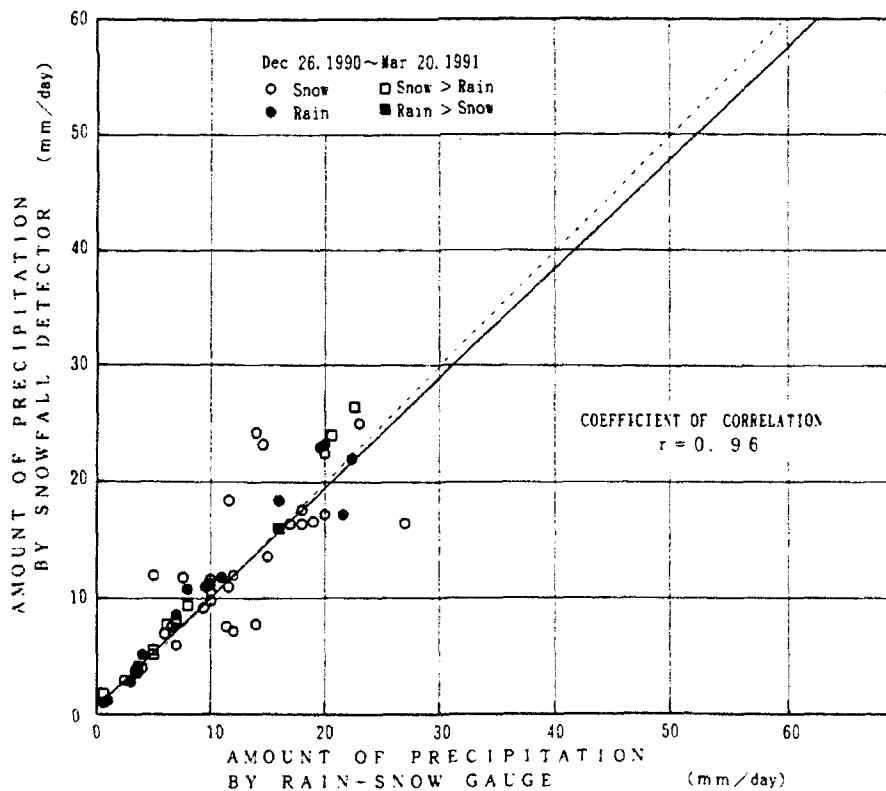


Figure 5. Comparison of precipitations per day with rain-snow gauge and snowfall detector.

comparing values of precipitation per day with this snowfall detector and the standard rain and snow gauges at the Japanese Meteorological Agency. The correlation coefficient between both measured values is 0.96. It has been proved that the correlation coefficient should be larger than this in the case of rain, and lower in the case of snowfall.

MEASUREMENTS

With the measuring equipment on the 15-m high rooftop of Nagaoka Technical High School, intensities of snow and rain precipitations have been measured per 1-minute intervals continuously for almost 3 months (missing 24 hours on February 4) from 16 December 1990 to 20 March 1991. Figure 6 shows a schematic of the measuring system, where measured values are read with the computer and recorded on a floppy disk. In addition, the precipitation could be measured as either snow or rain precipitation. Moreover, to find discriminations between rain or snowfall, a CCD TV camera was used to take photos every each 4 seconds, so that pictures of the external field could be stored with video recording equipment.

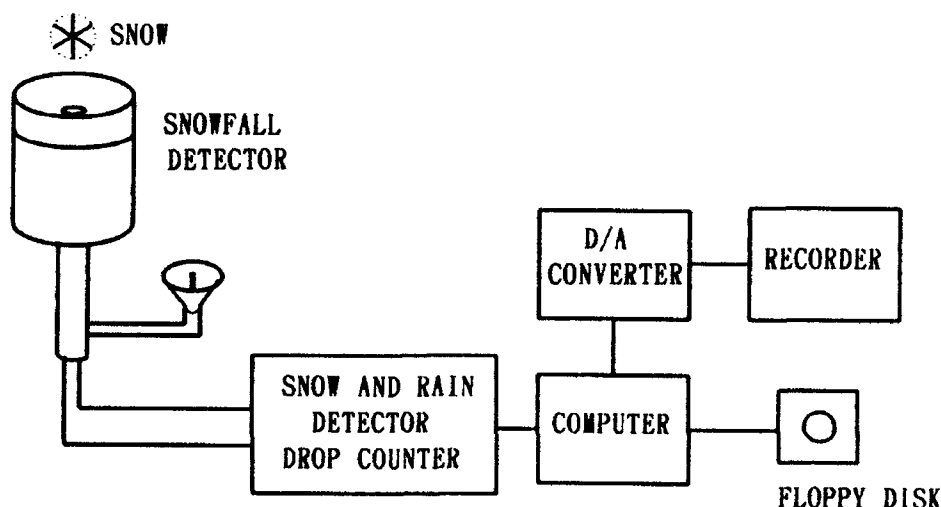


Figure 6. Schematic measuring system.

RESULTS

Snowfall intensities by time recording

Figure 7 shows a sample of snowfall intensity recording for the 1-minute measurement. With the measuring unit of 0.0070 mm, mentioned previously, the

output of snowfall intensity could be obtained by counting not less than one water drop for each one minute. Recording during the observation, it has been estimated that the maximum snowfall intensity was less than 0.35 mm/min.

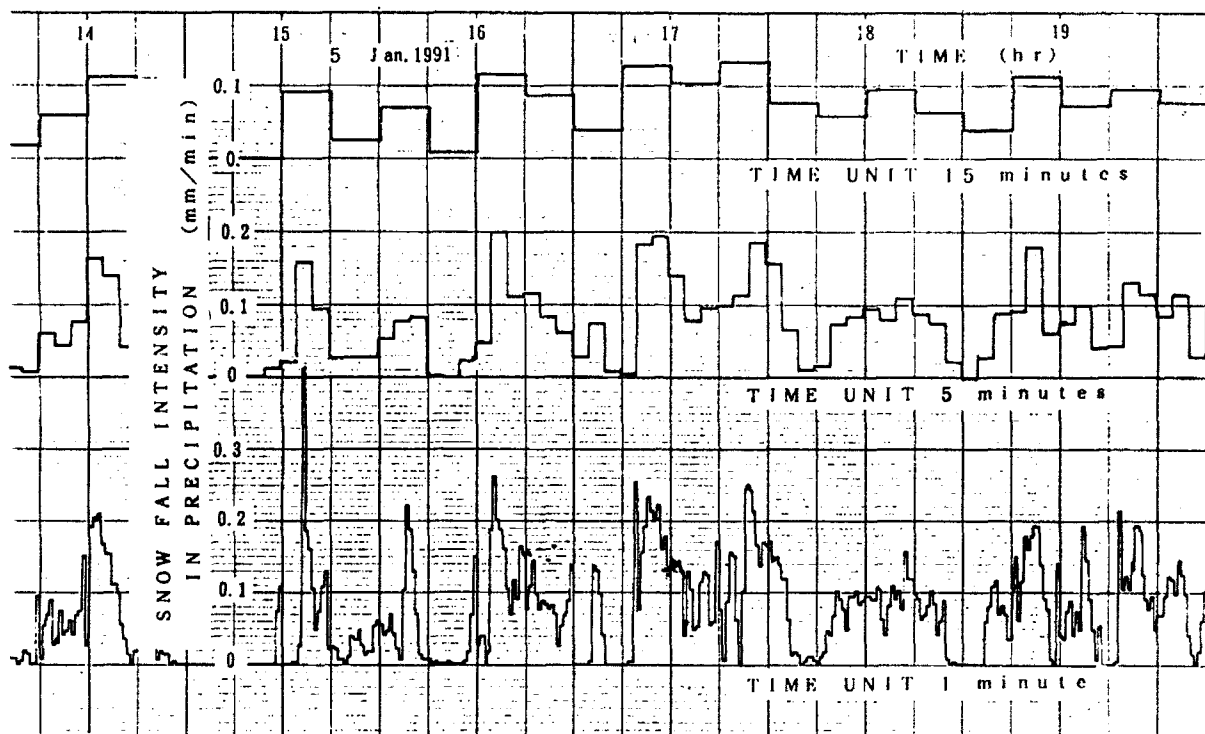


Figure 7. Sample record of snowfall intensity with detector.

Frequency of occurrence of separate snowfall intensity values.

Investigating the frequency of occurrence for each separate value of snowfall intensity, continuously recorded per one minute during the observation, the result of the distribution has been obtained as shown in Figure 8. The total frequency was given by 16153 numbers with an intensity of 0.0070 mm/min, which could be converted to the time of 269.2 hours. According to Figure 8, the more snowfall intensity increases, the more frequency of occurrence decreases exponentially. A regression equation of the relation between the snowfall intensity I and the relative frequency of occurrence F (%) percent could be given as equation (1).

$$F = F_0 \cdot \text{EXP}\{-K (I - I_0)\} \quad (\%) \quad (1)$$

where, $F_0 = 23.3$, $K = 38.0$, $I_0 = 0.0070$ mm/min
water drop numbers: $n = 1, 2, 3, \dots$

$$\text{and } I = n \cdot I_0$$

Under the snowfall intensity of 0.077 mm/min, the frequency of occurrence should be decreased linearly (Fig. 8). But, above the intensity, the frequency should be larger than the value given by this equation. This reason could be that the precipitated snowflake has not been melted instantaneously, and could be melted after a large amount of snowfall lied on the receptacle, because of the small heater power supply of 10-W setting at the receptacle for melting.

Moreover, the result calculating accumulated value F proved that 50 % of the total frequency occurred under the snowfall intensity of 0.056 mm/min, while 90 % occurred under the 0.070 mm/min. Then, recalculating values measured per one-minute unit to those per 5-minute unit, the result of frequency could be given by the distribution of frequency (Fig. 9). The same regression equation has been obtained for that related between the snowfall intensity, averaged by 1 min for the value per 5 min, and the relative frequency of occurrence F percent given by this figure.

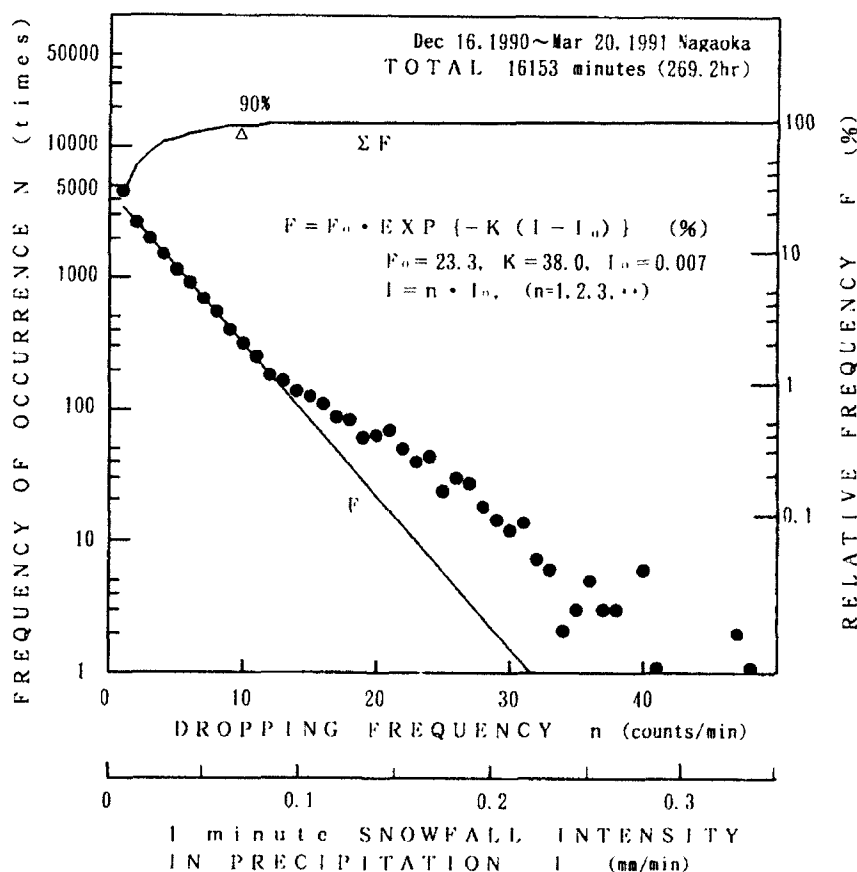


Figure 8. Frequency of occurrence for separate snowfall intensities per one-minute measure

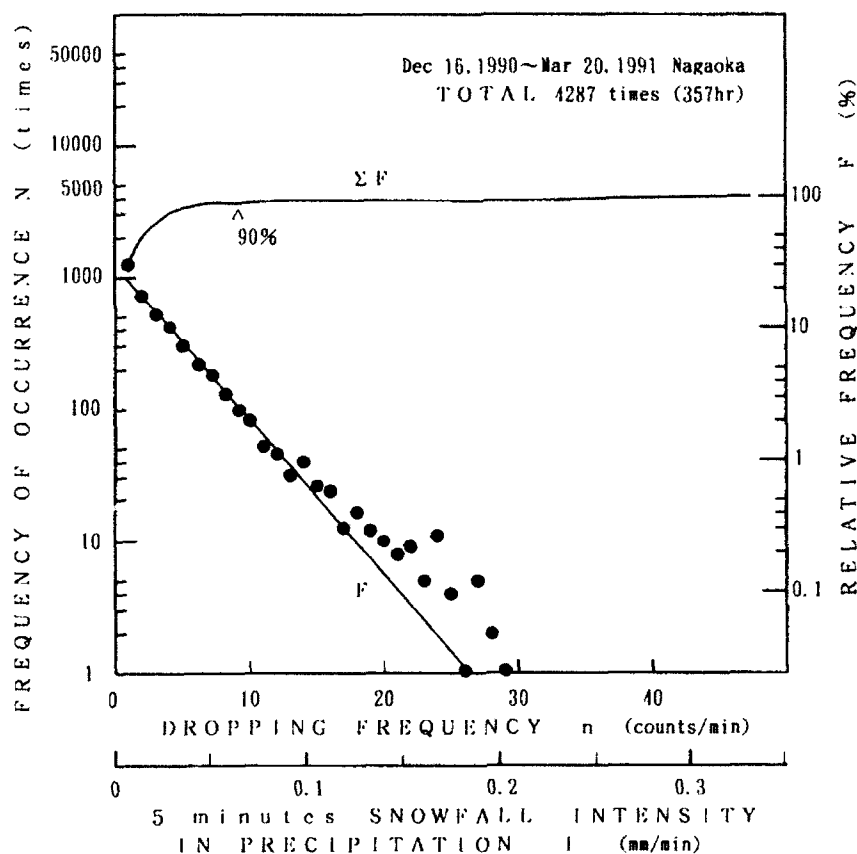


Figure 9. Frequency of occurrence for separate snowfall intensity per 5 minute measurement.

Correlations of the snowfall intensities measured with an electronic balance and the snowfall detector.

The mass of natural snowfall has been measured per 1 minute with an electronic balance for comparing to the snowfall intensity measured with the snowfall detector, during continuous a 240-min, interval from 19 to 23 hours, 8 February 1992.

The lag correlation coefficient between measuring time units from 1 to 5 min and lag times for 0, 1 and 2 times of the measuring time has been deduced for both measured values (Table 1).

In the case of the larger measuring time unit, the lag correlation coefficient increases more. However, according to this table, the increment is not so great. In addition, for any time unit, the more the lag time increases, the more the lag correlation coefficient decreases. This proves that the time rate value measured with the snowfall detector to that with the electronic balance should be estimated within 1 min.

Table 1. Lag correlation coefficient.

Feb 8, 1992 . 19:00 ~23:00

Lag Time (min)	Measuring Time Unit T (min)				
	1	2	3	4	5
0	0.978	0.977	0.981	0.983	0.990
1 • T	0.647	0.095	0.198	0.505	0.793
2 • T	0.573	0.383	0.278	0.396	0.510

Amount of precipitation;

Electronic balance : 4.7 mm

Snowfall detector : 5.9 mm

DISCUSSION AND CONCLUSIONS

Experimental results mentioned above are as follows. Even using a detector with such a simple structure, the mass of rain and snowfall intensities per short time could be measured for a long time. For the snowfall at Nagaoka during the observation, the frequency distribution of snowfall intensities has been obtained such that distribution can be expressed by equation (1). The more the snowfall intensity increases, the more the frequency of occurrence decreases exponentially. The maximum snowfall intensity has been estimated to a value below 0.35 mm/min. During the observation, 50 % of the total frequency occurred below the snowfall intensity of 0.056 mm/min, while 90 % occurred under the 0.070 mm/min. Above the snowfall intensity of 0.1 mm/min, it come apart from equation (1), because of a lack of heater power to melt the snowflakes, a point which must be improved.

Comparing values measured with the electronic balance and the detector, there is not so much a difference of correlations between them, even if the measuring time unit increases 1 to 5 min. In addition, if the simultaneous lag correlation coefficient (at 0 lag time) is at the maximum, even for any measuring time, then the time that with this detector to that with the electronic balance could be estimated within 1 min.

Because these measurments were made only during one winter, there is no evidence whether equation (1) has universality or not. Thus, more measurements have to be investigated. Based on these data, effective control

methods for snow melting with sprinkling water will be further studied.

REFERENCESE

Konishi, H., Endoh, T. and Wakahama, G., 1988.

A New Snow Guage Using an Electric Balance. JOURNAL OF THE JAPANESE SOCIETY OF SNOW AND ICE Vol. 50, No. 1, 3-7.

Tamura, M., 1990.

Snow and Rain Fall Frequencies in Nagaoka. JOURNAL OF THE JAPANESE SOCIETY OF SNOW AND ICE Vol. 52, No.4, 251-257.

The Use of Snow Survey Data in Determination of Ground Snow Loads

Douglas R. Powell
Lecturer, Department of Geography
Sonoma State University
Sonoma, California, U.S.A.

ABSTRACT

Snow surveying is a formal, scientific technique for forecasting stream flow from snowmelt in a particular watershed. At some 2,000 sites in the western United States, snow water equivalent data are measured and recorded with many records dating back over forty years. These data are valuable for determination of ground snow loads and are often the only reliable data in mountain terrain. The author draws from forty years of field experience in snow surveying in the western United States, Afghanistan, and Chile to discuss three major methods to obtain snow water equivalent data: the federal snow sampler, snow sensors, and gamma ray attenuation. Advantages and limitations of each method in using water equivalent data in the determination of ground snow loads are described, with much attention given to the federal sampler as a relatively inexpensive, portable and easily used tool for immediate measurement of snow depth, water equivalent and density at any place, at any time. Other applications of snow survey data to ground snow load determination are described with a brief comment upon the difficult problem of extrapolating data from a snow course or snow sensor to a particular project site.

INTRODUCTION

The purpose of snow surveying as a formal, scientific technique is to forecast stream flow from snowmelt in a particular watershed. For years in various snow accumulation zones in the United States and elsewhere in the world, attention was given to a practical, operational method of forecasting snow runoff, months in advance, in a given basin. The first successful use of snow surveying to forecast volumetric snowmelt on a major scale occurred in the Donner Pass - Lake Tahoe region in the central Sierra Nevada in the first decade of the 20th Century. This resulted from the pioneering efforts of James E. Church, a professor of classics at the University of Nevada in Reno, who is widely recognized as the Father of Snow Surveying. On his own initiative, without financial support for some years, he began measuring the water equivalent of snow accumulation in the vicinity of Mt. Rose (3,286 meters, 10,788 feet). He discovered a definite correlation between an index of water equivalent in the snowpack of the Lake Tahoe basin and the subsequent rise of the lake level from snowmelt runoff during April through July. In the spring of 1909, he successfully forecast how much the lake would rise from

snowmelt and thereby mitigated an intense dispute with a real potential for violence, between a hydroelectric power company and lakeside property owners as to how discharge from Lake Tahoe would be regulated at a dam across the outlet of the lake. After this practical demonstration of the efficacy of snow surveying, the technique spread throughout snow accumulation zones in California, then into all of the mountain states in the western United States, into western Canada and many other countries where snowmelt was a major component in streamflow.

For the past forty years I have been actively engaged in snow surveying, primarily in the southern Sierra Nevada in California but with three field seasons in Afghanistan and two in Chile to establish snow survey programs in those countries. I estimate I have spent a minimum of 1600 days at mid-to-high elevation in mountain terrain on snow measurement. This long experience does not qualify me automatically as an omniscient expert but does indicate considerable exposure to problems of snow data acquisition. I also had the privilege and good fortune to learn about snow surveying in the office and field from the founder of the science, James Church, who remained active well into his eighties. From this experience and research, I offer the following observations and suggestions about how snow survey data are gathered and may be used in ascertaining ground snow loads.

METHODS OF SNOW SURVEYING

The first essential activity of snow surveying is to gather data on snow water equivalent at particular sites in river basins where snow accumulation is significant. This work is conducted or coordinated by the State Department of Water Resources in California, and by the Federal Soil Conservation Service in other mountain states, in western United States and Alaska, with local offices in each state. In Canada, each province has a public agency for taking and coordinating snow surveys. These public offices then issue surface runoff forecasts for the snowmelt season for each river basin where measurements have been taken - usually as of February 1, March 1, April 1 and May 1; in some basins earlier, in some later. These forecasts are available to water users and planners and to any interested citizen.

There are about 2,000 sites in the United States where snow water equivalents are measured regularly, about 400 in California. Many of these sites have continuous data from the 1930's to the present, especially in California which has a few eighty-year records. These data are available at the above-mentioned offices for study and analysis. Although the measurement of snow water equivalent at these 2,000 sites, snow courses and sensors is employed primarily for stream flow forecasting, this parameter can be most valuable in the determination of ground snow loads at any site. These snow data are often the best, or even the only, reliable, long-term data source in mountainous regions or areas away from weather stations and can be immediately converted into ground snow loads of kPa or psf. Snow water equivalent from snow surveying data has been widely used in western United States for quantifying permissible roof snow loads in building codes and for mapping distribution of ground snow loads as in the state of Idaho (Sack and Sheikh-Taheri, 1986). It may be very helpful in snow engineering to be aware of the chief methods of acquiring snow water equivalent with advantages and limitations of each method.

Federal Snow Sampler

The federal snow sampler, sometimes referred to as the Mount Rose sampler, only a little modified from Church's original instruments of seventy to eighty years ago, is still the basic tool used for snow data acquisition in much of North America and the rest of the world. It is composed of sections of hollow aluminum tubes, generally 76 centimeters (30 inches) in length. The sampler, with sufficient sections coupled together to reach from the top of the snowpack to the ground, is pushed through the snow to the ground, acquiring a core of snow. The bottom section is fitted with a steel cutter tip with teeth to cut through dense snow and ice layers. The inside of the cutter tip is slightly smaller in diameter than the rest of the tube, which prevents the snow core from sliding out through the bottom when the sampler is lifted out of the snowpack. In the United States the diameter of the cutter tip is 1.485 inches; one inch depth of water of this diameter weighs exactly one ounce; thus a spring scale calibrated in ounces is used to determine the snow water equivalent of the sample in inches. A similar relationship can be used in the metric system to give the snow water equivalent in centimeters. Each tube has alternating narrow slots, roughly 12 centimeters in length, to which a driving wrench, with spreading metal arms, may be attached to provide leverage for getting the sampler through deep snow and ice layers. After the sampler is driven to the ground, the snow depth is recorded by reading the scale marked along the sampler's length; then the sampler is lifted out of the snow and weighed. By subtracting the weight of the empty sampler, the snow water equivalent of the core is obtained. In snow surveying, usually ten samples, 15 - 45 meters (50 - 150 feet) apart, are taken at each measuring site or snow course, which is given a specific name, such as Bishop Pass. These samples are averaged to obtain one value of snow depth and water equivalent for each snow course. From depth and snow water equivalent readings at each sample point, or for the entire course, density values can be readily calculated. Other variations of metal tube instruments are used but the federal snow sampler is by far the most common. Using the sampler effectively does not call for great technical skill or extraordinary physical strength (deep, dense snow may call for extreme exertion) but experience with all possible conditions, especially in difficult snow and adverse weather, is critical for consistent and reliable data. (More detail on field sampling can be found in California Department of Water Resources, 1985; and Powell, 1987). Figures 1, 2, 3 and 4 show samples being taken in the Sierra Nevada.

Following are some common and troublesome problems in using the federal sampler. To prove that the sampler has reached the ground at the bottom of snowpack, evidence of sand, dirt, or vegetation should be present on the teeth of the cutter. The length of the core within the tubes, observable from the tube slots, should be not less than 90% of the depth. Penetration of ice layers at the ground or within the snowpack, especially in deep snow, may be exasperating and time consuming. In the Sierra Nevada and elsewhere, internal ice layers usually form during periods of clear weather with accompanying melt-freeze metamorphism. When later buried by subsequent large snowfalls, these layers persist at depth, often well into the melt season. The cutter may clog, pushing snow aside when sampling, or snow may stick to the inner tube surface and be most difficult to remove. Cooling the sampler before use on the snow surface or in shade, or sampling in early morning or late afternoon may avoid or alleviate sticking problems, but not always. Ponding of water at the bottom of the snowpack during active snowmelt causes problems to which there may not be adequate answers.

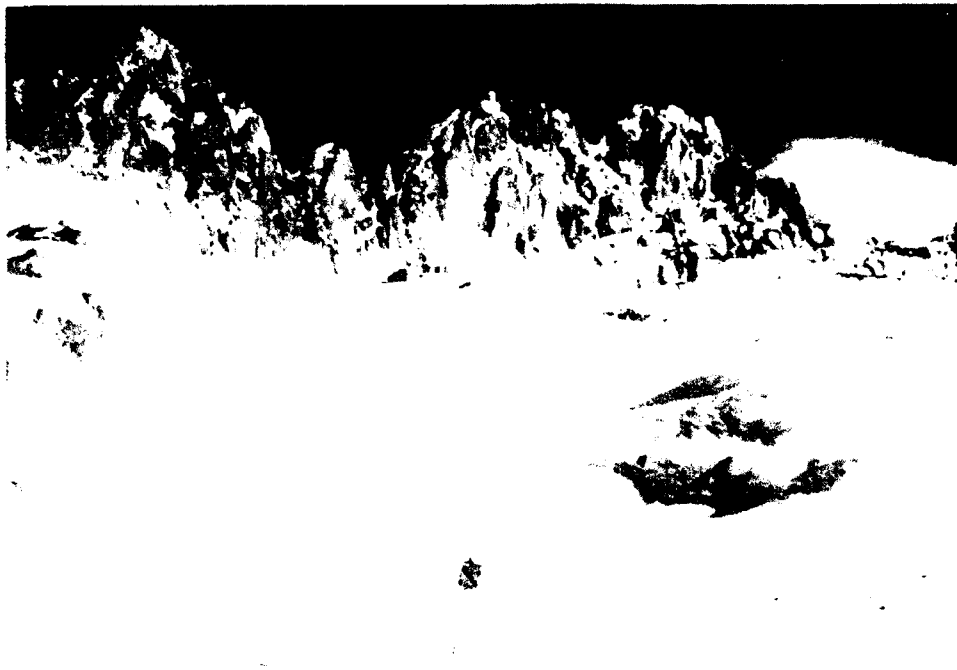


Figure 1. Bishop Pass snow course in the Kings River Basin, Sierra Nevada, California, elevation 3,400 meters (11,200 feet). The pipe and sign at middle bottom mark one end of the course with ten sample points, 45 meters (150 feet) apart.



Figure 2. Using the federal snow sampler at the Bullfrog Lake snow course, Kings River Basin, Sierra Nevada, California, elevation 3,300 meters (11,800 feet). The surveyor is holding the driving wedge to push the federal sampler through a snow depth of 4 meters (13 feet).



Figure 3. Weighing the federal sampler with a snow core at the Bullfrog Lake snow course. The snow water equivalent of this sample was 150 centimeters (60 inches).



Figure 4. Withdrawing the federal sampler in very deep snow, 750 centimeters (300 inches), at the Piute Pass snow course, San Joaquin River Basin, Sierra Nevada, California, elevation 3,400 meters (11,200 feet). Ten 75 centimeter (30 inch) tubes were used. Water equivalent of this sample was 325 centimeters (130 inches).

Various field tests by different agencies have concluded that the federal sampler over measures water equivalent by up to 10 - 12% in deep snowpacks (California Department of Water Resources, 1976; Western Snow Conference Metrification Committee, 1983). The California tests indicated the error increased with depth and density; other tests do not show significant correlation with density. There is no general agreement on causes for this overmeasurement: proposed explanations are that outside snow is forced into the tubes through the slots while the sampler is being driven through deep, dense snow, and the design of the cutter. The Western Snow Conference Metrification Committee Report (1983) provides a detailed analysis of a variety of snow samplers used in North America, and concludes that the federal sampler is the most utilitarian for deep snows in western United States, but recommends that design modifications and further field tests be performed on the cutter to correct possible overmeasurement. This report also gives design recommendations, specifications, and drawings about conversion of sampler equipment to the metric system. Many times in my own field experience, I am convinced the reverse is true - the sampler underweighs by pushing snow aside, especially by partial clogging at the cutter, and by not picking up light density snow, which may occur in layers even in deep snow. I would like more research into this matter, especially under variable field conditions. Users of the federal sampler should be aware of possible overmeasurement - or undermeasurement - particularly in deep snow. Many water equivalent readings from adjacent federal sampler and sensor sites have not conclusively shown the federal sampler consistently overweighs compared to the sensors (Suits, 1985).

Thus, there are problems in using the federal sampler. Most can be successfully solved or mitigated with persistence, experience and research. The advantages of the federal sampler are many and significant. In one quick and simple measurement, snow depth, water equivalent and density can be obtained at any given site, at any time of day or night. Snow water equivalent is a direct expression of ground snow load, immediately convertible into any measurement system. The equipment, sampler and scale is readily portable; one person can carry the necessary number of tubes for all but very deep snow. An improved carrying case for the sampler, which provides protection for the tubes and comfort for travel, has recently been developed in British Columbia, Canada (Gluns and Rose, 1992). In snow depths less than 2 meters, one person generally performs the measurement although two persons make the task easier. I have been involved in taking successful samples in the Sierra Nevada in depths of 12 meters with water equivalents of 350 centimeters. Deeper samples have been measured elsewhere, such as the Kenai Peninsula in Alaska. The equipment is relatively inexpensive, currently about \$ 2,500 for a complete set with eight tubes.

The federal sampler is indeed a versatile and valuable tool for determining ground snow load in all types of terrain, snow and weather conditions. It is also very useful in obtaining roof snow loads. Its portability means it can be taken on most roofs for sampling, although personnel safety and prevention of damage to roof surfaces are important considerations. It will not penetrate ice accumulations of any thickness, which presents special problems of roof snow load assessment. Another significant use of the sampler is for ground truth measurements on or in the vicinity of snow sensors. Snow survey agencies, such as the California Department of Water Resources and the Federal Soil Conservation Service, take many manual samples throughout the winter to check the accuracy of pressure pillows and other sensors. I highly recommend that any agency, company or individual working with ground and roof snow loads possess a federal

snow sampler or its equivalent. It can be used any time, any place, in nearly any weather by one or two persons. Taking samples in difficult snow and inclement weather may well be challenging and most unpleasant but I firmly believe that the understanding of snow by any person is much enhanced by exposure to all manifestations of its physical environment.

Pressure Type Snow Sensors

Since the 1960's other devices for measuring snow water equivalents have been increasingly used at snow survey courses and other locations where this information is desirable. Most commonly used are pressure type sensors called snow pillows or snow tanks. These are butyl rubber or stainless steel envelopes filled with an antifreeze solution. The snow above the surface changes pressure on the antifreeze fluid proportional to the weight of the water equivalent in the snowpack. The snow water load is read by a pressure transducer and the magnitude of this force can be telemetered to a central master receiving station such as Sacramento, California; Ogden, Utah; and Boise, Idaho. In California, the data are sent by radio to a Geostationary Operation Environmental Satellite (GOES) which is generally located 35,900 kilometers (22,300 miles) above the equator at 135 degrees west longitude, then relayed to a receiver terminal in Sacramento for storage or on-call use. The Soil Conservation Service transmits radio signals skyward, which are reflected downward from ionized meteorite trails in the upper atmosphere (80 - 120 kilometers above the surface of the earth) between the data sites and the master stations at Ogden and Boise. Both transmitting systems generally use solar panels for a power source.

The first snow pressure pillows employed were butyl rubber envelopes, commonly 3.66 meters (12 feet) in diameter, requiring up to 300 liters of antifreeze. These have been largely replaced by stainless steel tanks using far less antifreeze. Most of the steel sensors consist of four tanks (1.22 by 1.52 meters; 4 by 5 feet) placed alongside each other with a total surface area of 2.44 by 3.04 meters (8 by 10 feet). The steel units are often still called snow pillows, sometimes snow tanks, or just snow sensors. There are perhaps 700 such sensors operating presently in snow survey programs. The Soil Conservation Service operates over 500 of these which report air temperature and cumulative seasonal precipitation along with snow water equivalents. Figures 5 and 6 show installation of steel pillows in the Sierra Nevada.

These systems make daily readings of snow water equivalents possible. Snow depths are not recorded, so density readings are not available. Data from the sensors allow incremental contributions from individual storms, information lacking from once-a-month manual measurements. The temperature data may indicate whether the precipitation was snow or rain. Costly and time-consuming travel to the snow course is eliminated and, theoretically, the data are available in any weather.

There are problems. Pillows or tanks may leak. They may be slow in responding to quick changes in water equivalent, sometimes several days or more, particularly during heavy storms or rapid snowmelt. Bridging of the snow and accumulation of meltwater above the sensor may result in inaccurate data and the electronic equipment may malfunction. Unexpected heavy snow accumulations have sometimes buried the transmission equipment, with a cessation of reporting when much needed. Vandalism or animal activity (bears have a taste for antifreeze)



Figure 5. Installing a stainless steel snow pillow at the Dana Meadows snow course, Tuolumne River Basin, Sierra Nevada, California, elevation 2,925 meters (9,600 feet). Four tanks, 1.22 by 1.52 meters (4 by 5 feet), with a total surface area of 2.44 by 3.04 meters (8 by 10 feet), are placed alongside each other. The sensor is covered with about 5 centimeters of sod to protect its surface and to retain the first snowfall of the season.



Figure 6. Completion of installation of the steel pillow at the Dana Meadows snow course in the Sierra Nevada. The aerial at the top points towards the GOES satellite. Immediately below the aerial is the solar panel which is the energy source for transmission of water equivalent data. The people are being instructed in the installation of snow pillows.

can damage or destroy sensors in the summer months. Since the sensors measure snow at one point, the data are more subject to local aberrations of snow accumulation at that site, such as wind drifting, creep, and avalanching, than data from manually measured snow courses which have ten sample points.

A major purpose of introducing sensors for acquiring snow water equivalent in snow survey programs was to reduce or eliminate manual measurements. This reduction has not proceeded as rapidly as originally planned, partly because of the cost of installation and maintenance, partly because of problems of operation and some loss of confidence in the accuracy of the pillow data. In California, the data are used primarily at present to provide information about snow water equivalent increase between the monthly manual measurements. Many sensors are located on pre-existing snow courses and dual sets of water equivalent data, by federal sampler and telemetered sensor, are available. It may take ten to twenty years or more before forecasters establish sufficient confidence in sensor data in making surface runoff forecasts to justify elimination of the sampler data. Thus, manual federal sampler surveys may continue along with sensor snow water equivalent data for many years. Moreover, ground truth federal sampler measurements on and near sensors will continue indefinitely.

There have been a number of studies to test the accuracy of sensor snow water equivalent measurement, often by comparison with adjacent or nearby manual samples (Soil Conservation Service, 1978; Suits, 1985). Thus far, there have been no discernible, predictable differences between the two methods. Sometimes sensor results are higher than control federal sampler figures, sometimes lower. The two approaches to gathering snow water equivalent data appear roughly equal in accuracy and reliability.

Some implications of using sensor snow water equivalent data in determining ground snow loads are the following. Where and when available, sensor data can be used in much the same manner and with similar confidence as federal sampler data. Chief advantages are daily readings from sensors and observing incremental increases in snow water equivalent from particular storms. Main disadvantages are breakdowns and time lags in recording and transmission of sensor data; the fixed location and one point measurement of the sensors compared to the mobility of the samples; and the greater cost of installation and maintenance of the sensor. It should be pointed out that both methods have ardent supporters and detractors. In the future, a higher percentage of snow water equivalent data generated from sensor data in snow survey programs will probably occur.

Gamma Ray Attenuation

There are other automated and telemetered devices for ascertaining water equivalent at a given site. They operate on the principle of measuring the degree of attenuation by a snowpack of gamma radiation from a source to a counter. This can be calibrated in inches or centimeters of water. The most promising method of measuring gamma radiation is being developed by the Office of Hydrology, United States Weather Service, in Minneapolis, Minnesota (Office of Hydrology, National Weather Service, 1992). This depends upon measuring gamma radiation from an instrumented aircraft flying about 150 meters above the ground over a designated strip of terrain, roughly 16 kilometers long, 300 meters wide, in gentle

terrain; smaller areas are used in mountainous terrain. The designated strip is flown over without snow cover to acquire a background gamma radiation reading, then at various times during the winter with snow cover to measure the water equivalent from the degree of attenuation of the gamma ray radiation by the snowpack. This method of using gamma radiation has one serious limitation. If the water equivalent is about 100 centimeters (40 inches) or more, the radiation recorded by the counter drops down to amounts difficult to measure without major error. But these aerial surveys show much promise in generating snow water equivalent data over broad areas with low to moderate snowpacks - currently in gentle terrain, later in mountainous regions. Ground truth snow water equivalent measurements with snow tube samplers are taken to verify the data. The chief use of these aerial surveys for determination of ground snow loads will be to acquire average loads over extensive areas. Maximum readings will be lost in the average figures but some extremes could be ascertained by checking the ground truth measurements.

OTHER APPLICATIONS OF SNOW SURVEY DATA

Snow survey data can contribute information useful to snow engineering other than the direct measurement of ground snow loads. Each agency that conducts snow surveys maintains records of all surveys made, including figures for each sample point of each snow course. Detailed study and analysis of these records can divulge valuable information on snow densities, extreme depths, and water equivalents (one sample point may be much higher than the course average), the time of year of maximum accumulation, the intensity and frequency, the duration of significant storms, the extreme and high ground snow loads, and the variation of depth and snow water equivalent in short horizontal distances. Concerning this last point, I have found on snow courses in the Sierra Nevada that depth and snow water equivalent can double from one point to another within distances of 50 to 100 meters, the variance often being the same ratio from year to year.

There is the inevitable and difficult problem of extrapolating the data from snow courses and sensors to a particular building site or other location where these data are useful for ground snow load determination (Powell, 1988). In general, the closer the two are together, the better. This calls for the most careful comparison of the data site to the project site. The location and detailed descriptions of course and sensor sites, giving elevation, exposure/orientation, surrounding topography and vegetation are generally available from the measuring agency, and can be very helpful. Of particular value is the existence of more than one course or sensors in the area near the project site. This can be helpful in drawing ground snow load contours, using the measured sites as reference points, over an area large enough to include the project site. A thorough knowledge of and experience with the weather patterns and topography of the region are desirable. A personal reconnaissance of the snow survey sites and the project site under winter conditions is essential. There are no easy answers or concise formulas to this eternal problem of extrapolating data from one site to another, given the variable deposition and accumulation of snow in short distances. I again point out that snow survey data are often the only reliable data in mountainous areas.

CONCLUSIONS

Snow surveying is a technique for measuring snow water equivalent at particular sites throughout the snow accumulation season in order to forecast surface runoff during the snowmelt season. There are some 2,000 sites in the western United States where regular measurements are taken, many with continuous records of forty years or more. I have been actively engaged in snow surveying for forty years, primarily in the Sierra Nevada of California but with experience in Afghanistan and Chile and much contact with snow survey participants in other states and Canada. I have outlined the origin of snow surveying and three major methods by which snow water equivalent is obtained: the federal sampler, pressure sensors and aerial surveys. I have discussed the advantages and limitations of each method in using water equivalent data in the determination of ground snow loads with emphasis upon the federal sampler as an inexpensive, portable and simple tool for immediate measurement of snow depth, snow water equivalent and density, at any place and any time. Any agency, company or individual can make good use of the federal sampler for determination of ground snow loads. Snow survey data can be analyzed for valuable information other than water equivalent, and in much of western United States and Canada snow surveying is the only source of reliable snow data because of inaccessibility of terrain and lack of weather stations.

REFERENCES

California Department of Water Resources (1976) "*Snow Sensor Evaluation in the Sierra Nevada, California*," State of California, Sacramento, CA.

California Department of Water Resources (1985) "Snow Survey Sampling Guide," State of California, Sacramento, CA.

Gluns, D.R., and G. Rose (1992) "An Improved Carrying Case for Snow Tubes," Paper delivered at Western Snow Conference, Jackson, Wyoming. In press, "*Proceedings of the Western Snow Conference*", 1992.

Office of Hydrology (1992) "*Airborne Gamma Radiation Snow Survey Program and Satellite Hydrology Program, User's Guide, Version 4.0*," National Weather Service, Minneapolis, Minnesota.

Powell, D.R. (1987) "Observations on Consistency and Reliability of Field Data in Snow Survey Measurements," *Proceedings of the Western Snow Conference*, Vancouver, British Columbia, Canada 69-77, 1987.

Powell, D.R. (1988) "Determination of Ground and Roof Snow Loads at a Particular Site," *Proceedings of First International Conference on Snow Engineering*, Santa Barbara, California, July 1988, 456-461, United States Army Corps of Engineers, February, 1989.

Sack, R.L., and A. Sheikh-Taheri (1986) "*Ground and Roof Snow Loads for Idaho*," University of Idaho, Moscow, Idaho.

Soil Conservation Service (1978) "*Snow Sensor Evaluation*," United States Department of Agriculture, Soil Conservation Service, Washington, D.C.

Suits, R.D. (1985) "*California Snow Sensor Performance*," unpublished MS thesis, University of California, Davis, CA.

Western Snow Conference Metrification Committee (1983) "*Metrification of Manual Snow Survey Equipment*," Western Snow Conference, Portland, OR.

2

Structural Case Histories

Michael O'Rourke, Chairman



Surveying the depth of snow on roofs in Japan with the aid of a kite balloon. (Photograph provided by Shuji Sakurai.)

Effects of Roof Size and Heat Transfer on Snow Loads on Flat Roofs

P.A. Irwin*, S.L. Gamble*, R.N. Retzlaff* and D.A. Taylor†

*Rowan, Williams, Davies & Irwin, Inc., Guelph, Ontario, Canada N1K 1B8

†Institute for Research in Construction, National Research Council, Ottawa, Ontario, Canada K1A 0R6

ABSTRACT

The snow loading on roofs is affected by, amongst other factors, their size and shape and by heat loss through the roof from below. This paper reports on research, done under contract for the National Building Code of Canada, aimed specifically at quantifying the trends of snow loads versus roof size for varying rates of heat loss. The concern was with the very large flat roofs now being constructed and the lack of supporting data. Small roofs lose snow rapidly because they tend to be scoured off by wind. Large roofs retain snow longer because there is a relatively greater quantity to be transported over long distances before removal. Melting by heat transfer through the roof, therefore, is relatively more important for large roofs as a snow removal mechanism.

The studies have been undertaken using the finite-area element computer simulation technique on hypothetical flat roofed buildings in three Canadian cities with different climatic regimes: Edmonton which is a very cold city with moderate snowfall; Montreal which has larger snowfall and is not as cold; and St. John's Newfoundland which has a maritime climate characterized by heavy snowfalls and strong winds. The paper discusses the results of the computer simulations and compares them with Code provisions and available full scale data.

INTRODUCTION

Design snow loads on single and multi-level flat roofs are based on measurements of snow depths and densities taken during surveys and after collapses (e.g. Taylor, 1992, O'Rourke and Redfield, 1981, O'Rourke, Tobiasson and Wood, 1986)) and on the experience and judgement of the engineers on the Building Code committees. When flat roof surveys were started in Canada in 1966, most roofs were less than about 75 m in length although there were exceptions. In recent years, however, very large flat-roofed buildings have been built of dimensions 300 x 300 m and beyond and there is one in Ontario which is about 280 x 1000 m. Such roofs have not been surveyed and experience with them is limited.

Surveys are very expensive, take years to complete, 10 at least, and inevitably leave unresolved questions. To supplement field data and to answer the unresolved questions, efforts

have been made to develop analytical and computational approaches, based on wind tunnel tests, to estimate snow loads on roofs (Irwin and Gamble, 1988; Gamble et al., 1991 and Isyumov, 1971) and there has been some success with these. In particular, the Finite Area Element (FAE) method has been developed (see Irwin and Gamble, 1988; Gamble et al, 1991) and used to establish the trends described in this paper.

THE FINITE AREA ELEMENT (FAE) METHOD

Each roof is divided into many elemental areas. For each element, the predicted wind velocities one metre above the roof at the four corners (grid points) are used by the program to compute the snowdrift fluxes through the sides of each element. Thus the analysis proceeds hour by hour for an entire winter season of meteorological data, calculating the increase or decrease in the mass of snow in each element, as a result of snowfall, drifting, and melting.

Wind tunnel tests are usually used to determine the local wind speed and wind directions at each grid location on the roof - for 16 wind directions in 22.5 degree increments. It is possible, however, to specify the velocity patterns on simple roofs by other methods. In this study, no wind tunnel tests were done; the roofs were assumed to be flat with wind speeds and directions uniform over the entire roof. Although the general snow loadings were modelled, localized drifts caused by complex airflows close to the roof edges could not be modelled. These local drifts tend to be the same for the roof sizes studied and are covered implicitly by the current National Building Code of Canada (NBCC) (National Research Council of Canada, 1990) provisions for roofs of less than 75 m in length. Therefore for the present study of trends, this was not considered to be a serious limitation.

From the meteorological records of daily snowfall, which include information indicating heavy, medium, or light accumulations, the amount of snow falling onto an element in a given one hour period is estimated. Likewise, meteorological records for temperature, when combined with solar radiation data and building heat loss data, determine the melting rate for the snow in the element. Thus computations are made for the amount of snow melted in each element. If the snow surface has melted or it has rained, the snow is not available for drifting. As well, more snow cannot be scoured from an area than is available for drifting or has fallen, fresh, into the area. By stepping through the meteorological data in one-hour intervals, the increase in snow load as a result of snowfall, the redistribution of loads by drifting, and the reductions in load from melting are evaluated for all elements comprising the grid. The entire history of events in each element is computed for the number of years of meteorological records available for each roof location. Then a statistical analysis of the loads on each element is done to get predicted design loads.

THE STUDY

The paper describes a study in which the FAE method was used to examine the effects of the following parameters on the snow loads on 10 m high flat roofs in open and suburban exposure:

- a) Building size; Montreal, Edmonton, St. John's (square buildings 10, 40, 100, 300, 500 m on a side);
- b) Building shape; Montreal only (square vs rectangular 300 x 40, 40 x 40, 300 x 100, 100 x 100, and 200 x 300 m, with the prevailing winter winds aligned with the long side of each roof);
- c) Heat loss-roof insulation; Montreal and Edmonton (R infinite, R15, R5 BTU's); and
- d) Local climate - geographic location - (Montreal, Quebec; Edmonton, Alberta; St. John's, Newfoundland). Montreal has moderately high snowfall with moderate temperatures, Edmonton is cold (continental) with lower snowfall, and St. John's experiences a maritime climate with high snowfalls, strong winds and more winter rain (see Table 1).

The loads computed in the analysis were:

- a) average load - the largest average load over the whole roof,
- b) peak load - the largest average load in one roof bay (the bay sizes are 2.5 x 2.5 m for 10 x 10 m roofs; 10 x 10 m for 40 x 40 m roofs and 20 x 20 m for the rest), and
- c) step load - the maximum average load due to roof snow deposited on the ground just off the edge of the roof. No drifting along the ground was allowed.

Table 1. City Meteorological Normals Comparison (1951-80) and NBCC Ground Snow Loads

City	Total Yearly Snowfall mm H ₂ O	Total Winter ¹ Rainfall mm H ₂ O	Average Winter ¹ Temperature °C	Average Winter ¹ Windspeed km/hr	NBCC	
					S _e kPa	S _r kPa
Edmonton	136	5	-10.0	13.2	1.6	0.1
Montreal	235	108	-7.1	17.7	2.2	0.4
St. John's	359	311	-3.1	27.2	2.6	0.6

Notes: 1. Winter denotes the months of December to March inclusive.

Results of the Analysis

Effect of heat transfer and R value

Heat transfer through the insulation and into the snow on the roof will melt some snow and reduce loads. The effect of heat loss was investigated by simulating different R values of

roof insulation on five building sizes in Montreal and Edmonton. The following assumptions were made: the inside air temperature was 20 deg C and the outside convection coefficient was 33 W/m²K. The results in Table 2 indicate that the reductions in load compared to a perfectly insulated roof are relatively modest, a maximum of only 14 % for a 300 x 300 m R 5 roof in Montreal and as expected, less (5 %) for the colder climate of Edmonton. Smaller or exposed roofs tend to demonstrate less effects from reduced roof insulation. This is due to the shallower snowpack found on smaller or exposed roofs which provides less insulation than the deeper drifts found on larger or sheltered roofs. This effect is illustrated in Table 2 a).

Table 2. Effect of Heat Transfer - Roof Insulation

a) Montreal

R Value	Normalized Peak Snow Load $S/(S_r + S_d)$					
	40 m x 40 m Roof		100 m x 100 m Roof		300 m x 300 m Roof	
	Open Exposure	Suburban Exposure	Open Exposure	Suburban Exposure	Open Exposure	Suburban Exposure
Infinity	0.28	0.71	0.49	0.93	0.87	0.98
R 15	0.28	0.67	0.47	0.88	0.82	0.92
R 5	0.26	0.61	0.44	0.80	0.76	0.84

b) Edmonton - 300 x 300 m Building

R Value	Normalized Peak Snow Load $(S/(S_r + S_d))$	
	Open Exposure	Suburban Exposure
Infinity	0.85	0.95
R 15	0.84	0.93
R 5	0.81	0.90

The predictions by the FAE method may have tended to underestimate the load reductions due to melting since it was assumed that meltwater was soaked up by the snowpack up to the point where the pack could contain no more. Only thereafter could the meltwater drain away. The observations (O'Rourke and Redfield, 1981) imply a reduction in the order of 20 % due to heat transfer and this is reflected in the ASCE 7-88 standard (American Society of Civil Engineers, 1990).

Effect of roof size

Peak and average roof loads

The results of the analyses for the three cities are plotted in Figures 1 to 4. There is a trend to significantly larger peak and average snow loads as the roof size; in particular, the length

increases. Such a trend was expected because as a roof becomes very large, its size begins to approximate the ground and the roof load begins to approach that on the ground. Exposed ground, however, has reduced snow on it, and as Figure 1 shows, so does even a very large exposed roof. The snow is scoured off exposed roofs, bouncing along in a process called saltation and eventually blows over the edge.

The peak loads for roofs larger than 40 x 40 m are computed for 20 x 20 m bays which are big enough areas to control the design of columns, beams and slabs. Loads averaged over the entire roof (Figures 3 and 4) are of less importance to designers. It is interesting to note how similar the trends are for Montreal and Edmonton. The particularly strong winter winds at St. John's (see Table 1) result in the roofs with suburban exposure having the same peak and average loads as those with open exposure in Montreal and Edmonton. Roofs with open exposure in St. John's have much reduced loads due to the high speed of the winds causing drifting.

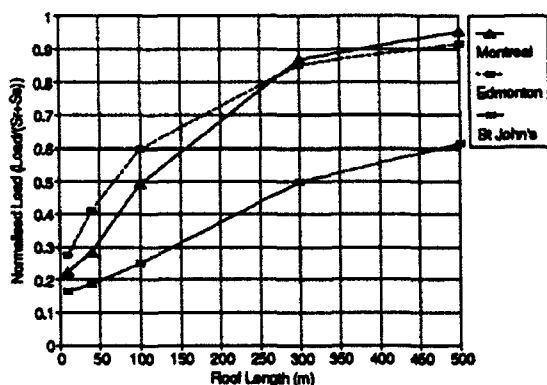


Figure 1. City Comparisons of Peak Snow Load - Open Exposure (Square Roofs)

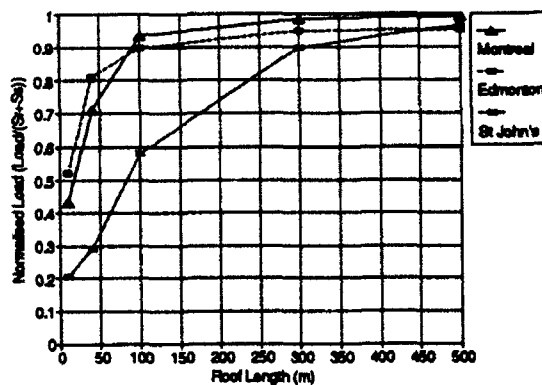


Figure 2. City Comparison of Peak Snow Load - Suburban Exposure (Square Roofs)

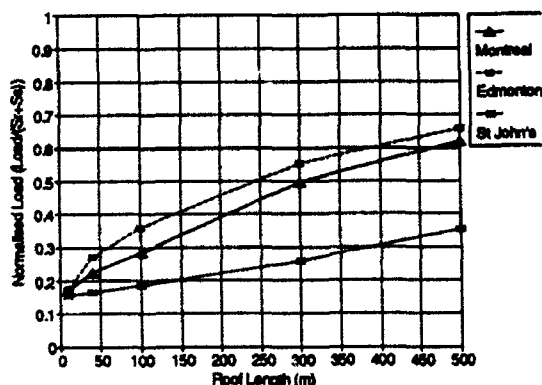


Figure 3. City Comparisons of Average Snow load - Open Exposure (Square Roofs)

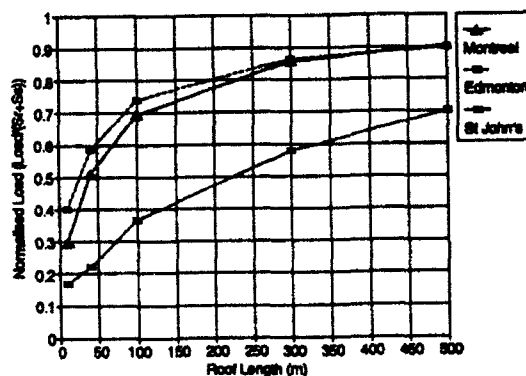


Figure 4. City Comparisons of Average Snow Load - Suburban Exposure (Square Roofs)

Step (drift) loads

The simulation allowed snow to drift off the roof and accumulate as a uniformly distributed mass of snow in a sheltered zone 20 m wide on the ground 10 m below the edge of the roof. For comparative purposes, the National Building Code of Canada (NBCC) would have an average amount of snow in a 20 m wide drift of about 1.3 ($S_e + S_r$). It can be seen in Figures 5 and 6 that the predicted step loads from the FAE simulations are sensitive to upper level roof size and to wind exposure. For roofs of up to 50 m length in suburban exposure in Montreal and Edmonton the predictions do not exceed the NBCC value of 1.3. However, for exposed conditions, or in the windier climate of St. John's the predictions indicate normalized step load of about 2.0 could occur at the edge of a 50 m long upper level roof (see Figure 5). For roofs longer than 50 m step loads several times higher than 2.0 appear possible. The predicted step loads are almost certainly overestimates of real life values because of the assumption that the step was 100 % efficient in capturing all snow drifting off the upper roof (some snow will be carried entirely away by the wind). However, it is noteworthy that in the Jordan Marsh roof collapse (M.A.Reidy Engineers, 1978) that the normalized step load is estimated to have been in the range of 4 to 4.5 for a roof length of about 100 m, which is consistent with the predictions for an exposed roof of that size.

Effect of roof shape

It is of interest to investigate whether a change in roof planform results in different snow loads. The expectation is that a narrower roof would lose more snow off the sides than a square roof when the wind direction shifts. Indeed that is what occurs. Table 3 illustrates that for a constant width, peak snow load

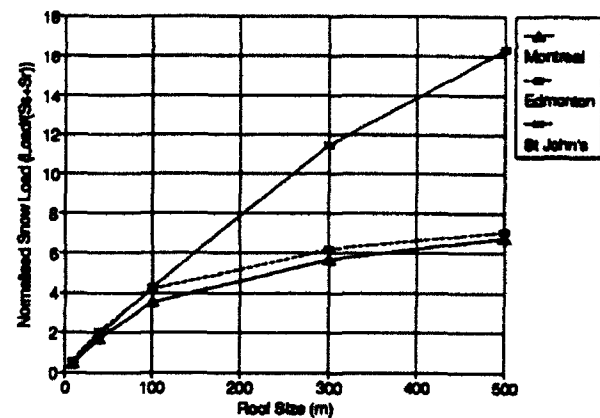


Figure 5. City Comparisons of Step Loads - Open Exposure (Square Roofs)

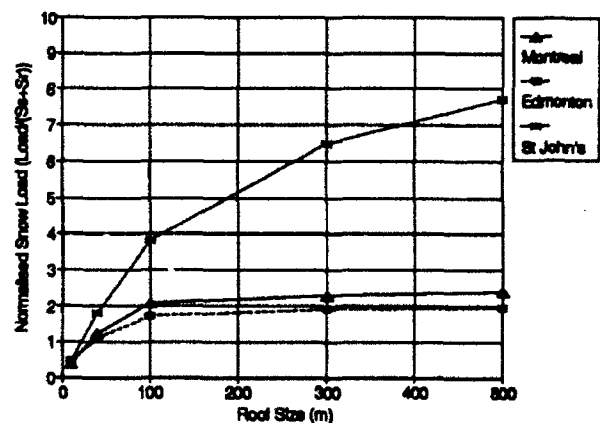


Figure 6. City Comparisons of Step Loads - Suburban Exposure (Square Roofs)

increases with building length. Further, it shows that as the width increases, so also does the peak load, although at an ever decreasing rate as the building approaches a square shape.

Table 3. Effect of Roof Shape

(a) 40 m Width

Roof Length (Along Predominant Blowing Snow Winds)	Peak Snow Load (kPa)
40 m (40 x 40 m)	0.74
300 m (300 x 40 m)	1.08

(b) 100 m Width

Roof Length (Along Predominant Blowing Snow Winds)	Peak Snow Load (kPa)
100 m (100 x 100 m)	1.28
300 m (300 x 100 m)	1.59

To be able to deal with roofs of different aspect ratios, a characteristic roof length would be advantageous. Such a characteristic length was obtained by comparing the amount of snow on the square and rectangular roofs. The characteristic length, l^* , defined as the length of the square roof that experiences the same design load as the rectangular roof, was found to be of the form

$$l^* = 2w - w^2/l \quad (1)$$

where w is the small dimension of the roof, and l the large. Figure 7 presents the combination of data taken from the three cities, for open and suburban exposures and for roofs of square and rectangular planform. The plot is in the form of normalized bay (peak) load versus the characteristic length of each roof simulated. As noted previously the peak bay load, the highest average in a bay, is of more interest to designers than the largest average load over the whole roof.

Superimposed on these results are possible design curves which rise above NBCC loads for roofs with characteristic lengths greater than about 75 m. Note that the value of the design load for small roofs (horizontal portion of the design curves shown in Figure 7) actually changes somewhat for different cities because of the varying contribution of the rain load, S_r . An average for the cities studied is shown in the figure. The design curves fit the data well for Montreal and Edmonton but are conservative for St. John's because, as noted before, the winds in St. John's are very high resulting in turbulent diffusion as a major mechanism of snow transport off the roof. Indeed because the analysis does not model turbulent diffusion, all the data (and possible design curves) may be conservative, especially for the larger roofs in open exposure. Note that

the design curves have been drawn to fall slightly below the FAE results (which were for zero heat transfer in this Figure) as an allowance for some heat transfer through typical roofs. For the same reason the curves level off at 0.95 rather than 1.0.

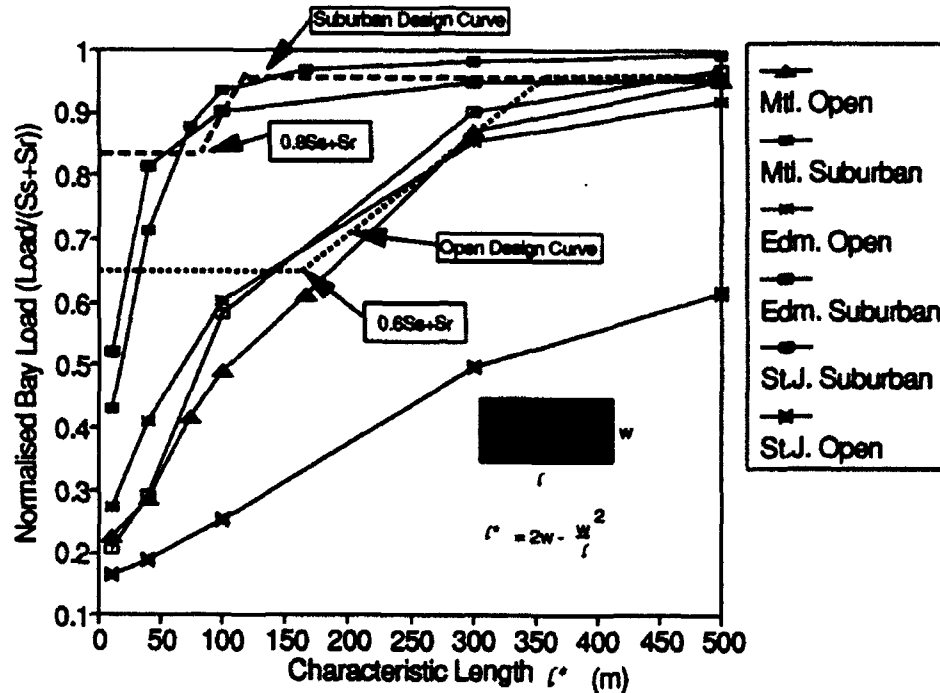


Figure 7. Load Reduction Factors and Recommendations

The influence of wind velocity is illustrated in Figure 8. This is an alternate presentation of the data in Figure 7 with the effect of wind speed prominent. Figure 8 accounts for the effects of exposure and building height on velocity. The velocity used was the average wind speed at the roof height. This value is obtained by finding the average (annual) wind speed, U_{avg} , in published wind normal tables for the geographic location and applying the following equation:

$$U_{roof} = U_{avg} \times (Z_{roof}/Z_{anem})^{\alpha} \quad (2)$$

where Z_{roof} = the height of the roof
 Z_{anem} = the height of the anemometer (usually 10 m)
 α = 0.14 for open exposure
 α = 0.25 for suburban exposure

Clearly the winter wind (Table 1) is more appropriate but not as readily available. Even without accounting for turbulent diffusion, Figure 8 highlights the importance of saltation at the higher wind speeds in reducing loads by transporting snow off roofs.

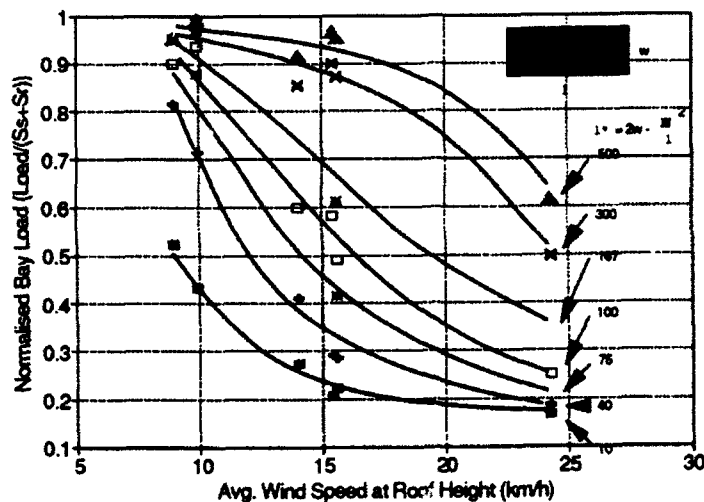


Figure 8. Load Reduction Factors - Alternate Presentation Accounts for Roof Size, Exposure, Height, and Average Annual Wind Speed

Conclusions

1. The analysis identifies a trend towards loads higher than those recommended in the 1990 NBCC Commentary on Snow Loads for roofs longer than about 75 m.
2. The wider a rectangular roof, the more snow load it attracts.
3. A characteristic length can be defined to obtain the snow loads on rectangular flat roofs in terms of an equivalent square roof.
4. Heat transfer effects for roofs of different heat loss were predicted to reduce roof loads by 5% to 15% for exposed and sheltered roofs respectively. The effect is less for smaller roofs because of the shallower snowpack found on these roofs. Actual reductions may be more, as the predictions are thought to be conservative.
5. For larger roofs, step loads much larger than those in the NBCC were identified, particularly for roofs exposed to strong winds. These are upper bound loads, however, in part because the analysis assumed the step to capture all snow drifting off the upper roof with 100% efficiency.

6. Despite the upper bound nature of the predicted step loads they indicate the need to take a further look at code provisions for steps, especially where the upper roof area is large and the site is exposed to strong winds. There is field evidence that in such situations exceptionally large step loads can indeed occur.

References

American Society of Civil Engineers, 1990, "Minimum Design Loads for Buildings and Other Structures", ASCE 7-88, 1990.

Gamble, S.L., Kochanski, W.K. and Irwin, P.A., 1991, "Finite-Area-Element Snow Load Prediction - Applications and Advancements", Proc. 8th International Conference on Wind Engineering, London, Ontario, Canada, July 8 - 12, 1991.

Irwin, P.A. and Gamble, S.L., 1988, "Predicting Snow Loading on the Toronto SkyDome", Proceedings First International Conference on Snow Engineering, Santa Barbara, California, July.

Isyumov, N., 1971, "An Approach to the Prediction of Snow Loads" Ph.D. Thesis, Faculty of Graduate Studies, University of Western Ontario, London, Canada.

M.A. Reidy Engineers, 1978, "The Blizzard, February 6-7, 1978, Evaluation of Snowdrift Loads on the Roof, Jordan Marsh Company Central Service Facility", Boston Massachusetts, February.

National Research Council of Canada, 1990, "Supplement to the National Building Code of Canada 1990", Associate Committee on the National Building Code.

O'Rourke, M., and Redfield, R., 1981, "Ground to Roof Conversion Factors: Uniform Loads", ASCE Preprint 81-074, New York, May 11 - 15, 1981.

O'Rourke, M. Tobiasson, W., and Wood, E., 1986, "Proposed Code Revisions for Drifted Snow Loads", ASCE J. Struct. Eng., Vol. 112, No. 9, pp. 2080 - 2092.

Taylor, D.A., 1992, "Snow on Two-Level Flat Roofs - Measured vs. 1990 NBC Loads", Can. J. Civil Eng. 19, 59 - 67.

Field Measurement and Characteristic Analyses of Snow Load on Flat Roofs

Hirozo Mihashi,* Toru Takahashi,[†] and Masanori Izumi*

*Department of Architecture, Tohoku University, Sendai 980, Japan

[†]Department of Architecture, Chiba University, Chiba 263, Japan

ABSTRACT

Snow load on the ground and flat roofs was measured every week for several years at more than 100 buildings in Tohoku District, Japan. Influencing factors on the ground-to-roof conversion factor were investigated and the formula of snow density introduced in the ISO draft '91 is critically discussed.

INTRODUCTION

Since the most available data for snow load are usually snow depth on the ground, it is essential to determine the ground-to-roof conversion factor and the snow density for designing buildings in snowy areas. So far, however, very little information has been published on the variation of the conversion factor for snow loads on roofs. O'Rourke and his co-workers (1982) analyzed data on ground and roof snow loads for 199 structures. They concluded that the conversion factor was most strongly influenced by the exposure of the structure but less influenced by the thermal characteristics of the structure. Moreover they did not recognize any observable difference in snow loads on sloped roofs between 0° and 35°. Høibo (1988) analyzed snow load data of about 200 buildings with gable roofs to propose a formula of the conversion factor as a function of slopes and ground snow load for different roofing materials.

In this study, weekly data of snow load on the ground and flat roofs were measured for two or three years at more than 100 buildings in the northeast part of the Honshu Islands (Tohoku District) in Japan. All the data are shown in other reports by authors (1985, 1989) and only the summary is presented in this paper.

MEASUREMENT PROCEDURES

The study was composed of two parts. In the first part, snow load and depth on the ground and flat roofs of 22 buildings in Yamagata prefecture were measured every week in 1984 and 1985. Snow samplers were used to measure the snow load. Only the typical results are presented in this paper, whose locations and the outline are shown in Figure 1 and Table 1, respectively.

In the second part, mainly snow depth on the ground and flat roofs of 99 buildings in Tohoku District were measured every week from 1986 to 1988. Among them, data of 47 buildings were used for factor analysis, whose locations and the outline are shown in Figure 2 and Table 2, respectively.

MEASUREMENT RESULTS AND DISCUSSION

Figure 3 shows the weekly variation of results measured in Yamagata prefecture in 1983

- 1984. Figures 3.1, 3.2 and 3.3 show variations of snow load, conversion factor and snow density ratio, respectively. In these results, the conversion factor was recognized to be strongly influenced by thermal characteristics. In case of unheated buildings, the conversion factor varied between 0.8 and 1.0 and the snow density ratio was almost 1.0. On the other hand, the conversion factor of 0.75 - 0.85 was measured for usually heated office buildings and the snow density was slightly lower than that of the former cases varying between about 1.0 and 0.8. For buildings with poor thermal insulation, the conversion factor gradually decreased up to 0.5 or even less, and the snow density ratio varied very roughly between 1.5 and 0.5. The variation was influenced by the snow intensity and the thermal insulation factor. In case of regularly heated buildings such as fire stations, the conversion factor decreased remarkably. In some cases, the snow load on roof was 30 to 50% larger than that on the ground. It might be caused by influences of wind.

These results revealed that once a year measurement gave very rough information and that only the continuous measurement could give a reliable data to determine the conversion factor. It was also pointed out that the influences of thermal characteristics of the roof were not negligible to conversion factors and that snow intensity should be considered when reduction of snow loads due to the thermal influence was performed.

Figure 4 shows the relation between the equivalent snow density and the maximum snow depth. The equivalent snow density was calculated from the relation between the maximum snow load and the maximum snow depth. In Figure 4, the mean values of meteorological data in Japan are shown with their variation ranges (Sakurai et al., 1982; Mihashi and Takahashi, 1988). The formula of snow density introduced in the draft of ISO 4355 that was proposed in USSR (1970) may give too large values for rather warm areas and for heavy snow areas above 2 m. In the draft of AIJ recommendation (1992), the following formula is adopted:

$$\rho = 125 \sqrt{d} + 185 \quad (\text{kg/m}^3) \quad (1)$$

Figure 5 shows the weekly variation of snow depth (on ground and roof) and the conversion factor, which is the result of the measurement in Part 2. In case of inland locations, the conversion factor varied between 1.0 and 0.7. On the hand, it varied between 0.5 and 0.3 in locations closed to the coast and very windy locations where the exposure effect might be dominant. Typical examples of snow drift are shown in Figure 6. In some cases where it rarely snows, the conversion factor was changeable and distributed between 1.0 and 0.5.

Multivariate statistical analysis was performed for those data in which twelve variables shown in Table 3 were chosen. Table 4 shows the factor loading matrix and accumulated contribution ratio. The first factor seems to be corresponding to the snow depth and the snowfall. The second factor may describe the exposure effect that correlates to the distance from the coast, the wind speed and geological conditions. The third factor corresponds to the thermal condition of the roof. The fourth and fifth factors are changed in 1987 and 1988. They describe the local wind conditions and the atmospheric temperature conditions. The former condition is influenced by parapets and the building height. The latter condition influences properties of snow. Figure 7 shows the relation between the factor-1 and the factor-2. Two years' measurement gives slightly different results but some qualitative tendencies are certainly recognized. These five factors can totally represent about 87% of flat roof snow depth.

CONCLUSION

The conversion factor is influenced by several factors. Only the continuous measurement could give reliable data to determine the conversion factor and the influences of thermal characteristics of the roof were not negligible. The formula of snow density proposed in USSR (1970) may give an overestimation for warm area and for heavy snow areas above 2 meters.

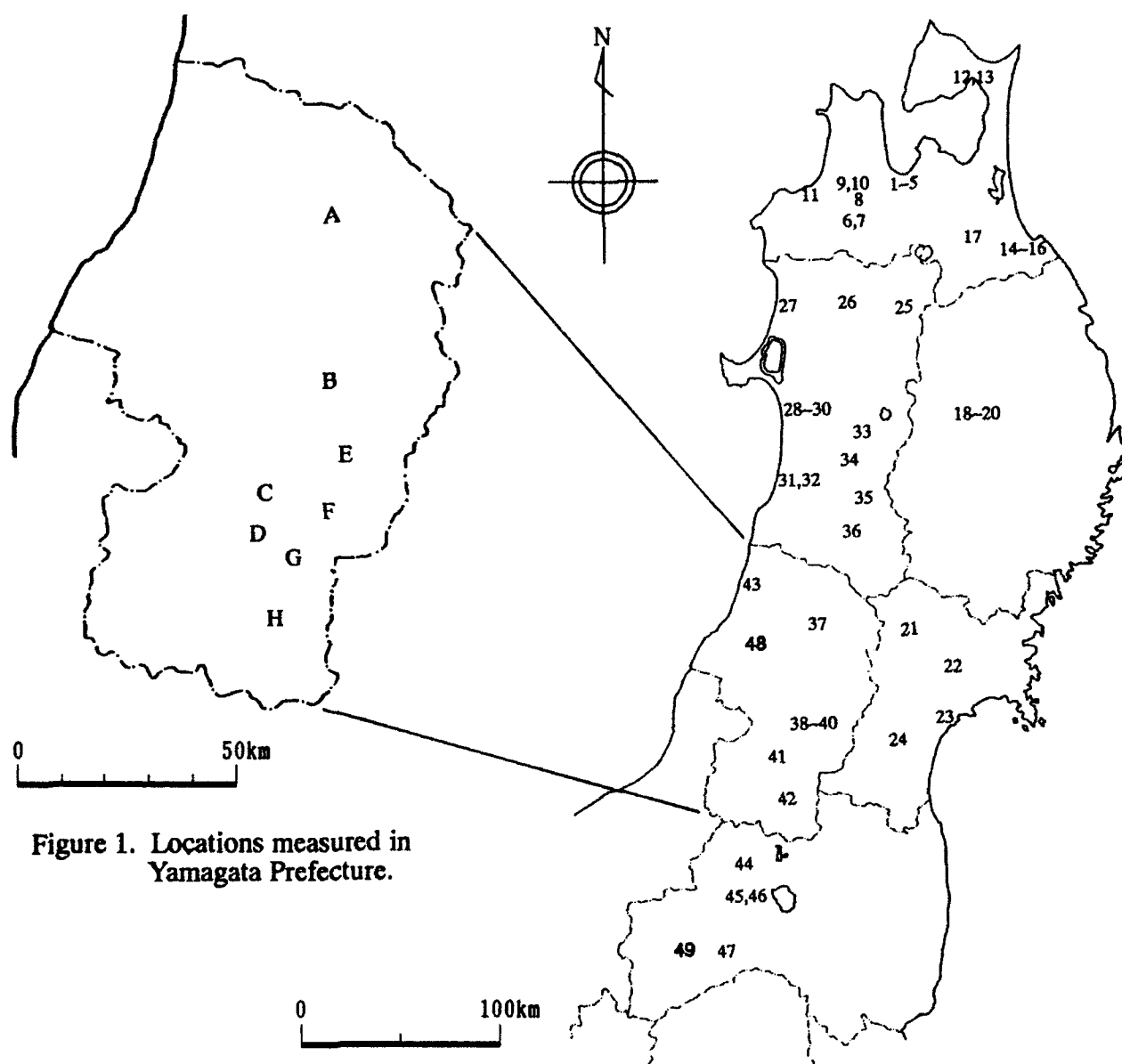


Figure 1. Locations measured in Yamagata Prefecture.

Figure 2. Locations measured in Tohoku District.

Table 1. Characteristics of observed buildings to measure snow load.

Site	Structure	Use	Year	Height	Slope	Parapet	Insulation	Heating	Ground
A Shinjo-3	RC 1	Obs. house	1969	3.72	1/100	-	-	nothing	lawn
B Kahoku	RC 4	House	1982	14.3	1/50	0.5	fpb. 30mm	partially	soil
C Shirataka	S 1	Nursery schl.	1982	3.9	1/100	0.15	fpb. 30mm	normally	soil
D Nagai	S 2	Kindergarten	1980	7.8	1/100	0.05	gw. 50mm	normally	soil
E Yanagata-1	RC 4	Office	1968	17.7	1/100	1.1	?	sometimes	cray
F Kaminoyama	RC 5	Office	1974	19.8	1/100	0.55	ceb. ?	normally	soil
G Nanyo	S 4	Office	1982	15.7	1/50	0.5	?	normally	cray
H Yonezawa-1	SRC 7	Office	1969	26.4	1/100	1.3	fpb. 25mm	partially	soil

ceb. : cemented excelsior board, fpb. : foamed polystyrene board, gw. : glass wool

Table 2. Characteristics of observed buildings to measure snow depth.

No.	Site	Structure	Use	Year	Height	Slope	Parapet	Insulation	Temperature
1	Aomori-1	RC 4	Office	1965	15.9	1/100	1.5	ceb. 25mm	17.0 (office room)
2	Aomori-2	SRC 8	Office	1984	29.7	1/80	1.15	fpb. 25mm	22.0 (corridor)
3	Aomori-3	RC 6	Office	1960	19.5	1/100	1.1	ceb. 15mm	21.0 (office room)
4	Aomori-4	RC 2	Office	1962	6.8	3/100	1.0	ceb. 25mm	25.0 (office room)
5	Aomori-5	RC 2	Office	1961	7.9	1/100	0.1	-	22.0 (office room)
6	Hirosaki-1	RC 2	Office	1973	7.1	1/100	0.3	fpb. 25mm	22.0 (office room)
7	Hirosaki-2	RC 3	Office	1964	9.0	1/100	1.1	ceb. 25mm	20.0 (office room)
8	Fujisaki	RC 2	Office	1968	7.1	1/100	0.15	fpb. 20mm	25.0 (office room)
9	Goshogawara-1	RC 2	Office	1984	7.9	1/100	0.7	fpb. 25mm	20.0 (office room)
10	Goshogawara-2	RC 3	Office	1983	12.2	1/62	1.45	fpb. 50mm	25.0 (corridor)
11	Ajigasawa	RC 2	Office	1980	7.9	1/50	0.35	fpb. 30mm	23.0 (office room)
12	Mutsu-1	RC 4	Office	1983	15.8	1/50	0.46	fpb. 30mm	24.0 (office room)
13	Mutsu-2	RC 2	Hall	1985	11.0	1/100	0.65	fpb. 30mm	18.0 (entrance hall)
14	Hachinohe-1	RC 4	Office	1963	5.2	1/100	0.9	-	19.0 (office room)
15	Hachinohe-3	RC 3	Office	1979	12.2	1/100	1.2	fpb. 25mm	12.5 (office room)
16	Hachinohe-4	RC 5	Office	1971	12.5	1/100	1.1	fpb. 25mm	21.0 (office room)
17	Towada	RC 3	Office	1981	12.3	1/50	0.5	fpb. 50mm	21.0 (office room)
18	Morioka-1	SRC 8	Office	1962	29.0	1/100	1.2	-	19.0 (office room)
19	Morioka-2	RC 3	Office	1964	11.2	1/100	1.8	ceb. 25mm	25.0 (office room)
20	Morioka-3	RC 2	Office	1976	7.2	1/100	1.5	-	20.0 (office room)
21	Narugo	RC 2	Office	1957	7.4	1/100	0.05	-	24.0 (office room)
22	Furukawa	CB 1	Office	1962	3.9	1/100	0.22	ceb. 25mm	20.0 (office room)
23	Shiogama	RC 3	Office	1960	11.5	1/90	0.85	fpb. 10mm	12.0 (waiting room)
24	Kamafusa	RC 3	Office	1970	13.3	1/100	0.45	fpb. 15mm	22.0 (office room)
25	Kazuno	RC 2	Office	1965	11.6	1/100	1.15	ceb. 12mm	20.0 (office room)
26	Takanosu-4	RC 3	Office	1970	11.9	1/100	0.5	fpb. 15mm	22.0 (office room)
27	Noshiro-2	RC 3	Office	1969	11.9	1/100	1.1	fpb. 15mm	23.0 (office room)
28	Akita-1	RC 4	Office	1964	15.5	1/85	1.15	ceb. 30mm	17.0 (office room)
29	Akita-3	RC 5	Office	1968	19.4	1/100	0.5	ceb. 25mm	24.0 (office room)
30	Akita-5	RC 6	Office	1959	24.7	1/100	1.25	-	21.0 (office room)
31	Honjo-1	RC 1	Office	1966	3.7	1/100	0.28	-	24.0 (office room)
32	Honjo-2	RC 3	Office	1963	11.7	1/100	0.6	ceb. 9mm	20.0 (office room)
33	Kakunodate	RC 1	Office	1966	4.0	1/100	0.1	-	27.0 (office room)
34	Omagari-2	RC 3	Office	1967	10.3	1/100	0.55	ceb. 15mm	24.0 (office room)
35	Yokote	RC 3	Office	1970	11.9	1/100	0.75	ceb. 15mm	24.0 (office room)
36	Yuzawa-2	RC 3	Office	1966	11.7	1/100	1.2	ceb. 15mm	21.0 (office room)
37	Shinjo-1	RC 3	Office	1982	11.9	1/100	0.6	fpb. 50mm	22.0 (office room)
38	Yamagata-1	SRC11	Office	1983	38.9	1/50	0.65	fpb. 50mm	20.1 (meeting room)
39	Yamagata-2	S 16	Office	1975	61.2	1/100	1.2	fpb. 25mm	22.0 (office room)
40	Yamagata-3	RC 6	Office	1983	25.2	1/100	1.1	fpb. 50mm	21.0 (office room)
41	Nagai	RC 5	Office	1981	20.6	1/100	0.8	-	20.5 (office room)
42	Yonezawa-1	SRC 7	Office	1969	26.4	1/100	1.3	fpb. 25mm	20.0 (kitchen)
43	Sakata-1	RC 5	Office	1964	18.9	1/100	0.4	-	21.0 (office room)
44	Kitakata	RC 3	Office	1978	11.5	1/50	0.6	fpb. 30mm	16.0 (office room)
45	Aizuwakamatsu-1	SRC 4	Office	1983	17.4	1/45	1.8	fpb.100mm	20.0 (office room)
46	Aizuwakamatsu-2	RC 3	Office	1970	9.8	1/100	1.15	ceb. 12mm	23.0 (office room)
47	Tajima	RC 4	Office	1971	14.3	1/100	1.2	-	24.0 (office room)

ceb. : cemented excelsior board

fpb. : foamed polystyrene board

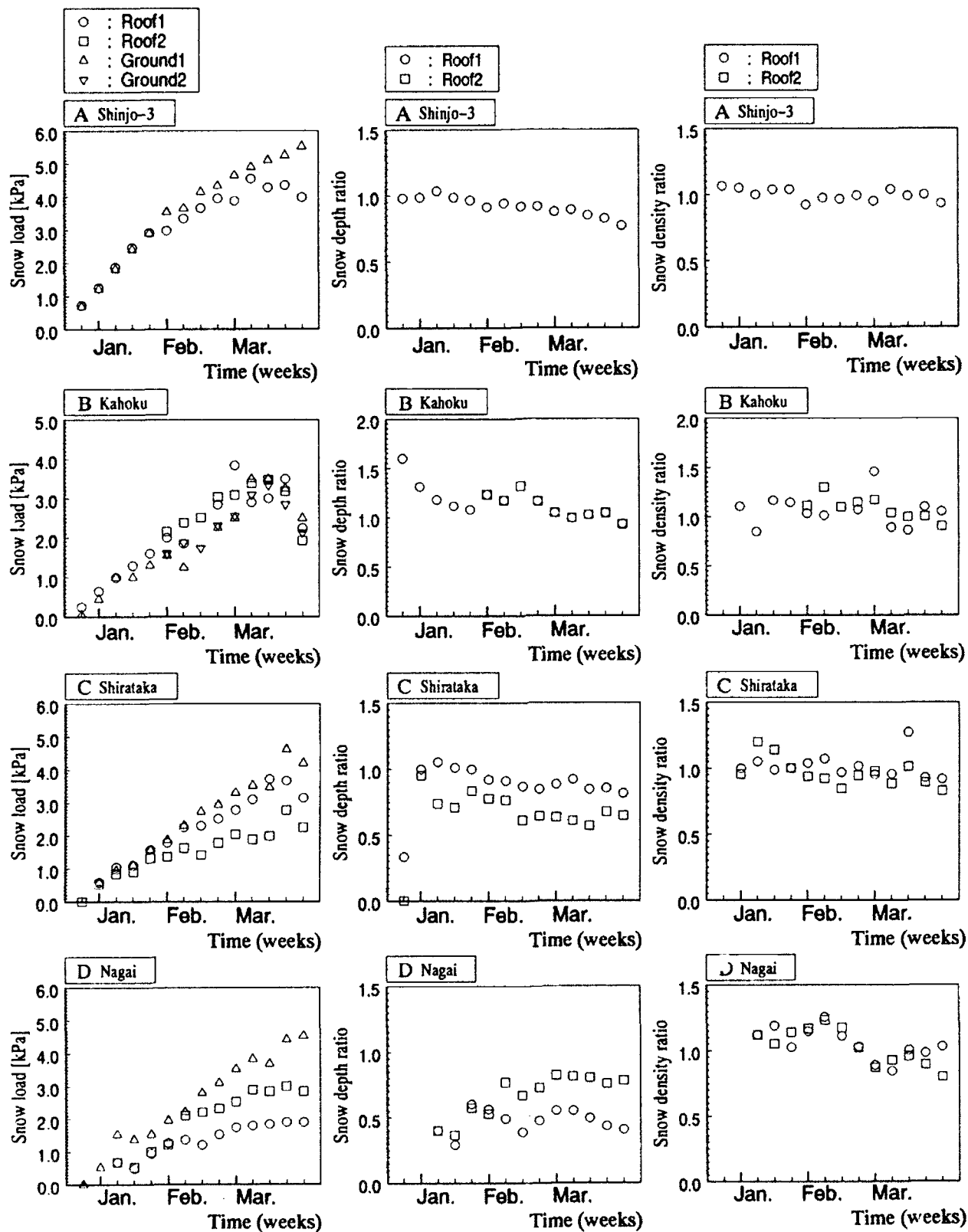


Figure 3.1.a. Variation of snow load.

Figure 3.2.a. Variation of conversion factor

Figure 3.3.a. Variation of snow density ratio.

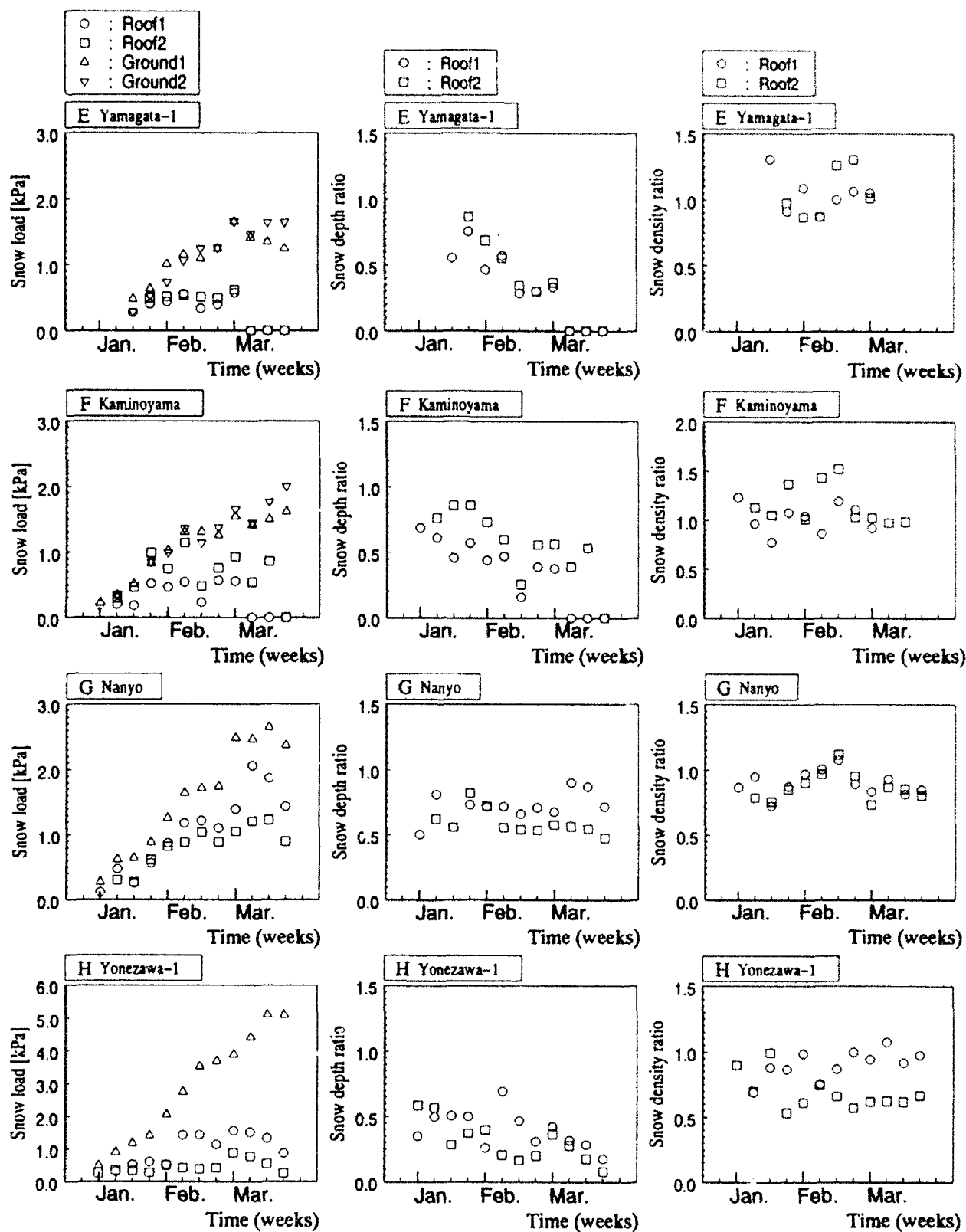
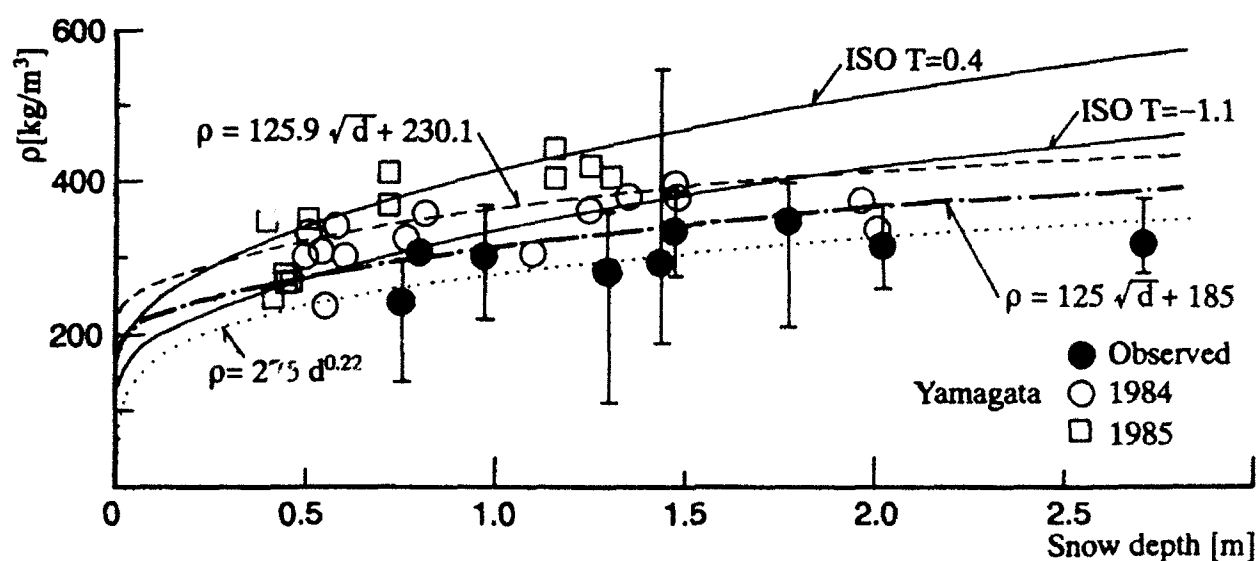


Figure 3.1.b. Variation of snow load.

Figure 3.2.b. Variation of conversion factor

Figure 3.3.b. Variation of snow density ratio.



	d_1 [m]	ρ_1 [kg/m ³]	d_2 [m]	ρ_2 [kg/m ³]	Dec.	Temperature Jan.	Feb.	Mar.	Wind [m/s]
1983 - 84									
Yonezawa	1.36	383.			-0.3	-2.9	-3.3	-1.4	2.3
Nanyo	0.77	329.			0.1	-4.5	-6.0	-2.4	1.9
Kaminoyama	0.56	238.	0.59	346.	0.5	-3.5	-2.9	-1.5	1.7
Yamagata	0.51	331.	0.55	307.	0.8	-2.4	-2.9	-0.5	1.5
Tendo	0.51	306.	0.61	305.	1.3	-1.6	-2.4	0.4	1.0
Funagata	2.02	339.							
Obanazawa	1.98	376.			-0.8	-3.2	-3.4	-1.4	2.8
Nagai	1.26	366.			-0.1	-3.3	-3.6	-1.4	2.0
Shinjo	1.48	380.			-0.4	-3.3	-3.5	-1.6	2.0
Nishikawa	1.48	392.			-0.3	-3.3	-3.5	-1.3	1.9
Sagae	0.82	360.			0.7	-1.9	-2.0	0.2	
Kahoku	1.10	308.			0.8	-1.9	-2.4	0.0	
1984 - 85									
Yonezawa	0.73	412.	0.73	367.	0.9	-3.6	-0.3	1.8	
Nanyo	0.48	267.	0.45	250.					
Kaminoyama	0.45	267.	0.42	250.					
Obanazawa	1.26	419.	1.31	405.	0.9	-3.8	-0.5	1.5	
Funagata	1.16	405.	1.16	439.					
Higashine	0.40	348.	0.51	357.	0.6	-4.5	-0.7	1.9	
Yamagata	-	-			1.2	-3.5	0.2	2.5	
Shinjo	-	-			0.9	-3.6	-0.7	1.2	

	Observed year	d	ρ	T	v
Hirosaki	(1965-74,82-85: 11)	0.76	237.	0.1	3.0
Fukui	(1984)	0.81	310.	3.0	3.0
Sapporo	(1964-83: 19)	0.98	308.	-2.7	1.5
Takada	(1962-80: 19)	1.30	281.	3.7	2.5
Yonezawa	(1958-75: 13)	1.45	294.	0.5	2.3
Shinjo	(1958-75: 13)	1.48	335.	-0.2	2.0
Obanazawa	(1958-75: 15)	1.79	341.	-0.1	2.8
Yuda	(1961-75: 12)	2.02	317.	-1.3	1.5
Tadami	(1962-76: 12)	2.73	320.	0.3	2.0

Figure 4. Relation between equivalent snow density and the maximum snow depth.

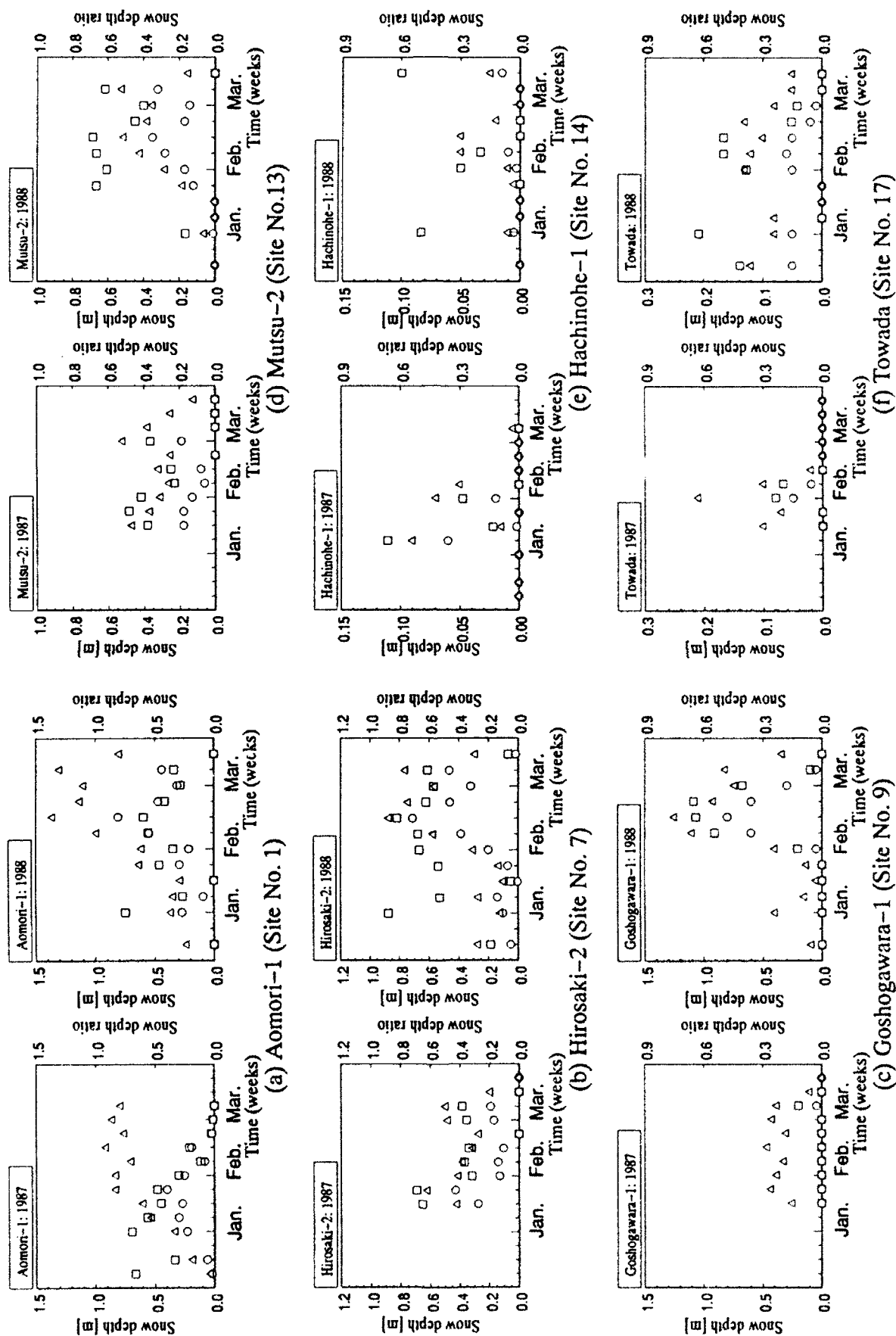


Figure 5.a. Variation of snow depth and conversion factor (Δ : ground, \circ : roof, \square : conversion factor).

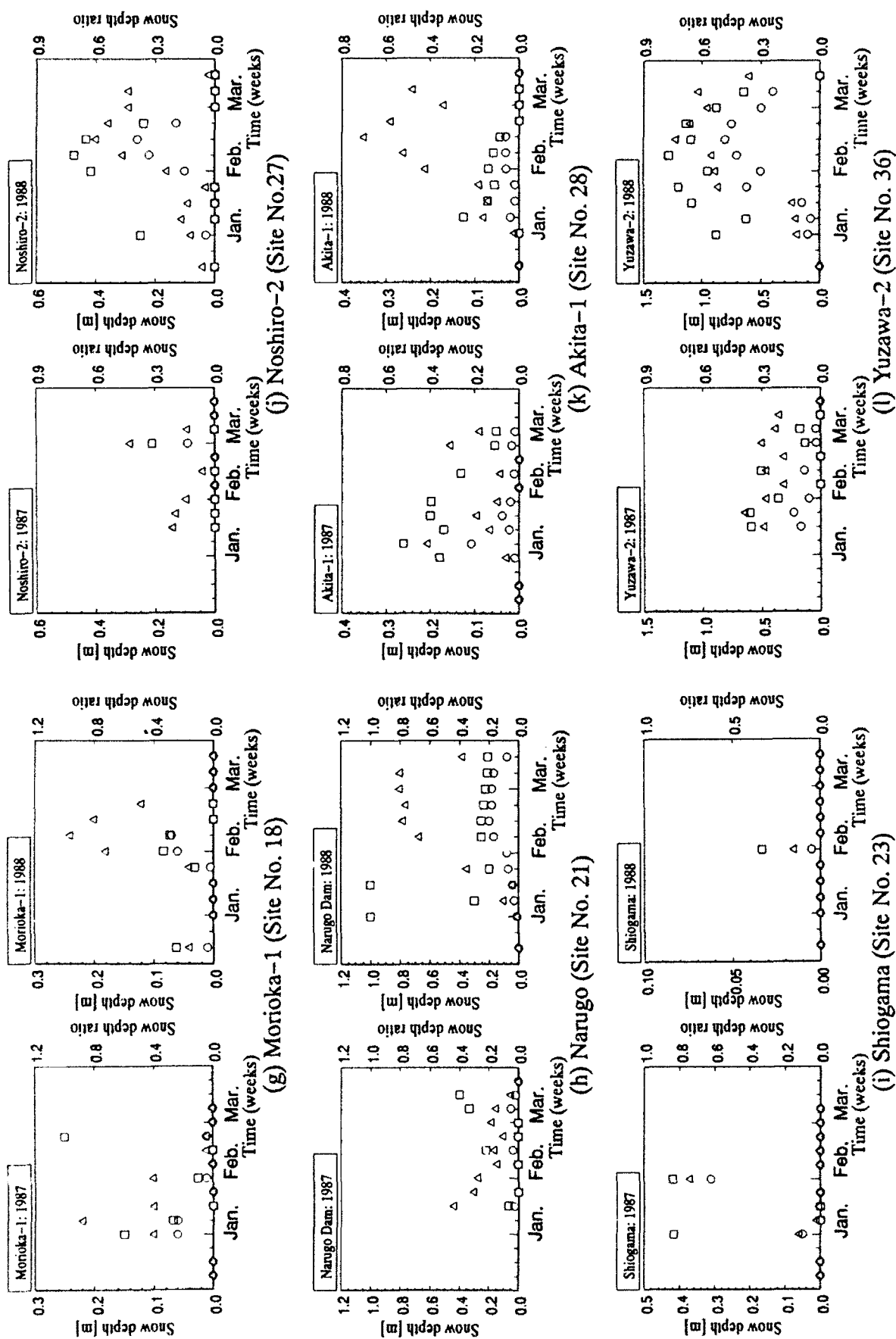


Figure 5.b. Variation of snow depth and conversion factor (△: ground, ○: roof, □: conversion factor).

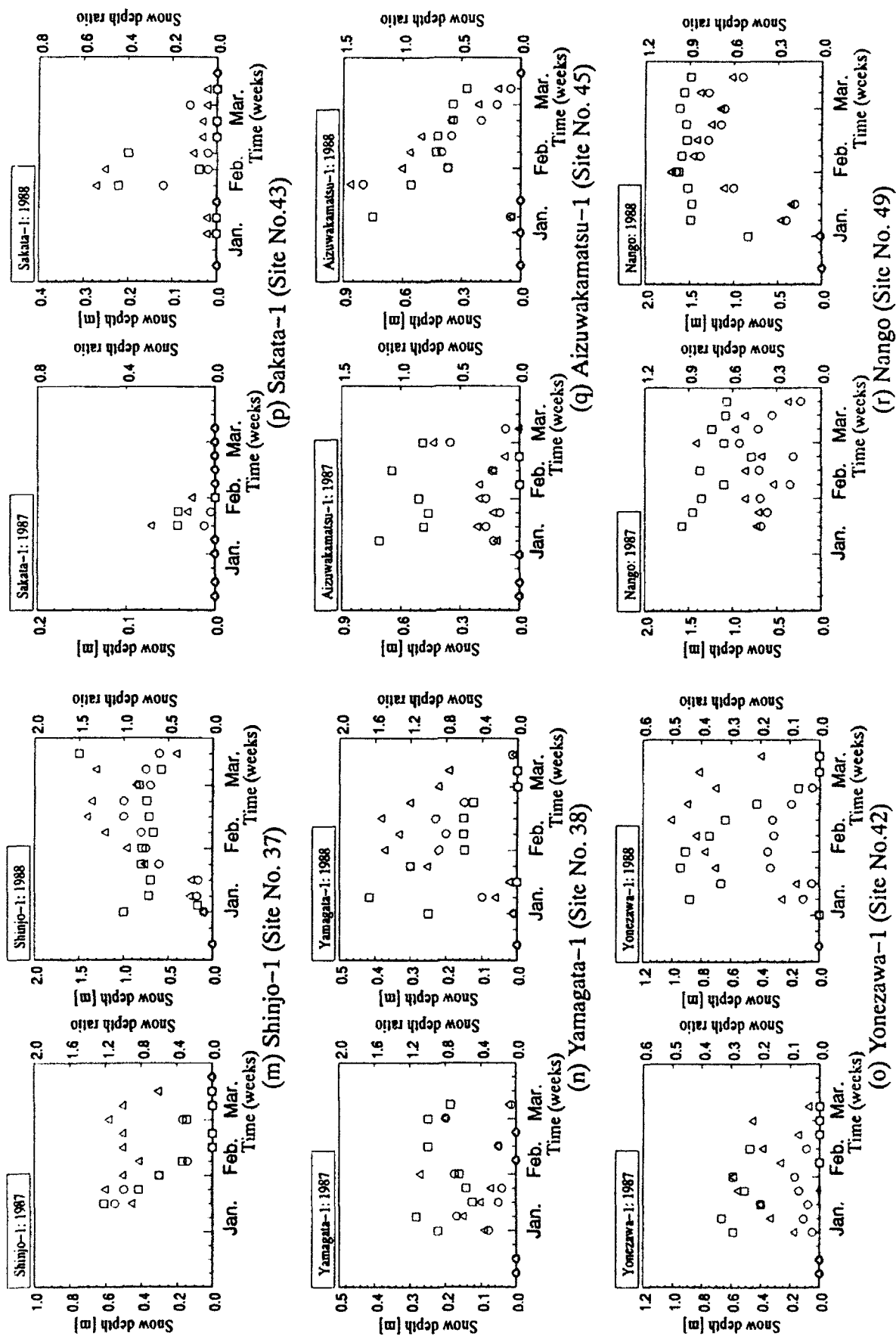


Figure 5.c. Variation of snow depth and conversion factor (Δ : ground, \square : roof, \square : conversion factor).

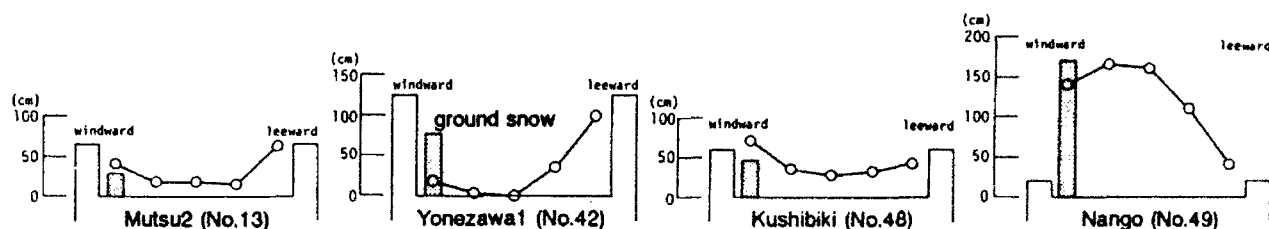


Figure 6. Typical snow drift on roof.

Table 3. Variables for factor analysis.

1 BLYEAR	:	Year the building was built.
2 HEIGHT	:	Height of the building.
3 PARAPT	:	Height of parapet or fence.
4 HINSLT	:	Thermal resistivity of the roof [$\text{m}^2\text{K/W}$].
5 ROOMHT	:	Average temperature of the room under the observation point on roof.
6 SEADIS	:	Distance from sea.
7 SNOWFL	:	Accumulation of daily snow fall in a week (Jan.27 - Feb.3).
8 SNOWDP	:	Ground snow depth of the observation day (Feb.3).
9 WINDMN	:	Average wind speed in a week (Jan.27 - Feb.3).
10 TEMPMN	:	Average temperature in a week (Jan.27 - Feb.3).
11 DEPRAT	:	Snow depth conversion ratio on the observation day (Feb.3).
12 DEVITN	:	Snow drift factor defined as below (Feb.3).

$$\text{DEVITN} = (\text{roof snow depth on leeward} - \text{roof snow depth on center}) / \text{ground snow depth}$$

Table 4. Factor loading matrix and accumulated contribution ratio.

	1987	FCT.1	FCT.2	FCT.3	FCT.4	FCT.5	1988	FCT.1	FCT.2	FCT.3	FCT.4	FCT.5
1 BLYEAR		0.001	-0.083	0.916	0.050	0.011		0.017	-0.147	-0.904	0.040	0.009
2 HEIGHT		-0.001	-0.116	0.322	-0.154	-0.572		-0.091	-0.002	-0.264	0.499	-0.543
3 PARAPT		0.011	-0.164	0.107	0.424	-0.772		0.032	0.136	-0.067	0.920	0.099
4 HINSLT		-0.046	-0.069	0.886	-0.140	-0.128		0.035	-0.094	-0.900	0.097	-0.108
5 ROOMHT		0.029	-0.145	0.147	0.209	0.676		-0.517	-0.084	0.021	-0.326	0.262
6 SEADIS		0.107	-0.929	0.090	0.164	-0.099		-0.182	-0.694	-0.013	0.497	0.027
7 SNOWFL		-0.929	0.018	0.059	0.036	0.008		-0.943	-0.075	0.072	0.038	0.095
8 SNOWDP		-0.969	0.001	0.043	0.089	-0.032		-0.891	-0.195	-0.096	0.144	-0.542
9 WINDMN		0.073	0.839	-0.163	0.220	-0.056		0.170	0.795	0.191	0.140	-0.023
10 TEMPMN		0.465	0.227	0.130	-0.703	-0.088		0.163	0.055	-0.031	-0.115	-0.867
11 DEPRAT		-0.091	-0.398	0.066	-0.774	-0.074		-0.080	-0.802	-0.078	-0.137	-0.000
12 DEVITN		0.430	0.474	0.153	0.290	0.052		0.472	0.312	-0.271	0.047	0.376
a.c.r.(%)		21.7	40.5	54.1	65.4	75.9		24.4	42.5	55.0	65.2	74.1

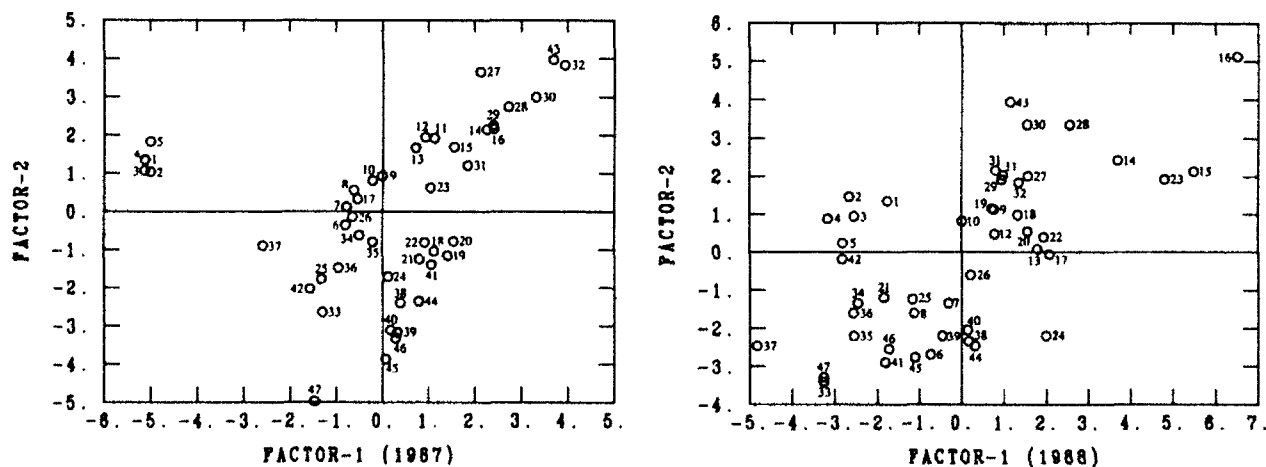


Figure 7. Relation between factor-1 and factor-2.

ACKNOWLEDGMENT

This study was performed as a collaboration project with the Ministry of Construction. Authors would like to thank Messrs. M. Konno and T. Matsumura for their assistance. These works were also assisted by Shinjo Branch of the National Research Center for Disaster Prevention Science and Technology Agency, and many administrative offices in Tohoku District.

REFERENCES

- Høibo, H. (1988) "Snow Load on Gable Roofs, Results from Snow Load Measurements on Farm Buildings in Norway," *First International Conference on Snow Engineering*, CRREL Special Report 89-6, 95-104, July 1988.
- Izumi, M., Mihashi, H., Sasaki, T. and Takahashi, T. (1985) "Fundamental Study on Roof Snow Loads Estimation," *Journal of Structural Engineering*, AIJ, Vol.31B, 59-72, March 1985.
- Izumi, M. et al. (1989) *Building Design and Snow Loads in Tohoku District*, Building and Repairs Association, Sendai, 101p. (in Japanese).
- Mihashi, H. and Takahashi, T. (1988) "Note on Determination of Snow Loads," *Proc. of the 4th Symposium on Snow Engineering*, 71-78, January, 1988 (in Japanese).
- O'Rourke, M.J., Redfield, R. and von Bradsy, P. (1982) "Uniform Snow Loads on Structures," *Journal of the Structural Division*, ASCE, Vol.108(ST12), 2781-2798, December 1982.
- Otstavnov, V.A. and Gokhberg (1970) "Promyshlennoe Stroitel'stvo," No. 9, Moscow, USSR.
- Sakurai, S., Joh, O. and Shibata, T. (1982) "The Maximum Snow Load on the Ground in Heavy Snow Areas," *Summary of Tech. Papers of Annual Meeting*, AIJ, 1149-1150, October 1982.

Roof Snow Observation and Application to House Construction

Tsutomu Nakamura,* Osamu Abe[†] and Seitaro Takada**

*Nagaoka Institute of Snow and Ice Studies, NIED
Suyoshi, Nagaoka 940, Japan

[†]Shinjo Branch of Snow and Ice Studies, NIED
Tokamachi, Shinjo 996, Japan

**Takada Architecture Corporation
Settaya, Nagaoka 940, Japan

ABSTRACT

Presented first are some snow features and snow problems of Japan: wide snow distribution from the north to the south, with dry and wet snow properties; the heavy amount of snow cover from which many snow problems arise, especially the problem of roof snow in urban areas; wide variation of the snow cover depth and the importance of the return period.

Results of roof snow observation for more than seven winters at Shinjo in the Tohoku area of Japan showed that the roof snow depth is mostly dependent on wind effects. If a building is isolated and the wind speed is high, the roof snow will be blown away. The ratio of the roof snow depth to the ground snow depth depends on the building height.

A series of wooden house designs based on snow knowledge and construction is introduced. The final house is the one where no roof snow removal work is necessary.

INTRODUCTION

Most of the residents who live in snowy area in Japan suffer from the heavy snowfall and deep snow cover though they could enjoy snow itself in winter. A heavy snowfall, which we call in Japanese GOSETSU, can produce much damage and sometimes became disastrous. There are snow avalanches in mountain areas, snow accretions, rimings and icings on the electric power lines and on trees, settling forces of the snow, drifting snow when snow is dry and wind is strong, roof snow problems especially in cities, etc. These snow and ice phenomena of the Gosetsu have killed persons, destroyed houses and produced other harmful effects. For example, the 36-Gosetsu killed 119 persons and destroyed 119

houses (in 1961), the 38-Gosetsu 231 persons and 1,735 houses (1963), the 52-Gosetsu 101 persons and 139 houses (1977), the 56-Gosetsu 152 persons and 466 houses (1981), and the 59-Gosetsu 131 persons and 189 houses (1984)(Regional Development Bureau, 1991). The roof snow problem is the one of the two biggest snow problems in Japan. In this article the deep snow cover in Japan is discussed, then case studies of the roof snow observation are introduced, and finally one example of a series of the house designs is introduced.

SNOW COVER IN THE JAPANESE ISLANDS

The Japanese islands are surrounded by sea and located at the middle latitudes. Therefore they receive a considerable amount of precipitation with an annual average of 1,750 mm over all of Japan. In winter Hokkaido island and the northwestern area of the Honshu island are covered with snow for the winter season (November to April).

The heavy snowfall is mainly caused by the winter monsoon (70%) which prevails in the northwesterly direction. Figure 1 shows the annual mean of the maximum snow depth on the ground for the years from about 1930 to 1945 (Central Meteorological Observ-

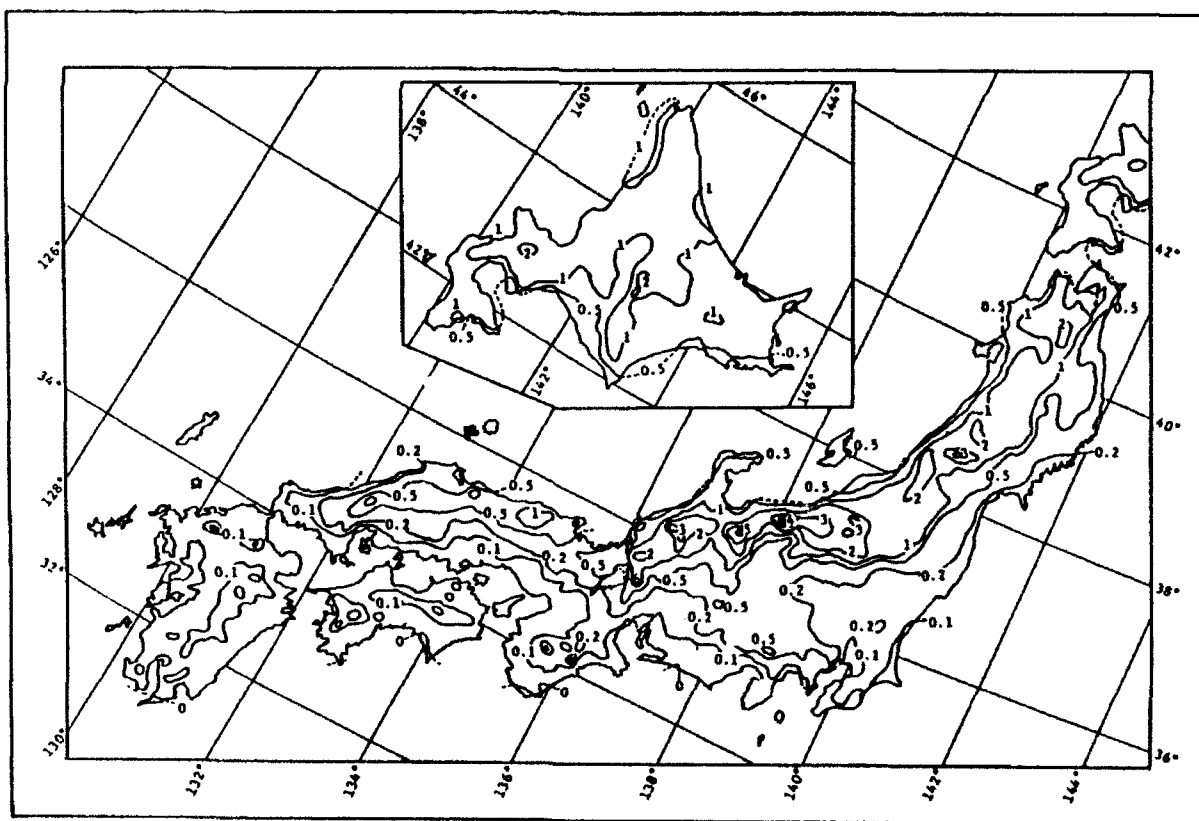


Figure 1. Annual mean of the maximum snow depth(m) on the ground in Japan (about 1930 to 1945. After Central Meteorological Observatory, 1949).

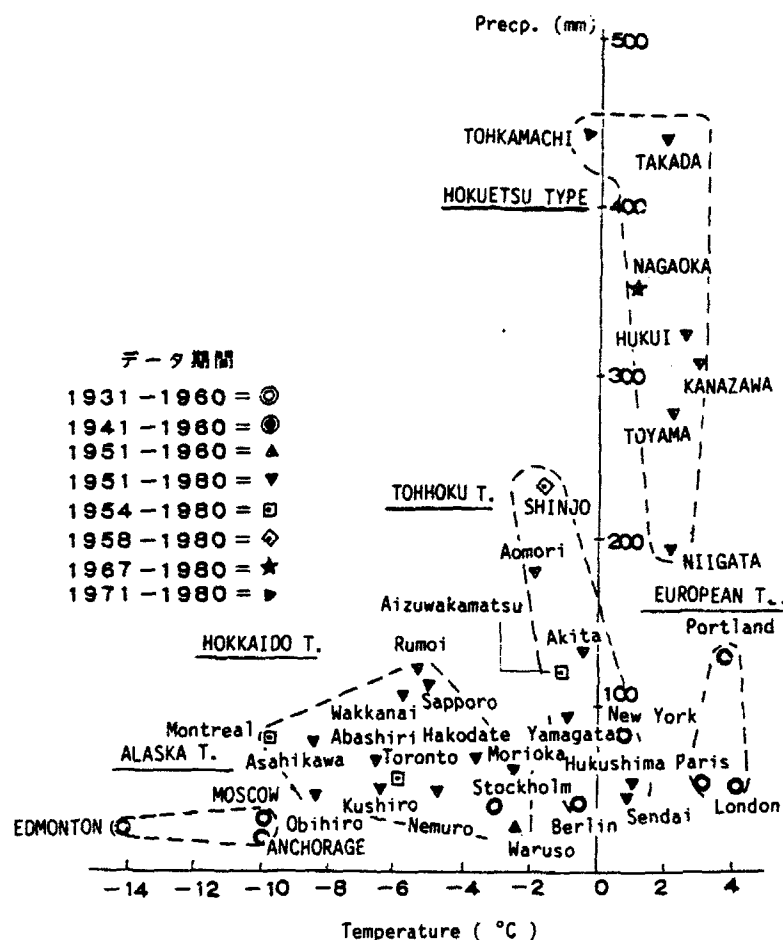


Figure 2. Distribution of cities on the Northern Hemisphere in reference to the mean air temperatures and the mean January precipitation (Minagawa et al. 1986).

atory, 1949). From this figure it is found that the deep snow depth area of more than 5 m is located at the center of the Honshu Island. Air temperatures over the Japanese Islands vary from the Hokkaido to the Kyushu Islands. For instance, mean air temperatures at Wakkanai of the northernmost city of the Hokkaido Island are -6°C on one hand, and the other hand $+9^{\circ}\text{C}$ in the southernmost point of the Kyushu Island in January. Physical properties of snow are strongly dependent upon the temperatures. Therefore it is difficult to have one general equation to sort out the snow problems over all the Japanese Islands. In these heavy snowfall areas there are many cities, towns and villages where 21 million people reside. Figure 2 shows the distribution of cities in the Northern Hemisphere in reference to the mean air temperatures and the mean January precipitation (Minagawa et al., 1986).

The snowfall varies daily, yearly and spatially. Figure 3 shows one example of the annual and daily variations of snow cover on the ground at Nagaoka in the Hokuriku district for the 1935/36 to 1990/91 winters. Each white figure corresponds to

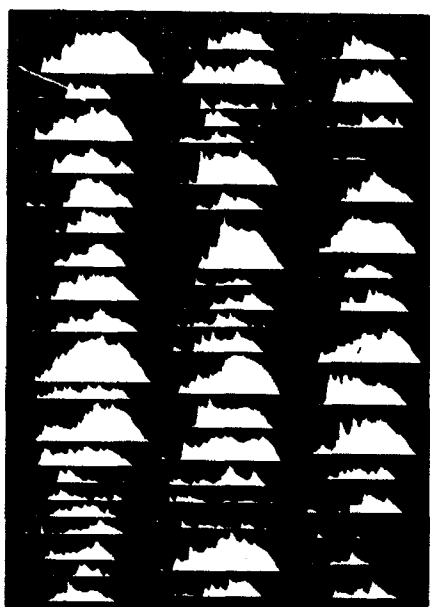


Figure 3. Annual and daily changes of snow depth on the ground at Nagaoka in Hokuriku district (1935/36 to 1990/91 winters). One figure corresponds to one winter.

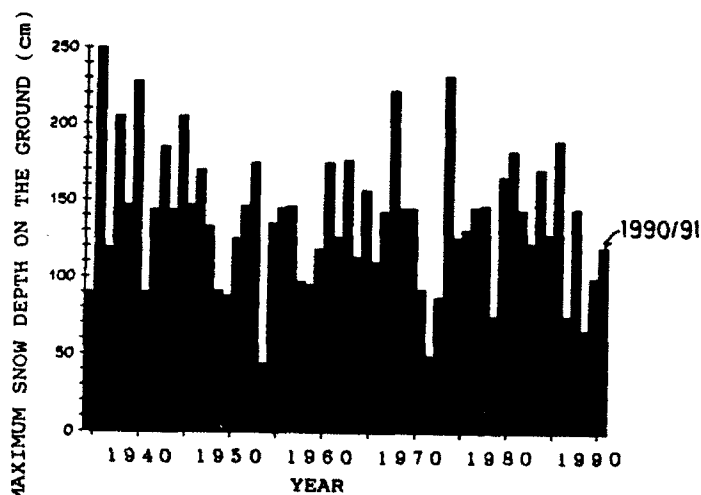


Figure 4. Annual variation of the maximum snow depth on the ground at Shinjo in Tohhoku district (1934/35 to 1990/91 winters).

each winter. It is shown in this figure that there is considerable annual variation. The standard deviation of the maximum snow depth on the ground at Nagaoka is calculated as 0.623 m and the one at Shinjo in the Tohoku area is found to be 0.448 m. The annual maximum snow depth variation is shown in Figure 4. The important and essential point of view for snow design is to consider the return period. Figure 5 shows four examples at Sanjo, Nagaoka, Takada and Koide in the heaviest area of the Hokuriku district. The figure shows that it is important to consider the return period of 100 years. In Japan the return periods of 30 years at the Ministry of Construction and of 100 years at the Railway Corp. are used for the snow design. If the return period is too short and the building is not strong enough, then we experience a sad situation like that shown in Figure 6, an example of destruction of a gymnasium.

ROOF SNOW OBSERVATION

It is important to observe and understand the phenomenon properly to solve any problem in a short time. Therefore we first started the roof snow observation and compared the results with those for the ground snow.

Figure 7 shows the location of the three buildings in Shinjo

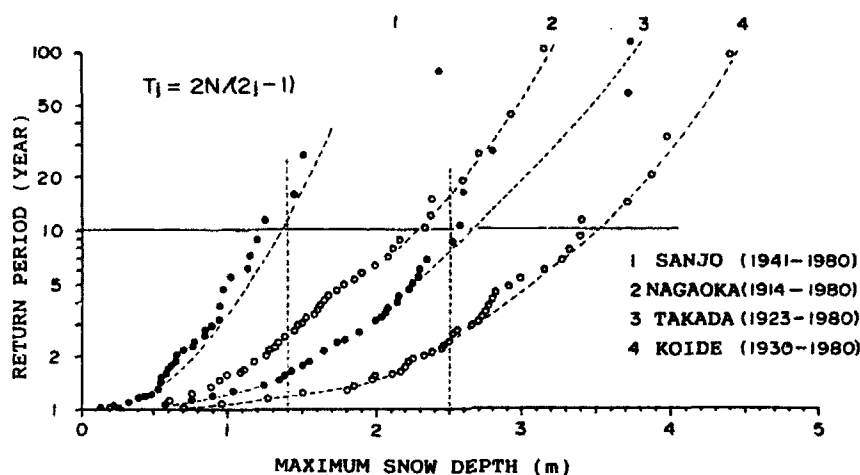


Figure 5. Return periods of the maximum snow depth on the ground at Hokuriku district of Japan (After M. Shimizu).

where roof snow observation was carried out (Nakamura and Abe, 1978, 1979). The prevailing wind direction is westerly as shown in the figure. The central building, Rc, is 9.7 m high and located at the windward of the store building, Rs, which is 5.7 m high. The distance between them is about 10 m. A lower building, Ro, 3.8 m high, is where snow and meteorological observations were made and is located 20 m from the central building. These three buildings have rather flat roof shapes, i.e., $\tan \theta$ is 8/100 for Rc, 4/100 for Rs and 2/100 for Ro. Ground snow observation was carried out at the location G_1 or G_2 shown in the same figure.

Figure 8 shows one example of the roof snow observation results compared with the ground snow observation. A reference level is taken at one specific snow layer close to the snow surface as shown in the figure. The numbers 1, 2, 3 and 4 correspond to the ground, G, storehouse, Rs, observation room, Ro and



Figure 6. Gymnasium destroyed by the roof snow weight (Photo taken by Dr. M. Higashiura on Feb. 18, 1975).

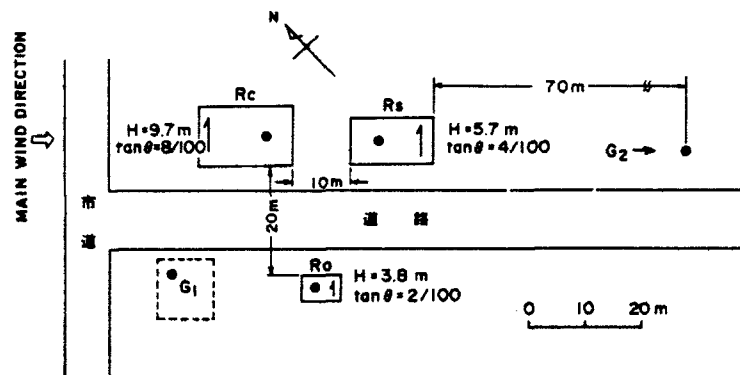


Figure 7. Location of the three buildings where roof snow observation was carried out (Nakamura and Abe, 1978).

central building, Rc, respectively. The hatching indicates missing snow compared with the roof snow depth of Rs. This comparison was made on Jan. 13, 1977. Figure 9 shows one example of comparison of roof snow depths on the three buildings and the ground snow depth for the whole winter of 1981/82 (Nakamura et al., 1984). This figure shows that the ground snow depth is the

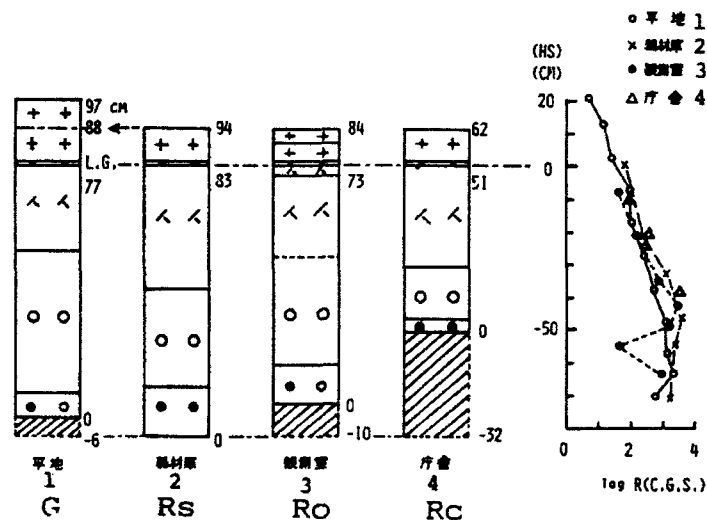


Figure 8. Comparison of the roof snow at the three buildings and of the ground snow (Nakamura and Abe, 1978).

highest among them, roof snow of Rs is secondary, then is that of Ro, and is smallest for that of Rc.

A comparison of the daily roof snow depth on the central building against the ground snow depth is shown in Fig. 10. The same sort of the observation and comparison were carried out for six winters. Table 1 summarizes the results of these observations (Nakamura et al., 1984). The result is shown as the ratio of the roof snow depth to the ground snow depth. The ratios are

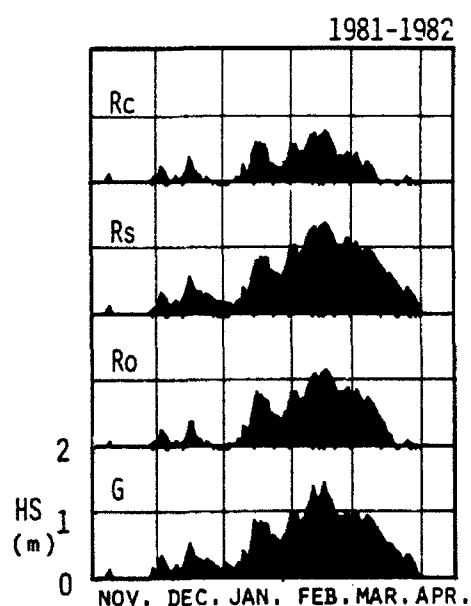


Figure 9. One example of the comparison of roof snow depth on the three buildings and the ground snow depth in 1981/82 winter (Nakamura et al., 1984).

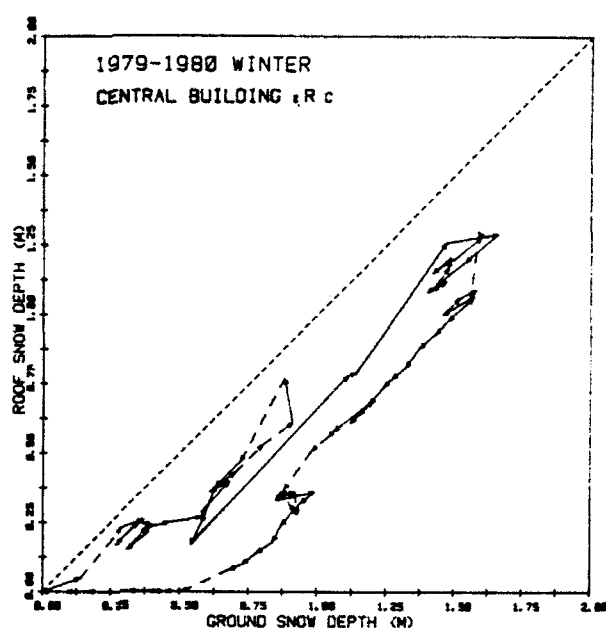


Figure 10. One example of the comparison between roof snow depth of the central building, Rc and ground snow depth in 1979/80 winter (Nakamura et al., 1984).

fairly well grouped into two categories depending on the winter snowfall conditions, i.e., a heavy or a weak snowfall year and a moderate snowfall year. During the six winters it was observed

Table 1. Ratio of the roof snow depth to the ground snow depth. The ratios are fairly well grouped into two categories depending on the winter snowfall condition, i.e., a heavy or a weak snowfall year and a moderate snowfall year.

Year		Ratio		
		Rc/G	Rs/G	Ro/G
Weak or heavy snowfall winter	1978~79	0.81	1.03	0.91
	1979~80	0.78	1.00	0.96
	1980~81	0.84	1.05	1.01
	Mean	0.81	1.03	0.96
Moderate snowfall winter	1977~78	0.54	1.03	0.80
	1981~82	0.58	1.05	0.88
	1982~83	0.57	0.97	0.75
	Mean	0.56	1.02	0.81

that drifting snow on the central building was transferred onto the roof of the store building when the westerly wind speed was strong. Therefore it is concluded that the reason why the ratio of the roof snow depth to the ground snow depth is close to 1 or sometimes a bit greater than 1 on the storehouse is due to the transfer of drifting roof snow from the central building and little snow melting at the roof snow base. At the storehouse no heater was used in the wintertime, though a small amount of snow melting of $0.62 \text{ mm} \cdot \text{day}^{-1}$ was calculated (Nakamura and Abe, 1978). It is concluded that the reason that the smallest roof snow depth

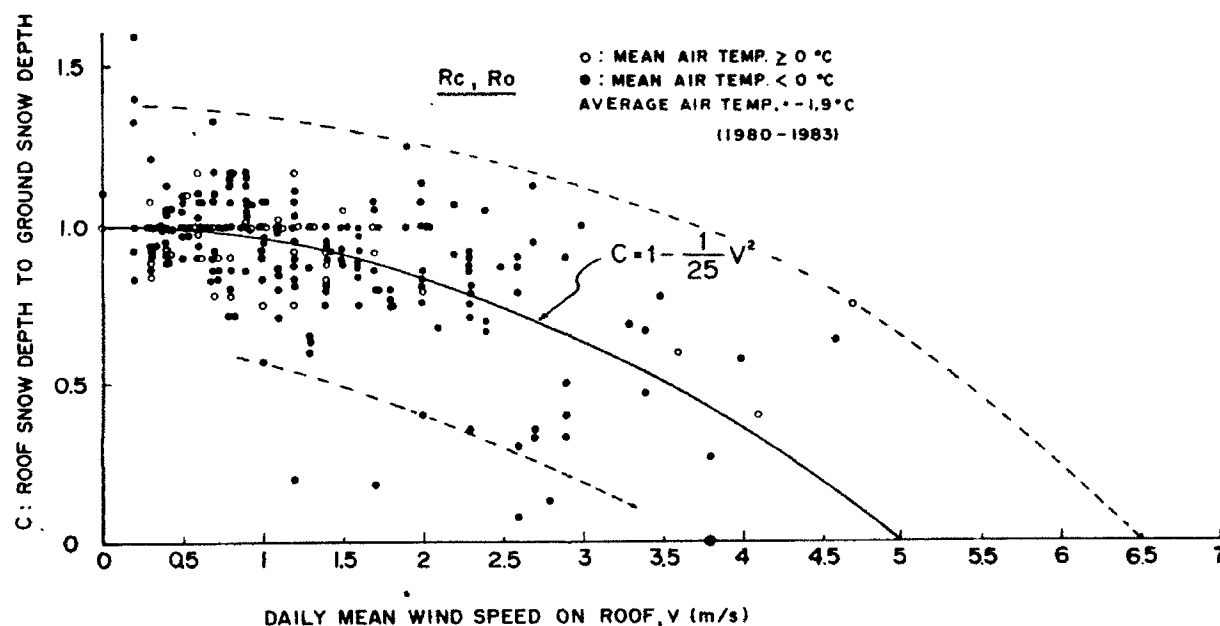


Figure 11. Relation between the ratio C , roof snow depth to ground snow depth and daily mean wind speed on roof (Abe and Nakamura, 1984).

was observed on the central building is due to the wind speed effect because the strongest wind speed among the three buildings must be observed as well as the partial roof snow melting of $2.9 \text{ mm} \cdot \text{day}^{-1}$ on the central building due to the heating in winter (Nakamura and Abe, 1978). The roof snow depth of the observation building was the smallest among the three buildings, and the amount was smaller than the ground snow depth. It is also concluded that the smaller roof snow depth is mainly due to wind. Therefore the effect of wind speed was surveyed and the result is shown in Fig. 11. The figure shows a relation between the ratio C , i.e., roof snow depth to the ground snow depth as a function of daily mean wind speed converted into the roof height based on the wind speed measured at the height of 5.5 m in the same Shinjo Branch yard. The figure shows that if wind speed on the roof became stronger than 6.5 m/s, then no roof snow will be observed on the roof though the wind speed variation is rather large.

Figure 12 shows the observational results of the more than six winters. The ratio of the maximum roof snow depth to the maximum ground snow depth as a function of building height is expressed in a function, R_h , for a heavy snowfall winter or a weak snowfall winter, and in another function, R_l , for a moderate snowfall winter in Shinjo for the sizes of these three buildings. These two equations must be in correspondence with the stronger wind speed and the weaker wind speed.

For the building construction, the more essential figure is the snow load. To convert the roof snow height to the roof snow weight, another relation is needed. Figure 13 shows the relation between the snow load and the snow depth at three different locations of Nagaoka, Shinjo and Sapporo. In the figure, F refers to February and M refers to March. Characters correspond to the date. Densities in the figure show an average of the whole snowpack on the ground.

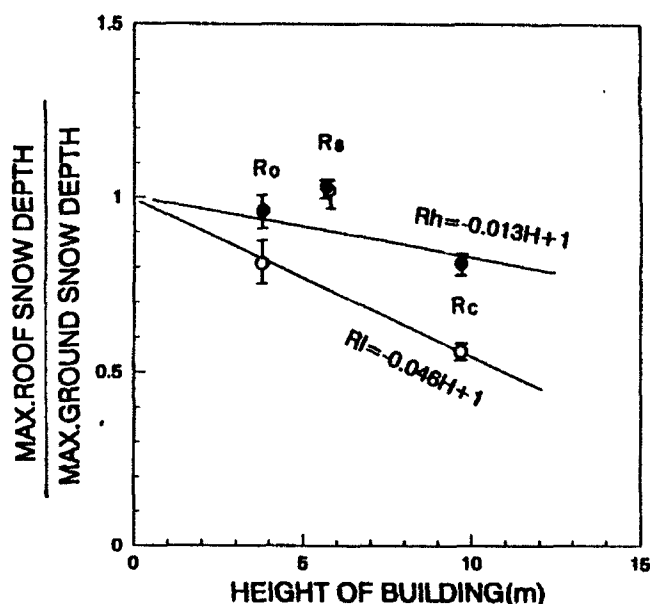


Figure 12. Ratio of the maximum roof snow depth to the maximum ground snow depth as a function of the building height for two different groupings of winters.

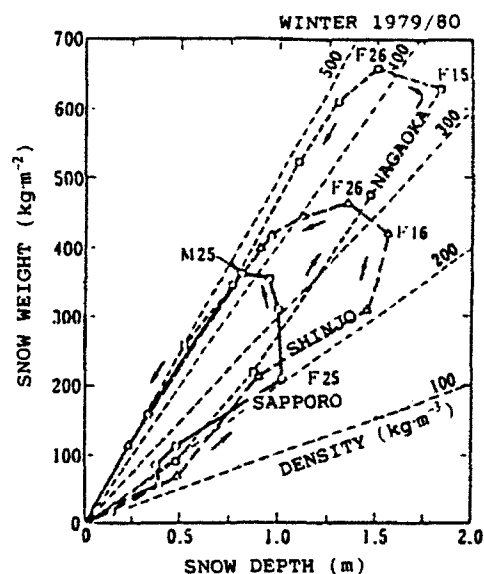


Figure 13. Circulation curve in correlation with the weight and depth of snow at three different points in Japan.

HOUSE CONSTRUCTION

When a building is designed for construction in a snow area, the roof snow load on the building and the snow removal method around the housing must be considered. If the average amount of snow is not so large, the design is much easier. One such example is shown in Fig. 14. The house was designed such that roof snow will slide down to two sides of the house, and the snow on

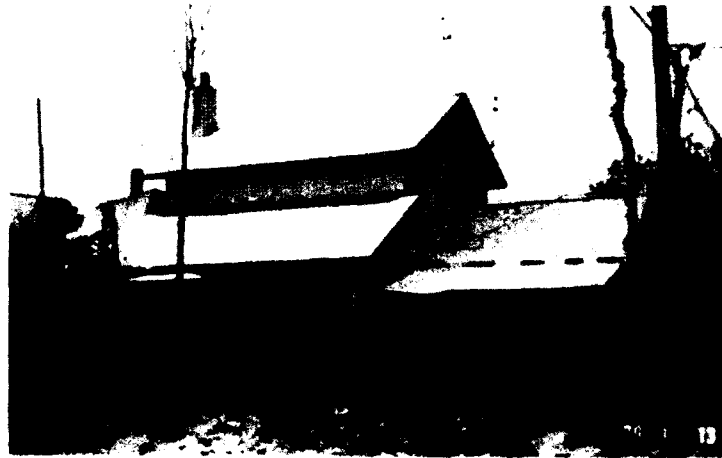


Figure 14. One example of a house designed for roof snow to slide down on to the ground (Hokkaido, built in 1960).

the ground was planned to be removed by manpower. While the residents were young this plan was good enough, but after they became old the removal of roof snow was very troublesome. Especially after a part of the house indicated by the dotted line was added, the problem became greater.

Figure 15 shows another example of a house where the roof snow was designed to be slid down to only one side of the house because much more ground snow was expected. The average ground snow depth was expected to be 1.5 m (at Shinjo in the Tohoku area of the Honshu Island). At the same time, the base concrete seen in the same figure was designed to be 1 m high which was higher than the usual. The situation in the winter is seen in Fig. 16. The roof snow has completely slid down onto the ground and has



Figure 15. House designed for roof snow to slide down onto the ground with 1 m high base (Shinjo, built in 1975).

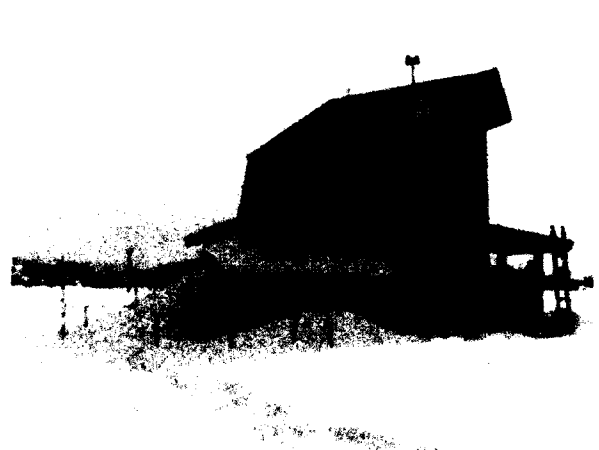


Figure 16. The same house in winter. This shows that the high base was justified.

piled up at one side of the house. Since the house was built in 1975 at Shinjo, many houses were built in the similar type in the city area. The only problem is how to remove the deposited roof snow on the ground because all windows are covered by the roof snow. To solve this problem two-thirds of the roof snow was tried to be kept on the roof by a roof snow stopper (a bar) for two winters. This 2/3 method (the first basic idea was given by Kawamata [1978]) worked well except for a slight creep deformation of the housing due to the snow load for a heavy snowfall winter of 1985. Therefore this slight deformation of the building must be countered by tough house construction.

The house shown in Fig. 17 was designed to keep all the roof snow on the house. The framework is shown in Fig. 18, which consists of four thick posts (0.15×0.15 m) at the center of the house (core structure), 12 posts (0.12×0.12 m) along the sides (kept in the walls), and four inclined (ascending) thick beams which work as braces in the roof. These beams are wooden, and the housing is essentially a wooden structure. The plan is shown in Fig. 19. Four thick circles show the core structure. Therefore the snow load is kept on the 16 posts evenly through four inclined beams partially. The maximum designed snow load is $525 \text{ kg}\cdot\text{m}^{-2}$ with roof snow depths of 2.5 m ($2.5 \text{ m} \times 300 \text{ kg}\cdot\text{m}^{-3} \times 0.7$).



Fig. 17 House Yajirobeh constructed for roof snow to be kept on the roof (Nagaoka, built in 1988).

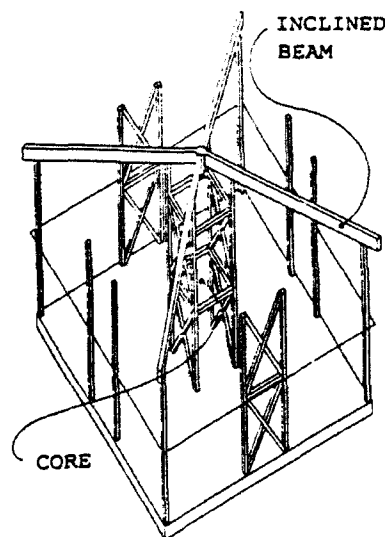


Fig.18 Framework of the house.

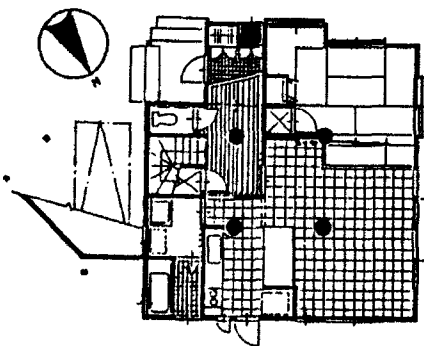


Fig.19 Plan of the Yajirobeh.



Fig.20 Yajirobeh in winter.

The coefficient of 0.7 is due to the house construction regulation. The slope of the main roof is 19.3 degrees ($\tan \theta = 3.5/10$). The housing (the nickname is Yajirobeh.) has some advantages, summarized as (1) unnecessary of roof snow removal, (2) snow cornice at the roof edges will not be formed because the roof edge was bent, (3) the roof snow will slide down onto the yards where no building is located, so the sliding roof snow should not harm to the neighbors even during earthquakes because the earthquake energy seems to be absorbed by roof snow (Nakamura et al., 1991), and (4) access to the outdoors is easier compared with the highly based housing. A roof-snow load sensor is fixed between the two posts of the house to measure a beam deflection due to overload of roof snow. Figure 20 shows the house in winter.

CONCLUSIONS

A wooden house which was strong enough for the roof snow design load of $525 \text{ kg}\cdot\text{m}^{-2}$ was designed and built. The house has been used in a heavy snowfall area of Nagaoka at the Hokuriku district. Since the house was built four winters have passed, but the housing has had no experience in heavy snowfall seasons. Eight of these houses have been built so far. This housing will be beneficial to the people in heavy snowfall areas. For the much deeper snow area, this housing might not be perfect. However experience in deep snow areas will keep us to reach to a better goal.

REFERENCES

- Abe, O. and T. Nakamura (1984) "Wind effect on the daily new snow depth on flat roofs", Rept. Nat. Res. Ctr. for Disaster Prevention, No. 32, pp. 73-87.
- Central Meteorological Observatory (1949) The climatography of snow in Japan, Snow Association of Japan, Tokyo, pp. 1-83.
- Kawamata, K. (1978) "One-thirds method for roof snow removal", KOKUSETSU, Vol. 6, No. 4, pp. 4-5.
- Minagawa, T., T. Sato, N. Yoshida and F. Sato (1986) Survey of the Roof Snow Removal Apparatus, Rept. Tohoku Elec. Power Co., No. 86010, 1-93.
- Nakamura, T. and O. Abe (1978) "Observations on vertical profiles of the snow cover on roofs and melting at the bottom of the snow cover", Rept. Nat. Res. Ctr. for Disaster Prevention, No. 19, pp. 219-228.
- Nakamura, T. and O. Abe (1979) Ibid. Draft Trans. 697, US CRREL, pp. 1-19.
- Nakamura, T., O. Abe, H. Nakamura, M. Higashiura and N. Numano (1984) "Comparison of the roof snow depth on three different types of buildings with the ground snow depth", Rept. Nat. Res. Ctr. for Disaster Prevention, No. 32, pp. 55-72.
- Nakamura, T., Y. Nohguchi, T. Kobayashi and K. Ootani (1991) Characteristics in vibration of experimental huts loaded with roof-snow, Abstracts of the AGU 1991 Fall Meeting, H31D-06.
- Regional Development Bureau (1991) Present situation and the consideration for the heavily snow covered area, pp. 1-416.

Survey of Roof Snow Depths by Aerial Photogrammetry

Shuji Sakurai,* Osamu Joh[†] and Takuji Shibata[†]

*Department of Architecture, Hokkaigakuen University, Sapporo 064, Japan

[†]Department of Architecture, Hokkaido University, Sapporo 060, Japan

ABSTRACT

The method of aerial photogrammetry is proved to be applicable in surveying snow depths on roofs over a broad area. First, measurement errors of roof snow depths by aerial photogrammetry are investigated. Then, examples are shown in applying to the measurements of snow depths on various types of roofs.

INTRODUCTION

Sufficient data on roof snow loads for structural design are not available because there is difficulty in measuring the intensity and distribution of snow load by climbing onto roofs. Especially on sloped roofs, snow sliding caused by the measurement technique makes the long-term measurement almost impossible in some cases. It is important to develop an efficient and accurate method for surveying roof snow loads. Here, the aerial photogrammetry is adopted in order to survey roof snow depths.

The present paper discusses the measurement accuracy of aerial photogrammetry for surveying roof snow depths. Furthermore, as examples, snow covers on the various types of roofs located in an assigned area of Sapporo are shown.

PROCESS FOR MEASUREMENT OF ROOF SNOW DEPTHS

Roof snow depths can be measured by subtracting the elevation value of roof surface from that of roof snow surface. Fig.1 shows how to survey the elevation values of roof surface and that of roof snow surface by aerial photogrammetry. As the pass points, manholes on the ground, which are near of the measured buildings, were in general selected in this study.

FEATURES OF AIRPLANE AND KITE BALLOON FOR AERIAL PHOTOGRAPHY

Airplane, kite balloon and unmanned-radio control helicopter are mainly used for aerial photography at the present time in Japan. In the present paper, airplane due to entrusting business and kite balloon, which can be controlled by users themselves, are selected. The airplane is especially suitable to take aerial photographs for broad area within a short time because of the superior mobile power. However, a chartered flight for aerial survey is expensive, and it has difficulty in photographing at any time and at any frequency. The kite balloon is suitable for the fixed point observation because the mobile power is not enough for taking photographs of broad area. As professional skills for operational technique are not necessary, it is possible to control the movements of the kite balloon by users themselves. Therefore, the necessary

expense is cheaper than airplane, and users can wait for the weather to become better condition suitable for photography. As the disadvantages of kite balloon, the photography time is influenced significantly by wind velocity, and it is difficult to confirm the coverage or the looking angle (see Remarks 1). Furthermore, surveying camera are confined by the mounting ability of the kite balloon.

INVESTIGATION OF MEASUREMENT ERRORS OF ROOF SNOW DEPTHS

Measurement errors of the aerial photogrammetry can be theoretically estimated from the relationship among the photo scale by flight, which is the ratio of focal length of surveying lens to the flight altitude, the measurement accuracy of the plotting instrument and the base-height ratio. However, measurement errors should be investigated in case of applying the aerial photogrammetry to survey the object with continuous curved surface without edges like snow cover. In the present paper, measurement errors of the aerial photogrammetry, which means the difference between the measured values of roof snow depths by the aerial photogrammetry and those by climbing onto the roofs, are investigated.

Table 1(a) shows photo scale by flight and range of photography overlapped by 60%, which are corresponding to three different flight altitudes by airplane. The surveying camera is RC-10(Wild). The lens is Aviogon(Wild), whose focal length is 213.8 mm. Table 1(b) shows photo scale by flight and range of photography overlapped by 60%, which are corresponding to three different flight altitudes by kite balloon. The surveying camera is MKWE (Hasselblad). The lens is Biogon(Hasselblad), whose focal length is 38.1 mm. As the plotting instrument, analytical stereoplotter DSR-11(Kern) was used. The measurement error of parallax difference is 0.01 mm. The base-height ratio is considered to be almost constant under the certain overlap.

Photographing by airplane

Snow depths, at 50 points on a flat roof as shown in Fig.2, were measured directly by climbing onto the roof. The mean value was 41 cm. Table 2 shows the results of the investigation on the effect of the flight altitude on the measurement errors of the aerial photogrammetry. To indicate the amount of scatter in the measurement errors, the mean values and the standard deviations are shown in the table 2. Figs. 3(a), (b) and (c) show the distribution of the measurement errors. When the assigned flight altitude is 300m, the dispersion of the errors is a normal distribution with the mean about 0 cm and the standard deviation of about 3 cm. From a practical point of view, the distribution of the measurement errors can be considered as a normal distribution with the mean 0 cm at the assigned flight altitude of both 500m and 800m. Then, the standard deviation is about 4 cm at 500 m assigned flight altitude and 5 cm at 800 m assigned flight altitude. These analyses show that the aerial photogrammetry by airplane is accurate enough for practical use to survey roof snow depths. The flight altitude is used properly within the necessary accuracy.

If the reflection of sunlight from the snow surface or roof surface causes halation (see Remarks 2) on the photograph, the measurement accuracy of the aerial photogrammetry will be influenced considerably. Table 3 shows the results of the investigation on the measurement errors by the halation. Figs. 3 (d),(e) and (f) show the distribution of measurement errors. The standard deviations with halation are about twice at each flight altitude in

these cases. However, it is difficult to determine quantitatively the relation between the degree of halation and the measurement errors. Further investigation about the technical plan against the halation is necessary.

On a shed roof, which is shown in Fig. 4, measurement errors of roof snow depths by the aerial photogrammetry were investigated in the same way as the flat roof above mentioned. The results at the assigned flight altitude of 300 m are shown in table 4. As it is obvious from Fig. 5, the dispersion of the errors is a normal distribution with the mean about 0 cm and the standard deviation of about 3 cm. The standard deviation is equal to that on the flat roof at the assigned flight altitude of 300m.

Photographing by kite balloon

Measurement errors of roof snow depths by kite balloon were investigated on a flat roof as shown in Fig. 6. The kite balloon is shown in Fig. 7, which is 2.1 m in maximum diameter, 4.5 m in total length and 4 kgf in maximum mounting weight. Table 5 shows the results of investigation on the effect of the flight altitude and on the measurement errors for the aerial photogrammetry. In practical application, the measurement errors can be considered as a normal distribution with the mean 0 cm at the assigned flight altitude of 20 m, 60 m and 100 m. The standard deviations at the assigned flight altitude of 20 m, 60 m and 100 m are about 3 cm, 4 cm and 6cm, respectively. Fig. 8 shows the distribution of the measurement errors for the assigned flight altitude of 100 m.

EXAMPLES APPLIED TO VARIOUS TYPES OF ROOFS

There is not enough basic data about snow depths on the various types of roofs for actual buildings. In this study, aerial photographs over an assigned area in Sapporo, Japan are taken by airplane at the assigned flight altitude of 300 m on February 4, 1991. Fig. 9 shows the assigned area which is open flat terrain located at longitude $141^{\circ}23'E$, latitude $43^{\circ}04'N$. Ten buildings in the area, which are warehouses of medium size with no heating inside, are selected in order to research the roof snow depths. They are numbered in Fig. 9. As shown in Figs. 10 and 11, the roof types are curved roofs with retainers, negative sloped roofs, gable roofs with retainers and flat roofs. The aerial photographs with snow cover are shown in Fig. 12. As shown in the figure, the administrators of the curved roofs have unfortunately removed the part of roof snow (numbered 3) just before taking aerial photographs. However, the snow density on the roof could be measured directly by climbing onto the roof. The average value is 0.25 g/cm^3 . The roof snow depths at A-A, B-B and C-C cross sections indicated in Fig. 12 are measured by aerial photogrammetry. The measured values at A-A cross sections are shown by solid lines in Fig. 10. The snow depths at B-B and C-C cross sections, which are not shown in the figure, approximate that at A-A cross section.

The ground snow depth on February 4, 1991, measured directly with a ruler at the park in the assigned area is 80 cm. Then, the average density of ground snow is 0.28 g/cm^3 . The ground snow depth is plotted in Fig. 10 by dash line for comparing with roof snow depth. As for the general meteorological conditions of the winter season, see Remarks 3 in the paper.

We can draw interesting conclusions according to the data at above mentioned three cross sections. The roof snow cover is distributed almost uniformly on the entire roof area for various types of roofs, and nearly equal to the ground snow depth except two curved roof. They are only a few examples.

However, these measured values are important as reference materials for structural design.

CONCLUSIONS

The present paper is concerned with the application of aerial photogrammetry for surveying roof snow depths. The results are as follows:

- 1) The aerial photogrammetry is accurate enough for practical use to survey roof snow depths. The airplane and the kite balloon should be properly selected according to the necessary accuracy, the range of photography and the expenses for measurements.
- 2) As examples, roof snow depths of 10 buildings with no heating inside located in an assigned area of Sapporo, Japan are surveyed on February 4, 1991. The types of roofs are curved roofs with retainers, negative sloped roofs, gable roofs with retainers and flat roof. The snow covers are nearly equal to the ground snow depth over the entire roof area except two gable roofs.

Further investigation about the technical plan against the halation is necessary because the measurement errors of aerial photogrammetry are influenced considerably by that on the photograph. The estimation of roof deflection is necessary under certain circumstances.

REMARKS

- 1) Dr.Koizumi has developed the photographic system of kite balloon with the equipments for monitoring device and positioning of the camera.
- 2) Snow surface and roof material cause the reflection of sunlight like a mirror in some cases. Strong light due to the reflection will penetrate the emulsion of the film and will be reflected by the polyester base of the film. Therefore, the image will not focused. This phenomenon is called halation. The cloudy weather should be selected for the meteorological condition of photography date.
- 3) General meteorological conditions by Sapporo District Meteorological Observatory during the winter of 1990-1991, which is about 5.6 km from the assigned area, were as follows: Continuous snow accumulation started on December 10 and finished on April 6. On February 4, i.e, the day when aerial photographs were taken, the ground snow depth was 84 cm. The maximum snow depth reached 125 cm on February 16. During 56 days from December 10 to February 3, the maximum value of daily snow falls was 36 cm and total value of those was 415 cm. The average value of daily mean temperatures during above mentioned 56 days was -0.8°C . During the above mentioned 56 days, the average value of daily mean wind velocities was 1.7 m/s and the daily maximum wind velocities were in the region of 2.4 m/s-7.9 m/s.

REFERENCES

- Sakurai, S., Joh, O. and Shibata, T. (1986) "Survey of Roof Snow Depths by Aerial Photogrammetry Part 1 Accuracy of the Measurement", Summary of Tech. Papers of Annual Meeting, AIJ, 47-48, August, 1986. (in Japanese)
- Sakurai, S., Joh, O. and Shibata, T. (1987) "Survey of Roof Snow Depths by Aerial Photogrammetry Part 2 Errors in the Measurement on Three Different Types of Roofs", Summary of Tech. Papers of Annual Meeting, AIJ, 1401-1402, October, 1987. (in Japanese)
- Sakurai, S., Joh, O. and Shibata, T. (1988) "Survey of Roof Snow Depths by Aerial Photogrammetry Part 3 Errors in the Measurement on a Flat Roof at Three Different Heights of Photographing", Summary of Tech. Papers of Annual Meeting, AIJ, 65-66, October, 1988. (in Japanese)
- Sakurai, S., Joh, O. and Shibata, T. (1989) "Survey of Roof Snow Depths by Aerial Photogrammetry with a Kite Balloon", Summary of Tech. Papers of Annual Meeting, AIJ, 49-50, October, 1989. (in Japanese)
- Sakurai, S., Joh, O. and Shibata, T. (1990) "Survey of Roof Snow Depths by Aerial Photogrammetry with a Kite Balloon Part 2 Errors in the Measurement on a Flat Roof", Summary of Tech. Papers of Annual Meeting, AIJ, 119-120, October, 1990. (in Japanese)
- Koizumi, T., Murai, S., Koike, T. and Manabe, H. (1986) "An Automated System and its Applications for Aerial Photography Using a Kite Balloon", Journal of Photogrammetry and Remote sensing, Vol. 25, 12-23, No. 3, 1986. (in Japanese)

Table 1. Flight Altitude, Photo scale by Flight and Range of Photography.

(a) Photography by Air Plane (Focal Length of Lens:213.8mm)

Flight Altitude	300m	500m	800m
Photo Scale by Flight	1/1400	1/2340	1/3740
Range of Photography (Overlapped by 60%)	131m×229m	219m×383m	350m×613m

(b) Photography by Kite Balloon (Focal Length of Lens:38.1mm)

Flight Altitude	20m	60m	100m
Photo Scale by Flight	1/520	1/1570	1/2630
Range of Photography (Overlapped by 60%)	11m×23m	34m×70m	57m×116m

Table 2. Measurement Errors of Roof Snow Depths (no Halation).
—Flat Roof by Air Plane—

Assigned Flight Altitude	300m		500m		800m	
	Photography without Snow Cover	Photography with Snow Cover	Photography without Snow Cover	Photography with Snow Cover	Photography without Snow Cover	Photography with Snow Cover
Photography Date	1987.11.14	1991.1.27	1987.11.14	1991.1.27	1984.6	1991.1.27
Actual Flight Altitude	269m	320m	482m	550m	820m	860m
Actual Photo Scale by Flight	1/1260	1/1500	1/2250	1/2570	1/3840	1/4020
Max. Error of Elevation at Control Points	3cm	3cm	3cm	2cm	—	3cm
Measurement Errors of Roof Snow Depths	n = 50 $\bar{e} = 0.2\text{cm}$ $\sigma = 3.1\text{cm}$		n = 50 $\bar{e} = 1.2\text{cm}$ $\sigma = 4.3\text{cm}$		n = 50 $\bar{e} = 0.4\text{cm}$ $\sigma = 5.0\text{cm}$	

n : Number of Measured Points
e : Mean of Measurement Errors
σ : Standard Deviation of Measurement Errors

Table 3. Measurement Errors of Roof Snow Depths (with Halation).
—Flat Roof by Air Plane—

Assigned Flight Altitude	300m		500m		800m	
	Photography without Snow Cover	Photography with Snow Cover	Photography without Snow Cover	Photography with Snow Cover	Photography without Snow Cover	Photography with Snow Cover
Photography Date	1987.11.14	1988.2.16	1987.11.14	1988.2.16	1984.6	1988.2.16
Actual Flight Altitude	269m	285m	482m	514m	820m	802m
Actual Photo Scale by Flight	1/1260	1/1330	1/2250	1/2400	1/3840	1/3750
Max. Error of Elevation at Control Points	3cm	3cm	3cm	5cm	—	4cm
Measurement Errors of Roof Snow Depths	n = 30 $\bar{e} = 0.3\text{cm}$ $\sigma = 6.7\text{cm}$		n = 30 $\bar{e} = 1.2\text{cm}$ $\sigma = 9.3\text{cm}$		n = 30 $\bar{e} = -3.3\text{cm}$ $\sigma = 9.5\text{cm}$	

n : Number of Measured Points
e : Mean of Measurement Errors
σ : Standard Deviation of Measurement Errors

Table 4. Measurement Errors of Roof Snow Depths (no Halation).
—Shed Roof by Air Plane—

Assigned Flight Altitude	300m	
	Photography without Snow Cover	Photography with Snow Cover
Photography Date	1987.4.9	1991.2.4
Actual Flight Altitude	365m	355m
Actual Photo Scale by Flight	1/1710	1/1660
Max. Error of Elevation at Control Points	4cm	6cm
Measurement Errors of Roof Snow Depths	$n = 42$ $\bar{e} = -0.1\text{cm}$ $\sigma = 2.9\text{cm}$	

n : Number of Measured Points
 \bar{e} : Mean of Measurement Errors
 σ : Standard Deviation of Measurement Errors

Table 5. Measurement Errors of Roof Snow Depths (no Halation).
—Flat Roof by Kite Balloon—

Assigned Flight Altitude	20m		60m		100m	
	Photography without Snow Cover	Photography with Snow Cover	Photography without Snow Cover	Photography with Snow Cover	Photography without Snow Cover	Photography with Snow Cover
Photography Date	1989.11.17	1990.1.27	1989.11.17	1990.1.27	1989.11.17	1990.1.27
Actual Flight Altitude	18m	19m	53m	56m	91m	89m
Actual Photo Scale by Flight	1/470	1/500	1/1390	1/1470	1/2390	1/2340
Max. Error of Elevation at Control Points	0cm	0cm	4cm	2cm	4cm	4cm
Measurement Errors of Roof Snow Depths	$n = 33$ $\bar{e} = -0.8\text{cm}$ $\sigma = 2.5\text{cm}$		$n = 33$ $\bar{e} = -0.9\text{cm}$ $\sigma = 3.7\text{cm}$		$n = 33$ $\bar{e} = 1.0\text{cm}$ $\sigma = 6.1\text{cm}$	

n : Number of Measured Points
 \bar{e} : Mean of Measurement Errors
 σ : Standard Deviation of Measurement Errors

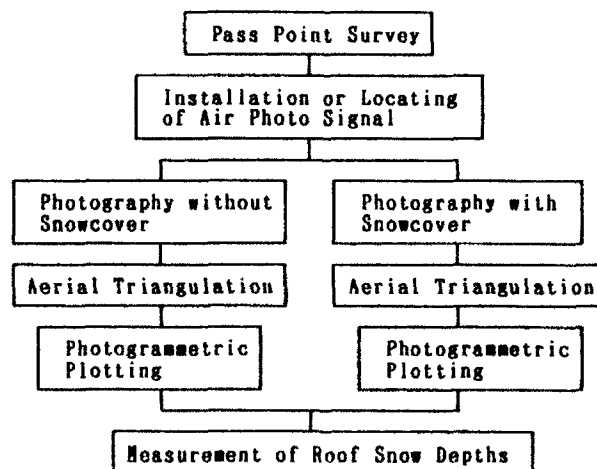


Fig. 1. Process for Measurement of Roof Snow Depths.

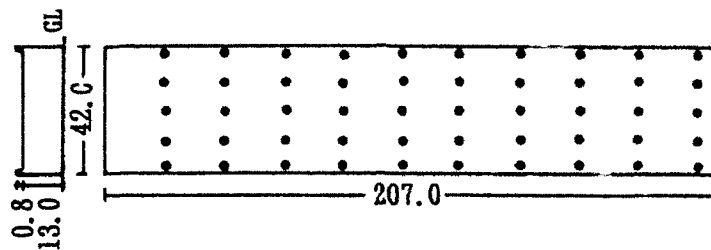
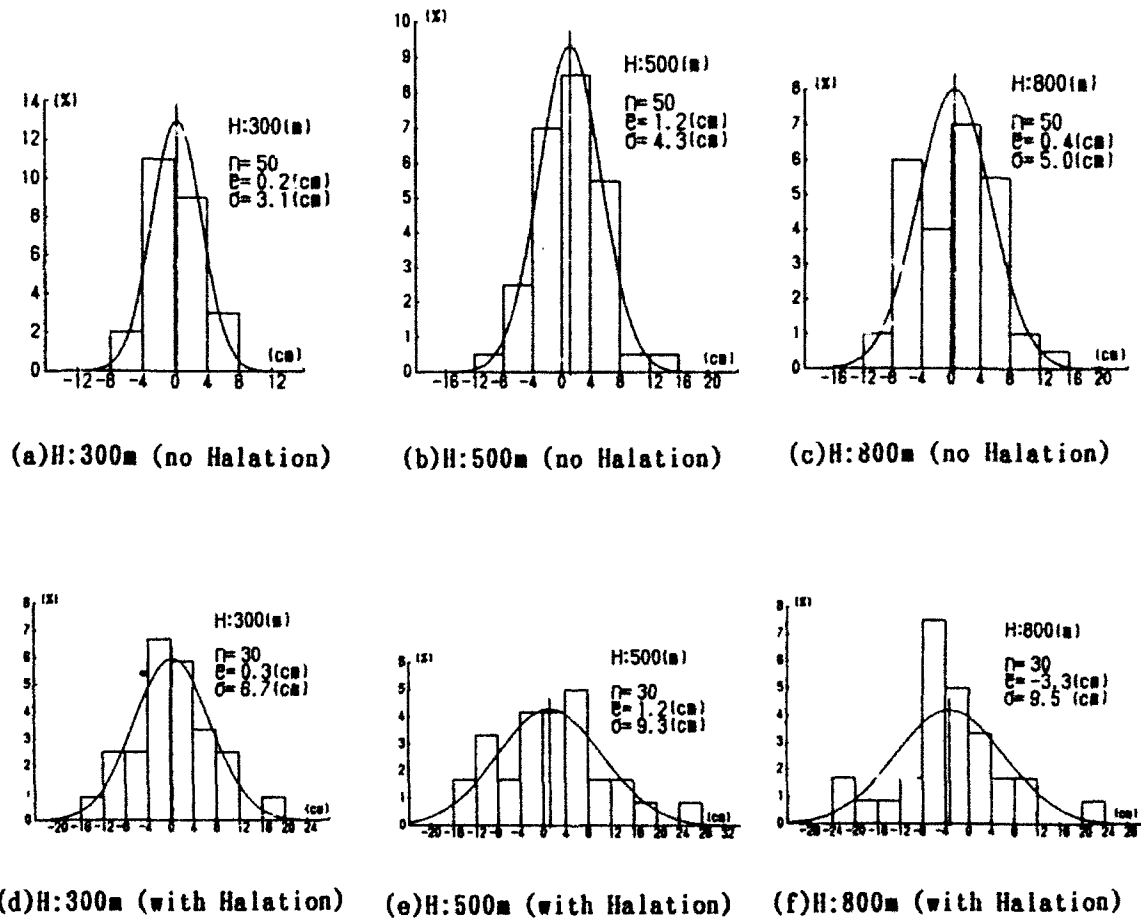


Fig. 2. Roof Plan, Cross Section and Measured Points.



H:Assigned Flight Altitude

Fig. 3. Distribution of Measurement Errors
 —Flat Roof by Air Plane—

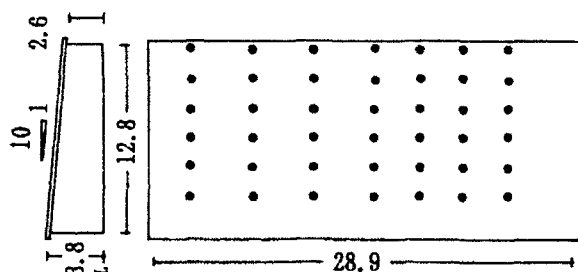


Fig. 4. Roof Plan, Cross Section and Measured Points.

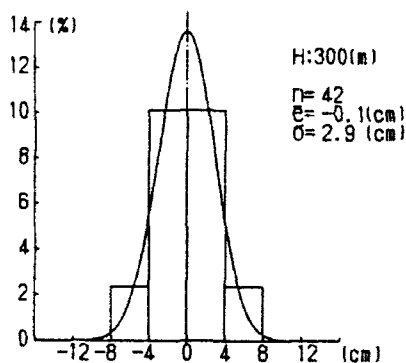


Fig. 5. Distribution of Measurement Errors (no Halation).
—Shed Roof by Air Plane—

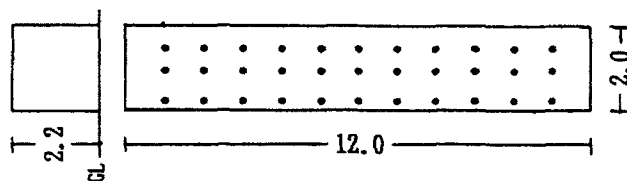


Fig. 6. Roof Plan, Cross Section and Measured Points.

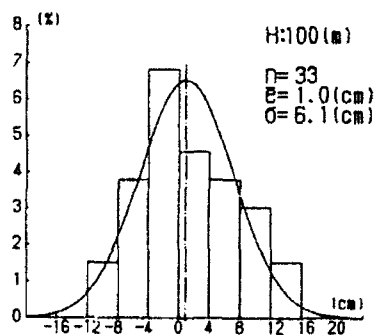


Fig. 8. Distribution of Measurement Errors (no Halation).
—Flat Roof by Kite Balloon—

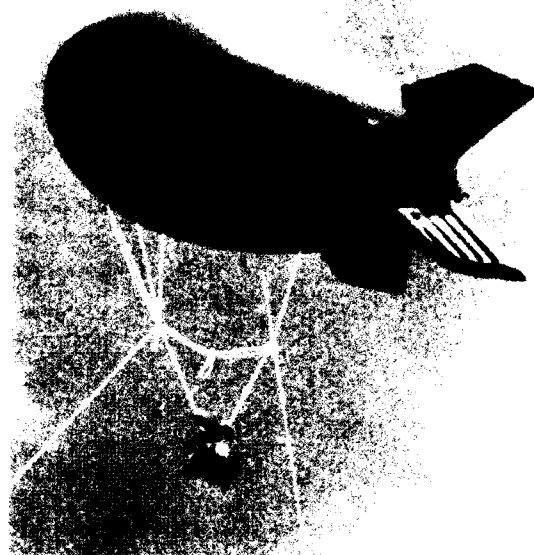


Fig. 7. Kite Balloon

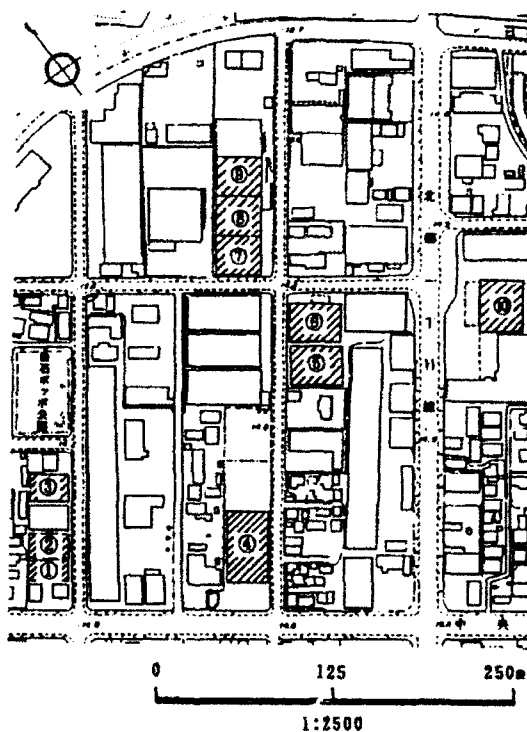


Fig. 9. Plan of the Measured Buildings.

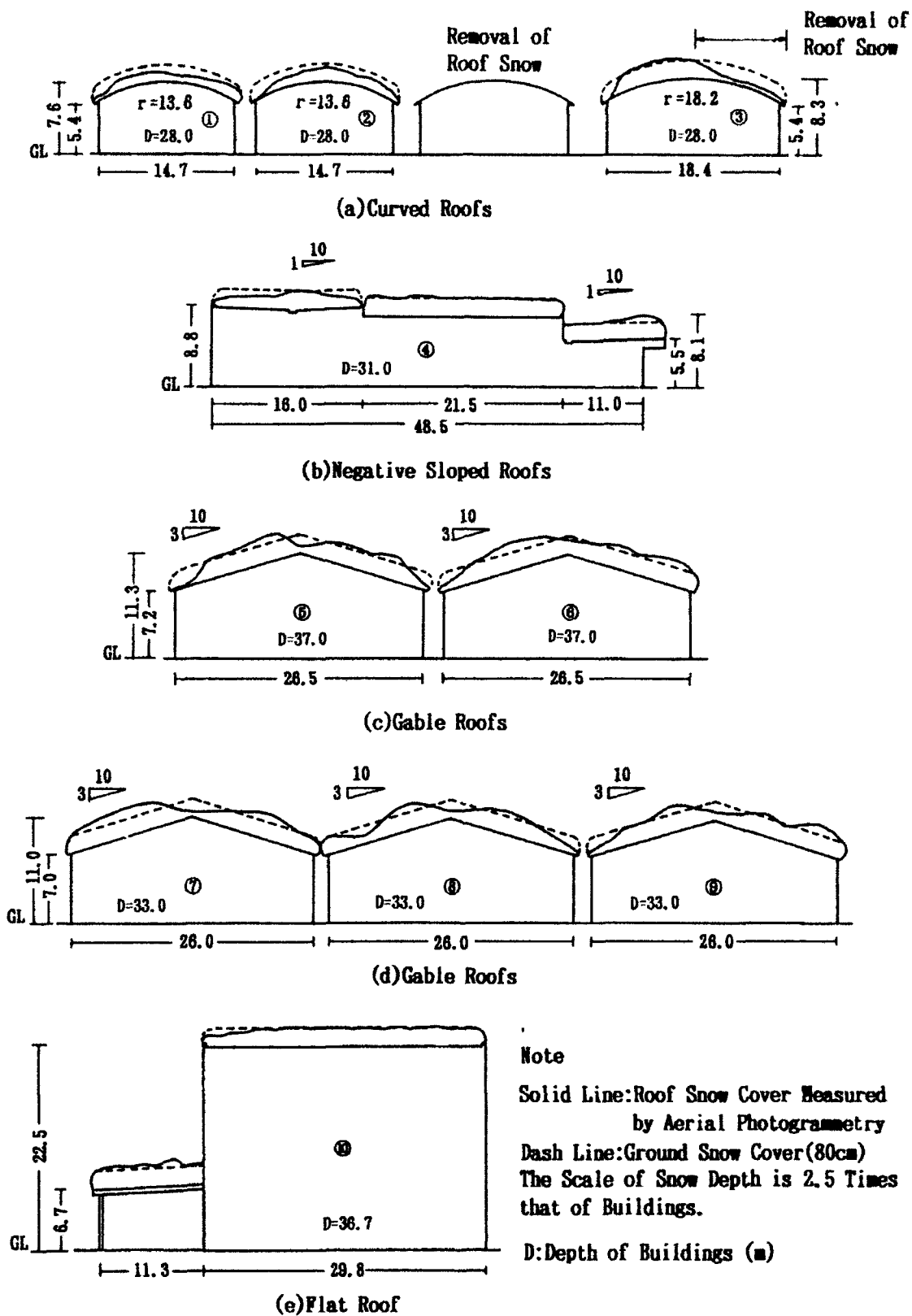
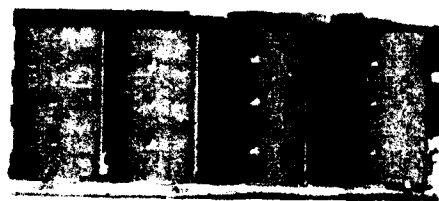
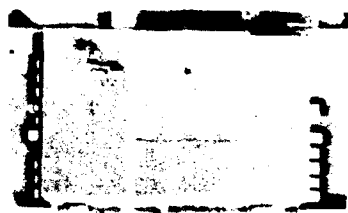


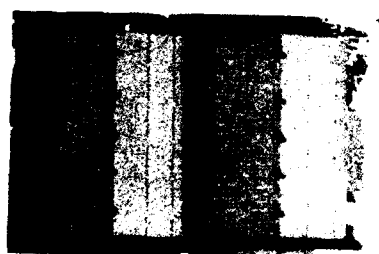
Fig. 10. Cross Sections of Buildings and Snow Covers.



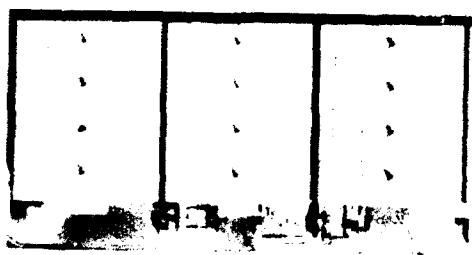
(a) Curved Roofs(1, 2, 3)



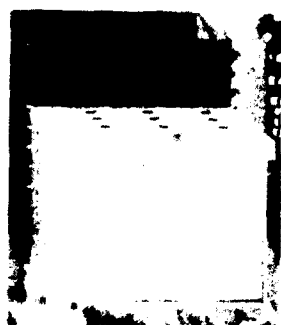
(b) Negative Sloped Roofs(4)



(c) Gable Roofs(5, 6)



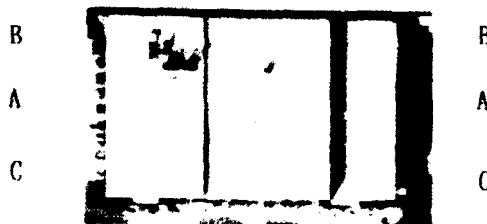
(d) Gable Roofs(7, 8, 9)



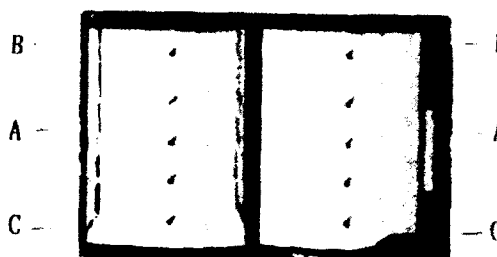
(e) Flat Roof(10)



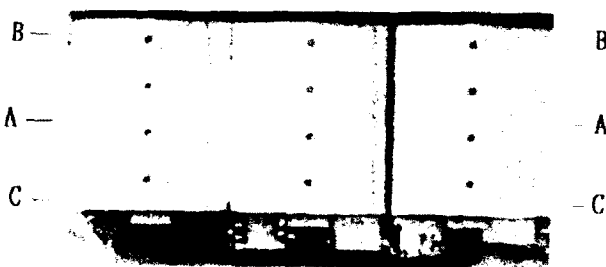
(a) Curved Roofs(1, 2, 3)



(b) Negative Sloped Roofs(4)



(c) Gable Roofs(5, 6)



(d) Gable Roofs(7, 8, 9)



(e) Flat Roof(10)

Fig. 11. Aerial Photographs without Snow Cover.
(Assigned Flight Altitude:300m)

Fig. 12. Aerial Photographs with Snow Cover.
(Assigned Flight Altitude:300m)

Wind Effects on Snow Accumulation on a Flat Roof

Jiro Suzuya,* Yasushi Uematsu[†] and Toshikazu Nozawa*

*Department of Architecture, Tohoku Institute of Technology, Sendai, Japan

[†]Department of Architecture, Tohoku University, Sendai, Japan

ABSTRACT

An unequal distribution of the snow on a flat roof has been investigated. The results were based on field measurements of roof snow. The measurement results were compared with the results of wind tunnel tests.

Measurements of the roof snow were carried out in the winter of 1991, for three months. Because the building used for measurement purposes had no air conditioning equipment, the lack of uniformity of the roof snow distribution was considered to be mainly caused by wind. Variations of wind speed and wind direction, during the period of the roof snow measurement, were recorded continuously.

Wind tunnel tests, using a reduced model of the building, were carried out. Crushed wheat was used as model snow particles, and two types of wind velocity profiles were chosen. Fitting the wind velocity profiles to the power law equation, the power law exponents were 0.15 and 0.20. The test wind velocity was varied from slightly lower than U_{th} to slightly higher than U_{th} , where U_{th} is the wind velocity at the threshold of particle movement.

Test results were compared with the field measurement results, and the model snow accumulations observed in the tests of the wind profile with $\alpha = 0.2$ power law exponent were found to be similar to the actual roof snow. The relationships between the distribution patterns of the model roof snow and wind velocity on the roof surface are also discussed.

INTRODUCTION

Although roof snow accumulations are not distributed uniformly on a flat roof, the snow load is ordinarily regarded as uniformly distributed in building design. When the snow load is treated as uniformly distributed, the total weight of roof snow tends to be overestimated. On the other hand, there is danger that the load of such structural members as purlins, which carry the load on small areas of the roof, is underestimated. To avoid such a potentially hazardous condition, it is necessary to grasp the actual condition of roof snow distribution. However, it is hard to estimate the lack of uniformity of the roof snow quantitatively.

In this paper, as a result of field observation, the transitions of the distribution patterns of roof snow are presented, together with wind data recorded at the site of the building. The process of formation of unequal roof snow distributions was investigated, based on the data obtained in the field observation and the data recorded at the meteorological station.

The lack of uniformity in roof snow is considered to be mainly caused by wind. Wind tunnel tests, in addition to field measurements, were carried out, using a reduced model of the building. When conducting a wind tunnel test, it is desirable that similarity between the field model and the test model be achieved. In the case of a wind tunnel test such as this, it was considered that the factors influencing similarity would be wind flow, the motion of the particle in

flow, and the motion of the particle on the accumulated snow surface. But it is difficult to satisfy all these conditions. In this study, the similarity of the wind flow was regarded as most important, and then two types of wind velocity profiles were chosen.

Comparing the actual condition of the roof snow with the wind tunnel test results, we discuss the predictability of partially concentrated snow loads on flat roofs.

FIELD OBSERVATION

Outline of Measuring Method

Roof Snow. The roof snow was measured on the roof of a building, located in the suburb of Aomori City, which is used for automobile inspection. The scale of the building is shown in Figure 1. The roof of the building is 6.5 m above the ground, and there are 60-cm-high parapets on the edge of the roof.

The areas surrounding the building are dotted with medium scale buildings, and the neighboring large buildings are more than 250 m away from the measured building.

The roof snow was measured every Saturday for thirteen weeks from December 1990 to March 1991. The snow depths were measured at nine points on the roof, as well as at two points on the ground, using measuring poles set at the points. These two points on the ground were in a grass-covered area, and sufficiently distant from the building. The arrangement of the measuring points is shown in Figure 2.

Wind. The wind measuring point was at the height of the building roof, 6.5 m above the ground, and 24 m away from the building in a northern direction. Wind speed and wind direction were recorded every ten minutes for the duration of the field observation. The data of wind direction and wind speed, averaged over 1.5 sec., were saved in an automatic data acquisition system.

Results

Distribution of the Roof Snow. The roof snow was observed in January, February and in early March, and the depths of the roof snow, measured within this time, are shown in Figure 3. The roof snow changed day after day; it increased with snowfall, and decreased when there was no snowfall. Because the building wasn't air-conditioned, the decrease in roof snow was considered to be caused mainly by natural melting. The depth of the roof snow peaked three times that winter, and the peak days were Jan. 12, Feb. 9 and Feb. 23. As a result of fresh snowfall, the roof snow depth increased uniformly. The unequal snow accumulations were formed not only by the process of melting but also by wind.

Wind Speed and Wind Direction at the Building Site. Large values for wind speed were recorded in winter at the building site. In January, about 20-m/s wind speeds were recorded in the morning. In February, there were a few cases of high wind speed in the middle of the month, but in the latter part of the month, high wind speeds were recorded often. Figure 4 shows the relative frequency distribution of the wind speed every week, in which snowfalls were observed. The number of measurements taken in a week is 1008. The wind direction at the building site fluctuated narrowly, and the principal wind direction was from the north.

The Climate of the City in the Winter. As a way to introduce the weather in the winter, the data concerning snowfall, ground snow and temperature are shown in Figure 5. These data were recorded at Aomori meteorological station, which is located about 2 kilometers from the building used in the observation to the northeast.

The average temperatures of the days in January were around 0°C. On a few days in the latter part of the month, the temperature rose above 0°C. In February, the movement of the

temperatures was similar to that in January. In the latter part of February the temperature fell below 0°C.

The snowfalls were observed mainly in early January and early February. Figure 6 shows the total amount of snowfall; it reached 500 cm in total. The ground snow observed at the meteorological station that winter was below average.

WIND TUNNEL TEST

Test Procedures

Test Equipment. An open circuit wind tunnel with a 100-cm-high and 140-cm-wide test section was used. A reduced model of the building on a scale of 1/200 was set up in the test section.

Artificial grass and the small wooden cubes were used as rough elements, to make optional wind velocity profiles. Figure 7 shows the profiles of wind velocity and turbulence intensity. The power law exponents are 0.15 for the former and 0.20 for the latter. The reference wind velocity U_r was measured at 60 cm above the wind tunnel floor.

The crushed wheat was used as model snow particles. The powder box was attached to the ceiling of the wind tunnel, across its width. The bottom of the powder box consisted of two sheets of acrylic plates, and both plates had many slits at regular intervals. The upper plate vibrated by means of a miniature motor, and the model snow fell down uniformly. The model snow scattering system was designed following a system used by Dickay and Srivastava (1988).

The model snow depth was measured using a laser displacement sensor attached to the stem of a traversing mechanism (Figure 8). Driving this mechanism, the sensor moved in two directions, and we could measure the depth at the appointed points with an accuracy within 0.01 mm.

The Properties of Model Snow Particles. The particles passing through a 0.5-mm sieve were used in the test. The distribution of the particle's size used is shown in Table 1.

Table 1 Distribution of the particle's size

Size (μm)	Percentage
500 - 300	43.46
300 - 150	26.26
150 - 125	3.34
125 - 106	8.91
106 - 75	11.43
75 - 38	3.53
< 38	3.07

To examine the properties of crushed wheat used as model snow, some preliminary examinations were carried out.

The densities of the particles were obtained by measuring the weight of crushed wheat lumps, which were made in a vacuum under pressure of 1 ton/cm².

To measure the terminal velocity of the particles, two sets of laser detection sensors installed in a long vinyl tube were used. As Figure 9 shows, the two sensors were fixed to the wall of the vertically erected tube, with a distance of 100 cm. Dropping a handful of the particles from the top of the tube, the two sensors detected the falling particles, and the differences of detection time between both sensors were recorded.

The properties of the crushed wheat used as model snow, their density, terminal velocity and average size, are tabulated in Table 2.

To determine the test wind velocity, the wind velocity at the threshold of particle movement was measured. The movement of particles, uniformly distributed on the flat plate fixed at

the height of the model roof, 3.2 cm high above the wind tunnel floor, started at 3 m/sec – a reference wind velocity.

Similarity Requirement. In verifying the similarity to actual conditions, the data about the properties of the actual snowfalls are indispensable. Since it was difficult to examine the snowfalls for the duration of the field observation, we use the snow data that had previously been presented in literature, which are tabulated in Table 2.

At the site of the observed building, wind speeds of about 20 m/s (averaged over 1.5 sec.) were recorded at the height of the roof. This value of wind speed is considered to be equivalent to an 11 m/s mean wind speed, adopting 1.8 as the value for gust factor. In the wind tunnel test, under conditions of $U_r = 3.0$ m/s test wind velocity and a 0.20 power law exponent, the equivalent wind velocity at the height of the model roof is calculated as 1.1 m/s.

Table 2 Properties of Actual and Model Snow

		Actual Snow	Model Snow
Particle Size	D cm	0.1 ~ 1.0	0.01 ~ 0.05
Particle Density	ρ_p kg/cm ³	100~ 300	1,310
Terminal Velocity	U_t m/s	1.0 ~ 2.0	1.0

By using the numerical data of the model and the actual snow into formulas for similarity conditions, the extents to which the wind tunnel tests satisfied the requirements for similarity to actual conditions are discussed as follows:

- (a) Similarity on the particle terminal velocity U_t to wind velocity U_0 : Because the terminal velocities of both particles are nearly equal, the requirement is satisfied when the wind velocities were equal both in the test and in field.
- (b) Similarity of inertia force of the particle to its gravity force: This condition is represented by equality of the following parameter in field and in test.

$$\sqrt{U_0^2 \rho_p / L g (\rho_p - \rho)}$$

Where L : characteristic overall dimension.

ρ : the density of the fluid.

g : the acceleration of gravity.

To satisfy this condition, the wind speed in the field must be eleven times higher than the test wind velocity.

- (c) Similarity of the critical surface shear stress to the gravity force acting on the particle: The condition is represented by equality of the following parameter in field and in test.

$$\sqrt{u_{*}^2 \rho / D (\rho_p - \rho)}$$

Where u_{*} : friction velocity at the threshold of particle movement.

To satisfy this condition, the friction velocity at the threshold of particle movement must be in a ratio of 3 : 2 between model and actual snow.

Close verifications of similarity requirements were difficult to obtain due to a lack of accurate data about actual snow. Although it is difficult to satisfy all similarity requirements simultaneously, the requirements (b) and (c) were roughly satisfied in the present test.

Results

Figure 10 shows the distributions of the model snow accumulation. The tests were performed at the reference wind velocity of $U_r = 2.0$ and 3.0 m/s, for the wind profiles of $\alpha = 0.15$ and 0.2 . The contour represents the ratio of the snow depth between roof and ground.

Figure 11 represents the results for the tests at higher wind velocities, that is, the reference wind velocity was 3.5 and 4.0 m/s, for the wind profiles with a power law exponent $\alpha =$

0.15. It took a considerably long time to obtain a sufficient model snow accumulation for precise measurement.

DISCUSSION

The remarkable features of the observed roof snow accumulations were as follows:

- (a) The snow distributed almost symmetrically about the north-south axis of the roof, but the depth was slightly larger on the east side than on the west side.
- (b) The snow depth was larger on the leeward (south side) of the roof than on the windward (north side), and it increased uniformly in the wind direction.
- (c) The roof snow depths were sometimes larger than that on the ground.

Comparing the observed roof snow with the wind tunnel test results, it is seen that the model snow distributions for $\alpha = 0.2$ resemble the actual distribution pattern.

To compare the observed results with the test results quantitatively, the model snow depths at the nine points corresponding to the field measurement were chosen. The ratios of the maximum to the average depth of the nine points were calculated. They were between 1.2 to 1.9 for the actual snow and 1.6 to 1.9 for the model snow, if the one extremely large value was excluded. The roof snow depth, measured at the end of the week in which we had no snowfall, was small, and the ratio is extremely large as a result.

While the model snow accumulations tended to concentrate at the central part of the roof, the actual snow depth at the central part was smaller than at the both sides (east and west). The tendency of the model snow to concentrate at the central part of the roof was remarkable in the test results of higher wind velocity.

The model snow distributions obtained in the tests for a wind profile of $\alpha = 0.15$ are different from those obtained in the tests where $\alpha = 0.2$, in some respects. Comparatively thick snow depths were observed at the central point of the windward side of the roof, for tests where $\alpha = 0.15$. However, in tests where $\alpha = 0.2$, the depth of snow decreased as it moved in a windward direction so that a deposit wasn't observed on the windward side.

To examine the difference in the distribution patterns of the model snow between the both test results, the wind velocities near the roof surface of the model building, at 2.5 mm above it, were measured. Figure 12 represents the results of measurements: Figure 12(a) is for the wind profile where $\alpha = 0.15$ and Figure 12(b) for $\alpha = 0.2$. The wind velocity at both the east and the west side are higher than at the central part of the roof. As for the north-south direction (wind direction), the wind velocity is increasing in the leeward side. In the test results for the wind profile where $\alpha = 0.15$, there was a low wind velocity area at the central part of the windward side of the roof. The snow depths are larger in this area, and a deposit was formed there. The surface wind velocity and model snow depth increase in the leeward direction. It is considered that there is a reattachment line of the separated flow near the deposit.

CONCLUSIONS

The observations of snow accumulations on a flat roof, together with the measurements of the wind at the site, were carried out during one winter. The high wind speeds were recorded frequently, and about 20% of the data recorded in each week indicated wind speeds higher than 20 m/s (averaged over 1.5 sec). The unevenness of the roof snow distribution developed with the passage of time after a snowfall. Snow depth increased on the leeward side of the roof.

Wind tunnel tests about the roof snow accumulation on the model building were carried out to examine the wind effects on the roof snow distribution. In the tests, using a 1/200 scale model building, crushed wheat was used as model snow, and two types of the wind profiles were chosen. It is difficult to satisfy all similarity requirements in the tests, but in the tests for the wind profile where $\alpha = 0.2$, the model roof snow accumulations resembled the actual one.

It is thought that the ratio between the maximum roof snow depth and the average depth is, ordinarily, less than 2, based on the results of the field observation and the wind tunnel tests.

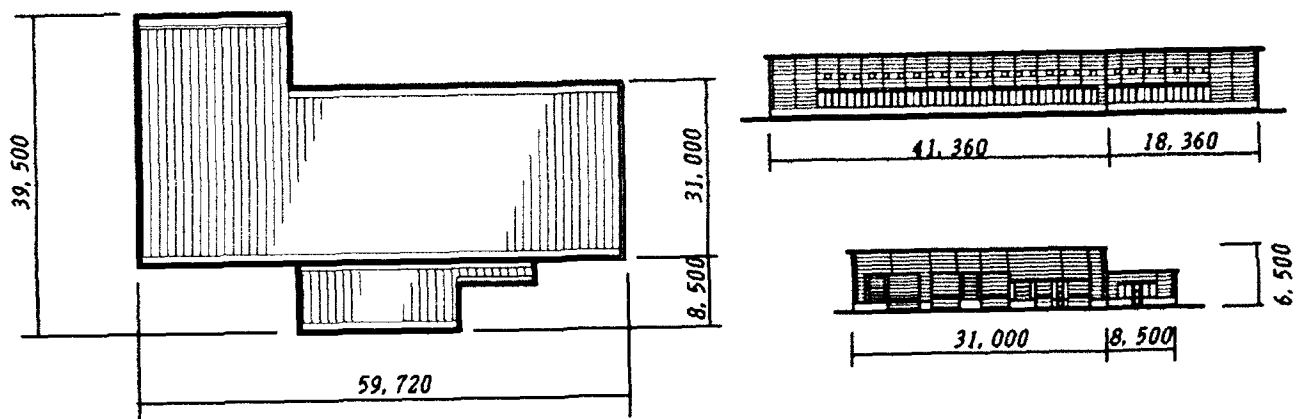


Figure 1. Scale of the building.

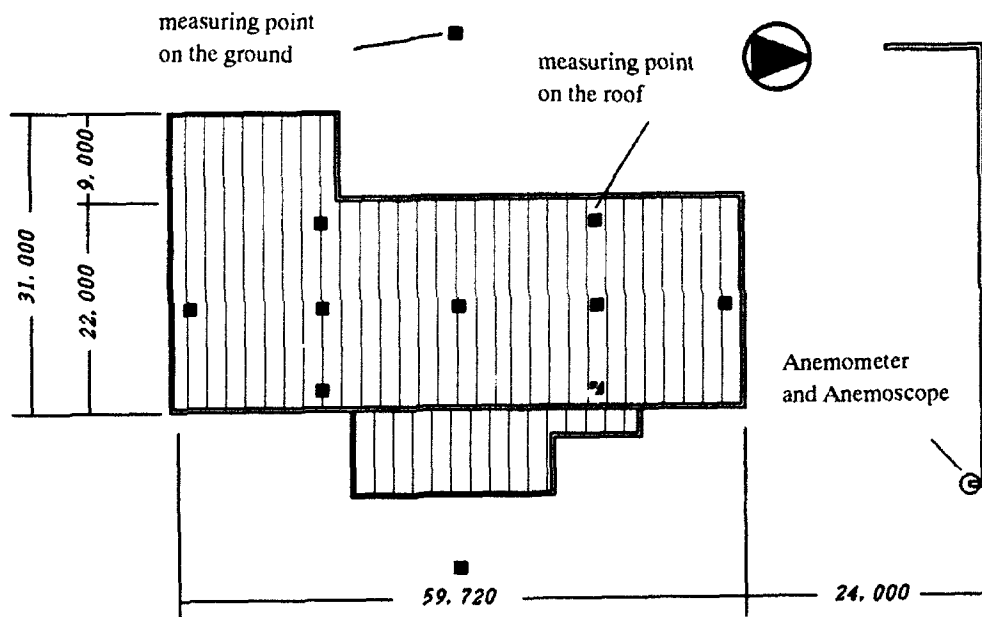


Figure 2. Arrangement of the measuring points.

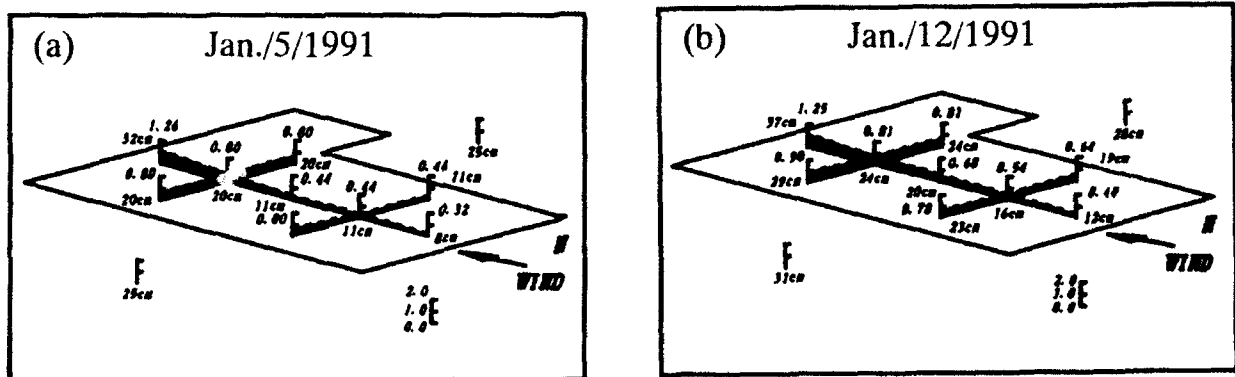


Figure 3. Depth of the roof snow.

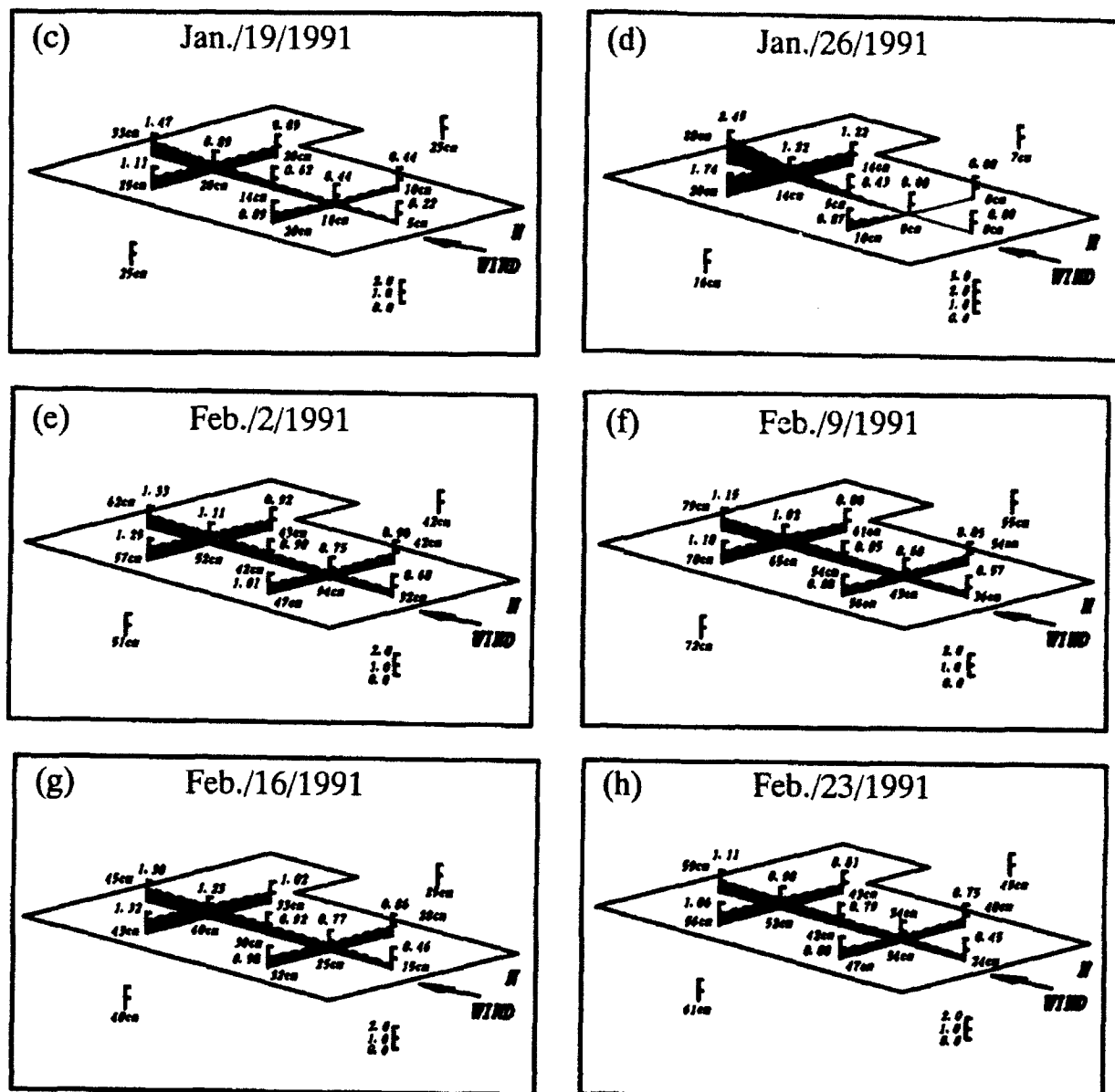


Figure 3. (continued) Depth of the roof snow.

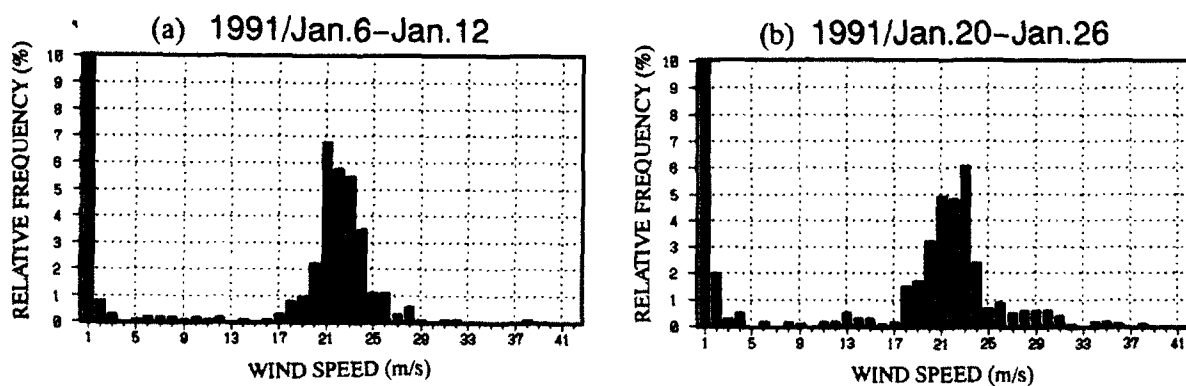


Figure 4. Frequency distribution of the wind speed.

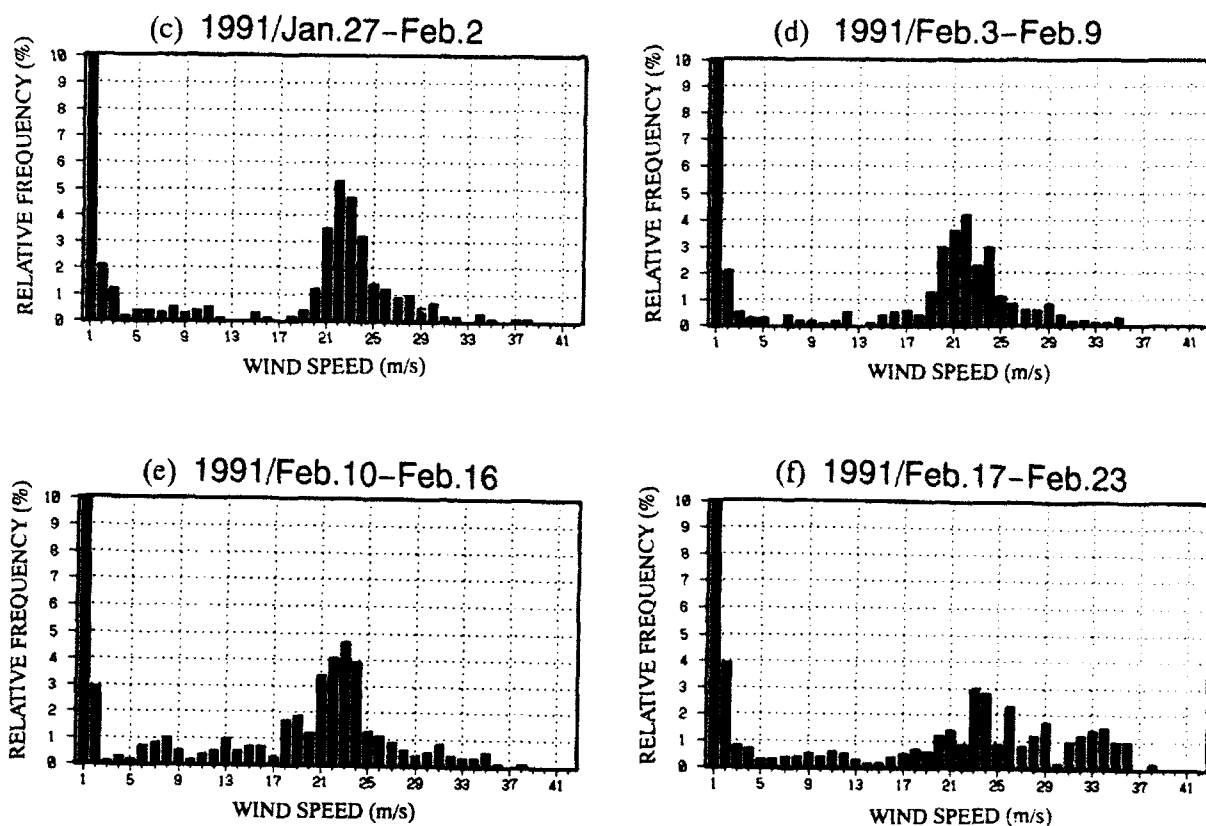


Figure 4. (continued) Frequency distribution of the wind speed.

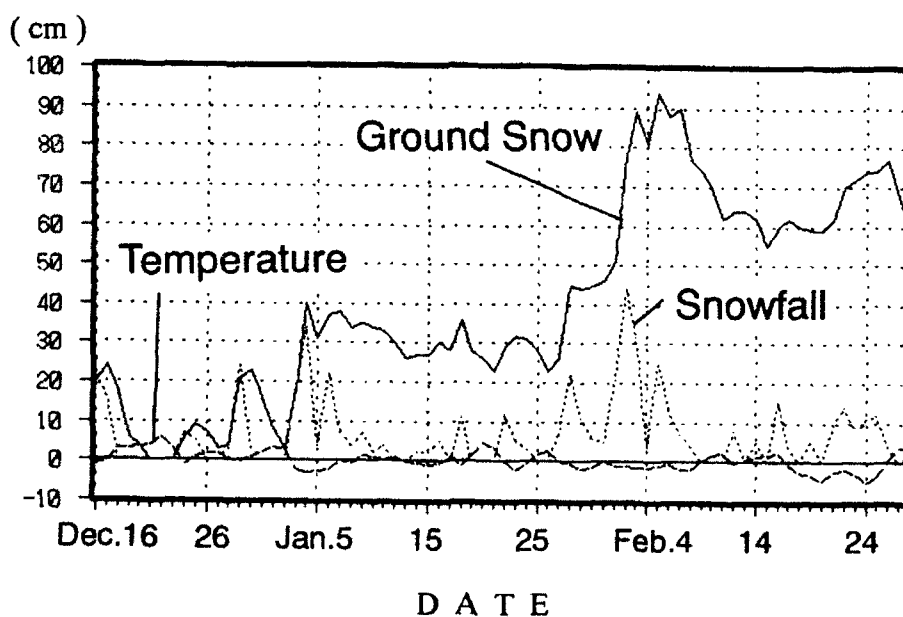


Figure 5. Meteorological Record in the Winter.

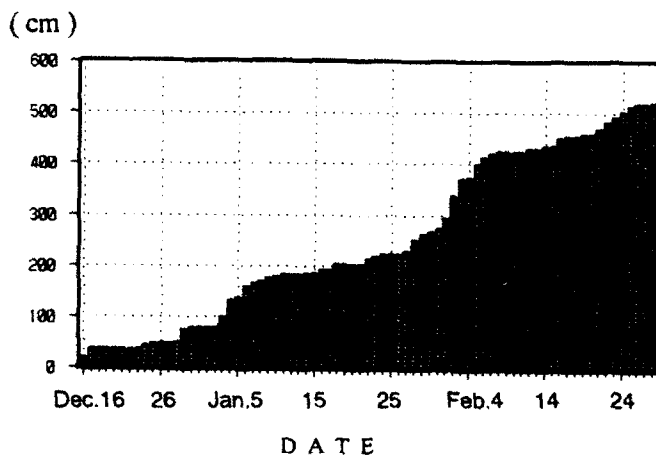
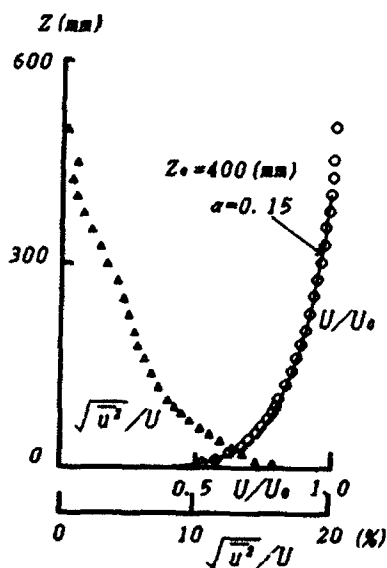
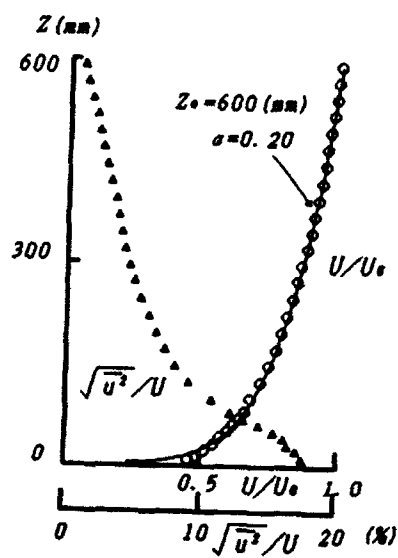


Figure 6. Total amount of snowfall.



(a) $\alpha = 0.15$



(b) $\alpha = 0.20$

Figure 7. Profiles of wind velocity and turbulence intensity.

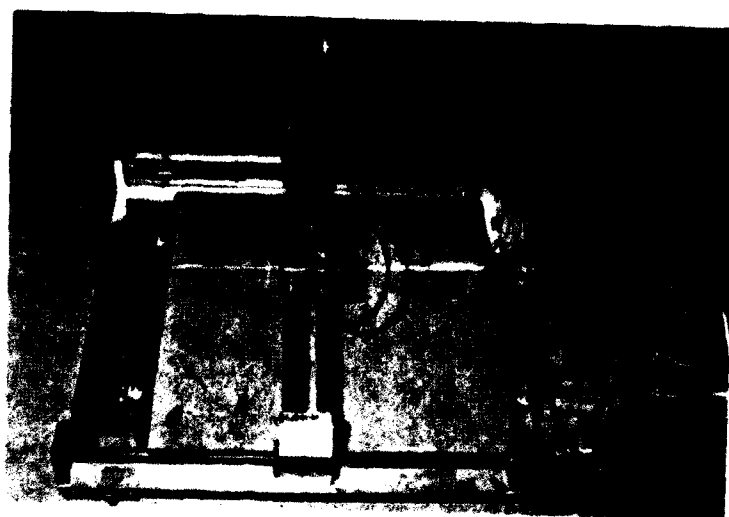


Figure 8. Traversing mechanism.

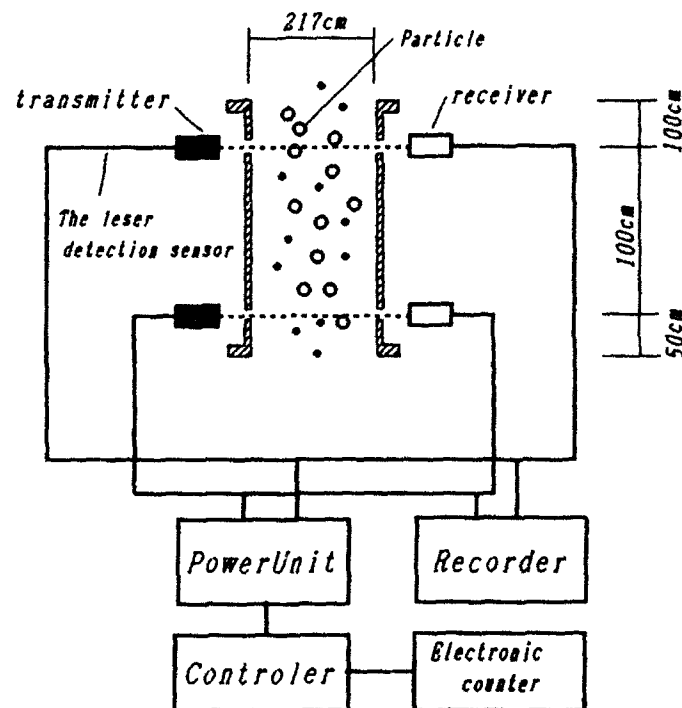


Figure 9. Measurement of the terminal velocity of particles.

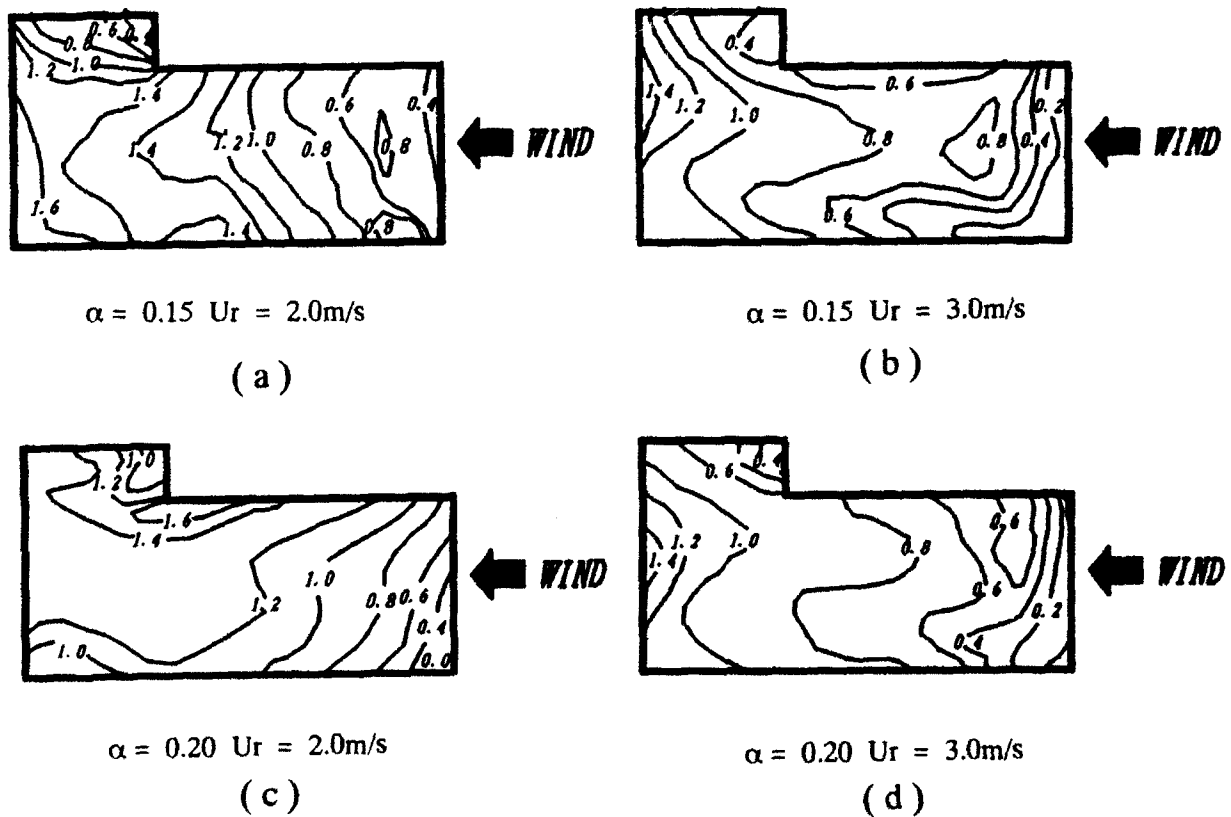


Figure 10. Distribution pattern of the model snow.

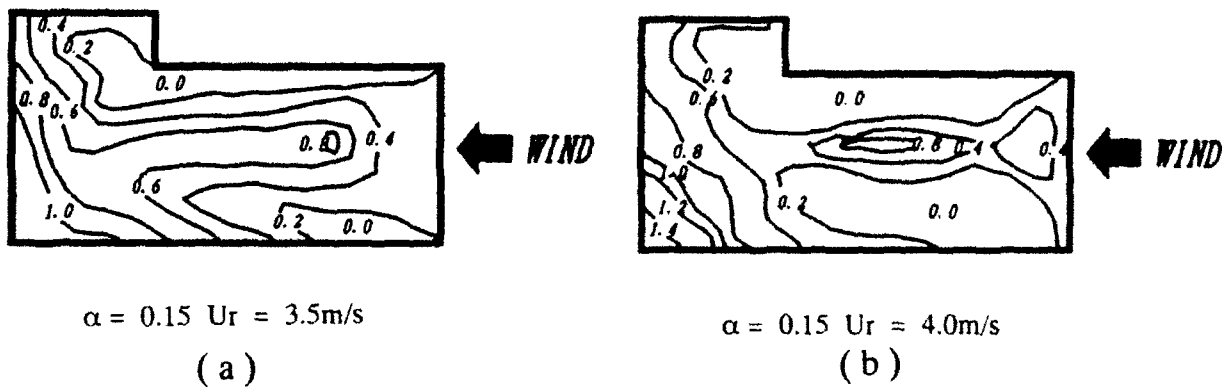
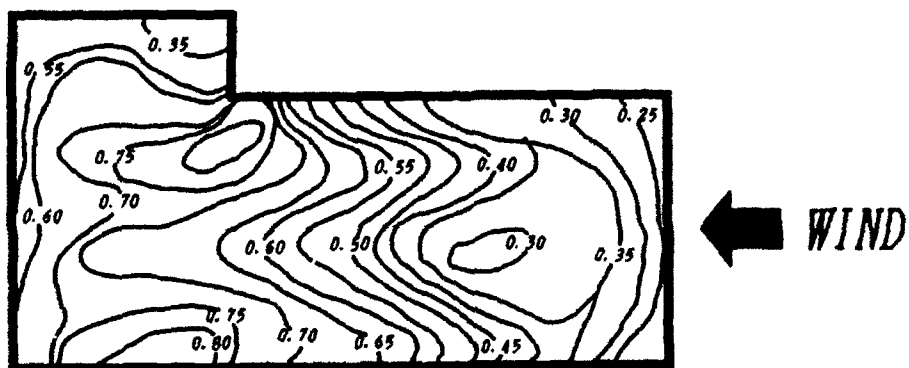
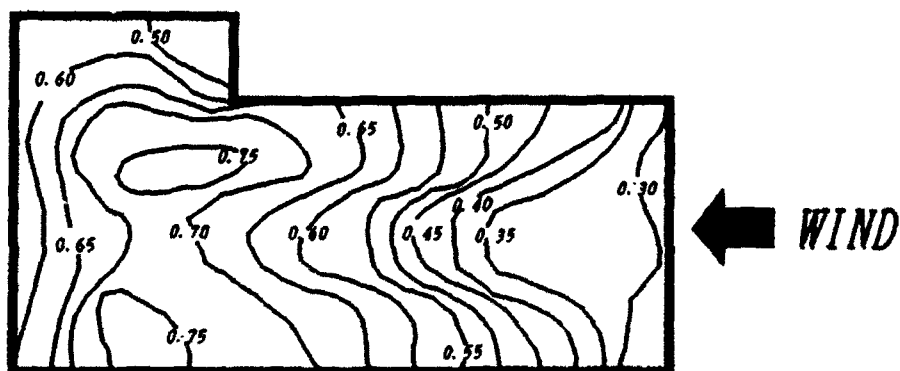


Figure 11. Distribution pattern of the model snow.



(a) $\alpha = 0.15$



(b) $\alpha = 0.20$

Figure 12. Wind velocities near the roof surface of the model building.

ACKNOWLEDGMENT

The authors wish to express their appreciation to the members of the Aomori Snow Study Circle (Representative; Shozo Yamakawa) for their cooperation in the field measurement.

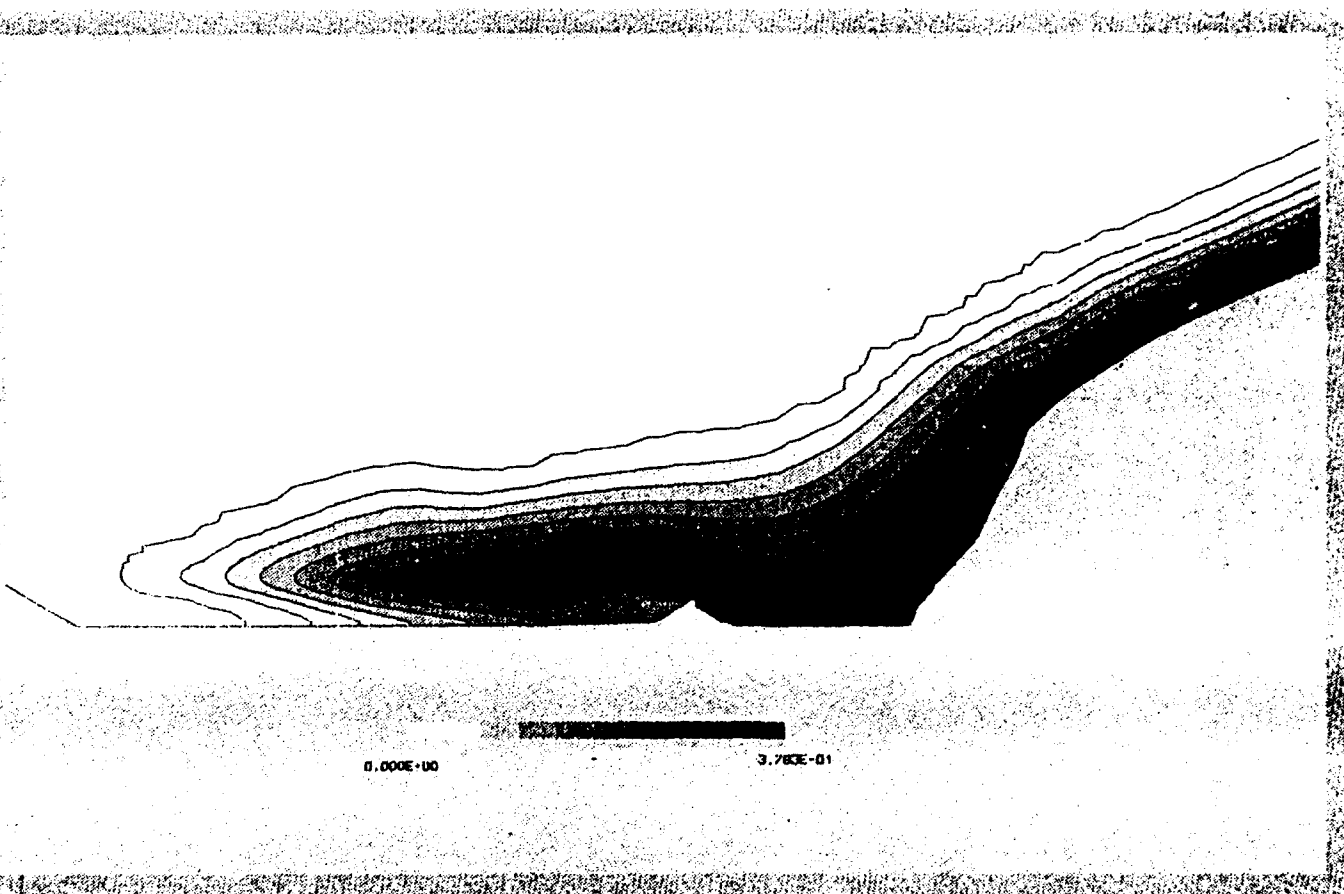
REFERENCES

- Dickey, R. and Srivastava, N.K. (1988) "Minimizing Snow Accumulation around the Entrance of a Building, An Experimental Case Study," *First International Conference on Snow Engineering*, CRREL Spcl. Rpt. 89-6, 243-255, Hanover, NH.
- Isyumov, N., Mikitiuk, M. and Cookson, P. (1988) "Wind Tunnel Modeling of Snow Drifting, Application to Snow Drifting," *First International Conference on Snow Engineering*, CRREL Spcl. Rpt. 89-6, 210-226, Hanover, NH.
- Isyumov, N. and Mikitiuk, M. (1990) "Wind Tunnel Model Tests of Snow Drifting on a Two-Level Flat Roof," *Journal of Wind Engineering and Industrial Aerodynamics*, 36, 893-904, Elsevier Science Publishers B.V., Amsterdam
- Iversen, J.D. (1988) "Modeling Drift Geometry in Wind Tunnel," *First International Conference on Snow Engineering*, CRREL Spcl. Rpt. 89-6, 227-231, Hanover, NH.
- Japan Contraction Machinery Association (1977), *Handbook of Snow Protection Engineering*, Morikita Shuppan, Tokyo, (in Japanese)
- Kind, R.J. (1990) "Mechanics of Aeolian Transport of Snow and Sand," *Journal of Wind Engineering and Industrial Aerodynamics*, 36, Elsevier Science Publishers B.V., Amsterdam
- Mikitiuk, M. and Isyumov, N. (1988) "Variability of Snow Loads on Large-Area Flat Roof," *First International Conference on Snow Engineering*, CRREL Spcl. Rpt. 89-6, 142-157, Hanover, NH.
- O'Rourke, M. and Garanakos, I. (1988) "Modeling Wind Effects on Drifting," *First International Conference on Snow Engineering*, CRREL Spcl. Rpt. 89-6, 178-187, Hanover, NH.
- Petersen, R.L. and Cermak, J.E. (1988) "Application of Physical Modeling for Assessment of Snow Loading and Drifting," *First International Conference on Snow Engineering*, CRREL Spcl. Rpt. 89-6, 276-285, Hanover, NH.
- Sant'Anna, F.M. and Taylor, D.A. (1990) "Snow Drift on Flat Roofs: Wind Tunnel Tests and Field Measurements," *Journal of Wind Engineering and Industrial Aerodynamics*, 36, Elsevier Science Publishers B.V., Amsterdam
- Tomabechi, T. (1985) "Geometry of Snow Accumulation on Roofs in Cold Winter Regions," *Doctoral Thesis*, Tohoku University, (in Japanese)

3

Analytical Modeling

Peter Irwin, Chairman



*Simulation of snow concentrations in a vertical section of a powder avalanche flowing over a defense structure.
(From the paper by Brandstätter, Weiser and Schaffhauser, this volume.)*

Three-Dimensional Simulation of Powder Avalanches

W. Brandstätter,* K. Weiser* and H. Schaffhauser†

*FBVA—Institute für Lawinenkunde, Hofburg, A-6020 Innsbruck, Austria

†AVL—List GmbH., Kleiststrasse 48, A-8020 Graz, Austria

ABSTRACT

The paper presents the physical and mathematical background of a three-dimensional theoretical model, which can be used to simulate the dynamics of powder avalanches very accurately. It is based on the fundamental differential equation system which governs the conservation of mass, momentum and snow concentration. The effects of turbulence are taken into account via a two-equation turbulence model. A comparison between computed results and measurement data obtained from a 3-dimensional model experiment are presented. Furthermore the application of the model to a real avalanche is demonstrated.

INTRODUCTION

Over the last few decades the alpine regions have experienced a significant increase of their recreational attraction and economical growth. Consequently, exposure of the public to potential hazards has grown and has called, among other things, for effective protection measures against avalanche accidents. In this respect, the knowledge about the avalanche formation, its dynamics and its behaviour in the runout zone is of extreme importance. However, little progress has been made in the past with respect to this. The main reasons are two-fold; firstly experimental investigations have been, and remain difficult for obvious reasons and secondly limitations of computational tools permitted only the use of very simple one-dimensional theoretical models which lead to unsatisfactory predictions about real avalanche dynamics.

A review on avalanche dynamics models is given in /11/. It summarizes the research in this area over the last thirty years in developing models for quantifying avalanche velocities, pressures, and related quantities. Hence no further discussion on this topic will be given in this paper. Instead, the remainder of the paper will concentrate on a new approach to modeling the dynamics of avalanches which became feasible with the advent of powerful supercomputers and workstations. It is concerned with the solution of the system of fundamental partial differential equations which

in a general form describe the conservation of mass, momentum and snow concentration in three dimensions and time. The effects of turbulence are taken into account via a two-equation turbulence model.

A brief description of the mathematical background and the numerical solution method employed follows. Subsequently its computer implementation is discussed and a comparison between computed results and measurement data obtained from a 3-dimensional model experiment are presented. Finally the application of the model to a real avalanche is demonstrated.

DESCRIPTION OF THE METHOD

The powder snow avalanche is considered as the flow of an unsteady compressible, turbulent 3-dimensional fluid suspended in air [11]. This flow is governed by gravity as the driving force and entrainment of the ambient air.

Equations Governing Fluid Dynamics

Based on the above assumptions, fundamental differential equations which govern the conservation of mass, momentum and snow concentration in Cartesian tensor notation can be written as:

$$\frac{\partial \bar{p}}{\partial t} + \frac{\partial}{\partial x_j} (\bar{p} \bar{u}_j) = 0 \quad (1)$$

$$\begin{aligned} \frac{\partial \bar{\rho} \bar{u}_i}{\partial t} + \frac{\partial}{\partial x_j} (\bar{\rho} \bar{u}_j \bar{u}_i) = & - \frac{\partial \bar{p}}{\partial x_i} + \frac{\partial}{\partial x_j} \left[\mu_t \left(\frac{\partial \bar{u}_i}{\partial x_j} + \frac{\partial \bar{u}_j}{\partial x_i} \right) - \right. \\ & \left. \frac{2}{3} \left(\mu_t \frac{\partial \bar{u}_m}{\partial x_m} + \bar{p} k \right) \delta_{ij} \right] + \bar{\rho} \bar{c} g \end{aligned} \quad (2)$$

$$\frac{\partial \bar{\rho} \bar{c}}{\partial t} + \frac{\partial}{\partial x_j} (\bar{\rho} \bar{c} \bar{u}_j) = \frac{\partial}{\partial x_j} \left(\frac{\mu_t}{\sigma_c} \frac{\partial \bar{c}}{\partial x_j} \right) \quad (3)$$

where mean values are denoted by overbars (-) and u_i is the velocity in direction x_i , p is pressure, δ_{ij} is the Kronecker delta, g the gravitational acceleration and μ and σ_c are viscosity and Prandtl number, respectively.

Turbulence Model Equations

The turbulent viscosity μ_t is obtained from differential transport equations for the turbulent kinetic energy k and its dissipation rate ϵ , to which it is linked by

$$\mu_t = C_\mu \rho \frac{k^2}{\epsilon} \quad (4)$$

where C_μ is an empirical coefficient. The value of this and other such coefficients appearing in the turbulence model are given in Table 1. The transport equations are of the general form

$$\frac{\partial(\bar{\rho}k)}{\partial t} + \frac{\partial}{\partial x_j} (\bar{\rho} \bar{u}_j k) = \frac{\partial}{\partial x_j} \left(\frac{\mu_t}{\sigma_k} \frac{\partial k}{\partial x_j} \right) + \mu_t G_{ij} - \frac{2}{3} \frac{\bar{\partial} u_m}{\partial x_m} \left(\mu_t \frac{\bar{\partial} u_m}{\partial x_m} + \bar{\rho} k \right) - \bar{\rho} \epsilon \quad (5)$$

$$\frac{\partial(\bar{\rho}\epsilon)}{\partial t} + \frac{\partial}{\partial x_j} (\bar{\rho} \bar{u}_j \epsilon) = \frac{\partial}{\partial x_j} \left(\frac{\mu_t}{\sigma_\epsilon} \frac{\partial \epsilon}{\partial x_j} \right) + C_1 \frac{\epsilon}{k} [\mu_t G_{ij} - \frac{2}{3} \frac{\bar{\partial} u_m}{\partial x_m} (\mu_t \frac{\bar{\partial} u_m}{\partial x_m} + \bar{\rho} k)] - C_2 \frac{\bar{\rho} \epsilon^2}{k} + C_3 \bar{\rho} \epsilon \frac{\bar{\partial} u_m}{\partial x_m} \quad (6)$$

Here

$$G_{ij} = \frac{\partial u_i}{\partial x_j} \left(\frac{\partial u_i}{\partial x_j} + \frac{\partial u_j}{\partial x_i} \right) \quad (7)$$

and σ_k , σ_ϵ , C_1 , C_2 and C_3 are further empirical coefficients.

Table 1: Empirical Coefficients and Prandtl Numbers

C_1	C_2	C_3	C_μ	σ_ϵ	σ_k	σ_ϵ
1.44	1.92	-0.373	0.09	1.0	1.0	1.22

The above equations have their origins in a model described by Launder and Spalding /7/ which was originally developed in the context of incompressible flows, and subsequently extended to the compressible case by several researchers /9,13/.

The mass fraction of snow termed the "snow concentration" c is defined as

$$\bar{c} = \frac{\bar{m}_S}{\bar{m}_S + \bar{m}_A} \quad (8)$$

where m_s and m_A denote the mass of snow and air respectively. Consequently a value of $c = 0$ means that only air is present whilst $c = 1$ corresponds to a flow situation where only snow is existing. Based on this, the mean density ρ is linked to the snow density ρ_s and the air density ρ_A via

$$\bar{\rho} = \bar{\rho}_A + \bar{\rho}_S \quad (9)$$

and

$$\bar{\rho}_S = \bar{c} \bar{\rho} \quad (10)$$

or

$$\bar{\rho}_A = (1 - \bar{c}) \bar{\rho} \quad (11)$$

Boundary and Initial Conditions

The no-slip condition is prescribed along the bottom surface of the avalanche via special shear-stress formulae derived from boundary layer theory, as described in /10/. The implications of this approach are also used to appropriately modify the equations for k and ϵ in this region.

At the start of each computation everything is assumed to be at rest and a snow layer of prescribed initial height is placed in the area where the avalanche originates. The actual dimensions of this volume as well as the initial snow density ρ_s are based on observations or measurements. Immediately after the start of the computation this snow volume starts to move under the influence of gravity.

Numerical Solution Procedure

Solution of the system of partial differential equations (1) to (6) can be obtained using the computer program FIRE /1,3/ developed at AVL. A brief description of the underlying numerical method is provided.

The differential equations are first recast into a general non-orthogonal coordinate frame. The resulting differential equation system is then discretized adopting the finite volume approach and employing a second order differencing scheme /14/ for approximations of the spatial derivatives and the Euler-implicit differencing scheme for the temporal derivatives.

This procedure reduces the differential equations to algebraic equations which are solved iteratively by an ICCG-method /6/ in a forward marching fashion at discrete time levels.

Computer Implementation

The computation itself can be divided into 3 distinct stages, namely pre-processing, main fluid mechanics calculation and post-processing. The pre-processing in turn can be sub-divided into 3 stages. A brief description of how to perform a typical flow computation now follows.

First a surface model of the avalanche slope and associated buildings, dams, etc., is generated. This is currently done by digitizing isolines of constant height from maps for the former and by taking data available from design drawings for the latter. Figure 1 shows an example of a cut-out of a complete surface model of an avalanche slope and a dam supposed to protect a motorway.

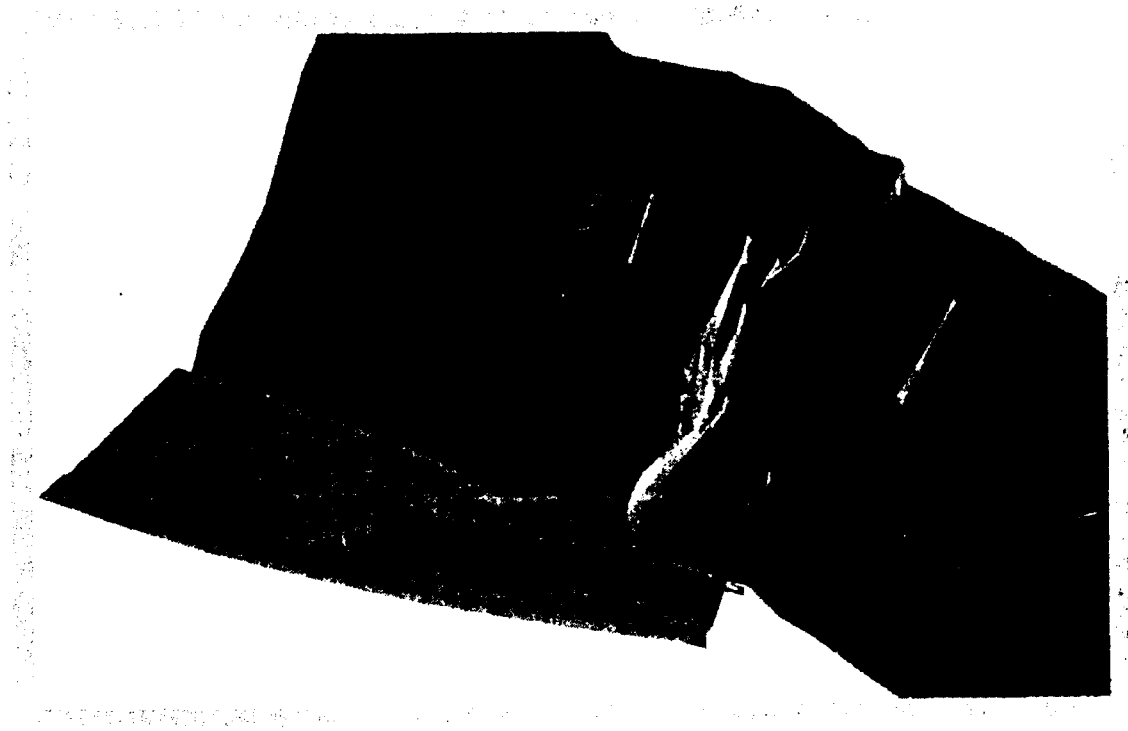


Figure 1: Part of the Avalanche Slope and the Protective Dam

The next step comprises the interactive generation of the actual computational mesh (volume mesh) which forms the basis of the finite volume analysis. The procedure is as follows:

Sufficiently far away from the actual region of interest (avalanche slope) boundaries for the flow domain are assumed to exist. This domain is then "filled" up with mesh cells and the linkage of all these cells is established. Figure 2 shows a cut-out of the complete computational mesh used to study the 3-dimensional motion of a powder avalanche.

Apart from the geometric and linkage information any fluid dynamics calculation requires additional information and initial and boundary conditions as shown in Figure 3. Together with some information used to control the solution sequence of the main code these are supplied in an interactive fashion.

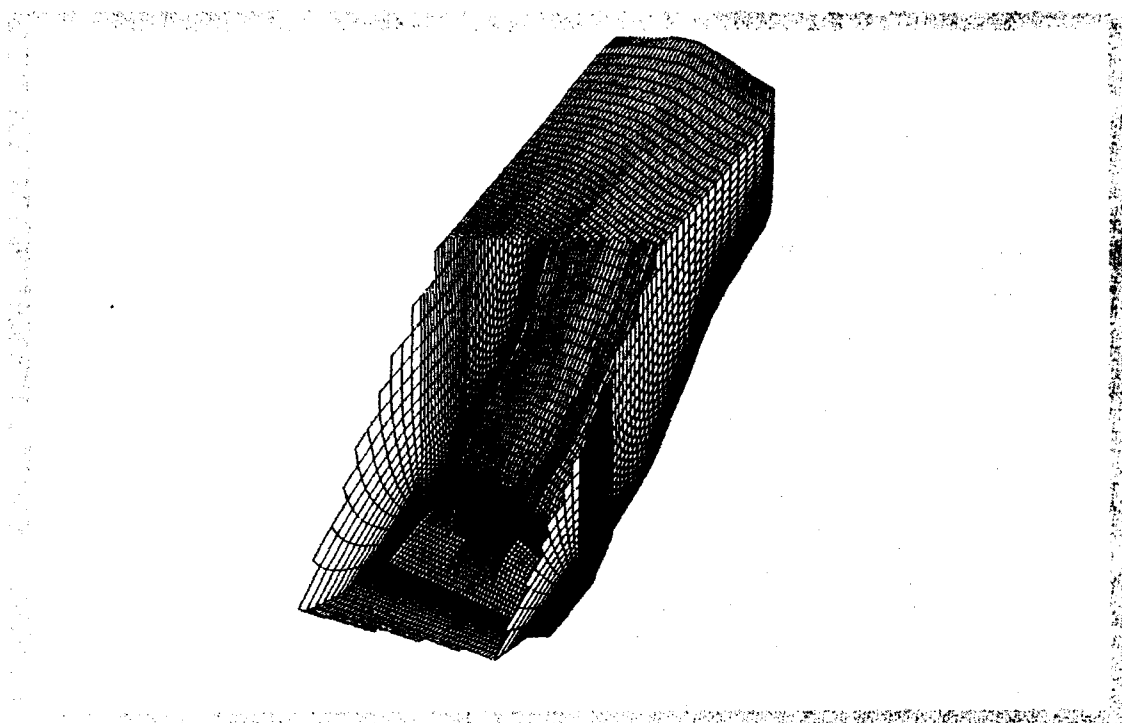


Figure 2: Cut-out of the Complete Computational Mesh

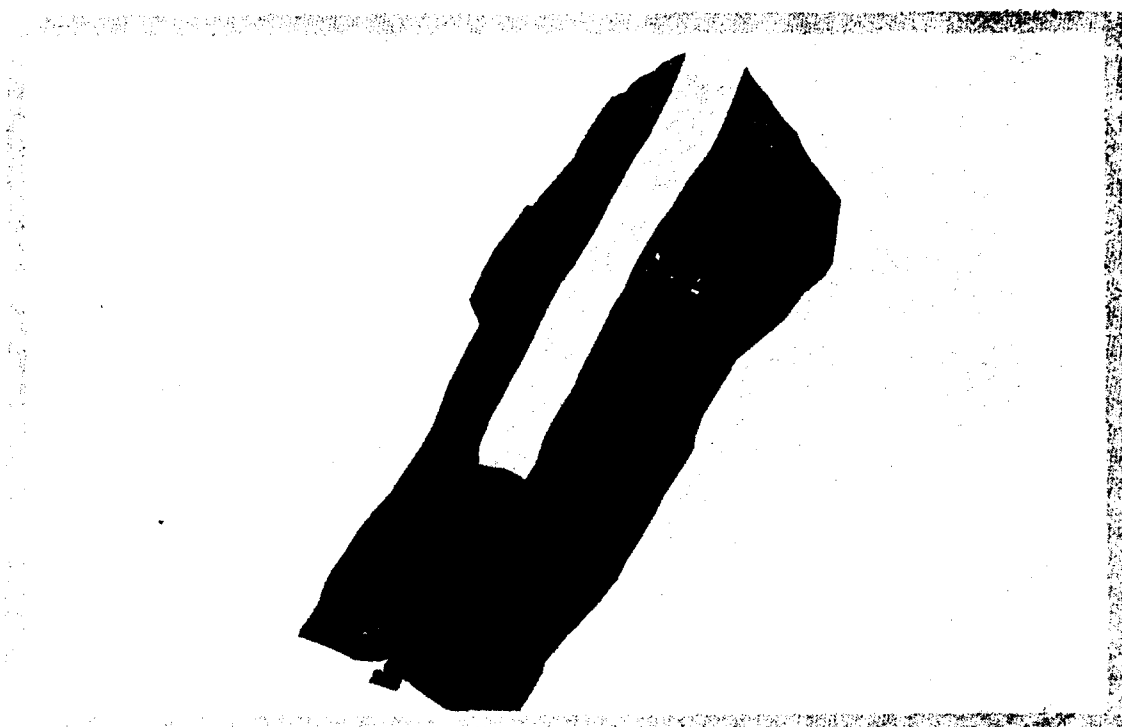


Figure 3: Definition of Boundary Conditions

The main fluid mechanics calculation can demand substantial computing resources due to the size and complexity of the algebraic equations resulting from discretizing equations (1) to (6). Therefore until recently the solution of the main equation systems was mostly performed on mainframes or supercomputers. However, the advent of powerful workstations and servers (their speed sometimes already exceeding that of mainframes) provides a cost-effective alternative and it is already feasible to run large problems on these hardware platforms.

Regarding the post-processing, the most demanding requirement is for a compact and informative means of displaying the results of the calculations. In the case of avalanche simulations this is accomplished by temporal information regarding the size, velocity and dynamic pressure within the avalanche and its periphery. Additionally integral quantities such as the total pressure force exerted on buildings are of interest.

VALIDATION OF THE MODEL

Field measurements concerning the motion of real powder snow avalanches are difficult, remain scarce and are mostly qualitative. Therefore a number of research centres in the past developed physical models in water tanks concerning 2-dimensional flow situations /5,12/ or most recently 3-dimensional flows /2/. The latter experiments were carried out in a water tank with glass walls containing an inclined plate as shown in Figure 4. Dyed salt solutions with a density of $\rho = 1070 \text{ kg/m}^3$ were used as a dense fluid. This fluid was released with zero velocity from a box located at the upper end of the inclined plate. Flow measurements were made from photographs taken at regular time intervals.

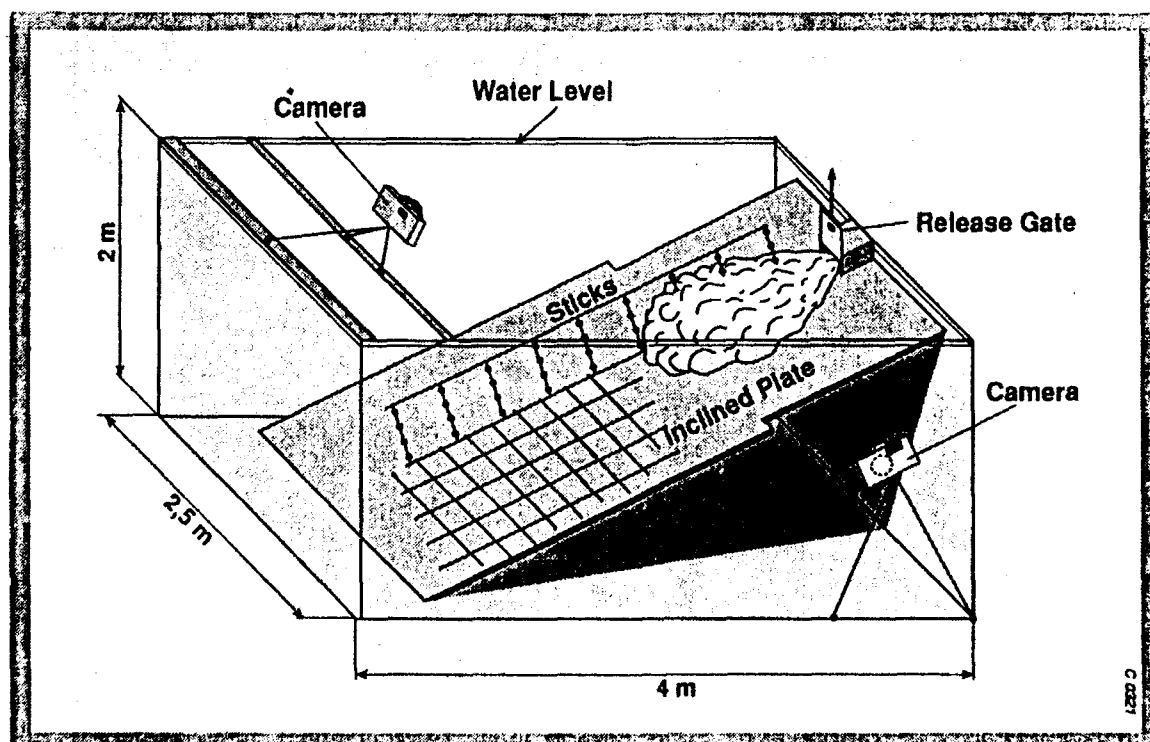


Figure 4: Water Tank - Experiments of P. Beghin and X. Olgne

Typical computational results prevailing at one time-step in the "symmetry-plane" of the laboratory avalanche are depicted in Figs. 5 and 6.

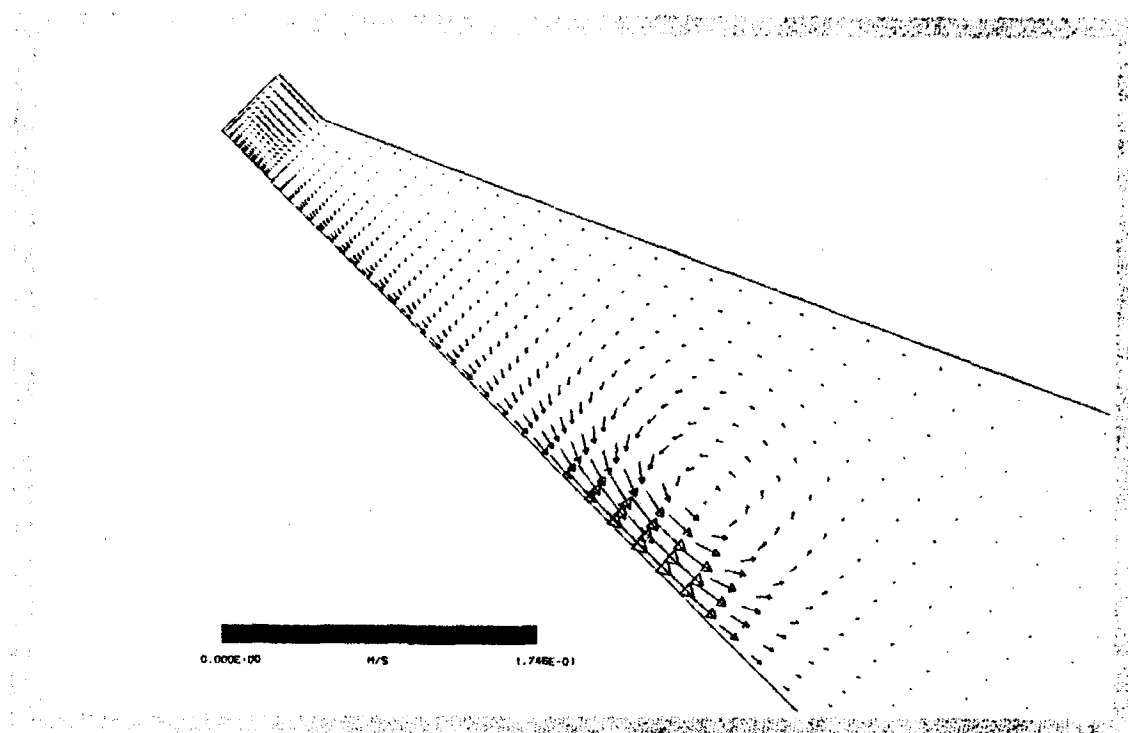


Figure 5: Computed Mean Velocity Field in the Symmetry Plane for a Plate with an Inclination Angle of 45 deg.

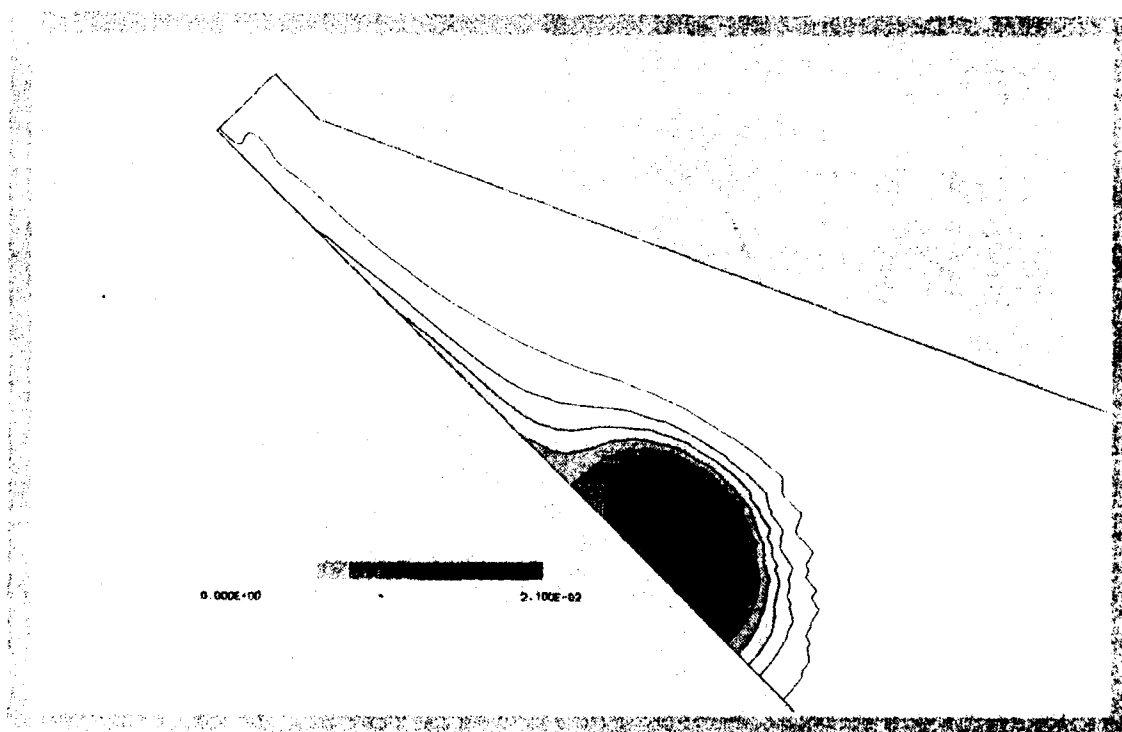


Figure 6: Computed Mass Fraction of the Dyed Salt for a Plate Inclination Angle of 45 deg.

A comparison between computational results and experimental data regarding the height and the width of the "avalanche" with respect to two different plate inclination angles is shown in Figs. 7 and 8. It is evident that excellent agreement can be found.

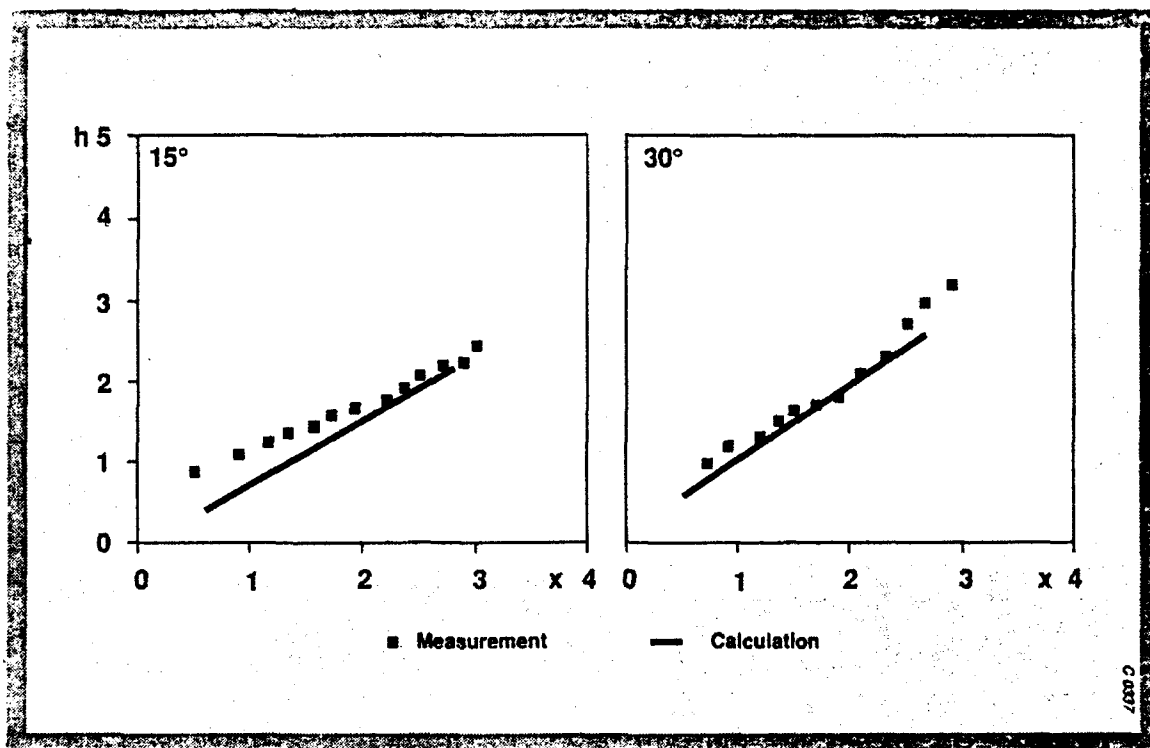


Figure 7: Height of the Flow as a Function of Distance from the Release Gate

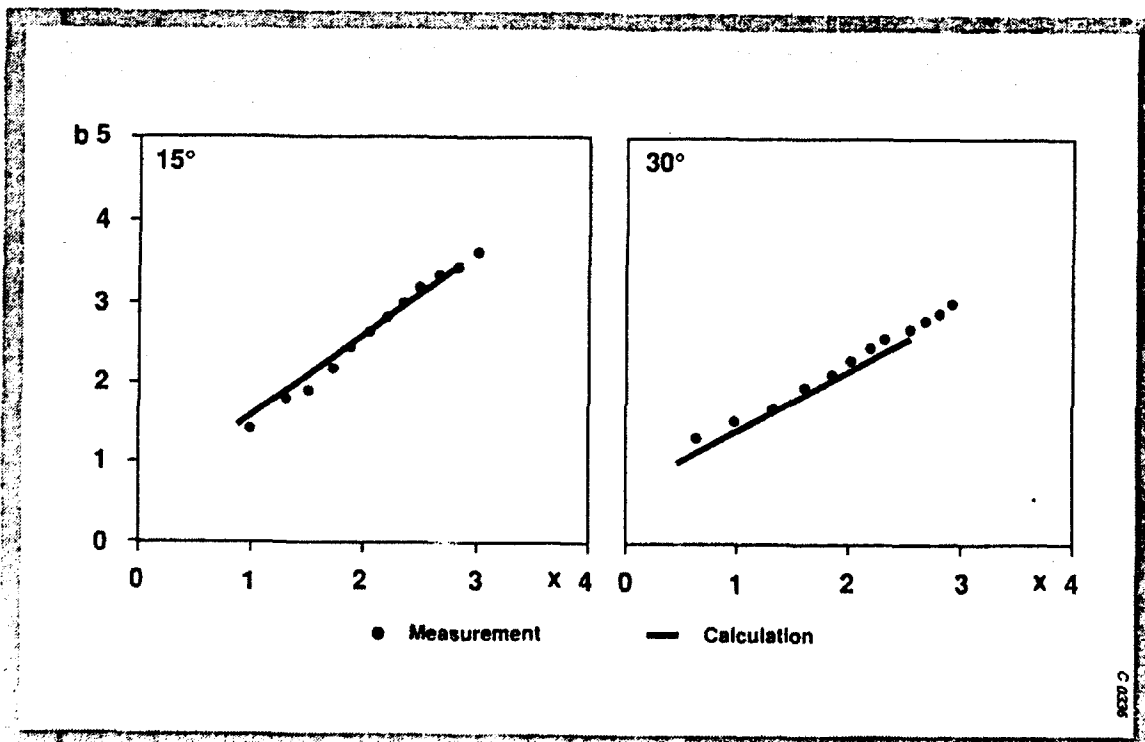


Figure 8: Width of the Flow as a Function of Distance from the Release Gate

With regard to the front velocity of the dyed salt solution good qualitative agreement between experiments and computations can be observed as shown in Figure 9.

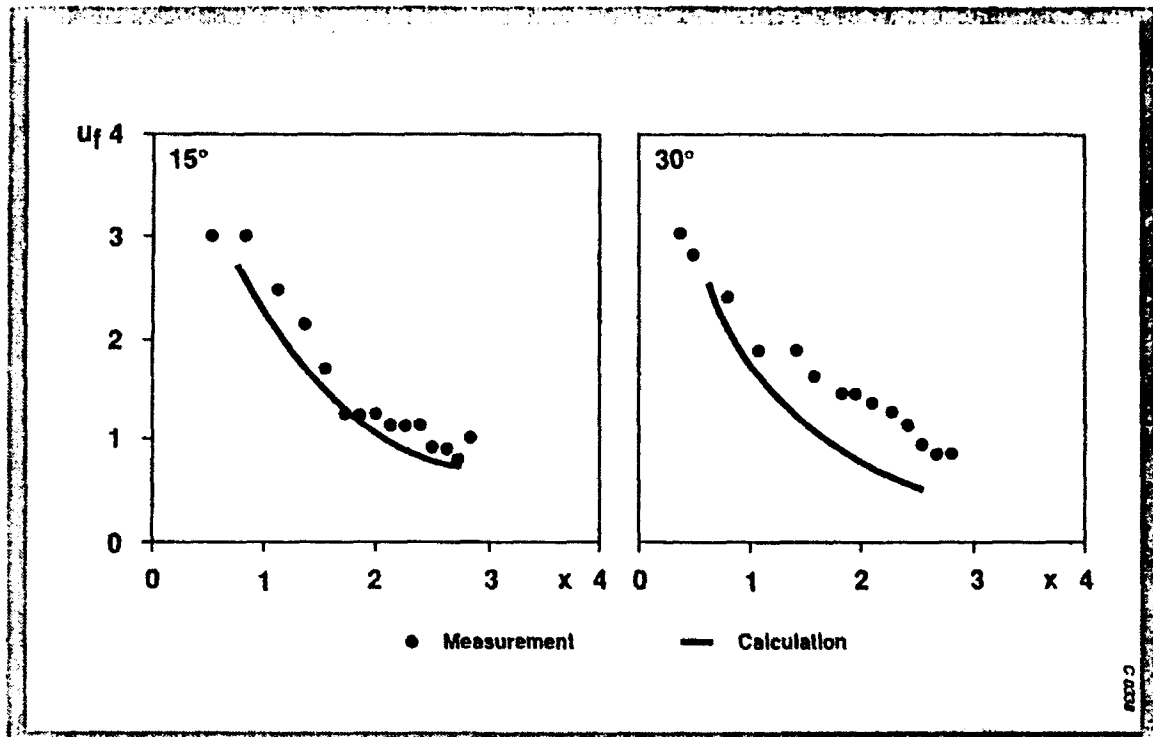


Figure 9: Front Velocity as a Function of Distance from the Release Gate

APPLICATION OF THE MODEL

As already indicated only scarce information is available to validate the model via "real life" problems. However, a first attempt was made in a forthcoming paper /4/ and hence no further effort with respect to this is made here. Instead of this, the following example should serve to demonstrate the application of the model to a problem occurring frequently during the design of motorways in Tyrol (Austria). Since environmental protection groups are opposing conventional avalanche fences which are located on top of the mountain in the starting area of an avalanche, alternative ways to protect human beings, houses and roads have to be found. One way is to build dams at the bottom of mountains as shown for example in Fig. 1. This of course raises immediately questions about the right location and dimension of the dam for effective protection. Three-dimensional simulations in such a case can serve at least as guidelines for the design of these dams.

Figure 3 shows the complete surface model of the avalanche slope, whose attitude is 2373 m. The avalanche is initiated in the

shaded area with a mean density of $\rho_s = 10 \text{ kg/m}^3$. This corresponds to a total snow mass of 3700 tons.

Lack of space prohibits showing the avalanche motion at successive time steps and hence attention is focused only to that point when the avalanche reaches the dam at the bottom of the mountain and when the largest dynamic pressures P_D , defined as

$$P_D = \frac{\bar{\rho}}{2} \bar{u}_i^2, \quad (12)$$

in the area surrounding the dam are occurring.

The mean velocity distribution in a vertical cut plane through the middle of the dam is shown in Figure 10. It gives a clear impression of the enormous height of the avalanche (approximately 100 m), and maximum velocities can be found to be around 70 m/s. However, it can be seen that in this region the motorway is protected reasonably well. The corresponding snow concentration is depicted in Figure 11 and it is evident that the largest values occur between the slope and the dam. The highest dynamic pressures can also be found in this area and on top of the dam (Figure 12).

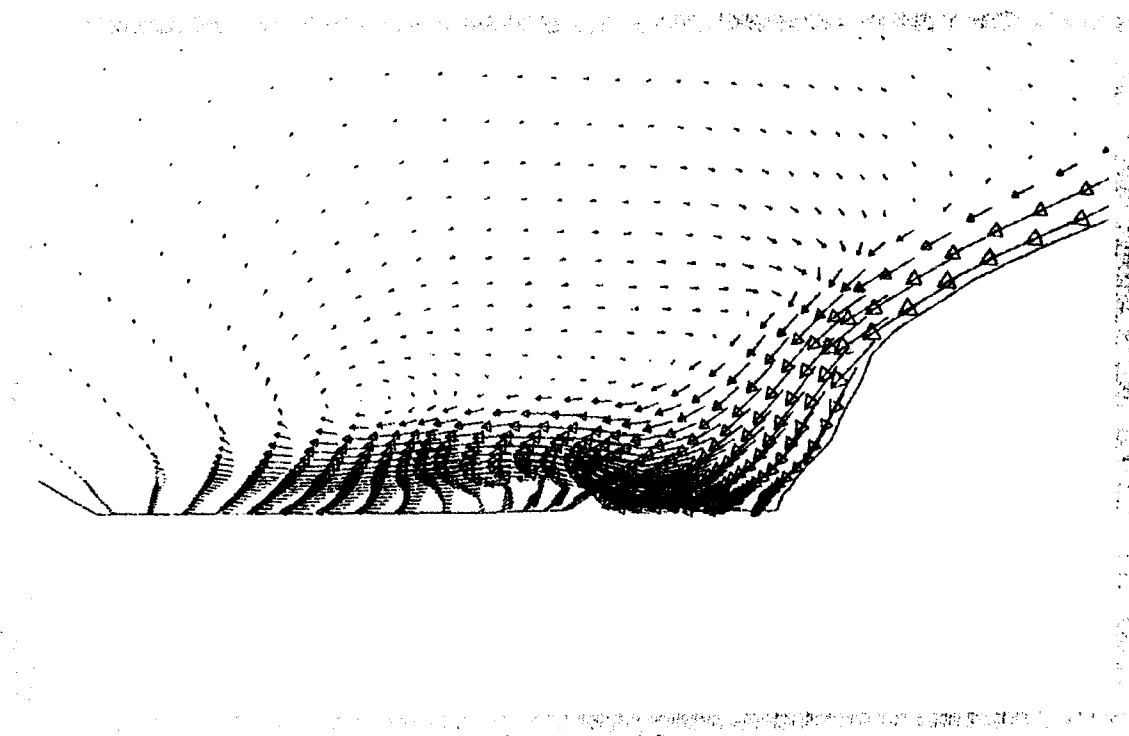


Figure 10: Mean Velocity Distribution in a Vertical Cut Plane
(Maximum Velocity = 70 m/s)

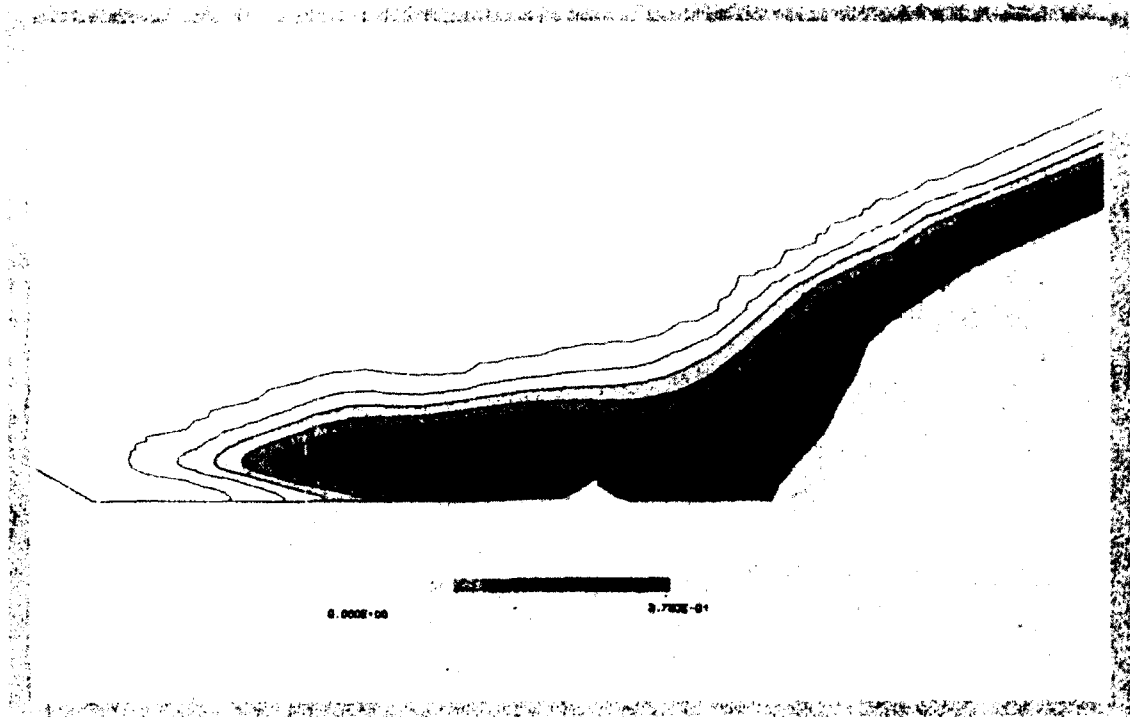


Figure 11: Snow Concentration Distribution in a Vertical Cut Plane

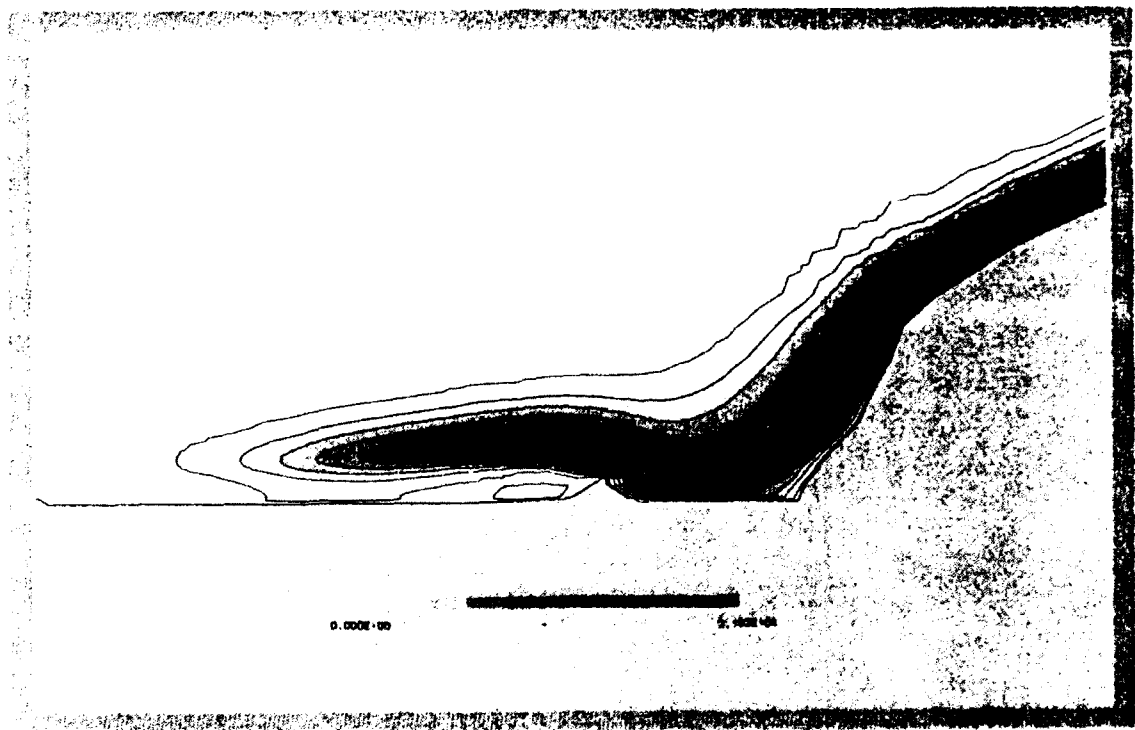


Figure 12: Dynamic Pressure Distribution in a Vertical Cut Plane

Figure 13 shows a front view of the dam base and a part of the avalanche slope. It is obvious that parts of the avalanche (indicated by the black high snow concentration region) are passing the dam on one side, i.e., that the length of the dam is too short. This can also be seen in Figure 14, where the dynamic pressure distribution is displayed.

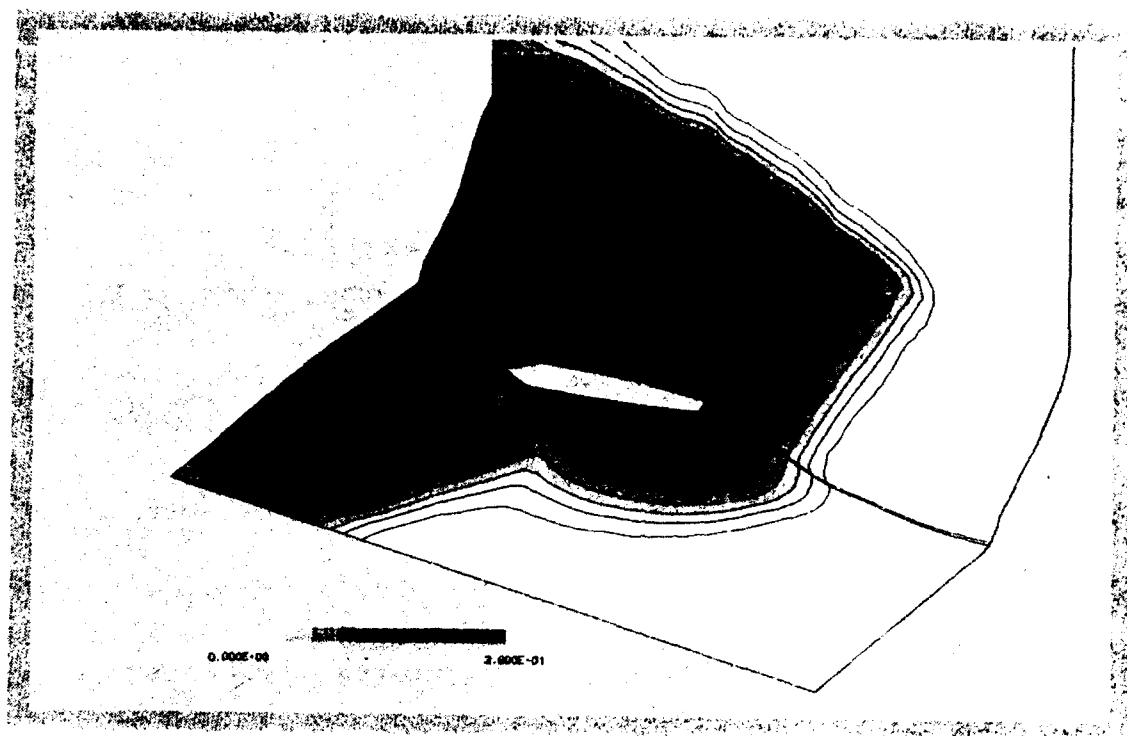


Figure 13: Snow Concentration around the Dam Base

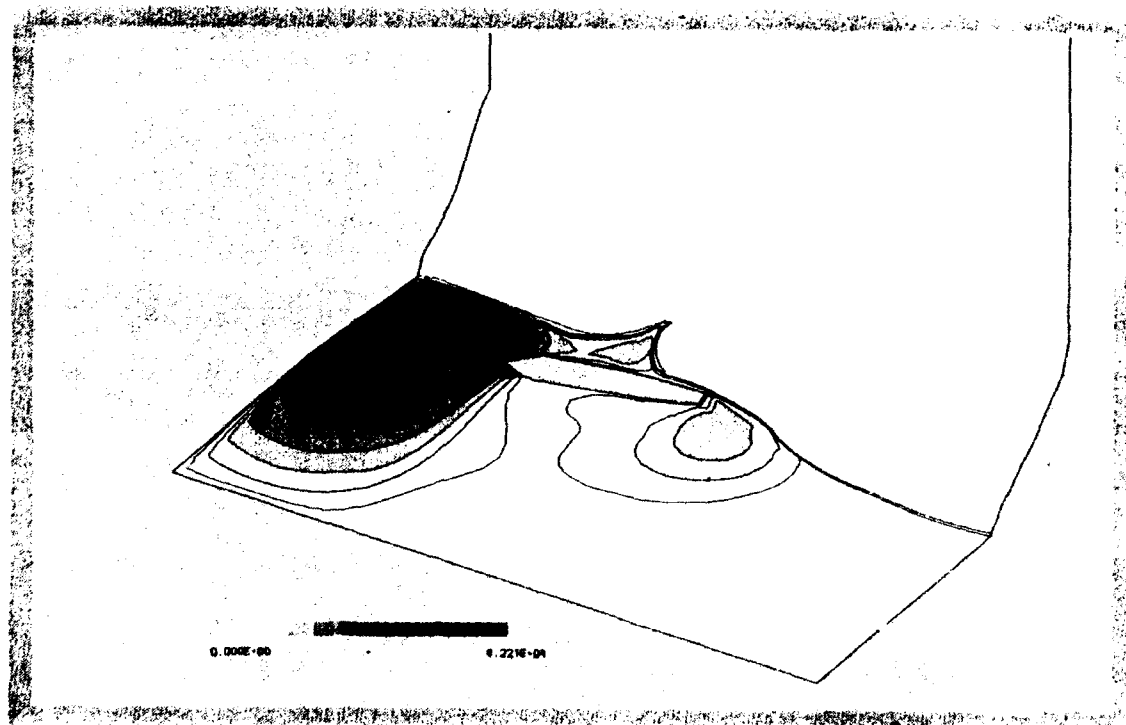


Figure 14: Dynamic Pressure Distribution around the Dam Base

DISCUSSION

This paper has described the first stages in the development of a theoretical model and its computer implementation for calculating the dynamics of real snow avalanches. Currently the model is applicable only to the motion of powder snow avalanches.

The further development of the model is focusing on a number of aspects. Probably the most difficult point is concerned with the principal mechanisms responsible for transition from a dense snow at rest into a flowing avalanche and its subsequent transition to a powder avalanche. Later on, when the avalanche enters the track and sufficient air entrainment is occurring to produce a dilute, turbulent powder avalanche cloud, in practically all cases a flowing part close to the ground still remains. To, at least, partially remedy these weak points the development of an Eulerian 2-phase model is currently under development.

When the avalanche is sliding downhill the processes of snow entrainment and sedimentation compete. As the terrain gradient diminishes, the avalanche emerges into the runout (or deposition) zone where expulsion of entrained air, snow particle sedimentation, and energy dissipation result in deceleration and ultimate cessation of motion. A first attempt to model these effects was suggested in /8/ and it will be implemented in the near future.

It has to be stated that, although in its present form the model is not capable of taking all the above-mentioned physical phenomena into account, the results obtained so far are encouraging.

ACKNOWLEDGEMENTS

The authors would like to thank Dr. P. Sampl for assistance in preparing this paper.

REFERENCES

- /1/ Bachler, G., Brandstätter, W., Ennemoser, A., Ennemoser, C., Mayer, R., Pachler, K., Steffan, H. and Wieser, K., "FIRE-Instruction Manual Version 3.3, AVL-List GmbH., Graz, Austria, 1992.
- /2/ Beghin, P. and Olagne, X., "Experimental and Theoretical Study of the Dynamics of Powder Snow Avalanches", Cold Regions Science and Technology, 19, 1991.
- /3/ Brandstätter, W., "Dreidimensionale Simulation turbulenter Innenströmungen im Automobilbau", VDI-Berichte Nr. 816, 1990.

- /4/ Brandstätter, W., Hagen, F., Sampl, P. and Schaffhauser, H., "Dreidimensionale Simulation von Staublawinen unter Berücksichtigung realer Geländeformen", Zeitschrift für Wildbach- und Lawinenverbauung, 1992.
- /5/ Hermann, F., "Experimente zur Dynamik von Staublawinen in der Auslaufzone", Versuchsanstalt für Wasserbau, Hydrologie und Glaziologie der ETH Zürich, Mitteilung VAW 107, 1990.
- /6/ Kershaw, D.S., "The Incomplete Cholesky-Conjugate Gradient Method for the Iterative Solution of Systems of Linear Equations", J. of Comp. Physics 26, 1978.
- /7/ Launder, B.E. and Spalding, D.B., "Mathematical Models of Turbulence", Academic Press, London, 1972.
- /8/ Parker, G., Fukushima, Y and Pantin, H.M., "Self-Accelerating Turbidity Currents", J. of Fluid Mechanics, Vol. 171, 1986.
- /9/ Reynolds, W.C., "Modelling of Fluid Motions in Engines - An Introductory Overview", Combustion Modelling in Reciprocating Engines, Ed. J.N. Mattavi and C.A. Amann, Plenum Press, New York, 1980.
- /10/ Schlichting, H., "Grenzschichttheorie", Verlag G. Braun, Karlsruhe 1982.
- /11/ Tesche, T.W., "A Three Dimensional Dynamic Model of Turbulent Avalanche Flow", International Snow Science Workshop, Lake Tahoe, California, October 22-25, 1986.
- /12/ Tochon-Danguy, J.C. and Hopfinger, E.J., "Simulation of the Dynamics of Powder Avalanches", Symp. Mécanique de la Neige, Actes du Colloque de Grindelwald, Avril 1974, IAHS-AISH.
- /13/ Watkins, A.P., "Flow and Heat Transfer in Piston/Cylinder Assemblies", Ph.D. Thesis, University of London, 1977.
- /14/ Yee, H.C., "Construction of Explicit and Implicit Symmetric TVD Schemes and Their Applications", J. of Comp. Physics 68, 1987.

Snow Load Prediction in the Andes Mountains and Downtown Toronto

FAE Simulation Capabilities

C.J. Williams, S.L. Gamble and W.W. Kochanski

Rowan, Williams, Davis & Irwin, Inc.
Guelph, Ontario, Canada N1K 1B8

A method for predicting snow loads on large roofs with complicated wind flows and drifting patterns was initially developed by RWDI to determine appropriate snow loads for the complex roof shape of a retractable roof stadium. The method was first described in detail at the First International Conference on Snow Engineering (Irwin and Gamble, 1988). Scale model wind tunnel tests to determine the local velocity field over the roof, and a computer program to examine the snow load time histories in elemental areas on the roof are the key components of the Finite Area Simulation (FAE) method. Drifting snow, falling snow, rainfall, temperature and solar insolation are considered by calculating, in time steps of from one to three hours, the snow loads in each elemental area for many years of meteorological data. The resulting load histories in each element are then used to determine the overall load and non-uniform load distributions appropriate for structural design.

FAE simulations were used recently to predict the snow loads on an industrial building the Andes mountains, which is an area of extremely high snow loads, and on a load sensitive glazed atrium in downtown Toronto. The wind tunnel tests required to determine the wind speed variations over the two roofs resulting from roof shape and surrounding buildings in Toronto, and from the surrounding mountainous terrain of the Andes are discussed.

The simulations give many useful insights into the way different factors influence the snow accumulations in these two areas, which represent two global extremes in terms of snow load potential.

INTRODUCTION

Building codes, such as the National Building Code of Canada, can adequately determine snow loads for most situations. The consulting engineering firm of Rowan, Williams, Davies & Irwin Inc. (RWDI) was recently asked to provide snow loads for two cases which could not be assessed using building codes because, in the first case:

- the subject roof is located in an area of extreme snowfall in the Andes mountains and is sheltered from the prevailing winds by the surrounding topography,

and in the second case:

- the roof is a complex shape surrounded by high-rise buildings in downtown Toronto and is glazed with a considerable heat loss through the roof.

Snow loads were produced for these two contrasting cases using the FAE simulation method developed by RWDI for prediction of snow loads on a large span roof of abnormal shape (Irwin and Gamble, 1988). This method uses scale model wind tunnel tests to define the wind velocity patterns over the roof and surrounding areas, and computations based on these patterns to determine how snow will drift over the roof. The cumulative effects of drifting over a winter season are considered by using detailed local meteorological records of wind direction, wind speed and snowfall to compute the snow redistribution at three hour intervals for the entire winter. Other important variables such as solar insolation, air temperature, heat loss through the roof, drainage of meltwater through the snowpack, etc. are allowed for in the computation. Long term snow loads are predicted by repeating the above computation for up to twenty five years of data and then using extreme value plots.

This paper discusses the setup of FAE simulations for the above two cases, presents some of the results of the FAE calculations to demonstrate the versatility of the calculation method and provides snowload information on these two contrasting cases. The details of the FAE calculation method are not presented as this information can be found in other references (Gamble, Kochanski and Irwin, 1991).

THE ANDES MOUNTAIN INDUSTRIAL BUILDING

The collapse of a portion of the stepped roof of an industrial building, which is shown in Figure 1, at a mine site and the requirement to assess snow loads for the redesign initiated the study. The site is located due east of Santiago, Chile, near the border with Argentina at an elevation of 3,500 metres in the Andes mountains where annual snowfalls in excess of 14 metres have occurred in recent years. It was considered inadvisable to use a building code approach because of the extreme snowfalls and the abnormal wind flows created by the local topography.

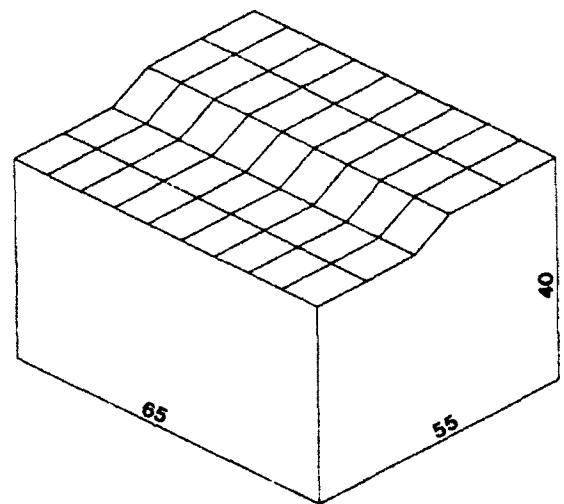


Figure 1. Andes Mountain Industrial Building

Wind Tunnel Tests

To assess the effects of the severe local topography on the wind conditions around the mine site, a 1:2000 scale topographic model was constructed from the contour plans of the area. A photograph of the test model is shown in Figure 2. The construction of the scale model was necessary to relate the wind conditions recorded at the local meteorological station to those that are present around the study building. The test model was placed in a boundary layer wind tunnel where wind blowing over the model simulates wind blowing over the actual site. Wind speeds and local wind directions were recorded for 16 wind directions (i.e. north, northeast...northwest) using surface wind speed sensors at 5 locations around the site.

FAE Setup

An orthogonal grid for the FAE simulation was laid out as shown in Figure 1 for the study building with 45 area elements. As the roof consisted of a simple stepped configuration the local wind speeds near the roof were estimated based on the results of previous wind tunnel tests conducted on similar structures, and on our knowledge of the wind flow patterns around those structures. Flow visualization during the wind tunnel test was also used to confirm these estimates. For the flat areas of the roofs, the local wind velocities were assumed to be uniform and about 0.7 times the local velocity in the vicinity of the buildings. Wind speeds in the step region of the roof were assumed to be zero to simulate the accumulation of snow in the roof step. Local wind directions at each grid intersection were all assumed to be in the same direction as the approaching wind direction in the vicinity of the buildings. Each intersection of the grid lines was assigned x,y,z co-ordinate values.

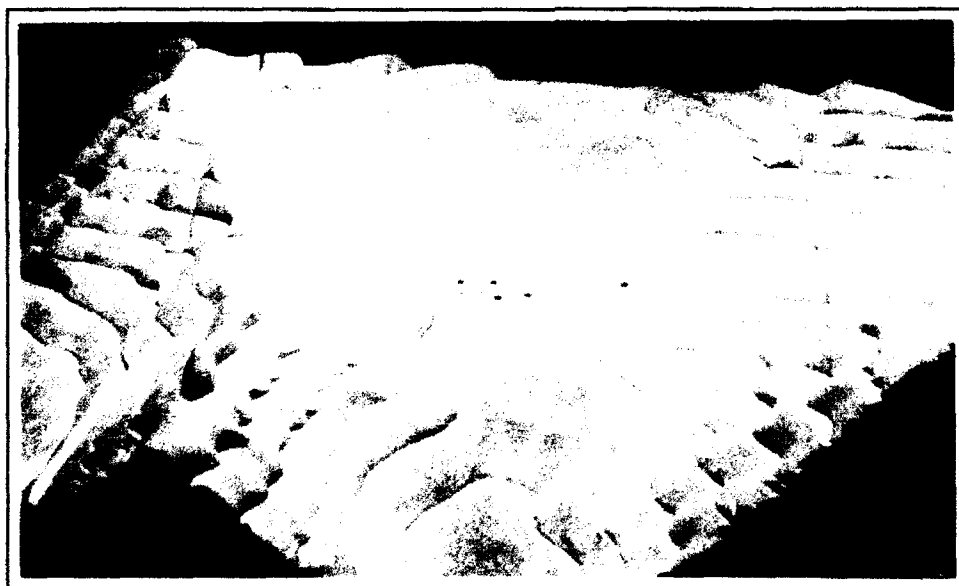


Figure 2. Topography Surrounding Mine Site

Ground Snow Load

The simulation was first run to calculate the ground snow load that would be encountered at the mine site using the local meteorological information obtained from data taken from the mine site. The simulated peak ground snow loads for each year of the 10 year period are shown in Figure 3. As can be seen, the ground snow loads are high for years 1982 and 1987, with values of 14.5 kPa and 10.8 kPa respectively.

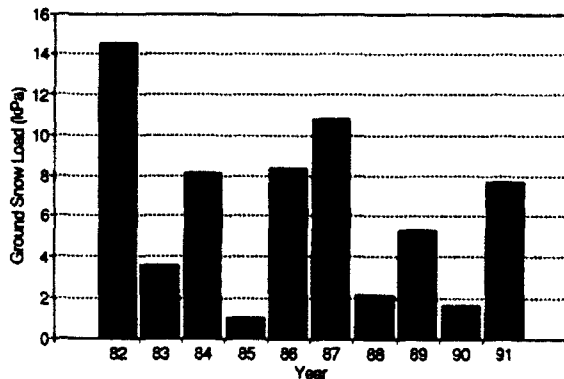


Figure 3. Ground Snow Load History

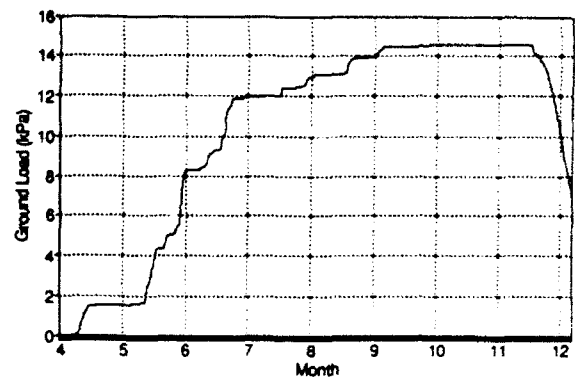


Figure 4. Ground Snow Load - 1982 Time History

The FAE method also allows the time histories of the ground snow loads for individual winters to be determined. A time history consists of the accumulated amount of snow on the ground at each three hour period of a particular winter. The winter of 1982 is shown in Figure 4 and it can be seen that from May to June there was a sudden increase in the ground snow load over a short period of time. This snow remained on the ground until subsequent storms deposited more snow at which point a maximum was reached in November. After that point, significant melting took place over a short period of time as a result of a warming trend.

The 20 and 30 year ground snow loads were determined from the extreme value plot (Fisher-Tippet Type I distribution) presented in Figure 5. As can be seen from the plot, the 20 year return ground snow load is 17.2 kPa and the 30 year return load is 18.9 kPa.

The ground snow loads found with the simulation are quite large, although not without precedence in alpine regions. Taylor (1988) considers snow loads found at high altitudes on the west coast of British Columbia, Canada. In this study, 30 year return ground snow loads of 32 kPa were predicted.

Study Building Roof Loading Simulation

The simulation was then run for the study building for the ten years of meteorological data available. Information about the building geometry, local wind speeds and local wind directions are used by the FAE model to carry out the simulation. For each elemental area created on the roof, the increase in snow load as a result of snowfall, the redistribution of the

load by drifting (local wind speed and direction), and the reductions in load from melting (due to the ambient air temperature) were calculated for each three-hour interval. Critical load conditions, such as the maximum overall snow load on the roof or maximum snow load in each elemental area was determined for each year of data.

Calibration of Computer Simulation

In order to provide a calibration of the computer simulation the results of the FAE simulation, using the 1991 data set, were compared to field measurements taken on various roofs shortly after the building collapse in July 1991. The following tables summarize the comparisons:

Location	Measured Snow Load (kPa)	Simulated Snow Load (kPa)
Lower Roof (electrical building)	12.5	13.0
Upper roof (industrial building)	8.2	7.7

It can be seen from this data that the FAE simulation calibrated well to the field data obtained from the study building.

Snow Load

From the snow simulations carried out, the maximum snow loading for each element on the roof was determined for each of the ten years of meteorological data. From the distributions simulated, it was verified that for the 20 and 30 year return periods, there was more than enough snow transport to completely fill the wedge-shaped volume in the roof step region of the building. It was noted from the time history plots that this occurs fairly early in the year after which it is still possible to accumulate virtually all the ground snow load on top of this drift in the step region. The FAE simulation therefore illustrated that in the worst case loading scenario the ground snow load for extreme years would directly add to the load produced by filling of the step region. An illustration of this loading case is shown in Figure 6. The result is a peak snow load found in the central region of the roof step of 25.4 kPa for the 20 year return period and a load on the flat section of the roof of 17.2 kPa.

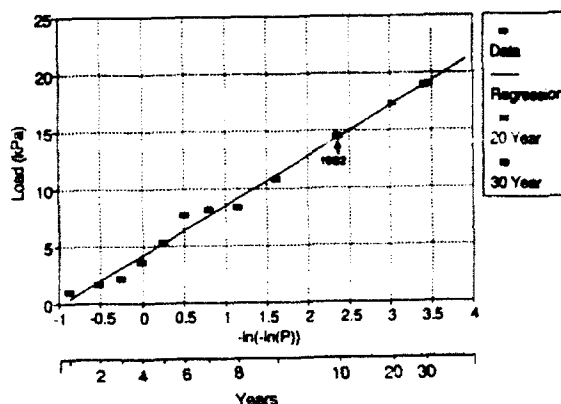


Figure 5. Extreme Value Plot - Ground Snow Load

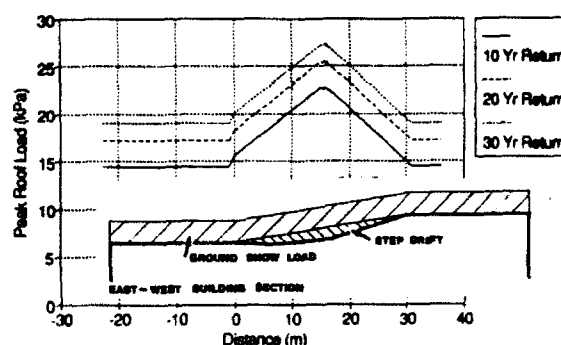


Figure 6. Peak Loads - Ground Load plus Step Load

Melt Water Effects

Melt water migration was also considered in the analysis. The meltwater is caused by two different processes:

1. Melting from the top of the snow pack due to warm atmospheric conditions.
2. Melting from the bottom of the snowpack due to heat loss from the roof.

The simulation showed that the melt water caused by atmospheric conditions is retained within the deep snow pack on the building roof. Since this water is merely absorbed, it is not free to migrate and, therefore, will not change the loads on the roof. Significant amounts of water are not released until rapid melting occurs in the spring.

The concern over melt water on the roof generated by heat loss through the building is how the water redistributes itself due to the roof slopes. It is assumed that the melt water generated on the flat sections of the roof stays in place, thus not changing the load. However, on the sloping stepped section of the roof, the potential exists for the water to run down the slope and pool at the bottom, causing an increase in load at the base of the slope.

To illustrate the effect of the melt water migration, two possible scenarios were simulated. The following assumptions were made: inside building temperature at the roof level is 10°C; snow temperature at the roof-snow pack interface is 0°C; roof insulation of 50 mm expanded polystyrene panel; and roof insulation effectiveness reduced by 25% due to air leakage around the panels.

Scenario 1. Water movement down the slope with drains

In this situation, the melt water from the slope runs down the slope and is assumed to be effectively drained from the lower part of the roof. The net effect of this situation is a modest lowering of the loads in the step region. As seen in Figure 7, the peak loads in the sloped region are reduced by about 3 kPa.

Scenario 2. Water movement down the slope without drains and with ice dams

In this situation, the melt water runs down the slope and is retained in the step region. This retention would be the result of blocked drains or the buildup of an ice dam to contain the water. As can be seen in Figure 7, there is a modest reduction in load on the slope (3 kPa) but a large increase in load at the base of the slope where the water pools. The magnitude of this load peak is dependent on the exact geometry of the ice dams and the roof drains, but for this example, the 20 year peak load value can be increased as much as 12 kPa.

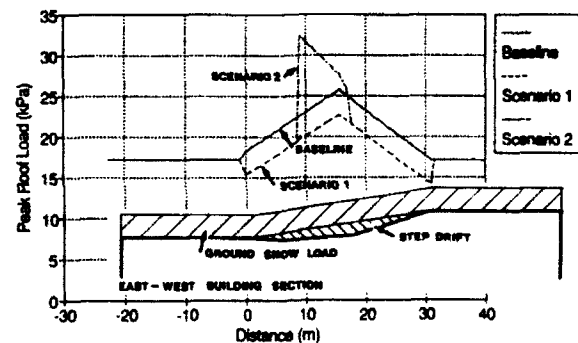


Figure 7. Peak Step Loads - Snow plus Meltwater

Apart from providing roof loading and design information on the effects of heated drains, a regular snow removal program was also discussed with the client.

COMMERCIAL BUILDING IN DOWNTOWN TORONTO

As a result of the complex geometry of the glazed roof under consideration in this case and the close proximity of adjacent low-rise and high-rise buildings, an FAE simulation was conducted to determine appropriate snow loads for the roof, taking into account the properties of the roof and the surrounding environment.

FAE Model Setup

Due to the effect of the surrounding buildings on the wind flows that occur in the area a 1:500 scale model of the study site was constructed and tested in RWDI's water flume wind/snow simulator for 8 key wind directions. In the water flume a water flow over the model is adjusted to simulate atmospheric wind flow and white silica is introduced into the water flow to simulate drifting snow (Irwin & Williams, 1983). The objectives of these tests were a) to determine how snowfall is deposited on the roof for various wind directions, b) to determine how snow drifts from one roof to another roof, and c) to give preliminary indications of where major snow accumulations occur due to drifting. The model used for these tests is shown in Figure 8. The scale model was then modified in order that the relative distribution of falling snow on the roof could be measured for different wind directions. This modification consisted of constructing a honeycomb of small cells in the roofs in order to trap falling sand(snow) thus preventing the sand(snow) from drifting. In this way the falling snow depth on the roof could be related to the ground snow depth. Ground snow is defined as the accumulation of snow that would occur in an open flat area, where it is unaffected by surrounding structures and wind. The snow simulation was calibrated against the ground snow load of 1.8 kPa for Toronto.

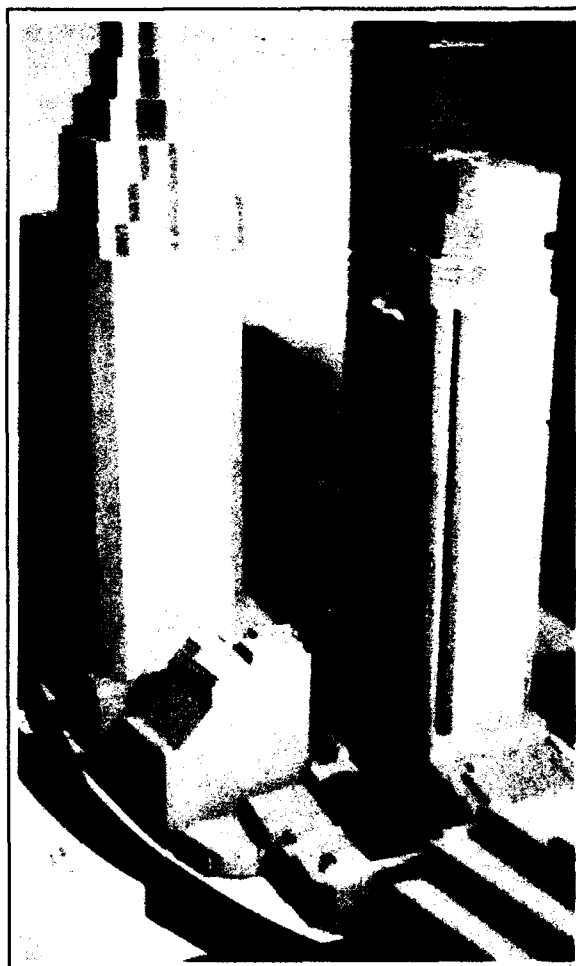


Figure 8. Downtown Toronto Glazed Roof
- 1:500 Scale Model

An FAE model of the drifting on the study roof and the various surrounding roof surfaces was then established. The model included roof surfaces that were adjacent to the study roofs in order that snow could drift from these adjacent roof surfaces onto the study roof. Essentially the roof was divided into 540 elemental areas by an orthogonal grid system.

Wind Tunnel Tests

A 1:200 scale model of the study site was then constructed and surface wind speed sensors were installed on the roof surfaces at key locations. The model was tested in RWDI's boundary layer wind tunnel to obtain wind speed ratios at each sensor location for 16 wind directions. In order to determine the direction of the wind at the various sensor locations, lightweight wind vanes were placed in the sensor holes. The direction of the wind was then visually determined and recorded for 16 directions. This model is shown in Figure 9. The 1:200 scale normally would have been sufficient to obtain a velocity distribution over the roof surface; however, because of the numerous peaks and valleys on the roof, the 1:200 scale model could not provide an accurate velocity profile down into the valleys. Therefore, a larger 1:50 scale model was constructed and tested in the wind tunnel. These data were then combined with the data from the 1:200 scale model test, that took into account the effect of surrounding buildings, to produce an overall velocity distribution on the roof. The 1:50 scale model is shown in Figure 10.

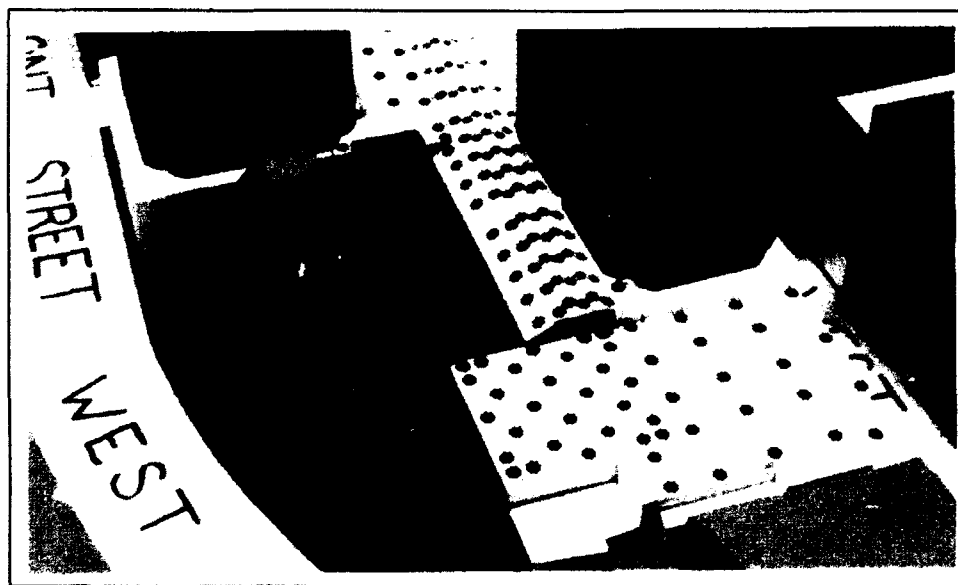


Figure 9. 1:200 Scale Model

FAE Simulation

From the predicted wind velocities at the four corners of each elemental area, the snowdrift fluxes across the four sides of the element were computed and the increase or decrease in the mass of snow in each elemental area, as a result of drifting, was computed.

From the meteorological records of daily snowfall the amount of snow falling onto the element in a given three-hour interval was estimated. Likewise, meteorological records for temperature, when combined with solar radiation data and building heat loss data, determine the melting rate for the snow in the element. Thus computations were made for the amount of snow melted in the element. By stepping through the meteorological data, the increase in snow load as a result of snowfall, the redistribution of load by drifting, and the reductions in load from melting, were evaluated in a detailed manner for all 540 elements.

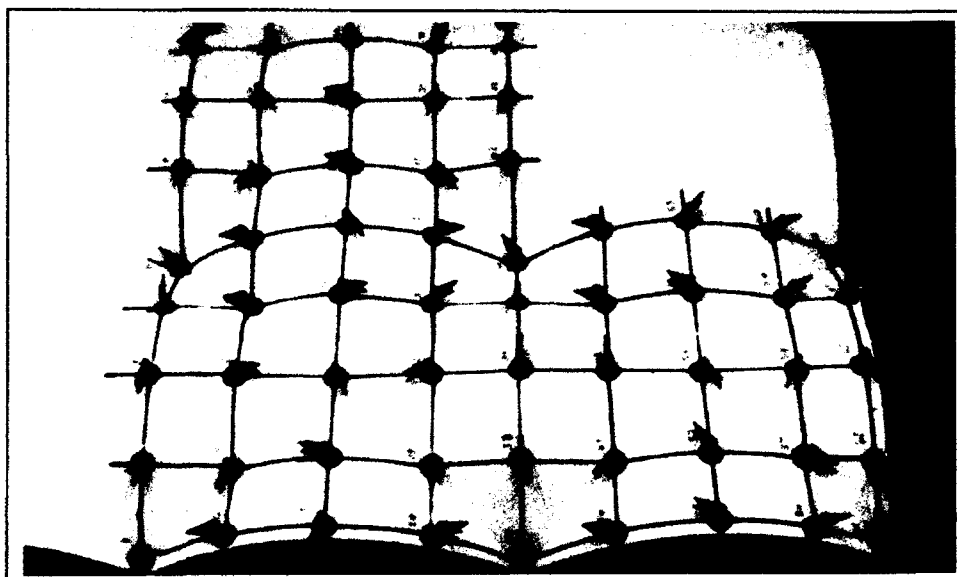


Figure 10. 1:50 Scale Model

ADDITIONAL FAE CONSIDERATIONS

Absorption of Rain

The amount of rain that snow can retain without the rain draining out of the snow is a highly variable quantity, depending heavily on whether or not there are ice layers in the snow. The computer simulation assumed that the snow could retain up to 50% of its own weight of liquid water before the water drains out.

Melting

The melting of snow is a complex phenomenon affected by air temperature, wind, direct short wave solar radiation, indirect radiation, long wave radiation and latent heat transfer. Depending on the thermal insulation of the building envelope, a certain amount of heat will escape from inside the building. A portion of this heat will warm up the snow or ice layer, and the rest (depending on the hardness and thickness of the layer) will escape to the outside air. If the sun comes out, the snow or ice will absorb solar radiation, causing further warming. When

the warming raises any of the snow or ice layer to the melting point, melting will occur. The resulting rate of melting will change continually as the outside temperature and the depth of the snow and ice layer changes. It is therefore continually recalculated by the simulation.

Heat Loss Through the Glazed Roof

For the study roof, the glass was assumed to be double glazed and the interior temperature was assumed to be 21°C. The simulation assumed that the interior temperature will be maintained at the desired level. If there is a situation of a power failure it was assumed that it will not last for a long period of time as this is a commercial building. The cool-down period in the event of a power failure would generally be slow enough and the normal melting rate a slow enough process that a power failure would not be critical to the outcome of the snow loads on the roofs.

Sliding Snow

A layer of snow on a sloped roof may harden after a time under exposure to wind and fluctuating temperatures. The snow will slide as soon as its weight is sufficient to overcome the adhesion to the roof surface. If the snow is dry, the required weight can be quite high depending on the slope angle and the roof material. If the snow is not dry, and a liquid film exists between the roof structure and the snow layer, there will be very little adhesion. In that case, sliding will occur freely on most smooth surfaces, regardless of the slope angle and the weight of the snow layer. A liquid film will exist at the snow-roof interface only if the temperature there reaches 0°C.

Snow Load Predictions

The loading on the roof for a uniform distribution is presented in Figure 11. As a result of snow blowing onto the study roof from an adjacent higher roof an increase in snow loads along the edge of the study roof was noted, particularly at the corner zone which had a maximum uniform snow load of 2.1 kPa. Loading in the central areas of the roof is primarily a result of the roof shape. The fairly deep valleys (2.5 m) act as traps for the snow where snow can easily drift in but cannot drift out. If the snow is allowed to slide towards the centre of each area concentrated snow loads of 3.8 kPa in the central area and 5.8 kPa could result as shown in Figure 12. A recommendation arising from the study was to install snow guards in the valleys, to prevent snow from sliding, and heat traced drains at the bottom of each valley to prevent meltwater from accumulating.

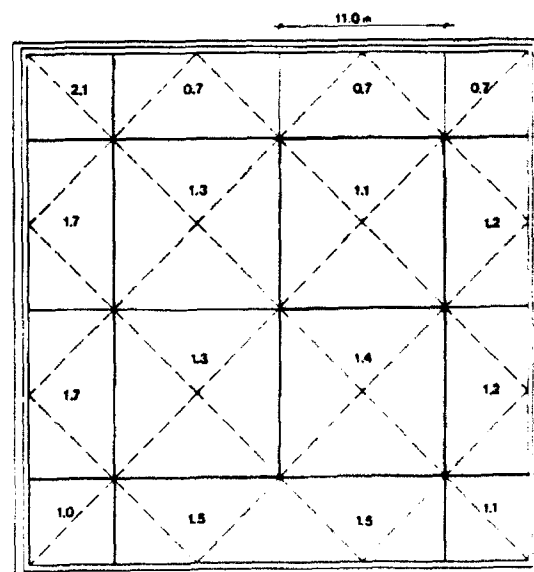


Figure 11. Uniform Distribution - 30 Year Snow Load (kPa)

REFERENCES

Gamble, S.L., Kochanski, W.W., Irwin, P.A., 1991, "Finite Area Element Snow Loading Prediction - Applications and Advancements", Proceedings International Conference on Wind Engineering, London, Ontario, Canada.

Irwin, P.A. and Gamble, S.L., 1988, "Predicting Snow Loading on the Toronto SkyDome", Proceedings First International Conference on Snow Engineering, Santa Barbara, California.

Irwin, P.A. and Williams, C.J., 1983, "Applications of Snow Simulation Model Tests to Planning and Design", Proceedings Eastern Snow Conference, Vol. 28, 40th Annual Meeting, Toronto.

Taylor, D., 1988, "Roof Snow Loads in Deep Snow Regions", Proceedings First International Conference on Snow Engineering, Santa Barbara, California.

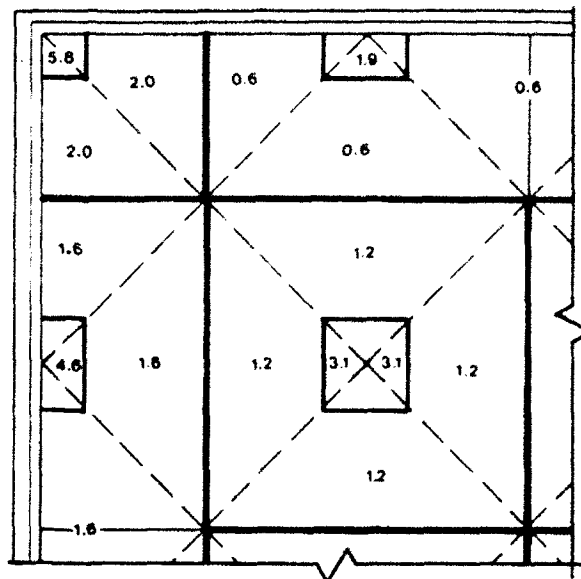


Figure 12. Loading Assuming Sliding
- 30 Year Snow Load (kPa)

Investigations on Snow Disasters and Development of a Disaster Potential Index

Takeshi Ito

Akita National College of Technology
1 Bunkyo-cho, Iijima, Akita-shi, Japan 011

ABSTRACT

This research aims to summarize winter conditions using meteorological parameters. Cold and snow are attributes of winter weather in the world's cold and snowy regions. Factors influencing them are mainly air temperature, the duration of sunshine and the quantity of snow. To analyze winter weather in snowy regions, a statistical potential index was proposed. The index (I_c) consists of seven meteorological parameters. Various kinds of data were collected for the period of 1891 to 1990 from Japanese observatories in snowy regions. The proposed index shows that 1945 was the maximum value, which means the most severe winter, and 1989 was the mildest winter since weather observation began. To evaluate the index synthetically, a principal component analysis was performed, and the analytical results showed that the proposed index is useful and coincides with the snow disasters that have occurred in the past.

INTRODUCTION

In recent years, new kind of snow disasters have been increasing due to the development of transportation methods, the spread of dwelling areas and the changes in many social conditions.

We should objectively consider these phenomena. With respect to snow, the time of snowcover, amount of snow, and the occurrence of heavy snowfalls depends on the individual region. By generalizing these phenomena in one term, a statistical characteristic potential index for each point can be made.

However, weather phenomena have physical dimensions and therefore, for the purpose of evaluating them to the same standard, their variations were standardized into random variables (Z -scores) and T -scores. Next, correlation analysis was carried out. As a result, seven parameters were selected to make the index " I_c " as is defined in the next section.

This paper describes an attempt to precisely define the relation

between winter weather circumstances and snow disasters using proposed index "Ic" and the results of principal component analysis..

To calculate Ic, data were collected from Japanese observatories in snowy regions for the period of 1891 to 1990. Using time series analysis of Ic, 1945 showed the maximum value, which means the most severe winter. On the other hand, 1989 showed the minimum value, which means the warmest winter since weather observation began. In recent years, this index has had a tendency to decrease. If a value is >2.5 , snow disasters occur somewhere in Japan. This coincides with past data and with results of principal component analysis.

AN INDEX OF WINTER WEATHER CIRCUMSTANCE

A world-famous heavy snowfall region exists in Japan even though it is located at relatively low latitude.

In 1956, the Japanese Government made a law to relieve problems caused by low air temperature and frequent heavy snowfalls. The law was made with two parameters: the air temperature and the quantity of deposit snow.

However, referring to snow, the time of snowcover, the occurrence of sudden heavy snowfalls, the quantity and the quality of snow depend on the individual region. Because of these different conditions in each point, various types of snow disasters are frequent in spite of the comparatively small area involved.

Fig.1 shows the trend of damages due to natural disasters in Japan, in which the largest number are caused mainly by typhoons, heavy rainfalls, mud flows, and earthquake. Snow disasters are relatively small; however, the damage appears in every year as is shown in Fig.2. According to this figure, remarkable damages were observed over the whole Japanese archipelago in 1963.

In recent years, snow disasters with more than 100 persons killed appeared in 1981 and 1984. From the record, new types of damages especially affecting older persons are gradually increasing.

Fig.3 shows a distribution map of the average of annual maximum depth of snowcover (Smax) in Japan and patterns of daily changes of snow cover at the largest Smax recorded in the past. As is shown in the figure, each point has a regionality. That is, from the view point of snow disasters, the time of snowcover, the occurrence of sudden snowfalls, and the quantity of deposit snow depend on the regions. In addition to these, if we take other factors, such as those very close to the real lives in the snowy regions, a new characteristic index will be made.

For this purpose, we tried several times to choose characteristic parameters that emphasize the winter weather. As a result, the following

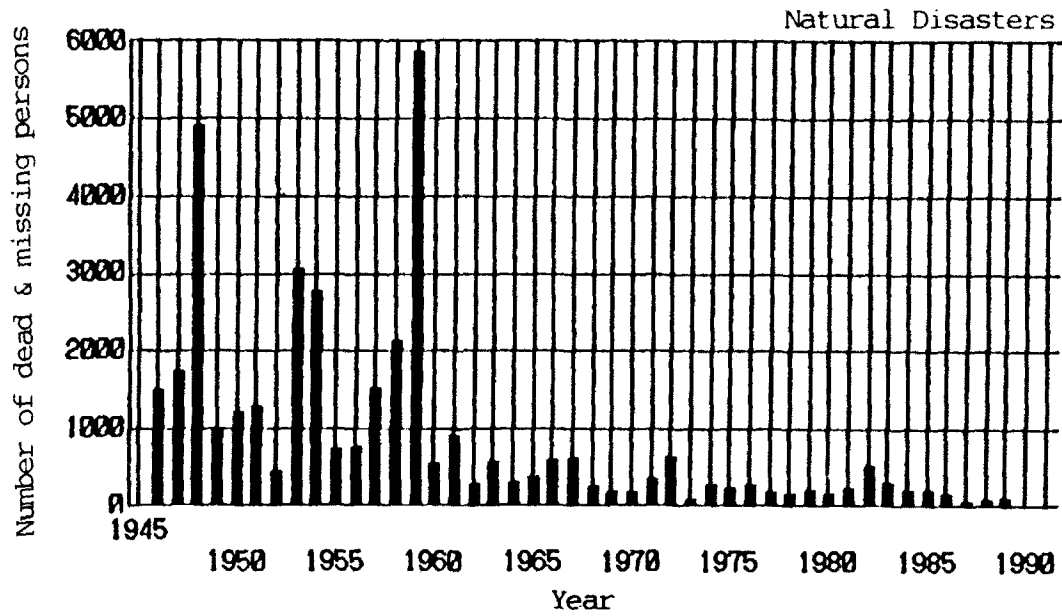


Fig.1 Number of dead and missing persons due to natural disasters in Japan.

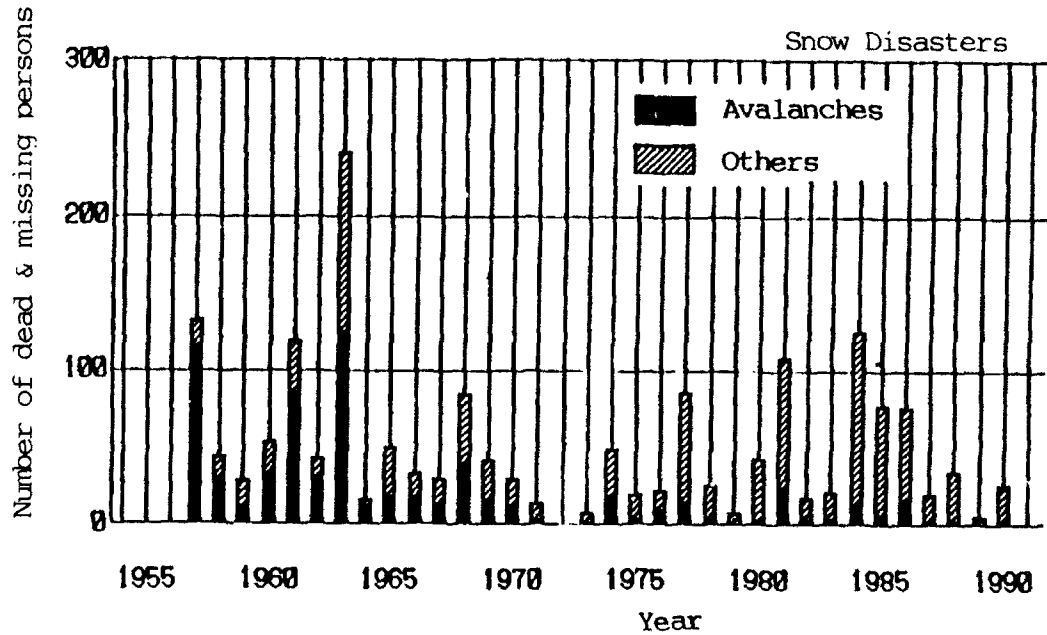


Fig.2 Number of dead and missing persons due to snow disasters in Japan.

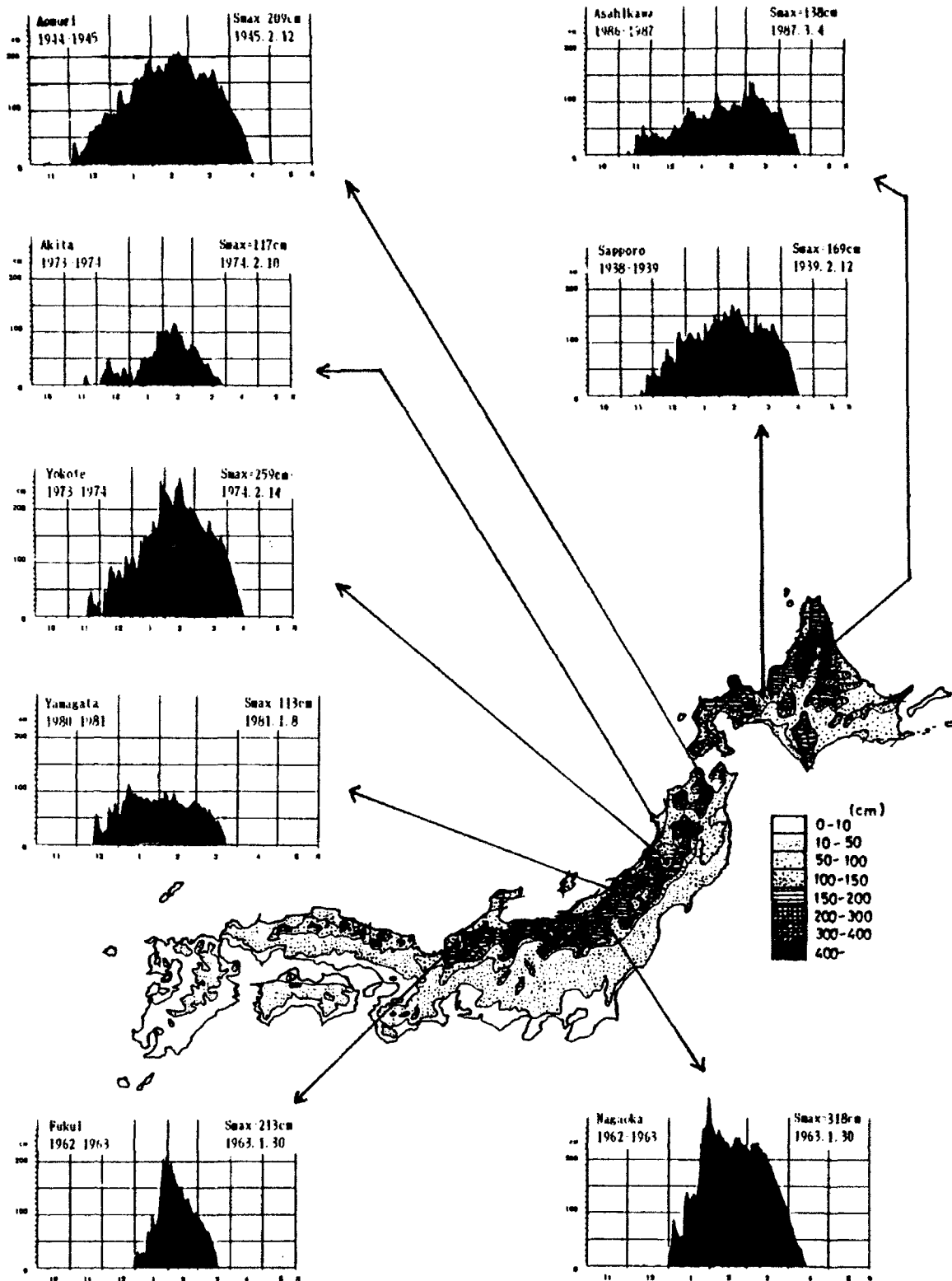


Fig.3 Distribution map of average of maximum depth snowcover(Smax) and patterns of daily changes of snowcover of the laegest values observed in the past.

seven parameters were selected to make the index.

$$Ic = (Smax + St + Snt + D_{10} + Is) / (Tmin + Sd) \quad (1)$$

Ic is a function of these parameters arranged this way. In which, $Smax$ = annual maximum depth of snowcover, St = accumulation of daily maximum depth of snowcover, Snt = positive differences of snowcover depth between the current day and the day before, D_{10} = number of days of snowcover depth more than 10 cm, Is = sudden snowfall factor referring to regional warning values, $Tmin$ = average of daily lowest air temperature, and Sd = cumulative hours of daily sunshine duration in January and February.

However, weather phenomena have respective physical demensions. Therefore, for the purpose of evaluating them to the same standard, we have to standardize their variations into random variables Ti (Z-scores) and then T-scores.

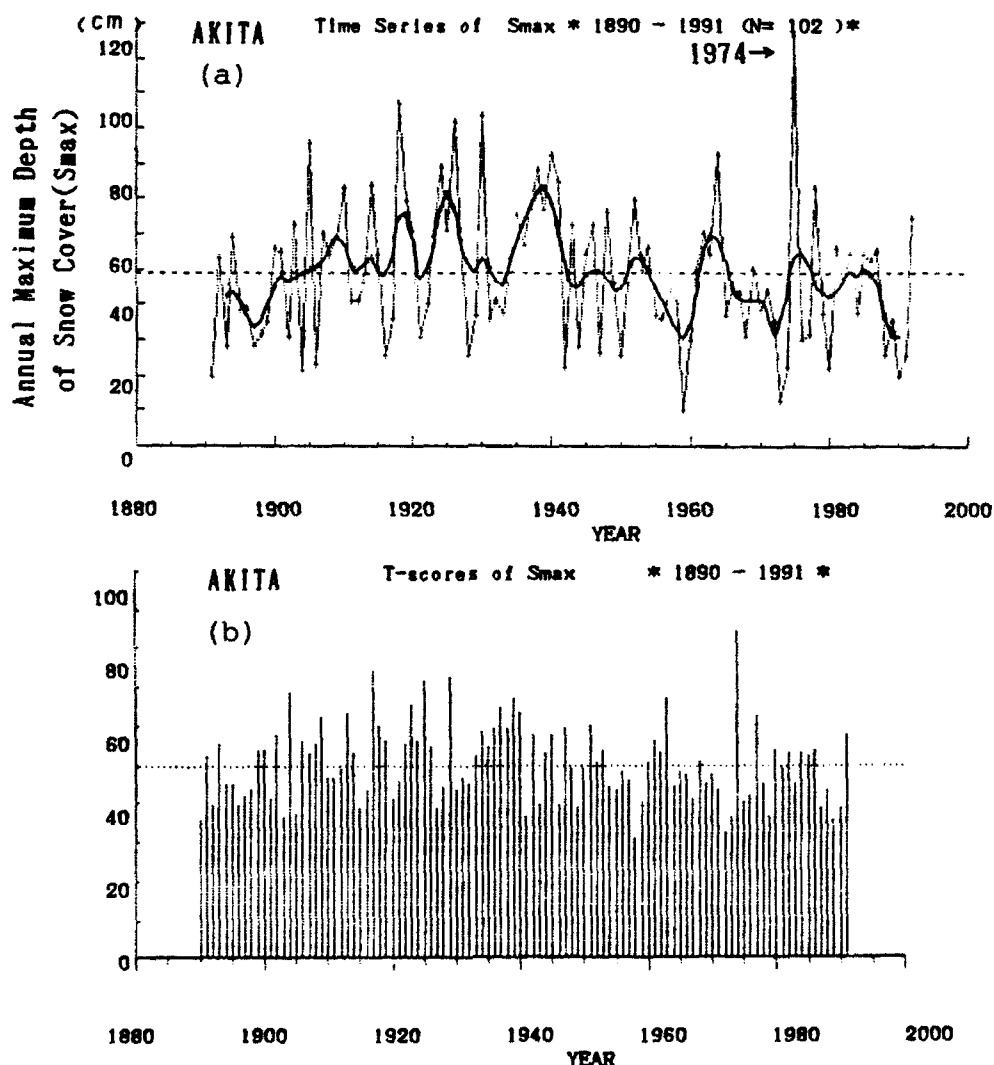


Fig.4(a) Time series of $Smax$ values (original data).
(b) Time series of T-scores of $Smax$ values.

Each value was calculated as follows:

$$T_i = (Y_i - \bar{Y}_i) / \sigma, \quad T\text{-scores} = 50 + 10 \times T_i \quad (2)$$

where, Y_i :original data, \bar{Y}_i :mean value of Y_i , and σ :standard deviation.

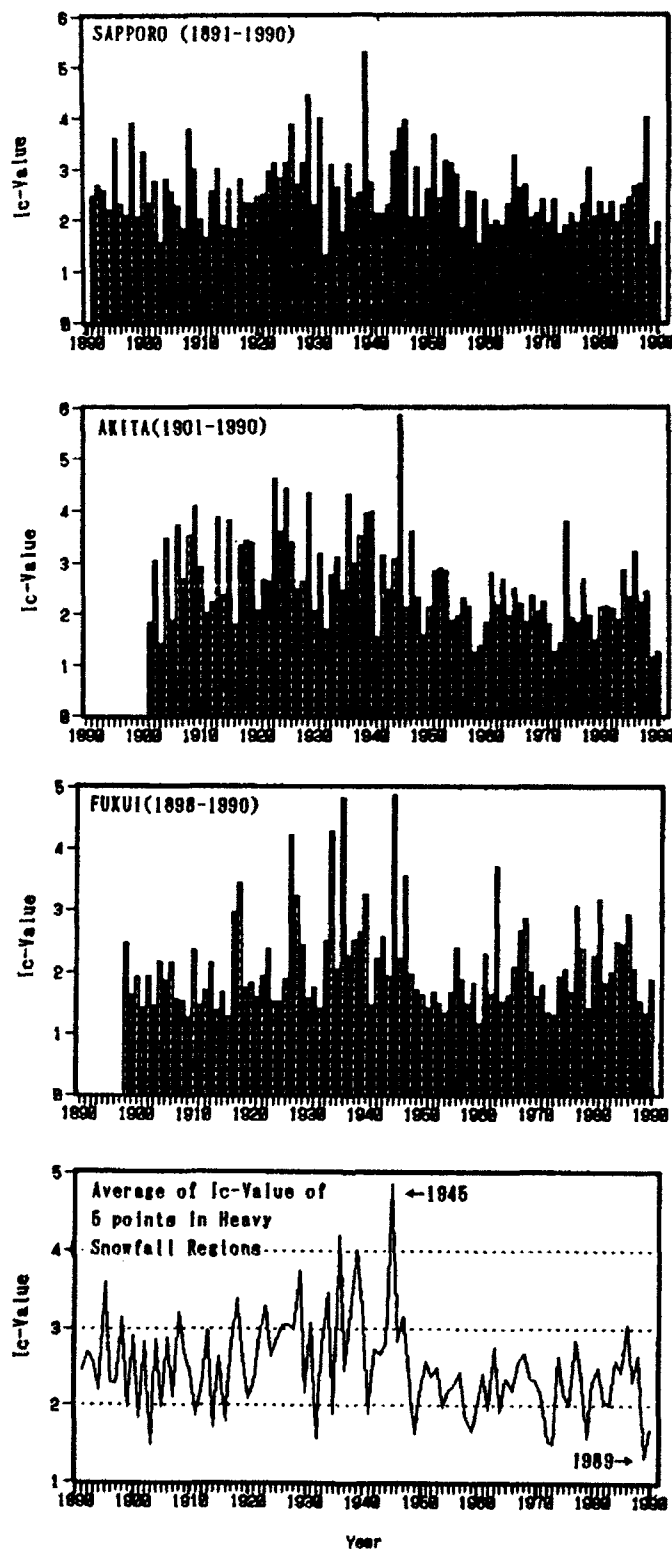


Fig.5 Time series of proposed index "Ic" and its 5 points (Sapporo,Aomori, Akita, Nagaoka, Fukui) values.

This "Ic" probably can be expressed as the index for winter weather circumstances of each year.

According to correlation analysis, these parameters were divided into two groups as shown in eq.(1); the parameters in the same group are positive to each other, but the two group are negative to each other. For the calculation Ic, a lot of meteorological data were collected from Japanese observatories in snowy regions during the period of 1891 to 1990. Fig.4(a) shows an example of time series of original Smax data in Akita, and Fig.4(b) shows their T-scores which were used for Ic calculation.

In consequence of time series analysis of Ic, as shown in Fig.5, 1945 showed the maximum value in most places, on the other hand, 1989 showed the minimum value which means mildest winter since weather observation began. From these figures, it is found that sever winters generally exist before 1945. In recent years, this index has a tendency to decrease.

This is very similar to the number of snow disasters; for example, avalanches have occurred in Japan as shown in Fig.6.

Consequently, the proposed index is concluded as an useful index to evaluate the winter weather environment in the snowy regions.

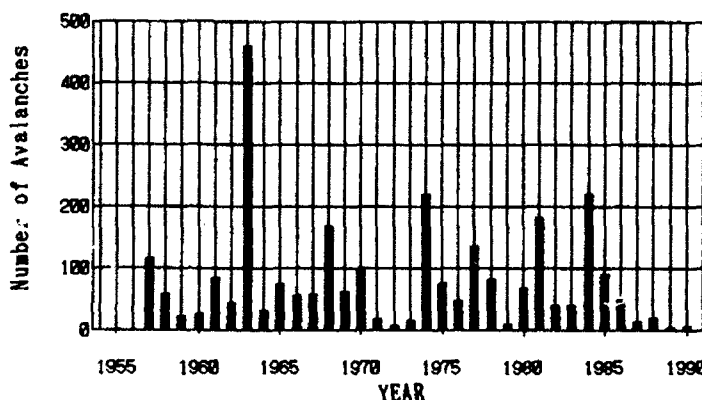


Fig.6 Number of avalanches in Japan(1957-1990).

PRINCIPAL COMPONENT ANALYSIS TO THE PROPOSED PARAMETERS

It may be possible to use the method of principal component analysis (PCA) to evaluate the parameters mentioned above. This is one of the multiple regression methods and is effective for investigating these various parameters together. The values of synthetic characteristics of these parameters by the analysis are expressed in the following.

$$\begin{aligned}
 Z_{(1)} &= a_{11}x_1 + a_{12}x_2 + a_{13}x_3 + \dots + a_{1p}x_p \\
 Z_{(2)} &= a_{21}x_1 + a_{22}x_2 + a_{23}x_3 + \dots + a_{2p}x_p \\
 &\dots \dots \dots \\
 Z_{(m)} &= a_{m1}x_1 + a_{m2}x_2 + a_{m3}x_3 + \dots + a_{mp}x_p
 \end{aligned} \tag{3}$$

Fig.7 shows the results of PCA to the data of Sapporo in the period

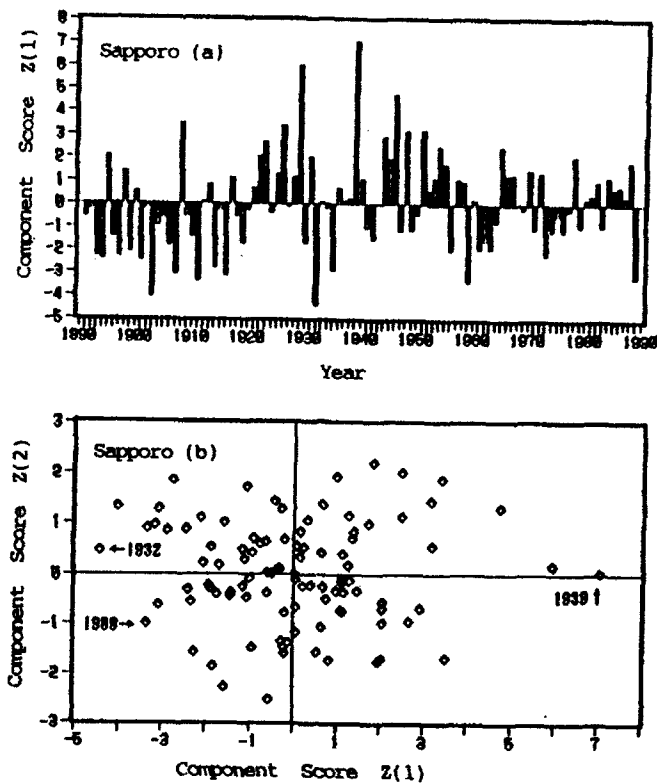


Fig.7(a)Time series of 1st principal component scores $Z_{(1)}$ at Sapporo City
(b)Coordinate expression of $Z_{(1)}$ and $Z_{(2)}$ scores at Sapporo City.

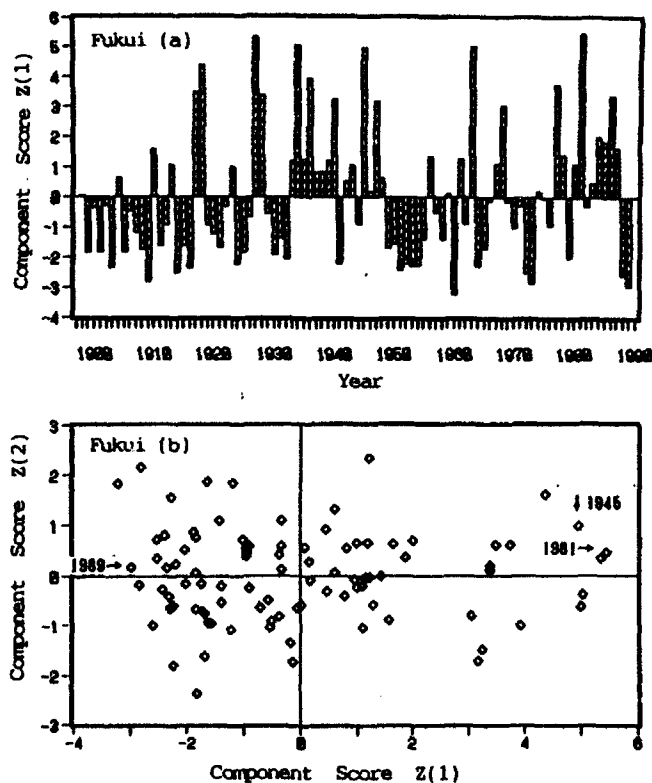


Fig.8(a)Time series of 1st principal component scores $Z_{(1)}$ at Fukui City.
(b)Coordinate expression of $Z_{(1)}$ and $Z_{(2)}$ scores at Fukui City.

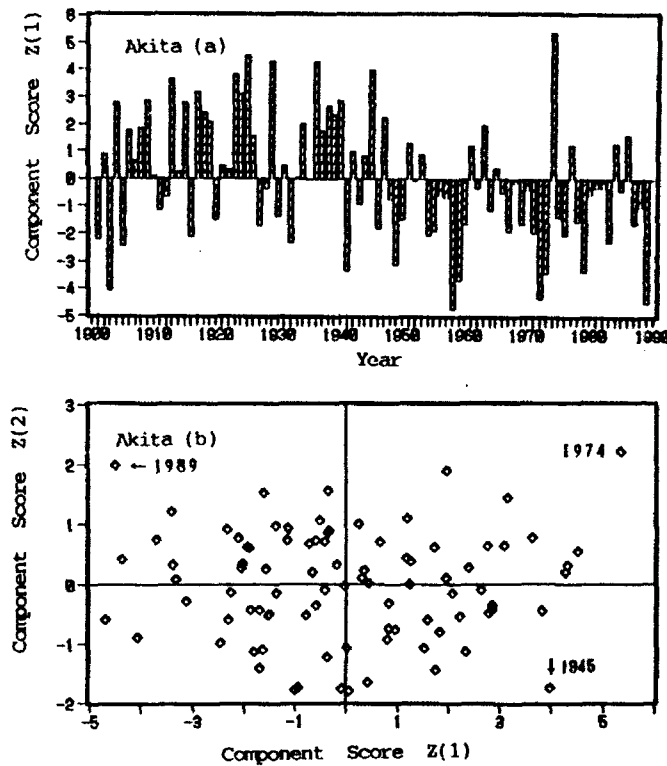


Fig.9(a)Time series of 1st principal component scores $Z(1)$ at Akita City
(b)Coordinate expression of $Z(1)$ and $Z(2)$ scores at Akita City.

of 1891 to 1990. In the figures, Fig.7(a) represents the time series of the first principal component score $Z_{(1)}$. Though its contribution is 59.53%, the analysis shows that the first rank is 1939. This teaches us that 1939 was the most severe winter in Sapporo (ITO, T., 1991). In fact, the largest S_{max} value was recorded in this year.

As is seen in Fig.5, both analytical results coincided with I_c values on the whole; However, from contribution of $Z_{(1)}$, it is not enough to express the characteristics of winter weather in Sapporo. Thus the second principal component $Z_{(2)}$ is necessary for an additional expression. Contribution of $Z_{(2)}$ is only 15.44%, but the cumulative contribution becomes 74.97%. Therefore, as it is nearly 3/4 to the whole, winter weather circumstance at Sapporo may be explained by both $Z_{(1)}$ and $Z_{(2)}$ as expressed in the following form:

$$Z_{(1)} = 0.4353 \cdot S_{max} + 0.4700 \cdot St - 0.1493 \cdot Tave + 0.3757 \cdot D_{10} \\ + 0.4595 \cdot Is - 0.0732 \cdot Sd + 0.4589 \cdot Snt \quad (4)$$

$$Z_{(2)} = 0.1226 \cdot S_{max} - 0.0407 \cdot St + 0.7607 \cdot Tave - 0.2298 \cdot D_{10} \\ + 0.1531 \cdot Is - 0.5606 \cdot Sd + 0.1188 \cdot Snt \quad (5)$$

Fig.7(a) shows a scatter diagram of the coordinate $Z_{(1)}$ and $Z_{(2)}$. From the factor loading of $Z_{(2)}$, air temperature is weighted for its characteristics. The years belonging in the first quadrant probably could be expressed such such the year observed much of deposit snow and remarkable low air temperature. The same tendency is also recognized in the Fig.5.

Fig.8 shows the case of Fukui City. In this case, the contribution of $Z_{(1)}$ is 69.12%, and considering $Z_{(2)}$, the cumulative contribution becomes 81.34%. The first rank is 1945 and the second rank is 1981. This coincides with Ic values.

Similarly, Fig 9 shows the case of Akita City. According to the analysis, $Z_{(1)}$ scores show that the first rank is 1974 when the largest Smax was recorded. The mildest winter was 1989 in the past and the contribution of $Z_{(1)}$ was 73.50%.

In this way, PCA showed very similar results to Ic values. From Ic values and the results of PCA, it was recognized that Smax, Tmin(Tave), and Sd were fairly weighted parameters for expressing the winter weather conditions.

CONCLUSIONS

A new attempt to indicate winter weather conditions using meteorological parameters was carried out. In this case, proposed index "Ic" is very useful to this evaluation. Because the details of past snow disasters are unknown, Ic is a proper index connecting snow disasters, and it will give some suggestions on how snow disasters occurred in the past.

As was seen in the analytical results, the Ic value indicated well the tendency of winter weather conditions depending on the individual region. Consequently, if we retrace the past conditions, this method is very useful for revealing the past phenomena.

Results of PCA and Ic values were similar to each other; however, the PCA method is somewhat complex to use. Thus, we prefer to take Ic values.

REFERENCE

ITO,T(1991) "Investigations On Snow Disasters and Their Prevention Processes Based On Data Analysis", Report on disaster-prevention potentials and their historical changes studied on the basis of data and records(The Japanese Ministry of Education Grant No.02201118:Chief Investigator, Prof. Shinjirou MIZUTANI, Nagoya University). 93-133,1991(in Japanese with English abstract).

Estimation of Daily Snow Mass on the Ground Using Air Temperature and Precipitation Data

Seiji Kamimura and Teruyoshi Umemura

Nagaoka University of Technology
Nagaoka, Niigata, Japan

ABSTRACT

In order to effectively operate snow-removal or snow-melting systems in heavy snowfall areas, supposing a suitable ground-to-roof coefficient is given, a simple degree-day method for calculating snow mass is proposed. The calculation treats only two types of data observed by the Meteorological Agency, air temperature and precipitation, and a coefficient determined uniquely on the place of estimation.

The principle of this method is as follows: First we define D_n as

$$D_n = \sum_{i=0}^n P_i - M_n$$

where P_i is daily precipitation, and M_n snow mass per unit area on n 'th day after the starting day of calculation. Next we plot the D_n against accumulated daily mean air temperature, ΣT , and then we find that the relationship between D_n and ΣT is well approximated by two kinds of linear relations with gradients, a^+ for $T > 0$ °C and a^- for $T < 0$ °C. Then we calculate today's snow mass using yesterday's cumulative snow mass, M_{n-1} , as:

$$M_n = M_{n-1} + P_n - (a^+ \text{ or } a^-) T_n.$$

Surveying the snow mass data observed at Nagaoka City for 3 years and Tokamati City for 15 years, the values of a^+ and a^- have been determined as 4.7 and 1.0 kg/(m²K) for Nagaoka and 4.3 and 0.93 kg/(m²K) for Tokamati, respectively. The calculated results with these coefficients show that the accuracy of the calculation is satisfactory for the estimation of roof snow mass.

INTRODUCTION

In the heavy snowfall areas it is desirable to know daily snow mass on house roofs in order to effectively operate snow-removal or snow-melting systems. Generally their systems operate with the snow depth on the roof, but it is considerably difficult to estimate the accurate load on a building only by the snow depth because the snow density fluctuates daily.

In designing a building, the snow load on the roof is estimated with statistical data of natural snow cover depth and density measured by meteorological agencies and some

accommodation factors. For example the Japanese architectural standard shows such an estimating procedure as to multiply the maximum ground snow depth by the snow density with the factor of roof gradient, and these values are locally and statistically determined beforehand.

Daily fluctuation of snow mass can be calculated by the heat balance on snow surface. For example, Yamazaki et al. (1991a and b) have recently reported a precise calculation of the snow metamorphism for 90 days using meteorological data and considering the heat balance on the snow surface, the internal heat conduction, the liquid water flow and the densification. This method requires a great deal of meteorological data and calculation. A considerably simple method has been recently presented by Sugaya (1990) who calculated a daily mass of snow by using a simulation model including only four meteorological factors: air temperature, shortwave radiation, wind velocity and precipitation. The results have a fairly good agreement with the direct measured data in Joetsu and Nagaoka City, Japan. His calculation, however, has a difficulty in appropriately determining the albedo and the time of runoff of the snowcover.

The degree-day method, which is based on the linear relationship between snow-melting mass and accumulated air temperature during a given period of time, has been used widely for estimating the amount of snow-melting. Using this method, Motoyama (1990) recently calculated the daily fluctuation of snow depth with only two meteorological data: air temperature and precipitation. Some parameters are, however, required to be determined empirically or by trial and error.

In the present paper we propose a simpler degree-day method in which two types of meteorological data, air temperature and precipitation, are used with a parameter which is locally determined beforehand. This method enables us to estimate today's snow mass on a roof only by calculation when a suitable ground-to-roof coefficient is prepared.

DEFINITION OF ACCUMULATED SNOW MASS REDUCTION, D_n , AND ITS RELATION TO DEGREE-DAY

The calculation starts at an arbitrary day before the beginning of snowfall. First we define an accumulated quantity D_n at n 'th day after the starting day as follows:

$$D_n = \sum_{i=0}^n P_i - M_n \quad (1)$$

where P_i is i 'th day's precipitation (mm), M_n snow mass per unit area (kg/m^2) on n 'th day and we call D_n "accumulated snow mass reduction" as it is similar to the amount of runoff. Figure 1 shows the daily change of D_n , ΣP_i and M_n which were observed at the Nagaoka Institute of Snow and Ice Studies during the 1985-1986 winter. In these observations, a pressure pillow was used for measuring the snow mass.

According to the time in Figure 1, we can see that D_n is equal to ΣP before December 9th when the snow mass M_n did not appear: because precipitation was liquid water only and promptly flew out. After that day, the precipitation included snow water. In the beginning of January, precipitation was mostly snow having no liquid water. Then the snow mass reduction D_n no longer increased but slightly decreased. This decrease seems due to the condensation of humidity on the snowcover. The snow mass increased until March 3rd when the snow-melting period began. In the snow-melting period, the runoff from snowcover became greater and greater: M_n was decreasing rapidly. Accordingly, D_n increased rapidly and finally met ΣP on April 23rd when M_n became zero, the snowcover having disappeared.

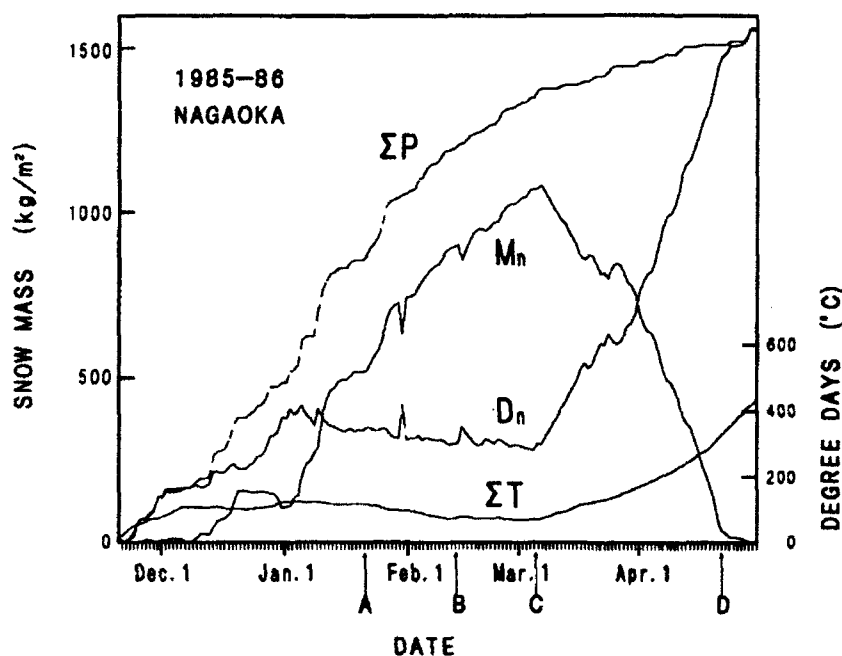


Figure 1. Daily variation of ΣP , M_n , D_n and ΣT observed in 1985-86 in Nagaoka Institute of Snow and Ice Studies.

The degree-day value is ΣT which is the accumulated value of mean daily temperature measured together with snow mass at the laboratory mentioned above. We can easily recognize the similarity of the two curves of D_n and for ΣT . Then taking ΣT in the horizontal coordinate and D_n in the vertical coordinate, we have plotted all the data already shown in Figure 2, where we can see that they are almost expressed by two straight lines, A-B and C-D. ΣT decreases from

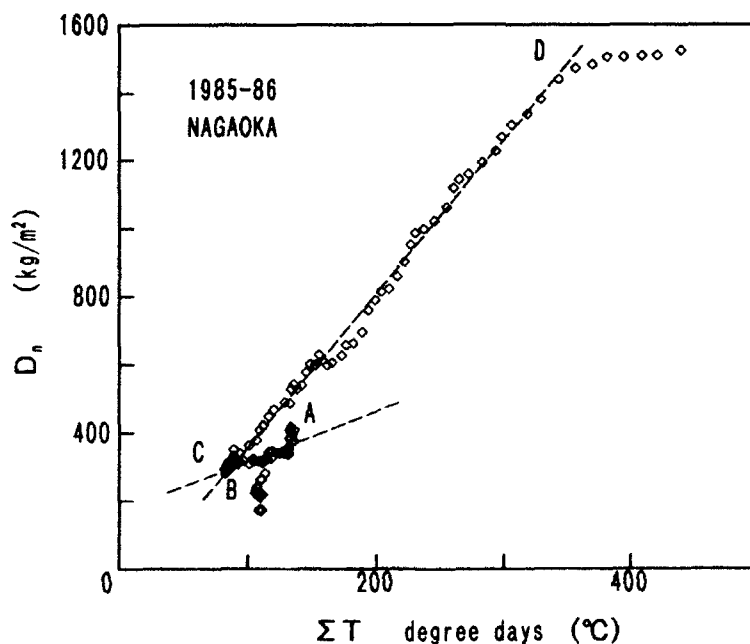


Figure 2. Relationship between ΣT and D_n of the data shown in Fig. 1.

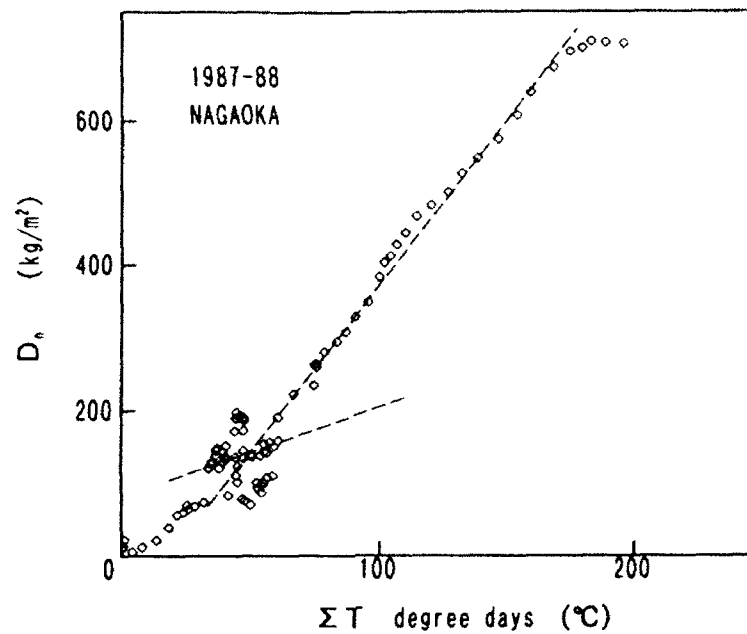


Figure 3. Relationship between ΣT and D_n of the data in 1987-88 in Nagaoka Institute of Snow and Ice Studies.

A to B and increases from C to D, where A, B, C and D correspond the days shown in Figure 1. This means that the mean daily temperatures are under the melting point of ice during the

Table 1. Linear coefficients of snow mass reduction, D_n , to degree-day, ΣT is drawn from the data observed in Nagaoka and Tokamati: a^+ for positive temperature days and a^- for negative temperature days.

year	coef. a^-	drawn period	correl. coef.	coef. a^+	drawn period	correl. coef.
Nagaoka						
1985-86	1.04	Jan. 21-Feb. 12	0.801	4.71	Mar. 5-Apr. 20	0.995
1987-88	0.935	Feb. 7-Feb. 23	0.752	4.77	Mar. 10-Apr. 7	0.996
Tokamati	-			3.98		
1975-76	3.88	Jan. 19-Jan. 30	0.880	4.06	Feb. 15-Apr. 16	0.986
1976-77	0.739	Dec. 27-Feb. 23	0.725	4.41	Mar. 7-Apr. 20	0.995
1977-78	0.729	Jan. 16-Feb. 26	0.440	4.42	Mar. 15-Apr. 29	0.997
1978-79	-	-	-	3.98	Feb. 6-Feb. 28	0.970
1979-80	2.67	Jan. 8-Jan. 27	0.504	4.42	Mar. 20-Apr. 20	0.995
	1.78	Feb. 6-Feb. 22	0.676	-	-	
1980-81	1.07	Dec. 27- Feb.	0.551	5.27	Mar. 13-May 3	0.992
1981-82	0.740	Jan. 28-Feb. 11	0.204	4.26	Feb. 27-Apr. 5	0.992
1982-83	1.09	Feb. 7-Feb. 16	0.134	3.49	Mar. 19-Apr. 14	0.995
1983-84	0.351	Dec. 25-Feb. 20	0.373	4.55	Mar. 24-May 10	0.997
1984-85	1.04	Dec. 24-Jan. 31	0.488	4.41	Mar. 12-Apr. 20	0.994
1985-86	0.601	Jan. 6-Feb. 12	0.297	4.13	Mar. 6-Apr. 27	0.993

period A-B, being nearly zero during B-C and over zero during C-D. Owing to the linear relations shown in Figure 2, D_n can be calculated with the two equations for A-B and for C-D.

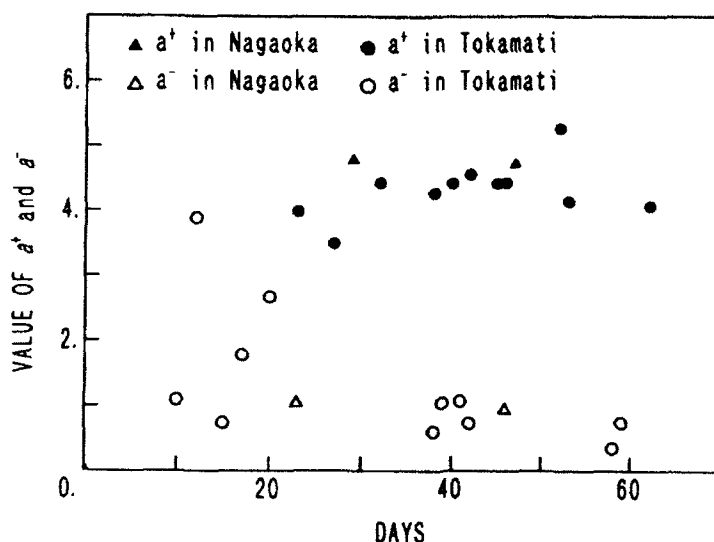


Figure 4. Dependence of the coefficients, a^+ and a^- , on the consecutive days of period taken for its determination.

Figure 3 shows the data observed at the same place in another year; two kinds of linear relations can be seen. When we write the linear relations in a form, $D_n = a\sum T + b$, we recognize that the linear coefficients a in Figure 2 and Figure 3 are almost the same. Then we plot the data observed at another place: Tokamati City which is 40 km far from Nagaoka City. At each place we can draw two coefficients, a^+ for positive temperature days and a^- for negative temperature days, for consecutive days when the temperature is either positive or mostly negative. This results are shown in Table 1. In general a^+ 's have nearly constant values and high correlation coefficients, while a^- 's sometimes have distinctively large values in Tokamati data, e.g. in 1975-76 and 1979-80. We recognize these data are taken for relatively short periods. Then taking the period in the horizontal coordinate, and a^+ and a^- in the vertical coordinate, their relations are shown in Figure 4, which shows that if we omitted the data for a shorter period than 20 days we can regard a^+ and a^- as each being constant. The mean values of a^+ are 4.7 for Nagaoka and 4.3 for Tokamati, and a^- are 1.0 for Nagaoka and 0.93 for Tokamati.

CALCULATED SNOW MASS AND ITS COMPARISON WITH OBSERVED ONE

We estimate today's mass of snow by calculation. First we define daily snow mass reduction and substituting equation (1) in it:

$$\Delta D_n = D_n - D_{n-1} = P_n + M_n - M_{n-1}. \quad (2)$$

Introducing the linear relation elucidated in the preceding section, it follows that:

$$\Delta D_n = \left(a \sum_{i=1}^n T_i + b \right) - \left(a \sum_{i=1}^{n-1} T_i + b \right) = a T_n \quad (3)$$

where a and b are the constants in the linear relation. From equation 2 and equation 3 the mass on n 'th day (today) is straightforward,

$$M_n = M_{n-1} + P_n - a T_n. \quad (4)$$

This equation means that today's mass, M_n , is calculated by using the mass accumulated by yesterday, M_{n-1} , and the precipitation, P_n , and temperature, T_n , observed today, together with a constant, a , which, as already mentioned, is expressed as follows:

$$a = \begin{cases} a^+ & (T_m \geq 0) \\ a^- & (T_m < 0) \end{cases} \quad (5)$$

Using the equation (4) and the mean values, a^+ and a^- , derived in the preceding section, calculation and its comparison to the observed snow mass are carried out. Their results are shown in the following.

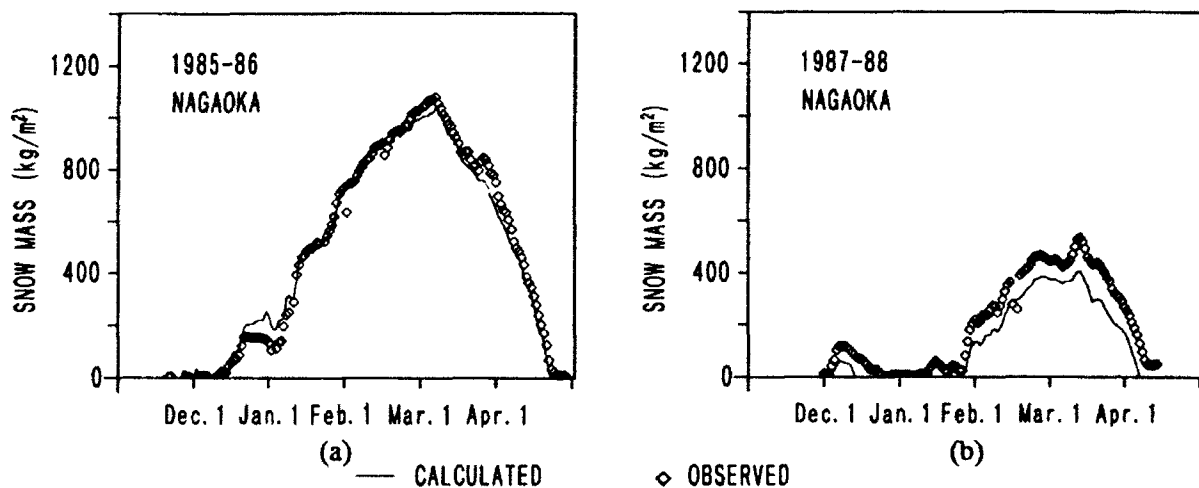


Figure 5. Calculated and observed snow mass in Nagaoka.

Table. 2. Comparison of the characteristic snow data calculated with that observed in Nagaoka.

	Maximum snow mass kg/m²		Snowcover starting day		Snowcover ending day	
	Observed	Calculated	Observed	Calculated	Observed	Calculated
1985-86	1081	1070	Dec. 9	Dec. 10	Apr. 23	Apr. 21
1986-87	406	366	Jan. 9	Dec. 27	Mar. 29	Mar. 30
1987-88	535	446	Nov. 29	Jan. 5	Apr. 8	Apr. 5

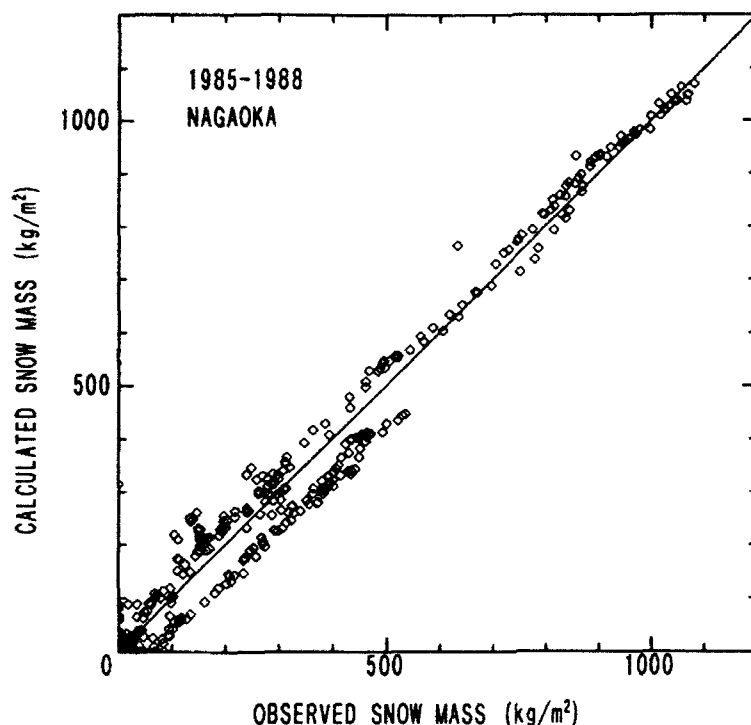


Figure 6. Comparison between calculated and observed snow mass in Nagaoka for three years, 1985-88: standard deviation is 66.1 kg/m^2 .

Result and discussion for the data in Nagaoka City

Taking the mean values of a^+ and a^- as 4.7 and 1.0 respectively, calculations are carried out for 3 three years in Nagaoka. Figure 5(a) shows the calculated values (solid line) and the daily observed values (diamond mark) in the winter, 1985-86. The agreement between the calculated values and observed values is quite good except for the days from Dec. 12 to Jan. 9. This agreement is due to the fact that the values of a^+ and a^- are the same as that obtained from only the data in this year. Figure 5 (b) shows another comparison for the data in the winter, 1987-88; in this year the compared values have the largest deviation in 3 years in Nagaoka. Nevertheless the deviation is so small that may bring no problem in practical use, e.g. a determination of the operation time of snow-removal or snow-melting system. Figure 6 shows the comparison of snow mass between the calculated and the observed for 3 years in Nagaoka. The standard deviation of these data is 66.1 kg/m^2 which is rather large in the starting period of snowcover but it is not so large in the later period when snow-removing or melting operations are required. Table 2 shows the comparison of the characteristic snow data of every 3 years. The agreement between the calculated values and the observed values is fairly good.

Result and discussion for the data in Tokamati City

Taking the mean values of a^+ and a^- as 4.3 and 0.93 respectively, calculations are carried out for 15 three years in Tokamati. Figure 7 (a) shows the calculated snow mass and the daily

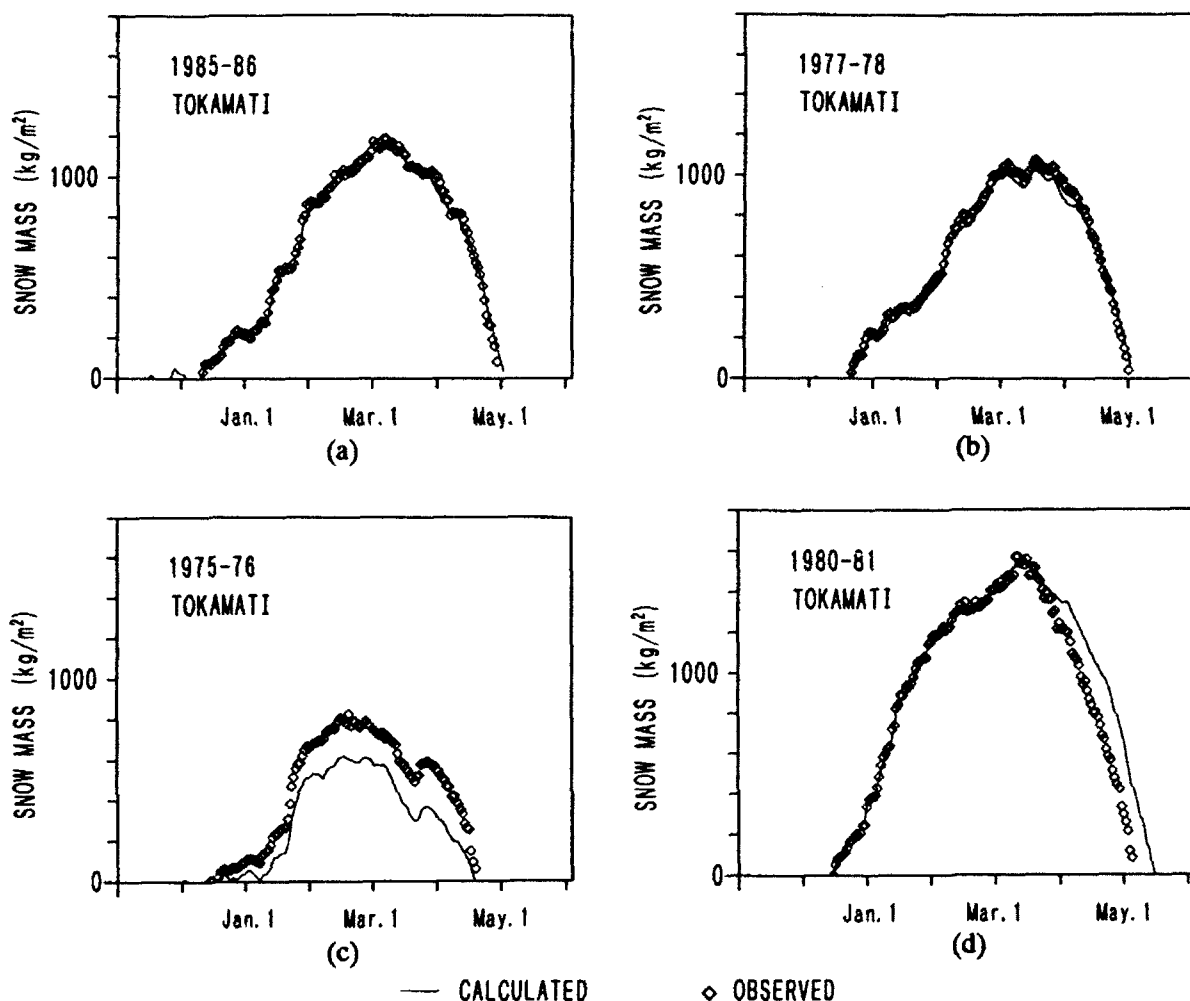


Figure 7. Calculated and observed snow mass in Tokamati.

observed snow mass in 1985-86 when the best agreement is obtained, and Figure 7 (b) in 1977-78 when the second best agreement obtained. The agreements are so good that no explanation may be necessary. Figure 7 (c) shows the comparison of the snow masses in 1975-76 when the worst agreement is obtained, and Figure 7 (d) in 1980-81 when the second worst agreement was obtained. As to the worst correlation, the reason of this disagreement is not well understood yet. As to the second worst data, in 1980-81 the disagreement occurred during the few days in March through April, near the ending day of snowcover. Much rain and not snow fell during those days in spite of relatively low air temperature.

All the data for 15 years in Tokamati are plotted in Figure 8. We can see there is good agreement between calculated and observed snow mass except for 3 years: two positively deviating data fits which are for 1980-81 mentioned above and 1983-84; and one negatively deviating data fit for 1975-76 mentioned above. The standard deviation of total calculated data from the observed data is 90.4 kg/m^2 . The characteristic snow data in Tokamati is shown in Table 3. In 1975-76

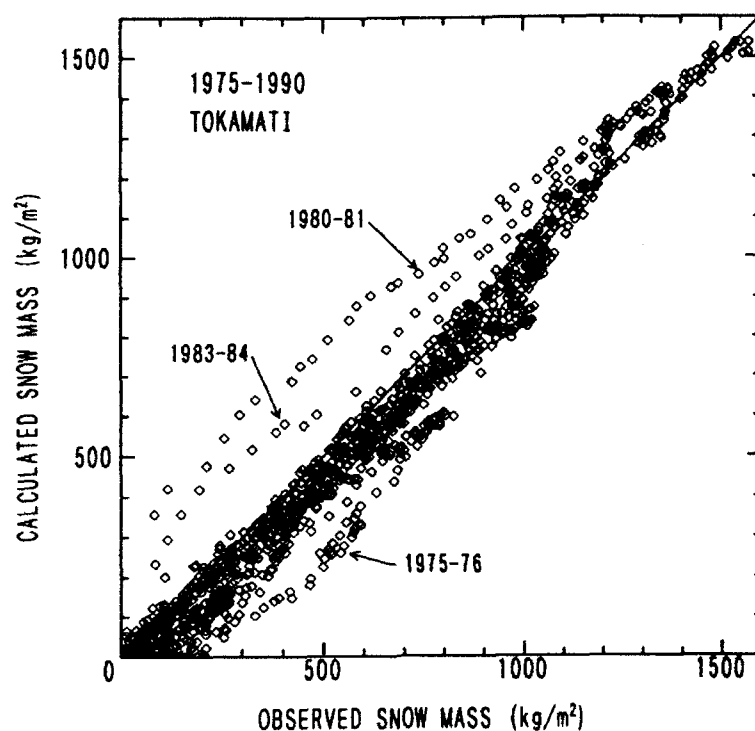


Figure 8. Comparison between calculated and observed snow mass in Tokamati for three years, 1985-88: standard deviation is 90.4 kg/m².

Table. 3. Comparison of the calculated and observed snow data in Tokamati.

	Maximum snow mass kg/m ²		Snowcover starting day		Snowcover ending day	
	Observed	Calculated	Observed	Calculated	Observed	Calculated
1975-76	824	618	Dec. 17	Dec. 17	Apr. 16	Apr. 14
1976-77	1051	1037	Dec. 27	Dec. 10	Apr. 20	Apr. 19
1977-78	1078	1028	Dec. 20	Dec. 20	Apr. 29	Apr. 29
1978-79	270	172	Dec. 20	Dec. 12	Mar. 23	Feb. 27
1979-80	854	756	Jan. 8	Jan. 8	Apr. 20	Apr. 21
1980-81	1571	1551	Dec. 14	Dec. 15	May 3	May 11
1981-82	495	421	Jan. 7	Jan. 7	Apr. 5	Apr. 2
1982-83	732	660	Dec. 31	Dec. 31	Apr. 14	Apr. 11
1983-84	1372	1442	Dec. 15	Dec. 12	May 10	May 14
1984-85	1026	890	Dec. 17	Dec. 23	Apr. 20	Apr. 19
1985-86	1190	1210	Dec. 10	Dec. 10	Apr. 27	Apr. 28
1986-87	620	565	Dec. 22	Dec. 21	Apr. 9	Apr. 7
1987-88	702	620	Jan. 6	Jan. 1	Apr. 15	Apr. 14
1988-89	161	149	Jan. 25	Jan. 25	Mar. 2	Mar. 4
1988-89	431	347	Dec. 31	Jan. 1	Mar. 14	Feb. 27

much disagreement appears in the term of maximum snow mass, in 1980-81 in snowcover ending day, and in 1983-84 there is a little disagreement in all 3 terms.

General discussion

The most notable characteristic of the present method is that only one parameter is necessary and is determined for each area. And the parameter is separated in two kinds depending on air temperature. There is an option to vary the threshold of air temperature to attain better agreement. For example, if we take 0.5 °C as the threshold, the agreement is a little improved in both data in Nagaoka and Tokamati; however, we do not yet know either the best value or its dependence on the observation area. Without this modification, that is with the threshold at 0 °C, we consider the agreement is satisfactory for practical use.

The dependence of error, δa , in a on the error, δM_n , of calculated value of M_n is easily derived from the equation (4) as

$$\delta M_n = \frac{\partial M}{\partial a} \delta a = -T_n \delta a, \quad \text{kg/(m}^2\text{d)}. \quad (6)$$

If 0.1 of δa is involved in a^* and \bar{a} , the maximum error in M_n is -400 (the maximum of ΣT) \times 0.1 = -40 kg/m² for a^* and $-(-100) \times 0.1 = 10$ kg/m²; these gives no problem in practical use.

CONCLUSION

A degree-day method with two kinds of parameters which is determined uniquely on site has been proposed and proved valid with Nagaoka and Tokamati data. When a suitable ground-to-roof coefficient is given, this method has an enough accuracy to estimate a snow mass on the roof from only daily air temperature and precipitation data given by the Meteorological Observatory.

ACKNOWLEDGMENT

We are indebted to Nagaoka Institute of Snow and Ice Studies of the National Research Institute for Earth Science and Disaster Prevention who offered the observed data of snow in Nagaoka, and the Tohkamachi Experiment Station Forestry and Forest Products Research Institute for the observed snow data in Tokamati.

We thank Secom science and Technology Foundation whose grant supported this research.

REFERENCES

- T. Yamazaki, T. Sakuraoka, T. Nakamura and J. Kondo (1991a) "A study of snow metamorphism: I Model description", *J. of the Japanese Society of Snow and Ice*, Vol. 53(2), 115-123, June 1991. (in Japanese)
- T. Yamazaki, T. Sakuraoka, T. Nakamura and J. Kondo (1991b) "A study of snow metamorphism: II Observation and simulation", *J. of the Japanese Society of Snow and Ice*, Vol. 53(2), 125-133, June 1991. (in Japanese)

H. Sugaya (1990) " Micro meteorological studies on the snowpack evolution in the hokuriku region: Measurements and modeling", *Bulletin of The Hokuriku National Agricultural Experiment Station*, No. 31, 43-64, December 1990. (in Japanese)

H. Motoyama (1990) "Simulation of seasonal snowcover based on air temperature and precipitation", *J. of Applied Meteorology*, Vol. 29, 1104-1110, November 1990.

Simulation on Depth of Newly Fallen Snow Based on AMeDAS Data

Yutaka Yamada and Takashi Ikarashi

Nagaoka Institute of Snow and Ice Studies, NIED, STA
Nagaoka, Niigata, Japan

ABSTRACT

This paper describes a simulation to estimate depth of daily newly fallen snow from data such as snow depth, precipitation and air temperature that are recorded by the automatic meteorological data acquisition system (AMeDAS) established by the Meteorological Agency of Japan and/or snow information systems developed in the snow country by local governments.

The simulation of two conventional methods and new rain gage method were conducted using the same data that are obtainable by AMeDAS.

In order to simulate by this new method, density of newly fallen snow is necessary. We first investigate to obtain a parameter of density. Results are still not satisfactory compared to the best conventional method; however, there is a possibility to improve this new method.

INTRODUCTION

New snow depth has been manually measured on snow boards at nine o'clock in the morning for many years in Japan. But meteorological observation systems at most of the local observation stations changed from manual operation into automatic meteorological data acquisition system (AMeDAS). At that time observation of daily new snow depth was abolished, and only snow depth has been measured every one hour with a wireless automatic snow depth meter.

Since then the stations have substituted the daily new snow depth for a value that is the sum of the positive difference of snow depth measured at every one hour. This substitution value is recorded on the monthly weather report by the Meteorological Agency. The daily difference of snow depth at 9 o'clock is also recorded on the local monthly weather report.

New snow density is an important practical quantity for snow removal operation on roads, surface snow avalanche prediction and others. The AMeDAS is a national observation network. Of

more than 1,300 stations, about 200 are equipped with a super-sonic snow depth gage and at other stations rain gage data are available.

It would be very useful if we could utilize the AMeDAS to get new snow data information. For this reason, we investigate the method of new snow depth estimation.

The simulation of two conventional methods and a new rain gage method were conducted using the same data that are obtainable by AMeDAS. In order to conduct simulation by this new method, density of newly fallen snow is necessary. We first investigate to obtain a parameter of density.

ERROR OF CONVENTIONAL ESTIMATION METHOD

First, the error of estimating daily new snow depth from snow depth data is discussed. Meteorological and snow data including snow depth and precipitation measured hourly were used in this error analysis of estimated new snow depth.

These data were collected from the original register of ground meteorology observed by the Nagaoka Institute of Snow and Ice. To compare the estimated new snow depth with the daily new snow depth, data were examined for three winter seasons from 1988/89 to 1990/91 (e. g., Yamada et al., 1989 and others). These new snow data were observed once a day at 9 o'clock.

Snowpack is formed by piles of new snowpack that come from newly fallen snow on the ground. Therefore, the simplest estimation methods are the two conventional methods which use only a snow depth meter.

These methods include the method of daily difference of snow depth and the method of the sum of positive difference of hourly snow depth. We will first compare these two estimation methods, which are both based on the difference of snow depth with the manually observed daily new snow depth, and discuss the problem of this method.

a. Daily difference of snow depth

This method substitutes the daily new snow depth for the difference of snow depth that is measured between the standard time and estimation time.

Comparison of this estimated value and the new snow depth measured on snow board is shown in Figure 1. These data only include a new snow depth greater than 8 cm, which is routinely measured at 9 o'clock.

The correlation coefficient of this method is 0.79. The absolute positive error is very low and most large errors are negative. In extreme cases, value of new snow depth is negative.

The main reasons of this negative error and negative new snow depth are due to the material property of snow that shrinks after accumulation. Namely, densification of the underlying layer causes the error. Further, large negative errors occurred in the period when snowfall continued several days.

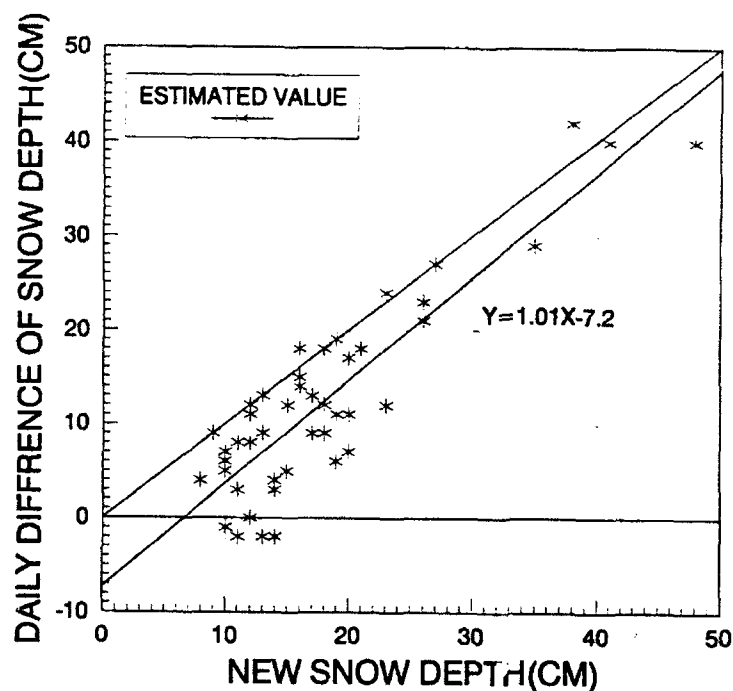


Figure 1. Relationship between daily difference of snow depth and new snow depth.

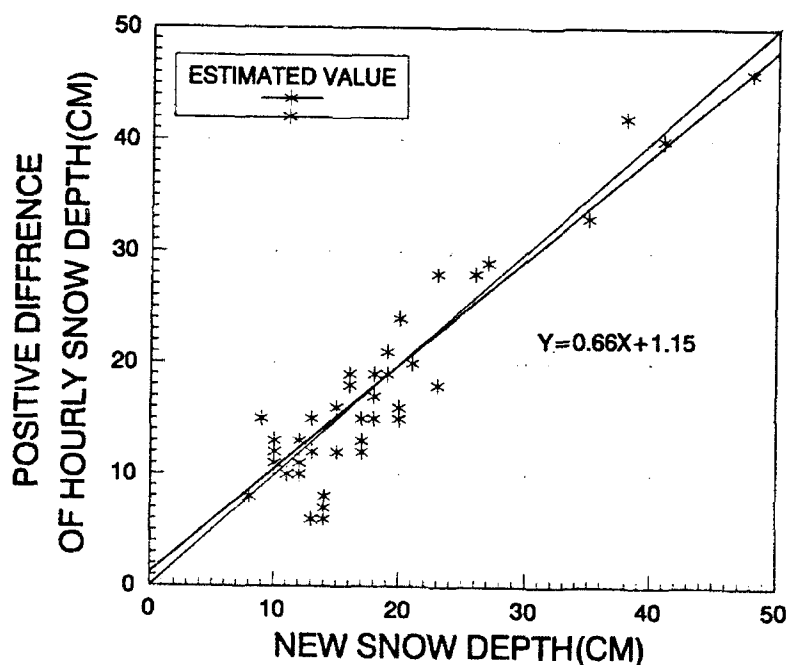


Figure 2 Relationship between positive difference of hourly snow depth and new snow depth.

b. Positive difference of hourly snow depth

This method estimates the new snow depth by summing up the positive increment of hourly snow depth differences.

As snow is a volumetric viscous compressible material, snow depth occasionally does not increase but sometimes decreases, even during snowstorms according to the condition and quantity of the older newly fallen snow layer. An study that is based on viscous compression model to estimate depth of snow has successfully been conducted (Motoyama and kojima, 1985; Motoyama, 1990), but such approach to estimate new snow depth has not been practically successful.

The positive difference method is considered to revise the error of the method of daily difference of snow depth by adding only positive hourly differences.

In the Figure 2, a comparison of estimated value of this method and the observed new snow depth is shown. By this revision, the extent of the error reaches the range of $\pm 5\text{cm}$ and estimated value fits linear curve. The correlation coefficient of this method is 0.66. This means that the revision of snow densification by removing negative differences of hourly snow depth worked better compared to the method of daily difference of snow depth. But there is still some negligible error and no physical meaning for correction as this is an empirical method.

NEW SNOW DENSITY

snow density will be used later as a parameter to convert water equivalent of snow measured by rain gage into new snow depth.

For this purpose, the density of new snow was investigated by measuring the depth and the water equivalent. New snow depth was measured on a snow board ($45 \times 45 \text{ cm}^2$) board having a scale in the center) and the water equivalent of new snow was measured by snow board or rain gage. The accuracy of this method (Table 1) was examined by the tests of significance with observed new snow density (Yamada, 1990).

TABLE 1. Comparison of new snow density statistics by two methods (ND: number of data, MOD: mode, $\mu 1$: simple arithmetic mean, STD: standard deviation, $\mu 2$: depth weighted mean, SK: skewness, KU: kurtosis)

Method	ND	MOD g/cm ³	$\mu 1$ g/cm ³	STD g/cm ³	$\mu 2$ g/cm ³	SK $\times 10^{-0.4}$	KU
Snow board	229	0.09	0.083	0.022	0.082	5.1	2.3
Rain gage	221	0.06	0.079	0.024	0.074	5.4	2.0

The frequency distribution of new snow at twenty-two cities in Japan is shown in Figure 4. In this figure, the relative frequency distributions of new snow density at each station are arranged, from the north, left to right and up to down. Therefore, at the top left, Wakkanai is located at the most northern place, and the bottom right, Hikone, is located at the most southern place.

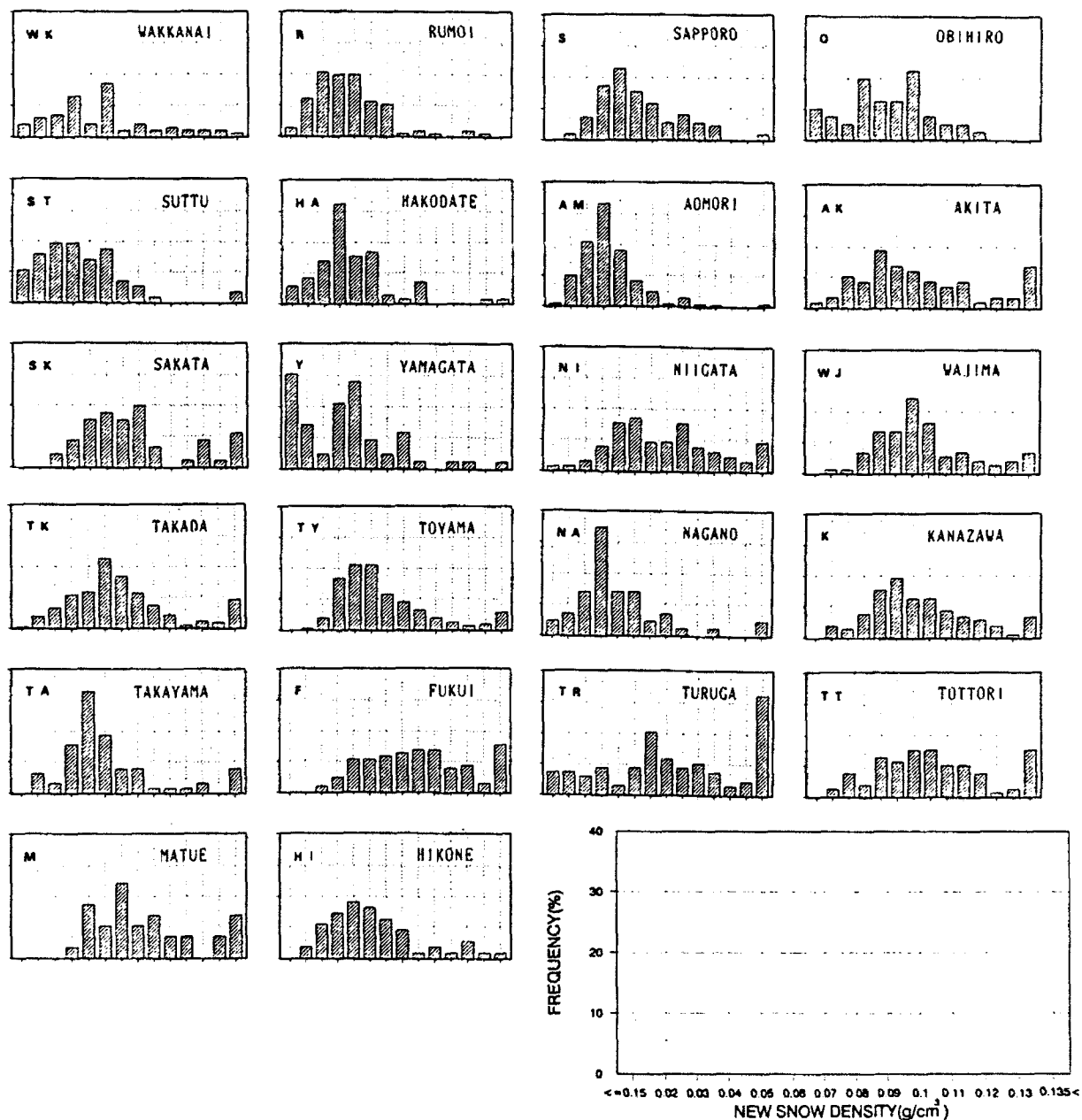


Figure 3. Relative frequency of new snow density along the Japan Sea (Observation periods are six and twelve hours).

In Figure 4, average density increases as north latitude decreases. Maximum average density appeared in Fukui (F) in the Hokuriku district, and minimum average density at Aomori (AM) in the Tohoku district. Wherever north latitude exceeds about 41° (Aomori[AM]), average densities are relatively small (generally speaking, less than 0.06 g/cm^3). However, even in the southern region where north latitude is smaller than 41° , there were some stations in which density was smaller than 0.06 g/cm^3 (Yamagata(Y), Nagano(NA), Takayama(TA), and Hikone(HI)). These stations are all located in the inland, high altitude basin.

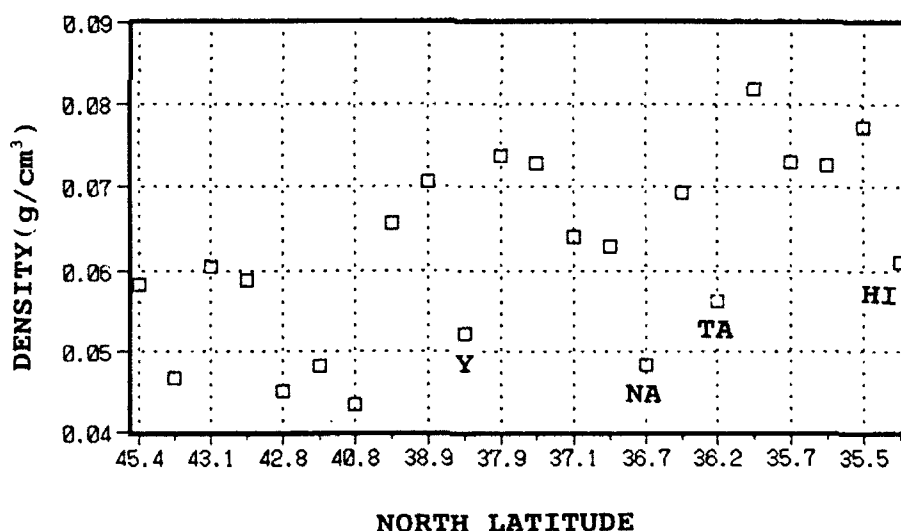


Figure 4. Relationship between average density of new snow and north latitude.

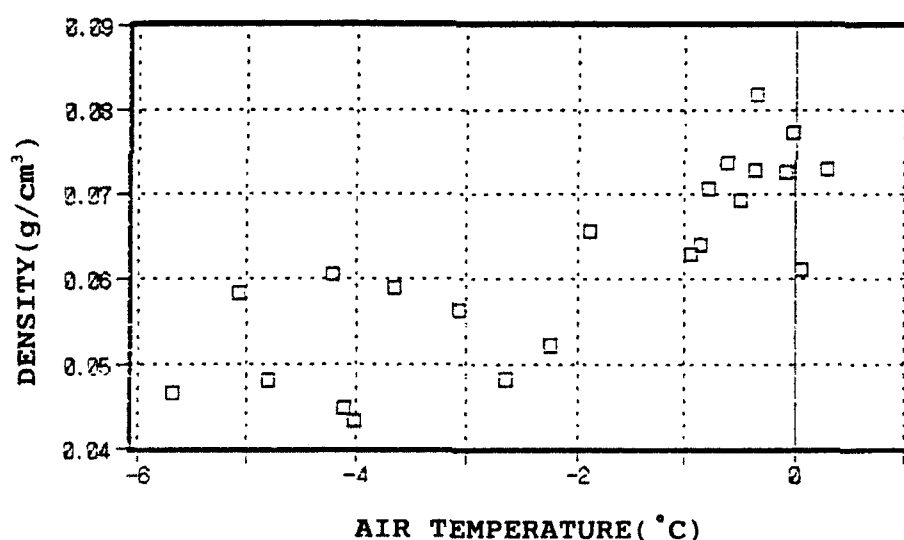


Figure 5. Relationship between average density of new snow and air temperature.

Relationship between average density and air temperature. (Figure 5) shows that at the station wherever air temperature is below -2°C , average density is smaller than 0.06 g/cm^3 . It seems, from Figure 5, that the regionality of new snow density depends mainly on air temperature. But Figure 4 shows north latitude has about the same influence.

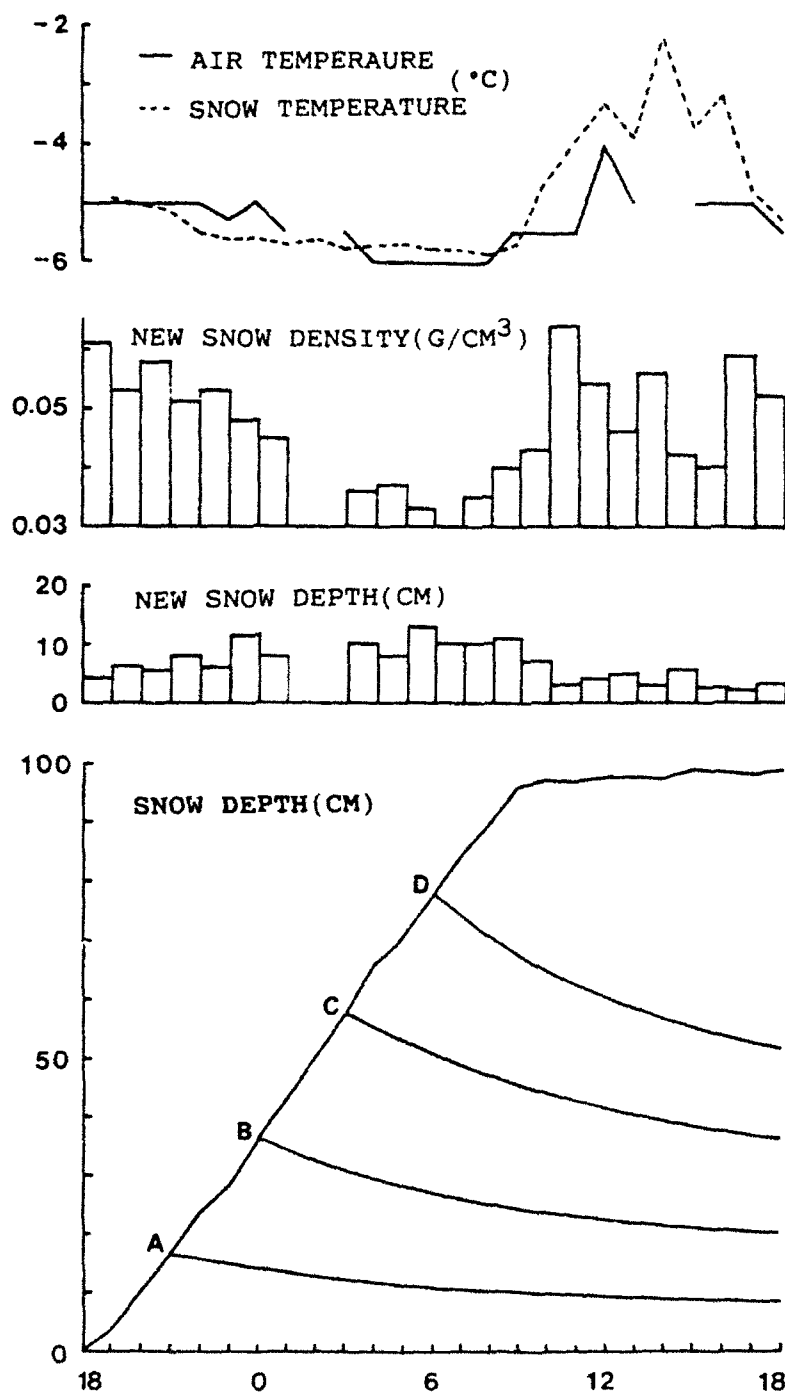


Figure 6. Observation on short period new snow density.

To apply and to check the rain gage method, new snow density for short periods during continuous snowfall is needed. For that purpose, 24 hours of continuous observations of settlement of boundary every 3 hours and new snow density every one and three hours was conducted at Nakasato village (elevation 400 m), Niigata Prefecture. Several observations were conducted during winter seasons of 1989/90 and 1990/91.

Figure 6 shows an example of one cycle observation when depth of daily new fallen snow amounted to 110 cm. New snow density which accumulated for one hour, ranged from 30 kg/m³ to 65 kg/m³ and average density was 46 kg/m³, while average density for three hours was 50 kg/m³.

RESULT

The rain gage method estimates the new snow depth to convert to solid precipitation by using new snow density.

Example of this method is shown in Figure 7 for the same data set for Figure 1 and Figure 2. Here new snow density is assumed as the mode, 90 kg/m³, according to the new snow density investigation on the snow board. The correlation coefficient of this method was 0.66 which is the same value as that of the method of positive difference of hourly snow depth. The results of estimation by this method fit well globally to the observed new snow depth. However, scattering of data was relatively larger.

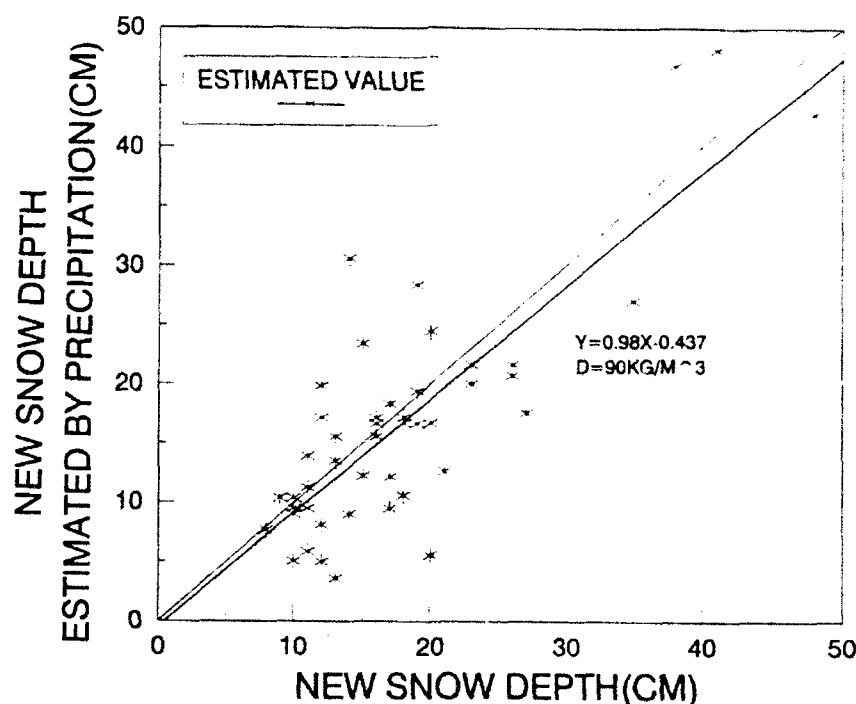


Figure 7. Relationship between new snow depth estimated by precipitation and new snow density.

The problems of this revision method are the trapping efficiency of the rain gage and new snow density. As is well known, when one uses a rain gage for measuring solid precipitation, the trapping efficiency of the meter is sometimes low especially in the strong wind periods or regions, because of lightness of snow crystals (Gray and Male, 1985; International organizing committee for WMO solid precipitation measurement intercomparison, 1985).

On the former problem of the trapping efficiency, it is recognized that accumulated solid precipitation over long periods is about the same as the water equivalent of snow cover (Yamada, unpublished). Therefore, error caused from this effect exists, but is small and seems to follow some regular rule.

On the latter problem, in order to apply the rain gage method, local characteristics of new snow density distribution (Yamada, 1990) show that determination of new snow density is important to improve the rain gage method.

CONCLUSION

The simulation of two conventional methods and the new rain gage method were conducted using the same of data that are obtainable by AMEDAS.

In order to conduct simulation by this new method, density of newly fallen snow is necessary. We first investigate to obtain a parameter of density. New snow density changes widely according to the local condition that especially depends on air temperature.

Results are still not satisfactory comparing to the best conventional method; however this new method can be improved by determining the appropriate new snow density and revising trapping efficiency. As a concluding remark, the newly proposed rain gage method could be as successful as the method applying the viscous compression model.

ACKNOWLEDGEMENT

I wish to express my gratitude to Dr. T. Nakamura, director of our institute and my colleagues for their apt suggestions and instructive encouragement. This research was supported by the budget of Science and Technology Agency (Development of snow information system in the highway: group leader Dr. T. Nakamura).

REFERENCES

Gray D. M. and D. M. Male (1981) "Handbook of snow", Pergamon Press.

International organizing committee for WMO solid precipitation measuring method intercomparison(1985) "WMO instrument and observation method", First Session, Norrkoping.

Motoyama, H., and E. Kojima, (1985) "Estimation model for the depth of a dry snow cover based on the viscous compression theory of seasonal snow cover (in Japanese with English Summary)", Low Temp. Sci. Ser. A, 44, 15-25

Motoyama, H. (1990) "Simulation of Seasonal Snowcover Based on Air Temperature and Precipitation" ,J. of Applied Meteor. Vol. 29, 1104-1110.

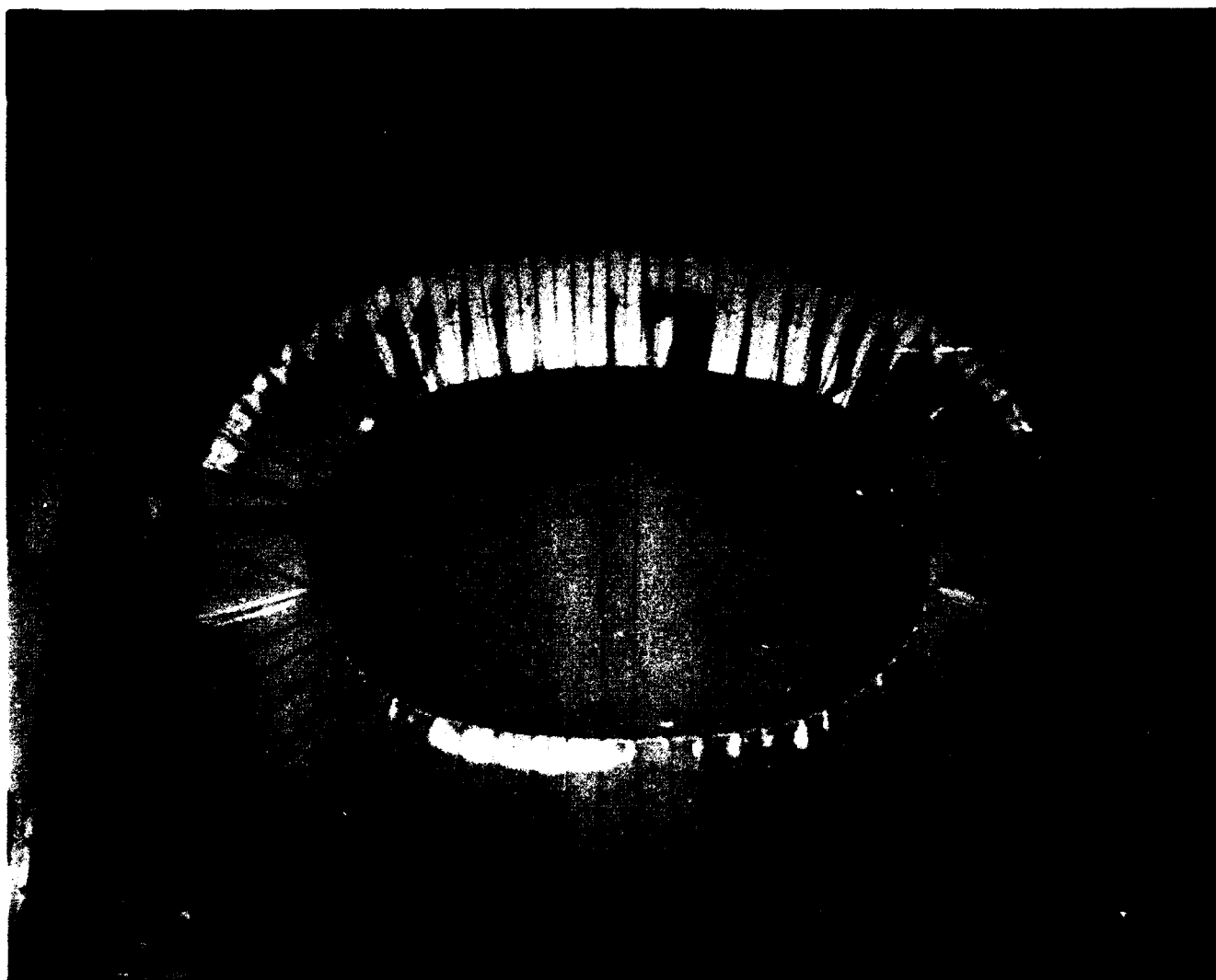
Yamada Y. and others(1989) "Data on snow Cover in Nagaoka(13), Nov.1988-Apr.1989 (in Japanese with English abstract)", Rev. of Res. for Disaster Prevention 138, pp.12.

Yamada, Y. (1990) "Distribution of new snow density in Japan", 5 th International Workshop on Atmospheric icing on structures. B5-2, 1-7.

4

Experimental Modeling

Nicolas Isyumov, Chairman



Model of the new Turin, Italy, stadium showing patterns of snow drifting. Pine sawdust was used to simulate snow in this French wind tunnel. (Photograph provided by Jerzy Wianecki.)

Wind Tunnel Modeling of Snow Accumulations on Large-Area Roofs

Nicholas Isyumov and Michael Mikitiuk

The Boundary Layer Wind Tunnel Laboratory
The University of Western Ontario
London, Ontario, Canada

ABSTRACT

The exact modelling of snow transport and accumulation requires the simulation of the turbulent boundary layer characteristics of the wind and the similitude of inertia, gravity, aerodynamic, interparticle and particle-to-bed forces between the prototype and model snows. This is extremely difficult. To move forward, some "relaxation" of the strict scaling laws is unavoidable. The snow load formation process is dominated by the aerodynamic influence of the structure and its immediate surroundings. As a result, it becomes paramount that the overall aerodynamics of the process are properly simulated. On the other hand, it is possible to accept some approximations in the modelling of particle properties.

INTRODUCTION

This paper examines the use of wind tunnel model studies to predict snow accumulations which can occur on roofs. The concern is for structural performance and the emphasis is therefore on situations which can lead to extreme loads. Both during and after a snowstorm, wind action plays an important role in shaping the roof snow deposits and determining their magnitudes. This is largely an aerodynamic process and the success of its study in wind tunnel or water flume models depends largely on the degree of similarity of the kinetics of the process, which can be achieved at a reduced scale.

While the modelling of detailed features of the process is extremely difficult, if not impossible at a reduced scale, wind tunnel model studies can capture the main essence of the problem. Approximations or "relaxations" of strict modelling requirements which are necessary to achieve practicable simulations at a reduced scale in a wind tunnel are discussed in this paper. Examples are presented to illustrate the importance of the various parameters of the process. Emphasis is on large-area roofs which generally tend to be flat or of low slope and frequently have multiple levels. For such roofs, it becomes particularly important to representatively model the transport of snow by wind action, as this will determine the magnitudes and distributions of drifts. Local loads due to snow drifts can be substantially greater than uniformly distributed or average snow loads and are therefore a concern to designers.

SNOW LOAD FORMATION PROCESS

To move forward with the discussion of modelling procedures, it is useful to first examine the problem under consideration. The consequences of a particular snowstorm on the roof snow load can be summarized as follows:

Consequences of Snowstorm "i"

$$\left(S, S_d, x_d, y_d, \dots \right)_i = \text{function} \left\{ \begin{array}{l} \bullet \text{ Characteristics of Storm} \\ \quad \Delta S, \rho_s, \Delta S/\Delta t, \Delta t, V, \alpha \\ \bullet \text{ Physical Properties of the Snow} \\ \bullet \text{ Siting of Building (including approach terrain,} \\ \quad \text{local topography, surrounding buildings)} \\ \bullet \text{ Building Geometry} \\ \bullet \text{ Snow Accumulations on Roof Prior to Storm} \\ \quad \left(S, S_d, x_d, y_d, \dots \right)_{i-1} \end{array} \right.$$

Here S and S_d are measures of the uniformly distributed and drift snow loads on the roof; x_d and y_d are coordinates describing the distribution of S_d ; ΔS , $\Delta S/\Delta t$, Δt and ρ_s are respectively the magnitude, rate, duration, and density of the snowfall; and V and α are the speed and direction of the wind.

Most wind tunnel model studies are carried out to simulate the effects of single snowfalls, usually chosen to represent an extreme snowstorm and possible drifting episodes which may follow. The consequences of such an event depend on the characteristics of the storm, the physical properties of the snow phase and the effects of wind action. The latter depends on the speed and direction of the wind, the building geometry, its immediate surroundings and the roughness of the approach terrain.

Depending on local climatic conditions, such a single event may not necessarily lead to an extreme snow loading condition. In many situations, extreme snow loads are the consequence of the cumulative effects of a number of storms. This is clearly a much more difficult problem as it involves effects which cannot be studied in a wind tunnel. For example, extreme snow loads may involve:

Formation of Extreme Snow Loads

$$\left(S_{\max}, x_{\max}, y_{\max}, \dots \right) = \text{function} \left\{ \begin{array}{l} \bullet \text{ Cumulative effects of individual snowfalls} \\ \bullet \text{ Redistribution, depletion and compaction} \\ \quad \text{of snow by drifting} \\ \bullet \text{ Sliding from sloped surfaces} \\ \bullet \text{ Effects of rainfalls} \end{array} \right.$$

- Sublimation, melting, refreezing
- Metamorphosis "aging"
- Runoff, ponding
- Icing, ice dams
- Other

Here S_{\max} is the magnitude of extreme snow loads; and x_{\max} and y_{\max} are coordinates describing the distribution of S_{\max} .

How does one best estimate loads in situations where maxima result due to the cumulative effects of a number of individual snowfalls, modified by wind action, rainfall and various thermodynamic effects? Physical models are unavoidable to properly allow for the aerodynamic influence of the building and its surroundings. Their effectiveness, however, is limited to periods during which the snow remains "driftable". Numerical models are needed to properly allow for the effects of snow melting, the superposition of rain and the action of thermodynamic factors. Hybrid procedures, including both physical and numerical models, are advantageous in such situations.

Given the complexity of the process, it is apparent that some simplifications are necessary in order to move forward. The remainder of this paper deals with the physical modelling of the effects of individual snowstorms, as well as situations where it is reasonable to assume that the snow remains "driftable". This is a reasonable approach for relatively short periods (several days) with subfreezing temperatures.

STRICT SIMILARITY REQUIREMENTS

The similarity requirements for physical model studies of snow drifting and accumulation have been extensively reported in the literature (Refs.1,2,3,4,5,6,7,8,9). Many modelling approaches have attempted to achieve similarity of snow particle motion during drifting of the ground snow cover, which at common wind speeds is dominated by saltation. Additional requirements appear when it becomes necessary to maintain similarity of airborne snow particles.

Motion of Surface "Snow" Particles

Similarity of the forces on a particle due to the action of the surface shear force and the restoring action of gravity is achieved by maintaining equality of the densimetric Froude number

$$\frac{\rho u_*^2}{(\rho_s - \rho)gd} = \text{constant} \quad (1)$$

where ρ , ρ_s , u_* , g and d are respectively the air density, the density of the snow particles, the critical or threshold values of the friction velocity u_* , the acceleration of gravity and the snow particle diameter.

Strictly speaking this requirement assumes that $\frac{d_m}{d_p} = \frac{H_m}{H_p}$, where H is a characteristic building dimension and subscripts m and p respectively denote model and prototype quantities. This is not realizable and $\frac{d_m}{d_p}$ tends to be substantially greater than $\frac{H_m}{H_p}$. An alternative approach is to maintain similarity of the densimetric Froude number based on building dimensions, namely

$$\frac{\rho_s v^2}{(\rho_s - \rho)gH} = \text{constant} \quad (2)$$

and to scale flow velocities so that

$$\frac{u^*}{u_*} = \text{constant} \quad (3)$$

To improve similarity of saltation, Kind (Ref. 8) suggests the additional requirements of

$$\frac{u_*^3}{(2gv)_m} > 30; \text{ and } \frac{\rho_s}{\rho} \geq 600 \quad (4)$$

where v is the kinematic viscosity of air.

Motion of Airborne Snow Particles

Similarity of gravity and fluid forces on a particle is achieved when

$$\frac{W_f}{v} = \text{constant} \quad (5)$$

where W_f is terminal velocity of the snow particles

Similarity of particle inertia and gravity forces is achieved when

$$\frac{\rho_s v^2}{(\rho_s - \rho)dg} = \text{constant} \quad (6)$$

Due to the practical difficulty of modelling d_m , H is used as the characteristic dimension. Also $\frac{\rho_s}{\rho}$ is typically much greater than unit. As a result, the requirement of equation (6) is replaced by,

$$\frac{v^2}{Hg} = \text{constant} \quad (7)$$

Similarity of particle inertia and fluid inertia forces is achieved when

$$\frac{\rho_s}{\rho} = \text{constant} \quad (8)$$

Studies carried out at the Boundary Layer Wind Tunnel Laboratory (Refs. 4,5,6) have indicated the importance of achieving a representative simulation of flow in the atmospheric boundary layer (particularly its lower layer), and the flow field in the immediate vicinity of the

roof. The flow similarity requirements are comparable to those needed for most wind engineering studies of buildings and structures (Ref. 10) and can be summarized as follows:

Similarity of Approach Flow

- i) Mean velocity profile
- ii) Structure of turbulence
- iii) Consistently scaled lengths

$$\lambda_L \approx \frac{Z_{om}}{Z_{op}} \approx \frac{Z_{gm}}{Z_{gp}} \approx \frac{L_{um}}{L_{up}} \approx \dots$$

L_u is the integral-length scale of the longitudinal component of turbulence.

Similarity of Building Aerodynamics

- i) Consistent scaling of all lengths

$$\frac{H_m}{H_p}, \frac{B_m}{B_p}, \dots = \lambda_L, \text{ as established in the scaling of approach flow.}$$

- ii) Similarity of aerodynamic features including characteristic lengths of vortices, separation bubbles, etc., or similarity of the Reynolds number (Re) regime

Sharp-edged Bodies

$$\frac{V_H H}{\nu} > 10,000$$

where V_H is the mean wind speed of the approach wind at the height of the roof.

Curved Shapes

Full similarity never achieved. (For all aerodynamic studies of curved shapes, the results obtained with small-scale models have to be interpreted when converting to full scale. Similarity with full-scale experience is the best indicator of representative scaling.)

In addition to the similarity of the building under study, it is necessary to ensure that the aerodynamic influence of surrounding buildings is properly allowed for.

Similarity of the Effects of the Near Field

- i) Consistent scaling of surroundings using λ_L
- ii) Minimum Reynolds number for adjacent buildings

Additional detailed characteristics of the snow phase, which can seldom be properly satisfied in small-scale physical model studies, include similarity of particle/surface forces, the angle of repose, the metamorphosis of the snow, sublimation, melting and refreezing, compaction, etc.

APPROXIMATE SCALING

In reviewing the above requirements, it becomes apparent that while it is possible to achieve a good simulation of natural wind, it is extremely difficult to maintain strict similarity of the various particle forces. It is particularly difficult to achieve proper Froude number scaling which is required to maintain the relative equality of inertia to gravity forces acting on the snow particles, see equations (1,2,6,7). An additional difficulty surfaces with Froude number-scaled experiments. The wind tunnel speeds become low and it is difficult to achieve fully developed turbulent boundary layer flow and to satisfy minimum Re requirements.

The deposition, transfer and accumulation of snow on roofs and in the vicinity of buildings are dominated by the aerodynamics of such buildings. Snow accumulates in areas of aerodynamic shade and its transport is dominated by turbulent mixing and the convective action of the flow. To model this process at a reduced scale in the wind tunnel, it is essential to achieve a good overall similarity of the mean and turbulent flow fields. In addition, it is necessary to achieve similarity of the trajectories of particles, both while airborne and when drifted by the wind along the roof. There are indications that precise scaling of the Froude number is not essential and that acceptable modelling can be achieved by maintaining similarity of the "bulk" hydraulic properties of the snow phase. The main requirements for such approximate similarity becomes:

- i) Similarity of the flow (approach and effects of near field)
- ii) Similarity of aerodynamics of buildings (for sharp-edged bodies $\frac{V_H H}{\nu} > 10,000$)
- iii) Similarity of the bulk hydraulic properties of the snow phase, $u_{*t}, W_f, \rho_s, \rho$
- iv) Requirement that the saltation hop length of model snow $l \ll H$, and $l \ll B$

where H and B are characteristic dimensions of the roof.

While it appears that strict Froude number scaling can be relaxed (Refs. 2,5,6) it is important to ensure that the saltation hop length of the model snow is substantially smaller than the characteristic dimensions of the roof. To achieve this, it is desirable to use as large a geometric scale as possible and it becomes advantageous to carry out tests in large cross-section wind tunnels.

TIME SCALING

The scaling of time in the wind tunnel becomes important when examining the consequences of a particular snow storm. The modelled characteristics of the storm would include V_H , the mean wind speed at roof level, α , the wind direction, the amount of snowfall during the storm ΔS , as determined by the depth of snow resulting at a location away from the influence of the model building, and the duration of the snowstorm Δt . It is necessary that

$$\left(\frac{\omega \Delta S}{\Delta t} N_H \right)_m = \left(\frac{\Delta S}{\Delta t} N_H \right)_p \quad (9)$$

Correspondingly

$$(\lambda_t)_{\text{Snow Phase}} = \lambda_L \lambda_V = (\lambda_t)_{\text{flow}}$$

where $\lambda_L = H_m/H_p$ and $\lambda_V = u_{*m}/u_{*p}$.

This requires that the nondimensional time for both the flow and the snow phase must be equal

$$\left(\frac{u_* t}{H}\right)_m = \left(\frac{u_* t}{H}\right)_p \quad (10)$$

For a consistent model, the time scale of the growth of snow deposits on and around the roof should equal the time scale of the model flow. A mismatch would result in an incorrect or distorted modelling of the overall process. While the arguments for a common time scale are obvious in situations of falling snow, the same time scale must also hold when considering snow drifting on the roof surface. The time scale for the snow transport during periods without snowfall can be obtained from the similarity of the mass flux of the drifting snow. For a consistent simulation of the mass flux of the model snow phase it is necessary that

$$\left(\frac{q_s}{\rho u_* H}\right)_m = \left(\frac{q_s}{\rho u_* H}\right)_p \quad (11)$$

where q_s is the snow flux within a unit lane.

This results in a time scale of

$$\left(\frac{u_* t}{H}\right)_m \left(\frac{\rho}{\rho_s}\right)_m = \left(\frac{u_* t}{H}\right)_p \left(\frac{\rho}{\rho_s}\right)_p \quad (12)$$

If $\left(\frac{\rho}{\rho_s}\right)$ is maintained constant as suggested above, equation (12) reverts to equation (10), derived for falling-snow conditions.

More complicated time scales have been suggested in the literature for the modelling of saltation transport of snow. These are difficult to physically justify as this would result in a time scale of the snow phase which differs from that for the flow. Clearly the time-scaling question requires further study and full-scale snow flux measurements over roofs are needed to allow comparisons with model values.

SOME RESULTS

Studies of snow accumulation on roofs, carried out at the Boundary Layer Wind Tunnel Laboratory using the above approximate approach, have examined the use of a number of possible model snow materials. These have included sand, ground walnut shells, sawdust, and various finely ground cereals. Of these, bran with a typical particle diameter of about 0.5mm has been found most effective. The physical properties of this material have been reported elsewhere (Refs. 5,6). Some of the trends observed in these studies of large area roofs are as follows:

Effects of Geometric Scale

Studies have been carried out at several geometric scales, in order to examine the consequence of relaxing strict Froude number scaling. Depositions on a large two-level roof,

studied at scales of 1:100 and 1:400, have been found to be similar. These tests were carried out in two different wind tunnels with representatively-scaled turbulent boundary layer flows in each case. The same model snow was used in these two simulations. The good observed similarity in the deposition patterns suggests that differences in Froude Number scaling are not appreciable, at least within this range of variation. In both cases, the saltation hop length of the model snow particles was substantially smaller than characteristic dimensions of the roof.

Effects of Wind Speed

The effects of wind speed are demonstrated in Figure 1. This diagram shows changes in the model roof snow layer after a period of drifting at different wind speeds. Prior to each test, the roof was covered with a similar depth of snow, denoted as D . Here d is the change in depth measured from the initial conditions. At time $t=0$, $\frac{d}{D}=0$ and $\frac{d}{D}=-1$ means that all the initial model snow has been removed. V_R is the mean speed of the approach wind at the height of the roof and V_{R_t} is its value at the threshold of drifting. Most numerical studies of the formation of drift snow loads omit the wind speed as a variable. Figure 1 clearly shows how important wind speed is in determining the rate at which material will be transported and, consequently, the snow depositions which can result due to particular drifting and/or snowfall episodes.

Unusual Drift Distributions

Wind tunnel model studies indicate that snow drifts on large-area roofs can substantially differ in magnitude and distribution from the idealized triangular drifts contained in most building codes. Figure 2 shows the drift formed on the lower portion of a two-level roof for a quartering or skewed wind. In such situations, corner vortices tend to shape the form of the drifts downstream of corners and at changes in geometry. As seen in Figure 2, the drift at the corner has a substantially longer downstream extent in comparison to other locations along the step. In situations where there is an ample supply of snow on the roof, such quartering drifts have been observed to be of substantial magnitude. Also, their downstream extent can be greater than the triangular drift lengths recommended in codes.

Duration of Periods With Snow Drifting

Since wind speed is a dominant variable in the shaping of roof snow loads, the duration of periods with appreciable drifting becomes an important parameter. Figure 3 shows results taken from an experiment in which a two-level roof was covered with a uniform model snow deposit, after which the wind was turned on and changes of the roof snow deposit were observed. Figure 3 shows the model mass snow flux per unit width at different locations along the roof and at three different times from the start of the experiment. This snow flux, denoted by q_s , is normalized by $\rho L V_R$, where L is the length of the upper roof. Also shown, is the local rate of change of the snow depth $\frac{\Delta d}{\Delta t}$ divided by the reference velocity V_R . It is important to recognize that the flux is not constant along the length of the roof. In this case the wind is from left to right and the flux is negative (a net loss) on the high portion and positive (net gain) on the low portion of the roof. The snow flux varies substantially with the amount of snow available and diminishes with time on the upper roof which has lost much of its snow towards the end of the test. Figure 3 clearly shows that the magnitude and the extent of the drift formed on the lower roof vary substantially

with duration of drifting. This demonstrates the importance of considering not only the wind speed but also the duration of expected strong wind conditions when estimating maximum drift loads on roofs.

Effect of Terrain Roughness

Substantial differences in snow deposition can be obtained on the same roof in different types of terrain. A change in terrain roughness has several significant influences. First, changing the roughness of the approach flow influences the overall aerodynamics of the roof and consequently changes the distribution of flow patterns and locations and extents of regions of aerodynamic shade. Second, changes in the structure of the turbulent flow alters the entrainment rate of snow particles and hence the transport of material for the same mean wind speed. This importance of terrain roughness has been previously reported (Refs. 4,6,11) and is shown in Figure 4. Substantially larger transport rates are observed for the urban case for the same normalized mean wind speed at roof level. The mean wind speed in each case is normalized by its corresponding threshold value at which model snow particle transport was observed to commence. Figure 4 also demonstrates that the functional dependence of the snow flux on wind speeds is substantially greater than that for transport by saltation alone, which is proportional to wind speed cubed.

Special Aspects of Large-Area Roofs

There are a number of special aspects to the formation of snow loads on large-area roofs. Their large plan dimensions result in longer drift transport distances. Consequently, longer times are required to clear such roofs by wind action. As a result, only partial clearing of the roof may occur during particular weather conditions. Correspondingly, there is a greater potential for non-uniform snow accumulations or drifts. In addition to a longer time constant for clearing the roof by wind action, large-area roofs also have longer drainage times for melt and rainwater. As a result, there is a greater potential for ice buildup.

The longer time constant of large-area roofs makes their extreme values more dependent on the cumulative effects of several snow storms. Studies have been carried out at the Boundary Layer Wind Tunnel Laboratory in which the cumulative effects of an approximately two-week period with below-freezing temperatures and appreciable snowfalls were studied in the wind tunnel. The model roof was exposed to a series of model snow storms, each scaled in magnitude and duration to correspond to actual weather conditions. Because of the cold temperatures, it was assumed that the full-scale snow would remain driftable during this entire period. The results of this wind tunnel simulation were in good agreement with available full-scale observations.

CONCLUDING REMARKS

The exact modelling of snow particle motion at reduced scales in wind tunnels and water flumes is extremely difficult. A particularly demanding requirement is the scaling of the Froude number which results from strict similarity arguments. Snow accumulations on roofs are dominated by the aerodynamics of the building itself and particle transport within its immediate vicinity is substantially different from that in open snow fields. As a result, it is possible to relax some of the strict modelling requirements for saltation transport and still achieve a good overall

similarity. This paper suggests that progress can be made with model studies in which only an overall or "bulk" similarity of the snow phase is achieved. In such studies, the primary similarity requirements become:

- i) the modelling of the mean and turbulent flow fields to which the roof is exposed,
- ii) the modelling the bulk hydraulic characteristics of the snow phase including its drifting threshold, its terminal velocity, and the ratio of the bulk snow to air densities.

Well-documented, full-scale data are needed to verify these simplifying assumptions and to improve the overall confidence of the modelling process.

REFERENCES

- 1) Anno, Y., "Requirements for Modelling of a Snowdrift", Cold Regions Science and Technology, Vol. 8, 1984.
- 2) Anno, Y., "Froude Number Paradoxes in the Modelling of a Snowdrift", Cold Regions Science and Technology, Vol. 10, 1985.
- 3) Irwin, P.A. and Williams, C.J., "Application of Snow-Simulation Model Tests to Planning and Design", Proc. Eastern Snow Conference, Toronto, Ontario, Vol. 28, June 1983.
- 4) Isyumov, N., "An Approach to the Prediction of Snow Loads", The University of Western Ontario, Ph.D. Thesis, London, Ontario, Canada, 1971.
- 5) Isyumov, N., Mikitiuk, M. and Cookson, P., "Wind Tunnel Modelling of Snow Drifting - Applications to Snow Fences", Proc. of the First International Conference on Snow Engineering, Santa Barbara, California, July 1988.
- 6) Isyumov, N. and Mikitiuk, M., "Wind Tunnel Model Tests of Snow Drifting on a Two-Level Flat Roof", Jrnl. Wind Engineering and Indust. Aerodynamics, Vol. 36, 1990.
- 7) Iversen, J.D., "Small-Scale Modeling of Snowdrift Phenomena", Proc. Int. Workshop on Wind Tunnel Modeling Criteria in Civil Engineering Applications, Gaithersburg, Maryland, April 1982.
- 8) Kind, R.J. and Murray, S.B., "Saltation Flow Measurements Relating to Modelling of Snow Drifting", Jrnl. Wind Eng. and Indus. Aerodynamics, Vol. 10, pp. 89-102, 1982.
- 9) Kind, R.J., "Snowdrifting: A Review of Modelling Methods", Cold Regions Science and Technology, Vol. 12, 1986.
- 10) ASCE Manual of Practice on "Wind Tunnel Model Studies of Buildings and Structures", Manual No. 67, 1987, New York, N.Y.
- 11) Mikitiuk, M. and N. Isyumov, "Variability of Snow Loads on Large-Area Flat Roofs", Proc. of the First International Conference on Snow Engineering, Santa Barbara, California, July 1988.

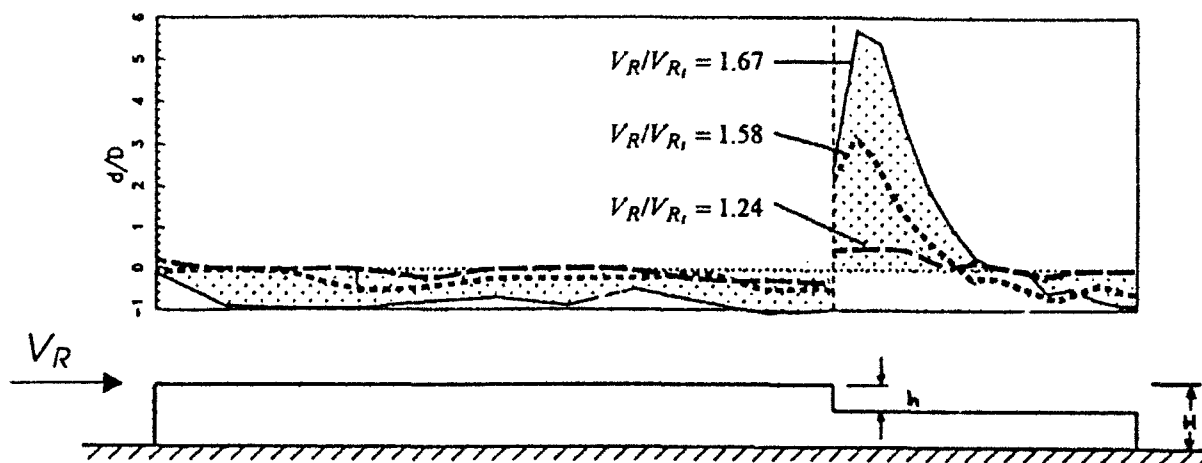


Figure 1 Changes to Snow Accumulation Patterns on a Two-level Roof in Urban Terrain after an 18-Hour Full-Scale Period with Drifting at Three Different Wind Speeds; D , is the Initial Snow Depth

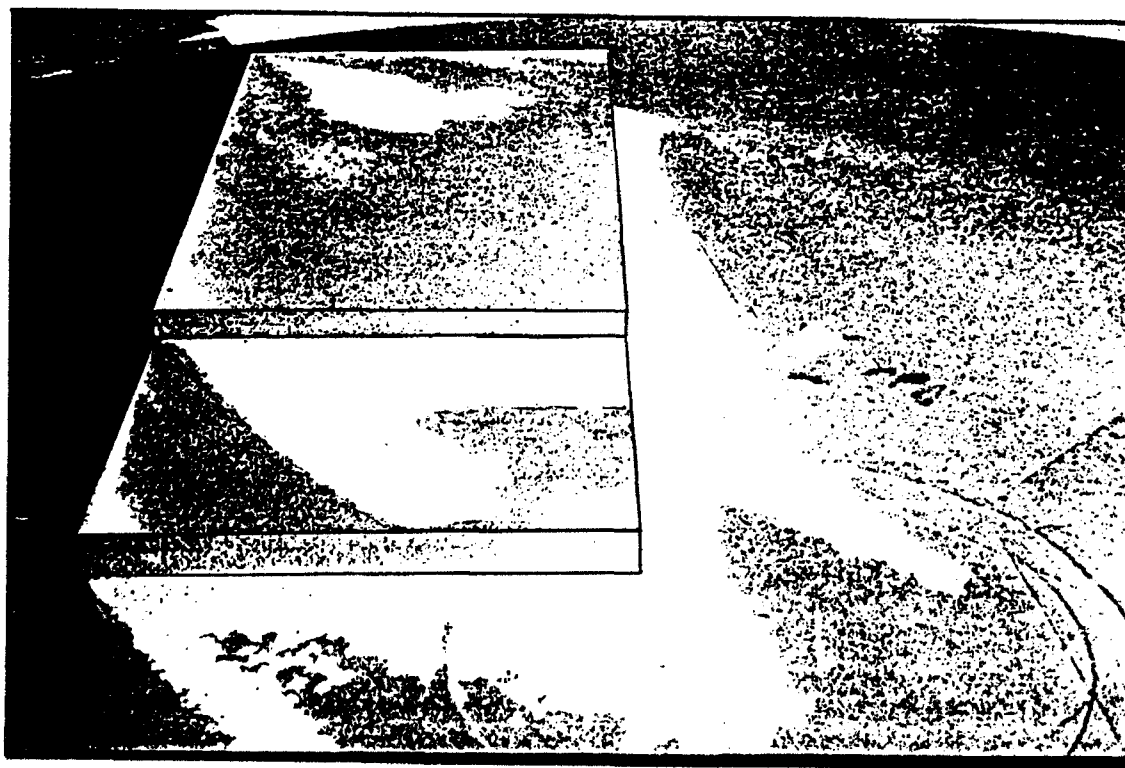


Figure 2 Drift Accumulation on a Two-Level Roof for a Quartering Wind

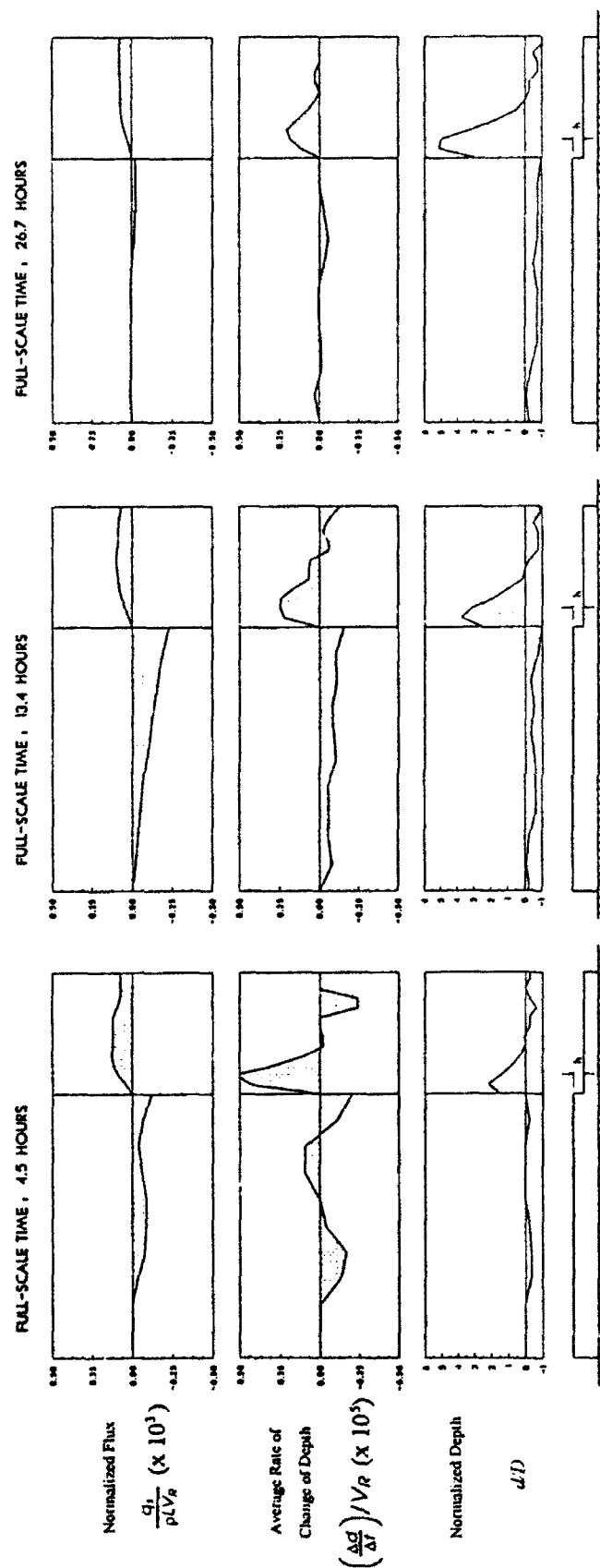


Figure 3 Variations of Snow Flux, Deposition Rate and Snow Depth for a Two-Level Roof in Urban Terrain at Different Times after the Start of Drifting,
 $V_R / V_{R_i} = 1.48$

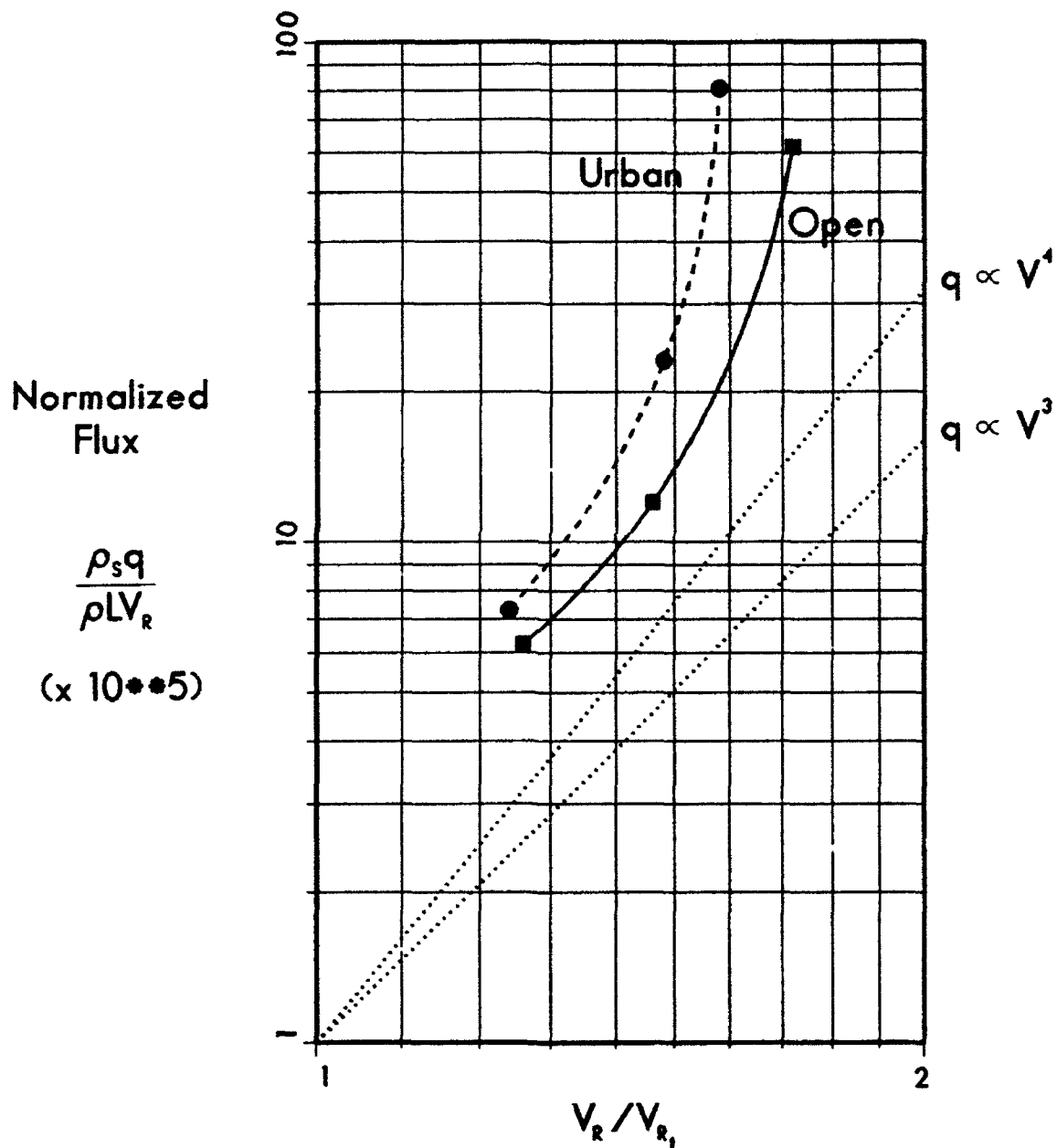


Figure 4 Snow Transport Within a Unit Lane Over the Upper Portion of a Two-Level Roof in Urban and Open Terrains, L is the Length of the Upper Roof

Laboratory Studies of Snow Drifts on Multilevel Roofs

Michael O'Rourke and Neal Weitman

Rensselaer Polytechnic Institute
Troy, New York

ABSTRACT

This paper describes ongoing laboratory research on triangular snow drifts at backward facing roof steps. A multilevel roof with the upper level roof located upwind of the lower level roof, with wind perpendicular to the roof step is considered. The laboratory experiments are conducted in the RPI flume, in which the flow of water simulates wind and crushed walnut shells simulate snow.

The objective of the research program is to develop basic knowledge about drifting of roof snow. Specifically, the threshold speed, transport rate of upper level roof snow and the trapping efficiency of a backward facing roof step are determined. The paper describes the RPI water flume and instrumentation used in the program as well as results to date.

INTRODUCTION

Snowfall during calm conditions leads to relatively uniform snow loads on a building's roof. However, the roof snow will be redistributed if sufficient wind is present during or after the snowfall. For example, for the multilevel roof shown in Fig. 1, wind blowing from left to right results in a triangular drift at the change in roof elevation. For wind blowing from left to right, the roof elevation difference H corresponds to a backward facing step. As observed by Tabler (1975), triangular drifts tend to form at backward facing steps. The source of snow for drifts at a backward facing step is primarily snow on the upper level roof. These roof drifts can become quite large and hence are important for the structural design of roof members. In point of fact, approximately 75% of all snow-related roof failures are due to drifts on multilevel roofs.

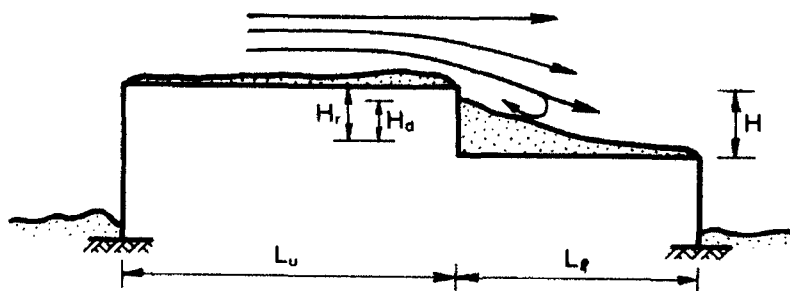


Figure 1 Triangular Drift at Backward Facing Roof Step

Empirical relationships for the expected height of triangular drifts on multilevel roofs have been developed. These relationships are the result of multiple regression analyses of actual roof drift case histories obtained from field surveys, failure investigations and insurance company files. Admittedly this data base is skewed towards large drifts because of the sources of the case histories. Large triangular drifts are typically associated with large upper level roofs adjacent to smaller lower roofs (i.e., a large, high roof, manufacturing space adjacent to a smaller, low roof, office space).

Based on approximately 160 case histories O'Rourke et al. (1986) proposed the following relationship for triangular drifts on multilevel roofs

$$H_d = 0.43 \sqrt[3]{L_u} \sqrt[4]{P_g + 10} - 1.5 \leq H_r \quad (1)$$

where H_d is the expected surcharge drift height in feet, L_u is the length of the upper level roof in feet, P_g is the ground snow load in psf, and H_r is the effective elevation difference, that is, the elevation difference, in feet, between the upper level roof and the uniform snow, if any, on the lower level roof. This relationship is the basis for multilevel drift load provisions in the 1987 BOCA code, the Massachusetts State code, ASCE standard 7-88, and the proposed ISO standard. Note that Eq. (1) make intuitive sense in that the drift height is a function of the appropriate snow source. That is, triangular drift height at a backward facing step in Eq. (1) is a function of the amount of snow per unit area and the length of the upper level roof. Equation (1) also indicates that not all of the "available snow" end up in the drift. For example, using reasonable estimates for the density of snow and the length of the drift, Eq. (1) suggests that the cross sectional area of a triangular drift is roughly 20% to 30% of the available snow as quantified by L_u and P_g . This introduces the concept of the trapping efficiency of a roof step. Although Eq. (1) matches fairly well the case history data, it does not include all the parameters which influence drift size.

Three items are needed in order for a roof drift to form. These are; (1) a geometric irregularity, (2) a source of driftable snow and (3) wind velocity sufficient to cause drifting. For triangular drifts at backward facing steps, the roof step is the geometric irregularity and snow on the upper level roof is the primary snow source. However, wind is needed for redistribution of snow into the drift.

Using multiple regression analysis, O'Rourke and Galanakis (1990) show that the surcharge height H_d of the triangular drift is related to the diagonal length of the upper level roof L_d , the effective roof elevation difference H_r and a blizzard intensity factor BI through the relationship

$$H_d = 0.119(H_r)^{.411}(L_d)^{.498}(BI)^{.235} \leq H_r \quad (2)$$

The primary difference between Eqs. (1) and (2) is that wind speed during and after snowfalls is considered explicitly in Eq. (2). The blizzard intensity factor BI is the maximum value over a three day period of the product of snow deposition and wind speed above a threshold.

$$BI = (h_i \cdot w_i)_{\max} \quad (3)$$

where h_i is the deposition or amount of snow in inches which fell during a three day period, and w_i is the area, with units of knot-days, of the wind speed above a threshold versus time graph for a three day period.

As defined above, the blizzard intensity BI is a function of a threshold speed. This recognizes the fact that winds of a certain velocity are needed for snow transport by creep (snow particles rolling along the surface), saltation (snow particles bouncing along the snow surface) or in suspension. From the multiple regression analysis a threshold speed of 3.98 knots (2.0 m/sec) was found to yield the best match between predicted and observed drift heights.

Blizzard intensity is evaluated for a three day period. The three day period was chosen to represent a reasonable upper bound for the duration of a blizzard. In addition old snow, at least in the East and the Pacific Northwest, tends to form a crust which inhibits drifting. Hence winds which occur three or four days after snow deposition are unlikely to result in significant drift formation.

It is author's opinion that no further useful information can be developed through multiple regression analyses of a collection of multilevel roof drift case histories. Detailed studies of the drift formation mechanism are needed for further improvements in drift load prediction methodology.

Wind blowing from left to right in Fig. 1 with a sufficient speed V would generate snow transport at the upper roof level due to creep, saltation, and particles in suspension. The transport can be quantified by a snow transport rate $G(t)$. Some of this transported snow will end up in the drift. The percentage of the transported snow which ends up in the drift can be quantified by the trapping efficiency $E(t)$ with $0 \leq E(t) \leq 1.0$. Since the length of the drift at a backward facing step is typically four to six times the drift height (i.e. linearly proportional to H_d), the change in the surcharge drift height is given by

$$\Delta H_d = H_d(t) - H_d(0) \propto \left[\int_0^t G(t) \cdot E(t) dt \right]^{\frac{1}{2}} \quad (4)$$

The authors feel that Eq. (4) can serve as the basis for a physical model of the drift formation process founded on mechanics, as opposed to empirical models founded on statistical analysis of drift load case histories.

The purpose of the research program described herein is the experimental determination of the transport rate $G(t)$ and the trapping efficiency $E(t)$ using scale models of multilevel roofs with backward facing steps in a water flume. Subsequent sections will describe the laboratory equipment, similitude considerations, the experimental procedure, and results to date for $E(t)$ and $G(t)$.

LABORATORY EQUIPMENT

The experiments described herein were performed in a 7.6 m (25 ft) long, 0.76 m (2.5 ft) wide, and 1.22 m (4 ft) deep open-channel water flume at Rensselaer. Two water pumps produce a maximum possible flow of 0.64 m/sec (2.1 ft/sec). One of the pumps can be throttled, so the flow rate can be altered during testing. A window is present where the models are placed which allows side viewing of the experiment in progress.

Velocity recordings are taken with a Swoffer Instruments Model 2100 Current Velocity Meter. It provides current measurements from 0.03 to 7.6 m/sec (0.1 to 25 ft/sec). The display has three averaging periods of 5, 20, and 90 seconds. A 5.1 cm (2 in) propellor is located at the end of the sensor wand and drives a rotor containing fiber-optic

bundles. This in turn creates a pulse that is proportional to the propellor RPM. The pulses are counted and processed to display the average interval velocity. Calibration of the meter was performed in the RPI towing tank.

Wooden building models were built to test in the flume. Some are scaled versions of benchmark case histories where failures due to drifting have occurred. The standard building model which was used for most of our tests to date, has a scale of 1:30 and is shown in Fig. 2. It corresponds to a prototype multilevel roof having upper and lower roof lengths, L_u and L_l of 18.3 m (60 ft), an upper level roof height of 6.1 m (20 ft) and a roof step, H , of 3.05 m (10 ft).

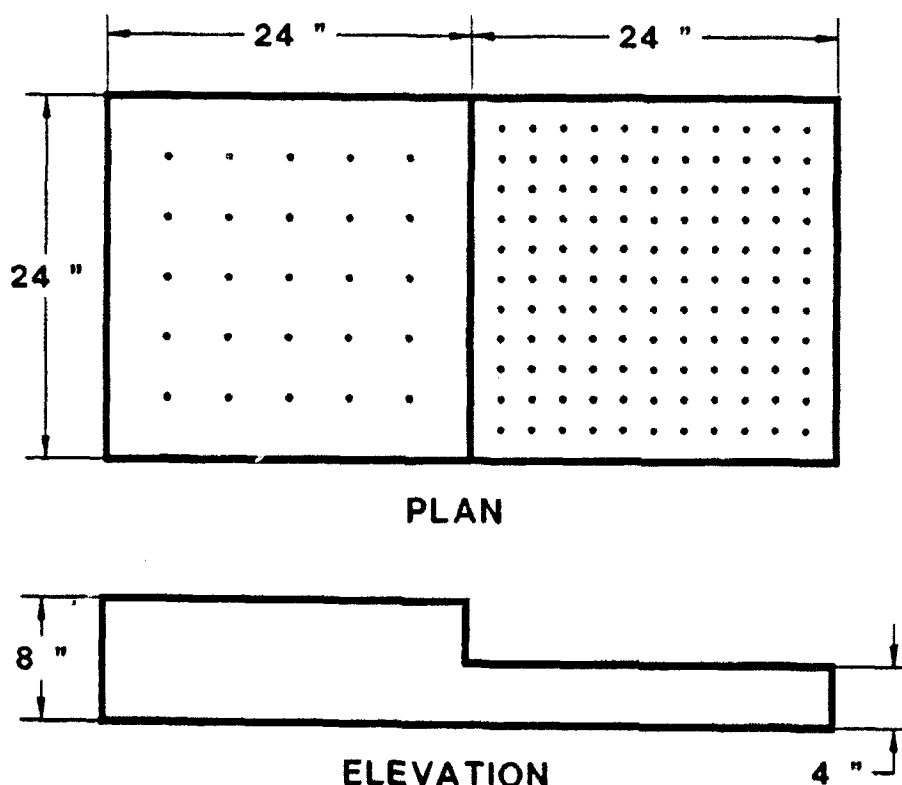


Figure 2 Standard Multilevel Roof Model with 1:30 Scale

Both the upper and lower roofs are painted with grids in order to facilitate the data taking process. A four inch grid is used on the upper roof, while a two inch grid is used on the lower. The tighter grid is used since the drift formed on the lower roof is of greater interest.

SIMILITUDE CONSIDERATIONS

Isyumov (1971) suggests modeling in which the ratio of the particle terminal fall velocity W and the particle threshold shear velocity U^* are the same for both model and prototype.

$$\frac{W_m}{W_p} = \frac{U_m^*}{U_p^*} \quad (5)$$

Above and in the following equations, the subscript m indicates the model while p indicates the prototype.

Our model particle selection is based on Eq. (5). Values for the terminal fall velocity and the threshold shear velocity for the snow in air prototype, W_p and U_p^* respectively, are available in the Handbook of Snow (Gray and Mallet, 1981). For loose dry snow in air the ratio W_p/U_p^* is 5.0.

After a few trials we choose crushed walnut shells in water as the model. The terminal fall velocity for a sphere as given by Raudkivi (1976) is

$$W = \frac{4}{3} \frac{d^2 g (\rho_s - \rho)}{24 \nu \rho} \quad (6)$$

when d is the mean particle diameter, g is acceleration due to gravity, ν is kinematic viscosity, ρ is fluid density, and ρ_s is particle density taken as the total unit weight of a submerged particle. For crushed walnut shells in water with $d = 0.02$ in (0.05 cm) and $\rho_s = 75.7$ pcf, (11.9 kN/m³) the terminal fall velocity W_m is 0.102 ft/sec (3.11 cm/sec). An experimental check using a graduated cylinder with a diameter of 6 cm yield $W_m \approx 0.08$ ft/sec (2.44 cm/sec).

The threshold shown velocity for a particle in water as given by Raudkivi (1976) as

$$U^* = 0.2 \sqrt{\frac{\rho_s - \rho}{\rho} g d} \quad (7)$$

For crush walnut shells, Eq.(7) gives $U^* = 0.0218$ ft/sec (0.66 cm/sec). This value was checked experimentally by measuring the fluid velocity of 0.365 ft/sec (11.1 cm/sec) at 2 in (5.0 cm) above the upper level roof for movement of walnut shells on the upper roof. The threshold shear was then back calculated assuming a logarithmic velocity profile given by Martins (1989).

$$\frac{U}{U^*} = 2.5 \ln\left(\frac{y}{d'}\right) + 8.5 \quad (8)$$

when U is the fluid velocity at a distance y above the surface for initial particle movement and d' is size of the roughness elements taken as the depth of walnut shells on the upper roof. For $U = 0.365$ ft/sec (11.1 cm/sec) and $y = 2$ in (5.0 cm), the value of U^* from Eq. (8) is 0.0305 ft/sec (0.93 cm/sec) which is somewhat higher than the theoretical value.

Using theoretical values for the walnut shell in water model, the W_m/U_m^* ratio equals 4.68 which is close to the snow in air prototype. Prototype and model properties are summarized in Table 1.

Property	Prototype Snow in Air	Model Walnut in Water
Diameter d(in(cm))	0.0197 (0.05)	0.02 (0.051)
Density ρ_s (pcf(kN/m ³))	3.12 (0.49)	75.7 (11.9)
Terminal Fall Velocity W(ft/s(cm/sec))	2.46 (75)	0.102 (3.11)
Threshold Shear Velocity U*(ft/s(cm/s))	0.492 (15.0)	0.0218 (0.66)
W/U*	5.0	4.68

Table 1 Properties of Prototype and Model

In order to maintain dynamic similarity, the densimetric Froude number for the walnut shell/water model should match that of the snow/air prototype. According to Iverson (1982), the densimetric Froude number provides a better correlation of deposition rate, than does the basic Froude number. That is, using the densimetric Froude number, dynamic similitude requires

$$\left\{ \frac{\rho U^*{}^2}{\rho_s gh} \right\}_p = \left\{ \frac{\rho U^*{}^2}{\rho_s gh} \right\}_m \quad (9)$$

where h is a characteristic height.

Since the above equation is a function of both the particle and medium densities, the medium velocity, and the scale, it will provide a basis for the scaling of prototype velocities to the model velocities in the future when we attempt to replicate benchmark case histories.

The geometric scale chosen for the model was based upon typical upper level prototype roof heights (approx. 20 ft (6.1 m)) and the depth of water in the flume at various flow velocities. At a slow velocity of 0.10 ft/sec (3.05 cm/sec) the water depth is roughly 12 in (0.30 cm) while at a high velocity of 0.70 ft/sec (21.3 cm/sec) the water depth is roughly 15.5 in (39.4 cm). For an 8 in (20.3 cm) upper level model roof height there is at least 4 in (10.2 cm) of water over the top of the roof even at low velocities. The 8 in (20.3 cm) model dimension corresponds to a 20 ft (6.1 m) prototype dimension for the geometric scale of 1:30 which we used.

EXPERIMENTAL PROCEDURE

An initial volume of dry walnut shell is placed on both upper and lower levels of the model and spread evenly. The flume is then filled slowly so as to not disturb the particulate. When the water level has reached a desired height of roughly 11 in (28 cm), the pump is throttled so as to maintain a constant fluid velocity for the duration of the test. The experiments thus simulate a wind storm following a snowfall.

When the test is completed the flume is allowed to drain slowly, so as to not disturb the drift that has formed. The drift depth measurements are then taken at each node of the grid on both upper and lower roofs. The wet walnut shells are then removed from the upper roof, and the volume is measured once it has been allowed to dry. The volumetric and mass transport rates are then calculated. Knowing the amount of particulate that has left the upper roof, and the volume of the surcharge drift, the trapping efficiency of the roof step is determined.

EXPERIMENTAL RESULTS

This section presents experimental results to date from our water flume tests. Figure 3 shows as a function of the test duration, the total amount of material transported from the upper level roof for water velocities of 0.15, 0.20 and 0.25 ft/sec (4.6, 6.1 and 7.6 cm/sec). The water velocity was measured at a spot 8 in (20 cm) above the flume floor and 24 in (61 cm) upstream of the upstream wall of the model. Note that each data point in Fig. 3 represents the results of one complete test. This is, because of the experimental procedure described in the previous section, we are not able to determine the amount of material which left the upper level roof at various times during an individual test, but only the total amount transported by the end of the test.

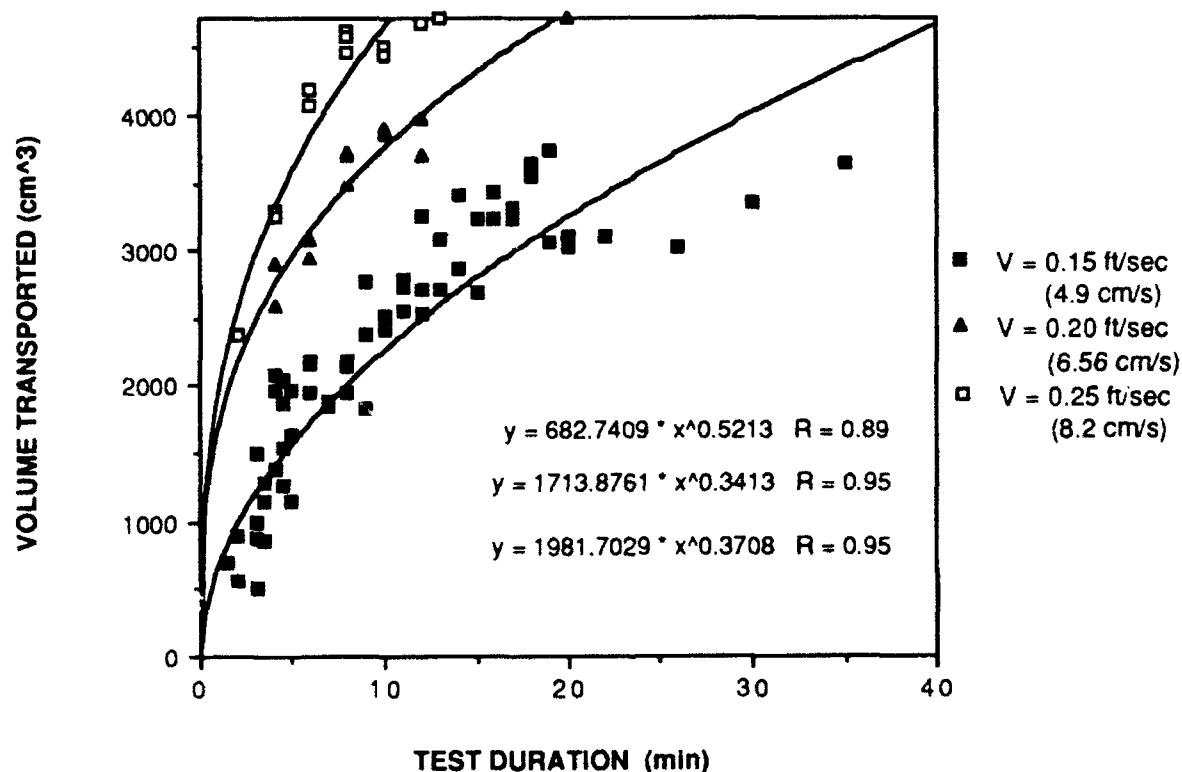


Figure 3 Volume Transported from Upper Level Roof versus Test Duration for three Water Velocities ($L_u = 24$ in (61 cm), initial particle depth = 0.5 in (1.27 cm))

Velocity Variation

As one would expect, the total transport is an increasing function of both test duration and water velocity. Note that the test results shown in Fig. 3 were all for an initial walnut shell depth of 1/2 in (1.3 cm) on both the upper and lower level roofs. Hence the maximum possible transport (ie total volume initially on the upper level roof) is 4720 cm³, and for $v = 0.25$ ft/sec (7.6 cm/sec) the upper level roof is clean after about 12 min.

Curves, also shown in Fig. 3, were fit through data points for each of the three water velocities.

The slope of the curve through the data points yields the volume transport rate, $G(t)$, with units of cm³/min. The volume transport rate is shown in Figure 4 for the standard model with upper roof length, L_u , of 24 in (61 cm). for the three water velocities. Note that the initial transport rates are largest towards the beginning of the test and decrease as material is removed from the upper level roof. That is, the transport rate is largest when the upper roof is fully covered with walnut shells.

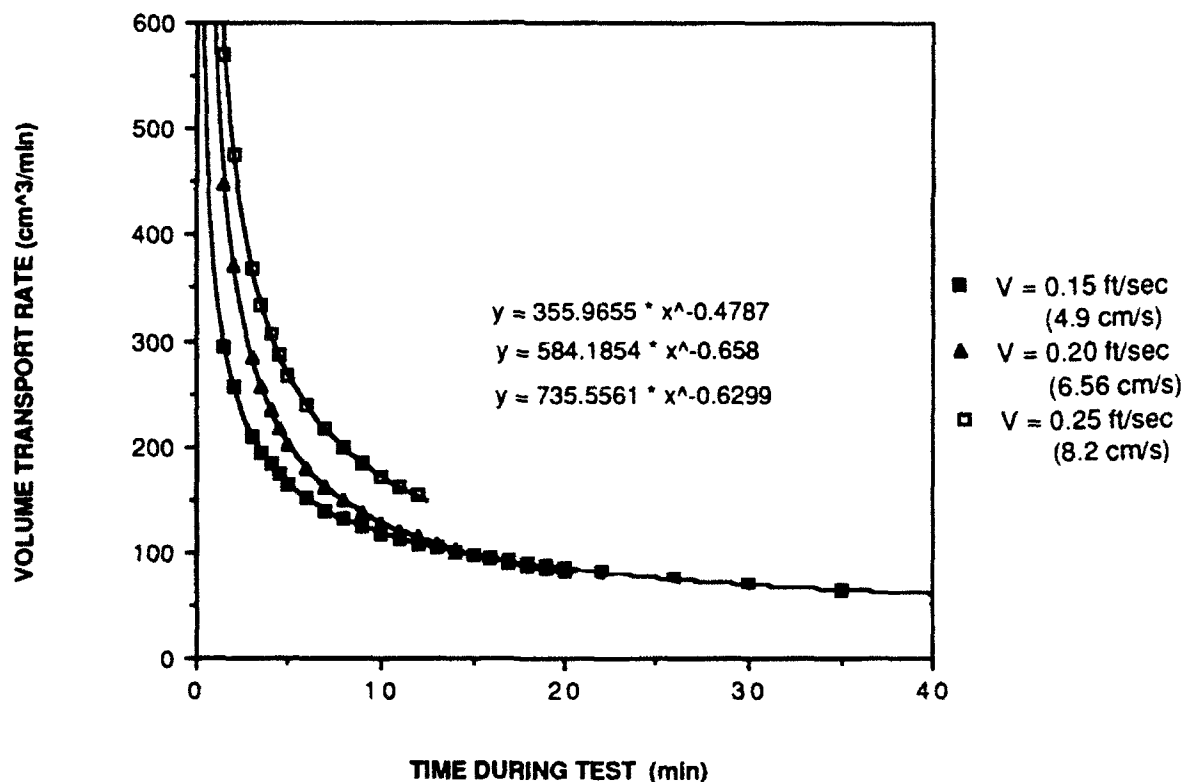


Figure 4 Volume Transport Rate versus Time for three Water Velocities ($L_u = 24$ in (61 cm), initial particle depth = 0.5 in (1.27 cm))

For the high water velocity of 0.25 ft/sec (7.6 cm/sec), the data points in Figure 3 correspond to test durations of about 4 to 12 min. and for those times the transport rate varies from roughly 300 to 150 cm³/min. For the low velocity of 0.15 ft/sec (4.6 cm/sec), the transport rate varies from roughly 200 to 100 cm³/min for times between 4 and 12 min.

As noted above, the drift surcharge volume was measured after each test. As defined herein, the surcharge drift is the volume of the roughly triangular drift above the initial depth of walnut shells on the lower level roof. Figure 5 show measured surcharge drift volumes for various test durations at a water velocity of 0.15 ft/sec (4.6 cm/sec). As one might expect the drift size is an increasing function of test duration and water velocity. That is for a 10 min test the drift volume is about 1600 cm³ for the 0.15 ft/sec (4.6 cm/sec) velocity, but about 2500 cm³ for $V = 0.25$ ft/sec (7.6 cm/sec).

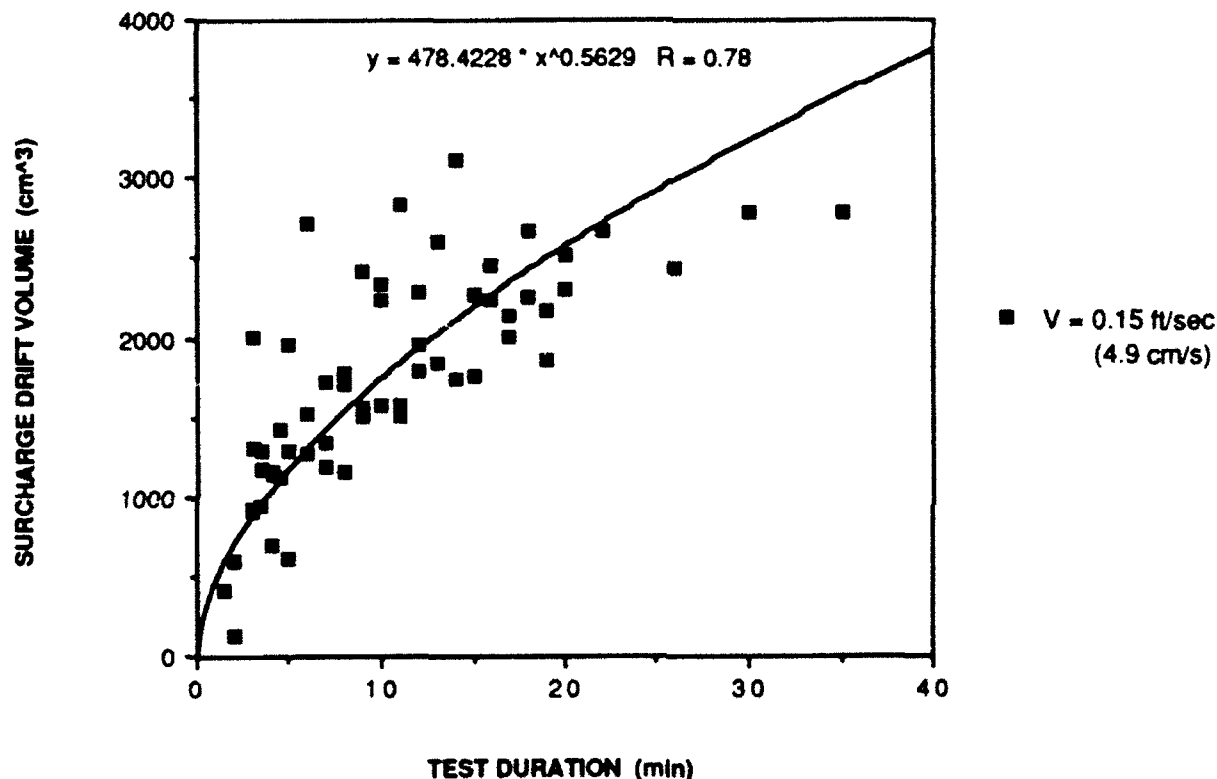


Figure 5 Surcharge Drift Volume versus Test Duration for Water Velocity of 0.15 ft/sec (4.6 cm/sec) ($L_u = 24$ in (61 cm), initial depth = 0.50 in (1.27 cm))

As with Fig. 3, the data points were fit with a curve. However, there is more scatter of data points about the curve in Fig. 5 than those in Fig. 3. The slope of the curve in Fig. 5 is the change in the drift volume per unit time. Herein we define the trapping efficiency as the change in the drift volume per unit time (ie slope of Fig. 5) divided by the transport rate (as shown for example in Fig. 4). The trapping efficiency for the standard model with $L_u = 24$ in (61 cm) is shown in Fig. 6 as a function of time for the three water velocities. Note that the trapping efficiency is a decreasing function of velocity. That is for a velocity of 0.15 ft/sec (4.6 cm/sec), the trapping efficiency of a backward facing step is about 80%, while for velocities of 0.20 and 0.25 ft/sec (6.1 and 7.6 cm/sec) it is less than 60%.

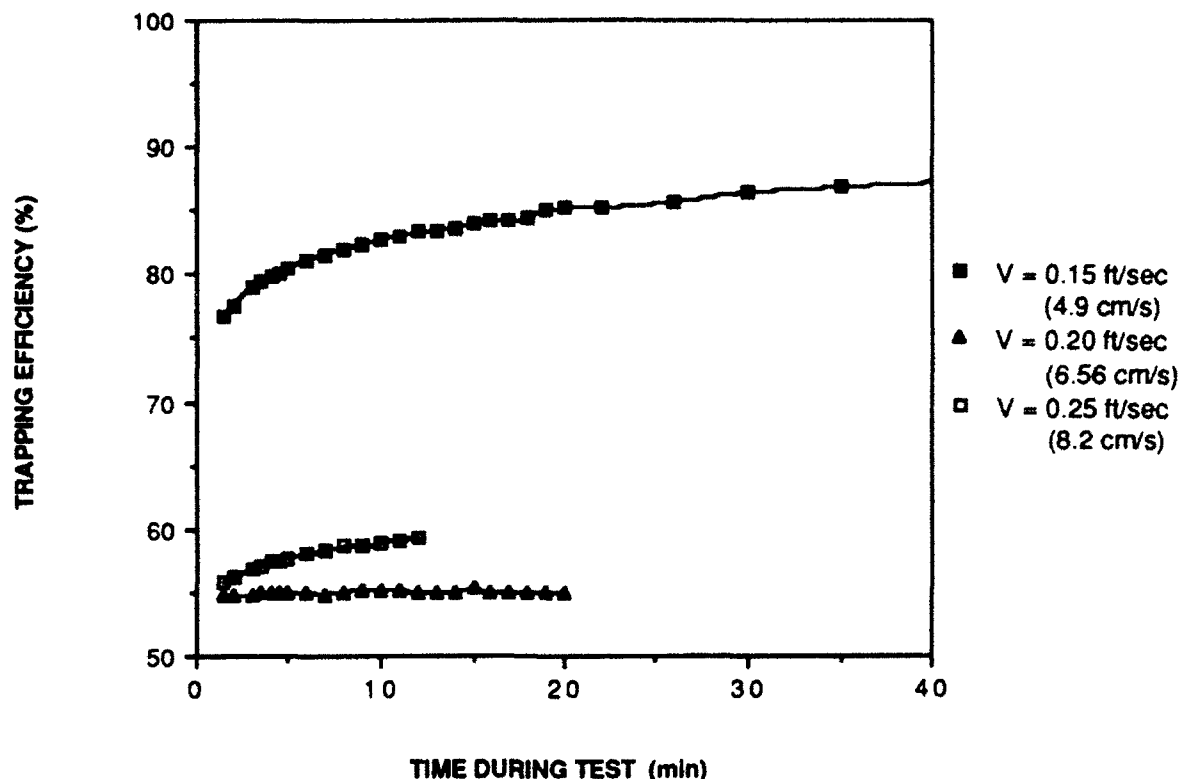


Figure 6 Trapping Efficiency versus Time for three Water Velocities ($L_u = 24$ in (61 cm), initial particle depth = 0.5 in (1.27 cm))

Length Variation

As mentioned previously, most tests were done on our standard building model shown in Fig. 2 with an upper roof length of 24 in (61 cm) and a lower roof length of 24 in (61 cm). However, we also performed some tests with upper roof length of 12 in and 36 in. Figure 7 shows the volume transport rate for a water velocity of 0.15 ft/sec (4.6 cm/sec) versus time for the three values of L_u . Note that the transport rate is a decreasing function of time as mentioned previously and an increasing function of roof length.

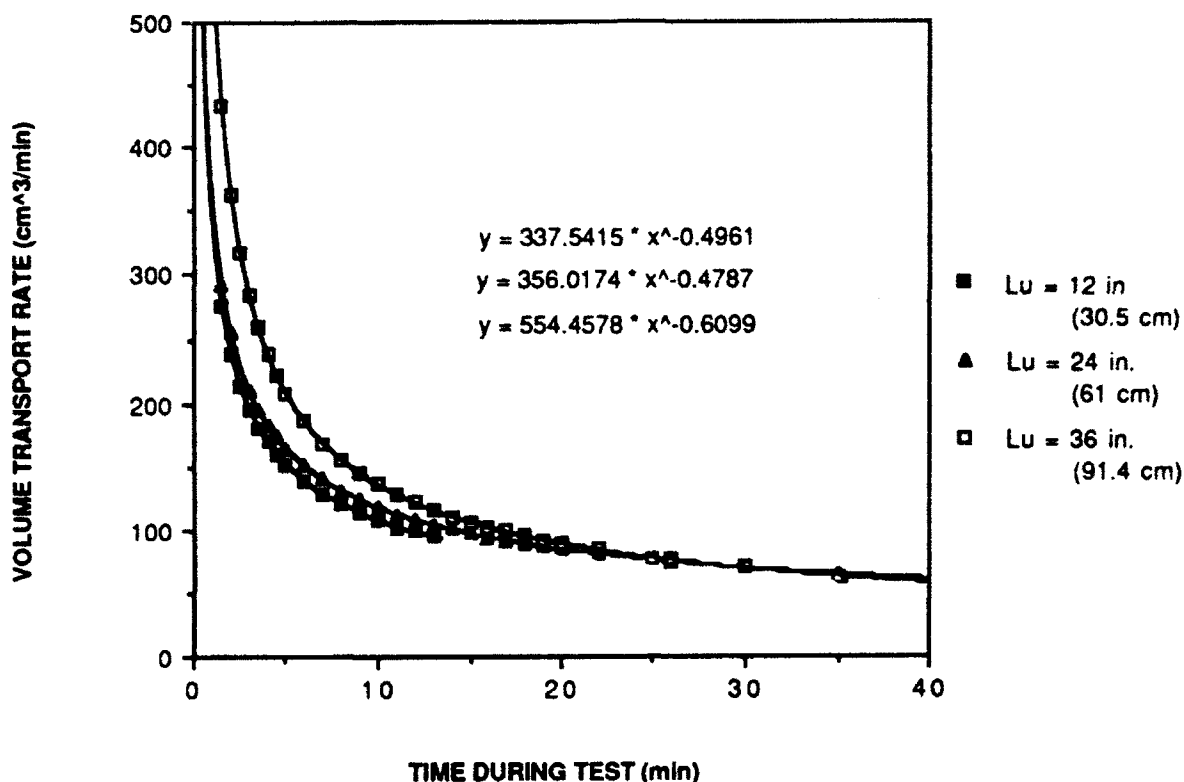


Figure 7 Volume Transport Rate versus Time for three Upper Roof Lengths ($V = 0.15$ ft/sec (4.6 cm/sec), initial depth = 0.50 in (1.27 cm))

SUMMARY AND FUTURE PLANS

This paper presents preliminary results from model tests conducted using the Rensselaer water flume. The objective of the test program was to develop fundamental knowledge concerning snow drifts at backward facing roof steps. In the tests, the actual snow in air prototype was simulated using a crushed walnut shells in water model. The walnut shells were chosen such that the ratio of particle terminal fall velocity to the particle threshold shear velocity was similar between the model and prototype.

At this point two specific elements were investigated, the volume transport rate for material leaving the upper level roof and the trapping efficiency (percentage of transported material which ends up in the lower level roof drift). Results suggest that the transport rate is a decreasing function of time and an increasing function of water velocity and the length of the upper level roof. The trapping efficiency appears to be a decreasing function of water velocity.

In the future, we intend to test at higher water velocities to eliminate problems of dune formation on the upper level roof which is more common at lower water velocities and for longer upper level roof lengths. We also plan to determine the effects of the initial depth of walnut shells on the roof, the roof step height H , and length of the lower level roof L_1 on the transport rate and trapping efficiency. In addition, we will measure the water velocity flow pattern over the model roof profile and then compare the measured transport rates with theoretical values. We also plan to quantify the trapping efficiency as a function of the relative size of the triangular drift. Finally we intend to compare measurements from the water flume experiments with three full scale case histories.

ACKNOWLEDGEMENTS

The research presented herein was supported by the National Science Foundation (NSF) through grant No. BCS-90-14499. However, the finding and conclusions are the authors alone and do not necessarily reflect the views of NSF.

REFERENCES

Gray, D., and Male, D., (1981) "Handbook of Snow; Principles, Processes, Management and Use" Pergamon Press Canada Ltd., 776 p.

Isyumov, N., (1971), "An Approach to the Prediction of Snow Loads", Ph.D. Dissertation to the Faculty of Engineering Science, The University of Western Ontario, London, Canada.

Iverson, J.D., (1982) "Small Scale Modeling of Snow-Drift Phenomena", Wind Tunnel Modeling for Civil Engineering Applications, Gaithersburg, MD, April.

Martins, R., ed. (1989), "Recent Advances in Hydraulic Physical Modeling", NATO ASI Series, Vol. 165, Lisbon, Portugal.

O'Rourke, M., Tobiasson, W., and Wood, E., (1986) "Proposed Code Provisions for Drifted Snow Loads". J. Structural Engineering, ASCE, Vol. 112, No. 9, September, pp. 2080-2092.

O'Rourke, M., and Galanakis, I., (1990) "Roof Snowdrifts Due to Blizzards". J. Structural Engineering, ASCE, Vol. 116, No. 3, March, pp. 641-658.

Raudkivi, A. J., (1976), "Loose Boundary Hydraulics", Pergamon Press, Oxford.

Tabler, R., (1975), "Predicted Profiles of Snowdrifts in Topographic Catchments". Paper presented at Western Snow Conference, Coronado, CA.

Development of a Wind Tunnel for the Study of Snowdrifting

Kuniaki Toyoda* and Tsukasa Tomabechi†

*Department of Mechanical Engineering

†Department of Architecture

Hokkaido Institute of Technology, Sapporo 006, Japan

ABSTRACT

A closed circuit wind tunnel with a working section of 1000 mm wide and 800 mm high has been developed for the study of snowdrifting at The Cold Regions Technical Center, Hokkaido Institute of Technology. The wind tunnel was designed so that the velocity profile on the floor of the test section was controllable in correspondence to the atmospheric boundary layer on the ground. The blizzard was simulated by blowing the activated clay particles through the specially designed multi-nozzle. The snowdrift geometries around various structures were measured with the laser displacement sensor. The traversing of the sensor and the data acquisition were automatically controlled by a personal computer, the data being processed to show the three-dimensional snowdrift geometries. The system was very efficient in obtaining the details of snowdrift. The snowdrift geometries around the models of snow fences and buildings were measured reasonably. These results suggest that the wind tunnel and the measuring system are very useful for the study of the snowdrifting.

INTRODUCTION

Blizzards cause serious snowdrifting problems on roads and around structures. Since the snowdrifting is caused by the wind, the phenomenon should be investigated on the basis of fluid mechanics. From a point of fluid mechanics, the natural blizzard is a very complicated phenomenon with a broad band of flow and snow conditions. Thus the data obtained from the field experiments are affected by various conditions, and it is impossible to discuss the effect of a special condition from the data. Moreover, it is very difficult to develop a general law from the data obtained on the different field conditions.

In order to experimentally analyze snowdrifting, it is necessary to control and keep constant the experimental conditions, especially the flow conditions, and to discuss the results on clearly defined conditions. Therefore, we have developed a wind tunnel to simulate the snowdrifting around snow fences and buildings.

The specifications for the design of the wind tunnel were as follows:

- (1) Enough space of test section to simulate the details of snowdrift.

- (2) Controllable velocity profile similar to the atmospheric boundary layer.
- (3) Suitable material as model snow.
- (4) Clean laboratory environment.
- (5) Constant experimental condition for a long-run experiment.
- (6) Efficient measurements of the complicated three-dimensional snowdrift geometries.

EXPERIMENTAL APPARATUS AND PROCEDURES

The closed circuit wind tunnel developed is shown in Figure 1. The tunnel was set up vertically to keep enough free space at the laboratory. The fan is driven by a three-phase 7.5-kW motor and the rotation speed is controlled by the frequency inverter, producing the wind speed up to 12 m/s in the test section. The side walls and roof of the 1000-mm-wide and 800-mm-high test section were made of removable transparent acrylic plates. The circular turning table of 800 mm diameter was installed on the floor in the test section. Three rows of stainless screen with a mesh size of 10 mm x 10 mm were set upstream of the test section, and the additional control screens with various mesh sizes smaller than that of the main screens were installed upstream of the main screens as shown in Figure 2 to control the velocity profile in the test section.

To simulate a blizzard, the activated clay particles were used as the suitable model snow particles (Anno, 1981). The properties of the particles are as follows: the apparent bulk density is 0.4-0.5 g/cm³, the angle of repose is 40-50 degrees, and the size ranges between 1-10 μ m. The particles were mixed with the compressed air and ejected at the upstream of the screens through the multi-nozzle shown in Figure 3. The same amount of air injected in the wind tunnel from the nozzle was exhausted through the exhaust duct with a small blower to relieve pressure inside of the wind tunnel.

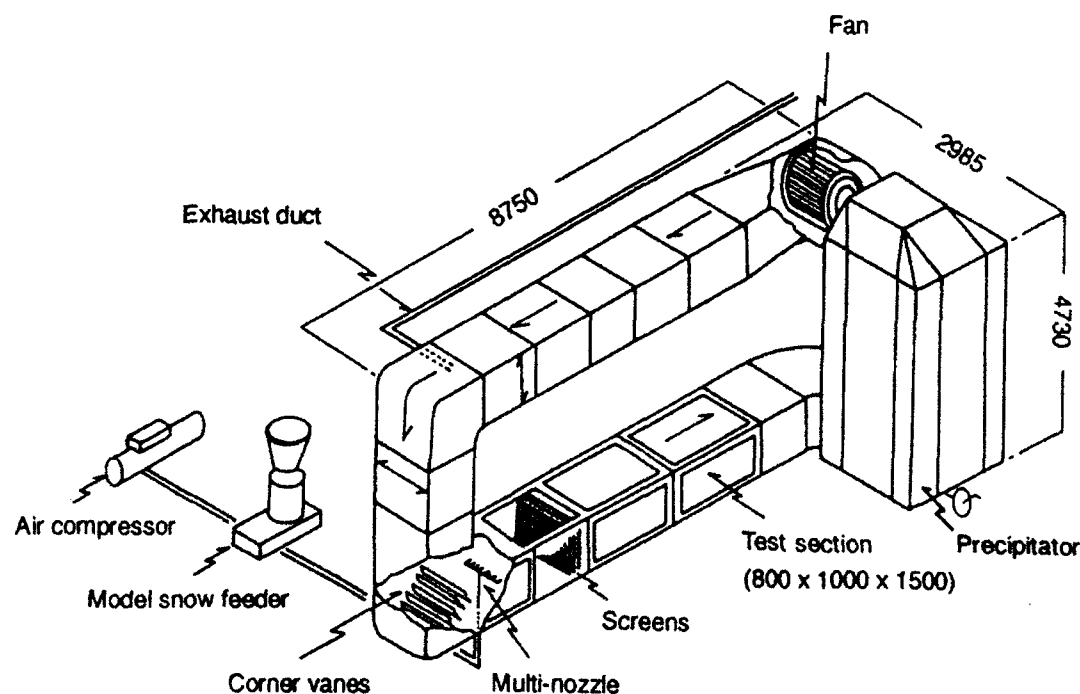


Figure 1. Wind tunnel.

A large duct of 1.5m x 1.5m x 4.75m was connected between the test section and the fan to accumulate the activated clay particles by the gravity force effect, which prevented the inflow of particles to the fan and thus the change of the wind tunnel performance owing to particle deposit in the wind tunnel except the test section. This is a very important consideration in a long run experiment.

The velocity profiles in the test section were measured with a Pitot tube. The snowdrift geometries around snow fences and buildings were measured with a laser displacement sensor attached to the computer-controlled three-dimensional traversing mechanism shown in Figure 4. The acquired data were stored in a personal computer and processed quickly to produce the three-dimensional snowdrift geometries. The total time of the data acquisition and processing was 40 minutes for two thousand measuring points.

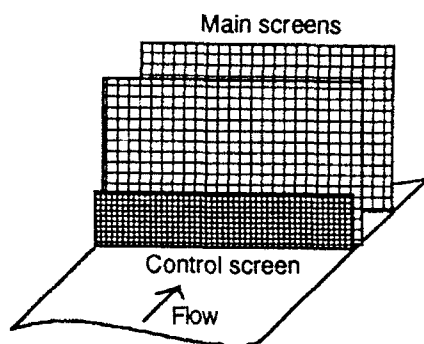


Figure 2. Screen combination to control the velocity profile.

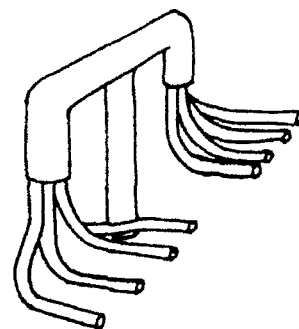
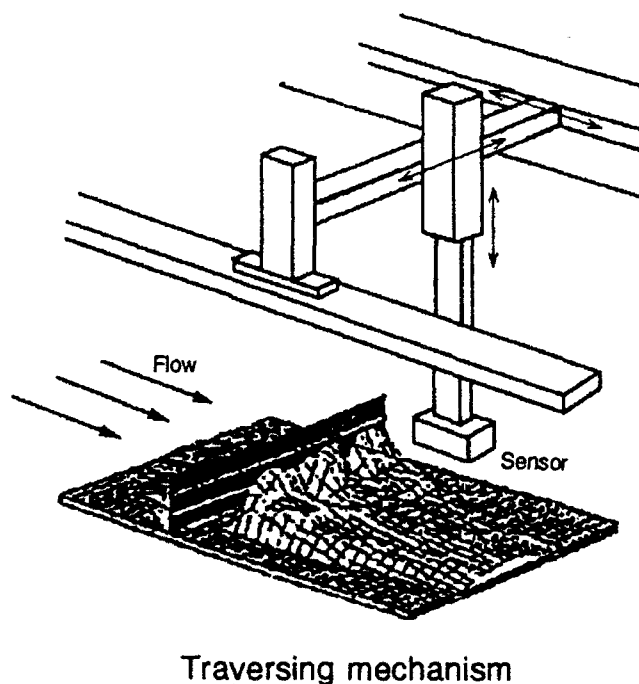
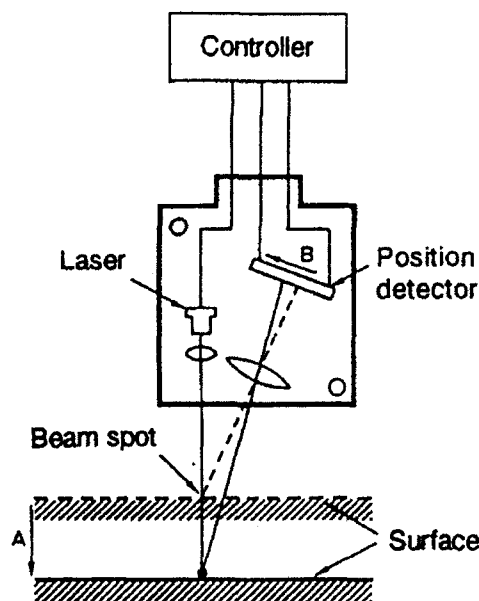


Figure 3. Multi-nozzle.



Traversing mechanism



Laser displacement sensor

Figure 4. Traversing mechanism and laser displacement sensor.

RESULTS AND DISCUSSION

The vertical and horizontal velocity profiles across the center of the test section are shown in Figure 5, which shows the uniform velocity field except in the boundary layer regions near the walls. The boundary layer profile on the floor of the test section was confirmed to be same in the spanwise direction except near the side walls. The boundary layers on the floor with and without the velocity control screen are shown in Figure 6. The distance (Z) and the velocity (U) are nondimensionalized by the reference location ($Z_r=250$ mm) and the reference velocity (U_r) at $Z=Z_r$. In the figure, the power law velocity profile ($U/U_r=(Z/Z_r)^{1/n}$) is shown by the solid line. The controlled velocity profile corresponds to the power law profile with $n=10$, which suggests that the velocity profile is similar to the atmospheric boundary layer over the smooth ground covered with snow (Shiotani, 1981).

If the reference height (Z_r) is assumed as 10 m for the atmospheric boundary layer, the similarity scale ratio between the wind-tunnel and atmospheric boundary layers is $R=250/10000=1/40$. Thus, considering the similarity of the flow field, the models of snow fences and buildings used in the experiments were scaled down to 1/40 of the prototypes. The scale was large enough to get the detailed snowdrift geometries around the models.

The reference velocity in the atmospheric boundary layer was estimated by the turbulence similarity law (Nemoto, 1963) as follows:

$$(U_r)_m/(U_r)_n=\{(Z_r)_m/(Z_r)_n\}^{1/3}$$

where U_r and Z_r are the reference velocity and height of the boundary layers, and the subscripts m and n mean model and natural conditions. Since in the experimental conditions $(U_r)_m=7$ m/s and $(Z_r)_m/(Z_r)_n=R=1/40$, $(U_r)_n$ is estimated as 24 m/s.

The snowdrift geometry around a snow fence with zero porosity and the bottom clearance of one sixth of the fence height H is shown in Figure 7. The experiment started after spreading enough activated clay particles over the floor of the test section, and the running time of the wind tunnel was one hour. The number of measuring points is $46 \times 41=1886$ and the space of points is 10 mm. The scanning time required over all points was 37 minutes, and the measurement system worked very efficiently.

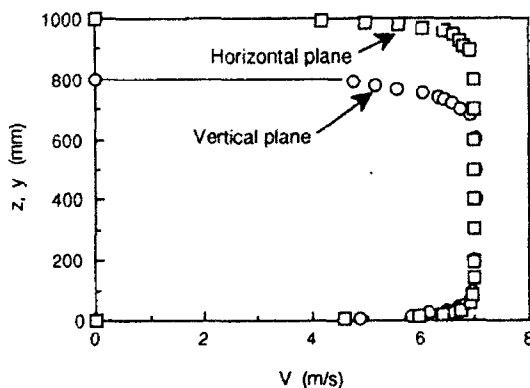


Figure 5. Velocity profiles in the test section.

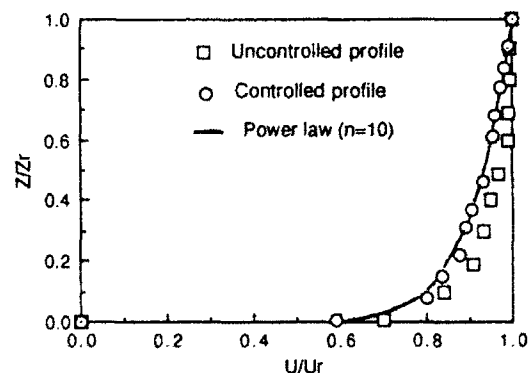


Figure 6. Boundary layer profiles.

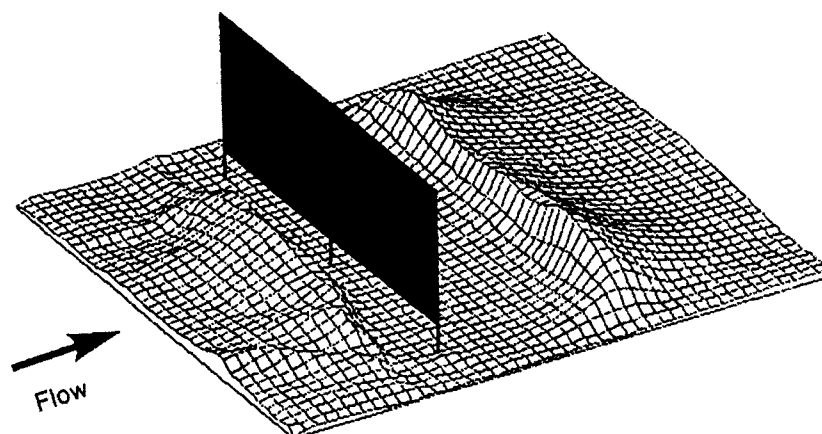
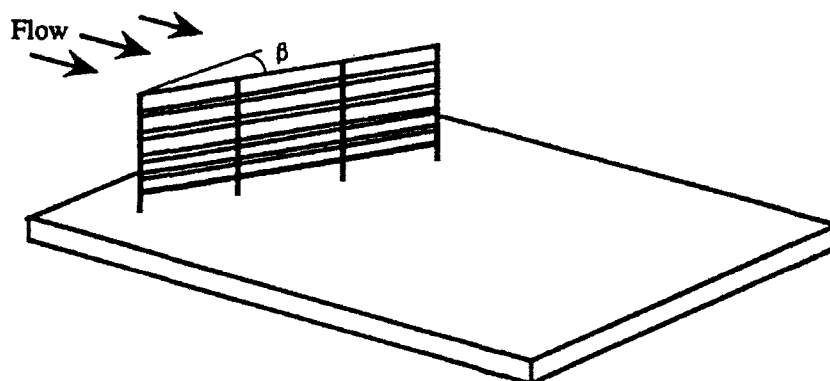
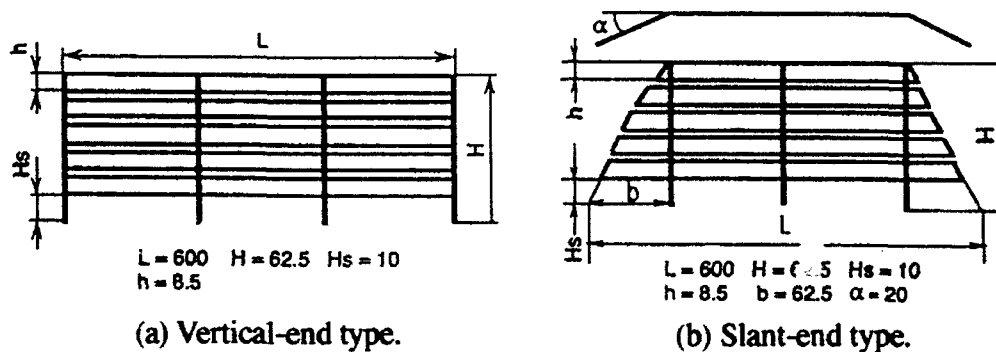


Figure 7. Snowdrift around a snow fence with zero porosity.



(c) Setting of snow fence.

Figure 8. Snow fence shapes.

The effects of flow direction and end shape on the snowdrift were investigated using the snow fences shown in Figure 8. Two types of end shape were used: vertical-end and slant-end. The effect of flow direction on the snowdrift around the vertical-end fence is shown in Figure 9. The result shows that the snowdrift decreases significantly with increasing β . The results of the slant-end fence are shown in Figure

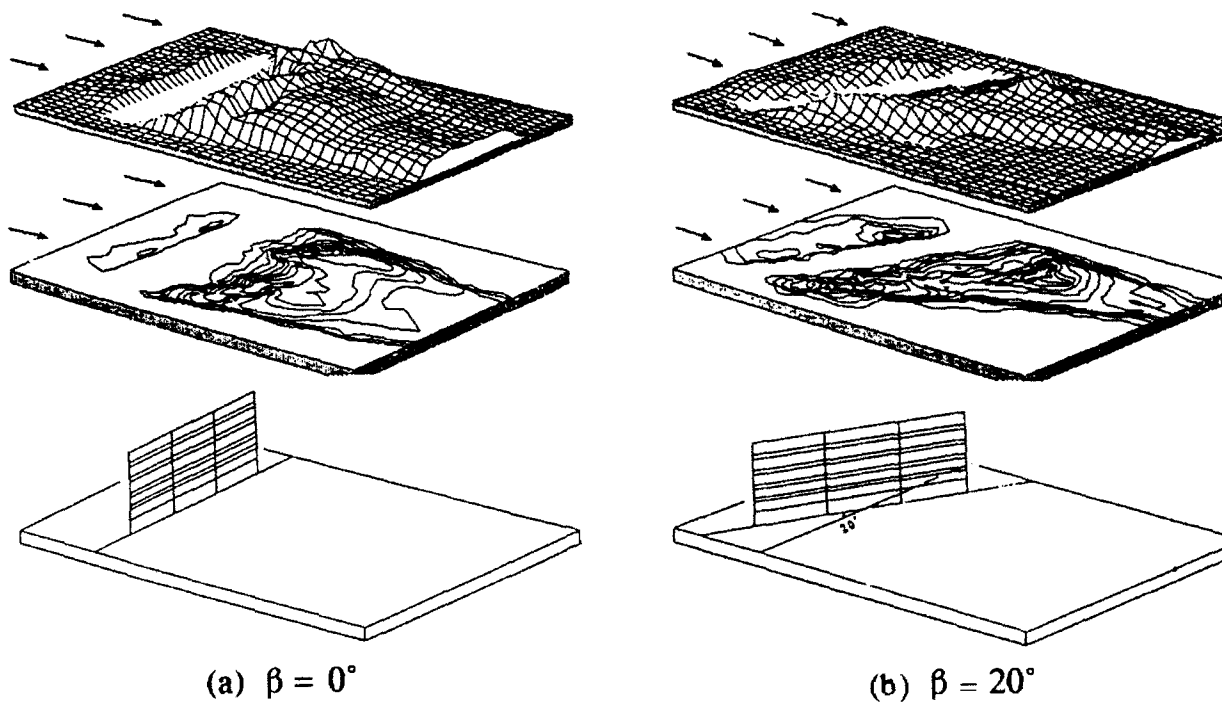


Figure 9. Snowdrift around the snow fence with vertical ends.

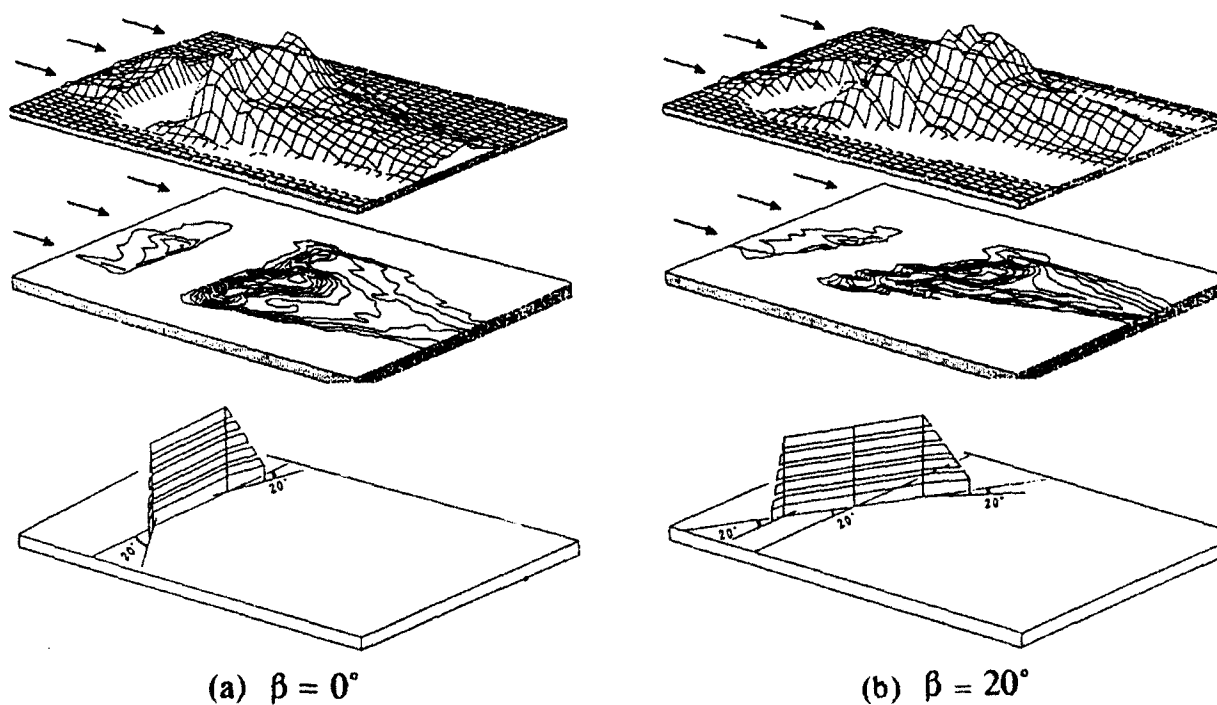


Figure 10. Snowdrift around the snow fence with slant ends.

10. In comparison with the vertical-end fence, the location where the snowdrift is the highest is 25% closer to the snow fence, the height of snowdrift is 25% higher, and the amount of the snowdrift is 10-12% larger. The difference may be owing to the different flow patterns originating from the end shapes; the dynamics of the vortical structures seems to play an important role in the flow pattern behind the fences. It is surprising that the amount of snowdrift behind the slant-end fence is still large at $\beta=20$ degrees. These results suggest that the performance of the slant-end fence is better than that of the vertical-end fence.

The snowdrift around a building model is shown Figure 11. The geometry is drawn as a half side of the spanwise width since the geometry is symmetric in the direction. The snowdrift geometry is reasonable and corresponds to the flow pattern characterized by flow separation and vortical structure.

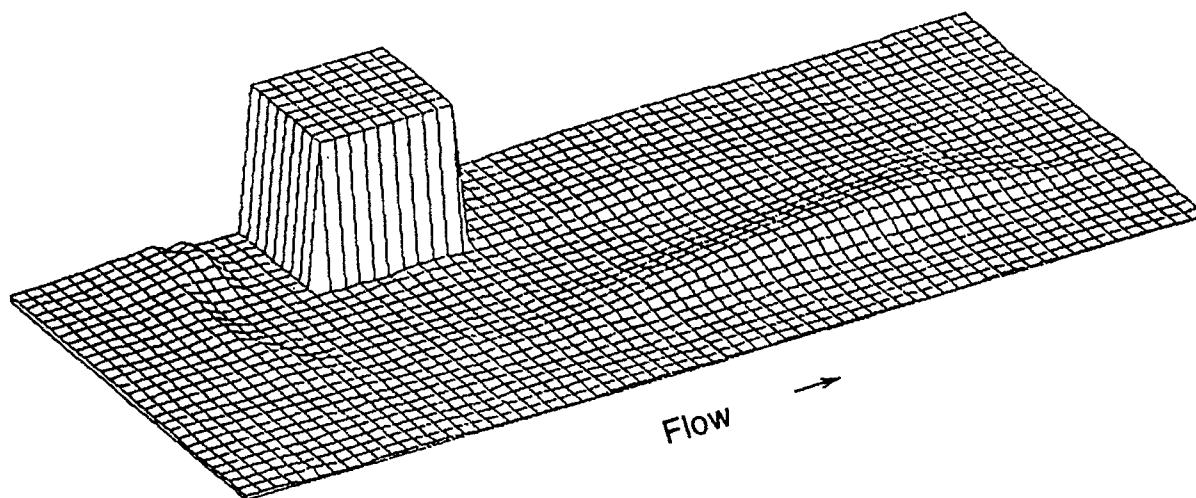


Figure 11. Snowdrift around the building.

CONCLUSIONS

The wind tunnel was developed to simulate the snowdrifting around structures, and the performance was confirmed by measuring the snowdrift around snow fences and a building. The results show that the snowdrifting is reasonable, and that the computer-controlled measurement and data-processing system is very efficient. The effects of flow direction and end shape on the snowdrift around the snow fences were investigated using the wind tunnel. The results show that the effect of flow direction on the snowdrift is significant for the vertical-end fence, and that the amount of snowdrift behind the slant-end fence is larger than that behind the vertical-end fence and is less affected by flow direction.

Although the developed wind tunnel is very useful to study the phenomena related to a blizzard, it needs more improvement to simulate the natural conditions. The gust in the natural wind might play an important role in the snowdrift, and

therefore a special device for generating gusts should be added to the wind tunnel. Natural snow particles have various sizes and moisture contents; the properties of which are required for the model snow. Thus we need more suitable model snow than the activated clay particles which simulate only the dry snow.

Regarding to the method of experimental analysis, since a blizzard is a typical phenomenon of two-phase flow, the two-phase flow approach is desirable to study snowdrifting. In the analysis, the interactions of snow particles and flow are a key point to shedding light on the details of the snowdrifting. Such an analysis by computer simulation is also expected.

REFERENCES

Anno, Y., and T. Konishi (1981) "Modeling the Effect of a Snowdrift-preventing Forest and a Snow Fence by Means of Activated Clay Particles," *Cold Regions Science and Technology*, Vol. 5, 43-58.

Nemoto, S. (1963) "Similarity Law of Wind Tunnel Experiments to Natural Wind," *Journal of the Society for Aeronautical and Space Science*, Vol. 11 (116), 272-278, Sept. 1963 (in Japanese).

Shiotani, M. (1981) "Characteristics of Strong Wind," *Kaihatsu Sha* (in Japanese).

Excess Loads on Flat Roofs of Buildings With and Without Parapets Under the Action of Wind and Snow

J. Wianecki* and A. Chevallier†

*Scientific Adviser and Expert in Aerodynamics of Structures

†Head of Aerodynamics Laboratory

Centre Expérimental du Bâtiment et des Travaux Publics

78470 St. Remy Les Chevreuse, France

ABSTRACT

The research and investigation for the experimental determination of the accumulation of snow under the action of wind is made possible by the use of a special wind tunnel designed and built at the C.E.B.T.P in 1975, called the "Wind tunnel for studying the accumulation of snow due to wind", in short the SANEV. It is located at St-Rémy-lès-Chevreuse on the Saint Paul estate, a picturesque stretch of country about 30 km south of Paris, where several research stations are in operation. A brief description of this installation, unique in France, is given. The starting point for research and investigation was indicated by work in Rumania. This shows that the study on models of the influence of wind on accumulations of snow is feasible, provided there is a possibility of establishing a similitude between the action of wind and the physical and mechanical properties of snow.

Since the greatest accumulation of snow occurs when the snow is dry and powdery, instead of using dry snow during testing, it is possible to use powdered materials insensitive to heat, for example, pine sawdust.

The paper includes the results of research on the experimental determination of excess loads corresponding to accumulation of snow under wind action on a flat roof of a building, first with no parapet, then with parapets of two different heights.

INTRODUCTION

The research and investigation for the experimental determination of the accumulation of snow under the action of wind is made possible by the use of a special wind tunnel designed and built at the C.E.B.T.P in 1975, called the "Wind tunnel designed for

studying the accumulation of snow due to wind", in short the SANEV. It is located at St-Rémy-lès-Chevreuse on the Saint Paul estate, a picturesque stretch of country about 30 km south of Paris, where several research stations are in operation. The detailed description of this installation, unique in France is given in reference (Wianecki, 1975).

This research and investigation were based initially on Rumanian research in this field (Mateescu and Negoita, 1969), (Mateescu and Popescu, 1974).

This work had shown that the study on models of the influence of wind on accumulations of snow is feasible, provided there is a possibility of establishing a similitude of action of wind and of the physical and mechanical properties of snow.

Since the greatest accumulations of snow occur when the snow is dry and powdery, it is possible to use powdered materials insensitive to heat, instead of using dry snow during wind tunnel testing.

Different materials have been used during this research, such as ground diatomite, ground asbestos, crushed ampore, sandust, foamed polystyrene and bakelite, in the form of particles varying in size from 0,1 to 0,3 mm.

Analysis of the Rumanian work using all these materials lead to the conclusion that the best material to simulate the phenomenon of snow accumulation is pine sawdust with a grain size around 0,2 mm.

The test procedure, which we call the Rumanian method, was then defined as follows:

- Phase 1 : free fall of a layer evenly distributed over the whole roof surface in the absence of wind
- Phase 2 : application of wind at a speed which must be greater than the speed at which grains of artificial snow are entrained

This speed was determined experimentally in our SANEV Wind Tunnel at 2.19 m/s. The Rumanians had used a speed of 2.25 m/s during their tests. Thus the initial parameters (material and particle diameter) were identical.

It must be noted that the speed at which real wind entrains snow particles is about 6 m/s.

Moreover, the maximum speed of real wind which brings about complete scattering of snow on a roof is approximately 16 m/s.

Real accumulations of snow therefore form in a relatively narrow range of wind speeds, i.e., $6 \text{ m/s} < v < 16 \text{ m/s}$, which corresponds on models to a range of

approximately $2 \text{ m/s} < v < 5 \text{ m/s}$.

DESCRIPTION OF THE SANEV WIND TUNNEL

The perspective view of the SANEV (see Figure 1), shows the five principal parts :

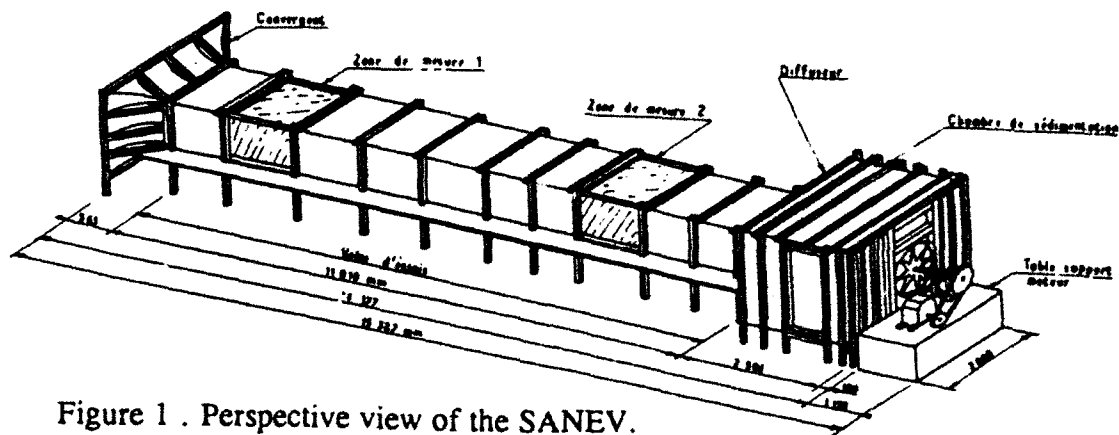


Figure 1 . Perspective view of the SANEV.

The convergent : length 0.563 m, measuring 1.60 m x 2.5 m at the entrance and 0.80 m x 1.25 m at the outlet, which represents a coefficient of contraction of $\alpha = 4$.

<u>The test tunnel</u>	height	0.8 m
	width	1.25 m
	length	11.01 m

The two measuring zones 1 and 2 are transparent ("perspex") and provide access at the sides and at the top of the tunnel.

The diffuser 0.5 m

<u>The sedimentation chamber</u>	length	2 m
	height	1.6 m
	width	2.50 m

in which a filter with a $\phi 200 \mu\text{m}$ sieve has been placed at a distance of 1.25 m from the diffuser outlet.

The support stand accommodating the motor, the mechanical speed variator and the shaft and turbine (power of the motor = 15 kW).

From a mechanical point of view, this wind tunnel operates like a special type of Eiffel tunnel, i.e., the air drawn in by the turbine passes through the 14.177-m-long tunnel

and the air current returns in the surrounding premises. Maximum speed attainable in the bare tunnel is 13 m/s.

By placing different obstacles whose size and density can vary according to the roughness required on the floor of the tunnel, it is possible to reproduce in the best conditions of similitude the main characteristics of natural wind in the lower layers of the atmosphere.

The vertical gradients of average speed, the intensities and scales of turbulence, the energy spectrum of wind can thereby correspond to different type of sites :

- large urban centre (high turbulence)
- suburb (medium turbulence)
- coastal areas (low turbulence)

Figure 2 shows the interior of the tunnel towards the convergent with the model of the new Turin stadium (Italy) placed in the second measuring zone and the roughness layers corresponding to a suburban site.



Figure 2. Model of the new Turin stadium placed in the second measuring zone.

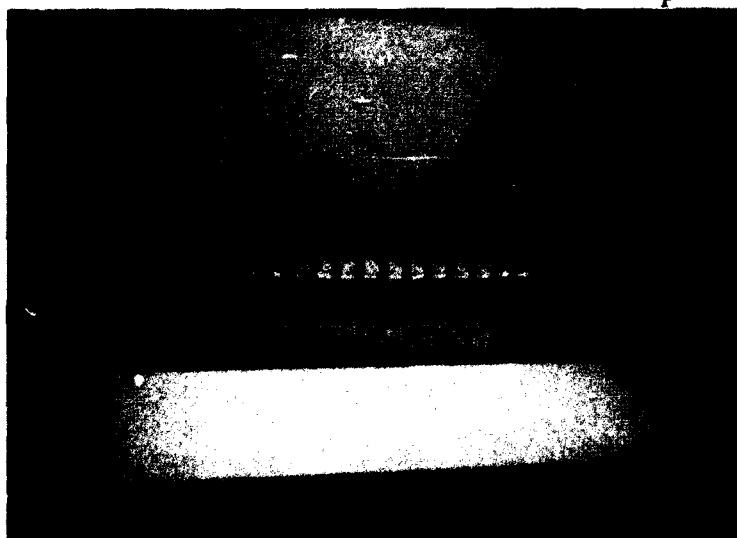


Figure 3. Side view of zone 2 with thickness measurement gauge and the reference device.

The lateral view of zone 2 in Figure 3 shows the measurement gauge for the thickness of the layer of artificial snow with the reference device.

Figure 4 presents an aerial type view after the test to identify the areas bared before undertaking the localized quantitative measurements using the gauge illustrated in Figure 2.

Several subjects of research and investigations have been carried out in this wind tunnel since 1975.

This paper will now present the results of research on the experimental determination of excess loads corresponding to the accumulations of snow under the action of wind on the flat roof of a building with no acroterion, then with an acroterion of two different heights.

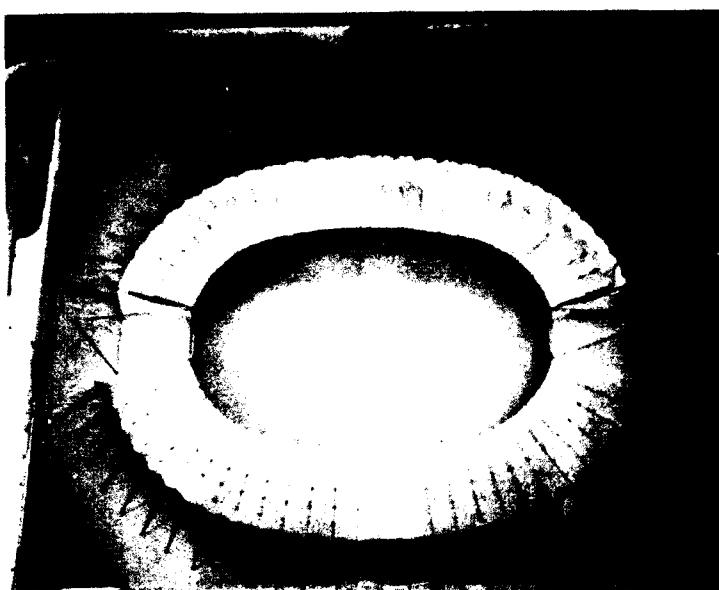


Figure 4. Aerial type view of the model of the new Turin stadium after testing.

DESCRIPTION OF THE MODEL AND ITS PLACING IN THE SANEV WIND TUNNEL

The 1/50 scale model represented a building with the following dimensions

length	30 m
width	10 m
height	12 m

The model therefore measured 600 x 200 mm, height 240 mm, was built of plywood. The parapets (height 5 and 10 mm) were made of thermo-adhesive strips.

The model was placed on the turntable in the second testing zone. This turntable offers the possibility of placing the model under different angles of incidence exposed to a wind.

RESEARCH PROGRAMME

Three wind directions were examined : 0° , 45° and 90° . For each of these incidences, the model was subjected to two wind speeds $v = 2.53 \text{ m/s}$ and $v = 3.10 \text{ m/s}$, each for 20 minutes and each for three different models :

- 1) without parapet
- 2) with a 5 mm parapet (representing a 25 cm full-scale upstand)
- 3) with a 10 mm parapet (representing a 50 cm full-scale upstand).

So the test considerations include :

- 3 models x 3 angles of incidence x 2 speeds

= 18 different tests for which the testing duration is always 20 minutes.

All these tests were carried out on a smooth roof surface (plywood painted black).

A mesh comprising 65 measurement points was traced on the roof of the model (Figure 7 and 8).

Each test began with an application of free falling artificial snow without wind. A check was then made with the measurement gauge to ensure uniformity of thickness of the 5 mm layer in compliance with the mesh.

Once prepared, the model was then subjected to wind at a well-defined speed ($v_1 = 2.53$ m/s or $v_2 = 3.10$ m/s) during a constant time $t = 20$ mn.

Measurement of thickness at 65 points and also photographs were taken at the end of each test.

TESTING

At first we tried to identify two speeds such that the first entrains the particles without excessive displacement, and a second displaces the "snow" more completely without however sweeping it all away.

The minimum speed of entrainment (2.19 m/s) of the particles brought about very definite displacements for wind directed along an angle of incidence of 45° , but for incidences of 0° and 90° , the particles were not displaced. We were therefore increased this first speed to $v_1 = 2.53$ m/s so that the artificial snow was slightly transported for $I = 0^\circ$ and 90° . We determined experimentally the second speed $v_2 = 3.10$ m/s in such a way that the roof not be totally "swept" in any case.

TEST RESULTS

The processing of measurements of thickness of snow accumulation due to wind was carried out with three approaches :

- localized accumulation index

$$i_{a,p} = \frac{e_k}{e_{\text{réf}}}$$

where e_k is the thickness of the layer in mm at point k
 $e_{réf}$ is the reference thickness equal to 5 mm

- index of linear accumulation

$$i_{a,l} = \frac{\frac{\sum_{k=1}^n e_k}{n}}{e_{réf}}$$

where e_k is the thickness of the layer in mm in n points located on the same straight line l .

- index of surface area accumulation

$$i_{a,s} = \frac{\frac{\sum_{k=1}^n e_k}{n}}{e_{réf}}$$

where e_k is the thickness of the layer in mm in n points located on the same surface.

To obtain the distribution of excess loads on the flat roof, we simply multiply these indexes of localized, linear or surface area accumulations by the excess load of snow per square metre of horizontal projection in the given site, in compliance with the national codes of each country.

The four photographs in Figures 5, 6, 7 and 8 serve as examples.

$I = 90^\circ$
 $v = 2.53 \text{ m/s}$
 $t = 20 \text{ min}$

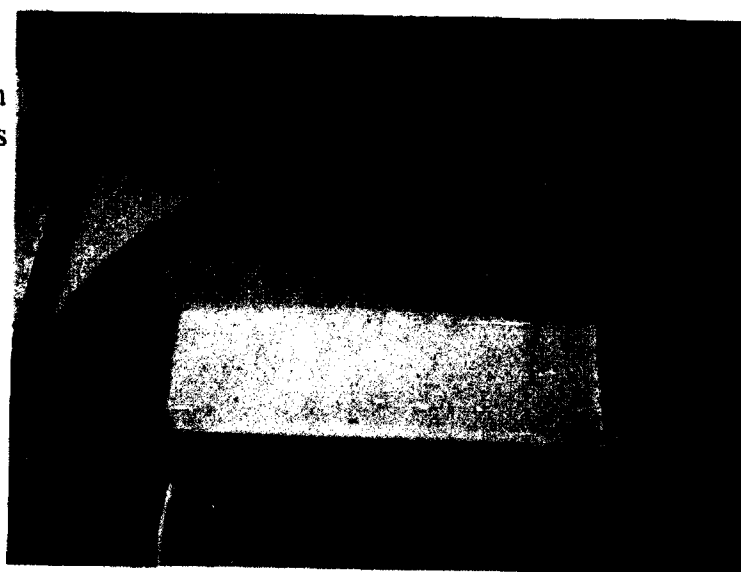


Figure 5. 10 mm parapet.

$I = 90^\circ$
 $v = 3.10 \text{ m/s}$
 $t = 20 \text{ min}$



Figure 6. 10 mm parapet.



$I = 45^\circ$
 $v = 2.53 \text{ m/s}$
 $t = 20 \text{ min}$

Figure 7. 10 mm parapet.

Also as examples we show the indexes of localized accumulation (Figure 9), linear accumulation (Figure 10) and surface area accumulation (Figure 11)

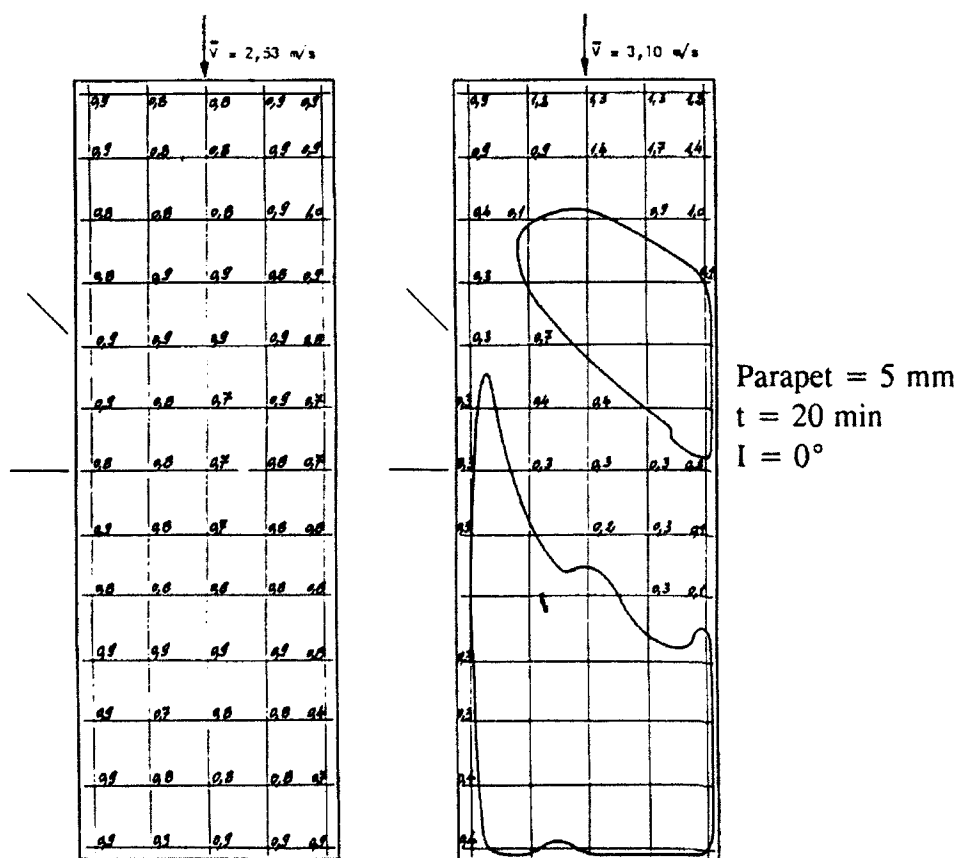


Figure 9. Indexes of localized accumulation.

Parapet = 5 mm
 $t = 20 \text{ min}$
 $I = 0^\circ$

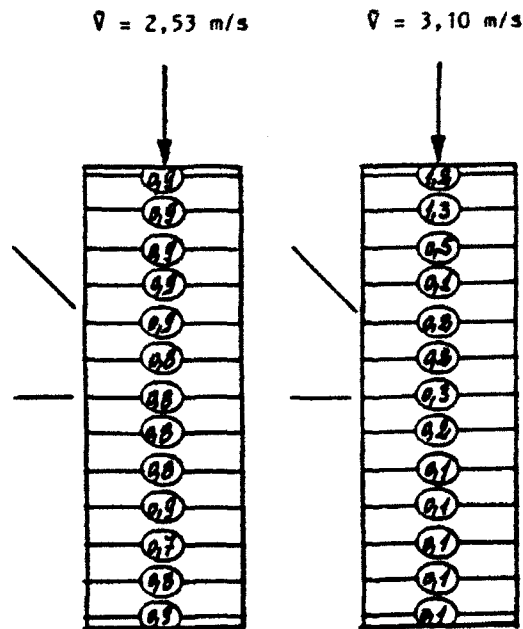


Figure 10. Indexes of linear accumulation.

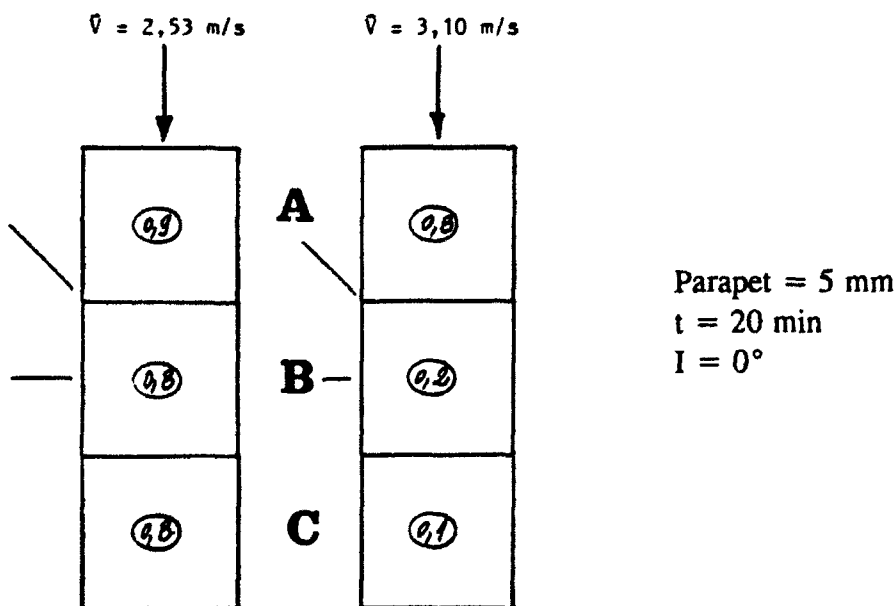


Figure 11. Indexes of surface area accumulation.

The indexes for surface area accumulation $i_{a,s}$ are the only ones which will serve directly for the determination of excess loads of snow. This is why we present them for all the cases dealt with in Table 1.

Table 1 - Indexes of surface area accumulation on the flat roof of an average building

I	no parapet						parapet 5 mm						parapet 10 mm					
	v = 2.53 m/s			v = 3.10 m/s			v = 2.53 m/s			v = 3.10 m/s			v = 2.53 m/s			v = 3.10 m/s		
	A	B	C	A	B	C	A	B	C	A	B	C	A	B	C	A	B	C
0°	0,8	0,7	0,8	0,6	0,2	0	0,9	0,8	0,8	0,8	0,2	0,1	1,0	0,9	0,9	1,0	0,3	0,4
45°	0,3	0,4	1,0	0	0,3	1,0	0,3	0,6	1,2	0,1	0,3	1,2	0,3	0,5	1,4	0	0,2	1,3
90°	0,8	0,8	0,8	0,4	0,6	0,6	0,9	0,9	0,9	0,9	0,8	0,8	1,0	1,0	0,9	0,9	0,7	0,8

The similitude relationships (Mateescu and Negoita, 1969) to establish the link between the model and the prototype (that is to say to real structure) were obtained from dimensional analysis (m indicates model, p indicates prototype).

The speed scale is expressed as follows :

$$k_v = \frac{v_m}{v_p} = \left(\frac{c_{x,p}}{c_{x,m}} \cdot \frac{D_m}{D_p} \cdot \frac{\rho_{n,m}^{1/2}}{\rho_{n,p}} \right)^{-1} = (k_{c_x}^{-1} \cdot k_D \cdot k_{\rho_n})^{1/2} = \frac{1}{3.14}$$

In this equation we use the following expressions :

$c_{x,p} = 0.6$ the drag coefficient of a particle of snow corresponding to the Reynolds number :

$$Re_p = \frac{v_p \cdot D_p}{14.5 \cdot 10^{-6}} = 4.6 \cdot 10^2$$

$c_{x,m} = 2.1$ the drag coefficient of a particle of snow corresponding to the Reynolds number :

$$Re_m = \frac{v_m \cdot D_m}{14.5 \cdot 10^{-6}} = 29$$

D_p the diameter of a spherical particle of snow equal to 1 mm

D_m the diameter of a spherical particle of artificial snow equal to 0.2 mm

$\rho_{n,m}$ the specific gravity of artificial snow equal to 0.163

$\rho_{n,p}$ the specific gravity of snow equal to 0.092

As regards the time scale, it is expressed in the following way :

$$k_t = \frac{t_m}{t_p} = k_v^{-1} \cdot k_1$$

where : k_v is the scale of speeds equal to $\frac{1}{3.14}$

k_1 is the geometrical scale of the model equal to $\frac{1}{50}$

Therefore we have two scales :

$$k_v = \frac{v_m}{v_p} = \frac{1}{3.14}, \text{ whence } v_p = 3.14 v_m = 3.14 \times \begin{cases} 2.53 = 7.9 \text{ m/s} \\ 3.1 = 9.7 \text{ m/s} \end{cases}$$

and

$$k_t = \frac{t_m}{t_p} = 3.14 \cdot \frac{1}{50} = \frac{1}{15.92} \text{ whence } t_p = 15.92 \times 20 \text{ min} = 320 \text{ min} = 5.3 \text{ hours}$$

CONCLUSIONS

Analysis of Table 1 shows that :

- 1°) the influence of the speed of wind on the distribution of snow on surfaces A, B and C is high, both for roofs with or without parapets, for $I = 0^\circ$ and 45° , whereas it is low and tends towards a uniform distribution, emphasized by the presence of parapets, for $I = 90^\circ$.
- 2°) the envelopes of the indexes of surface area accumulation, whatever the incidences and speeds, indicated in Table 2 below, show the influence of the presence and of the height of the parapet.

Table 2

Flat roof	A	B	C
no parapet	0,8	0,8	1,0
parapet 5 mm	0,9	0,9	1,2
parapet 10 mm	1,0	1,0	1,4

REFERENCES

C. MATEESCU and A. NEGOITA "Recherches roumaines concernant la surcharge de neige", Annales de l'ITBTP, n° 259 - 260, juillet - août 1969.

C. MATEESCU and H. POPESCU "Accumulations de neige sur les constructions - Etude expérimentale sur modèles", Annales de l'ITBTP, n° 317, mai 1974.

J. WIANECKI "Aérodynamique des Bâtiments et des Ouvrages d'Art - IV. Banc d'essais d'accumulation de la neige due au vent, Annales de l'ITBTP, n° 338, avril 1975.

5

Snow Control

Colin Williams, Chairman



Removing snow from a roof in the Sierra Nevada of California. (Photograph by Richard Flood.)

Static Friction of Roofing Materials Against an Ice Mass

Masatomo Watanabe* and Kazunobu Mirai†

*Department of Architectural Engineering, Hachinohe Institute of Technology, Hachinohe, Japan

†Department of Architecture, Faculty of Engineering, Tohoku University, Sendai, Japan

ABSTRACT

Values of static friction, changes of friction values caused by temperatures and effects of surface properties of roofings on the static frictions were studied experimentally. Eight roofing materials were selected as samples because of their wide variety of surface roughness and hardness. Measurements of static friction were carried out by a device which was made for the purpose of testing the friction angle. Ice blocks linked by a lead weight with multiple nails were utilized as a sliding ice mass. Four temperature levels were examined to find the friction changes caused by changes in temperature. Surface roughness values of standard parameters and fine roughness were measured for the purpose of finding the roughness effects against ice mass.

From this study, it is clarified that each roofing material has specific friction values against ice, and that friction values generally decrease with increasing temperatures, and that static friction depends mainly on the fine roughness parameter R_{zf} , which can be obtained by small cut-off value measuring upon R_z (ISO roughness parameter).

INTRODUCTION

Snow slides, snow loads and snow refreezings on pitched roofs cause various types of damage to various building elements. In the heavy snow regions of Japan, therefore, various architectural ideas of roof-snow removals have been attempted to prevent those snow damages. The removal of roof snows by utilizing sliding snow actions is one of the most useful methods for pitched roofs. In order to build snow-removal roofs utilizing snow sliding successfully, the characteristics of many resisting forces concerned with slides of roof snow must be clarified. The static friction of roofing materials is a very important one.

Much of the prior research on frictional forces of roofing materials against snow or ice has been carried out on slippery roofings such as colored metal sheets. Maeda (1979) was

the first to attempt the experimental discussions on the static friction of a metal roofing, and recently Ueno et. al. (1987) made an experimental discussion using several metal roofings and an ice block. In those articles, however, the effects of the surface characteristics upon the static friction were not discussed fully.

The adhesive theory of the friction mechanism of ice (Tushima 1980) gave us the important suggestion that surface properties of roofing materials such as roughness and hardness could have important influences on the friction of ice or snow on roofs. So, effects of surface roughness and hardness on the friction were analyzed in our study.

EXPERIMENTAL PART

Roofing Samples

A brief outline of eight roofing samples is shown in Table 1. Those samples are selected in consideration of the two surface properties of roughness and hardness. Roughness properties of those samples can be separated into a smooth (sample sign: M-02, M-11, M-12 and G-01) and a rough group (sample sign: M-13, G-03, C-02 and X-03). Hardness properties of the samples are separated into a soft (sample sign: M-11, M-12, M-13 and X-03) and a hard group (sample sign: M-02, G-01, G-02 and C-02).

In comparing surface roughness the values of roughness parameter R_z ("ten point height of irregularities" of ISO and JIS) are used, and in surface hardness the values of the elastic constant E of the surface materials are utilized. Table 2 shows the values of roughness and hardness of roofing samples. The size of roofing samples for experiments was approximately 25 cm \times 50 cm.

Measurements of Static Friction

If the friction angle θ (degrees) can be measured, the coefficient μ_s of static friction is given as $\mu_s = \tan \theta$. The static friction was measured by the method of testing the friction angle θ using the device that was built in the form of the slanting board method in this study. A side view of this testing device is shown in Photo 1. In this device, a slanting board is lifted up by a wire, and lifting speeds are controlled by a rolling-up disk. In this study, the lifting speed is maintained at approximately 10 seconds per 1 degree of slope angle.

The sliding ice mass of 8.4 N is formed by three ice blocks and a lead weight with many nails. Side and bottom views of this ice mass are shown in Photo 2. The ice blocks are fixed in a triangular arrangement by multiple nails that are molded into the lead weight (right picture of Photo 2.). The total contact area of ice mass with the roofing surface is 9 cm² (1.5 cm \times 2.0 cm \times 3 blocks), and the maximum contact force between the ice and roofing surface is approximately 0.9 N/cm² at the slope angle 0°.

Measurements were carried out in a cold room, and the friction was tested at four temperature levels of -10°, -5°, -1° and +3 °C.

Table 1. Outline of of roofing materials selected as samples.
Type of roofing material, surface condition and
thickness are shown.

Sample Sign	Roofing Type	Surface Condition	Thickness(mm)
M-02	Cold-Rolled Steel Sheet	Dull Texture	1.5
M-11	Colored Steel Sheet	Painted Glossy Blue	0.6
M-12	Colored Steel Sheet	Painted Dull brown	0.6
M-13	PC-Ply* ¹ Steel Sheet	Embossed Pattern	0.6
G-01	Float Glass Sheet	Completely Smooth	2.7
G-03	Patterned Glass Sheet	Embossed Pattern	5.6
C-02	Asbestos-Cement Shingle	Fine Sand Adhered	5.0
X-03	Lauan Plywood	Nearly Straight Grain	12.0

*¹ Polyvinyl Chloride Ply

Table 2. Specific values of surface roughness and hardness of
roofing samples

Sample Sign	Roughness Parameter		Surface Material and Hardness	
	* ¹ Rz(μ m)	* ² Rz _f (μ m)	Surface Material	* ³ E (N/cm ²)
M-02	6.6	4.0	Mild Steel	2.1×10^7
M-11	2.8	1.4	Thermoplastic	$2 \sim 5 \times 10^5$
M-12	3.9	1.8	Thermoplastic	$2 \sim 5 \times 10^5$
M-13	26	3.5	Thermoplastic	$2 \sim 5 \times 10^5$
G-01	0.2	0.05	Sodium Glass	$5 \sim 9 \times 10^6$
G-03	78	3.6	Sodium Glass	$5 \sim 9 \times 10^6$
C-02	152	39	Cement Concrete	$1 \sim 3 \times 10^6$
X-03	54	26	Red Lauan	$4 \sim 7 \times 10^6$

*¹ Roughness parameter Rz measured by standard cut-off value.

*² Rz_f is measured by 0.25 mm cut-off as fine roughness parameter.

*³ Values of elastic constant showed in general engineering book.



Photo 1. Device made for the measurements of static friction. Left photo shows the front view, and right shows a testing state.

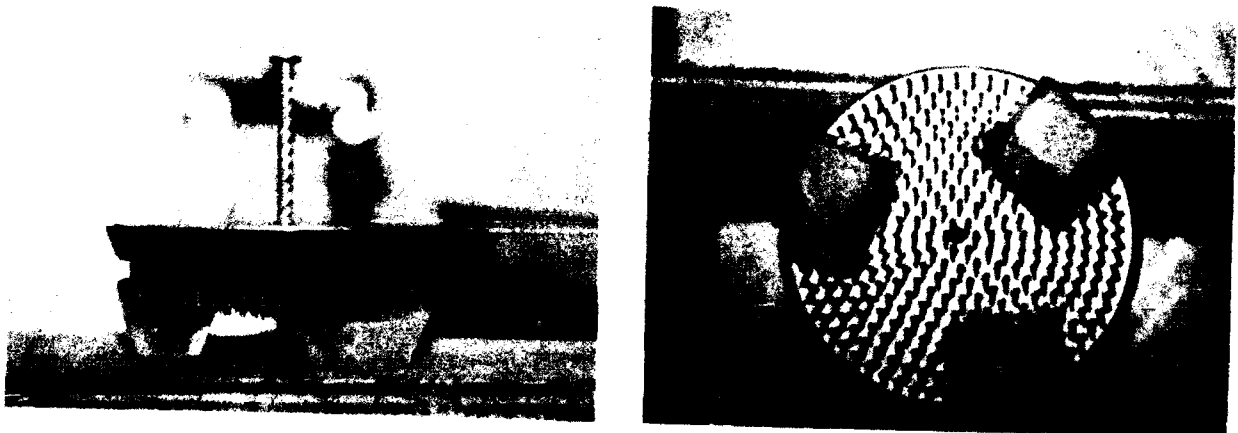


Photo 2. Sliding ice mass formed by ice blocks and a lead weight with multiple nails. Left photo shows a side view, and right shows the triangular arrangement of three ice blocks.

Measuring Roughness Parameter

Main roughness parameters of Ra ("arithmetic mean deviation" of JIS surface roughness), Rz ("ten point height of irregularities" of ISO and JIS surface roughness) and the profile curve of surface roughness are measured by a electric surface analyzer of the pickup type (JIS B 0651) on all of roofing samples. The parameters of Ra and Rz are measured under the condition of a low cutting filter of 0.25 mm cut-off in order to clarify the fine roughness of real contact surfaces to ice, and each fine roughness parameter is named as Raf and Rz_f correspondingly in this study. The Rz_f values of roofing samples obtained by this measuring are shown in Table 1.

RESULTS AND CONSIDERATIONS

Measured Static Friction

In measuring the static friction μ_s , six measurements of μ_s are repeated on each combination of the samples and the temperature levels, and the error in range of testing temperature is controlled to within $\pm 1.5^\circ\text{C}$ in the cold room. The averages and the standard deviations of six μ_s values measured in all experimental condition are shown in Table 3. The statistics of experimental μ_s values indicates that each roofing material has specific μ_s , and that the standard deviation of μ_s values is generally small in smooth roofings, but somewhat large in rough surface roofings.

The typical patterns of μ_s changes that are caused by temperature changes are shown in Fig. 1. The μ_s values of smooth surface roofings decrease directly with the increase of temperatures (diagrams of G-01 and M-12), but the μ_s values of rough roofings do not decrease in temperature higher than 0°C (diagrams of C-02 and X-03). The phenomena of μ_s increasing or not changing at warmer temperature can be explained that the contact surfaces of ice are deformed by melting into the figure of the rough surface, and a resisting force created by surface biting between ice and roofing. However, this resisting force is effective only for a short time, because the ice soon melts away.

Effects of Roughness and Hardness on Friction

The effect of surface roughness and hardness on the static friction is analyzed by variance analysis in two-way classification, and the variance analysis is carried out using the μ_s data of the lowest temperature level of -10°C . It is expected that the μ_s data of -10°C level would have a larger effect on surface hardness, because the hardness of ice increases with decreasing temperatures. A hypothetical grouping of roofing samples on surface roughness and hardness, and the μ_s value of each sample at -10°C is shown in Table 4.

The results of the variance analysis are shown in Table 5. The results indicate that the effect of surface roughness is highly significant (level 99%), but the surface hardness is of no significance. That is to say, the surface roughness is the most important property that influences the static friction of roofing materials against an ice mass.

Table 3. Average and standard deviation of static friction μ_s between roofings and an ice mass.

Sample Sign	* ¹ Level -10°C		* ¹ Level -5°C		* ¹ Level -1°C		* ¹ Level +3°C	
	* ² Av.	Std. Dev.	* ² Av.	Std. Dev.	* ² Av.	Std. Dev.	* ² Av.	Std. Dev.
M-02	0.27	0.03	0.25	0.08	0.17	0.02	* ³ 0.01	---
M-11	0.19	0.01	0.13	0.03	0.05	0.01	* ³ 0.01	---
M-12	0.24	0.01	0.15	0.01	0.07	0.01	0.02	0.00
M-13	0.09	0.01	0.10	0.01	0.04	0.01	* ³ 0.01	---
G-01	0.18	0.02	0.16	0.02	0.06	0.02	* ³ 0.01	---
G-03	0.08	0.01	0.08	0.02	0.04	0.00	0.19	0.04
C-02	0.68	0.15	0.46	0.07	0.39	0.06	0.41	0.04
X-03	0.70	0.07	0.67	0.13	0.48	0.15	0.71	0.08

*¹ Error of temperature is controled to within $\pm 1.5^\circ\text{C}$.

*² Average of six times measuring μ_s .

*³ Fixed angle 0.5° is used in approximatly 0° friction angle.

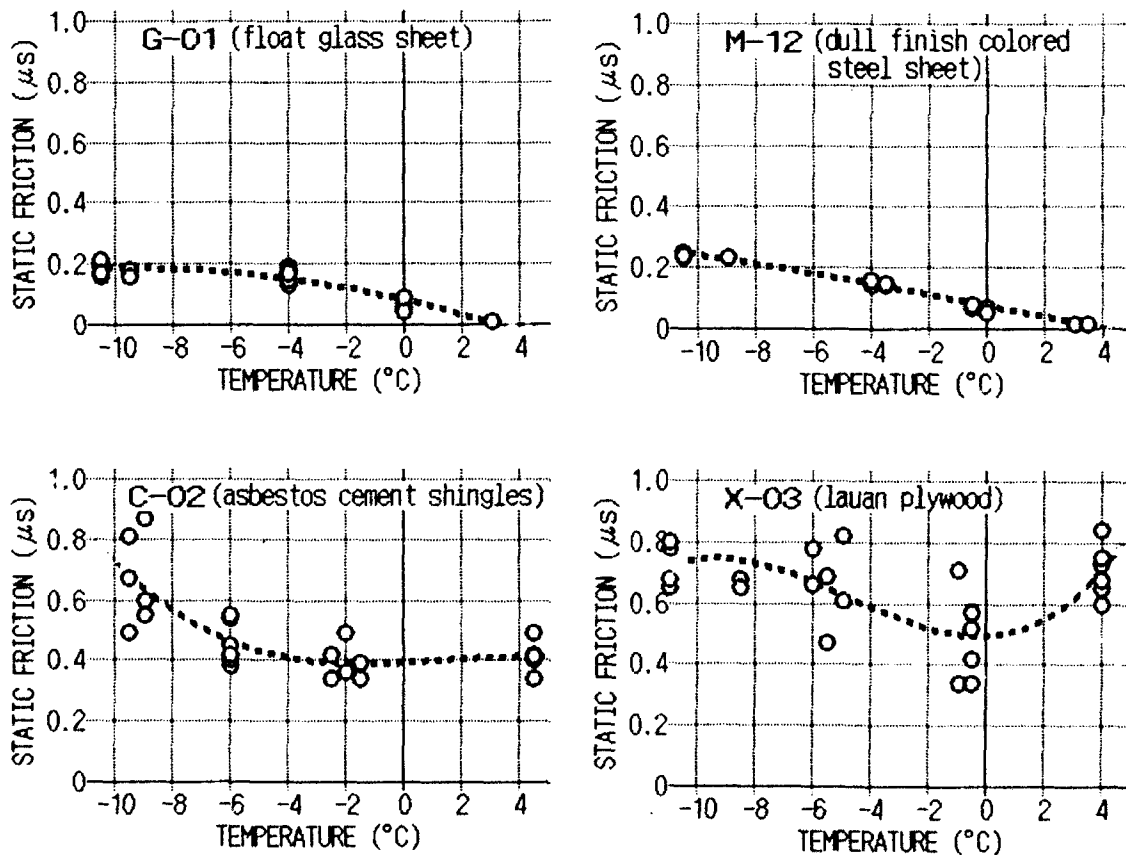


Fig. 1. Typical patterns of μ_s changes caused by the temperature change.

Table 4. Hypothetical grouping of roofing samples in variance analysis on surface roughness and hardness. The μ_s data of -10 °C were utilized in the analysis.

^{*3} Hard Samples		μ_s	^{*4} Soft Samples		μ_s
^{*1} Rough samples	C-02	0.67	X-03		0.70
	G-03	0.08	M-13		0.09
^{*2} Smooth samples	M-02	0.27	M-12		0.24
	G-01	0.18	M-11		0.19

^{*1} $R_{zs} \geq 10(\mu m)$ ^{*2} $R_{zs} < 10(\mu m)$ ^{*3} $E \geq 10^6(N/cm^2)$ ^{*4} $E \leq 10^5(N/cm^2)$

Table 5. Results of variance analysis on surface roughness and hardness. Roughness has a significance level of 99 %.

Factor		Square Sum	Freedom	Variance	Ratio
Roughness	Variation	0.419	3	0.140	F=559**
	Residuals	0.001	4	0.002	
	Sum	0.420	7		
Hardness	Variation	0.000	1	0.000	F=0.00
	Residuals	0.420	6	0.070	
	Sum	0.420	7		

** 99% level significance

Table 6. Correlation coefficients between roughness parameters and static friction μ_s . Rzf has the highest correlations with μ_s at all temperatures.

	Roughness Measured by ^{*1} Standard Cut-Off Value		Roughness Measured by ^{*2} Small Cut-Off Value	
	Ra	Rz	Raf	Rzf
μ_s Values in -10°C	0.293	0.303	0.596	0.766
μ_s Values in - 5°C	0.216	0.217	0.435	0.646
μ_s Values in - 1°C	0.218	0.218	0.538	0.833
μ_s Values in + 3°C	0.698	0.696	0.814	0.846

^{*1} Ra and Rz are measured by JIS and ISO cut-off value.

^{*2} Raf and Rzf are measured by small cut-off value of 0.25 mm.

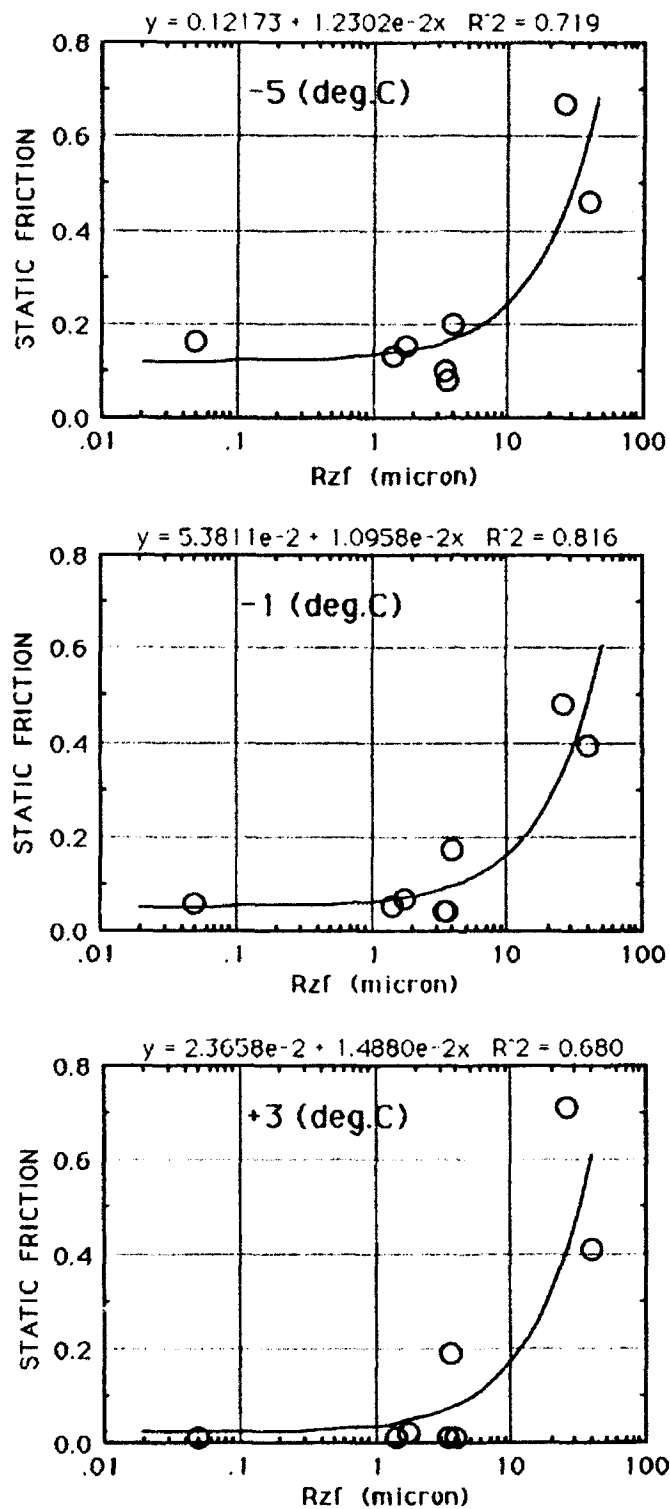


Fig. 2. Relationship between static friction and Rzf value in each temperature condition.

Relationships between Roughness and Static Friction

The analysis of correlation coefficients between roughness parameters and static friction μ_s was carried out. The correlations between four roughness parameters (R_a , R_z , R_{af} and R_{zf}) of all temperature levels (-10° , -5° , -1° and $+3^\circ\text{C}$) were examined, and results of correlation coefficients of all combinations are listed in Table 6. The results indicate that the correlation coefficient between roughness values and μ_s values is higher in fine roughness parameters (R_{af} , R_{zf}) than those of standard parameters (R_a , R_z), and the R_{zf} that was measured by 0.25 mm cut-off take the highest coefficients with the μ_s at all temperature levels.

The correlation analysis suggests that the static friction of roofings against ice can be mainly estimated by the values of R_{zf} . Therefore, the regression analysis between R_{zf} and μ_s was tried on each temperature case. Regression curves of R_{zf} versus μ_s upon three temperature levels of -5° , -1° and $+3^\circ\text{C}$ are shown in Fig. 2 by way of example. Those diagrams indicate that all of regression curves fit in the simple equation, and if the R_{zf} values are greater than approximately $10\text{ }\mu\text{m}$, the static friction of roofing materials tends to rise steeply in any temperature condition. Thus, it can be defined that aslippery roofing has less than approximately $10\text{ }\mu\text{m}$ R_{zf} , and a rough surface has greater than $10\text{ }\mu\text{m}$ R_{zf} .

CONCLUSIONS

In this experimental study on the static friction of roofing materials, the following important findings are clarified:

1. The methods to measure the static friction of roofing materials against ice that were used in this study were simple in mechanisms and easy to operate.
2. Static friction of roofing materials against ice varied widely, but each roofing material took specific friction values.
3. Static friction of roofing materials against ice decrease generally as temperature increases for smooth surface roofing, but not necessarily for rough surface in higher temperatures than 0°C .
4. Static frictions of roofing materials against ice mainly depends upon the surface roughness and not upon the surface hardness.
5. Roughness parameters evaluated by utilizing the small cut-off of 0.25 mm have higher correlation coefficients with static friction than those by the standard cut-off.
6. Static frictions of roofing materials against ice can be assessed by a fine roughness parameter R_{zf} is obtained by 0.25 mm cut off measuring upon R_z ("ten-point height irregularities" of ISO roughness parameter).

REFERENCES

- Maeda, H. (1979) "Conditions of Snow Sliding on Metal Sheet Roof," Journal of Japanese Society of Snow and Ice, Vol.41, No.3, 199-204, September 1979 (in Japanese).
- Sack, R.L., Arnholtz, D.A., and Haldeman, J.S. (1987) "Sloped Roof Snow Loads Using Simulation," Journal of Structural Engineering, Vol. 113, No. 8, 1820-1833, August

1987.

- Tusima, K. (1975) "A Review on Mechanisms of Friction of Ice," *Journal of Society of Lubrication Engineering*, Vol. 21, No. 5, 287-294 (in Japanese).
- Tusima, K. (1980) "Friction of Plastic Ball on Single Crystals of Ice," *Journal of Society of Lubrication Engineering*, Vol. 25, No. 7, 450-457 (in Japanese).
- Taylor, D.A. (1987) "Snow on Sloping Roof," *Proceedings 1987 CSCE Centennial Conference*, Vol. 1, 145-158, May 1987.
- Tamura, M., Hirayama, I., and Miyauchi, S. (1990) "A New System for Controlled Snow Sliding on a Roof," *Journal of Japanese Society of Snow and Ice*, Vol. 52, No. 2, 81-90, June 1990 (in Japanese).
- Tomabechi, T., Yamaguchi, H., Itou, T., and Hoshino, M. (1991) "Fundamental Study on Sliding of Snow on Roof of Membrane Structure," *Journal of Structural and Construction Engineering*, Architectural Institute of Japan, No. 425, 99-105, August 1991 (in Japanese).
- Ueno, M., Takashima, K., Takamura, H., and Fukumoto, H. (1987) "Characteristics Evaluation of Steel Roof Sheet for Snow Sliding," *Journal of Japanese Society of Snow and Ice*, Vol. 49, No. 9, 131-137, September 1987 (in Japanese).
- Watanabe, M., and Hirai, K. (1987) "Study on Friction between Roofing Materials and Snow: Static Friction between Staple Roofing Materials and Ice Blocks," *Journal of Snow Engineering*, No.3, 1-11, June 1987 (in Japanese).
- Watanabe, M., Yamakawa, S., Tsukidate, T., and Tsukinaga, Y. (1988) "A Study on Roof Building System for Snow Damage Protection in Timber House," *Jutaku Kentiku Kenkyujoho*, No.14, 333-350, March 1988 (in Japanese).
- Watanabe, M., and Hirai, K. (1988) "Study on Friction between Roofing Materials and Snow: Sliding Velocity and Kinetic Friction Occurred in Friction Angle," *Journal of Snow Engineering*, No.9, 1-12, December 1988 (in Japanese).
- Watanabe, M., and Hirai, K. (1988) "Study on Snow Sliding Properties of Roofing Materials: Dynamic Friction between Staple Roofing Materials and Ice Block," *Summaries of Technical Papers of Annual Meeting*, Architectural Institute of Japan, 21-22, October 1988 (in Japanese).
- Watanabe, M., and Hirai, K. (1989) "Study on Snow Sliding Properties of Roofing Materials: Roughness Characteristics of Roofing Materials," *Summaries of Technical Papers of Annual Meeting*, Architectural Institute of Japan, 365-366, October 1989 (in Japanese).
- Watanabe, M., and Hirai, K. (1990) "Study on Snow Sliding Properties of Roofing Materials: Evaluation of Static Friction by Surface Roughness," *Summaries of Technical Papers of Annual Meeting*, Architectural Institute of Japan, 451-452, October 1990 (in Japanese).
- Watanabe, M. and Hirai, K. (1991) "Study on Snow Sliding Properties of Roofing Materials: Roughness and Friction of Colored Metal Sheet," *Summaries of Technical Papers of Annual Meeting*, Architectural Institute of Japan, 21-22, October 1991 (in Japanese).

Specifying Snow Melting System Performance

William L. Fyall and Dana L. Hart

Raychem Corporation, Menlo Park, California, U.S.A.

ABSTRACT

Slippery sidewalks, stairs and automobile ramps continue to be a hazard in cold regions. As energy costs rise and safety concerns increase, it becomes more important for engineers and designers to make thoughtful tradeoffs between system performance and operating cost. The data required to understand snow melting system performance have been widely published for many years, but interpreting this data has been difficult.

A simple graphic presentation of the required power input for various geographical locations and operating conditions provides the key to understanding and specifying snow melting effectiveness. The graphic data allow engineers to quickly evaluate performance in return for a given power input and make appropriate tradeoffs.

INTRODUCTION

Automatic snow and ice removal using embedded pavement heating systems is common in sidewalks, ramps, stairways, emergency exits, handicapped entrances, decorative patios and helicopter landing pads. Automatic systems contribute to increased safety and convenience while reducing maintenance costs.

Current design practice in the United States is to specify a snow melting system power requirement based on experience or an interpretation of the guidelines published by the American Society of Heating, Refrigerating and Air Conditioning Engineers, Inc. (ASHRAE). The ASHRAE guidelines are in turn based on studies published by William P. Chapman in the early 1950's. Chapman's classification system is detailed in the footnote to Figure 2 in the 1987 HVAC Systems and Applications Handbook (ASHRAE, 1987). Chapman defines three classes of snow melting system performance based on the frequency distribution of required system output for historical weather records for a given city. Data are presented for 33 American cities.

Chapman's important contribution was to recognize that there is a characteristic required snow melting power frequency distribution for each geographical location. Snow falls at various temperatures, wind speeds and rates and these conditions vary from year to year, but over a long period snowfall in a given area occurs with a characteristic signature.

Although Chapman's frequency distribution data have been available for many years through the ASHRAE Systems Handbooks, it is rarely used. This valuable data has been ignored because terminology introduced by Chapman unnecessarily complicates understanding it and because the power classification system derived from the data is unrealistic in today's energy environment.

An alternate to Chapman's power classification system has been in use with electric snow melting systems for about three years. The alternate method stresses specifying expected performance rather than power and is based on a graphic presentation of the required power frequency distribution.

Throughout the following discussion, values are given in Inch-Pound (IP) units followed by the International System of Units (SI) in parentheses to conform to the format followed in the ASHRAE Handbooks. Table A4 located in the Appendix presents selected conversion constants to assist readers in converting from IP to SI units.

SPECIFYING PERFORMANCE

It is common practice to specify a snow melting system in terms of power output only. The system is specified for 30, 40 or 60 watts per square foot ($320, 430$ or 645 W/m^2) of pavement based on whether the application is residential, commercial/industrial or critical. The basis for this specification is a misunderstanding of Chapman's classification system. The practice ignores substantial regional differences in snowfall patterns. It tends to produce systems which are oversized and waste energy and to mislead designers about the degree of safety their systems are providing.

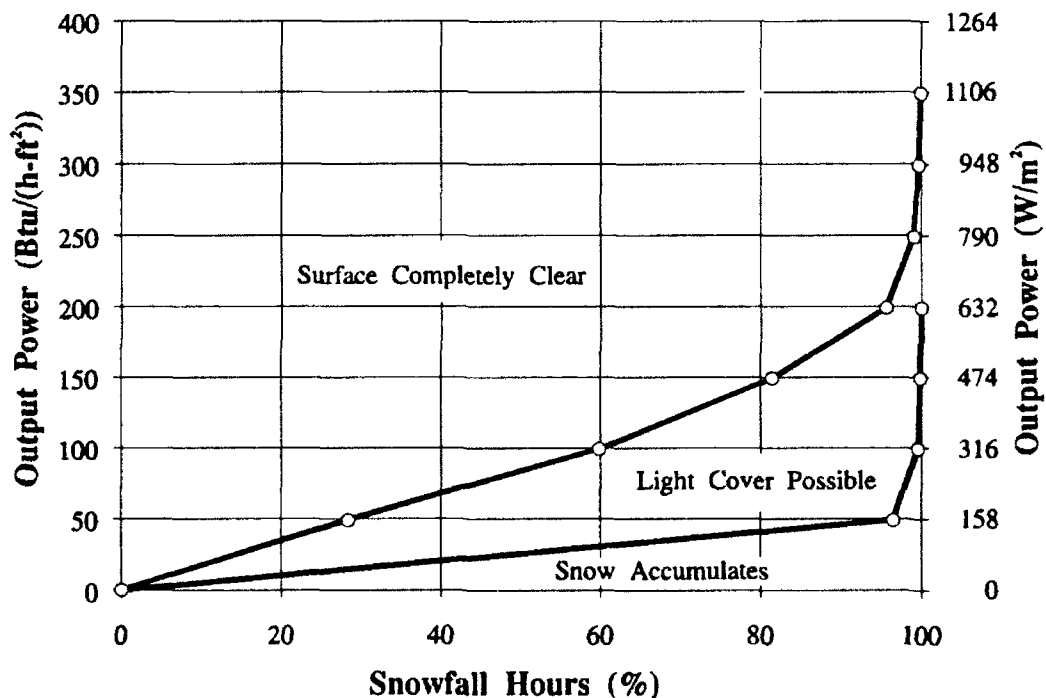


Figure 1: Snow Melting Performance

Table 1: Snow Melting System Classification Criteria

	ASHRAE Handbook	Minneapolis (1980-1989)
Class I design, Btu/(h-ft ²) (W/m ²)	63 (199)	76 (240)
Class II design, Btu/(h-ft ²) (W/m ²)	155 (489)	244 (770)
Class III design, Btu/(h-ft ²) (W/m ²)	254 (801)	330 (1041)
Maximum output for $A_r=0$, Btu/(h-ft ²) (W/m ²)	155 (489)	244 (770)
Maximum output for $A_r=1$, Btu/(h-ft ²) (W/m ²)	313 (987)	400 (1262)
Mean snowfall, hours	203	153

Note: See text for a definition of free area ratio, A_r

An alternate approach which we have used on over 200 snow melting projects stresses specifying expected performance using a graphic representation of the ASHRAE frequency distribution data to translate performance into power. The ASHRAE frequency distribution data for a given city are plotted on a cumulative frequency distribution graph. Figure 1 shows such a graph for Minneapolis, Minnesota. The graph contains two curves which show required output power as a function of percentage of snowfall conditions. The area above the upper curve is labeled "surface completely clear." Operation on or above the upper curve represents a condition where snow melts immediately upon contacting the pavement. The area below the lower curve is labeled "snow accumulates," because operation on or below the lower line represents a condition where the output of the system is less than that required to melt all of the falling snow and accumulation results. When system operation is in the area between the curves, the pavement will have some slush or snow on it, but the snow depth will not be increasing.

Designers pick an operating point based on the percentage of snowfall conditions for which they expect the surface to be completely clear. Prudent tradeoffs are necessary. The operating point should be high enough that snow is prevented from accumulating for nearly 100% of conditions, but low enough to avoid excessive energy costs. In contrast, the system performance level is predetermined when Chapman's classification system is used. A Class I system is one designed for the 98th percentile of the lower curve. A Class II system is designed for the 100th percentile of the lower curve, and a Class III system is designed approximately for the 98th percentile of the upper curve.

Approximately 90% of the snow melting projects we have completed over the last three years have been designed to maintain the surface completely clear for 80% of snowfall conditions. We recommend choosing an operating point between 75% and 98%. If the system is under powered, dynamic response is slow and there is a risk that the pavement will ice at low temperatures even with the heating system energized. As the operating point is increased beyond 98%, energy costs rise much more rapidly than perceptible improvements in performance. Systems sized for the 80th percentile of the frequency distribution provide a good compromise between effectiveness and operating cost.

Several questions arise when system performance is specified. Is the frequency distribution of required power truly characteristic for a city? Under what conditions will the specified performance be inadequate? How does the actual performance compare to that of a system designed to Class I, Class II and Class III criteria?

Table 2: Distribution of Required System Output

Required System Output Btu/(h-ft ²) (W/m ²)	Free Area Ratio=0		Free Area Ratio=1	
	ASHRAE Handbook %	Minneapolis (1980-1989) %	ASHRAE Handbook %	Minneapolis (1980-1989) %
0-49 (0-156)	96.5	94.4	28.4	25.3
50-99 (157-313)	3.1	4.9	31.4	34.3
100-149 (314-471)	0.3	0.6	21.7	21.0
150-199 (472-629)	0.1	0.0	14.1	14.0
200-249 (630-787)		0.1	3.5	2.0
250-299 (788-944)			0.6	1.0
300-349 (945-1102)			0.3	0.3
350-399 (1103-1259)				0.1
400+ (1260+)				

Note: See text for a definition of free area ratio, A_r

MINNEAPOLIS WEATHER STUDY

To answer these questions we monitored an 80th percentile system installed near Minneapolis, Minnesota. Minneapolis was chosen because it has the most severe winter weather of any major US snow melting system market. In addition to following the performance of actual systems, we recalculated the required power frequency distribution using historical weather data and Chapman's power equations.

Weather data were purchased from the National Weather Service¹ for the months of November through March for the years 1980 to 1989. The information was supplied on IBM-compatible disks in ASCII comma-separated variable text format. It was manipulated and analyzed using a spreadsheet program. The data required for the simulation are dry-bulb temperature, wind speed, relative humidity and precipitation recorded hourly.

For each hourly period in which the air temperature was less than or equal to 32°F (0°C) and the precipitation was equal to or greater than 0.01 in (0.25 mm) water equivalent, the required snow melting power was calculated using the following equations²:

$$q_s = 2.6s(32 - t_a) \quad (1)$$

$$q_m = 746s \quad (2)$$

$$q_e = h_{fg}(0.0201v + 0.055)(p_{ws} - p_{av}) \quad (3)$$

$$q_h = 11.4(0.0201v + 0.055)(33 - t_a) \quad (4)$$

$$q_o = q_s + q_m + A_r(q_e + q_h) \quad (5)$$

¹Copies or selections of almost 200 different climate data sets are available from the National Climatic Data Center, Federal Building, Asheville, NC 28801-2896 (telephone: 704-259-0682). For this weather study, hourly temperature, relative humidity and wind speed data were taken from file TD-3280 and hourly precipitation data from file TD-3240.

²The SI form of these equations is given in the ASHRAE HVAC Systems and Applications Handbook (ASHRAE, 1987) and the ASHRAE Fundamentals Handbook (ASHRAE, 1989).

$$p_{av} = 2.036 \phi [\exp\{ C_1/T + C_2 + C_3T + C_4T^2 + C_5T^3 + C_6T^4 + C_7 \ln(T) \}] \quad (6)$$

where:

- q_s = sensible heat, Btu/(h-ft²)
- q_m = heat of fusion of snow, Btu/(h-ft²)
- q_e = heat of evaporation, Btu/(h-ft²)
- q_h = combined radiation and convection heat loss, Btu/(h-ft²)
- q_o = required snow melting power, Btu/(h-ft²)
- s = snowfall rate in equivalent inches of water, in
- v = wind velocity, mi/h
- p_{av} = vapor pressure of moist air at ambient temperature, in-Hg
- h_{fg} = 1075.9 Btu/lb, enthalpy of saturated vapor at 33°F
- p_{ws} = 0.188 904 in-Hg, saturation pressure of water vapor at 33°F
- t_a = ambient temperature, °F
- A_r = free area ratio, dimensionless
- ϕ = relative humidity, dimensionless
- T = $t_a + 459.67$, °R

and:

- C_1 = -1.021 416 462 E+04
- C_2 = -4.893 503 01
- C_3 = -5.376 579 44 E-03
- C_4 = 1.920 237 69 E-07
- C_5 = 3.557 583 16 E-10
- C_6 = -9.034 468 83 E-14
- C_7 = 4.163 501 9

Equations (1) through (5) are the ASHRAE snow melting equations developed by Chapman. Equation (3) differs slightly from the ASHRAE form in that it incorporates a computed value for the saturation pressure of water, p_{ws} , at a 33°F film temperature rather than the constant given by ASHRAE. Equation (6) uses ASHRAE's saturated vapor pressure expression (ASHRAE, 1989) to compute water vapor partial pressure, p_{av} .

The frequency distribution of required outputs developed by Chapman (Chapman, 1956) and published by ASHRAE, was calculated from Equation (5) by solving the equation for values of free area ratio, A_r , of zero and one. Free area ratio is defined by Chapman as the ratio of the snow-free area to the total heated area. A ratio of one corresponds to a heated slab which is completely clear of snow, while a ratio of zero indicates a heated slab which is completely covered by a thin layer of snow and slush. A ratio between zero and one occurs when the slab is supplying at least enough heat to meet the sensible and heat of fusion needs of a particular set of snowfall conditions, but is failing to supply all of the additional heat needed to meet the evaporation, conduction and radiation losses of the slab.

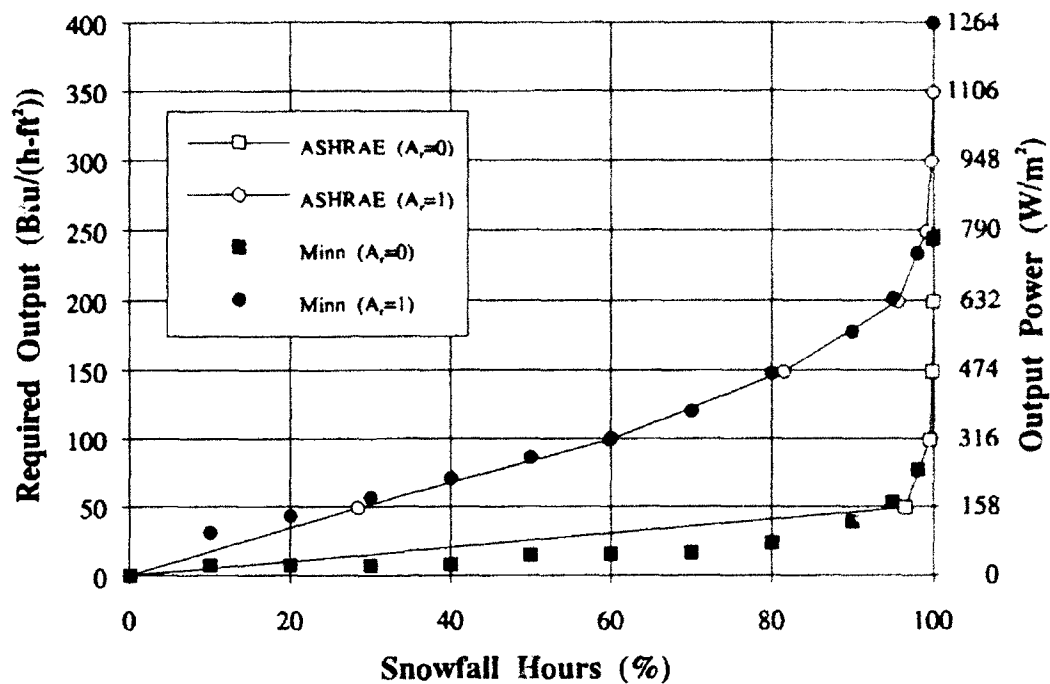


Figure 2: Required Output Frequency Distribution

Table 2 shows the study data compared to published ASHRAE data. The data are plotted in the form of a cumulative frequency distribution in Figure 2. The Minneapolis frequency distribution for 1980-1989 is very similar to that prepared by Chapman based on 1940-1949 data. However, the required outputs for Chapman's classification system computed from this data are significantly different. Table 1 summarizes ASHRAE classifications recalculated using the study data. Because the ASHRAE classification is based on maximum required output (except for Class I), the occurrence of a single severe storm during this period increased the Class II and Class III criteria by 30% and 57% respectively.

The study revealed interesting snowfall details. The mean temperature during snowfall for the period was 21°F (-6°C) which is significantly higher than the mean winter temperature. During this period there were 1529 hours of snowfall, an average of 153 hours per year compared to an average of 203 hours reported by Chapman. There were 124 hours of snowfall when the temperature was at or below 5°F (-15°C) and 50 hours of snowfall at or below 0°F (-18°C). The minimum temperature at which snow fell was -14°F (-26°C), while the highest wind speed during snowfall was 34.5 mi/h (55.5 km/h). Table A2 in the Appendix summarizes the winter weather for the study period.

PERFORMANCE FAILURE

A system designed to operate at the 80th percentile of the required output power frequency distribution can be said to fail roughly 20% of the time. The Minneapolis study provides insight into how the system performs even when it is not supplying enough power to melt the snow immediately.

Table 3: Performance Failure of an 80th Percentile Design

Date	Time	Temp	Wind	RH	Precip	q(s)	q(m)	q(e)	q(h)	A _r =0	A _r =1
	LST	°F	Knots	%	[1]	[2]	[2]	[2]	[2]	[2]	[2]
27-Dec-82	18	30	15	85	7	0.4	52.2	21.2	13.7	52.6	87.5
27-Dec-82	19	29	11	92	8	0.6	59.7	14.7	14.1	60.3	89.2
27-Dec-82	20	29	15	89	7	0.5	52.2	21.2	18.3	52.8	92.3
27-Dec-82	21	29	16	89	5	0.4	37.3	22.4	19.4	37.7	79.5
27-Dec-82	22	29	16	85	5	0.4	37.3	25.3	19.4	37.7	82.4
27-Dec-82	23	28	20	89	11	1.1	82.1	30.8	29.5	83.2	143.5
28-Dec-82	0	28	22	85	18	1.9	134.3	37.2	32.1	136.2	205.5
28-Dec-82	1	26	28	92	32	5.0	238.7	47.7	56.1	243.7	347.5
28-Dec-82	2	26	24	92	25	3.9	186.5	41.5	48.7	190.4	280.5
28-Dec-82	3	25	27	96	7	1.3	52.2	46.6	62.0	53.5	162.0
28-Dec-82	4	25	27	100	9	1.6	67.1	42.8	62.0	68.8	173.5
28-Dec-82	5	24	23	88	8	1.7	59.7	50.2	60.2	61.3	171.7
28-Dec-82	6	24	26	92	2	0.4	14.9	52.6	67.3	15.3	135.3
28-Dec-82	7	23	25	88	2	0.5	14.9	57.6	72.2	15.4	145.2
28-Dec-82	8	21	25	85	4	1.1	29.8	66.2	86.6	31.0	183.9
28-Dec-82	9	18	22	82	2	0.7	14.9	68.2	96.4	15.6	180.2
Jan-83	7	32	14	85	1	0.0	7.5	14.5	4.3	7.5	26.2

[1] Precipitation in hundredths of inches of water equivalent

[2] Btu/(h·ft²)

In Minneapolis, an 80th percentile system is required to produce 148 Btu/(h·ft²) (466 W/m²). For the study period, the power requirement exceeds this 306 hours in 10 years or 30.6 hours per year. During this time snow is not melted immediately, so that some slush and snow cover the pavement. For two hours during this period the system output is less than that required to supply the heat of fusion of the falling snow and snow begins to accumulate. Table 3 shows the power requirements during that period of failure. Accumulation began at 1:00 AM; however, accumulation would have stopped during the hour beginning at 3:00 AM when the system output was more than required to supply the heat of fusion.

FIELD EXPERIENCE

The simplified approach to specifying snow melting performance by specifying only the percentage of snowfall conditions for which snow will melt immediately has been in use for three years with success. We have followed one project with particular interest. A college near Minneapolis installed an 80th percentile system in the summer of 1991 in a handicapped entrance ramp. The system was in operation October 31, 1991 when a record-setting snow storm hit the area. In four days the storm set 100-year records for the greatest snowfall in 24 hours and the greatest total snowfall for a single storm. Table A3 shows the calculated power distribution during that storm.

The output distribution indicates that the design output was exceeded nine hours during the storm, but the owners of the system reported that the electric snow melting system kept the pavement clear during the entire storm. The maximum required output for a free area ratio of one

was 196.7 Btu/(h-ft²) (620.5 W/m²), while the maximum output for a free area ratio of zero was 120.6 Btu/(h-ft²) (380.4 W/m²). During the only period when the system output was exceeded for two or more consecutive hours, the calculated evaporation loss was 34% or more of the total and the calculated convection loss 55% or more of the total. Since the ramp is sloped for drainage and shielded from the wind by plants and buildings, it is likely that the actual evaporation and convection losses were lower than calculated.

CONCLUSION

Minneapolis winter weather from 1980 to 1989 was studied to compare the frequency distribution of required snow melting output to published ASHRAE data and to examine the power requirements between the 98th and 100th percentile of the distribution. Although there were fewer hours of total snowfall compared to the 1940-1949 period, the frequency distribution was remarkably similar. Our limited test seems to confirm Chapman's hypothesis that snowfall occurs with a characteristic power signature.

We found significant differences in the 98th to 100th percentile of the frequency distribution compared to Chapman's data. The severe storms which influence this part of the distribution are relatively rare, and a 10-year sample of weather data is insufficient to capture them. Since Chapman's classification of snow melting systems is based entirely on the behavior of 98th to 100th percentile power requirements, we recommend against using it to specify snow melting system performance. Our experience with over 200 projects shows that systems specified to provide a completely clear surface for approximately 80% of snowfall conditions provide a good compromise between performance and operating economy.

REFERENCES

- ASHRAE (American Society of Heating, Refrigerating and Air Conditioning Engineers, Inc.), 1987, "Snow Melting", 1987 ASHRAE Handbook - Heating, Ventilating, and Air-Conditioning Systems and Applications, ASHRAE, Inc., Atlanta, Georgia.
- ASHRAE (American Society of Heating, Refrigerating and Air Conditioning Engineers, Inc.), 1989, "Psychrometrics", 1989 ASHRAE Handbook - Fundamentals, ASHRAE, Inc., Atlanta, Georgia.
- Chapman, William P., 1952, "Design of Snow Melting Systems", Heating and Ventilating, 96-102, April, 1952.
- Chapman, William P., 1956, "Calculating the Heat Requirements of a Snow Melting System", Air Conditioning, Heating and Ventilating, 67-71, September, 1956.

APPENDIX

Chapman's classification system places emphasis on the 98th to 100th percentile of the output frequency distribution. The Minnesota study shows that extremely high power requirements at the upper end of the frequency distribution are due primarily to increased convection losses caused by low temperatures and high wind speeds.

Table A1: Required Output - 98th to 100th Percentile

DATE	Time	Temp	Wind	RH	Precip	q(s)	q(m)	q(e)	q(h)	A _r =0	A _r =1	%
	LST	°F	Knots	%	[1]	[2]	[2]	[2]	[2]	[2]	[2]	
25-Dec-85	22	7	18	69	2	1.3	14.9	76.9	139.7	16.2	232.8	98.0
1-Feb-89	23	-2	14	79	2	1.8	14.9	66.1	151.2	16.7	233.9	98.0
1-Dec-85	15	15	22	88	6	2.7	44.8	71.6	115.7	47.4	234.7	98.1
3-Mar-85	14	22	26	81	11	2.9	82.1	68.7	82.3	84.9	235.9	98.2
2-Feb-89	15	-4	14	71	1	0.9	7.5	68.2	159.8	8.4	236.4	98.2
5-Feb-84	1	11	23	84	1	0.5	7.5	84.2	147.2	8.0	239.4	98.3
20-Jan-82	14	11	17	84	8	4.4	59.7	64.3	112.4	64.0	240.8	98.4
2-Feb-89	6	-5	13	75	3	2.9	22.4	64.0	154.1	25.3	243.4	98.4
1-Dec-85	19	8	20	73	2	1.2	14.9	82.1	147.5	16.2	245.8	98.5
7-Jan-89	20	7	20	87	2	1.3	14.9	79.0	153.4	16.2	248.6	98.6
20-Jan-82	11	8	13	84	12	7.5	89.5	54.0	101.4	97.0	252.4	98.6
1-Dec-85	17	10	20	80	5	2.9	37.3	77.2	135.7	40.2	253.1	98.7
8-Jan-89	7	2	18	79	1	0.8	7.5	79.0	166.6	8.2	253.9	98.8
1-Dec-85	16	12	24	84	3	1.6	22.4	85.7	146.1	23.9	255.7	98.8
25-Dec-85	23	7	20	84	3	2.0	22.4	79.9	153.4	24.3	257.7	98.9
2-Feb-89	9	-6	15	71	1	1.0	7.5	73.3	178.7	8.4	260.4	99.0
8-Jan-89	5	2	19	79	1	0.8	7.5	82.9	174.7	8.2	265.9	99.0
2-Feb-89	1	-3	16	75	2	1.8	14.9	75.4	174.5	16.7	266.6	99.1
10-Feb-81	13	-2	17	65	1	0.9	7.5	80.5	178.8	8.3	267.7	99.1
7-Jan-89	23	4	20	76	2	1.5	14.9	85.6	171.1	16.4	273.1	99.2
8-Jan-89	2	2	20	79	1	0.8	7.5	86.8	182.9	8.2	278.0	99.3
8-Jan-89	6	2	20	79	1	0.8	7.5	86.8	182.9	8.2	278.0	99.3
1-Dec-85	20	7	22	80	3	2.0	22.4	88.4	167.1	24.3	279.8	99.4
28-Dec-82	2	26	24	92	25	3.9	186.5	41.5	48.7	190.4	280.5	99.5
1-Dec-85	23	6	22	69	2	1.4	14.9	93.1	173.6	16.3	282.9	99.5
8-Jan-89	3	2	21	76	1	0.8	7.5	91.4	191.1	8.2	290.8	99.6
8-Jan-89	0	3	22	79	3	2.3	22.4	93.5	192.8	24.6	311.0	99.7
2-Feb-89	2	-4	19	79	2	1.9	14.9	87.7	208.6	16.8	313.0	99.7
5-Feb-84	2	8	28	76	1	0.6	7.5	110.1	200.3	8.1	318.5	99.8
5-Feb-84	5	1	23	79	2	1.6	14.9	99.5	214.1	16.5	330.2	99.9
28-Dec-82	1	26	28	92	32	5.0	238.7	47.7	56.1	243.7	347.5	99.9
5-Feb-84	4	2	30	76	1	0.8	7.5	126.6	264.7	8.2	399.5	100.0

[1] Precipitation in hundredths of inches of water equivalent

[2] Btu/(h·ft²)

The study of Minneapolis weather reveals interesting detail about winter weather. It is commonly believed that snow rarely occurs below 20°F (-7°C). The study shows that the mean temperature during snowfall in Minnesota is only 21°F (-6°C) and that snow occurs down to -14°F (-26°C). The study confirms that it is both very cold and very windy during snowfall in Minneapolis.

Table A2: Minneapolis Weather During Snowfall 1980-1989

	ASHRAE Handbook	Minneapolis (1980-1989)
Mean wind speed during freezing periods with no snowfall, mi/h (km/h)	11.1 (17.9)	
Mean temperature during freezing periods with no snowfall, °F (°C)	16.9 (-8.4)	
Fraction of winter hours below freezing, %	70.8	61.1
Mean winter temperature, °F (°C)		24.1 (-4.4)
Mean winter wind speed, mi/h (km/h)		11.1 (17.9)
Mean winter relative humidity, %		71.4
Mean temperature during freezing periods, °F (°C)		16.9 (-8.3)
Mean wind speed during freezing periods, mi/h (km/h)		10.6 (17.1)
Mean relative humidity during freezing periods, %		72.1
Mean temperature during snowfall, °F (°C)		21.0 (-6.1)
Mean wind speed during snowfall, mi/h (km/h)		13.4 (21.6)
Mean relative humidity during snowfall, %		84.3
Mean snowfall, equivalent inches of water (mm)		0.024 (0.61)
Lowest temperature during snowfall, °F (°C) (4-Feb-82)		-14.0 (-25.6)
Hours of snowfall with temperature less than 0°F (-18°C)		50
Hours of snowfall with temperature less than 5°F (-15°C)		124
Highest wind speed during snowfall, mi/h (km/h) (5-Feb-84)		34.5 (55.5)
Greatest snowfall during one hour, equivalent inches of water (mm)		0.32 (8.1)
97-1/2% Winter dry bulb temperature, °F (°C)		-10.0 (-23.3)
99% Winter dry bulb temperature, °F (°C)		-16.0 (-26.7)
97-1/2 percentile temperature during snowfall, °F (°C)		-1.0 (-18.3)
99 percentile temperature during snowfall, °F (°C)		-5.0 (-20.6)
80 percentile required output power when $A_r=1$, Btu/(h-ft ²) (W/m ²)		147.8 (466.2)
80 percentile required output power when $A_r=0$, Btu/(h-ft ²) (W/m ²)		23.6 (74.4)
98 percentile required output power when $A_r=1$, Btu/(h-ft ²) (W/m ²)		232.8 (734.4)
98 percentile required output power when $A_r=0$, Btu/(h-ft ²) (W/m ²)		76.4 (241.0)

Table A3 shows the computed power requirement for a record-setting snow storm which hit the Minneapolis area on October 31, 1991. The storm dropped 18.5 in (470 mm) of snow in one 24-hour period and 28.4 in (721 mm) total, setting 100-year records. During this storm an electric snow melting system producing 148 Btu/(h-ft²) (466 W/m²) was reported to have kept the pavement clear during the entire storm.

The calculated power requirement exceeded the installed power 7 hours the night of November 2. Although it is unlikely that anyone was on site to observe the heated ramp, it is probable that the ramp was clear. The largest component of the calculated heat loss is convection. Since the ramp is located among buildings and trees, it is shielded from the wind and true convection losses are probably less than the calculated losses. Analysis of the power requirements of this storm shows that it is not the quantity of snow or the duration of snowfall which determines the maximum demands on the snow melting system, but the contribution of wind and temperature to evaporation, convection and radiation losses from the slab.

Table A3: Record-Setting Minneapolis Snow Storm - 1991

Date	Time	Temp	Wind	DP	Precip	q(s)	q(m)	q(e)	q(h)	A _r =0	A _r =1
	LST	°F	Knots	°F	[1]	[2]	[2]	[2]	[2]	[2]	[2]
31-Oct-91	1251	30	6	28	6	0.3	44.8	8.1	6.6	45.1	59.8
31-Oct-91	1351	30	8	29	7	0.4	52.2	6.3	8.2	52.6	67.1
31-Oct-91	1450	30	11	29	5	0.3	37.3	8.1	10.6	37.6	56.2
31-Oct-91	1550	30	9	29	6	0.3	44.8	6.9	9.0	45.1	60.9
31-Oct-91	1655	31	7	29	4	0.1	29.8	3.9	4.9	29.9	38.7
31-Oct-91	1755	31	8	30	5	0.1	37.3	4.3	5.5	37.4	47.2
31-Oct-91	1855	31	13	30	5	0.1	37.3	6.3	8.1	37.4	51.9
31-Oct-91	1955	31	12	30	7	0.2	52.2	5.9	7.6	52.4	65.9
31-Oct-91	2054	32	9	30	14	0.0	104.4	2.4	3.0	104.4	109.8
31-Oct-91	2155	32	11	29	6	0.0	44.8	2.8	3.5	44.8	51.1
31-Oct-91	2255	32	15	29	11	0.0	82.1	3.6	4.6	82.1	90.3
31-Oct-91	2355	32	12	30	9	0.0	67.1	3.0	3.8	67.1	73.9
1-Nov-91	0051	31	15	30	7	0.2	52.2	7.1	9.2	52.4	68.7
1-Nov-91	0151	31	16	30	5	0.1	37.3	7.6	9.7	37.4	54.7
1-Nov-91	0250	31	19	30	12	0.3	89.5	8.8	11.3	89.8	109.9
1-Nov-91	0350	30	21	29	14	0.7	104.4	14.1	18.5	105.2	137.8
1-Nov-91	0450	30	21	28	12	0.6	89.5	14.1	18.5	90.1	122.8
1-Nov-91	0550	29	18	28	16	1.2	119.4	16.1	21.5	120.6	158.2
1-Nov-91	0652	30	24	28	14	0.7	104.4	15.9	20.9	105.2	142.0
1-Nov-91	0750	30	22	28	13	0.7	97.0	14.7	19.3	97.7	131.7
1-Nov-91	0850	29	23	28	10	0.8	74.6	20.0	26.8	75.4	122.2
1-Nov-91	0950	30	22	27	12	0.6	89.5	14.7	19.3	90.1	124.2
1-Nov-91	1050	30	24	27	6	0.3	44.8	15.9	20.9	45.1	81.9
1-Nov-91	1150	29	25	26	2	0.2	14.9	21.6	28.9	15.1	65.6
1-Nov-91	1250	29	25	25	4	0.3	29.8	21.6	28.9	30.2	80.6

Table continued on following page

Date	Time	Temp	Wind	DP	Precip	q(s)	q(m)	q(e)	q(h)	A _r =0	A _r =1
	LST	°F	Knots	°F	[1]	[2]	[2]	[2]	[2]	[2]	[2]
1-Nov-91	1350	29	23	26	3	0.2	22.4	20.0	26.8	22.6	69.4
1-Nov-91	1450	28	24	25	6	0.6	44.8	25.5	34.8	45.4	105.7
1-Nov-91	1550	27	24	25	5	0.7	37.3	30.0	41.7	38.0	109.7
1-Nov-91	1655	27	23	23	7	0.9	52.2	28.8	40.2	53.1	122.1
1-Nov-91	1755	26	22	23	8	1.2	59.7	31.7	45.0	60.9	137.6
1-Nov-91	1854	25	22	24	7	1.3	52.2	35.5	51.4	53.5	140.4
1-Nov-91	1953	24	26	22	7	1.5	52.2	45.6	67.3	53.7	166.6
1-Nov-91	2055	24	24	22	4	0.8	29.8	42.3	62.6	30.7	135.6
1-Nov-91	2154	24	20	21	7	1.5	52.2	35.9	53.1	53.7	142.7
1-Nov-91	2254	23	22	20	2	0.5	14.9	42.6	64.3	15.4	122.3
1-Nov-91	2355	23	25	18	2	0.5	14.9	47.9	72.2	15.4	135.5
2-Nov-91	0150	20	21	17	1	0.3	7.5	50.1	80.1	7.8	138.0
2-Nov-91	0250	20	22	15	2	0.6	14.9	52.2	83.6	15.5	151.3
2-Nov-91	0350	19	22	14	2	0.7	14.9	55.2	90.0	15.6	160.8
2-Nov-91	0450	17	23	11	1	0.4	7.5	63.2	107.1	7.9	178.1
2-Nov-91	1050	15	23	7	1	0.4	7.5	68.4	120.5	7.9	196.7
2-Nov-91	1150	16	23	8	1	0.4	7.5	65.8	113.8	7.9	187.5
2-Nov-91	1654	17	23	11	1	0.4	7.5	63.2	107.1	7.9	178.1
2-Nov-91	1854	17	18	10	1	0.4	7.5	50.7	86.0	7.9	144.5
3-Nov-91	0150	15	18	10	1	0.4	7.5	54.9	96.7	7.9	159.5
3-Nov-91	0250	15	16	9	1	0.4	7.5	49.5	87.2	7.9	144.7
3-Nov-91	0350	14	15	9	1	0.5	7.5	48.5	87.1	7.9	143.5

[1] Precipitation in hundredths of inches of water equivalent

[2] Btu/(h-ft²)

Table A4: Selected SI Unit Conversions

Multiply	By	To Obtain
Btu/(h-ft ²)	3.155	W/m ²
Btu/lb	2.326	kJ/kg
in	25.4	mm
in-Hg (0°C)	3.386	kPa
knots	1.852	km/h
mi/h	1.609	km/h
W/ft ²	10.764	W/m ²

1981 ASHRAE Handbook - Fundamentals, ASHRAE, Inc., Atlanta, Georgia

Snow Removal from a Pantiled Roof Using Electrically Heated Roof Tiles

Yoshio Higashiyama, Kazutoshi Asano,* Akihiko Miyano[†] and Yutaka Murata**

*Department of Electrical Information and Engineering, Faculty of Engineering
Yamagata University, Yonezawa, Yamagata 922, Japan

[†]Professor Emeritus, Nagoya Institute of Technology, Nagoya, Aichi, Japan

**Yoken Co., Ltd., Gohtsu, Shimane, Japan

ABSTRACT

A snow sliding method for snow removed from a pantiled gable roof has been investigated since January 1989 at Yonezawa in northern Japan using an electrically heated roof tile (SMERT), which is a pantile with an electric heater deposited on its undersurface. In order to obtain the fundamental and practical data for energy saving operation of the SMERT, snow sliding tests have been carried out by changing the arrangement of the SMERTs and unheated tiles as well as input power. The time variations of the surface temperature of the tiles and the amount of meltwater were monitored during the experiments. Snow sliding strongly depends on the surface temperature of roof tiles and would likely occur at a temperature above 2 °C, regardless of whether or not the tiles are heated. Snow meltwater plays a significant role in increasing the surface temperature of unheated tiles and thereby snow sliding occurs on the roof.

INTRODUCTION

Snow melting method using an electric heater has been widely used. However, melting snow on a whole roof requires a huge amount of energy and results in high operating costs. Heaters are mainly installed at eaves of a roof covered with steel roofing to prevent ice formation and the collapse of eaves. However, the application of an electric heater for a pantiled roof yields a problem, that is, heating a pantile with a heater placed on sheathing is inefficient due to the presence of air spacing. One method of overcoming such a disadvantage is to attach an electric heater to pantile and to heat tiles directly. The experiments using a pantile with an electric heater were carried out two decades ago (Association of Construction Mechanizing of

Japan, 1977). The results showed the good performance of snow melting, though the problems on fabrication of reliable tiles and on the energy saving operation have remained.

On the other hand, a new snow-melting electrically heated roof tile (SMERT) has been recently developed. It has a thin electric heater coated on the undersurface of a conventional pantile with plasma spraying. Presently, the technical problems such as manufacturing method, stability of a heater, and roofing methods of SMERTs have been solved. However, how to operate SMERTs at low operating cost or low input energy has remained the present concern. Since the area of one tile is small relative to the whole roof area and one piece of SMERT is regarded as one element, a combination of SMERTs may essentially constitute of a linear or planer heater at an any position on the roof according to the purpose: snow melting, snow sliding, and prevention of icicles.

Performance tests on snow removal have been carried out at a model house in Yonezawa, Japan, since January 1989, especially focusing on snow sliding (Higashiyama et al., 1991). Since it is necessary to lower the operating cost and the initial installation cost, the whole roof is not covered with the relatively expensive SMERTs. We proposed the tile arrangement consisting of lines of heated tiles and unheated ones alternatively. Here, test results in the winter of 1990/1991 are examined and analyzed in detail. The influence of the surface temperature of roof tiles on the snow sliding are discussed from practical and physical aspects.

EXPERIMENTAL

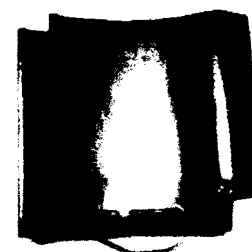
Roof Tiles

The snow-melting electrically heated roof tiles (SMERT) is shown in Figure 1. Every pantile is roofed partially overlapped so that the contact area of a pantile with a snow cover is 275 mm x 230 mm. The U-shaped thin heater, which has an area of 200 mm x 50 mm, is formed by plasma deposition on the center position of the undersurface of a conventional pantile. The SMERT to be installed at the first line of the eave has a heater deposited near the edge of the tile to prevent icicle formation. The heater area is completely covered with a thin film of an electrical insulator. For the tests in the 1990/91 season, a 12-mm-thick thermal insulator was used to improve heat efficiency as shown in Figure 1(c).

Since the nominal input power of a heater was designed to be 20 W using 100 V_{AC} commercial power, the electric resistance of a heater was set at approximately 500 Ω . Input power to a piece of SMERT was varied from 6 to 20 W by adjusting the applied voltage.

Test Roof

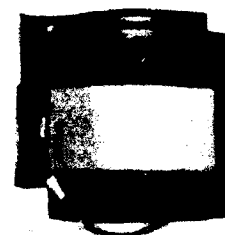
A gable-roof house as shown in Figure 2 was built on an experimental basis in the Yonezawa campus of Yamagata



(a) Upper surface



(b) Heater



(c) Thermal insulator

Figure 1. Snow melting electrically heated roof tiles.

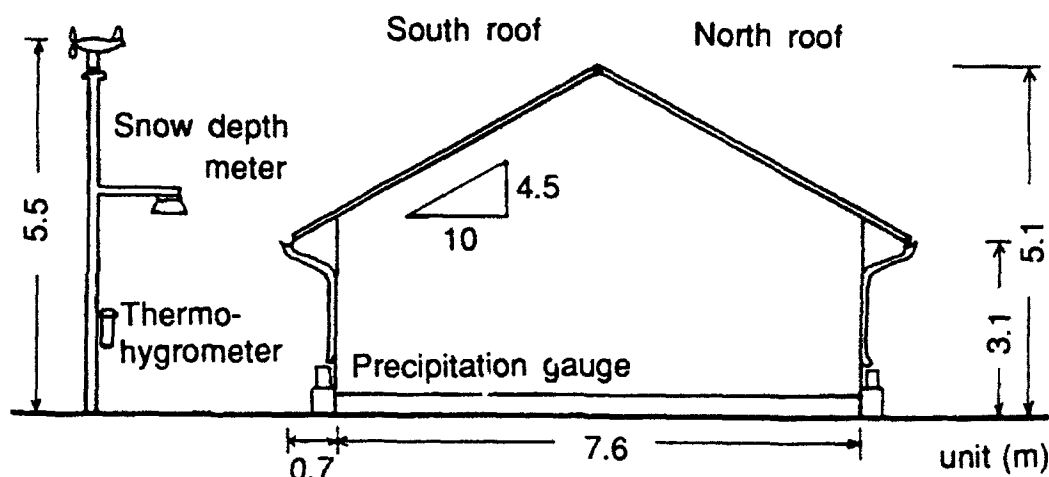
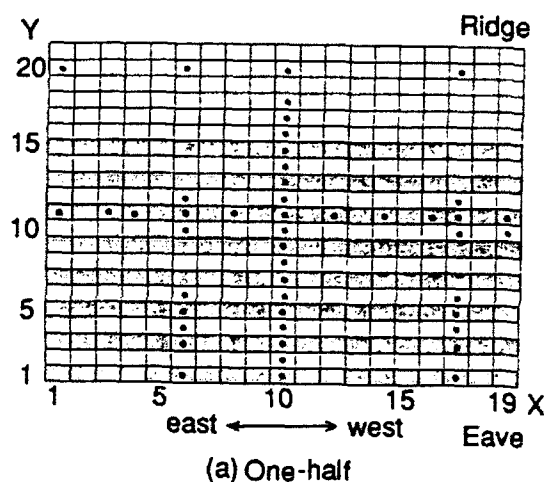


Figure 2. Test house.

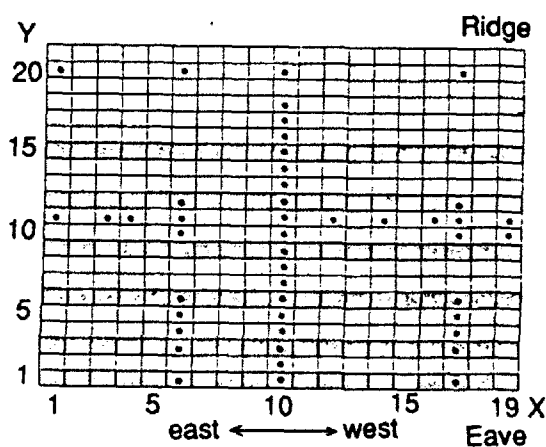
University. The roof area is 52 m^2 (5.3 m in the direction of the eaves \times 4.9 m from the eave to the ridge \times 2 faces). The angle of the roof is 24° . The roof facing north was designed for the snow sliding experiment and the one facing south was for the snow melting experiment. Each roof surface is covered with 399 pantiles, 19 columns \times 21 rows as shown in Figure 3. The position of each pantile is represented by a row and column. The column number is denoted by the letter X in the direction of the eave (from east to west), and the row number is denoted by the letter Y in the direction from the eave to the ridge.

Figure 3 shows two example arrangements of heated and unheated roof tiles on the snow sliding roof. In order to turn each row of SMERTs on or off independently, all of the SMERTs placed in the same row are connected in parallel to the power supply, except that the two ends and each row has its own electrical switch.

Figure 3(a) shows the one-half arrangement in which half of the roof tiles are heated. In the one-half arrangement, the rows of heated and unheated tiles alternate. In the one-third arrangement shown in Figure 3(b), one row of heated tiles and two rows of unheated tiles are repeatedly arranged except near the eave.



(a) One-half



(b) One-third

• Thermocouple

Figure 3. Example of the arrangement of the heated tiles on the roof.

Test Method and Observing System

When snow depth on the roof reached around 200 mm, the SMERTs were turned on manually at a desired input power, usually in the evening to prevent snow melting due to sunshine. After the occurrence of snow sliding, the SMERTs were turned off.

The surface temperature of the heated and unheated tiles was measured with thermocouples at the positions shown in Figure 3. The data were collected with a YOKOGAWA HR2500E data acquisition system every 10 minutes along with meteorological factors such as outside ambient air temperature, humidity, snow depth, wind velocity and direction. Since the amount of melt water is an important index related to the input energy for snow melting, all of the melt water flowing down from the roof was collected with a gutter and guided directly into a precipitation gauge as illustrated in Figure 2.

The time variation of roof snow cover was monitored with a video camera set to record for 1 sec out of every 60 sec to grasp the time of occurrence of snow sliding and movement of the snow cover, which was compared with the time variations of the surface temperature of the roof tiles.

OCCURRENCE OF SNOW SLIDING

The test results in three snow seasons are summarized in Table 1. A SMERT used in each season is slightly different in electrical resistance, heater material, shape, and thermal

Table 1. Summary of snow sliding test for three snow seasons

Test No.	Date (M/D/Y)	Rate of SMERT	Input Power (W)	Minimum Temperature (°C)	Roof snow depth (mm)	Time to slide (hours)
88-D1	1/29/89	1/2	20	-1.4	300	13
88-D2	2/ 3/89	1/4	20	-5.0	200	***
88-D3	2/11/89	1/2	10	-11.0	50	***
89-D1	12/20/89	1/3	20	-2.3	200	14
89-D2	1/ 4/90	1/3	10	-2.5	300	17
89-D3	1/ 7/90	1/3	15	-1.7	350	23
89-D4	1/20/90	1/3	10	-14.0	150	***
89-D5	1/25/90	1/2	10	-9.2	400	***
89-D6	2/ 2/90	Y1, Y3	20	-11.7	100	***
90-D1	1/ 5/91	1/2	20	-0.2	150	0.5
90-D2	1/ 7/91	1/2	20	-5.3	200	5.3
90-D3	1/18/91	1/2	15	-7.6	200	4
90-D4	1/28/91	1/2	10	-9.2	50	16
90-D5	1/30/91	1/3	10	-4.7	50	1.2
90-D6	2/ 3/91	1/3	10	-1.4	200	4.8
90-D7	2/ 5/91	1/3	8	-4.5	200	15.4
90-D8	2/ 7/91	1/3	6	-10.0	50	***
90-D9	2/25/91	1/2	6	-1.9	200	12.6

*** : no snow sliding

insulation, because of the year by year improvements. In the 1990/91 season, a SMERT attached with a thermal insulator was used. The *time to snow slide* in the last column of Table 1 is the time from turning SMERTs on to snow sliding and therefore represents the performance of the SMERTs under the given test conditions.

The surface temperature of pantiles significantly affects the occurrence of snow sliding. Here, as one successful example of snow sliding, the incidence of snow sliding in test #90-D2 is examined in detail below.

Snow Sliding

Figure 4 shows the change of roof snow cover taken with a video camera in test #90-D2 which was set at the one-half arrangement. Input power to one piece of SMERT is 20 W. In this test, the SMERTs were turned on at 17:30 in the evening and turned off at 10:30 the next morning. The roof snow cover slid down at midnight 5.3 hours after switching the SMERTs on.

In Figure 4(b), horizontal stripes appeared over the roof snow, showing that snow above the SMERTs melted. Snow above the eave slid down first as shown in Figure 4(c). Four minutes later, most of snow cover above the heated area slid down.



(a) Turn on



(b) 2 hours 40 minutes



(c) 5 hours 15 minutes



(d) 4 minutes later (c)

Figure 4. Occurrence of snow sliding taken with a video camera.

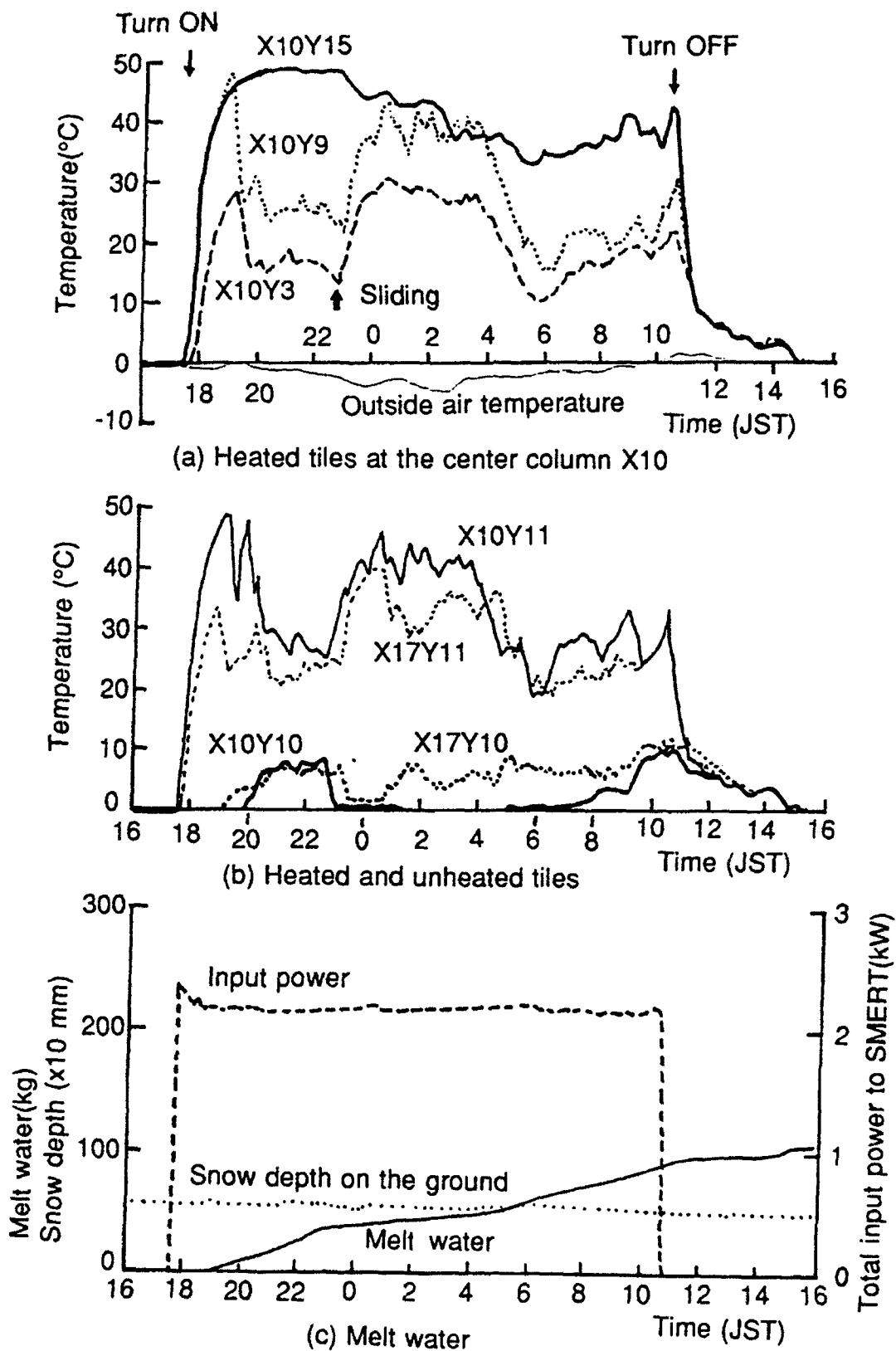


Figure 5. Time variation of the surface temperature of the roof tiles and the cumulative amount of melt water.

Surface Temperature of Roof Tiles

Figure 5 shows the time variations of the surface temperature of pantiles along with that of snow melt water. The changes of the surface temperature of the tiles correspond to the behavior of the roof snow cover and to the snow state above the roof tiles. Figure 5(a) shows the surface temperature of the tiles of X10Y3, X10Y9, and X10Y15 which are placed at column X10. The legend for each data plot in Figure 5 corresponds to the location of pantiles on the roof. They are expressed as the combination of X for row and Y for column number, referring to Figure 3. The SMERT X10Y15 is at the uppermost position among the rows of heated tiles in this test. The tile X10Y3 at the third row from the eave may be cooled with outside air from the back side of the sheathing at the eave, because of the rafter-supported eave.

As the SMERTs were turned on, their surface temperature started to rise gradually. As the temperature reached the maximum value (around 50 °C) one and half hours later, there was a sudden drop in temperature of both SMERTs X10Y9 and X10Y3, while the temperature of X10Y15 remained almost constant.

There is no doubt that the drop in temperature results from the flow of snow melt water from the upper portion of the roof. Figure 5(c) shows the time variation of cumulative quantity of melt water along with that of the total input power. The incidence of the sudden drop in the surface temperature coincides with the onset of flow of melt water. During the period that the melt water was flowing, the surface temperature of the SMERTs remained almost constant. In contrast, the surface temperature of X10Y15 located at the uppermost position remained at the maximum temperature, because little melt water would flow on it. After snow sliding, the surface temperature of the SMERTs rose again because of the absence of melt water.

Unheated Tiles

Figure 5(b) shows the time variations of the surface temperature of unheated tiles which were located at positions one row lower than the row of SMERTs. As snow melt water starts to flow, the surface temperature of the unheated tiles rises gradually. Melt water is heating up when flowing over the surface of the SMERTs and it makes the surface of the unheated tiles warm. As shown in Figure 5(b), the surface temperature of X10Y10 and X17Y10 reached around 7 °C. A sudden drop of temperature shows the occurrence of snow sliding.

DISCUSSION

Adhesive Force

Figure 4 shows one example of the behavior of the roof snow cover. The sliding manner is not always the same. Not all of the snow cover above the heated area slides instantly. In the tests for the 1988/89 and 1989/90 seasons, most of snow sliding occurred at the east side surface of the roof while snow at the west side surface remained.

In these two seasons, the surface temperature of the unheated tiles installed at the west side of the roof was always lower than that at the east side and the center. From the observations of the surface temperature of the unheated tiles and the events of snow sliding, the surface temperature of all the tiles was required to rise up to at least 2 °C to slide the roof snow cover for the one-half and one-third arrangement of heated tiles (Higashiyama et al., 1992).

Snow sliding would occur when the force of gravity acting on the snow mass along the roof slope overcomes the tensile resisting force of snow and the frictional and adhesive force of the roof snowpack against the tile surface. As snow melting progresses above the rows of the SMERT, the tensile force become smaller. The frictional force is much smaller than the adhesive force. Immediately before snow sliding, the roof snow pack would be sustained mainly by the unheated tiles and the cool regions of the heated tiles. Consequently, snow sliding using SMERT is deeply related to the adhesive force between the snow and the surface of the unheated tiles.

Figure 6 shows the relationship of ambient air temperature in a refrigerating bath and adhesive force of snow to the surface of a pantile. Adhesive force decreases with temperature and is almost zero at 1 °C. Thus, the fact that snow sliding occurs when the surface temperature rose to at least 2 °C can be explained with the temperature dependence of adhesive force. In practice, snow sliding phenomena would be more complicated due to the presence of melt water.

Effect of Thermal Insulation

It is until the 1989/90 season that the SMERTs without thermal insulating materials had been used. By using SMERT with the thermal insulator in the 1990/91 season, the time duration for snow sliding seems to have come shorter than before, although it is difficult to strictly compare every test result because of the difference of the test conditions such as snow depth, outside temperature, etc.

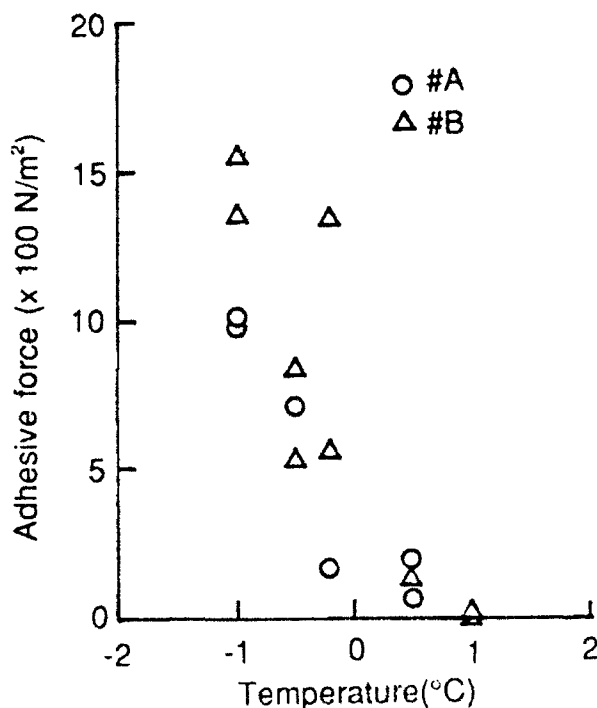


Figure 6. Dependence of adhesive force between the snowpack and a roof tile on air temperature.

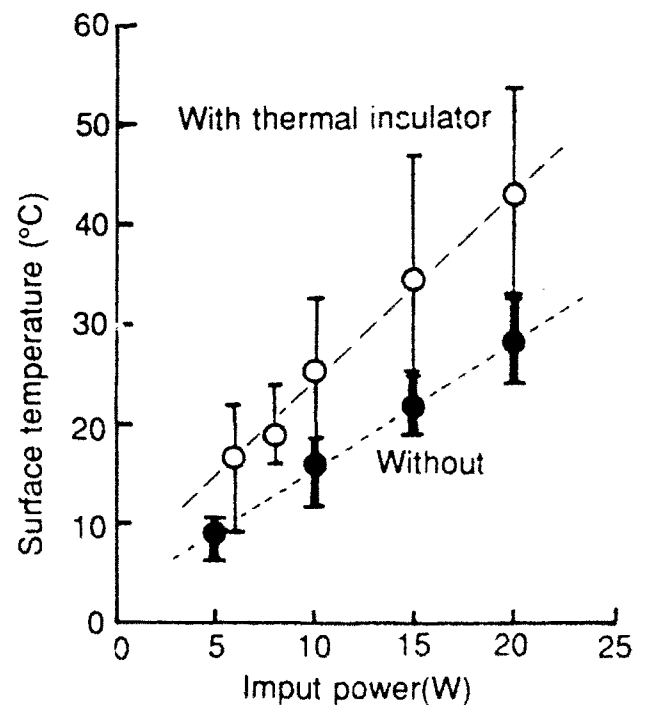


Figure 7. The relationship between the surface temperature and input power to a SMERT.

It should be pointed out that the surface temperature of the SMERT used in the tests of the 1990/91 season is certainly higher than before. Figure 7 shows the difference in surface temperature between SMERTs with and without thermal insulation for the same value of input power to the SMERT. These data have been obtained during practical snow sliding tests. The addition of a 12-mm-thick thermal insulator helps to reduce input power to approximately half for maintaining the same surface temperature.

The surface temperature increase is roughly proportional to the input power. The addition of the thermal insulator is equivalent to an increase in input power. The increase of surface temperature acts to make melt water warmer, thereby to heat the unheated tiles. Consequently, a SMERT with a heat insulator is useful to perform faster snow sliding and to save energy.

Melt Water and Ice

As described in the above discussion, snow sliding results from the increase of surface temperature of the unheated tiles with an assist of warm melt water, in sparse arrangement of SMERTs like as one-half or one-third one. However, melt water always has a risk of freezing, especially at the surface of unheated tiles. Freeze of melt water and formation of an ice dam significantly affect snow sliding even if the freezing area is negligibly small. Caution on snow melt water is required, especially on cold days and at one-third arrangement.

Figure 8 shows the frequency of outside ambient temperature during snowfall in the test site. It is clear that snow rarely falls when the outside temperature is below -5°C . This means that it is unnecessary to turn the SMERTs on when the outdoor temperature is below -5°C because of little snow accumulation, even if it is snowing. Such local meteorological conditions should be accounted for when the snow sliding system is used practically.

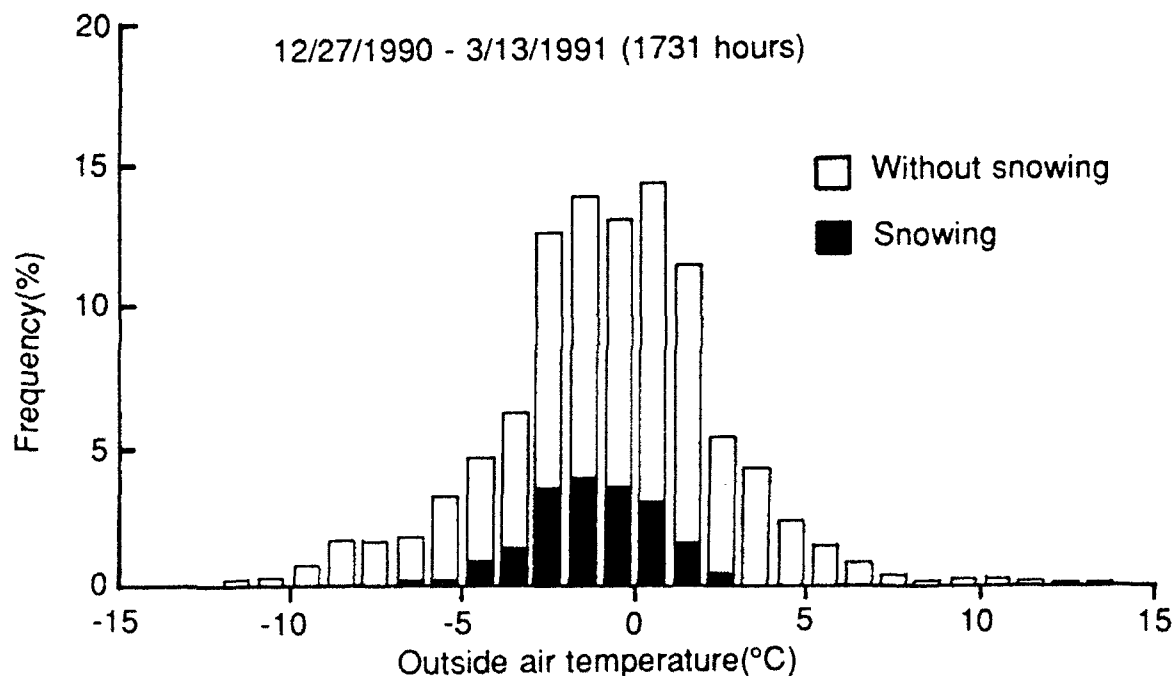


Figure 8. Snowfall frequency for the given value of outside air temperature.

CONCLUSION

The snow sliding performance using electrically heated roof tiles (SMERTs) has been examined for a model house. The SMERTs with a thermal insulator are effective in lowering the input power to a piece of SMERT and in initiating snow sliding earlier. To slide the roof snow effectively, the surface temperature of all of tiles needs to be at least 2 °C, regardless of the types of tiles and their positions. Melt water plays an important role of increasing the temperature of the unheated tiles in the sparse arrangements of the heated tiles.

ACKNOWLEDGEMENT

The authors wish to thank T. Bonkohara of Yoken Co. Ltd. for his useful discussion about the test methods, and also to thank H. Suzuki, H. Funaba and H. Matsuda for their help during the experiments.

REFERENCES

Association of Construction Mechanizing of Japan (1977) "Handbook of Snow Prevention Engineering", Morikita, Tokyo (in Japanese)

Y. Higashiyama, K. Asano, and A. Miyano (1991) "Snow sliding on a roof lined by the electrically heated roof-tiles" Proceeding of Snow Engineering, Vol. 7 (1), 9-18 January 1991 (in Japanese)

Y. Higashiyama, H. Funaba, K. Asano, and A. Miyano (1992) "Influence of the surface temperature of roof tiles on sliding snow by use of electrically heated roof-tiles", *ibid*, Vol. 8 (1) 3-11 January 1992 (in Japanese)

Removal of Snow from Membrane Structures

K. Otsuka and Y. Homma

Technical Research Institute, Obayashi Corporation, Tokyo, Japan

ABSTRACT

Experiments on snow slides on membrane structures were performed. The coefficient of starting friction and tensile strength of snow were investigated. Attempts on the artificial induction of snow slides on membrane roofs were also made by using a scale model of membrane structures. The snow sliding patterns on the full scale membrane structures due to snow slides induced by heating of the membrane were determined numerically based on the experimentally derived mechanical properties of snow. The results of the experiments and the numerical calculations support the idea of practical application of the artificial snow slides for the removal of snow from the full scale membrane structures.

INTRODUCTION

In constructing large span membrane structures in deep snow regions, snow cover on roofs becomes important to the structural design because it causes large loadings that may bring about the deflation of membrane roofs. Snow on membrane roofs also affects indoor luminosities because snow with a few centimeters in thickness can decrease the sunlight to a large extent and lower the indoor luminosities of membrane structures. The relatively high indoor luminosities in the daytime due to transmission of solar radiation through membrane roofs is one of the attractive aspects of membrane structures. For the above reasons, it is desirable that the snow cover on membrane roofs be removed as fast as possible after snow accumulation with some artificial methods.

Artificial methods for the removal of snow from the membrane structures, thermal methods and mechanical methods are considered to be used. In the thermal methods, the snowpack on roofs is removed by melting, while it is removed by artificially induced snow slides in the mechanical methods. The thermal methods have so far been widely studied and employed, which usually use warm air as the snow melter. Although the snow melting methods by warm air have worked fairly well, they take much time to remove snow completely and also consume a large amount of heat energy. In the mechanical methods, on the other hand, snow is not removed by melting it so that the amount of required energy will be much less than the thermal methods. Therefore, if the artificial induction of snow slides on the membrane roofs is possible, it will become a highly effective way for the snow removal.

In order to establish the artificial snow slides as a practical method for the snow removal from membrane structures, it is necessary to know the physical properties of snow, which are closely related to the mechanics of snow sliding on membrane roofs. We investigated them in a series of field experiments performed in Sapporo City over two winter seasons ('89-'91). Attempts to induce snow slides

artificially on membrane roofs were also made by using scale models of membrane structures for the purpose of examining the possibilities of snow removal by the artificial snow slides. Note that we define membrane as glass fibre cloth coated with ethylene-tetrafluoride throughout this study.

In this paper, we will describe the results of the experiments on the mechanical properties of snow and of the scale model tests on the performance of the removal of snow by artificial snow slides. Along with the experiments, a simple model for snow sliding on membrane roofs was developed based on the mechanical properties of snow obtained experimentally. The feasibilities of the practical use of artificial snow slides for full-scale membrane structures will be assessed with the model. The limitations and the problems which may arise in the applications of the method will be also briefly discussed.

MECHANICS OF SNOW SLIDES

Occurrence of snow sliding is governed by the balance of forces acting on a snow cover on roofs. Suppose a snow cover on a sloped membrane roof is exerted by several forces as shown in Figure 1. The snow cover is stabilized against sliding force G by resistance R and the internal tensile force I . Although the snow in the vicinity of the eave might be exerted by compressive force, it is neglected in this study for simplicity. Snow sliding will be initiated when the reduction of resisting force takes place. A single event of sliding of the whole snowpack at a time and successive, multiple slides of segmented snowpack can be observed. In the latter case, snow sliding is preceded by tensile fractures at multiple locations within the snow pack. At an arbitrary cross section C , tensile fracture occurs when the sum of the sliding force G and the resisting force R , which are acting on snow on the eave side of C , exceeds the tensile strength I at C , that is, $I < R + G$.

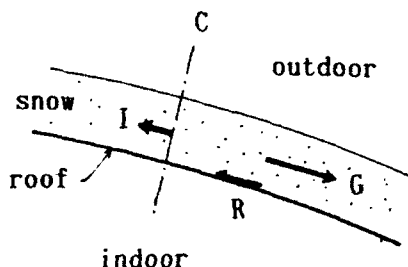


Figure 1. Forces acting on the roof snow cover.

The factor that most strongly affects the occurrence of snow slides would be the reduction of resisting forces between the snow and the roofs. In many cases, the reduction of resisting forces is caused by melting of snowpack at the snow-roof interface (Sack et al., 1987) due to warm ambient air or leakage of heat from inside the structure through the roof. Sliding can also be caused by wind suction (Lepage and Schuyler, 1988).

The magnitudes of the resisting forces under the bottom melting depend on the content of the meltwater which exists at the roof-snow interface and on the characteristics of snowpack near the roof (Tomabechi et al., 1991). The resisting forces under melting are the combination of adhesion and viscosity of meltwater and pure friction of snowflakes to the roof material. As snow melting progresses increasing the meltwater content, the viscous forces gradually become dominant

among those forces yielding the reduction of the resistance.

If the lowermost part of the snowpack is frozen to the roof before melting, the reduction of resisting forces resulting from the bottom melting will be considerably large. In that case, the meltwater tends more to concentrate at the bottom of the snowpack because the ice has a larger impedance to the infiltration of liquid water than snow. Since viscous force is smaller than adhesive force by more than an order of magnitude and substantially smaller than frictional force, the meltwater layer acts as a lubricant for sliding. Thus heating the snowpack frozen to the roof from below could produce the conditions favorable to sliding. Therefore, in consideration of this characteristics of an ice layer under melting, removal of snow by artificial slides will be possible to apply.

A METHOD OF THE REMOVAL OF SNOW BY ARTIFICIAL SNOW SLIDES

Based on the nature of the reduction of resisting forces of the ice layer

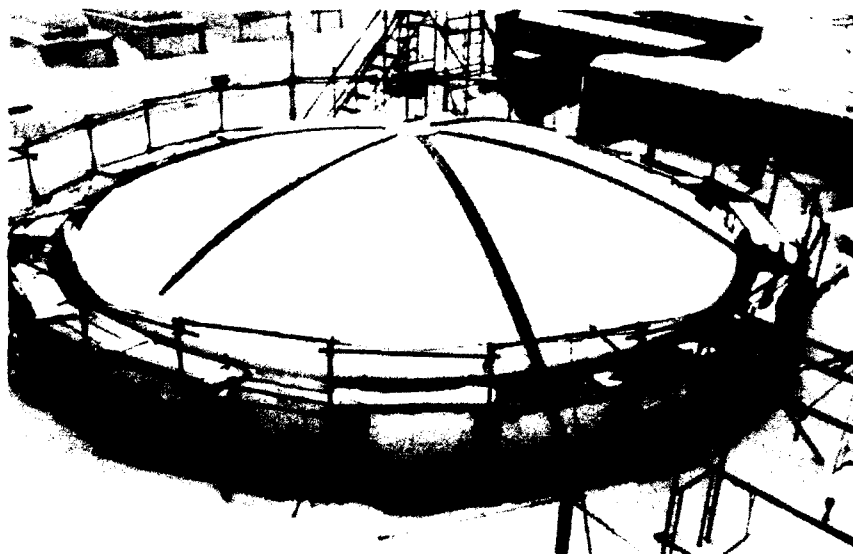


Figure 2. Scale model.

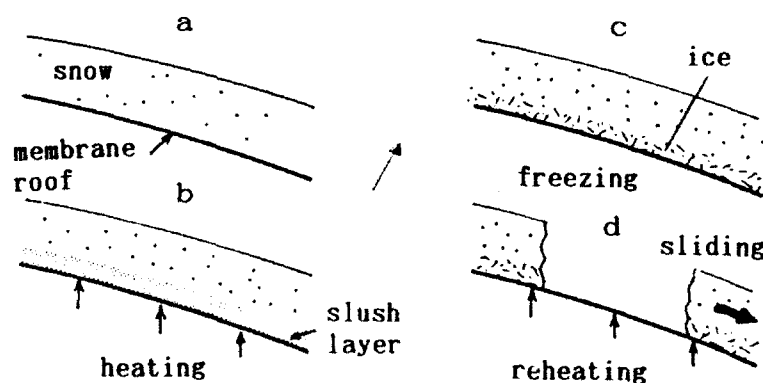


Figure 3. Artificial induction of snow slides

under the bottom melting, we attempted the artificial induction of sliding of snowpack on membrane roofs by making use of a scale model of membrane structures (Fig.2) in the field. The bases of the method are the artificial formation of an ice layer and the melt of the ice layer. To form the ice layer, the snowpack is initially heated from below long enough for a slush layer of a certain thickness to appear at the bottom. The slush layer is then cooled to freeze it. After completion of freezing, the frozen slush layer is heated again. The snow condition at the bottom of the snow cover produced in this way will become the one that is most favorable for snow sliding. The procedure described above is illustrated in Figure 3.

OUTLINE OF EXPERIMENTS

As shown in the previous section, resisting forces and tensile strength of a snow pack play a central role in the mechanics of snow slides. The coefficient of starting friction was examined as the measure of resistance of snowpack against sliding. Since a snowpack in the midst of bottom melting is our major concern regardless of whether it has an ice layer at its bottom or not, the coefficient of starting friction in this study does not include the effect of adhesion of ice to the roof surface.

The experiments conducted in this study are listed in Table.1. In the experiments on the coefficient of starting friction of snow, the experimental

Table 1. List of experiments

<u>Experiments</u>	<u>To be investigated</u>
Mechanical properties of snow	Coefficient of starting friction of <ul style="list-style-type: none"> · <u>frozen slush layer under bottom melting</u> · <u>slush layer</u> Tensile strength of <ul style="list-style-type: none"> · <u>fresh dry snow</u> · <u>frozen slush layer</u>
Scale model tests	Performance of the artificial snow slides

roof was introduced as shown in Figure 4. It is a wooden box with a single membrane roof whose walls and floor are thermally insulated. It has six fan heaters (600 W/heater) equipped on the floor that provide heat to the snow on its roof. The outer and inner surface temperatures of the membrane roof as well as the inside air temperatures were measured with thermocouples. The inside air is easily ventilated with the outside air. After snow has accumulated on the roof, it is inclined until the snow starts sliding at inclination of θ . The coefficient of starting friction is obtained as the tangent of θ .

Two types of snow conditions at the bottom of the snow are prepared prior to the every inclination of the experimental roof. One of them, hereafter referred to as the melt-only case, is the condition in which a slush layer is formed by heating. The other, the freezing-remelting case, is the one in which snow cover is made frozen to the roof through the heating followed by cooling, and then short-term heating was imposed again just before the inclination.

Tensile strength of snow was investigated by putting the ground snow very carefully into the snow container shown in Figure 5. The container consists of two pieces of the same size and shape. Tensile forces are imposed on the one piece of

the container and the other is fixed on the horizontal base. With the measurement of tensile force by a load cell at the moment when the tensile fracture occur at the test section, the tensile strength of snow is obtained.

The removal of snow by artificial snow slides was tested by employing a scale model of membrane structures, which is 10 m in diameter as shown in Figure 2. The roof of the model is composed of twelve single layer

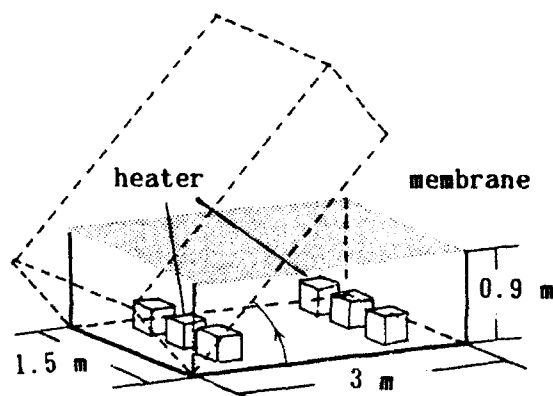


Figure 4. Experimental roof.

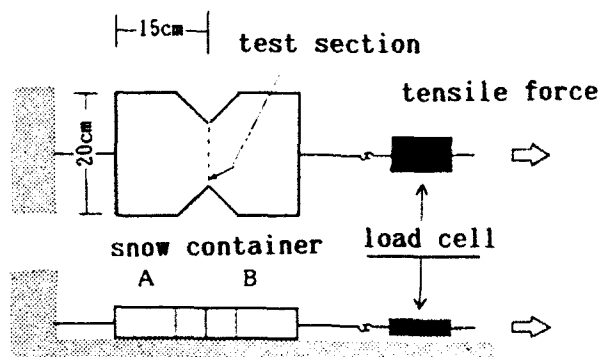


Figure 5. Measurement of tensile strength of snow.

membrane panels. The shape of the roof permits snow to smoothly slide off once the snow sliding takes place. The model has a warm air snow melting system. From an array of equally spaced outlets along the inside periphery of the model, warm air produced by the steam boiler is provided to the roof that warm the snow cover on the roof from below. Controlling the temperatures of the warm air jet is at our proposal. The temperatures of both the inner and outer surfaces of the membrane roof were measured by thermocouples attached to the roof and their real-time temporal variations were carefully monitored on the screen of a personal computer.

In all experiments in this study, fresh snow obtained within two days of last deposition was used. Snow containing much freezing rain or wet snow was also excluded. This is because under highly wetted snow falls, the ambient air temperature will be above freezing point, which prevents an ice from forming and as a result we inevitably resort to the thermal methods to remove the snow.

RESULTS OF EXPERINMENTS ON THE MECHANICAL PROPERTIES OF SNOW

Coefficient of Starting Friction

Through a number of measurements of the sliding angles for the two types of experimental types described above, gross features of the relations between the coefficient of starting friction and the snow load were obtained and shown in Figure 6. It is seen in this figure that there exists a large difference in the magnitudes of the coefficient of starting friction between the melt-only case and the freezing-remelting case in which the coefficient of starting friction is much less than that in the melt-only case for the same snow load. The small values in the freezing-remelting case indicate that the snow cover would start

sliding at the inclination of as large as 10° or so.

The decrease of the coefficient of starting friction with an increase of the snow load is recognized in both types of experiments as shown in the figure. The dependence of the coefficient of starting friction on snow load in the freezing-remelting case is much weaker than that in the melt-only case. It is probably due to the impedance of the ice layer to the infiltration of meltwater. The impermeability of the ice layer sandwiches the meltwater well between the roof and the ice; that is, the frictional properties become more independent of the snow load. On the other hand, due to the higher permeability of snow, the lubricant layer of meltwater will be formed more gradually in the melt-only case along with progression of compacting the snow near the bottom as the snow load increases, yielding the stronger dependence of the coefficient of starting friction on snow load. The results of the experiments suggest that it would be possible that snow sliding on membrane roofs are induced artificially by using the freezing-remelting technique.

The relations between the coefficient of starting friction μ and snow loads P (kgf/m^2) can be regressed by nonlinear fittings as follows.

$$\mu = 2.96 \exp(-0.657 P^{0.33}) \quad (\text{melt-only}) \quad (1)$$

$$\mu = 0.387 P^{-0.33} \quad (\text{freezing-remelting}) \quad (2)$$

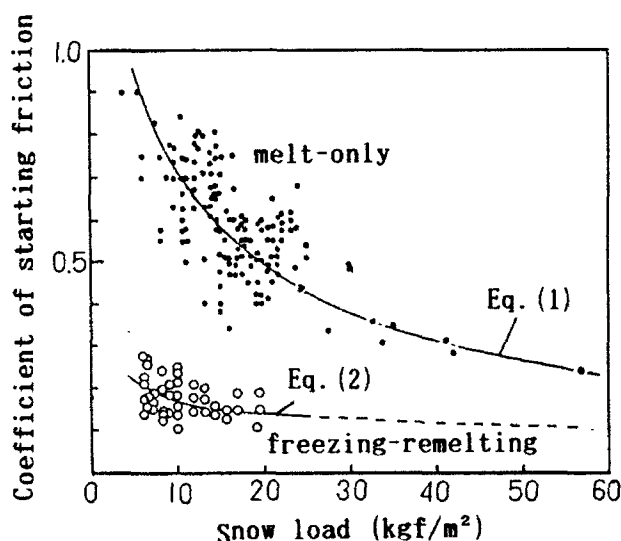


Figure 6. Relation between coefficient of starting friction and snow load.

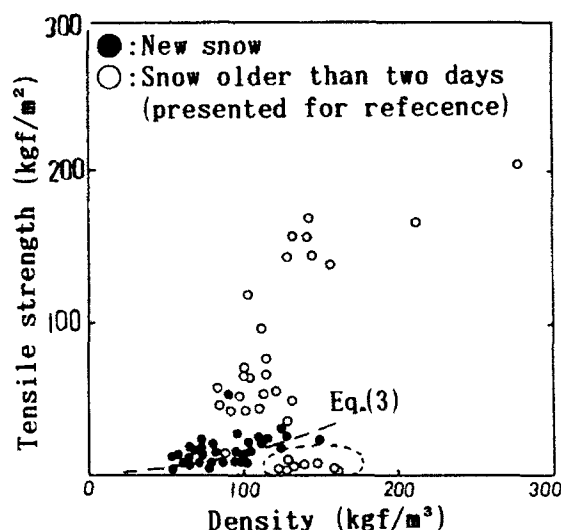


Figure 7. Relation between tensile strength of snow and snow density.

Tensile Strength

The tensile strengths obtained in the experiments are plotted against density in Figure 7. Positive correlation between the strength and the density is qualitatively agreed with the previous studies by many researchers. The tensile strength of dry snow σ_s (kgf/m^2) obtained in this study can be expressed as a

function of snow density ρ_s (kg/m^3) as follows.

$$\sigma_{*s} = 0.0506 \rho_s^{1.22} \quad (3)$$

Compared with the previous studies on the tensile strength of snow summarized by Mellor (1975), the tensile strength in our study is smaller than those presented in the Mellor's paper by more than an order of magnitude. This could be explained that in those studies they concerned mainly hardened and much older snow, which showed rather high densities (more than 300 kg/m^3) than the snow we used. As long as the roof snow to be removed by the artificially induced sliding is concerned, the strength obtained in this study would be most appropriate.

A small number of experiments on the tensile strength of the frozen slush layers were also carried out to infer their strength under the remelting stage of artificial snow slides. This is because the strength of the ice layer may be important in considering the mechanics of snow slides on the remelting stage since it has much greater strength than snow although the thickness of the ice is generally much smaller than that of the whole snow cover.

The tensile strength of a frozen slush layer has a variety of values ranging from $300 \text{ (kgf/m}^2\text{)}$ to more than $2000 \text{ (kgf/m}^2\text{)}$. The comparisons of the the ice artificially formed on the roof in the scale model tests with that made in the snow container suggest that the strength values between 300 and $1000 \text{ (kgf/m}^2\text{)}$ would be representative as the strength of the artificially formed ice layer.

RESULTS OF SCALE MODEL TESTS

The method of the artificial snow slides was tested in the field by using a scale model of membrane structures. The scale model tests were performed seven times. Five of them were highly successful, in which the snow cover was almost completely removed by artificially induced snow sliding. We present here the one of the successful cases conducted on February 6, 1991.

We had an accumulation of snow which was uniformly 7 cm in depth on the roof of the model in the evening of February 5. After snowfall stopped, the warm air snow melting system was set on. The snow cover was heated long enough for a slush layer of $1\text{-}2 \text{ cm}$ in thickness to be formed at the bottom of snow. After the initial heating was completed, the inside air was rapidly ventilated with the outside air to make the inside temperature lower quickly. The outdoor temperature was kept below the freezing point throughout the night, which permitted the slush layer to be turned into ice. Early the next morning, the snow cover on the model was heated again for a short period of time to form a thin meltwater layer at the of the roof-ice interface, which lowered the coefficient of starting friction to in a large degree. Within ten minutes after the onset of the reheating, snow sliding took place on one roof panel after another and the snow removal was completed in a few minutes as shown in Figure 8.

Snow removal by the artificial snow slides is successfully achieved when the ice can be adequately formed. The ice thickness and hardness would depend on the amount of heat supplied to the snow in initial heating and the heat removed from the snow in the subsequent freezing stage. In the experiments on the coefficient of starting friction described earlier, we found relations between the characteristics of the ice layer (thickness and hardness) and the heat budget of the lowermost portion of the snow cover in the heating-freezing process. Based on them, we determined the lengths of the periods of the initial

heating and freezing and the temperature of the air jet of the snow melting system. The results of the scale model tests were favorable and we can conclude



Figure 8. Artificial snow slides on the scale model.

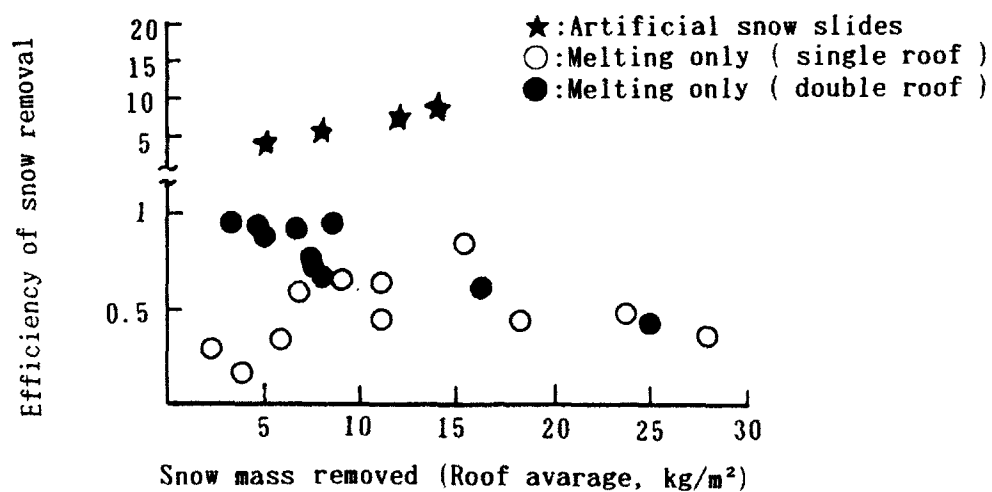


Figure 9. Efficiencies of removal of snow from the scale model.

that the method of artificial snow slides will be well applicable to full-scale membrane structures.

We compared the efficiencies of the snow removal by the thermal method with the artificial snow slide method. The efficiency of snow removal is defined as the ratio of the total snow mass to be removed to the amount of heat required for removing the snow completely. By the definition, it is possible that the efficiency of snow removal exceeds 1 for the artificial snow slides. The efficiencies obtained in the scale model tests regarding both methods are plotted against the total snow mass removed in Figure 9. Note here that the removal of snow by melting was also carried out more than twenty times during the whole period of the field experiments. Figure 9 shows the remarkably large efficiencies of the artificial snow slide method compared to the thermal method, which means that it would contribute significantly to the reduction of the cost of snow removal from the membrane structures.

NUMERICAL CALCULATIONS

A simple numerical model based on the mechanical properties of snow obtained in this study was developed to diagnose the locations of tensile fracture of snow cover on membrane roofs during the course of artificial snow slides. In this section, we consider the snow slides on the model roof as shown in Figure 10. It is an approximation of the individual roof panel of the scale model. The snow cover on the model roof is assumed to consist of an ice layer and a dry snow layer embedded on it, which corresponds to the state of the snow cover ready to be removed by the artificial snow slides. In order to diagnose the locations of the tensile fracture, the model roof is divided into thirty finite area elements ($\Delta\theta = 1^\circ$). Starting with the eave of the model roof, the following equations of balance of forces are successively applied to each cross section of snow cover at the boundary of neighboring area elements:

$$I_{j-1/2} = \{(D_s - D_i) \sigma_s + D_i \sigma_i\}_{j-1/2} W_{j-1/2} \quad (4)$$

$$G_{j-1/2} = \sum_j^{30} \Delta G_j \quad R_{j-1/2} = - \sum_j^{30} \Delta R_j \quad (5, 6)$$

where

$$\Delta R_j = \mu_j \Delta G_j \cot \theta_j \quad (7)$$

$$\Delta G_j = \{(D_s - D_i) \rho_s + D_i \rho_i\}_j W_j \sin \theta_j r \Delta \theta. \quad (8)$$

The meaning of each symbol of the above equations is given in Table 2. When

$$I_{j-1/2} < G_{j-1/2} + R_{j-1/2} \quad (9)$$

is satisfied, the occurrence of tensile fracture is diagnosed and then the snow cover on the eave side of cross section $j-1/2$ is removed by sliding. In the calculations, it is assumed that no stress is acting on the snow cover along the margin of the model roof.

Calculations were performed for the snow cover having the uniform depth of 10 cm and 30 cm, where the thickness of the frozen slush layer is set at 2 cm. The density of dry snow and the frozen slush layer are assumed to be 100 kg/m³ and 600 kg/m³ respectively. Equations (2) and (3) were used to relate the coefficient of starting friction to snow loads and the tensile strength of dry snow to

density. Three different values of 300, 600, and 900 (kg/m²) were assigned to the ice strength because we could not find the analytical relations between the strength of ice and its density.

The equations of balance of forces of snow cover were solved by varying the radius of the model roof from 10 to 100 m at intervals of 10 m. The resultant locations of snow lines expressed by the angular distance from the top of the roof are given in Fig.11, which is defined as the edge of the remaining snow cover after the snow slides (see Fig.12). The locations of snow lines calculated by the model fluctuate extensively with its size of the roof because the each snowline is not the result of a single snow sliding event but of several successive snow slides in segments (Fig.12). Therefore it is very difficult to

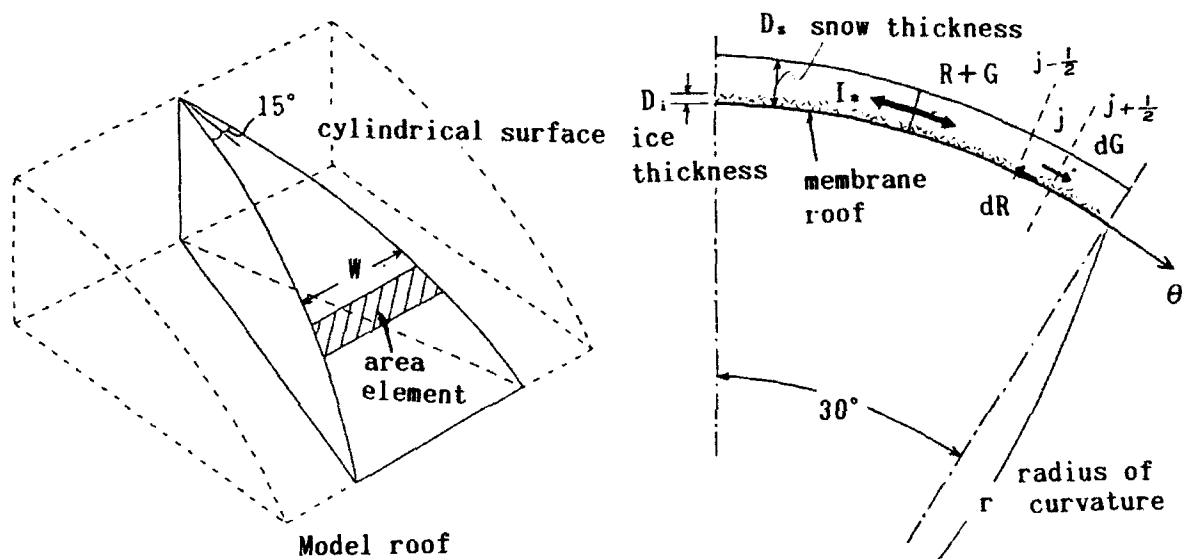


Figure.10 Model roof and processes included in numerical calculation.

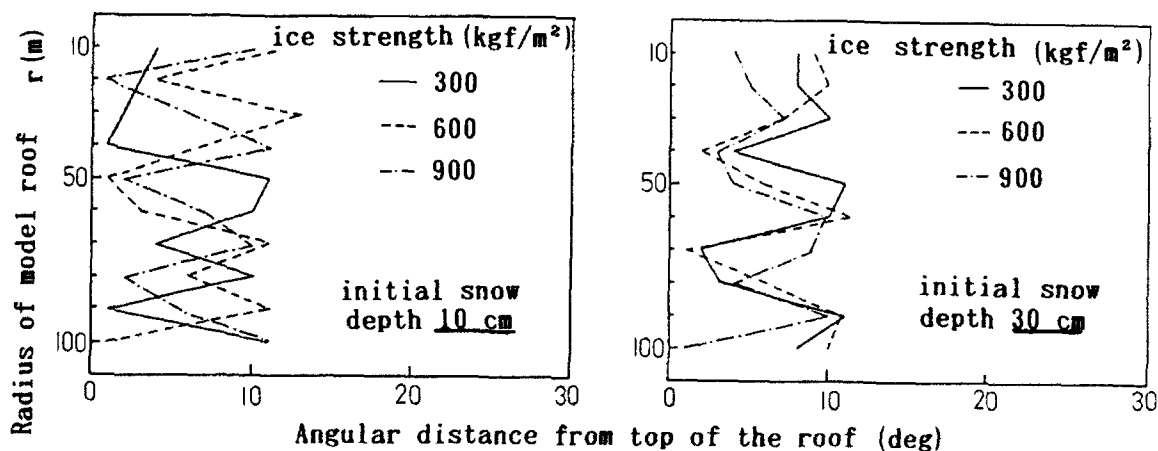


Figure 11. Variation of snow lines with size of model roof.

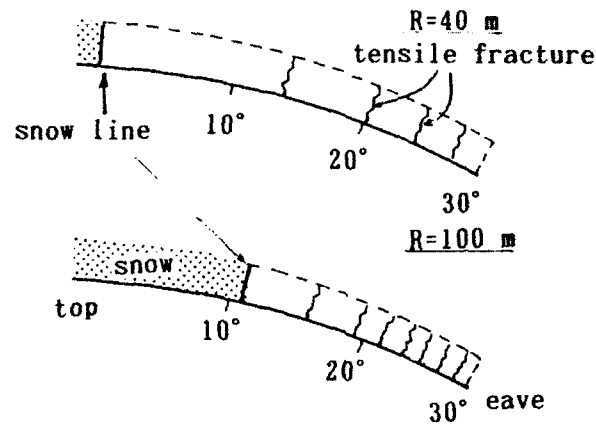


Figure 12. Segmentation of snow pack.

find any simple relations between the locations of snowlines and the size of the roofs as far as the calculations made here are concerned. If the minimum slope of the roof, however, is greater than about 10° , the almost complete snow removal would be possible to achieve. The results of calculations have shown that the application of the artificial snow slides to the full-scale membrane structures will be feasible.

DISCUSSIONS

Combining the results of the scale model tests with those of the numerical calculations, it has been shown that the method of artificial snow slides would be applicable to snow removal from membrane structures. Nevertheless, there are some limitations in the method for its practical use. Since the formation of an ice layer is the basis of this method, its application is restricted to the conditions of the weather where the air temperature is below zero. From this point of view, the method will work most efficiently in those areas where there are a sufficient number of freezing days available every winter, such as Hokkaido. But still, it sometimes snows at the air temperatures above the freezing point in the early winter and at the beginning of spring. Under such weather conditions, the thermal method will be more useful for the snow removal instead of the artificial snow slides. Therefore, either the mechanical method or the thermal method will be most relevant to according to the weather conditions, which will not bring any inconvenience since both methods demand the same snow melting device.

CONCLUDING REMARKS

A series of field experiments on the coefficient of starting friction and the tensile strength of snow were performed. These quantities are primarily responsible for snow sliding on the membrane roofs. Based on the mechanical properties of snow obtained in the experiments, a method for snow removal from membrane structures by the artificial snow slides was proposed and tested by using a scale model in the field. The scale model tests shows that the method will work well when the air temperature is sufficiently low for the formation of the ice layer at the bottom of the snow cover. The application of the method to

the full scale membrane structures is supported through simple numerical

Table 2. List of symbols.

W_j	:width of the area element j
ρ_s	:density of dry snow (100 kg/m ³)
ρ_i	:density of frozen slush layer (600 kg/m ³)
j	:the number of area element (1~30)
ΔG_j	:gravity acting on the snow on the area element j
ΔR_j	:resistance force acting on the snow on the area element j
$\mu = 0.387P^{-1/3}$:starting friction coefficient
$P = \{(D_s - D_i) \rho_s + D_i \rho_i\} \cos \theta_j$: snow load
$\sigma_{s,s} = 0.0506 \rho_s^{1.22}$:tensile strength of dry snow (kg/m ²)
$\sigma_{s,i}$:tensile strength of frozen slush layer (300, 600 and 900 kg/m ²)

simulations. Although the method has some limitations in terms of the air temperatures, we expected that it will reduce the costs for the snow removal from the membrane structures.

ACKNOWLEDGEMENT

The authors would like to thank Dr. T. Shibata (Professor of Hokkaido Univ.) and Dr. O. Joh (Assistant Professor of Hokkaido Univ.) for providing us with valuable advice throughout this study.

REFERENCES

- Lepage, M.F., and G.D. Schuyler (1988) "A simulation to Predict Snow Sliding and Lift-Off on Buildings," Proceedings of the First International Conference on Snow Engineering, 128-141, July 1988.
- Mellor, M. (1975) "A review of basic snow mechanics," Prc. Int. Symp. on Snow Mechanics, Grindeiwald, Int. Assoc. Hydrol. Sci. Publ. 114, pp. 251-291.
- Sack, R.L., D. Arnholtz, and J.S. Haldeman (1987) "Sloped Roof Snow Loads Using Simulation," Journal of Structural Engineering, American Society of Civil Engineering, Vol. 113, No. 8, 1820-1833.
- Tomabechi, T., H. Yamaguchi, T. Itou and M. Hoshino (1991) "Fundamental Study on Sliding of Snow on the Membrane Structure," Journal of Structural and Construction Engineering, Architectural Institute of Japan No. 426, 99-105 (in Japanese with English Abstract).

Engineering Studies on Pneumatic Conveying Systems of Snow

Toshiichi Kobayashi* and Motonobu Kumagai†

*Nagaoka Institute of Snow and Ice Studies, NIED
Suyoshi-machi, Nagaoka-shi, Niigata-ken, 940 Japan

†Kyushu Engineering Office, Kyushu Regional Construction Bureau, Ministry of Construction
Higashi Kushihara-cho, Jurume-shi, Fukuoka-ken, 830 Japan

ABSTRACT

This paper describes outdoor experiments on pneumatic conveying systems of snow. One of these systems conveys snow in its natural forms without any artificial processing, i.e., in dispersed granular or small block forms. Another system conveys snow in the form of snowballs which were formed by compressed air by another machine. Both experiments were conducted under the positive pressure condition. These experiments showed that a pneumatic conveying system of snow in dispersed granular or small block forms was effective at distances shorter than 500 m, and conveyance in the form of snowballs was effective at distances longer than 500 m.

INTRODUCTION

In order to remove snow from roads, several types of snow-removing machines are used in snowy regions in Japan. During the recent use of these machines, the main road traffic was hardly disrupted. However, it is difficult to remove snow from narrow streets and narrow areas around each house using these machines. Therefore, a snow removing channel system and a hydraulic conveying system for removing snow pipes are used in these areas, but they cannot be used in the region where no water is available. Therefore, studies of pneumatic conveying systems of snow have been carried out since 1985. These systems can be

mainly classified into four types as shown in Figure 1. Two types of them were investigated outdoors. One of these systems conveys snow in its natural forms, and the other conveys snow in the form of snowballs by compressed air; both are under the positive pressure condition.

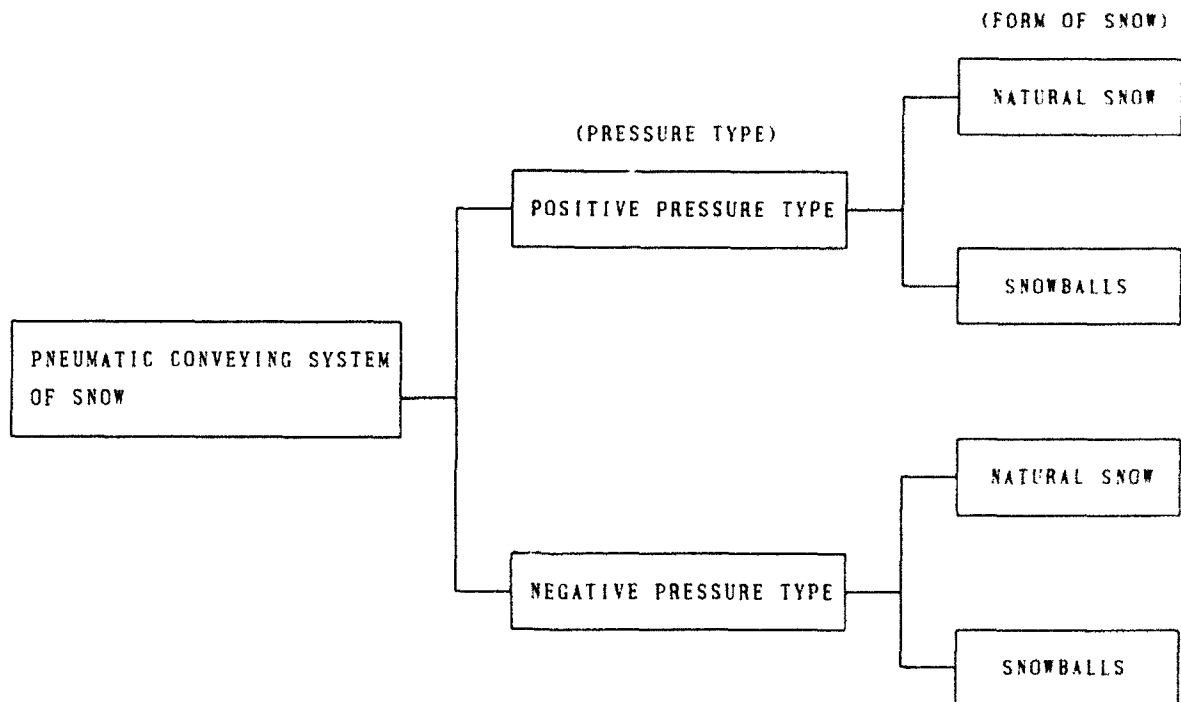


Figure 1. Pneumatic conveying system of snow.

EXPERIMENT FOR CONVEYING NATURAL FORMS OF SNOW

Methods

The equipment for conveying snow in its natural forms consists of a blower (22 kW, turbofan), a snow feeder and a pipeline (inner diameter: 250 mm, length: 20 m, a horizontally straight pipe). In order to keep air from blowing up from the feeder, a baffle plate is installed at the lower part of the feeder in the pipe (see Figures 2 and 3).

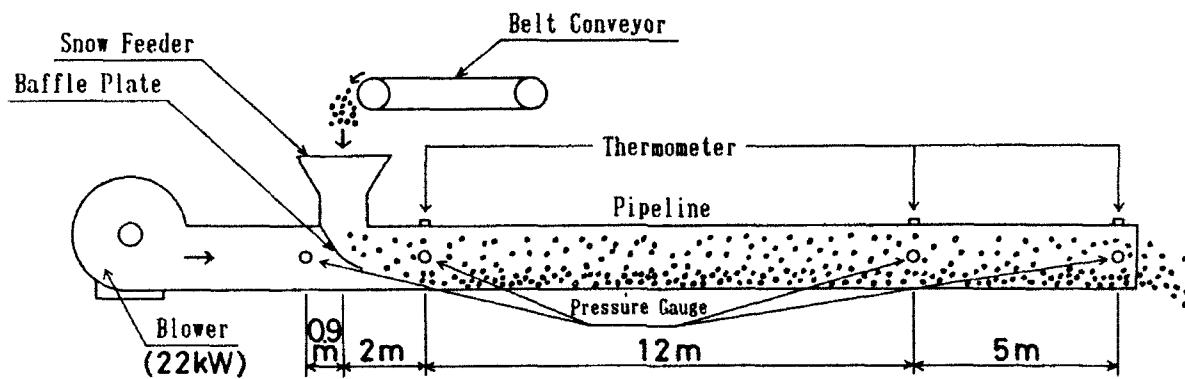


Figure 2. Schematic diagram of the experimental equipment for a pneumatic conveying system for natural snow.

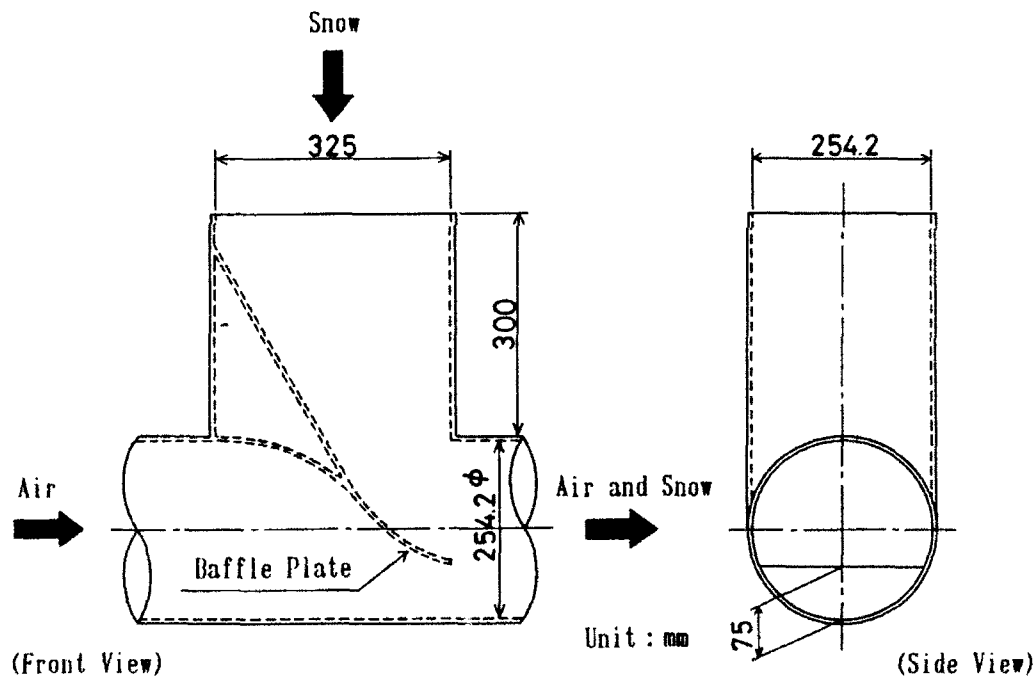


Figure 3. Drawing of the snow feeder.

Results

The pressure loss in the horizontally straight pipe when new snow was fed was approximately equal to that of the single-phase flow of air. The pressure losses at the air velocity of 30 m/s in a pipe are as follows: 34 Pa/m for new snow, 49~52 Pa/m for fine-grained snow and 64 Pa/m for granular snow (see Figure 4).

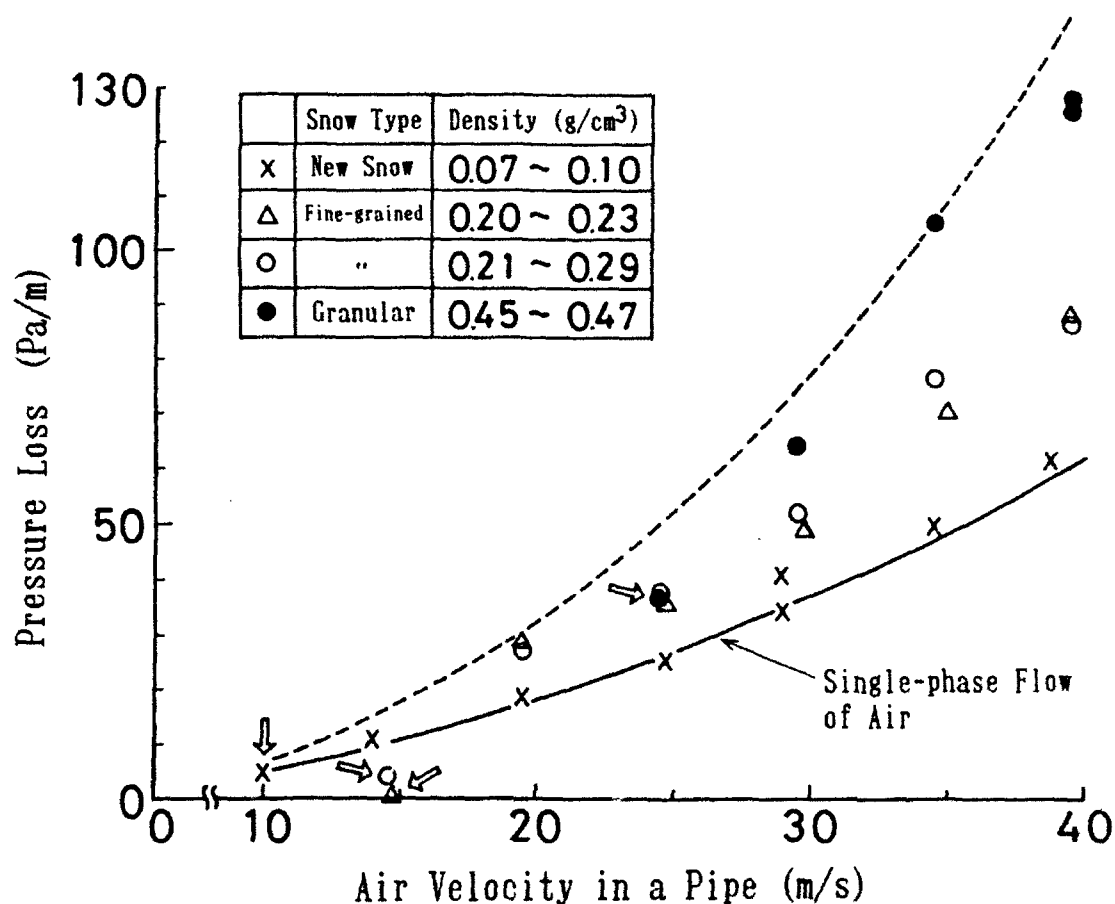


Figure 4. Relation between the pressure loss and the air velocity in a pipe obtained with the pneumatic conveying system for natural forms of snow.

The critical air velocities shown as arrows in Figure 4, under which no snow could be conveyed inside of a pipe, depended on the snow types, i.e., 10 m/s for new snow, 15 m/s for fine-grained snow and 25 m/s for granular snow. Therefore, it is concluded that air velocities in a pipe of more than 25 m/s are necessary to smoothly convey natural forms of snow.

EXPERIMENT FOR CONVEYING SNOW IN THE FORM OF SNOWBALLS

Methods

The equipment for conveying snow in the form of snowballs consists of a blower (22 kW, Roots blower), a snow compacting device, a snowball feeder and a pipeline (inner diameter: 150 mm,

length: 34 m, a horizontally straight pipe, two horizontally bent pipes and a vertically bent pipe, see Figures 5 and 6). The snow compacting device consists of an air compressor and two air cylinders (see Figure 7). Snowballs are made by compacting natural forms of snow.

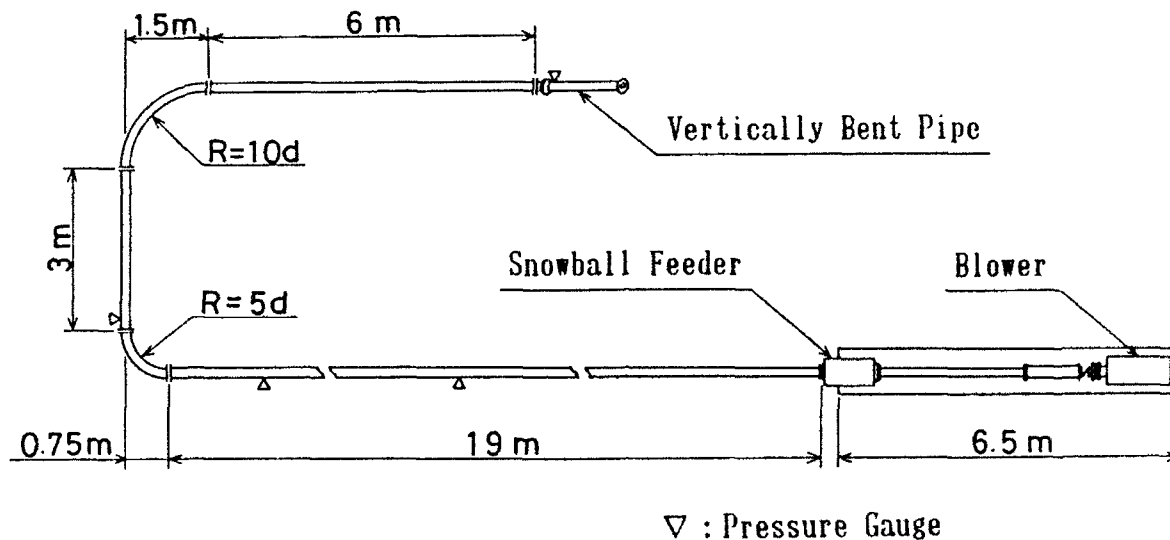


Figure 5. Schematic diagram of the experimental equipment for a pneumatic conveying system of snow in the form of snowballs (plan).

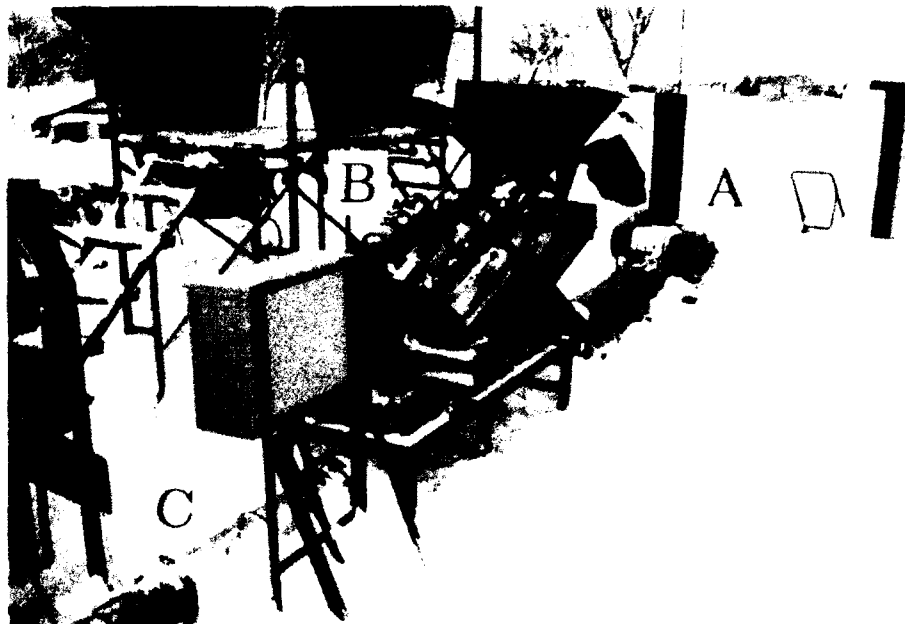


Figure 6. The whole view of the experimental equipment (A: blower, B: snowball feeder, C: pipeline).

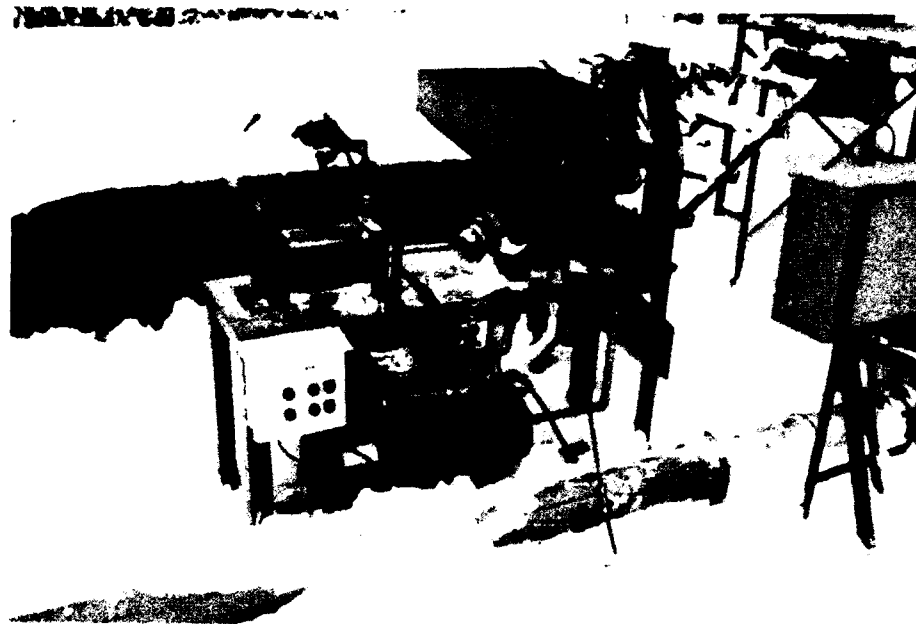


Figure 7. The snow compacting device.

The power to make snowballs

By the compressive stress (about 2 tons) which was generated by the air compressor, granular snow (density: 0.5 g/cm^3) was changed into snowballs (density: 0.9 g/cm^3 , diameter: 135 mm, weight: 1.2 kg). In order to produce snowballs at the rate of 20 t/h, the power of about 40 kW was needed, assuming that the efficiency was 50 %.

The pressure loss in a pipe

Horizontally straight pipe

Snowballs fed in a pipe moved smoothly as they slid on the bottom of the pipe at an air velocity of 7.5 m/s, but snowballs could not move in the pipe at an air velocity of less than 7.5 m/s. As shown in Figure 8, the pressure losses increased with the increase of the air velocities, and the amount of the pressure loss increased with the increase of the rate of the snowball transportation.

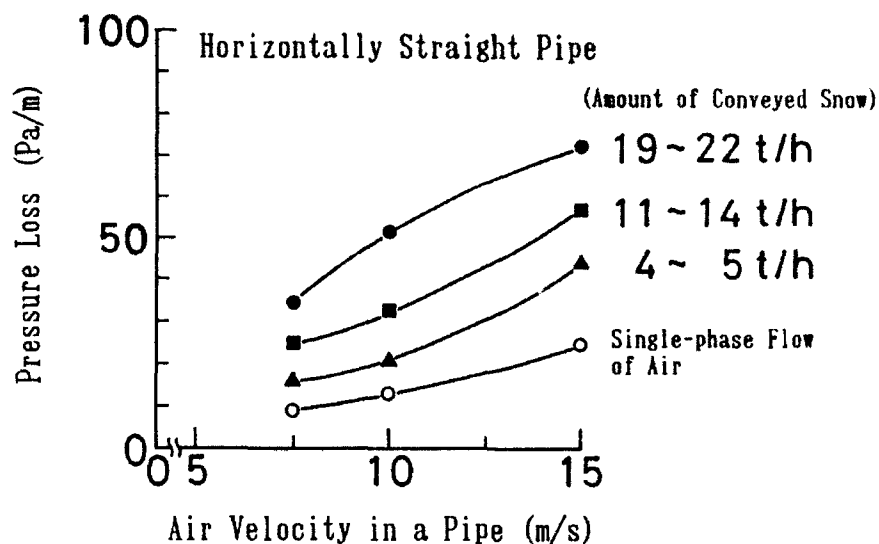


Figure 8. Relation between the pressure loss and the air velocity in a horizontally straight pipe obtained with a pneumatic conveying system of snow in the form of snowballs.

Horizontally bent pipe

The pressure loss in a horizontally bent pipe was 1.7~3.2 times as large as in a horizontally straight pipe. The radius of curvature of the bend is as follows: $R = 5d = 0.75$ m, where R is the radius of curvature and d is the inner diameter of the pipe. In spite of a rather sharp bend, snowballs moved smoothly in the pipe (see Figure 9).

Vertically bent pipe

The pressure loss in a vertically bent pipe (angle of inclination: 45° , length of the hypotenuse: 2 m) was 6~8 times (at an air velocity of 7.5 m/s), about 4 times (at 10 m/s) and about twice (at 15 m/s) as large as in a horizontally straight pipe. The lower the air velocity in a pipe, the higher was the pressure loss in a vertically bent pipe (see Figure 10). The reason for this is as follows. The pressure loss is defined by the difference of the air pressures between the inlet and the outlet of the pipe. The pressure at the outlet of the pipe is the atmospheric pressure; therefore, the pressure loss is proportional to the inlet pressure. The air velocity is proportional to the inlet pressure. If the air velocity is high, then the momentum of the air must be transferred into the snowball with less energy loss. Therefore, the pressure loss at the high air velocity is small,

and vice versa. Therefore, to convey snowballs to a higher level, it is necessary to increase the air velocity.

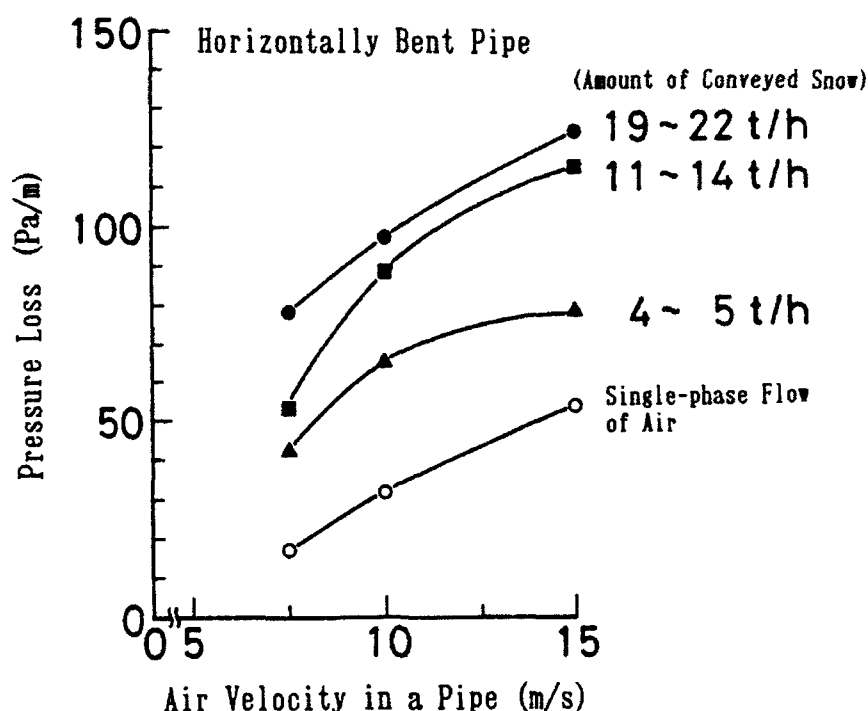


Figure 9. Relation between the pressure loss and the air velocity in a horizontally bent pipe obtained with a pneumatic conveying system of snow in the form of snowballs.

The suitable diameter of a snowball for conveying

In order to investigate the suitable diameter, snowballs of two different diameters, i.e., 135 mm and 90 mm, were conveyed in a pipeline. As a result, a 135-mm snowball could be conveyed at an air velocity of 7.5 m/s, but a 90-mm snowball could not be conveyed at that air velocity. Because the clearance between a 90-mm snowball and the wall of the pipe became bigger as compared with a 135-mm snowball, it is considered that the amount of air flow through the clearance increased and the snowball speed decreased. For this reason, the 90-mm snowball seems not to have been completely conveyed in whole pipe. It is, therefore, considered that the amount of air flow through the clearance needs to be decreased to convey snowballs efficiently, and the best clearance must be chosen. Otherwise the snowballs themselves will produce a blocking phenomenon. Therefore, it is considered that a 135-mm snowball, which is equivalent to 0.9 times the inner diameter of a pipe, is more suitable than a 90-mm snowball for conveying.

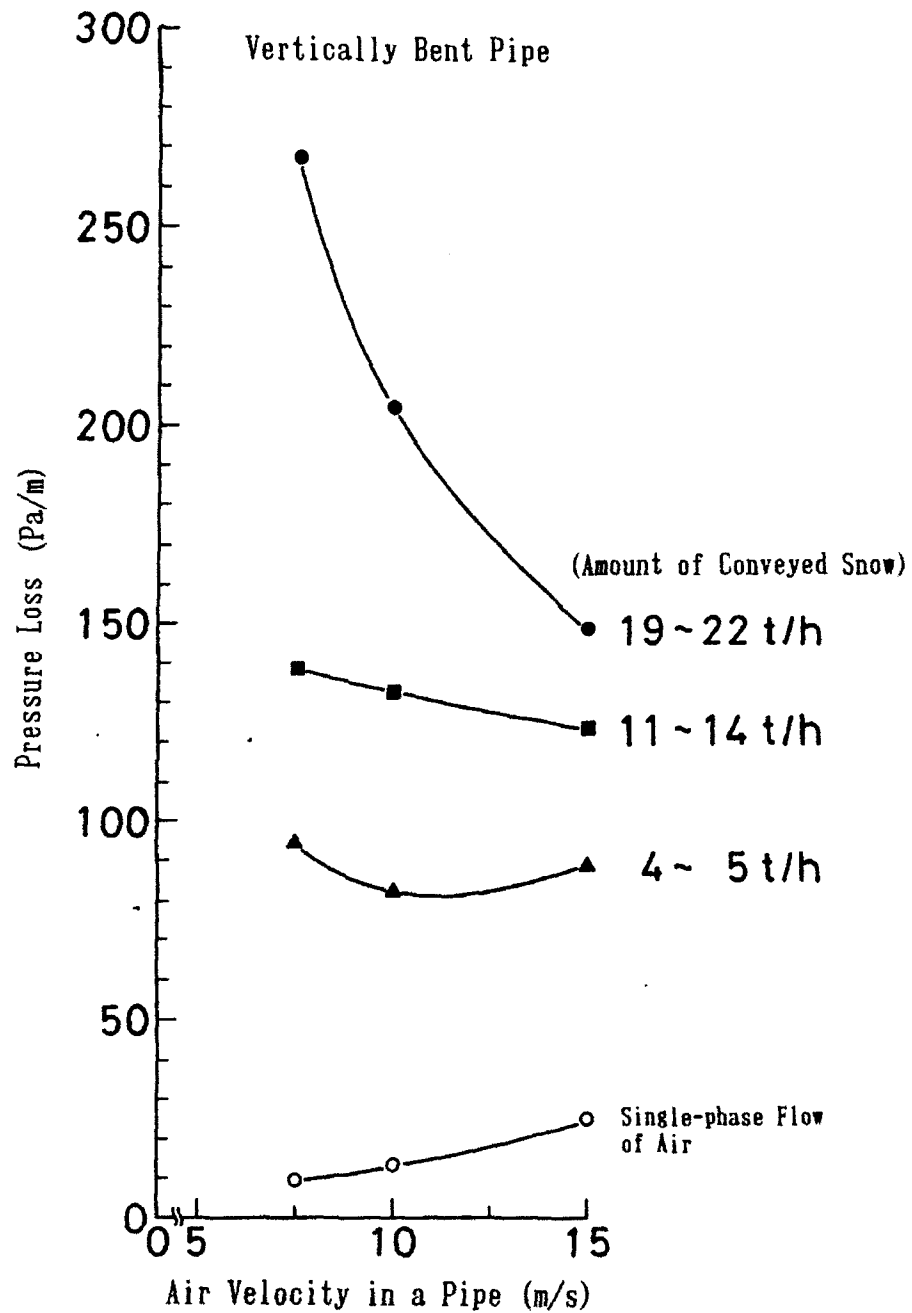


Figure 10. Relation between the pressure loss and the air velocity in a vertically bent pipe obtained with a pneumatic conveying system of snow in the form of snowballs.

DISCUSSION

Comparisons of the snow conveying power were made among four different types of snow conveying systems, i.e., a pneumatic conveying system in the form of natural snow, a hydraulic conveying system for removing snow pipes, a pneumatic conveying system in the form of snowballs and conveyance by dump trucks.

In these calculations, the only snow conveying power was calculated by four equations shown in Table 1, but the snow loading power into each piece of equipment was not included. However, in the case of a pneumatic conveying system in the form of snowballs, the snow compacting power was added. The conditions of these calculations are as follows:

- (1) Conveying snow 20 tons/hour of snow in the horizontally straight course.
- (2) An efficiency for conveying snow of 50 %. In fact, these conveying systems were different from each other in efficiency, but we did not have any reliable data; therefore, we supposed that they were all 50 %.
- (3) As the inner diameter of a pipe was 150 mm, the data published by Muramatsu and Hashimoto (1991) were used as the data for a pneumatic conveying system in the form of natural snow.
- (4) The power for conveying snow by dump trucks was calculated by assuming the trucks were running at a constant speed, but not at an accelerated speed.

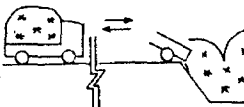
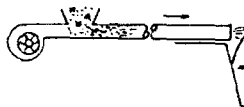
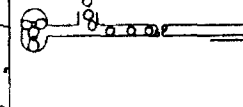
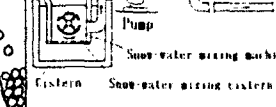
The results of these calculations are as follows:

- (1) To convey snow in the form of snowballs, the power to make snowballs was rather large, but the power to convey snowballs in a pipe is small compared with the other two systems if the conveying distance is more than 750 m (see Figure 11).
- (2) If we substitute 1 for the power for conveying snow by a dump truck for 1 km, the power for the other conveying systems of snow for 1 km is:
 - for a pneumatic system in the form of natural snow : 3.8,
 - for a hydraulic system in a pipe : 3.1,
 - for a pneumatic system in the form of snowballs : 2.4.

CONCLUSIONS

It is concluded that a pneumatic conveying system of snow in the form of snowballs will be best among these three systems, except for conveyance by dump trucks when snow must be conveyed

Table 1. Equations for calculating the power of four different types of snow transportation systems.

	Conveying of snow by dump trucks	Pneumatic conveying of snow		Hydraulic conveying of snow Solid-liquid two-phase flow
		Natural snow	Snowballs	
Schematic diagram				
Equations for calculating the power	$L = \frac{\mu \cdot v \cdot v + \left\{ \frac{A \cdot \gamma \cdot v^3}{g} \right\}}{102}$ <p> μ : Rolling resistance = 0.025 W : Weight of truck and snow = 4000+9500 = 13500kg v : Travel speed = $\frac{Q \times 2(\text{round}) \times (T/q)}{3600 \cdot t \times (T/q)}$ T : Conveying snow mass (t/h) q : loading snow mass = 4 ton/time t : loading time = 60 sec/time A : Projected area = 6.25 m² γ : Air density = 1.29 kg/m³ </p>	$L = \frac{P_0}{1730} \cdot Q \cdot \left\{ \left(\frac{P_0 + P}{P_0} \right)^{0.25} - 1 \right\}$ <p> P_0 : Atmospheric pressure = 101.36 Pa Q : Blast quantity = 19.4(m/s) × A × 60 = 20.6 m³/min P : Pressure loss per 1m = 196.1 Pa/m (at 23.7 t/h) 185.7 Pa/m (at 20 t/h) Q : Conveying distance (m) </p>	<p>Power for making snowballs</p> $L_1 = \frac{F \cdot S \cdot n}{102}$ <p>Power for conveying snowballs</p> $L_2 = \frac{P_0}{1730} \cdot Q \cdot \left\{ \left(\frac{P_0 + P}{P_0} \right)^{0.25} - 1 \right\}$ <p> F : Compressive stress by air = 2.2 ton S : Stroke of piston = 0.2 m n : Number of snowballs = W/q (number/sec) q' : Weight of a snowball = 1.2 kg P_0 : Atmospheric pressure = 101.36 Pa Q : Blast quantity = 7.5 m/s × A × 60 = 8 m³/min P : Pressure loss per 1m = 34.3 Pa/m (at 20 t/h) Q : Conveying distance (m) </p>	$L = 0.163 \cdot Q \cdot P \cdot d \cdot r$ <p> Q : Flow rate of two-phase flow = $\pi / 4 \cdot d^2 \cdot v$ = 3.2 m³/min d : Inner diameter of pipe = 0.15 m v : Current = 3 m/s P : Pressure loss = $0.068 \alpha \cdot \frac{Q \cdot v^2}{d^5} + 0.007 v \cdot \frac{Q \cdot v^2}{d^5}$ α : Volumetric concentration = $\frac{T}{Q \cdot P \cdot 60}$ = $\frac{20}{3.2 \times 0.3 \times 60}$ = 0.45 ρ : Snow density 0.3 g/cm³ γ : Water density 1 g/cm³ </p>

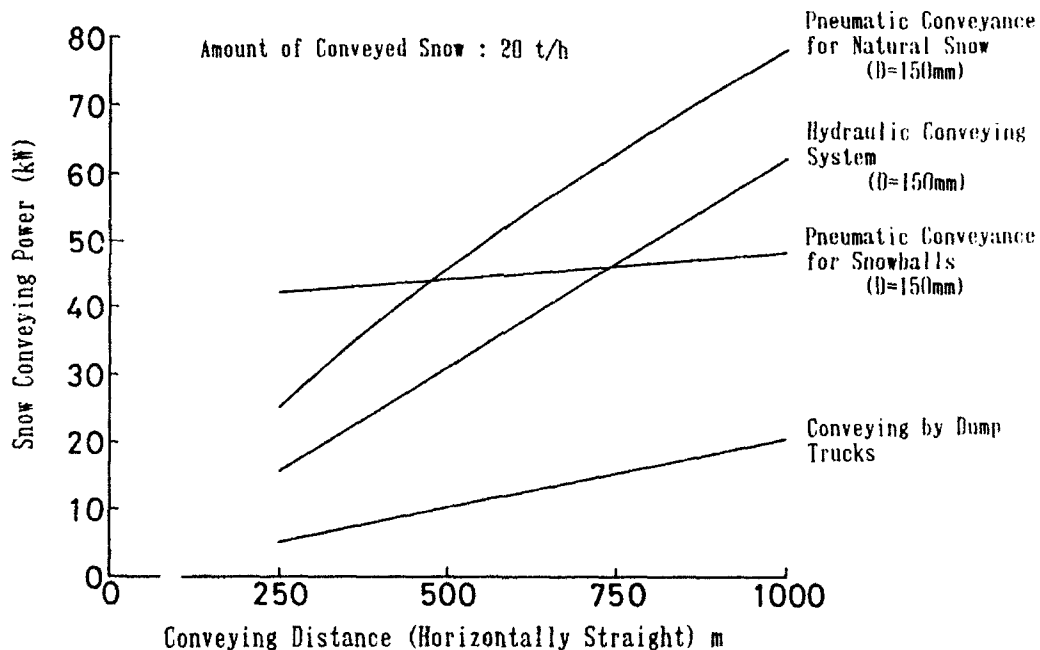


Figure 11. Comparisons of four different types of snow transportation systems.

for a distance of more than some hundred meters. On the other hand, a pneumatic conveying system of natural snow will be effective if snow will be conveyed in a distance of less than 500 m. Neither of these pneumatic conveying systems of snow needs large amounts of power, depending on the distances, nor any water source. Therefore, it is concluded that these systems will have practical use in the near future.

ACKNOWLEDGMENTS

The authors would like to thank Dr. T. Nakamura and Dr. Y. Nohguchi of the Nagaoka Institute of Snow and Ice Studies, NIED, for their useful suggestions.

REFERENCES

- Kobayashi, T., and Kumagai, M. (1989) "Experiments of Snow Removal Based on the Use of a Blower (1) - Pressure Loss in a Horizontal Straight Pipe -," The Report of the National Research Center for Disaster Prevention, 44, 105-121.
- Kobayashi, T. (1991) "Experimental Studies of Pneumatic Conveying System of Snow," Journal of the Japanese Society of Snow and Ice, 53-3, 211-216.
- Kumagai, M., and Kobayashi, T. (1989) "Experimental Studies of Pneumatic Conveying System of Snow in the Form of Lumps," Preprint of the Japanese Society of Snow and Ice 1989 Meeting, 528.
- Kumagai, M., and Kobayashi, T. (1990) "Experimental Studies of Pneumatic Conveying System of Snow in the Form of Lumps (2)," Preprint of the Japanese Society of Snow and Ice 1990 Meeting, 541.
- Kumagai, M. (1990) "Snow Conveying System Satisfied the Demands of the Age - Pneumatic Conveying System of Snow -," Summaries of the 15th. Meeting for Disaster Prevention for Snow and Ice, 43-50.
- Kumagai, M., and Kobayashi, T. (1992) "Experimental Studies of Pneumatic Conveying System of Snow in the Form of Lumps," Journal of the Japanese Society of Snow and Ice, 54-2, 153-158.
- Muramatsu, T., and Hashimoto, N. (1991) "The Experiments on Pipeline Transportation of Snow by Air," Civil Engineering Journal, 33-6, 56-61.

Hydraulic Transportation Machine Development for Snow Removal from Urban Areas

Teruyoshi Umemura

Nagaoka University of Technology, Nagaoka, Niigata, Japan

ABSTRACT

Hydraulic transportation machines are being developed in Japan for future construction of a snow removal pipeline system in an urban area with heavy snowfall. In early stage experiments, a snow feeder that feeds snow into the pipeline was a slurry pump with its inlet opening in a water pit. Now it has developed into a machine equipped with a stirring impeller for mixing snow and water. The present paper, laying the emphasis on vertical impeller snow feeders, describes the process of development which revealed the following:

- (1) A vertical impeller machine with straight blades can be used efficiently and safely by the residents.
- (2) Conventional slurry pumps work well for transporting the snow/water mixture.
- (3) The dimensions of a snow feeder should be determined by watching the critical fraction of snow to guard against blockage.
- (4) Control of the machine against blockage is required for improving the work time ratio of machine.

INTRODUCTION

In the northeast of Japan there are a number of heavy snowfall cities with more than 100 cm of snow cover. A large portion of the sidewalks and yards are left under the snow cover in winter while most roads are kept open by the daily operation of snow removing vehicles which have been well developed during these 40 years.

Snow melting pipe system are widely applied in those cities and are effective in eliminating the snow on sidewalks and yards, but unfortunately bring about land subsidence. Snow removing ditches are increasingly applied in several cities, though they require land gradients, plenty of water and a suitable river for dumping snow.

Thirteen years ago we proposed a system of snow removal, storage and air-conditioning use that should be required in a future city with heavy snowfall (Umemura et al., 1979; 1987b). In that system snow in the city is thrown into a snow feeder, mixed with water, transported to a snow reservoir in a suburban area, stored there and returned to the city in summer for air-conditioning as cooled water. Thus our study of hydraulic transportation of snow has started and continued so far.

We have already reported the fundamental characteristics of snow/water mixture flow (Shirakashi et al., 1989) and the development of snow fraction control devices (Kitahara et al., 1991), respectively. Hence another important of our study, that is the development of a snow feeder is described in this report.

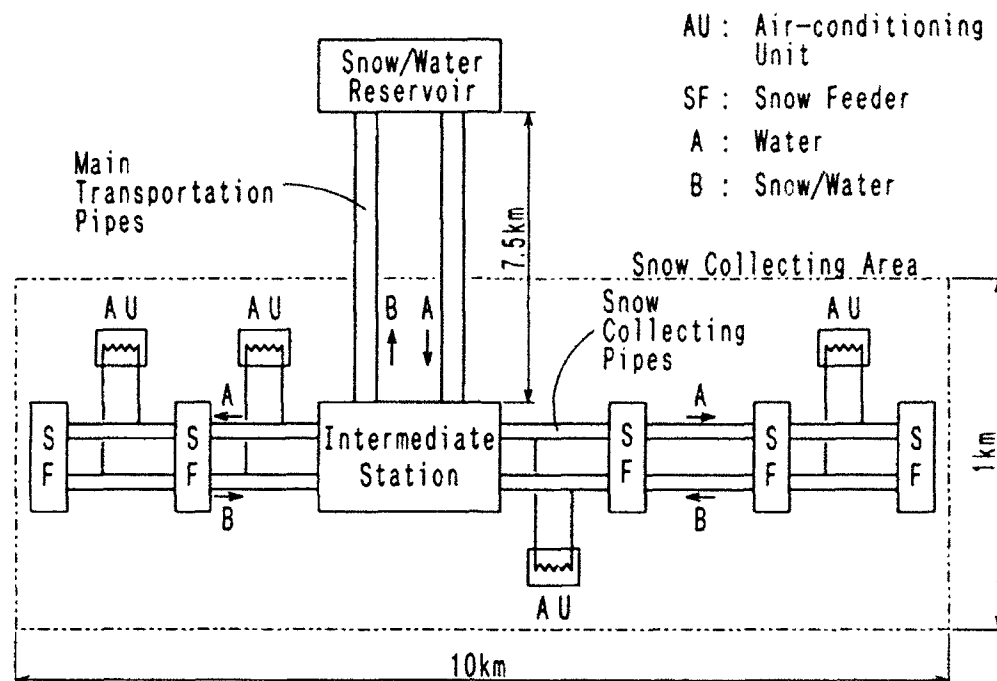


Figure 1. Schematic diagram of the integrated system of removal, storage and air-conditioning use of snow; after Umemura et al. (1979).

EARLY STAGE EXPERIMENTS FOR MACHINE DEVELOPMENT

The first attempt to transport snow with water through pipe was made in 1972 by Kawagoe and Shimobe (1972) for agricultural use. Figure 2 shows their experiment where snow is thrown into a hopper just above the inlet of a bladeless pump. The sucked snow and water is forced to form a mixture flow and delivered into the pipeline where they measured the pressure loss of the flow. They reported that granulated snow of density of 500 to 600 kg/m³ was able to be sucked and transformed into a mixture of 28 % snow mass (volumetric 60 %). There was, however, a great difficulty in sucking the snow, which might be the major reason of the abandonment of their experiment.

The Nagaoka Institute of Snow and Ice Studies made the second attempt in 1978 by Isobe et al. (1978). Figure 3 shows their experiment where a submerged snow receiver was placed in a drainage ditch. A slurry pump was placed out of the ditch as was a snow/water separator with a supporting stand so as to recycle the snow in the experiments. The maximum fraction of the mixture flow they attained is estimated at 35 % in solid mass. However, much difficulty in sucking still remained.

Kobayashi et al. (1981) of the above institute produced a snow/water mixing machine which has a stirring blade rotating round a horizontal shaft in a hopper container as in Figure 4. Snow and water are mixed and forced to the center of the container by the stirring impeller and sucked by a slurry pump. The impeller is similar to an auger of a rotary snow blower. Two kinds of impeller shown in Figure 4 were tested and it was concluded that the ribbon screw is much superior to the rake because adhesion and growth of snow are more likely to occur around the rake. This type of machine was developed to practical use as described later and is called a horizontal impeller snow feeder in contrast with the machine described in the following section.

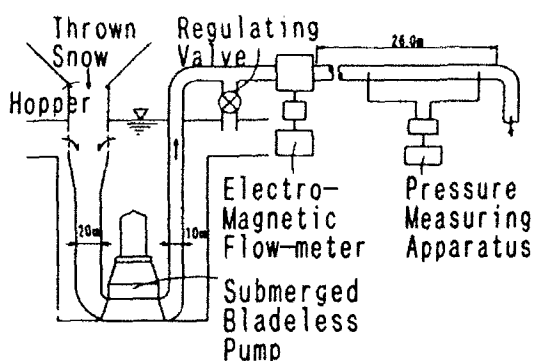


Figure 2. Schematic diagram of early stage experiment after Kawagoe et al. (1972).

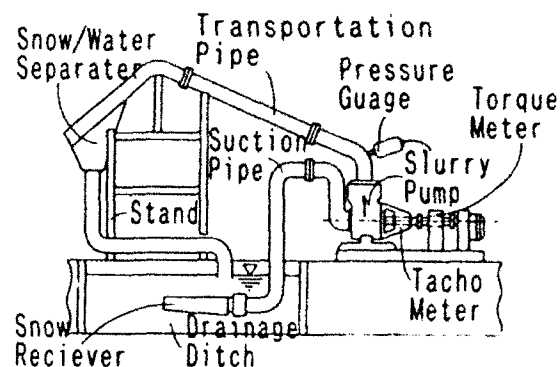


Figure 3. Schematic diagram of early stage experiment after Isobe et al. (1978).

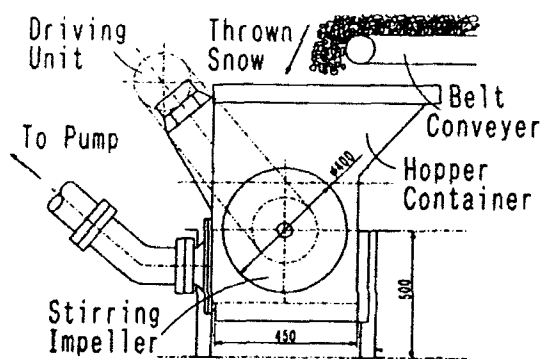
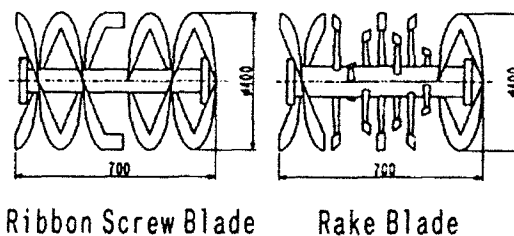


Figure 4. Snow/water mixing machine with horizontal impeller after Kobayashi et al. (1981).

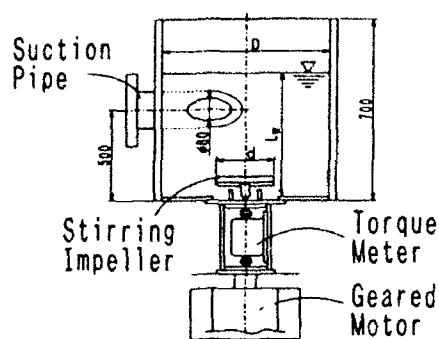


EXPERIMENTS FOR DEVELOPING VERTICAL IMPELLER SNOW FEEDER

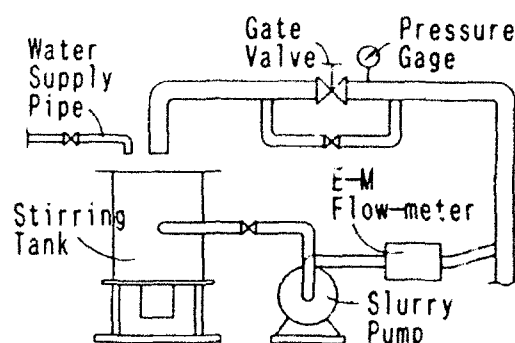
The proposed system (Figure 1) requires a new type of machine that mixes and feeds snow into the pipeline at a corner of a sidewalk or house yard when residents, e.g. housewives, throw snow into the machine. Therefore, safety and convenience are required, and the machine with a vertical stirring impeller seems the best because it is similar to household electric washing machines. The snow treating capacity required for a household snow feeder was estimated to be 1.0 to 3.0 tons of snow per hour.

Figure 5 illustrates the early stage experiments (Umemura et al., 1984): (a) the stirring tank, and (b) the experimental system. Snow thrown into the stirring tank is mixed with water by a rotating impeller with a horizontal axis, sucked by a slurry pump, flowing through the circulating pipe, and returned to the tank. The solid fraction in the snow/water mixture is measured at the outlet of the pipe by sampling and weighing, the flow rate by a electromagnetic flow meter.

Regulating the gate valve under a constant fraction of snow, we obtain the relation between the flow rate and the pressure, the so-called characteristics of the pump. Figure 6 shows



(a) the stirring tank



(b) the experimental system

Figure 5. Vertical impeller snow feeder used in the early experiments which revealed the critical snow fraction of stirring and the optimum dimensions of machine (Umemura et al., 1984).

what was measured for the slurry pump we used (Ebara SALG52). The delivery and the efficiency both decrease with increasing snow fraction. But the decrease is so slight that may not bring any difficulty in practical use.

Increasing the snow fraction with the other variables unchanged, we see the normal state of stirring (see Photo 1 (a)) suddenly breaks down, with a mass of snow separating from the stirred mixture and growing on the surface (Photo 1 (b)). The solid fraction at which the mass of snow begins to grow is called the critical solid fraction of stirring and denoted by $f_{s,c}$ in the present paper.

Most of the dimensions for designing a vertical impeller snow feeder are determined by experimentally measuring $f_{s,c}$ and the stirring power denoted by w (W/kg). Figure 7 shows a summarized result of experiments carried out to determine the optimum values of n , d/D and D/L_w . All the $f_{s,c}$ increase monotonously with increasing n and D/d , whereas $w/f_{s,c}$ does not increase monotonously but has arrests with increasing n and D/d . The arrests give the optimum values of the n and D/d . Those are at about 400 rpm and 2.5 respectively which were confirmed by the other experiments where the impeller diameter varied.

In order to design a better shape of a impeller, 10 shapes of blades shown in Figure 8 were tested in small-scale stirring experiments by measuring the mixing rate of snow as well as $f_{s,c}$ and $w/f_{s,c}$ (Umemura et al., 1987a). The following 3 shapes of blades were chosen and then tested further in the actual scale. These gave the followings: ribbon screws, straight-blade paddles and turbines having increasingly good performance in this order in view of $f_{s,c}$ and $w/f_{s,c}$. In terms of the mixing rate, however, straight-blade paddles, anchor blades, turbines and ribbon screws are better, in this order. On the other hand, blades inducing axial flow, e.g., pitched blade paddles or propeller blades or inducing centripetal flow, e.g., curved blade paddles or brumagin type

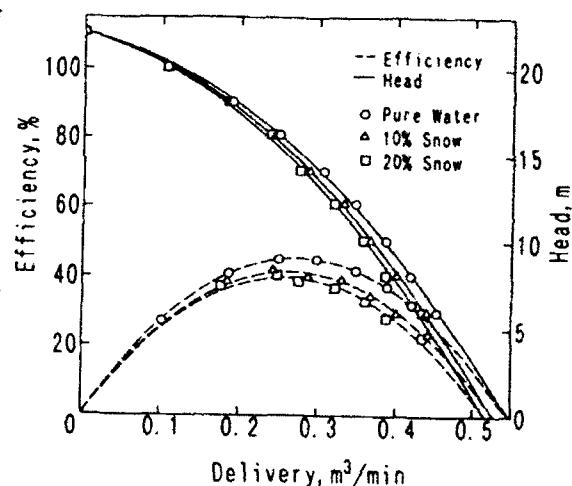


Figure 6. Characteristics of the slurry pump used in the early experiments (Umemura et al., 1984).

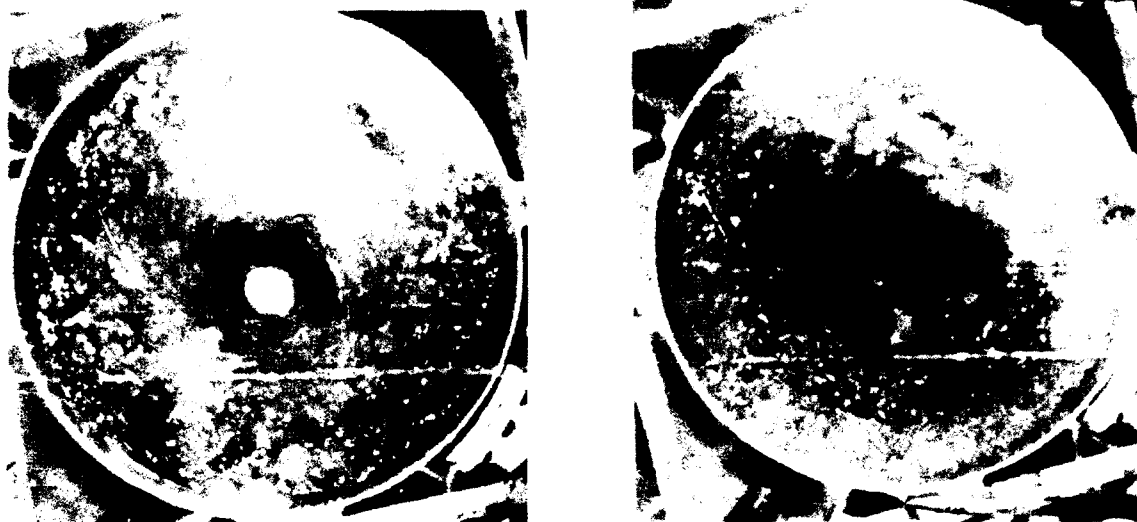


Photo 1. States of stirring (Umemura et al., 1984): when the snow fraction increases, the normal state (left) suddenly breaks down and changes to the critical state (right), where a ring of snow has grown along the inner wall of the tank.

impellers are worse for every aspect of mixing performance. In conclusion, a straight-blade paddle is recommended for the stirring blade of a snow feeder.

DEVELOPMENT OF PRACTICAL SNOW FEEDERS WITH VERTICAL IMPELLER

Design

We have designed a practical vertical impeller snow feeder which is illustrated in Figure 9 (Umemura et al., 1991): it is to be used by unspecified people who remove snow from sidewalks or private areas usually with a "snow dump," which is illustrated in Figure 10. According to the size of snow dumps the opening diameter of the snow feeder, D , has been decided to be 650 mm. Then the diameter of the impeller, d , is decided as 260 mm by using the above-mentioned relation, $D/d=2.5$; similarly, $n=610$ rpm and $V=0.10$ m³ are decided.

The slurry pump (Ebara 65FVQ52.2), that is to say a feeding pump, with a 2.2 kW motor and 65 mm transportation pipes are incorporated, which has a closer characteristic to that of a conventional water pump than what has been shown in Figure 6; e.g., the head is 10.4 m for the delivery of 0.32 m³/min

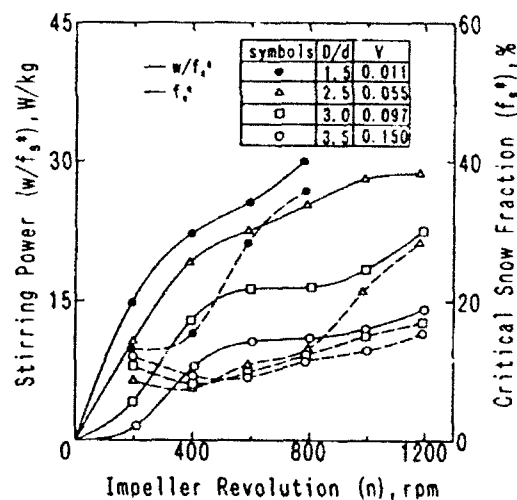


Figure 7. Changes of critical snow fraction, f_s^* , and the stirring power per unit mass of snow, w/f_s^* , with varying the impeller revolution, n , (Umemura et al., 1984); the tank diameter, D , and the meniscus height, L_w , vary in the experiment maintaining the relation, $D/L_w=1.7$, with a constant impeller diameter, $d=200$ mm. $V=\pi D^2 L_w/4$ and D/d are taken as the parameters.

and 9.3 m for 0.5 m³/min.

The practical snow feeder is installed in a narrow alley where neither removing vehicles nor melting system is available, but there is a neighboring small river for supplying water and dumping snow. The water raised by a submerged pump (Ebara 50BMS51.5) from the river is sent to the snow feeder through the pipe of 50 m length, and snow thrown into the tank by residents is mixed with the water in it. The snow and water are sucked by the feeding pump, and sent to the river, with pump performance measured by an electromagnetic flow meter. The level of the meniscus is controlled to be 560 through 650 mm in depth by operating the electro-powered gate valve.

Operation

In the vertical snow feeder, sometimes blockage occurs in the tank, the suction pipe or its neighborhood. The signs of blockage are the sound of stirring impeller, the appearance of the stirred mixture or the flow meter indicator. The researchers who know the signs of blockage can control the snow throwing rate while residents in general can not do this, so the frequency of blockage is quite different depending on the operators. Once blockage occurs, snow throwing should stop for more than few minutes to release it. Accordingly, the worktime ratio of the machine greatly depends on who is operating it.

Table 1 shows the operational data of the practical snow feeder. In the residents' operation, snow quality is not distinguished but in the researchers' operation it is divided into two: compacted and granulated and their densities are 0.2 t/m³ and 0.4 t/m³ on average, respectively, with 0.3 t/m³ postulated in the residents' operation. The numbers of throws are for the researchers' operation from January 29th to February 2nd in 1986, and for residents' operation for 25 successive days; during this period the accumulated snowfall was about 350 kg/m² and the depth of snowcover varied from 238 cm to 254 cm. Therefore, 31.3 tons of total snow mass thrown into the feeder (AB) corresponds to the mass of snowcover on the area of 424 m².

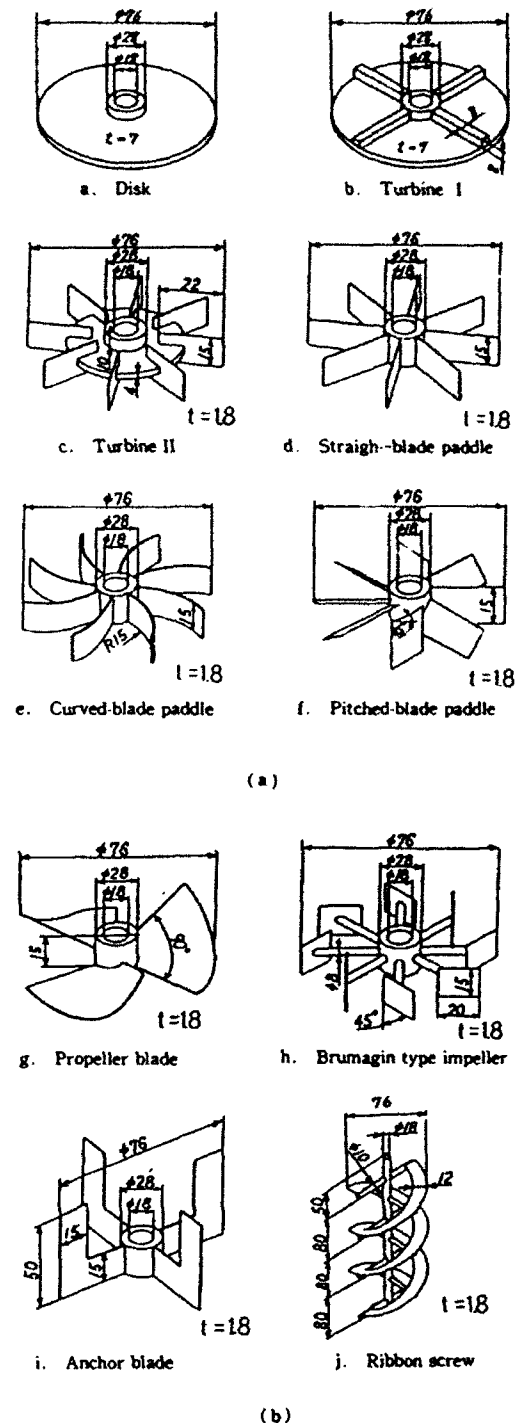


Figure 8. 10 shapes of blades tested in the small-scale stirring experiments (Umemura et al., 1987): enlarged blades of b, d, and j also showed good performance in the actual scale experiments.

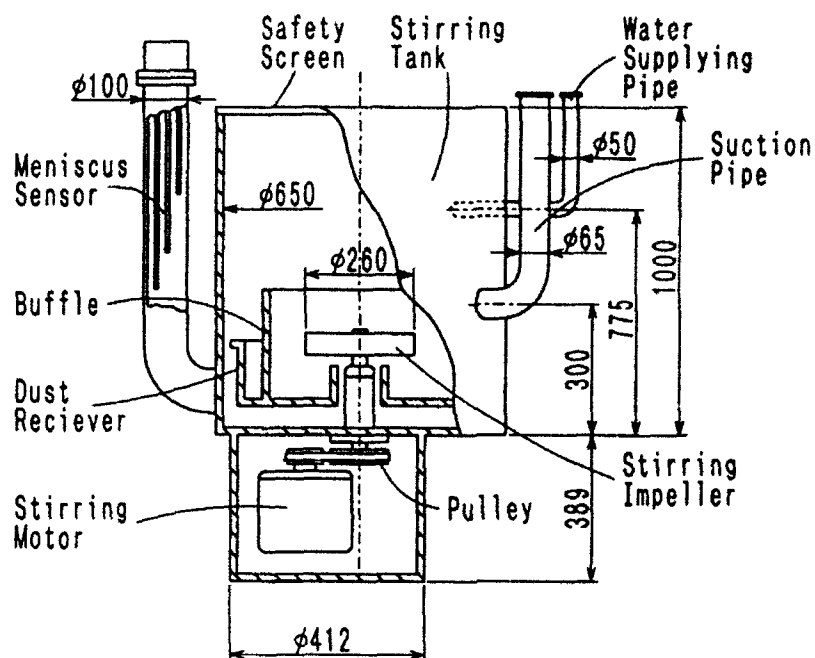


Figure 9. Vertical impeller snow feeder for practical use (Umemura et al., 1988); figures are expressed in mm.

The snow treatment capacities of the machine of 1.15 t/h for compacted snow and 2.65 t/h for granulated snow which were obtained by the researchers satisfies the design specification, but that by the residents, 0.43 t/h, is under the specification. In general, compacted snow is more likely to incur blockage: it requires a longer time interval for mixing with more water and more stirring power, which about doubles the times per unit of snow mass. The difference in snow treatment capacity between the researchers and the residents results merely from the frequent occurrence of blockage in the residents' operation. This evidence is recognized in all values in Table 1. It may be convenient to use a volumetric value instead of mass value because it makes all values for compacted snow and for granulated snow approximately same.

Improvement

To improve the performance against blockage, the machine has been equipped with two control devices: a device monitoring the electric stirring power which gives operators a warning signal to reduce the snow throwing rate when the power exceeds a threshold; and another device monitoring the flow rate of the snow/water mixture which gives operators another signal when the flowing rate falls below a threshold and operates the electric-powered gate valve to send a

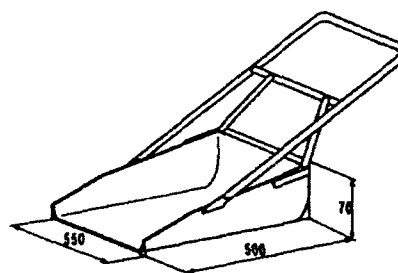


Figure 10. "Snow dump": a daily necessity for removing snow around houses in a heavy snowfall area in Japan.

given amount of water directly into the suction pipe. This operation is repeated several times until the flow rate rises again; i.e., the blockage is released. With the devices incorporated, the snow treating capacity of the machine is expected to rise to 2.6 t/h through 3.0 t/h, which was attained in researchers' operation, but has not yet been reached in residents' operation.

Table 1. Operation data of the practical snow feeder with vertical impeller: performed by researchers and by unspecified residents.

Operators	Researchers		Residents
Snow quality	Compacted	Granulated	Indiscriminate
Measured values :			
Number of throws (A)	195	420	1169
Mean mass per throw (B), kg	12.9	21.2	17.0
Apparent density of snow (C), t/m^3	0.2	0.4	0.3
Time of operation (D), h	2.19	3.36	46.18
Supplied water (E), t	20.6	29.1	362
Supplied power (F), kWh	9.58	15.1	19.3
Derived values:			
Snow treating capacity (AB/D), t/h	1.15	2.65	0.43
Time interval of throwing (D/A), s	40.4	28.8	142.2
Water consumption (E/AB), kg/kg	8.2	3.2	18.2
Mean solid fraction (AB/(AB+E)), kg/kg	10.9	23.8	5.2
Its volumetric value (AB/(AB+EC)), m^3/m^3	(37.8)	(43.3)	(15.4)
Power consumption (F/AB), Wh/kg	3.80	1.70	6.50

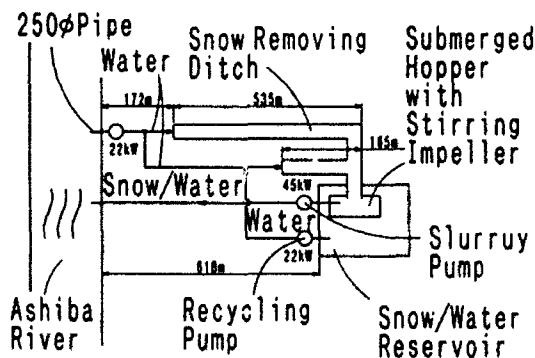


Figure 11. Hydraulic transportation system installed in Fukui Station for removing snow from the station to the Ashiba River after Akahoshi et al. (1985). A horizontal impeller snow feeder was used.

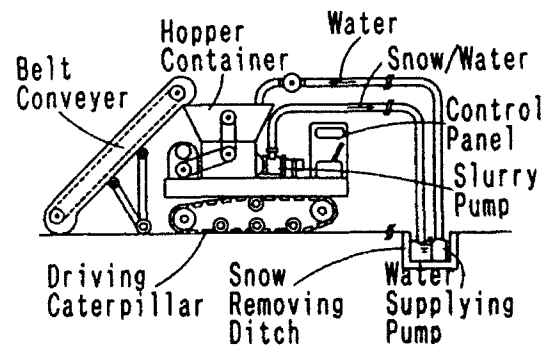


Figure 12. Movable snow removing apparatus produced by Isobe et al. (1985). A horizontal impeller snow feeder was used.

Comparison with other practical machines

Another machine with a horizontal impeller mentioned above has also been studied by other researchers: two trials have been made for practical use: Akahoshi et al. (1985) constructed

a pipeline for transporting snow removed in Fukui Station to the Ashiba River (see Figure 11) and Isobe et al. (1985) produced a movable machine for transporting snow from narrow places to a snow removing ditch or a wide road where conventional snow-removal vehicles run (see Figure 12). The specifications and performance of these machines are shown in Table 2. Where Fukui's are design values while the others measured. Although the snow treating capacity differs cumulatively by 4 times and by 5 times from Nagaoka's machine to Fukui's machine, the mean solid fractions measured are approximately same, i.e., 23.8 % and 24.9 %. Whereas power consumption per unit snow mass is greatly different between vertical and horizontal; this results from the nature of blades. Paddles used in the horizontal machine required relatively high rate of revolution, 610 rpm, while ribbon screw blades required only 60 rpm. Therefore, a horizontal machine seems preferable to a vertical machine from the viewpoint of power consumption.

Concerning blockage, nothing has been reported about horizontal machines; it may be the most important problem in the development of practical snow feeders with a horizontal impeller as well as with a vertical impeller. Safety and convenience are also their future problem.

Table 2. Comparison of practical snow feeders.

	Vertical, Nagaoka	Horizontal, Fukui	Horizontal, Movable
Snow treating capacity, t/h	2.65	11.2	64
Mean solid fraction, %mass	23.8	24.9	16.7
Power consumption, Wh/kg	1.70	0.53	0.76
Stirring impeller	Straight paddle	Ribbon screw	Ribbon screw
revolutions, rpm	410	179	60
pump capacity, l/min	180	750	6240
transporting dist., m	50	50-150	618

Fukui's values are values designed, but others measured for granulated snow.

SUMMARY

Through the development process of vertical impeller snow feeders, from the experimental machines to the practical machine, following facts have been revealed:

- (1) A vertical impeller machine with straight blades can be used efficiently and safely by the residents.
- (2) Conventional slurry pumps work well for transporting snow/water mixtures.
- (3) The dimensions of a snow feeder should be determined by watching the critical fraction of snow to guard against blockage.
- (4) The control of a machine against blockage is required for improving the work ratio of machines.

From the viewpoint of power consumption a horizontal impeller machine is superior to a vertical impeller snow feeder; however, blockage, safety and convenience are problems.

ACKNOWLEDGEMENT

The research has been conducted as projects of the Technological Development Center of the Nagaoka University of Technology since 1982. They were supported by Nagaoka City, Niigata Engineering Co. Ltd., Ebara Co. Ltd, Sato Engineering Co. Ltd., Maruiso Construction Co. Ltd. and Argos Co. Ltd. Also they have been supported by a Grant-in-Aid of Scientific Research of the Ministry of Education, Science and Culture. The author expresses his gratitude to the above sponsors and also to Prof. N. Hayakawa and Prof. M. Shirakashi who supported this research as leaders of the projects.

REFERENCES

- T. Akahoshi, T. Kimura, H. Ishimura and N. Yamamoto (1985) "Snow Removing Ditch of Snow/Water Mixture Transportation Type", *Tetsudo Doboku (Civil Engineering for Rail Way)*, Vol. 27(1), 8-12, 1985. (in Japanese)
- K. Isobe, S. Kobayashi and H. Miyaura (1978) "Study on Hydraulic Transportation System of Snow With Pipe", *S53 Proceedings, Japanese Soc. Snow and Ice*, P149, October 1978. (in Japanese)
- K. Isobe (1985) "Pipe Transportation System for Snow", *Yuki to Douro (Snow and Road)*, No. 2, 83-89, 1985. (in Japanese)
- N. Kawagoe and S. Shinobe (1972) "Snow Removing Trial by Transportation in Pipe", *9th National Symposium on Natural Disaster Science, Proceedings*, P103, October 1972. (in Japanese)
- T. Kitahara, M. Shirakashi, H. Taniuchi, A. Uchikura and A. Okada and N. Hayakawa (1991) "Development of Snow-Fraction Control Technique in Hydraulic Conveying of Snow", *ASME Proceedings, FED-Vol. 118, Liquid-Solid Flows*, 235-239, 1991.
- T. Kobayashi, I. Nohara and H. Kuriyama (1981) "On Snow Transportation in Snow/Water Mixed Phase (Part 2)" *S56 Proceedings, Japanese Soc. Snow and Ice*, P63, October 1981. (in Japanese)
- M. Shirakashi, A. Uchikura, T. Umemura, A. Okada, H. Taniuchi and N. Hayakawa (1989) "Hydraulic Conveying of Snow for Urban Snow Removal and Storage for Air Conditioning", *IAHR Proceedings*, B-375, August 1989.
- T. Umemura, I. Hattori, I. Gotoh, T. Tejima and M. Hattori (1979) "Studies on the Effective Use of Fallen Snow as a Cold Energy source 1. Proposal and Evaluation of Urban Air Conditioning System with Gathered Snow", *Tech. Report of Nagaoka Univ. of Tech.*, No. 1, 158-162, March 1979. (in Japanese)
- T. Umemura, S. Ohura, T. Tokuhiko, I. Hattori and A. Okada (1984) "Hydraulic Conveying of Snow II, Snow Feeder to Pipeline", *Seppyo (snow and Ice)*, Vol. 40(2), 51-58, June 1984. (in Japanese)

T. Umemura, K. Mineno, F. Kamemizu and Y. Seino (1987a) "Snow/Water Mixing Performance of Various Stirring Blades for a Vertical Type Snow Feeder", *Trans. JSME, Series B*, 53(491), 2037-2040, July 1987. (in Japanese)

T. Umemura, N. Hayakawa, M. Shirakashi, Y. Fukushima and Y. Kawahara (1987b) "A System of Urban Snow Removal and Storage Integrated with Air Conditioning", *Reports of Special Project Research on Energy. The Ministry of Education, Science and Culture, Japan. SPEY20*, 249-253, October 1987.

T. Umemura, T. Kobayashi, A. Hatakeyama, Y. Sato and M. Shirakashi (1991) "Development of Machines for Hydraulic Transportation of Snow Part 1", *Seppyo (Snow and Ice)*, Vol. 54(1), 19-25, March 1992. (in Japanese)

6 Mechanical Properties and Behavior

Wayne Tobiasson, Chairman



*Heavy snow load on avalanche defense structures in Japan and damage that has resulted in new design criteria.
(Photographs provided by Katsumi Katakawa.)*

Flow Characteristics of Snow-Water Mixtures in Horizontal Pipes

Mikio Sasaki,* Toshio Kawashima* and Hiroshi Takahashi†

*Hachinohe Institute of Technology, Hachinohe, Japan

†Department of Mining and Mineral Engineering, Tohoku University, Sendai, Japan

ABSTRACT

Experimental investigations of head losses and particle velocity distributions have been undertaken for snow-water and polystyrene particle-water mixture flows. Energy losses increase at lower velocities as those velocities decrease, but at higher velocities energy losses are close to that of pure water flows. The particle velocity profiles in a vertical plane at lower velocities are skewed considerably. The deformation of the profiles is the result of larger energy losses at lower velocities. As mean velocities increase, so do the slip velocities. Due to this increase of the slip velocities, particle segregation and migration disappears in higher velocities. The particle velocity distributions in a horizontal plane are nearly uniform and are hardly affected by mean velocity decrease. The particle velocity profiles in a vertical plane skew gradually with a concentration increase. The deviation of the profiles due to increased concentrations is the result of higher energy losses.

INTRODUCTION

The snow drain system has been investigated theoretically and first named by Sato and Shuto (1983 a,b). Snow drains, which are constructed along streets, are used as a hydraulic conveyor for removing snow in the districts of Japan where snowfall is heavy. When heavy snowfall occurs, snow is removed by mechanical power to both sides of the road. Almost all masses of snow on the streets are then thrown into the snow drain by manpower, and finally, they are transported by water flows to a natural river or a larger artificial open channel.

Usually, snow drains are in the form of an open rectangular channel constructed of concrete or pre-cast concrete. The width of the typical snow

drain is about 0.5 m. Water conveyed by an open channel or pumped from rivers is released into the snow drain to maintain its transport capacity.

Recently, the number of cities utilizing the snow drain has increased greatly, and many more cities are planning to build new snow drains. This is due to citizens' demands to use snow drains on their streets. However, there are many locations where such snow drains are not feasible due to lack of adequate slope to the roads. If a snow drain is constructed in such an area, and the terminus is lower than the final station, then snow conveyed by the drain is not transported by water flow from the terminus to the final station, i.e. a natural river or a larger open channel. However, the problem can be solved by a snow drain system relying not on the surface water flow but on water flow by pumping from the terminus to the final station. Therefore, we propose a snow drain system in which a pipeline is used in the final transportation of snow.

In designing a hydraulic snow transport system through pipelines, one of the most important practical problems is to estimate the pressure loss. Some researchers have investigated experimentally the pressure loss in snow-water mixture flows. However, the behavior of solid particles and the mechanics of energy losses have not yet been made clear, and therefore, extensive investigations are needed.

In this present study, our experiments use polystyrene particles to imitate the transport of snow in a pipeline, and to get accurate data regarding solid particle velocities in solid-liquid mixture flows. If the solid pump is set at the start station in the pipeline, the pump crushes snow blocks into much smaller ones. Hence, snow-water mixture flows become similar to polystyrene solid-water mixture flows.

In the present study, solid particle transport in multiphase flows is observed experimentally, and the behavior of solid particles and the mechanics of energy losses in snow-water mixture flows are investigated. Finally, the dynamics of snow-water and solid-water mixture flows are discussed.

EQUIPMENT AND METHODS

These experiments are facilitated by using three kinds of pipes with diameters $d = 39.7, 49.3$ and 49.7 mm. Figure 1 shows a schematic diagram of experimental polystyrene particle-water mixture flows. The diameters and specific gravities of polystyrene particles used in this study are $d_p = 3.21, 3.22$ and 3.09 mm, and $S = 0.86, 0.96$ and 1.04 , respectively. The test section shown in Fig.1 is 13 m in long, and is made of transparent acrylic pipes with diameters $d = 39.7$ and 49.7 mm. A part of the pipe is covered with a quadrilateral acrylic water jacket in order to eliminate the refraction of light by the curvature of the cylindrical pipe. Within the jacket, visual

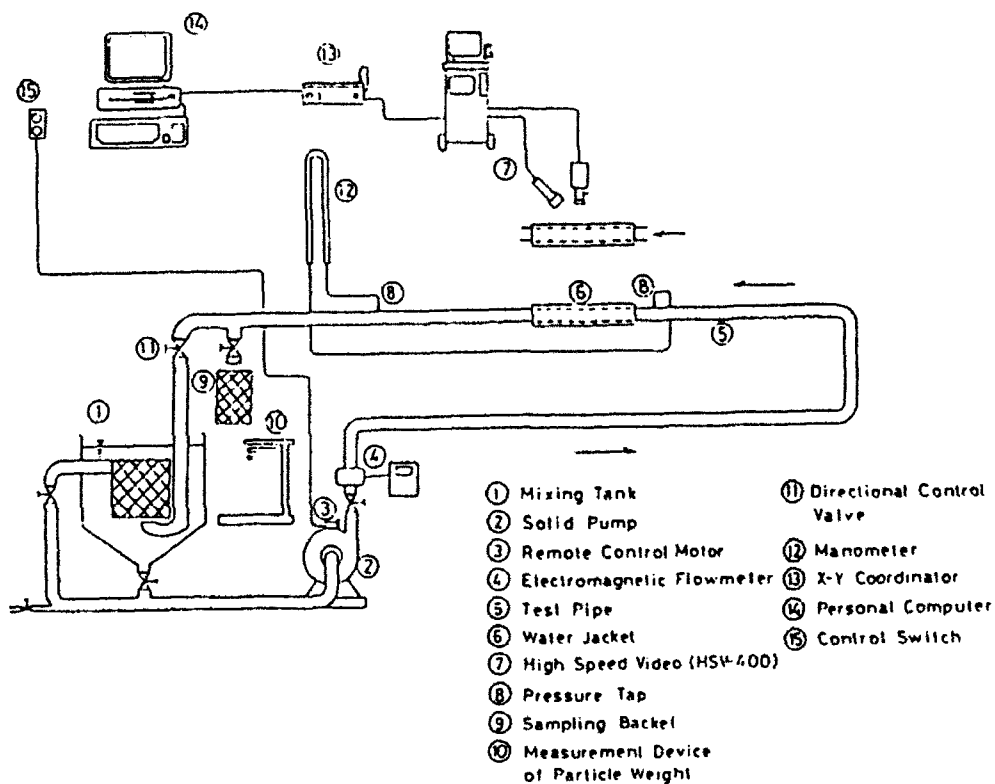


Fig.1 Schematic experimental equipment. Experiments with polystyrene particle-water mixture flows.

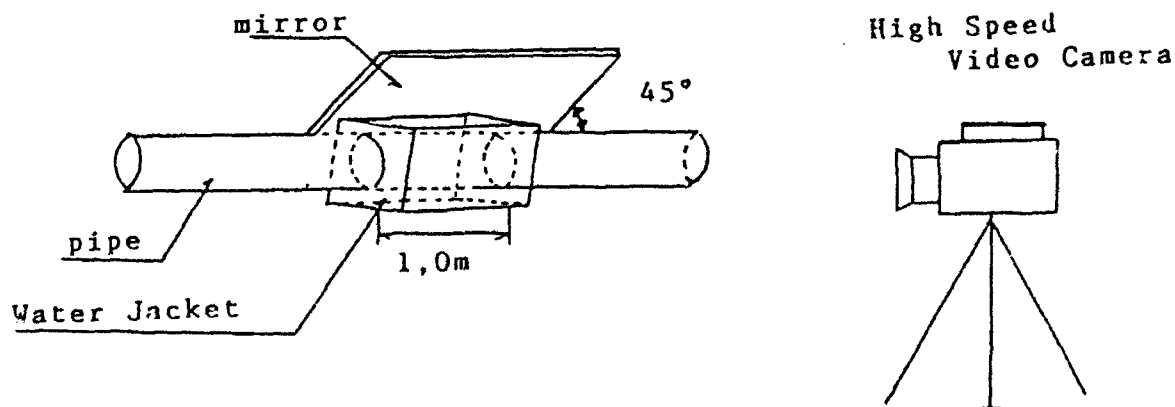


Fig.2 Device for measurements of particle velocities in a vertical and horizontal planes in water slurries of particles.

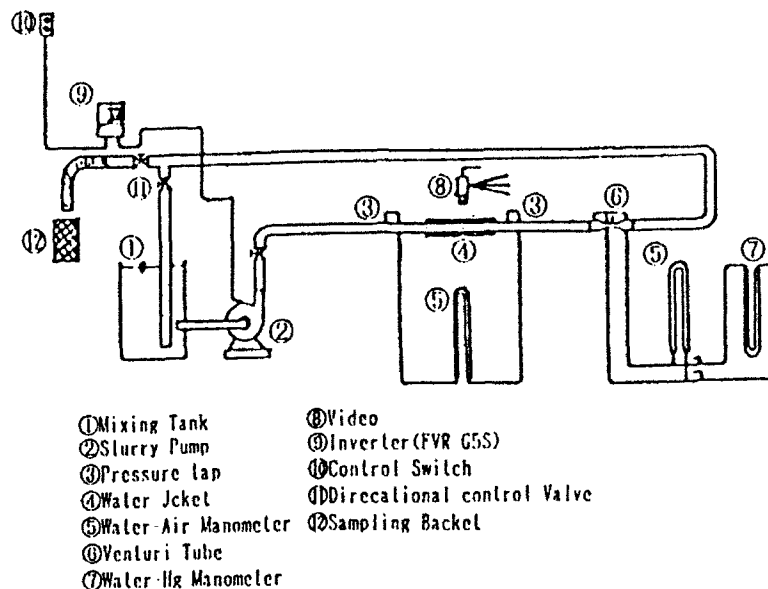


Fig.3 Schematic experimental equipment. Experiments with snow-water mixture flows.

observations of the behavior of particles were made with a high speed video camera with a maximum exposure speed of 400 fps. The shutter speed of the camera is 200 fps. (1/200 seconds), and it gives us satisfactory and clear pictures of the behavior of particle in these experiments. To ensure clear visual observation of the behavior of particles, a small fraction of the particles were painted with red coloring.

As shown in Fig.1, the particle trajectories were obtained by transforming the particle positions from a video image into time and space coordinates via the X-T coordinator, and the data of the particle trajectories were transmitted to a computer.

Figure 2 shows a device for observing the behavior of polystyrene particles in not only vertical but also horizontal planes at the same time. Thus, two-dimensional movements of particles are observed in water slurries of polystyrene particles.

Figure 3 shows a schematic for experimental equipment used in snow-water mixture flows. The test section for observations of snow-water mixtures is made of an acrylic pipe with the diameter $d=49.3$ mm. The specific gravities of snow in the pipeline and before the tests are $S = 0.827$ and $S = 0.418$ respectively. The snow concentrations range from 1.48 to 31.6% by volume. However, almost all experiments are at concentrations of 6% or less by volume.

EXPERIMENTAL RESULTS

Figure 4 shows polystyrene particle slurries at lower, middle and higher velocities in the horizontal pipeline. In the figure, z , V and C are the vertical distance from the pipe bed, the mean velocity and the solid concentration, respectively. The figure suggests that at lower velocities polystyrene particles migrate from lower layer to upper layer in the pipeline. On the other hand, at higher velocities no segregation occurs. In the present experiments, as the mean velocity decreases, solids and water in mixture flows become increasingly segregated. This implies that a particle's naturally buoyant force increases as the mean flow velocity decreases.

On the other hand, in experiments with water slurries of polystyrene particle with specific gravity larger than 1, the particles migrated from upper to lower layer in the pipe.

Figure 5 shows snow-water mixture flows at lower velocities. As shown in the figure, segregation and particle migration appear as well as polystyrene particle-water mixtures.

Figure 6 shows the relationship between the hydraulic gradient, i , and a modified Froude number, Fr_m , defined in the following equation (1).

$$Fr_m = Fr^2 / |1-S| \quad \text{where } Fr^2 = V^2 / gd \quad \text{-----(1)}$$

in which g is the gravitational acceleration and Fr is the Froude number.

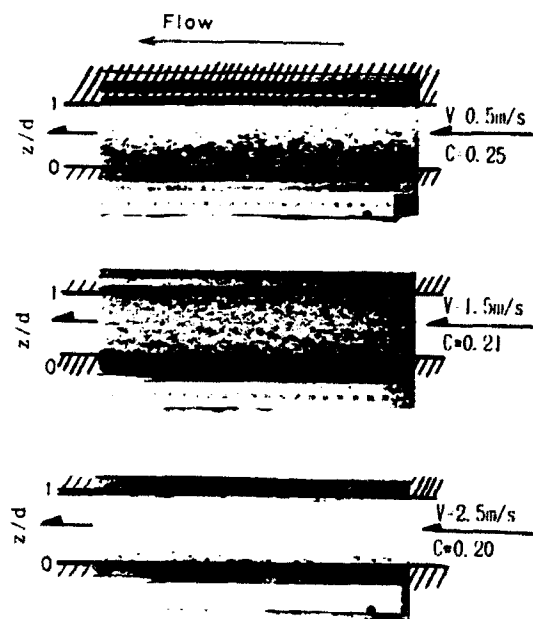


Fig.4 Polystyrene particle-water mixture flows in horizontal pipeline. In these pipes, white and black portions correspond to solid particles and water respectively. $S = 0.86$.

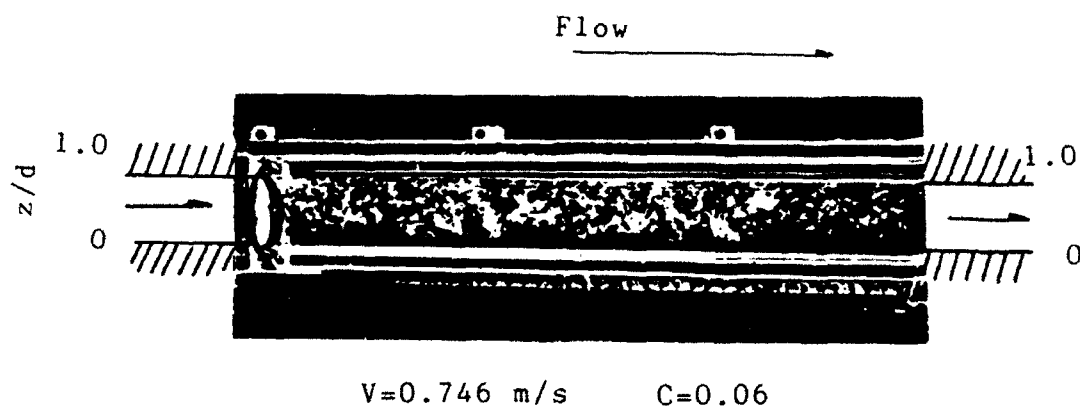


Fig.5 Snow-water mixture flows at lower velocities in horizontal pipeline.

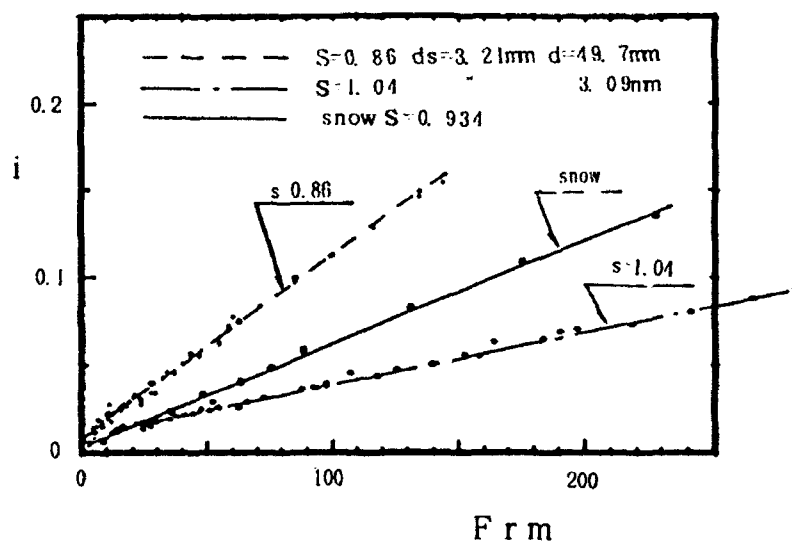


Fig.6 Relationship between hydraulic gradient, i , and modified Froude number, $Fr m$.

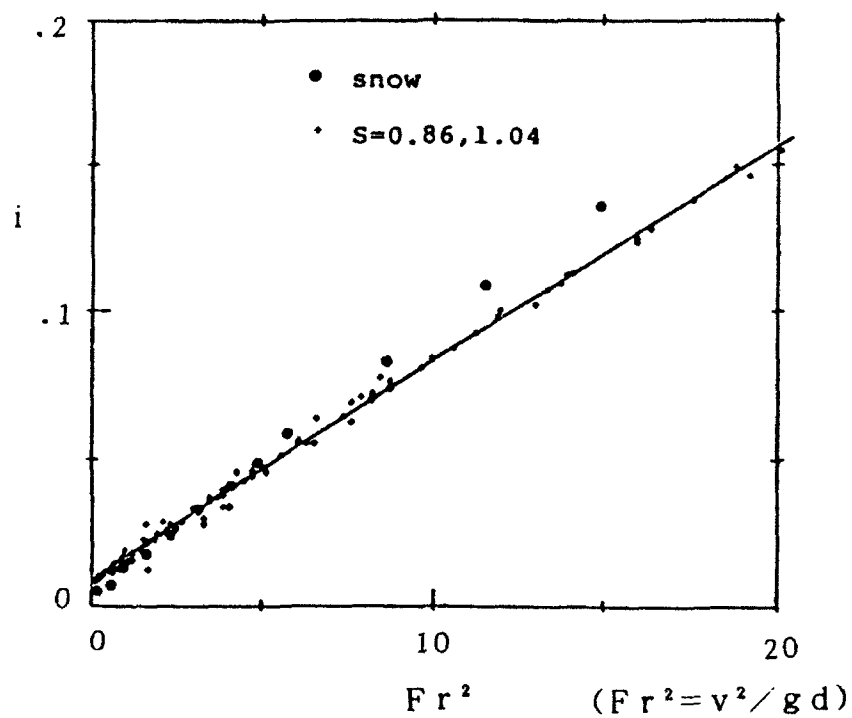


Fig.7 Relationship between hydraulic gradient and Froude number.

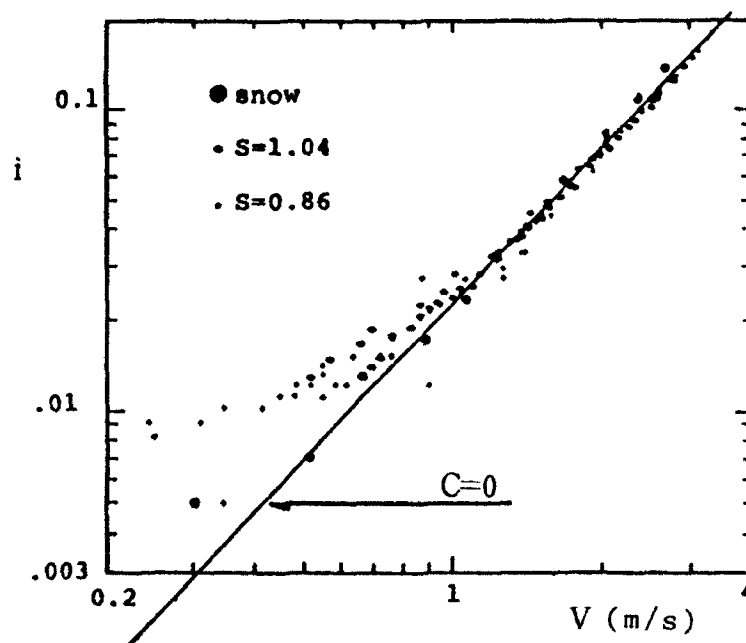


Fig.8 Relationship between hydraulic gradient and mean velocity.

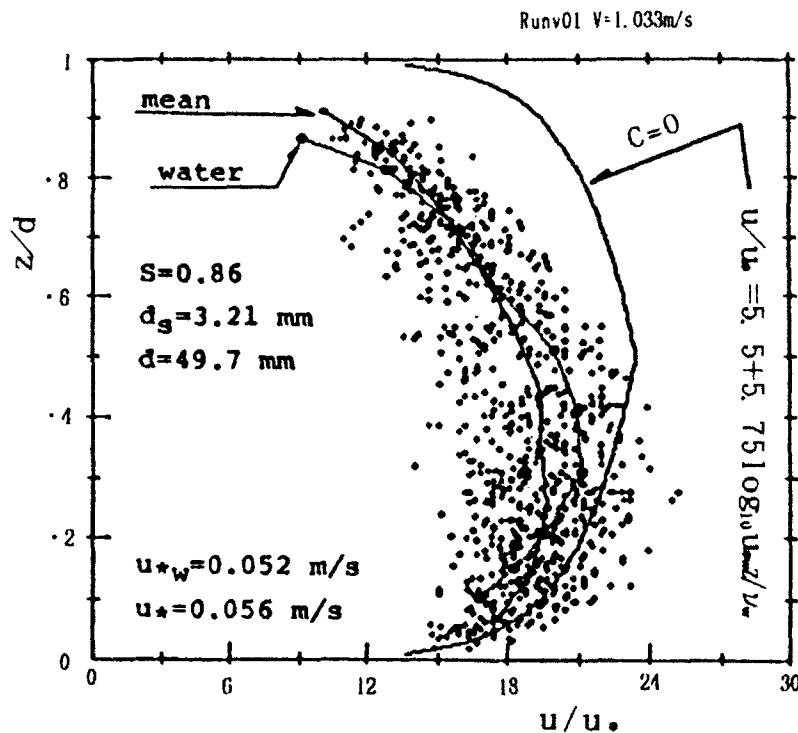
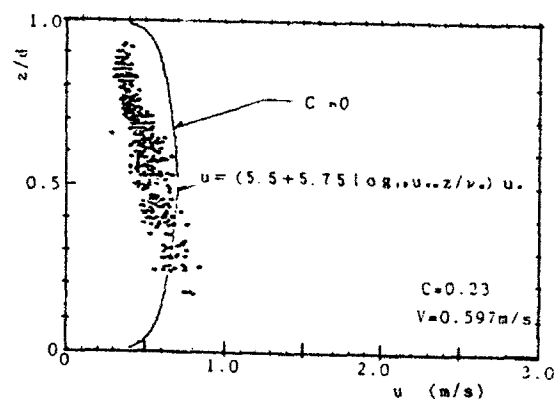
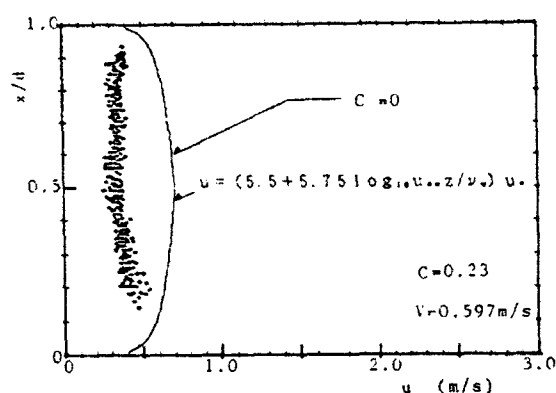


Fig.9 Particle velocities in vertical plane.

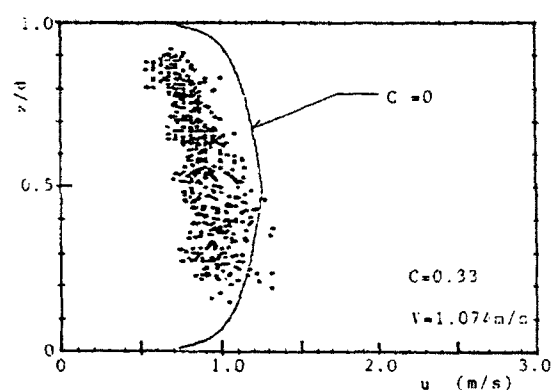
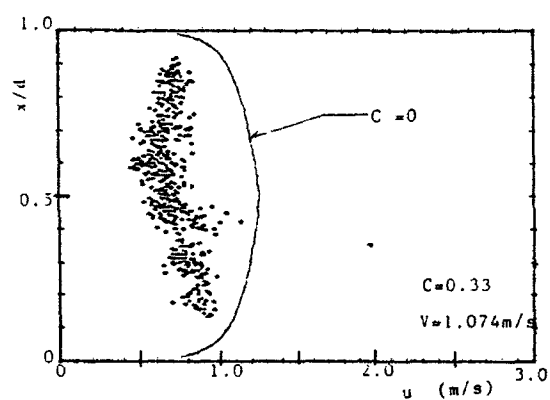
As shown in Eq.(1), the function F_{rm} is a parameter that represents the effects of the buoyant force in the flow field of the solid-liquid mixtures. Figure 6 shows that i increases as the value of $|1-S|$ increases. This means that i is directly proportional to $F_{rm} |1-S|$. Namely, the dominant parameter in solid-liquid mixture flows is not F_{rm} but Fr^2 .

Figure 7 shows the relationship between i and Fr^2 . It demonstrates that the i vs. Fr^2 results are linear except perhaps at the very lowest velocities. This characteristic of solid-liquid flows is represented clearly in Fig. 8. The figure suggests that, at velocities of 1 m/s and below, energy losses increase as the mean velocities decrease, and, at higher velocities, the hydraulic gradient is very similar to that at $C=0$, although the hydraulic gradient of snow-water flows is slightly larger than that of particle-water mixture flows. In snow-water mixture flows at velocities of 1 m/s and below, the i vs. V results are near those of turbulent pure water flows. This is due to solid concentrations which are less than 6% by volume.

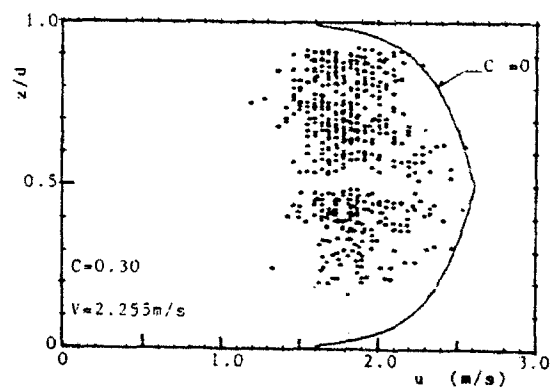
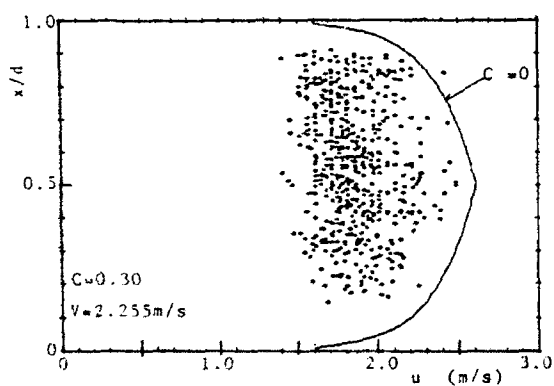
Figure 9 shows an example of particle velocity distributions obtained for a vertical plane, in which u_* is the friction velocity, ν_w is the kinematic viscosity and subscript w means water. The fluid velocity profile was measured with a Pitot tube. The profile perhaps represents the lowest limit value of the fluid velocity in mixture flows because the pressure head in the Pitot tube decreases due to particle collision with the top of



(a) Velocities in a horizontal plane. (b) Velocities in a vertical plane.
Fig.10 Particle velocities at lower velocities.



(a) Velocities in a horizontal plane. (b) Velocities in a vertical plane.
Fig.11 Particle velocities at middle velocities.



(a) Velocities in a horizontal plane. (b) Velocities in a vertical plane.
Fig.12 Particle velocities at higher velocities.

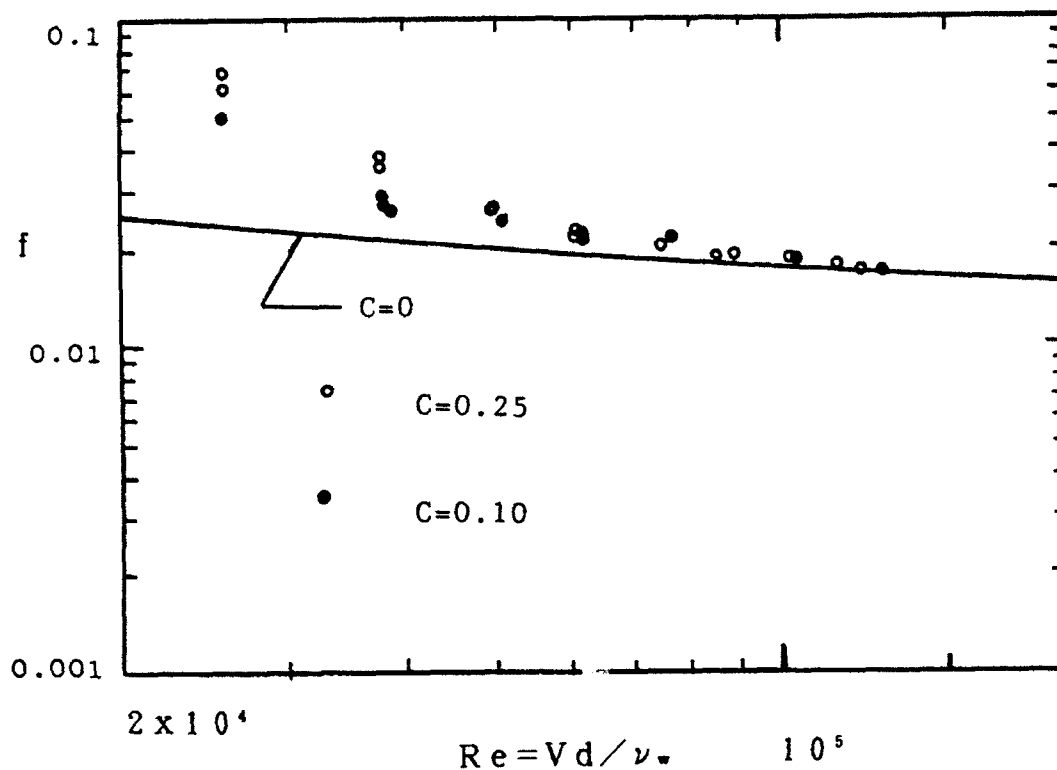
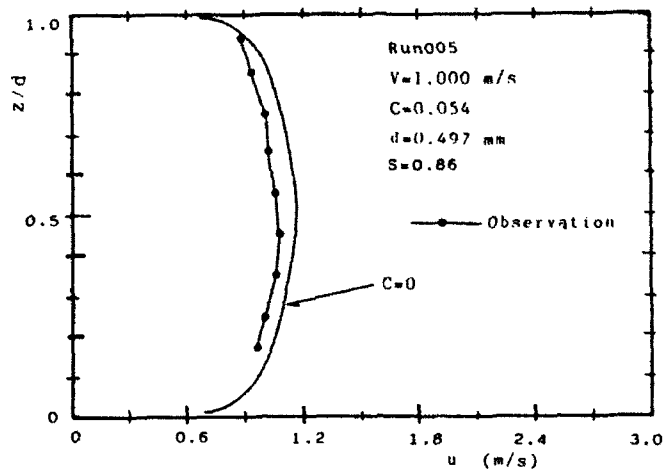


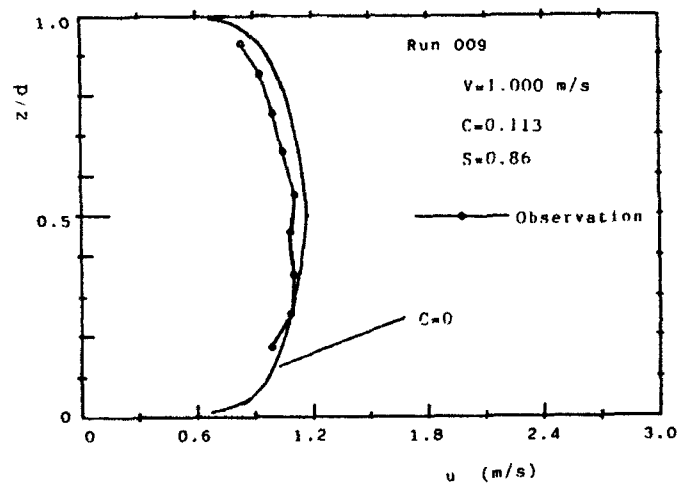
Fig.13 Relationship between friction factor and concentrations.

the tube. The solid line at $C = 0$ in Fig.9 shows the velocity profile of particles in the smooth turbulent flows, and the velocities pointed by term "mean" in Fig.9 are local velocities averaged within a small cross section given by dividing the cross section of the pipe into 10 equal parts. In comparing the velocity profiles of Fig.9, we see that particle velocities decrease in the upper region in which local solids concentrations are higher than in the lower region.

Figures 10, 11 and 12 display the particle velocities in solid-liquid mixture flows at the lower, middle and higher velocities, respectively, where x is the horizontal coordinate. These figures show that (1) velocity distributions obtained for a horizontal plane are nearly uniform and are hardly affected by a mean velocity decrease, (2) vertical velocity distributions vary, depending on the rate of velocity decrease, and the skew of the velocity profiles at lower velocities is considerable, thus the deformation of the velocity profile is the result of larger energy losses at lower velocities, and (3) slip velocities increase as the mean velocities increase; therefore, because the slip velocities are greater at higher velocities than at lower velocities, particle segregation and migration disappear as the mean velocities in the flow field of solid-water mixtures increase.



(a) Particle velocities at 5.4% solids by volume.



(b) Particle velocities at 11.3% solids by volume.

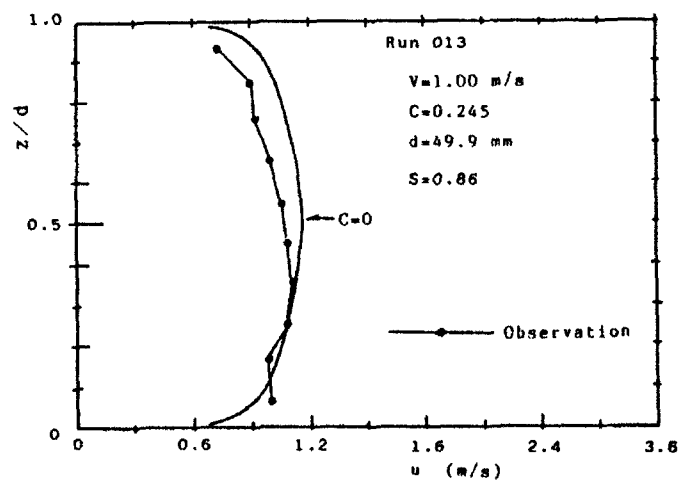


Fig.14 Particle velocities at the same bulk velocity for various slurry concentrations.

Figure 13 shows the relation between the friction factor f , and solid concentrations. The figure suggests that the higher the particle concentrations become, the larger the friction factor, especially in lower velocities.

To investigate the relationship between the friction factor and concentrations, we summarize the velocity profiles at the same velocity for various slurry concentrations. Figure 14 is an example of the results, in which only slurry concentrations are varied in experimental conditions. The figure reveals that the particle velocity profile skews gradually as concentrations increase. The deviation of the velocity distributions due to increased concentrations is the result of increased energy losses in solid-liquid mixture flows.

CONCLUSIONS

The characteristics of the behavior of particles in snow slurries and polystyrene particle slurries were studied experimentally. Using a high-speed video camera for visual observations, the particle velocity profiles and energy losses were examined in detail.

Within the scope of the present study, the following conclusions were derived using snow-water and polystyrene particle-water mixture flows in horizontal pipes:

- (1) Energy losses increased at lower velocities as velocities decrease, but at higher velocities, energy losses were close to that of turbulent pure water flows.
- (2) The particle velocity profiles in a vertical plane in lower velocities skewed considerably. The deformation of the profiles is the result of larger energy losses at lower velocities.
- (3) As the mean velocities increased, the higher the slip velocities became. The increase of the slip velocities eliminated the particle segregation and migration at higher velocities.
- (4) The particle velocity distributions in a horizontal plane were nearly uniform and were hardly affected by a mean velocity decrease.
- (5) The particle velocity profiles in a vertical plane deformed gradually as concentration increased. The deviation of the profiles due to the increased concentrations was due to increased energy losses.

ACKNOWLEDGEMENTS

We thank the Education Ministry of Japan for financial support of this work [Grant-in-Aid-for Scientific Research on Priority Areas 1991(03201137), Representative: Mikio Sasaki, Hachinohe Institute of Technology].

REFERENCES

- Sato T. and N. Shuto(1983a): The snow drain — a means of snow removal from city area — , Natural Disaster Science, Vol.5, No.1, pp.1-11.
- Sato T. and N. Shuto(1983b): Snow drain system — velocity formula for snow-laden water flow — , J. of Hydrosience and Hydraulics, Vol.1, No2, pp.9-16.

Mechanical Properties of High Water Content Snow

Shun'ichi Kobayashi, Kazoru Izumi, Yasuhide Ezaki and Masataka Tan

Research Institute for Hazards in Snowy Areas, Niigata University
Niigata, 950-21 Japan

ABSTRACT

High water content snow exists at boundaries between the roof and the snow, and between an impermeable ground and a snow cover. These snow avalanches caused by high water content snows. Therefore it is very important to understand the mechanical properties of high water content snow for prevention of these snow disasters. Two compression tests (tapping and uniaxial compression) were carried out to obtain some mechanical properties of the high water content snow. For the tapping tests the volume reduction rates by compression were decreased with increasing water contents up to saturation by water, and after saturation the reduction rates became constant. On the other hand, in the uniaxial compression test the breaking strength and the compressive viscosity were decreased. The breaking strength and the compressive viscosity were rapidly decreased with increasing water content. The snow showed a viscoelastic property up to water saturation, and a plastic property after the water saturation.

INTRODUCTION

Niigata Prefecture is known as one of the heaviest snowfall areas not only in Japan, but also in the world. The Asian winter monsoon from the Arctic brings heavy snow which is derived from the warm water of Japan Sea. Important characteristics of the snow in the Niigata area are its wetness and low strength. This snow frequently causes wet snow avalanches (Izumi, 1987), roof snow avalanches (they are of much higher frequency in the Niigata) and the slush flow or slush avalanche disasters that are rapid mass movements of water-saturated snow. Wakahama (1968) observed the metamorphism of snow immersed in water. According to the observations of Wakahama (1965, 1968, 1974), small ice grains are eliminated and the larger grains grow rapidly until they reach diameters in a range from 1 to 2 mm. This process is accompanied by a loss of strength between snow particles and an increase in density. Colbeck (1974, 1976, 1980) studied grain growth of wet snow theoretically. Tusima (1978, 1985) experimentally studied the grain

coarsening of snow particles saturated with pure water and Tusima and Raymond (1979) extended the study to impure water. They also analyzed grain coarsening as the process of growth and disappearance of grains caused by heat flow from relatively large grains to relatively small grain (Raymond and Tusima, 1979).

The above references to the metamorphism of wet snow suggest that a mechanical strength may be weakened and the compressibility of wet snow increased with increasing liquid water content. However, there are only a few works on mechanical properties under high water contents, e.g., Kinoshita (1963) and T. Kobayashi (1985). In order to clarify the mechanical properties of the high liquid water content snow, compression tests by tapping and uni-axial compression were carried out in a coldroom at a constant temperature, 0 °C.

METHODS

Tapping test

A simple compression test by tapping was applied to various kinds of wet snow. Mizuno and Kuroiwa (1966) studied the compression of dry snow by tapping. Figure 1 shows a tapping apparatus used in our experiments. Two cylindrical containers filled with snow particles were dropped repeatedly from two heights of 38 mm and 18 mm using an apparatus illustrated in Figure 1. As shown schematically in Figure 2, the initial volume of snow filled in the containers V_0 decreases exponentially with the number of taps N and tends finally to the definite value V_∞ . The equations have been defined for the strain of volume, γ and the number of taps, N (Mizuno and Kuroiwa, 1966):

$$\gamma = \frac{V_0 - V}{V_0} = \frac{a \cdot b^N}{1 + b \cdot N} \quad (1)$$

here V is the volume of snow at the tapping number N , and a and b are the numerical constants. Furthermore, Eq. 1 changes to the following form:

$$N/\gamma = \frac{1}{a \cdot b} + \frac{N}{a} \quad (2)$$

The Eq. 2 is presented schematically in Figure 3.

The numerical constants have the following physical meaning, namely, when N approaches infinity, then Eq. 1 becomes

$$\gamma_\infty = \frac{V_0 - V_\infty}{V_0} = a \quad (3)$$

As shown in Eq. 3, the constant a means the final strain of volume. Substituting of Eq. 3 into Eq. 1 gives,

$$b = \frac{V_0 - V}{N(V - V_\infty)} = 1/N_i \quad (4)$$

here N_i is the number of taps at which V equals to $(V_0 + V_\infty) / 2$.
Therefore the value b is closely related to the rate of compression by tapping.

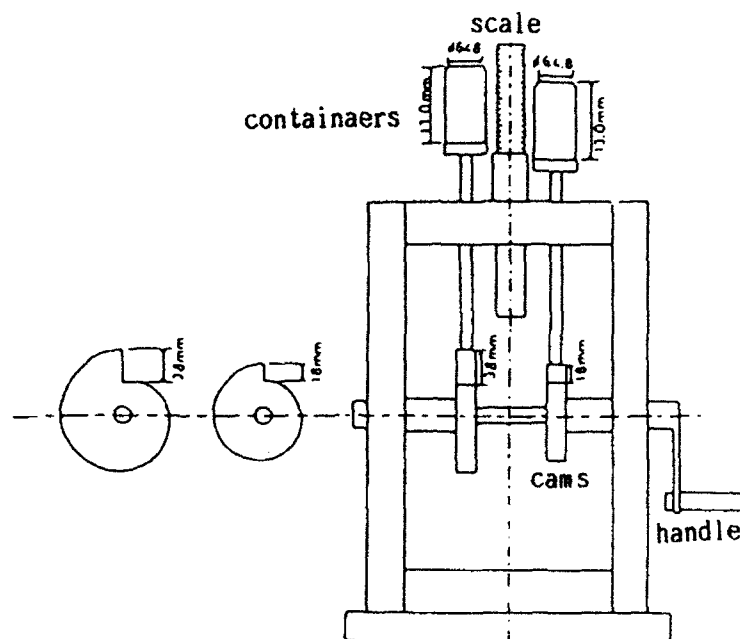


Figure 1. Schematic diagram of the equipment.

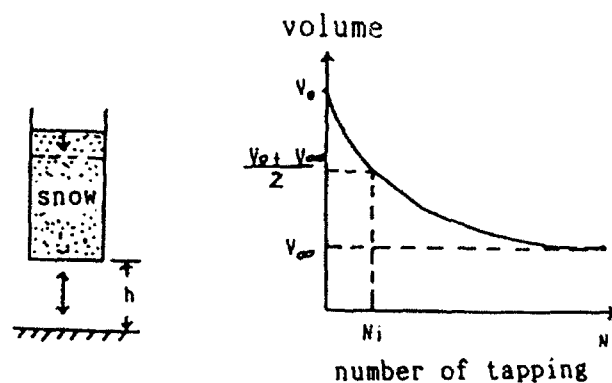


Figure 2. Schematic diagram of tapping.

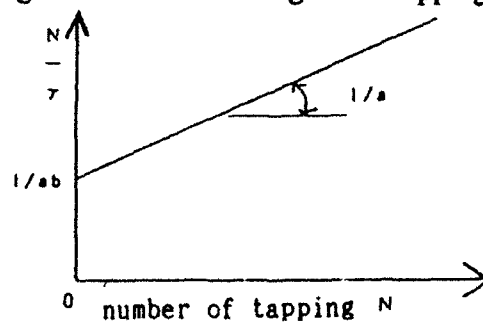


Figure 3. Schematic diagram of a relation between N/γ and N .

Uni-axial compression test

The snow pillars used in these experiments were 64.8 mm in a diameter and 131mm in an initial height, and the speed of compression was constant at 2 mm/min. The speed corresponds to a constant strain rate of $2.54 \times 10^{-3} \text{ sec}^{-1}$. The water with 0°C was added to the snow samples so that the weight ratio of water/snow of the samples reached the values of 0 % to 200 %. The compressive forces were registered electrically during the compression until the sample was compressed 30 mm. Figure 4 shows an example of the relation to the compressive force to the time in the case of new snow. In the figure the numbers mean weight ratio of water/snow in percentage. For a reference, the values of compressive strength were estimated from the force at a point of 15 % value of the strain. The compressive viscosity was calculated from our experiments using the following equation:

$$\eta = \sigma \rho / (d\rho/dt) \quad (5)$$

here η is the compressive viscosity ($\text{kPa} \cdot \text{s}$), σ is the compressive stress (kg/m^2), ρ is the snow density (kg/m^3) and t is the compressive time (sec).

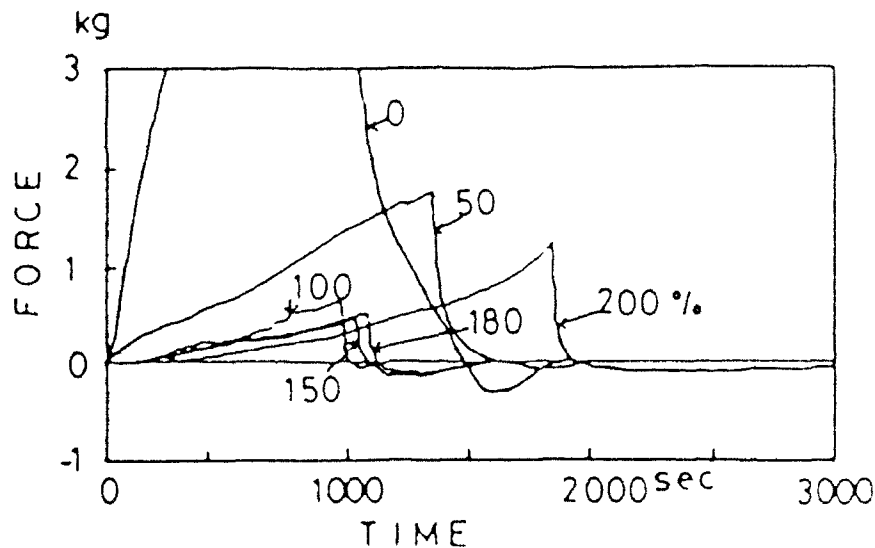


Figure 4. The relation of force to time (new snow)

EXPERIMENTAL RESULTS

Tapping compression test

The snow samples used in our tapping test are shown in Table 1. Four kinds of snow, i.e., new snow, compacted snow, granular snow and depth hoar snow, were used. The relation of snow density to tapping number in the cases of new snow and compacted snow is shown in Figure 5. In the figure the results of various liquid water contents are expressed in the case of two tapping

heights, i.e., (a) 38 mm and (b) 18 mm. From these results we can estimate the relation of N/γ to the tapping number N as shown in Figure 6, and the values a and b of various kinds of snow were determined from the inclinations of straight lines and the values of N/γ at which approaches zero in the figure (see Figure 3). Table 2 shows the values a and b of various snow samples under conditions of high liquid water contents. In general the numerical constants of various snow samples increased slowly with the increase in the weight ratio of water/snow.

Table 1. Snow samples used in tapping test.

	temp. (°C)	ρ (kg/m ³)	h (mm)	water content (%)
new snow	10	119	18	0, 50, 100, 150, 200, 220
		119	38	0, 50, 100, 150, 180, 200
compacted snow	10	218	18	0, 50, 75, 100, 125, 150
		218	38	0, 50, 75, 100, 125, 150
granular snow	0	417	38	0, 25, 50, 75, 100
	-10	429	38	0, 25, 40, 50, 60, 75
depth hoar	0	383	38	0, 25, 40, 50, 62.5, 75
	-10	392	38	0, 25, 50, 63, 70, 75

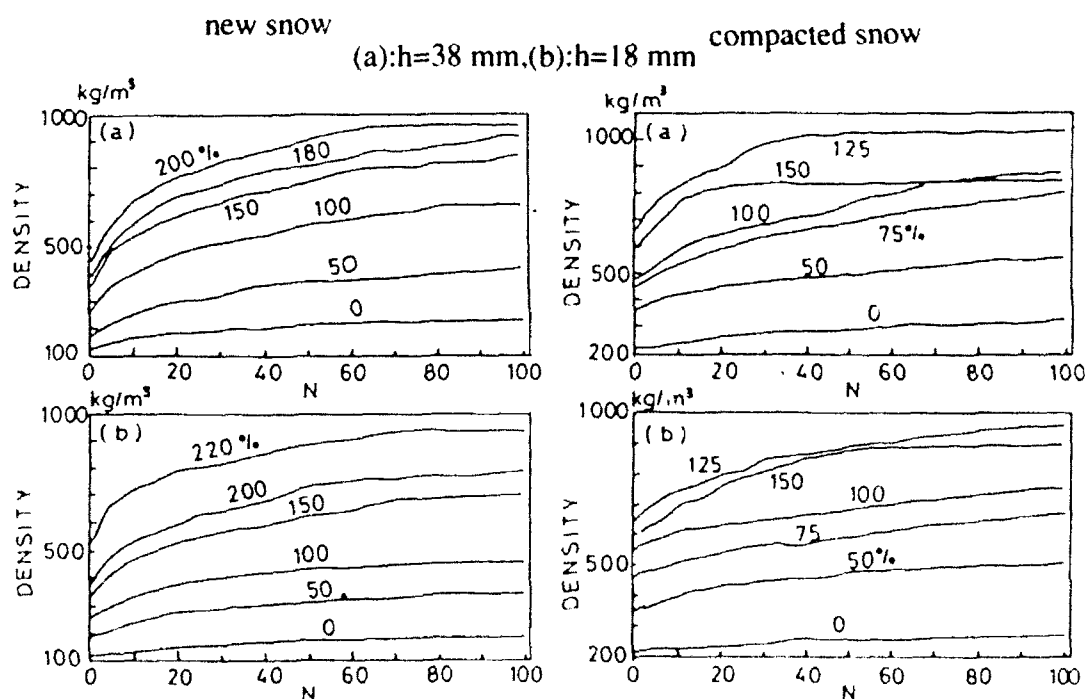


Figure 5. The relation of snow density to tapping number.

Uni-axial compression test

From Figure 3 the compressive force changed with time as shown by the curve in the figure, and the shape of the curve is almost the same as for plastic deformation (Kinosita,1960). However, the peaks corresponded to the forces at a point that the compression reached at 30 mm of the sample's length so that the force in wet snow is much smaller than that in dry snow.

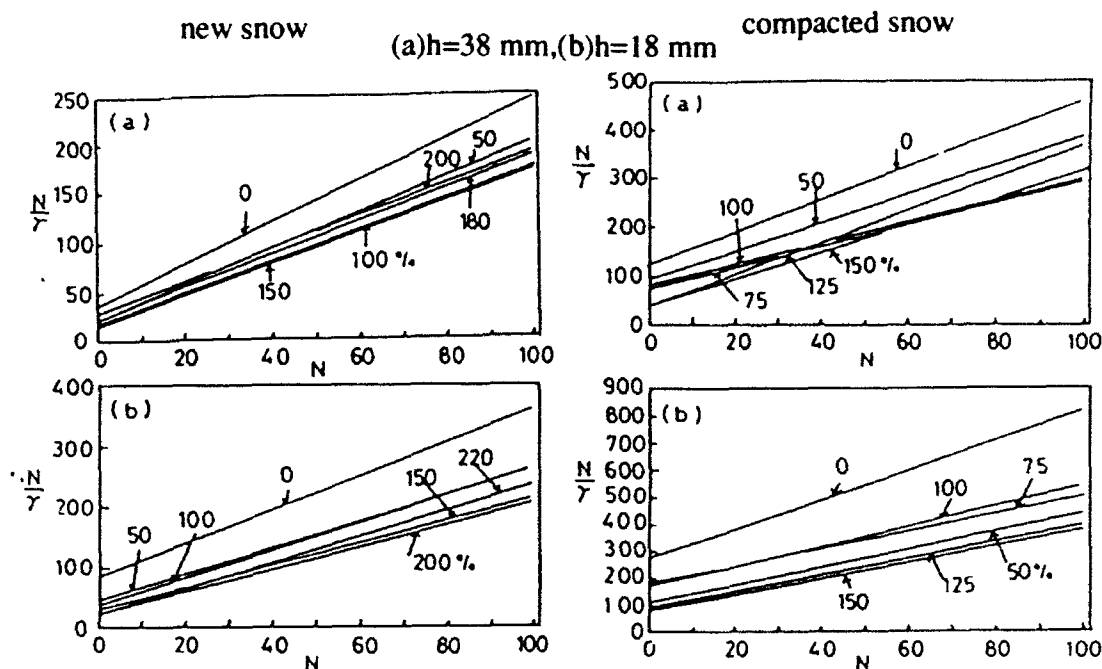


Figure 6. The relation of N/γ to tapping number N .

After the peak, the force decreased with increasing time because the load was released so that the force was also relaxed. Figure 7 shows the relation between the compressive strength at a point of 15 % strain and the snow density in the case of new snow and compacted snow. In the figure the unit of the strength is expressed. If we need a unit of stress then one should divide by 33 cm^2 of cross section of the snow sample. The compressive strength decreased quickly with increasing snow density which corresponds to the weight ratio of water/snow. Figure 8 also shows the relation between the compressive viscosity and the snow density. The compressive viscosity decreased quickly with increasing weight ratio of water/snow.

Kinosita (1963) discussed the compression of snow immersed in water of 0°C when the speed of compression was 2.9 mm/min . In his experiment, the density of snow before the immersion was 420 kg/m^3 , and the initial height and diameter of the snow pillar were 21.8 cm and 6.6 cm respectively. He also noted the relations between the compressive viscosity and the density of snow and showed that the viscosity decreases with increasing water contents and increases with increasing compressive speed.

Table 2. Numerical constants of various snow a and b.

(w:weight ratio of water/snow in %; h=tapping height)

(new snow)

W %	0		50		100		150		180	200		220
h mm	18	38	18	38	18	38	18	38	38	18	38	18
V_0 cm ³	428.5	428.5	428.5	428.5	431.8	425.2	431.8	431.8	418.6	421.9	426.9	408.7
V_{∞} cm ³	273.6	224.1	230.7	171.4	240.6	158.2	201.1	161.5	168.1	194.5	187.9	220.8
a	0.36	0.48	0.46	0.60	0.44	0.63	0.53	0.63	0.60	0.54	0.55	0.46
b	0.032	0.059	0.047	0.063	0.060	0.096	0.064	0.114	0.081	0.083	0.085	0.102

(compacted snow)

W %	0		50		75		100		125		150	
h mm	18	38	18	38	18	38	18	38	18	38	18	38
V_0 cm ³	431.8	431.8	431.8	431.8	435.1	435.1	431.8	431.8	425.2	421.9	431.8	431.8
V_{∞} cm ³	352.7	303.3	303.3	283.5	300.0	240.6	316.4	234.0	286.8	267.0	286.8	300.0
a	0.18	0.30	0.30	0.34	0.31	0.45	0.27	0.46	0.33	0.37	0.34	0.31
b	0.020	0.028	0.032	0.032	0.017	0.032	0.022	0.027	0.033	0.069	0.036	0.088

(granular snow)

W %	0		25	50	75	100	0	25	40	50	60	75
h mm	18	38	38	38	38	38	38	38	38	38	38	38
V_0 cm ³	431.8	431.8	428.5	428.5	428.5	428.5	428.5	428.5	428.5	428.5	428.5	428.5
V_{∞} cm ³	392.3	356.0	346.1	313.1	352.7	408.7	398.8	346.1	336.2	309.8	332.9	339.5
a	0.09	0.18	0.19	0.27	0.18	0.05	0.07	0.19	0.22	0.28	0.22	0.21
b	0.022	0.018	0.026	0.031	0.100	0.022	0.016	0.018	0.025	0.021	0.026	0.088
	store temp. 0°C						store temp. -10°C					

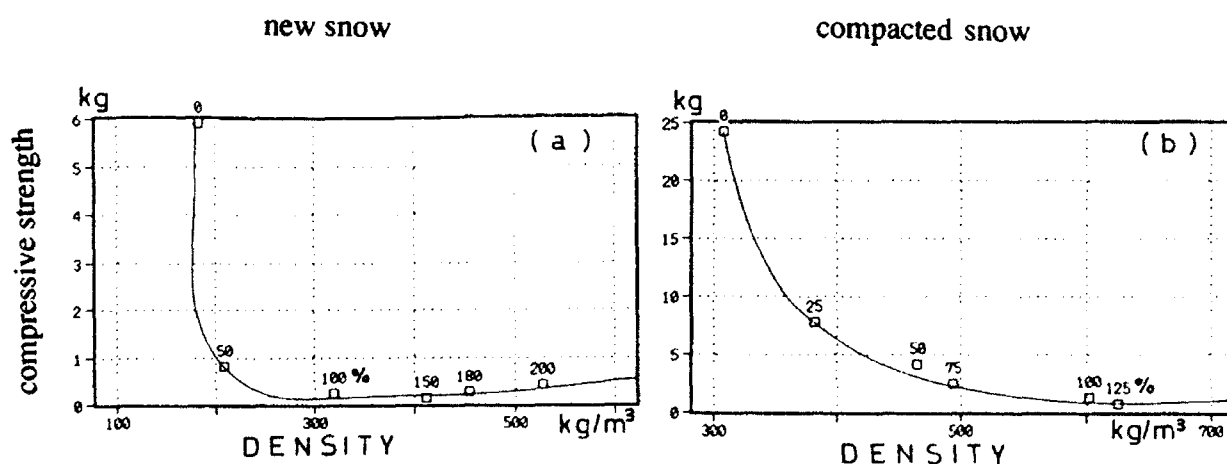


Figure 7. The relation of compressive strength at the point of 15% strain to the snow density or the weight ratio of water/snow.

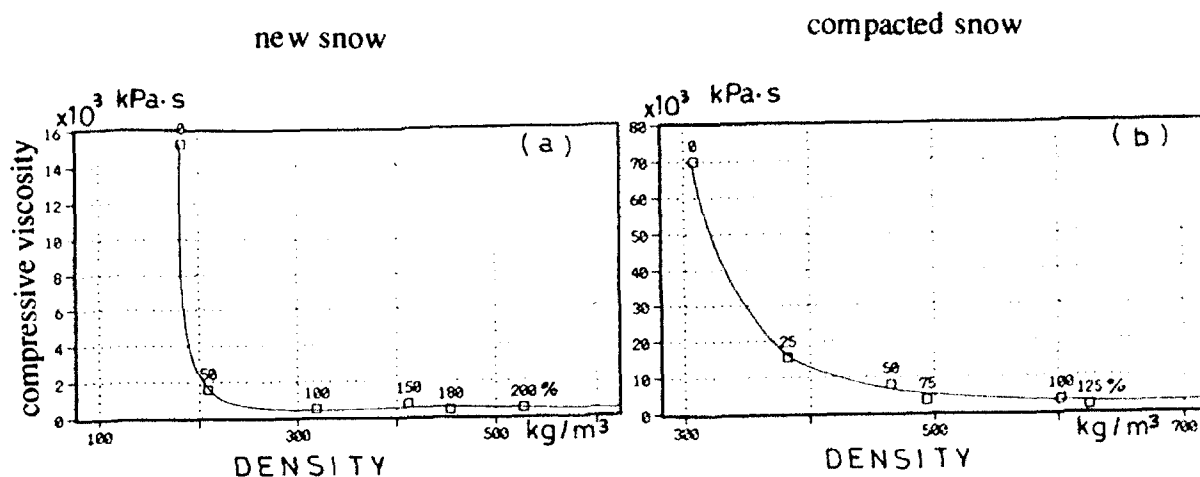


Figure 8. The relation of the compressive viscosity to the snow density or the weight ratio of water/snow.

CONCLUDING REMARKS

From the experiments with tapping tests and uni-axial compression tests of high water content snow, the following results were obtained:

- (1) The mechanical strength of deposited snow decreases with increasing water contents and the character of such snow will be changed from visco-elastic to plastic.
- (2) After the snow is saturated by water, the strength of such snow increases.
- (3) The compressive strength of wet snow increase with increasing initial dry snow density.

Moreover, it is more important to study the shear strength of water- saturated snow. Slush avalanches and slush flows are rapid mass movements of water- saturated snow and occur every year on the eastern slopes of Mt. Fuji in Japan, which causes deforestation near the timberline and natural disaster, (Anma et al.,1988). Recently some slush flow disasters also occurred in some small valleys, and people were killed by these slush flows. The biggest slush flow disaster in Japan was at Ohozikari, Aomori Prefecture, on March 22,1945. At that time, 88 people were killed and 2 Ohouses crushed by the slush flow. The shear strength of high water content snow must be known in order to research the mechanism of such slush flow occurrences.

REFERENCES

- Anma,S.,Fukue,M. and Yamashita,K.(1988)"Deforestation by slush avalanches and vegetation recovery on the eastern slope of Mt. Fuji,"International Symposion,INTERPRAEVENT,1988-GR AZ,Tagungspublikation,Band 2,Seite 133-156.
- Colbeck,S.C.(1974)"Grain and bond growth in wet snow,"International Association of Hydrological Sciences Publication ,No.114,51-61.

Colbeck,S.C.(1976)"Thermodynamic deformation of wet snow,"CRREL Report,76-44.

Colbeck,S.C.(1980)"Thermodynamics of wet snow metamorphism due to variations in curvature,"
Journal of Glaciology,Vol.26(94),291-301.

Izumi,K.(1987)"Studies on the hardness of wet snow and its decrease due to solar radiation
"Annual Report of Research Institute for Hazard in Snowy Areas, Niigata University,Vol.9,1-42
December 1987.

Kinosita,S.(1963)"Compression of snow immersed in water of 0 °C. 1,"Low Temperature
Science,Ser.A,21,13-22,(in Japanese with English Summary),December1963.

Kobayashi,T.(1985)"Vane shear strength of snow immersed in water(1)-Relation between vane
shear and immersion time,"Journal of the Japanese Society of Snow and Ice,Vol.47(2),55-62,
(in Japanese with English Summary),June1985.

Mizuno,U. and Kuroiwa,D.(1966)"Compression of snow particles by tapping," LowTemperature
Science,Ser.A,24,111-131,(in Japanese with English Summary),December1966.

Raymond,C.F. and Tusima,K.(1979)"Grain coarsening of water-saturated snow," Journal of
Glaciology,Vol.22(86),83-105.

Tusima,K.(1978)"Grain coarsening of ice particles immersed in pure water,"Journal of the
Japanese Society of Snow and Ice,Vol.40(4),155-156,December1978.

Tusima,K.(1985)"Grain coarsening of snow particles immersed in water and solutions,"Annals of
Glaciology,Vol.6,126-129.

Tusima,K. and Raymond,C.F.(1979)"Grain coarsening of snow saturated with solution,"Journal
of the Japanese Society of Snow and Ice,Vol.41(2),91-99,June1979.

Wakahama,G.(1965)"Metamorphism of wet snow," Low Temperature Science,Ser.A,23,51-66
(in Japanese with English summary),December1965.

Wakahama,G.(1968)"The metamorphism of wet snow,"International Association of Hydrological
Sciences Publication,No.79,370-379.

Wakahama,G.(1974)"The role of melt water in densification process of snow and firm",
International Association of Hydrological Sciences Publication,No.114,66-72.

Characteristics of Snow Pressure Acting on Avalanche-Preventive Fences

Katsumi Katakawa,* Chuichi Shimomura,[†] Mideya Ishikawa,**
Shunichi Hatae^{††} and Hiroshi Matsuda***

*Nakayama Steel Works, Ltd.

[†]Snow Research Center

**Nippon Steel Metal Products Co., Ltd.

^{††}Sumikin Metal Products Co., Ltd.

***Shinko Kenzai Ltd.

ABSTRACT

Japan is a heavy snow country, unparalleled in the world, and countermeasures against heavy snowfall have been taken by developing avalanche-preventive fences to protect public facilities such as roads and villages from snow avalanches.

For effective development and installation of avalanche-preventive fences, it is necessary to design these fences in consideration of the distribution form of snow pressure acting on avalanche-preventive fences.

Accordingly, the following examination was made:

- (a) By actually measuring snow pressure acting on avalanche-preventive fences in snowfall areas, a computation method of design load suitable for the characteristics of Japan's snow quality was examined.
- (b) A method of forecasting the form of the snow accumulated on avalanche-preventive fences, and a method of analyzing snow pressure acting on avalanche-preventive fences on the basis of the form of accumulated snow were developed as a means to easily survey the distribution form of snow pressure acting on avalanche-preventive fences. The measurement results obtained by these methods were examined in comparison with those of on-site observation.
- (c) Furthermore, using the results of (a) and (b), a design method based on the analysis results of snow-pressure distribution was examined.

1. DESIGN LOAD SUITABLE FOR JAPAN'S SNOW CHARACTERISTICS

1.1 Purpose of Survey

In Japan, the snow-pressure load acting on avalanche-preventive fences has traditionally been based on Swiss guidelines. After thaws, however, some fences are found damaged. This is presumably because Swiss glide factors for relatively low-density snow, which are not fully applicable for the relatively high-density snow seen in Japan, are used for designing avalanche-preventive fences. Accordingly, a field survey of glide factors suited for the characteristics of Japan's snow quality was made.

1.2 Method of Survey

A field survey of the snow-pressure load acting on avalanche-preventive fences and glide factors corresponding to slope conditions was made between 1987 and 1991 in the Joetsu district of Niigata Prefecture. The conditions of slopes surveyed are shown in Table 1.

Table 1. Conditions of slopes surveyed for snow pressure.

Location, structure symbol	Slope angle	Aspect	Vegetation of slope surface	Slope distance between structures
Eguchi A	35°	South	Long-bladed grass	18 m
B	35°	Northeast	Long-bladed grass	18 m
C	30°	South	Long-bladed grass	18 m
D	45°	South	Long-bladed grass	18 m
E	35°	South	Long-bladed grass	13 m
Doro A	40°	West	Bamboo	13 m
B	30°	West	Grass	10 m
C	35°	West	Grass	11 m
D	32°	West	Grass	24 m
E	35°	West	Grass	13 m
F	32°	West	Shrub	24 m
Uragawara	40°	South	Long-bladed grass	150 m
Matsunoyama	28°	Northeast	Long-bladed grass	20 m
Yamagata	32°	Northeast	Grass	25 m

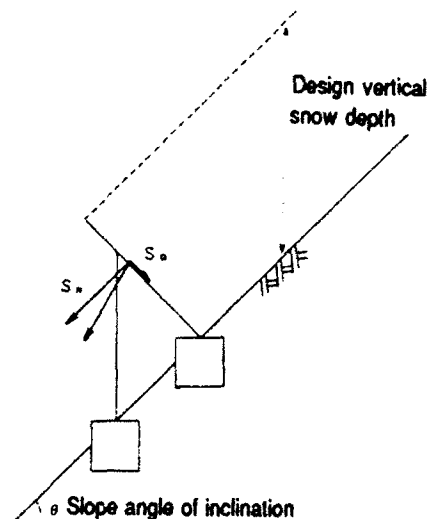


Figure 1. Snow pressure acting on avalanche-preventive fences.

Glide factors, N_2 , corresponding to slope conditions were calculated inversely from snow-pressure load by the following equation:

$$S_N = \gamma \cdot \frac{H^2}{2} \cdot K \cdot N_2$$

where S_N : component of the snow pressure parallel to the slope per unit length of supporting plane (t/m)

γ : average snow density of snowpack (t/m³)

H: snow depth measured vertically (m)

K: creep factor

1.3 Results of Survey

Glide factors, N_1 , in the Swiss guidelines are given in accordance with aspects and classes of soil, as shown in Table 2. Figure 2 shows the results of comparison of glide factors, N_1 , in the Swiss guidelines and glide factors, N_2 , obtainable from snow-pressure load. In this figure, the mark \bullet indicates the maximum of the differences between each N_1 and N_2 , and the straight line is the regression line of such maximum values. This indicates that values about 1.5 times the glide factors, N_1 , must be used in Japan. It is also clear from Figure 3 that the figure of about 1.5 times remains constant regardless of slope angles.

Table 2. Classes of soil and glide factor values.

Classes of soil	Values of glide factor, N_2	
	Aspect	
	North	South
Class I • big boulders ($d^* \geq 30$ cm) • terrain with more or less big outcroppings of rocks	1.8 (1.2)	2.0 (1.3)
Class II • surface covered with shrubs at least 1 m tall • well-exposed mounds covered by grass and tiny shrubs; the mounds must be at least 50 cm high • well-pronounced cow trails • boulder (d^* about 10-30 cm)	2.4 (1.6)	2.7 (1.8)
Class III • short grass with little shrubs (eric, rhododendron, calluna, alnus, shrub pines under 1 m in height) • small boulder ($d^* \leq 10$ cm) intermingled with grass and brush • only a few expressed mounds up to 50 cm tall overgrown by grass and little shrubs • grass with indistinct cow trails	3.0 (2.0)	3.6 (2.4)
Class IV • smooth, long-bladed grass • smooth outcropping rock plates with stratification planes parallel to slope • smooth scree mixed with earth • swampy depressions	3.9 (2.6)	4.8 (3.2)

d^* is the diameter of the blocks that determines the roughness of the soil surface.

Note: Figures in parentheses are those in Swiss guidelines.

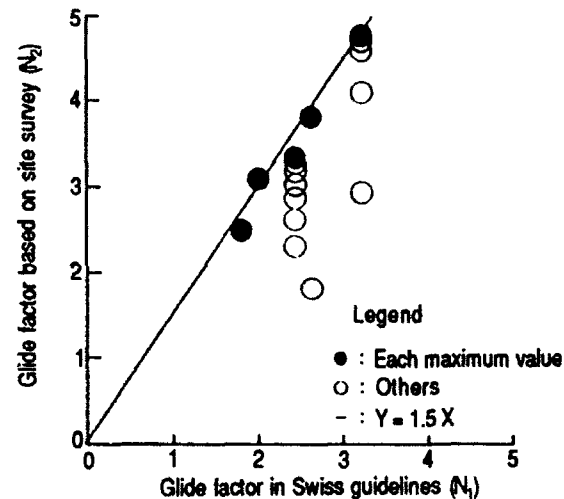


Figure 2. Comparison of glide factors.

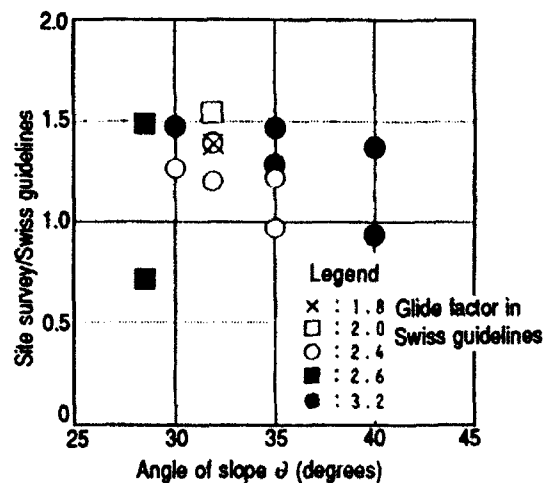


Figure 3. Glide factor and slope angle.

2. FORM OF SNOW ACCUMULATED ON AVALANCHE-PREVENTIVE FENCES

2.1 Purpose of Survey

For the analysis of snow pressure acting on avalanche-preventive fences, it is necessary to clarify the form of snow accumulated on the fences. Therefore, a method was proposed of forecasting the form of accumulated snow with a fluid theory, and the measurement results obtained by this method were compared with those of site measurement.

2.2 Method of Survey

The avalanche-preventive fences surveyed were on the upper part of a slope always exposed to winds. The situation is analogous to fences in a perfect fluid. The snow accumulated on the slope slides down slowly with the lapse of time, similar to the phenomenon in which a highly viscous fluid streams gently down a slope.

It was proposed to forecast the form of the snow accumulated on the avalanche-preventive fences from both the stream of a perfect fluid moving on and around the avalanche-preventive fences and the stream of a viscous fluid moving gently down a slope.

2.3 Results of Survey

Because the force of inertia is greater than gravity in a perfect fluid, and also because viscosity is greater than gravity in a highly viscous fluid, the following three equations hold for internal stress, p , and stream function, q , for both of these two streams:

$$\frac{\partial^2 p}{\partial x^2} + \frac{\partial^2 p}{\partial y^2} = 0 \quad \frac{\partial^2 q}{\partial x^2} + \frac{\partial^2 q}{\partial y^2} = 0 \quad \frac{\partial p}{\partial x} \cdot \frac{\partial q}{\partial x} + \frac{\partial p}{\partial y} \cdot \frac{\partial q}{\partial y} = 0$$

By analyzing these equations for a boundary condition with the slope and avalanche-preventive fences regarded as boundaries, and thus forecasting the form of the snow accumulated on the avalanche-preventive fences, the results as shown in Figure 4 were obtained. In this figure, C is the value given by the ratio of the vertical depth of the snow accumulated on an infinitely distant point of the slope to a design vertical snow depth for the avalanche-preventive fences.

Figure 6 shows the results of the examination of the

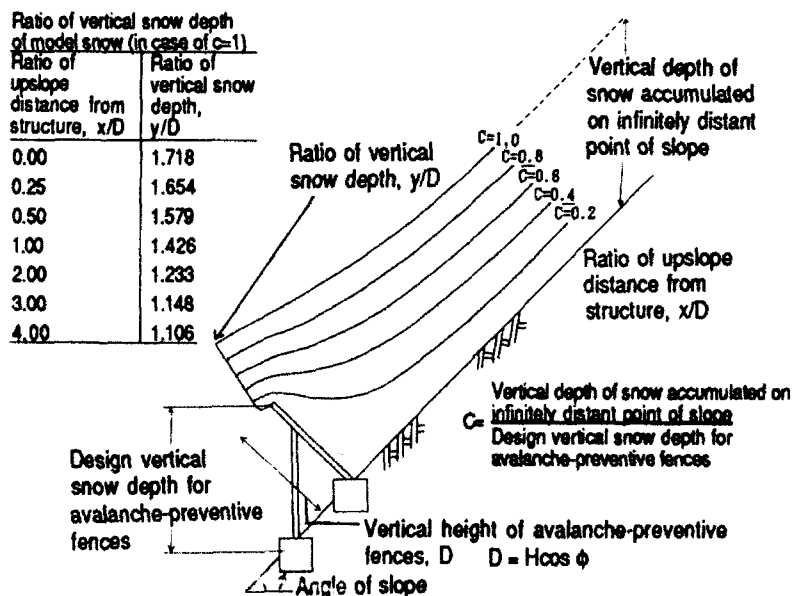


Figure 4. Form of snow accumulated on avalanche-preventive fences.

form of accumulated snow forecast by the fluid theory, as shown in Figure 4, in comparison with the results of site measurement of accumulated snow form (Figure 5). From this, it is evident that there is close agreement between the two results.

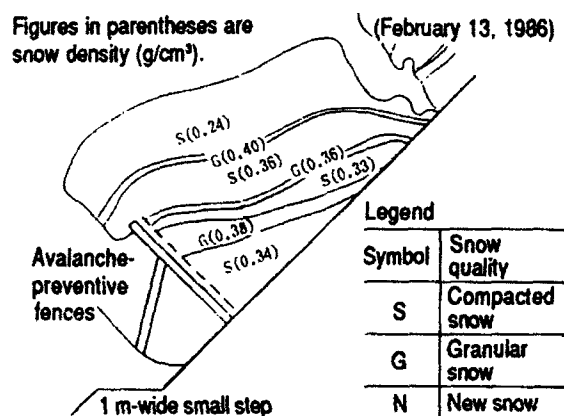


Figure 5. Results of snow cross-section measurement.

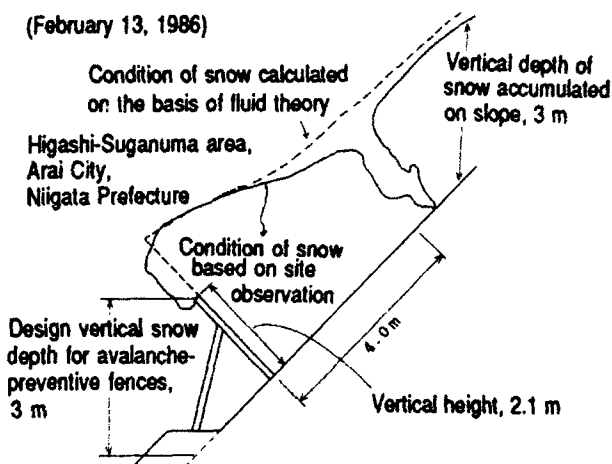


Figure 6. Comparison of forms of accumulated snow.

3. METHOD OF ANALYZING SNOW-PRESSURE DISTRIBUTION

3.1 Purpose of Survey

For surveying the distribution of snow pressure acting on avalanche-preventive fences, the most direct method is site measurement. But, since data on snow pressure are greatly affected by the weather and topographical conditions, collection of sufficient data for examination involves much time and huge costs. Accordingly, a snow-pressure simulation model using a three-dimensional finite element method was developed as a means to easily forecast the distribution of snow pressure on avalanche-preventive fences, and the measurement results thus obtained were verified by site measurements.

3.2 Method of Survey

The deformation of snow consists of elastic deformation as a solid property and plastic deformation as a liquid property. These properties can be approximated by the viscoelastic model as shown in Figure 7, and in the case of slow phenomena like a creep phenomenon, the ratio of change with time, $d\epsilon/dt$, of a strain, ϵ , is proportional to F/η_1 . Then, the snow accumulated on avalanche-preventive fences was divided into elements, and snow pressure acting on the fences was analyzed by means of the snow-pressure simulation model using the finite element method.

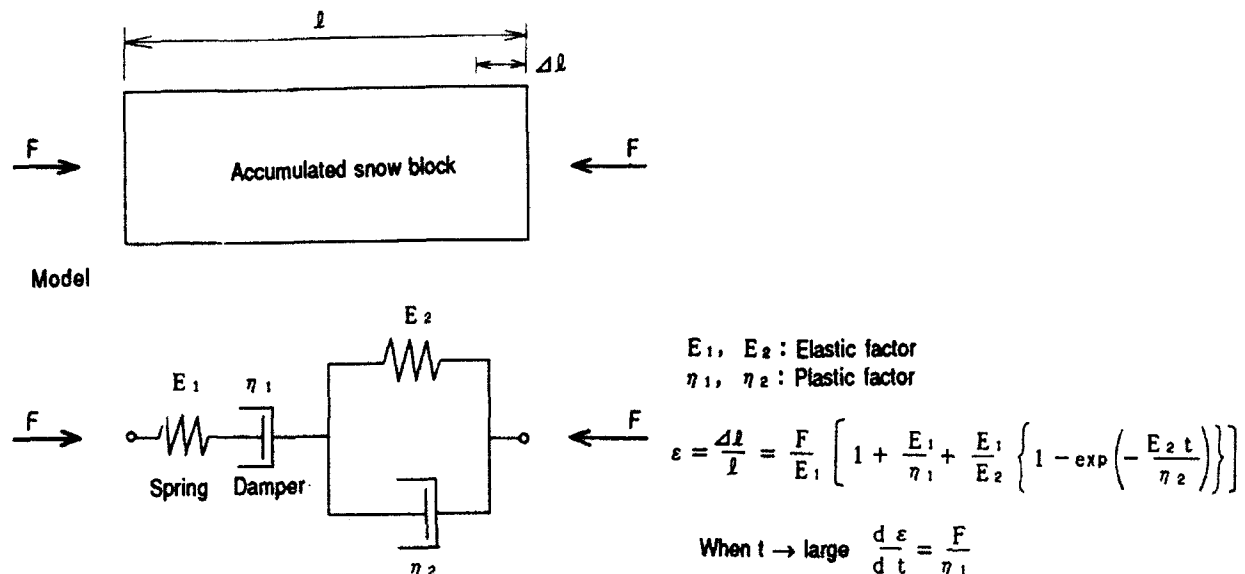


Figure 7. Viscoelastic model of snow.

3.3 Results of Survey

Snow in the state shown in Figure 5 was divided into elements, as shown in Figure 8, and snow pressure acting on avalanche-preventive fences was calculated using the snow-pressure simulation model. Two input factors in this computation were the form of snow and snow density. To ensure higher accuracy in the computation of snow pressure acting on the fences, the snow in the vicinity of the structures was divided into smaller elements, and the behavior of the snow (glide and creep) at the ends of the structures was reproduced for the computation. Figure 9 shows the computation results of snow-pressure distribution at section A-A in Figure 8, while Figure 10 indicates those at section B-B. These two results almost agree with the individual results of site measurement.

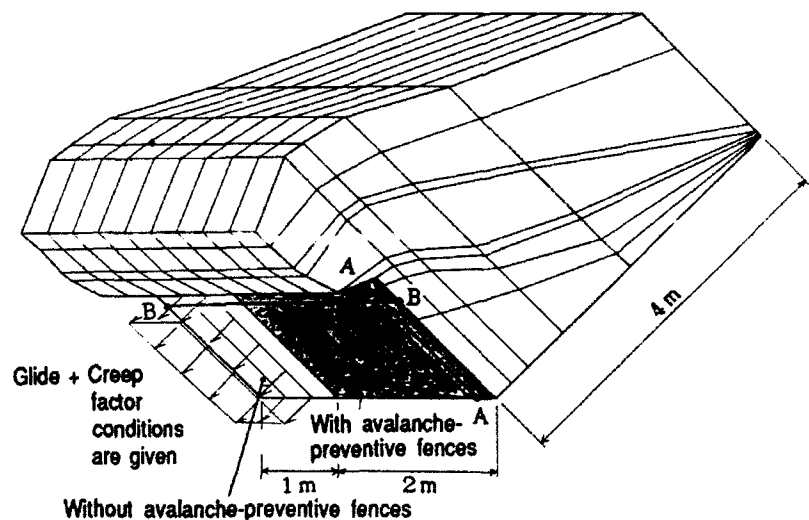


Figure 8. Divided elements used for snow-pressure analysis.

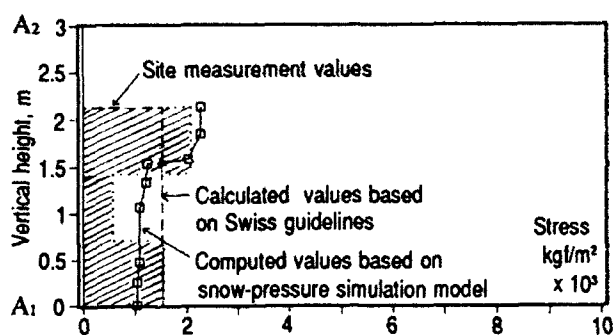


Figure 9. Snow pressure acting on avalanche-preventive fences (snow pressure distribution at section A-A).

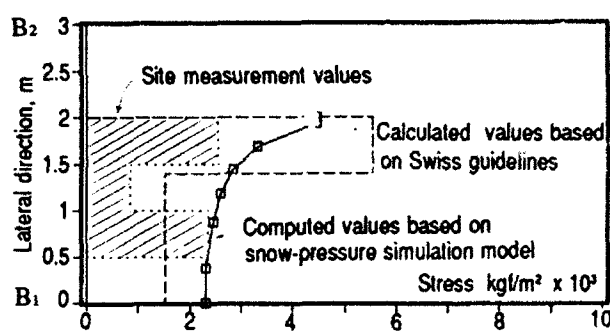


Figure 10. Snow pressure acting on avalanche-preventive fences (snow-pressure distribution at section B-B).

4. DESIGN METHODS BASED ON SNOW-PRESSURE DISTRIBUTION

4.1 Purpose of Survey

The best design method for avalanche-preventive fences is that based on the results of snow-pressure measurement at the site. But it is difficult to make site measurements in the case of great vertical snow depth and the like. The purpose of survey here was, therefore, to analyze snow-pressure distribution by use of the snow-pressure simulation model as described earlier and thus examine a more accurate design method.

4.2 Method of Survey

As for the distribution of snow pressure to be used for designing avalanche-preventive fences, the model snow forecast by the fluid theory was accumulated on avalanche-preventive fences and the distribution of snow pressure was examined in terms of the cases shown in Table 3, using the snow-pressure model. For the computation of the distribution, the slope was assumed to be of free-slip type, and forced glide and creep were created between the structures.

Table 3. Cases examined.

Factors	Range of examination
Design vertical snow depth	3, 4, 5 m
Angle of slope	30°, 40°, 50°
Snow density	0.30, 0.35, 0.40 t/m ³
Interval	1, 2, 3, 4, 5 m
Row space	3D, 4D, 5D, 6D
Inclination of structure	0°, 5°, 10°, 15°, 20°
Glide amount	Analysis undertaken assuming a free-slip slope, basically, and by varying glide amount

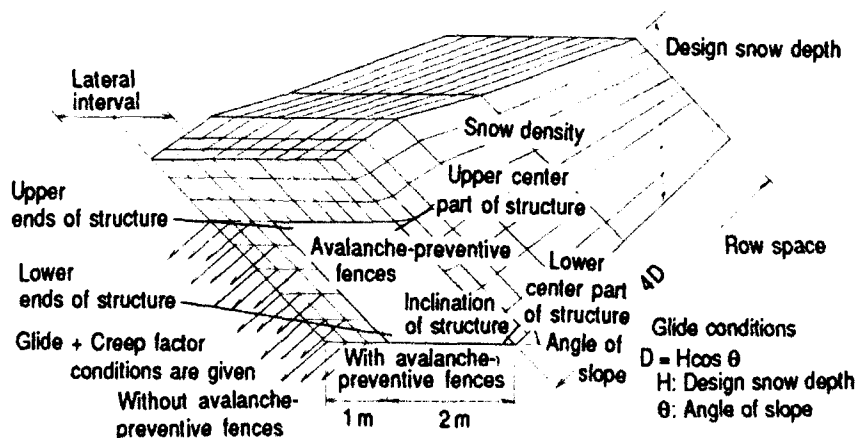


Figure 11. Factors in examination of distribution forms of snow pressure.

4.3 Results of Survey

Figures 12-15 show the computation results in the case of design vertical snow depth of 4 m, slope angle of 40 degrees, snow density of 0.35 t/m^3 , marshy slope with north aspect and interval (space between two structures measured across the slope) of 2 m. From this, it is considered that the adoption of Figure 16 as the distribution of snow pressure to be used for designing avalanche-preventive fences poses no problem.

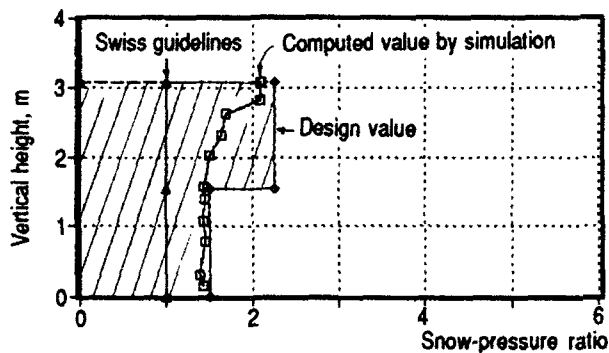


Figure 12. Snow-pressure distribution on avalanche-preventive fences (ends of structure).

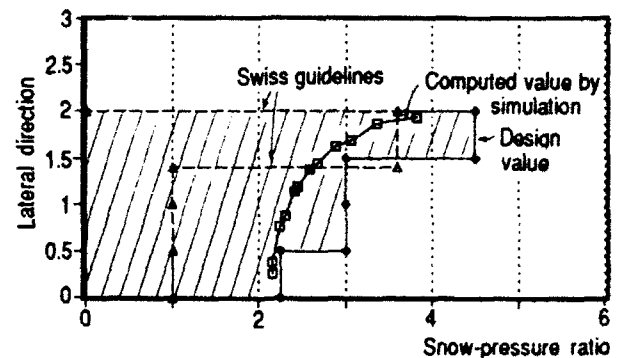


Figure 13. Snow-pressure distribution on avalanche-preventive fences (center part of structure).

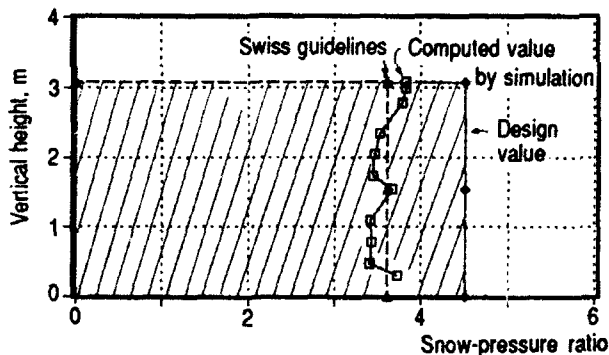


Figure 14. Snow-pressure distribution on avalanche-preventive fences (upper part of structure).

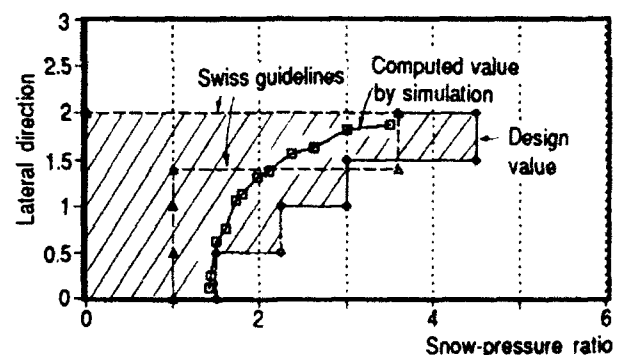
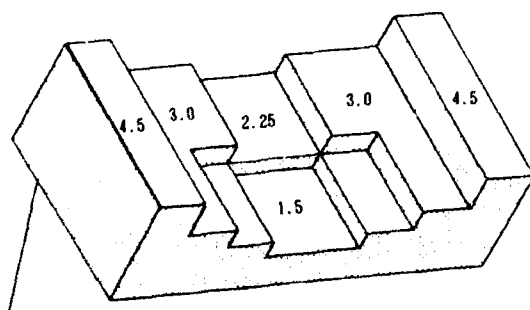
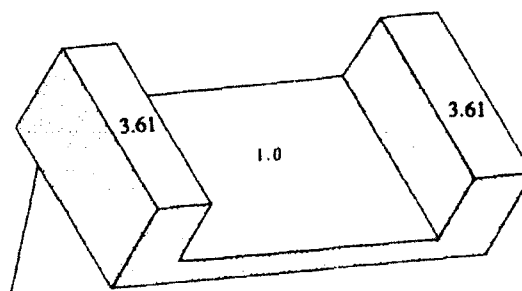


Figure 15. Snow-pressure distribution on avalanche-preventive fences (lower part of structure).



(a) Snow-pressure distribution as a result of examination



(b) Snow-pressure distribution in Switzerland (Swiss guidelines)

Figure 16. Comparison of design snow-pressure distributions.

It is confirmed that the design distribution of snow pressure shown in Figure 16 remains virtually unchanged, regardless of change in vertical snow depth, slope angle and snow density. It is also confirmed that Figure 16 meets the requirements for other factors, so far as the following requirements are satisfied.

- (1) Interval (space between the two structures measured across the slope): 2 m or less
- (2) Slope distance between structures: 5 times or less the vertical height of the structures

5. CONCLUSION

It was found through this research that, although it varies with slope angle and other factors, the snow-pressure load suited for the characteristics of Japan's snow quality is usually about 1.7 times the load calculated by the Swiss guidelines. This value is a result of both the reexamination of glide factors, leading to the figure of 1.5 times, and the reexamination of snow-pressure distribution.

The results obtained in this survey are expected to be put to practical use for preparing technical design guidelines for the installation of avalanche-preventive fences.

For reference purposes, this literature is part of the results of joint research by the Traffic Engineering Division and the Niigata Experimental Laboratory of the Public Works Research Institute, the Ministry of Construction and the Kozai Club, undertaken over a three-year period from 1989 to 1991.

Use of a Cold Energy Element in a Low-Temperature Storage System

Tetsu Suzuki

Professor, Niigata University
Niigata City, Japan

ABSTRACT

Utilizing winter's low temperatures, ice is manufactured in a box system built according to a specified constructional arrangement. Similarly, ice and snow may also be packed within the box system. As a whole, the system is laid out with multiple layers of covering which include rice hull materials that prevent heat entry. In addition, a special sheeting is used to reflect the sun's rays out of the system. The space created by this arrangement can then be used as a long-term low-temperature storage system. This paper, therefore, is aimed at giving an intermediate report of this low-temperature storage system, with an example of an ongoing in situ experiment.

1. INTRODUCTION

I wish to describe my recent work on the use of ice and snow. The world, including Japan as a part, contains vast cold regions. As such, during winter, a lot of cold energy from ice and snow can be obtained. This can be utilized to store foodstuffs such as potatoes, vegetables, etc., at a low temperature. However, melting occurs during spring, and while it is possible to continue the storage even during the summer season, the freezing facility, with its ability to prevent heat entry into the system, may entail a high initial cost. Likewise, in terms of electric consumption, running costs may also be high. In spite of these factors, utilization of cold energy for low temperature storage has great potential.

A prototype experiment on the use of ice is being conducted in Niigata University. Likewise, in Hokkaido and Asahikawa City, field facilities, measuring 8.5m X 8.5m X 2.5m, were also constructed and are now used for related experiments. China's Harbin City is also planning to start a similar experimental system to be operational by autumn this year.

2. METHODOLOGY

2.1. Construction of the Cold Energy Source (Fig. 1)

Using a container box made up of wood or related materials, we place a 10-cm thick layer of rice hulls on the inner bottom and vertical sidings. These rice hulls, having the ability to expand and contract, prevent heat entry into the box and are held in place by a waterproof sheeting. An appropriate quantity of water (about 5 to 10 cm deep) is poured into the box and allowed to freeze. The procedure is repeated until a big chunk of ice is produced. This serves as the basic

element of the cold energy. Likewise, in place of water, ice or snow can also be directly poured into the box.

2.2. Construction of a Low-Temperature Storage Space (Figs. 2 - 5)

In (A) of Fig. 2, an outline of the enclosure is illustrated. As shown in Fig. 3, the inside part is laid with the heat proofing materials (rice hulls with the sheeting). On the exterior side, a waterproof sheeting, which also reflects sunlight and ultraviolet rays, is used as a cover. The space, as enclosed by (A), can then serve as a low temperature storage space (B). The lower space in Fig. 4 and the upper space in Fig. 5 can, furthermore, be fully utilized. With the use of these extra spaces, a wider storage area can be achieved. Likewise, with the capability of (A) to be transported, its use as a family air conditioner or food storage system can be attained.

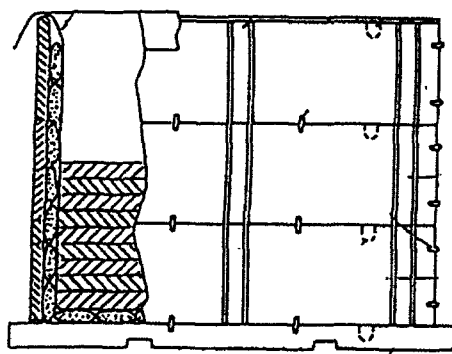


Fig.1 Cold energy source (A)

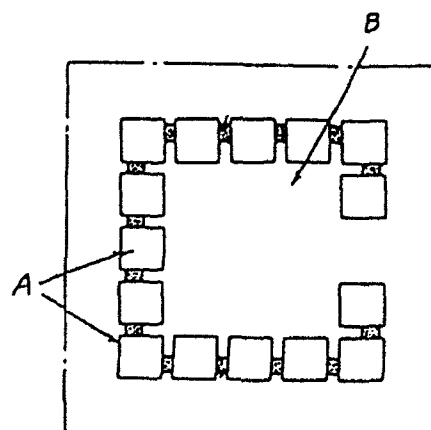


Fig.2 Plane figure

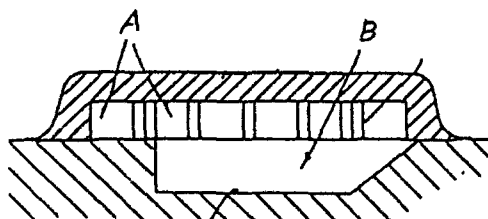


Fig.4 Vertical figure

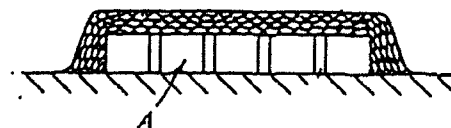


Fig.3 Vertical figure

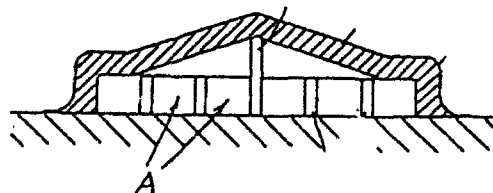


Fig.5 Vertical figure

3. IN SITU EXPERIMENTAL SAMPLE: ASAHIKAWA CITY

3.1. Overview of the Location (Figs. 6 -7)

Asahikawa City is located in Hokkaido - the northernmost island of Japan. It is an inland city characterized by subzero temperatures during winter. Manufacture of ice can best be

achieved during the winter season. However, a study on the degree of ice melting during summer is highly recommended. For this reason, Asahikawa City, which has a rather high summer temperature, has been chosen as the experimental site (Figs. 6 - 7).

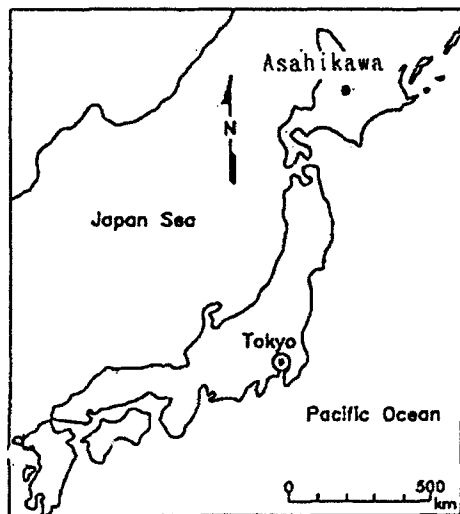


Fig.6 Map of Japan

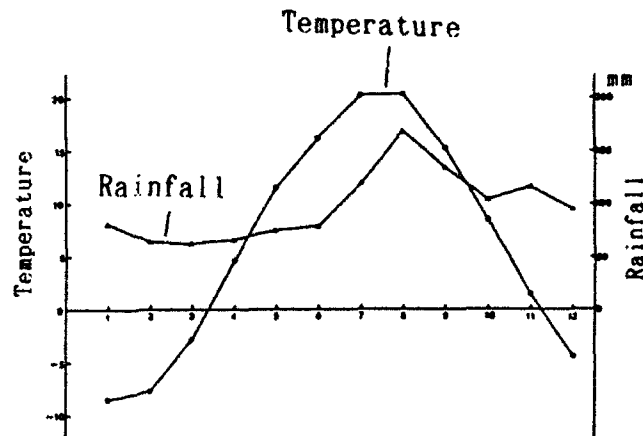


Fig.7 Average Temperature and Rainfall
(Asahikawa)

3.2. Arrangement of Cold-Energy Element (Fig. 8)

In the case of the Asahikawa project, a precast form or palette is used. The arrangement is as shown in Fig. 8.

3.3. Ice Manufacture

Due to the relatively warm winter season this year, and due to the fact that manufacture of ice was started in mid-February, a thickness of only 1.1 meters has been achieved.

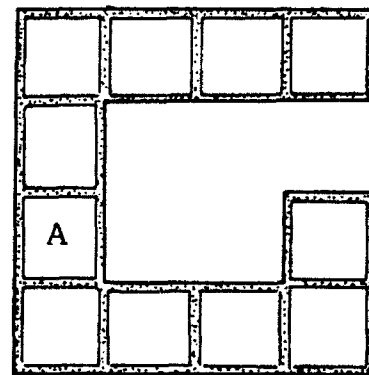


Fig.8 Plane figure

3.4. Structure of the Roofing System

To conform with experimental developments, the roofing system is built using constructional Types I to V.

3.5. Work Chronology

- ♦ Dec. , 1991 : Planning Decision.
- ♦ Jan. 25, 1992 : Project Started (construction of cold energy element and box system).
- ♦ Feb. 9, 1992 : Pouring of water for manufacture of ice.

- ♦ Feb. 26, 1992 : Construction of simple skeletal roofing system.
- ♦ March 20, 1992 : Placement of rice hulls on top of the skeletal roofing system (Type I).
- ♦ March 21, 1992 : Manufacture of last layer of ice. Total ice thickness reached about 1.1 m.
- ♦ April 6, 1992 : Placement of snow around the system periphery (Type II).
- ♦ April 21, 1992 : Type III construction.
- ♦ May 27, 1992 : Type IV construction.
- ♦ June 7, 1992 : Type V construction.

3.6. Influences in Type Variation

(A) Type I (Fig. 9)

Two layers of sheetings (upper and lower layers) are used as covering. However, when temperature is high, the temperature (11) on the surface of the upper sheeting and the temperature (10) under the upper sheeting are higher compared with the outside temperature.

(B) Type II (Fig. 10)

To reduce direct sun's rays by 50%, a shading net is placed on top of the upper sheeting. Using this method, temperatures (10) and (11) are decreased, approaching the outside temperature (12).

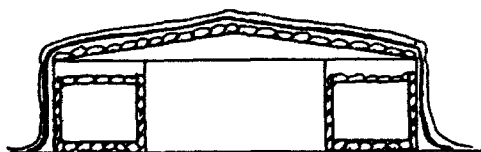


Fig.9 Vertical figure of Type I

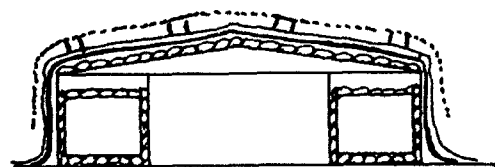


Fig.10 Vertical figure of Type II

(C) Type III (Figs. 11- 13)

With the two sheetings on top of each other, the heat that entered during the daytime will have the difficulty escaping during the nighttime. For this reason, rice hulls are placed between the two sheetings. When the outside temperature is high, the rice hulls' temperature (9) also increases. During nighttime, the outside temperature considerably decreases. However, the rice hulls' temperature does not have any substantial decrease.

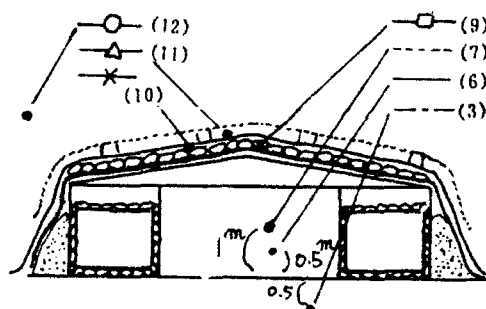


Fig. 11 Vertical figure

of Type III

(D) Type IV (Figs. 14

-15)

To decrease heat generated within the rice hulls, perforated pipes are placed underneath the rice hulls. Likewise, to minimize heat entry into the system, Styrofoam boards are placed on top of the lower sheeting. In spite of these innovations, there is no significant decrease in rice hulls' temperature during the nighttime. The cold-storage area, likewise, has a temperature increase.

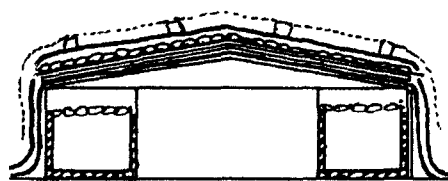


Fig. 14 Vertical figure

of Type IV

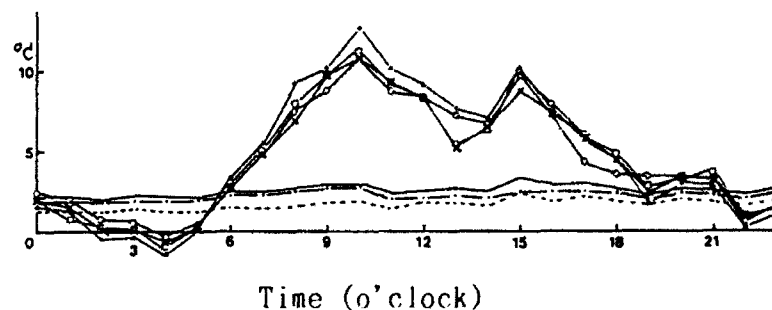


Fig. 12 Temperature (May 4)

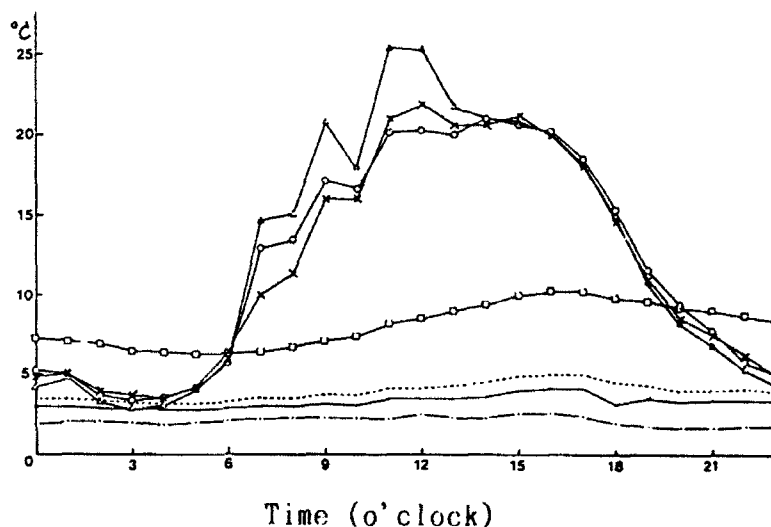


Fig. 13 Temperature (May 12)

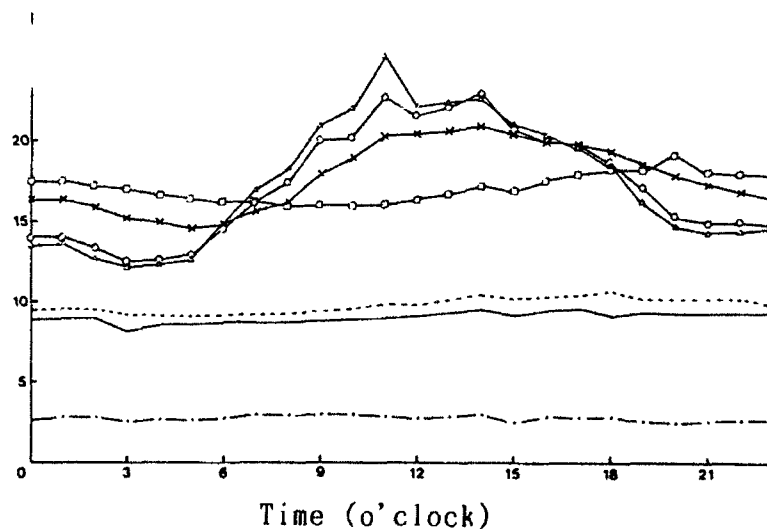


Fig. 15 Temperature (June 5)

(E) Type V (Figs. 16 - 17)

To allow proper circulation of air under the upper sheeting and within the rice hulls, which apparently have a higher temperature than the outside temperature, four sets of ventilators are placed on the topmost portion of the roofing system and perforated pipes are lined immediately under the upper sheeting.

Consequently, temperatures (10) and (11) start to decrease. Furthermore, to decrease the temperature in the inner cold-storage area, a part of the ice in the cold-energy element is exposed.

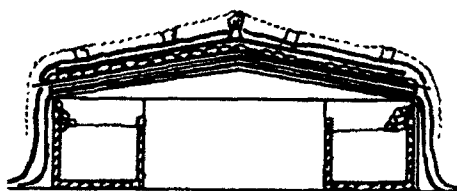


Fig.16 Vertical figure
of Type V

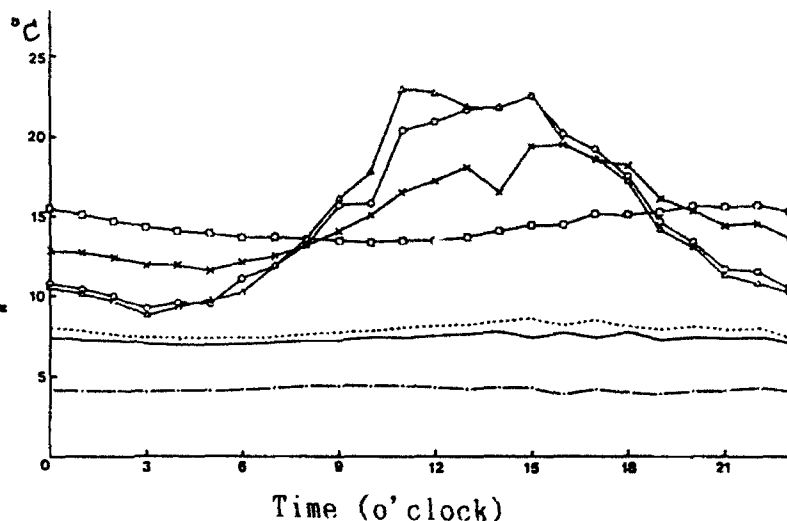


Fig.17 Temperature (June 16)

3.7 Ice Condition

From the overall perspective, at this point in time (June 17, 1992), ice has melted by 15%.

4. CONCLUSION

- (A) Total thickness of ice attained is 1.1 meters. About 80% is still being retained. The ice may last up to mid-July (Under ideal conditions, it may last up to early August).
- (B) If ice manufacture had been started in mid-January, a total thickness of 1.5 - 2.0 meters might have been achieved. This would last throughout the summer season.
- (C) If the setup had been done in a place where direct sunlight is minimal, e.g., the northern part of a hill or building, in a forest, etc., or if half of its height is embedded underground, more efficient results could have been obtained.
- (D) With proper improvement of the aforementioned simple methods, the following features can likewise be attained:
 - (1) It is easily built, readily extendable, reconstructible and transportable.
 - (2) It does not have any electric running cost.

- (3) Since it does not use any gas fuel, it is environmentally clean.
- (4) Since nature is the source, its use is sustainable ad infinitum. (Fossil fuel expires after a definite period of use, but ice and snow exist every year.)
- (5) Fossil fuel can be effectively used in areas other than low-temperature storage systems and, therefore, decreases environmental pollution and helps prevent global warming.
- (6) The project will be a boost to the development of the world's cold regions.
- (7) With the use of modern technology and with the world's cold regions as the project base, an ideal model for the construction of a low-temperature storage system can be developed.
- (8) As far as the cold-energy element is concerned, and in conformity with differences in the use of available materials, variations other than the box-type or container-type system can be used. For example, an air-mat container system can be utilized where the walls consist of materials that may be air inflated.

5. REFERENCES

- Kirkpatrick, D. L., M. Masoero, A. Rabi, C.E. Roedder, T.H. Socolow and T.B. Taylor (1985): "The Ice Pond - Production and Seasonal Storage Ice for Cooling", *Solar Energy*, 36, 5, 435-445.
- Kowata, H., Y. Sato, M. Nara, and S. Katayama (1989) "Ice Pond System for Application of Winter Coldness to Storage Cooling", *Proceedings of the Eleventh International Congress on Agricultural Engineering*, 2309-2316, 1989, Dublin.
- Vigneault, C. and H. McNicoll (1989): "Natural Ice Used to Refrigerate a Storage Building", *International Winter Meeting of American Society of Agri. Eng.*, Paper No. 89-1630.

7

Building Design

Ian Mackinlay, Chairman



*Seasonal features added to dwellings in Japanese snow country to create snow-free exterior spaces.
(Photographs by Ichiro Mizuno.)*

Design of North Cascade Visitor Center Located in Deep Snow Country

Robert G. Albrecht

Associate Professor, Department of Architecture
University of Washington, Seattle, Washington

ABSTRACT

A visitor center and rest room building were designed for Washington Pass in the Cascade Mountains of the State of Washington in the USA. The elevation of the site is 1670 meters. The buildings are to be located near the base of a moderate slope. Items which were considered in the design were roof design for heavy snow loads (13.1 kN/m^2), settlement forces due to the possibility of snow drifting over the entire building during the course of the winter, snow creep and glide forces from snow on the surrounding terrain since the buildings are to be located near the base of a slope, hydrostatic pressure due to snow against light framed walls, lateral forces on roof projections due to snow and the slope of the roof, and the consideration of the percent of the snow load which should be added to the building dead loads for seismic calculations.

INTRODUCTION

The North Cascades Highway is a scenic road through the Cascade Mountains of Washington State. It is open for travel only during the late spring, summer and early fall. One of the most scenic spots along this highway is a broad pass named Washington Pass located between the Granite Creek and Early Winters Creek drainages at an elevation of 1670 meters. At present there is a very limited visitor facility with a small display area and inadequate toilet facilities. The U.S. Forest Service requested the design of a visitor center building and a rest room building to be located

at this pass. The visitor center building is oriented with its long axis east-west so that it faces south toward the spectacular view of Early Winters Spires and the upper reaches of the Early Winters Creek drainage.

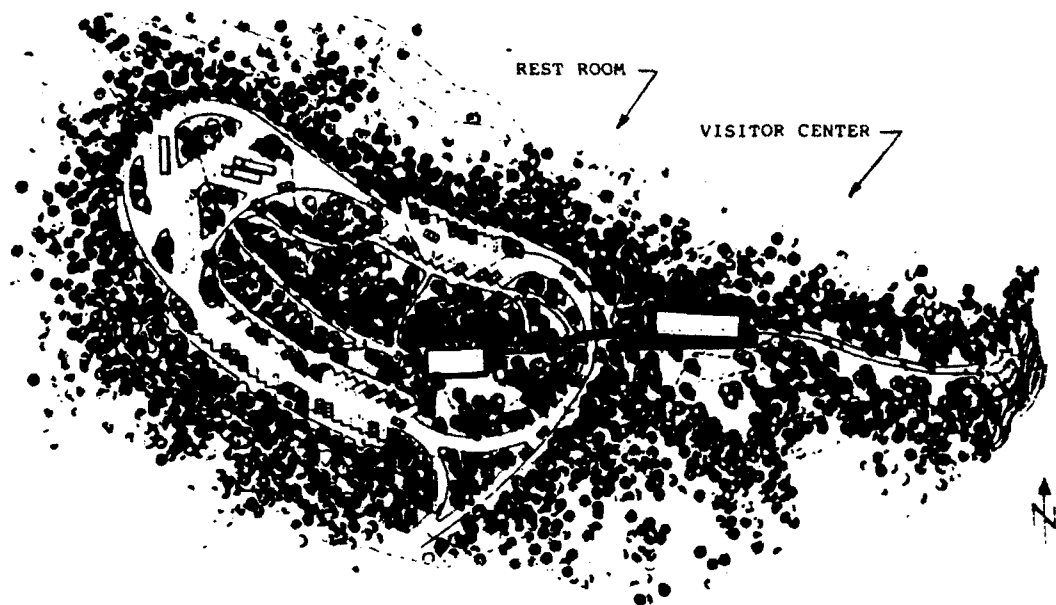
Both the visitor center building and the rest room buildings are lean-to form with a sloping shed roof supported at the low end by a wall and at the high end by columns. The heavy snow loads are carried by timber decking, large glued laminated beams and glued laminated columns. Lateral forces are primarily resisted by the reinforced concrete walls on the low side. A site plan for the visitor complex is shown in Figure 1. The visitor center building is on the east side of the site while the rest room building is on the west side of the site. A perspective sketch of the visitor center is shown in Figure 2. A photograph of the model of the visitor center building is shown in Figure 4.

SNOW PROBLEMS

The following is a quotation from the U.S. Forest Service advertisement for the design of the visitor center facility: "Washington Pass experiences temperatures from minus 30 degrees Fahrenheit (minus 34 degrees Centigrade) to 90 degrees Fahrenheit (32 degrees Centigrade). The average winter snow load is 243 pounds per square foot (11.6 kN/m^2), with a high of 275 pounds per square foot (13.1 kN/m^2). The station will be unheated throughout the winter. Washington Pass, 5477 feet elevation (1670 meters), is four miles (6.7 kilometers) from the Cascade Mountain divide: sometimes its weather follows the dry, sunny east-slope pattern, other times the pass experiences the overcast and precipitation of the western slope. The amount of sun and of snowfall varies widely from year to year." With this statement in mind, after study of the contour map and the architect's proposed organization of the site, the following snow country problems were identified:

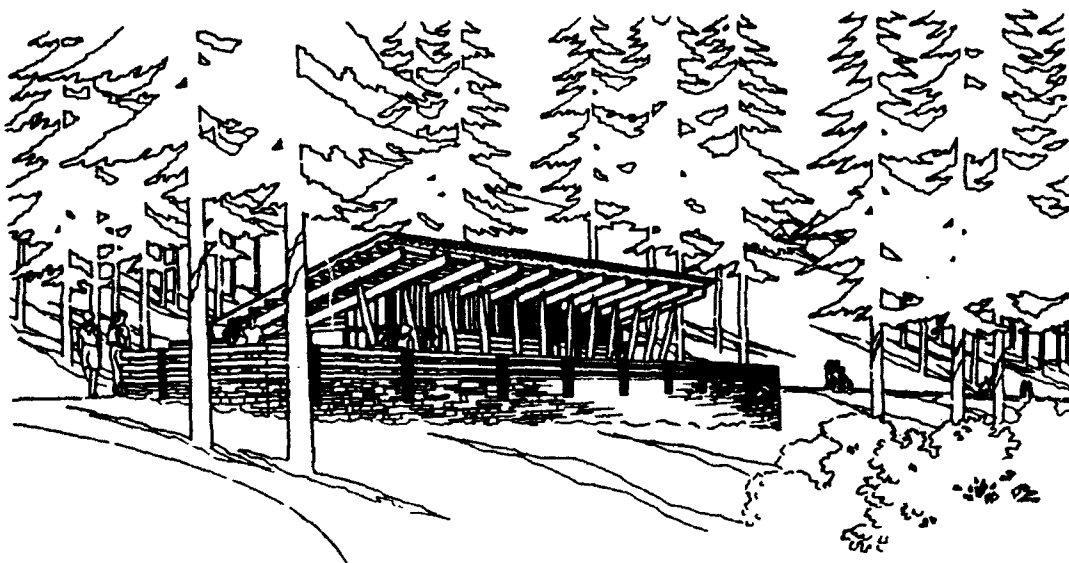
HEAVY SNOW ON THE ROOF:

Whereas the snow load of 13.1 kN/m^2 is not exceptional by Cascade Mountain pass standards (the snow load at Stevens Pass is 19.1 kN/m^2), the snow load at Washington Pass requires a considerable expenditure



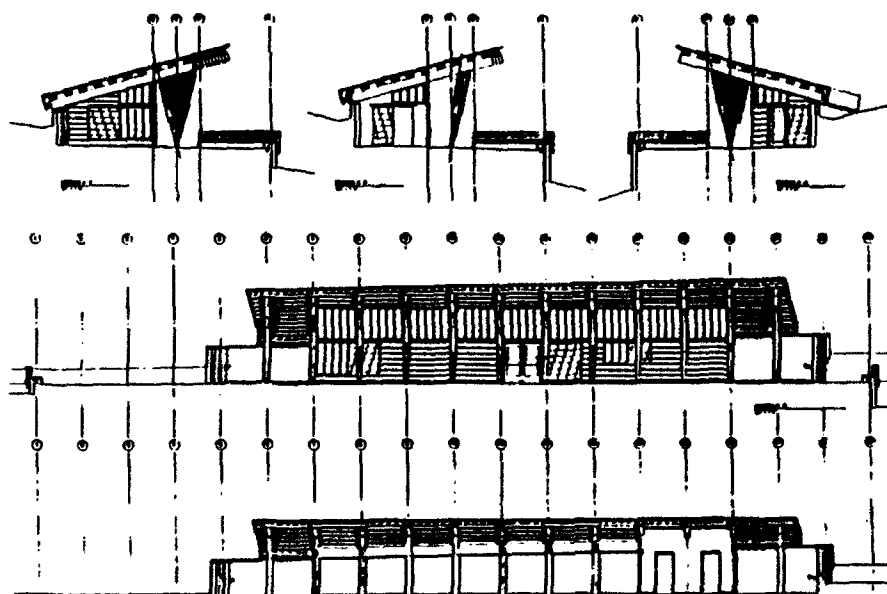
WASHINGTON PASS VISITOR CENTER
WINTHROP RANGER DISTRICT OKANOGAN NATIONAL FOREST, WASHINGTON

Figure 1



WASHINGTON PASS VISITOR CENTER

Figure 2



VISITOR CENTER BUILDING - SECTIONS

Figure 3

for the vertical load-bearing structure. The roof decking, purlins and beams are much stronger than one would expect to find in a typical Puget Sound Basin type structure. Not only are the purlins and beams heavy but the connections are also large. All of these elements will play a part in the appearance of these buildings.

SETTLEMENT PRESSURES:

At Washington Pass the expected snow depth under maximum snow conditions could be from 6.7 meters to 7.6 meters. Even though the highest point on the roof of the proposed visitor center is 5.2 meters above the ground, a strong connection between the ground snowpack and the roof snowpack could exist under deep snow conditions. When settlement occurs either due to thawing or spring conditions, this connection between the roof and ground snowpack can cause additional loading of the roof at the edges. A visitor center building in Mt. Rainier National Park which was located at approximately the same elevation as Washington Pass was severely damaged in 1950 due in part to snow settlement forces. Snow settlement forces were considered in the structural design of both the visitor center building and the rest room building, particularly in the areas of the overhanging roof.

SNOW CREEP FROM THE SURROUNDING TERRAIN:

Whenever snow lies on an inclined surface, it tends to creep downhill over periods of time. Buildings, particularly buildings kept unheated during the winter months, have been known to suffer horizontal displacements due to snow creep and glide where the average slope above the building has been less than fifteen degrees. At Washington Pass the slope from the proposed visitor center to the top of the east ridge of Cutthroat Peak is somewhat steeper than an average of 20 degrees. The visitor center building is located near the base of the slope and has the least amount of tree cover on its uphill side. The possibility of snow creep and glide forces was considered in the layout of the building. As shown in Figure 3, the wall on the uphill (north) side of the visitor center is a reinforced concrete cantilever

retaining wall. This north wall becomes essentially "dug into" the slope thus presenting very little surface area to incur snow creep forces. The existing fringe of trees shown on the site plan (Figure 1), will also provide some protection from these forces and will tend to eliminate forces due to glide. As shown on the site plan, the rest room building is proposed to be located about 67 meters from the base of the slope. There are two bodies of existing trees between the building and the base of the slope. Because of this protection, it was considered permissible to orient this building with its open side to the north (base of the slope). As shown in Figure 8, a low reinforced concrete wall is located on the north side of the building and should serve to block out any glide forces.

SNOW PRESSURES AGAINST LIGHT FRAMED WALLS:

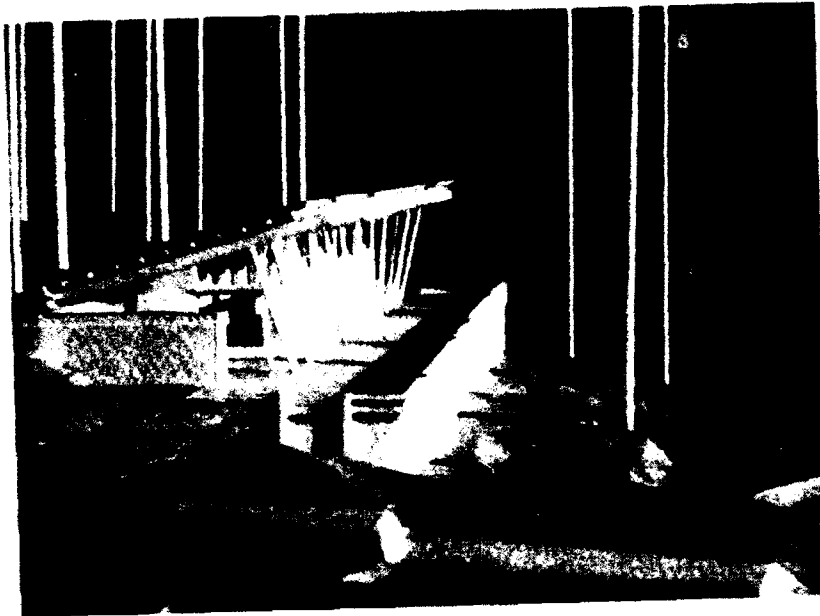
The light framed walls in both the visitor center building and the rest room building were designed to resist hydrostatic pressure due to snow.

LATERAL FORCES DUE TO SNOW ON ROOF PROJECTIONS:

Probably the least well-resolved problem with regard to snow forces is the large vent stack for the composting toilet located in the center of the shed roof of the rest room building (Figure 5 and Figure 7). Upon noting the location of this projection and its vulnerability to lateral forces due to snow, I requested that its location be changed. I was informed that the location of the vent stack was central to the architect's design. Furthermore, the composting toilet manufacturer informed the architect that the vent stack had frequently been put through the roof in other U.S. Forest Service installations. When I asked to see examples, I was sent a sketch of roof with the composting toilet vent stack located at the ridge of a gabled roof (where it should be).

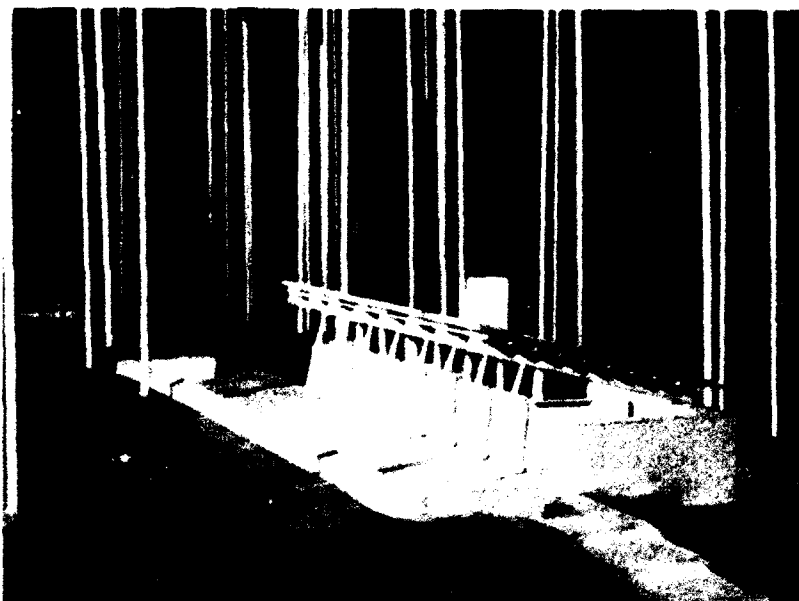
Since relocating the stack was an option which was not available, the courses of action considered were:

1. Build a splitter at the uphill edge of the stack. Since the roofing membrane is to be a standing seam metal roof, a splitter would not work very



WASHINGTON PASS VISITOR CENTER

Figure 4



REST ROOM BUILDING

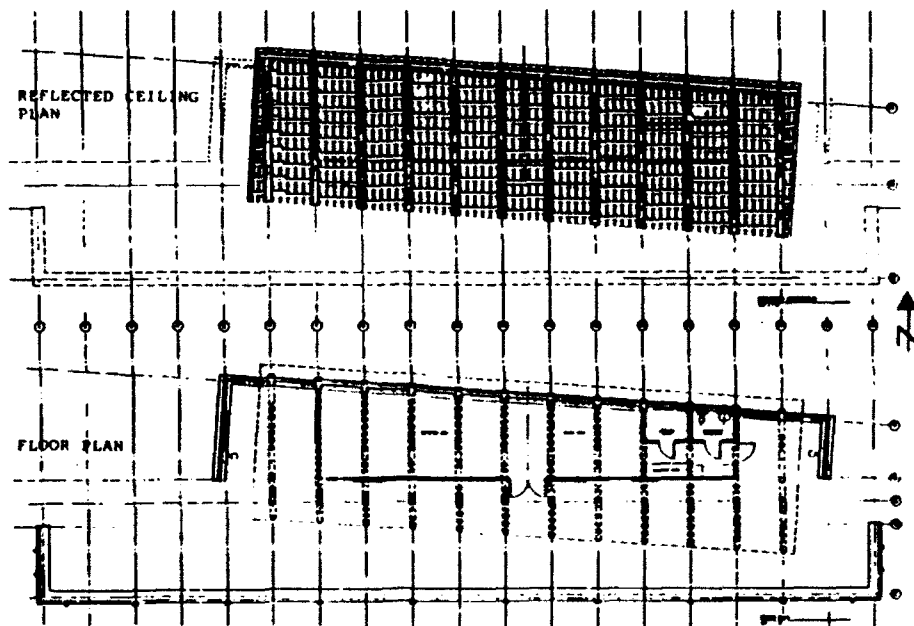
Figure 5

well. The standing seam metal roof tends to lock the snowpack into a set track of sliding and not allow it to split around an obstacle.

2. Build a cricket all the way to the uphill edge of the roof. This solution has some potential visual and waterproofing problems but is reasonably sure of working. In the final design, this may be the solution which will be adopted.
3. Make the stack and roof diaphragm strong enough to resist the forces. This solution was extensively explored in the preliminary design. The main problem was to determine the force which must be resisted by the vent walls (acting as shear walls) and the roof diaphragm due to snow gliding on the roof. The approach used was to obtain from the literature and from past experience a value for the shear strength of snow, and then to determine a reasonable potential failure surface based upon the length of the shed roof and the projected perimeter of the vent stack. By multiplying the area of the failure surface times the shear strength of the snow, a design force for the vertical shear panels, the roof diaphragm, and the retaining wall was determined. The force, although high, was such that it could be carried by these elements.

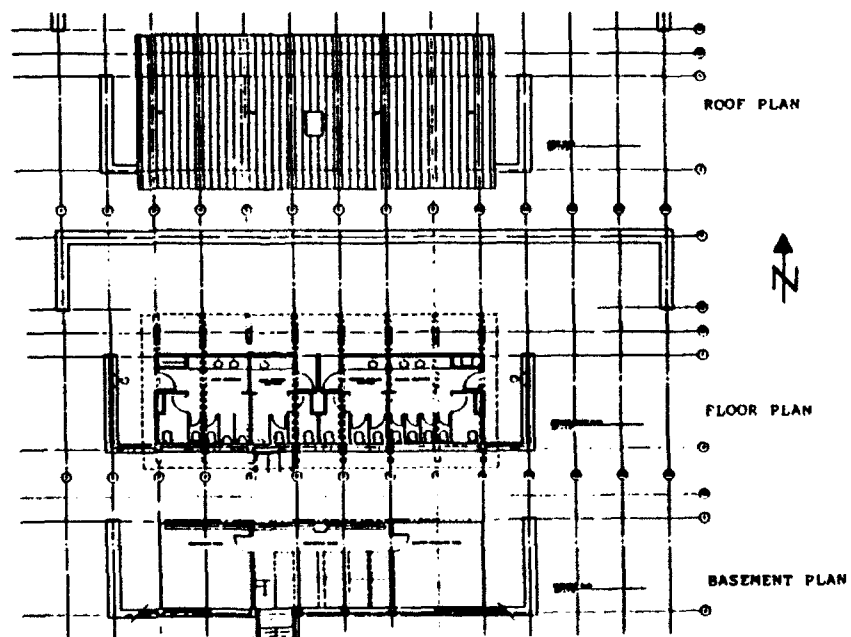
SEISMIC CALCULATIONS:

An important decision in doing seismic calculations for buildings to be located in deep snow country is to determine how much of the expected maximum roof snow load to add to the dead loads. The Uniform Building Code states that "Where the snow load is greater than 30 psf (1.43 kN/m^2), the snow load shall be included. Where considerations of siting, configuration and load duration warrant, the snow load may be reduced up to 75 percent when approved by the building official." Many cities, including Anchorage and Kodiak in Alaska, require only 25 percent of the snow load be added to the building dead load for seismic calculations. Seeking guidance for the design of the lateral force system of the Washington Pass visitor center and rest room buildings, I appreciated receiving a draft copy of a paper by O'Rourke and Speck entitled "Roof Snow



VISITOR CENTER BUILDING

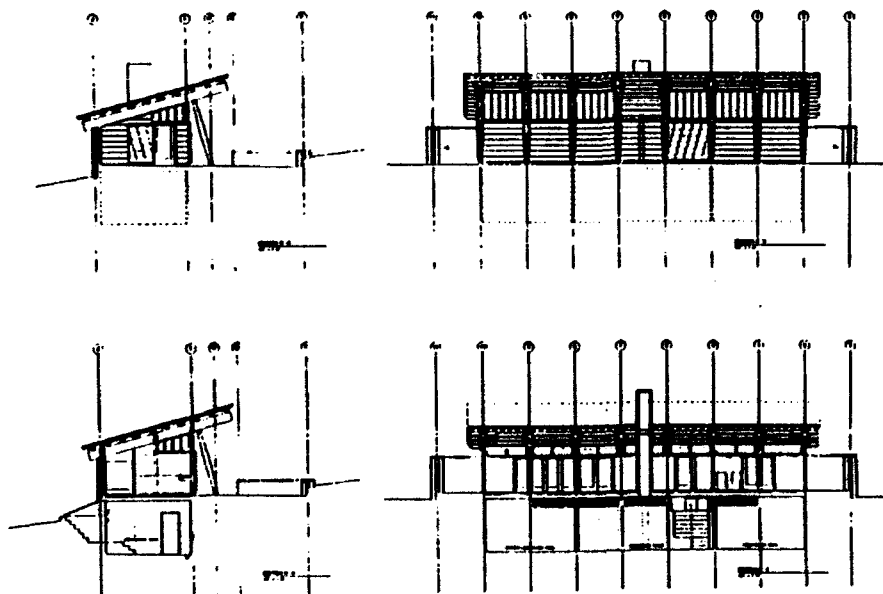
Figure 6



REST ROOM BUILDING

Figure 7

Load for Seismic Design Calculations." Their investigation was based in part upon data from Stampede Pass, a pass in the Washington Cascade Mountains with ground snow load conditions similar to those found at Washington Pass. Their conclusions would indicate that adding only 25 percent of the ground snow load to the dead load for seismic calculations would be reasonable. Accordingly, this is what was used for the structural design of the visitor facility at Washington Pass.



REST ROOM BUILDING - SECTIONS

Figure 8

Roof Snow/Ice Loads at North-Facing Roof Eaves Compared to Ground Snow Load Proposed Testing

Ian Mackinlay (FAIA) and Richard S. Flood (AIA/CSI)

Ian Mackinlay Architecture, Inc.
San Francisco, California, U.S.A.

ABSTRACT:

In deep snow country, a sloped roof design with overhanging eaves is a common occurrence, especially in residential structures. Ice dams, forming at the eaves, can add significant concentrated loads. Furthermore, ice dams frequently act as an obstruction to snow shedding off the sloping roof. When prevailing southerly winds drift snow onto north-facing roofs with ice dams, the snow build-up behind the ice dam can be substantial. The following proposed testing is intended to emulate these conditions. Two test structures will be built, one heated, the other unheated. Roof snow/ice weight will be measured and compared to ground snow load at the site. It is the authors' belief that data obtained will confirm their contention that under these conditions, roof snow/ice load will exceed ground snow load by a significant factor.

INTRODUCTION:

The Phenomenon of Ice Dams:

In regions of snowfall and freezing temperatures, ice dams form at the eaves of slope-roofed buildings. Roof snowpack primarily melts at the roof/snow interface. The roof surfacing material absorbs ultraviolet radiation and re-radiates the energy to the bottom of the snowpack. The roofing material also radiates interior building heat out through the roof, contributing to further melting of the snowpack. Melt water thus generated runs down under the insulating snowpack to the eave. Snowpacks 25 centimeters (10 inches) and thicker provide a high degree of insulating value, keeping the melt water from freezing. When the melt water emerges from under the insulating snow and encounters below zero C. air, the melt water freezes at the roof eave (Figure 1). This process continues and the resulting ice dam grows higher and higher.

During the ice dam's growth period, given equal volumes of snow, the concentrated load on the roof/eave structure is intensified compared to ground snow load, due to the high density of the ice and dammed water. Icicle growth from the ice dam adds additional load. The dam also acts as an obstruction to the upslope snowpack, preventing it from sliding off the roof. This increases overall roof snow loading as the roof snowpack is retained through succeeding snowfall events (Figure 2).

In some instances, creep can cantilever the ice well beyond the roof edge creating additional unbalanced load conditions (Figure 3). When the ice dam's grip on the roof finally is overcome by its own weight and the lateral force of retained melt water and upslope snow pressure, the ice dam comes crashing down tearing away at the eave structure and roof surfacing. Falling ice chunks are destructive and potentially life threatening to persons and property in the path of the falling ice. Ice dams also create severe architectural problems when dammed melt water permeates the roof envelope causing leaks into the building's concealed spaces and interior habitats.



Figure 1. Ice Dam. Note depth of the insulating snowpack above the ice dam.



Figure 2. Ice Dam as an Obstruction. Note how the ice dam forms a barrier to snow slide. Note hazard to entryway.



Figure 3. Cantilevered Snow/Ice Curl. Slow snow creep on a metal roof causes this type of unbalanced load.

Snow Load Codes:

The current 1991 edition of the *Uniform Building Code* (UBC) requires in Chapter 23, Section 2305(d), that snow loads, full or unbalanced, shall be used in calculating the design of structures where the snow loading will result in larger members or connections (than would otherwise be required). Further, this code section requires the Building Official (as defined in UBC Section 403) to determine the snow load. Unfortunately, the UBC does not spell out how "ground snow load" (as referred to in UBC Appendix, Chapter 23, Section 2342) is to be determined and, in the experience of the authors, it is often underestimated. In order to avoid disastrous roof collapse it is necessary to consider peak snowfall periods. The geometry and orientation of the roofs must be considered. It is also necessary to observe how the snow reacts to roofs and structures at the site being considered under natural rather than simulated or theoretical conditions. This test proposes such a natural approach.

The UBC permits roof snow loads over 97.65 kg/sq meter (20 psf) with roof slopes over 20 degrees (+- 4.33 in 12) to be subject to reduction depending on steepness. The authors contend this allowance is often unjustified. This code section also references UBC Appendix, Chapter 23 for alternative design. This Appendix is not a mandatory adoption requirement (in California) for local jurisdictions as is the basic UBC. Although this appendix chapter is more detailed than the basic code and serves as a guide to the design of buildings, structures and portions thereof, it still requires the Building Official to determine the ground snow load, although he can make adjustments when a registered engineer or architect submits substantiating data justifying the loads pertaining to a specific site. The appendix procedure also requires the roof snow load to be calculated according to Formula 43-1A which, for most buildings (except essential facilities, assembly occupancies over 300 and greenhouses), will result in roof snow loads ranging from 60% to 90% of the ground snow load determined by the Building Official. The authors believe that such reductions are rarely justified in north-facing roofs in the deep snow country where the snow depths on the roof exceed one foot. The proposed tests are intended to support this contention.

The special eave requirements of UBC Appendix, Chapter 23, section 2346 suggest the overhanging eave be designed for twice the calculated roof snow load. Therefore, the overhanging eave design load would be a factor of 1.2 to 1.80 of ground snow load after the allowable reductions in load are taken into consideration. The authors believe that while the UBC Appendix factors for overhanging eaves may be appropriate for sun drenched south- and west-facing eaves, these design factors do not address the significant roof load increase directly behind and upslope of the overhanging eaves, nor the perennially shaded north-facing eave condition (Figure 4). In addition, storm winds in the Sierra Nevada Mountains of California often come from the south or southwest, which strips snow from south-facing roofs and deposits it on north-facing roofs. This can add to the unbalanced load on the roof (Figure 5). The authors contend that the "ice dam" which forms at and near the eave of a north-facing roof prevents the snow on that roof from slipping off (Figure 5). Ice dams may even adhere tenaciously to the standing seams of metal roofs (normally thought to be 'slippery') and avalanche unexpectedly in times of general thaw. The result is that snow and ice loads may accumulate on north-facing roofs greatly in excess of ground snow load. The authors further contend that ice dams are larger and more persistent in heated than in unheated structures.



Figure 4. Unbalanced Snow Distribution. North-facing roof on right with about five times more snow than "sun-drenched" south-facing roof.



Figure 5. North-facing Eave with Ice Dam. Note ridgeline is free of snow while ice dam and southern winds build up snow on north-facing roof.

The other major code used in heavy snow areas of the United States, *Building Officials and Code Administrators, Inc. Building Code* (BOCA), permits a similar reduction of 60% to 90% from ground snow load, depending on various "exposure" and "importance" factors.

Purpose:

The test the authors propose has two simultaneous objectives. Its primary purpose is to demonstrate that the roof snow/ice load on north-facing roofs in the deep snow country, on the roof eaves and on the roof areas immediately upslope of the eave and, in fact, the entire roof area, can exceed by a significant factor the actual site ground snow load due to ice damming. A secondary purpose of this proposed test is to show the significance of building heat loss through the roof in the formation of north-side ice dams relative to natural freeze/thaw cycles in unheated structures. The American National Standards, *Minimum Design Loads For Buildings And Other Structures* (ANSI A58.1, 1982), Paragraph 7.4 permits a reduction in roof loads for "Warm Roofs" (ANSI Figure 8). This reduction is carried through to ASCE 7 - 88, which is a revision of ANSI A58.1, 1982. The authors believe that where ice damming occurs this reduction is unjustified and that testing will show that unheated structures are actually subjected to lower north-facing roof snow loads than are heated structures.

PROPOSED TEST STRUCTURES

- A. The authors propose to construct two side-by-side wood frame structures, each with a north-facing sloping roof terminating in an uninsulated and unheated eave. Structure geometry is intended to simulate an average one-story, shed roof portion of a typical home built in heavy snow country (Diagram 1).
1. Horizontal eave length to be 244 cm (8 ft).
 2. Downslope eave to project 25.4 cm (12 in) beyond wall.
 3. Roof pitch to be 4 in 12 (18.4 degrees).
 4. Roof to be 366 cm (12 feet) in length downslope from eave to ridge.
 5. Standard 11.47 kg/sq meter (235-lb) composition shingles in a dark brown color for roofing surface.
 6. Eave height to be approximately 305 cm (10 ft) above the ground.
 7. Structures shall be enclosed on all four sides with wood stud walls sheathed with plywood siding. Access doors will be installed on the south walls.
 8. The four corners of each structure will be supported by a 2268 kg (5000-lb) capacity weigh module. The weigh modules will be anchored to concrete spread footings.

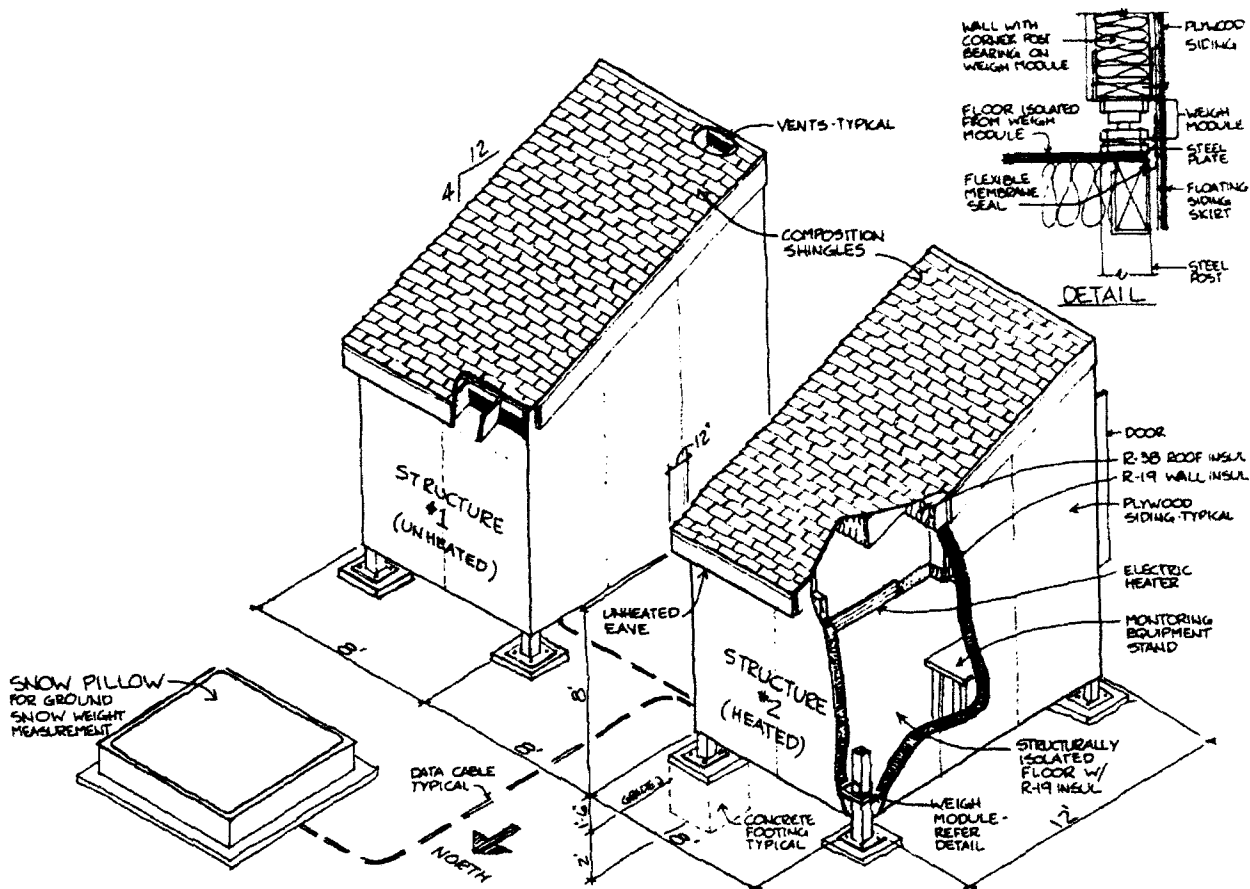


Diagram 1. Isometric View of Test Structures for Proposed Testing of Roof Snow/Ice Load at North-Facing Eave Compared to Ground Snow Load.

B. Structure #1 will be unheated and naturally ventilated. This structure will serve as a baseline sample for this site's natural environmental effects on the snow/ice formation on the north-facing roof. The authors anticipate some ice damming to occur at this structure's eave.

1. 30.5 cm. x 15.25 cm (12 in x 6 in) screen vents with .635 cm (1/4 in) mesh screen will be installed in each rafter space at both the eave and the ridge to ensure that the interior and exterior air temperature are approximately equal.
2. Structure will be uninsulated and unheated but will be caulked and weatherstripped to prevent undue interior water/ice intrusion.
3. A thermally and structurally isolated floor will be installed to provide a platform for passive data distribution equipment and to assure the roof snow load is accurately read by the instruments.
4. Electrical wiring for a 120 VAC outlet and overhead light will be installed.

C. Structure #2 will be insulated to conform to California Title 24 standards for residential construction. The interior will be heated to 21 degrees C (70 F).

1. Insulation will be in accordance with State of California energy standards:
 - a) Walls: R-19 batt insulation ($U=.0526$)
 - b) Roof: R-38 batt insulation ($U=.0263$)
 - c) Floor: R-19 rigid insulation ($U=.0526$)
2. Interior surfaces of the walls and underside of roof rafters will be sheathed with gypsum board taped and coated with latex paint.
3. Thermostatically controlled baseboard electric heating will maintain a nominal 21 degrees C (70 F) interior temperature.
4. Caulking and weatherstripping will be provided to minimize exterior air infiltration.
5. A thermally and structurally isolated floor will be installed to provide a platform for data monitoring equipment similar to that in structure #1.
6. Electrical wiring for 120 VAC outlet and overhead light will be installed. An exterior telephone line will be provided if remote monitoring is desirable.

TEST PERIOD

Testing will start in November of 1992 and continue until May, 1993. If this is a period of abnormally light snowfall or warm temperatures, the test will be continued during the next winter season and thereafter for several seasons as may be appropriate.

TEST LOCATION

The proposed tests will be performed on property owned by one of the authors, elevation approximately 1980 meters (6,500 ft) on the north shore of Lake Tahoe, California in the Sierra Nevada Mountains, approximately 38 degrees 30 minutes north latitude. This location normally has mid-winter ground snow loads of 488 - 1220 kg/sq meter (100-250 psf). At this location it is common to have 90 cm (3 ft) or more of snow on north-facing roofs during the winter. Normal winter air temperature is below freezing at night and above freezing during part of the day. Such conditions are favorable to the formation of ice dams.

PROPOSED INSTRUMENTATION

A. Roof Snow Loads

1. Weigh modules of 2268 kg (5000-lb) capacity at each of the four corners of each of the two structures. Analog output signals.

2. Power modules for each structure to convert weigh module analog output to high power digital output.
3. Controller with digital input and output plus PC/printer communication capability with display and calibration.

B. Ground Snow Load

1. Butyl rubber, antifreeze filled, snow pillow with a digitized output pressure transducer as used by the California State Department of Water Resources.
2. Backup: federal snow sampler.

C. Temperature

1. Temperature sensors with digital output capabilities for remote monitoring will be used to monitor interior air, interior ceiling, roof sheathing surface at eave, roof sheathing surface at ridge, outdoor air under eave and temperature at all building faces.
2. Temperature sensors with calibration capability.

D. Rain Gauge: rainfall gauge with digital output for remote monitoring of data.

E. Snowfall Gauge: snowfall gauge with digital output for remote monitoring of data.

F. Wind: combination wind speed and direction indicator with digital output for remote monitoring of data.

G. Control/Monitoring Equipment: to receive and store input signal data from the various sources. Ability to be programmed to initiate data sampling based on preset time basis with automatic increase in sampling rate due to changes in the environmental conditions being monitored. Personal computer with hard disk storage. Possible modem for remote monitoring.

DATA SAMPLING

- A. Roof and ground snow load: nominally twice daily. More frequent intervals during snow and rainfall conditions.
- B. Temperature: six times daily, two of which will correspond to snow load sampling.
- C. Rain and/or snowfall: during the event on an hourly basis.
- D. Wind: six times daily corresponding to temperature sampling.

DATA ANALYSIS

- A. Calculate average north eave snow weight in psf for each structure obtained from weigh module readings.
- B. Calculate average south ridge snow weight in psf for each structure obtained from weigh module readings.
- C. Calculate average total roof snow weight in psf for each structure obtained from weigh module readings.
- D. Correlate roof element average weight with ground snow weight obtained from snow pillow readings. Calculate roof snow/ground snow ratio factor.
- E. Correlate roof element weight differentials between structure #1 and structure #2. Calculate roof weight ratio factors between heated and unheated structures.
- F. Plot time versus data sample readings for all environmental parameters and establish curves. Correlate these curves against calculated roof element weight and ground snow weight. Analyze the corresponding relationships for patterns that may provide some means of predicting load fluctuations and the speed at which they may occur.

EXPECTED CONCLUSIONS: Assuming Three or More Feet of Snow on the Roof:

- A. North-facing eave snow load is expected to exceed ground snow load by a factor of approximately three for the heated test structure #2.
- B. North-facing eave snow for the unheated structure #1 is expected to be one and a half times ground snow load.
- C. The average load for the roofs of both structures is expected to exceed average ground snow load.

GOALS

If the expected conclusions can be verified, a case for code changes can be made. Such a change would improve the life safety of future construction. Furthermore, the test structure and data acquisition system would inevitably undergo refinements and could be made into a relatively simple, cost effective package that could be used at any deep snow locale to make site-specific roof snow load versus ground snow analyses. The authors suspect that the latitude, the snow depth and the daytime air temperature have a considerable effect on ice dam formation and thus on roof loading. The greater number of database sites available to the architectural and engineering community, the better the prospect for safe, well designed and constructed projects. Such tests, carried out over a number of years, will give the local Building Official an opportunity to have a realistic basis for determining snow loads on buildings.

REFERENCES

Uniform Building Code Standards, 1991 Edition, International Conference of Building Officials, Whittier, California.

Minimum Design Loads for Buildings and Other Structures, 1982 Edition, American National Standards Institute, Inc., New York, New York.

Basic Building Code, Building Officials and Code Administrators, International, Inc., Homewood, Illinois.

Re-Application of Traditional Architectural Schemes in the Snow Country

Ichiro Mizuno

Kanazawa Institute of Technology
Kanazawa, Ishikawa, Japan

ABSTRACT

The modernization of Japan in this century contributed to changing the nation into a science-and-technology oriented society, and it brought us economic prosperity. On the other hand, Japanese society became more homogeneous, and, as modernization continued, each region began losing its unique culture. The dominant information flow from the snowless area overwhelmingly influenced the architectural designs in the snow country, and the building designs and city plans that are less suitable for the snow country began appearing. The purpose of this paper is to report my study of many spatial schemes against snow in the snow country and my attempt to apply those schemes in modern architectural design and city planning.

I. SNOW IN HOKURIKU AREA

The Japan Sea side of central Honshu (the main island) is called 'Hokuriku.' The population in this area is approximately 5.5 million, including three big cities with over 300,000 people. The Hokuriku area has heavy snow every winter while the Pacific Ocean side does not. Thus, snow is a big obstacle for Hokuriku people. The average temperature seldom falls below five degrees below freezing, and the snow is wet and heavy.

II. ARCHITECTURE IN THE HOKURIKU AREA

The Hokuriku area has been inhabited since historical times, and the people in this area have developed their own unique way of life and environmental planning. However, due to the rapid modernization in this century, the people in the snow country have lost their uniqueness, and their lifestyle has become similar to the ones found in other parts of Japan. Owing to the new and better building materials and techniques in the field of architecture and city planning, the improved facilities and machines, and the advanced transportation and communication systems, we have built similar housing and comparable environments nationwide.

Recently we began to reconsider our nation's homogeneous appearance, and as a result productions of new designs that are appropriate for each region have begun. As a part of this work, I studied the old houses and cities in the Hokuriku area and found several traditional spatial schemes against snow.

Those are:

- yukigakoi* (covering to enclose a house)
- doma* (an earth-floored room)
- doen* (an earthen hallway)
- gangi* (a covered walkway like a corridor)
- hirairi* (a roof directed in parallel with the facing street)
- ryusetsuko* (a snow gutter)

These schemes gave me useful insight to design modern buildings with new materials. The following are examples.

III. CASE REPORTS

(1) Yukigakoi

Yukigakoi is a covering to enclose a building with wooden boards, straw or glass. It is removed when there is no snow. Both the *yukigakoi* used to cover the big windows in a living room or a dining room, and the one to be put up at the *genkan* (front door) area against the wind were popular. The function of *yukigakoi* is to produce a semi-outdoor space between the inside and the outside of a house. Here people can hang clothes to dry, store foods and firewood, keep tools, shovels, umbrellas and such, and move a dog house and *bonsai* plants indoors. The *yukigakoi* can also prevent snow from blowing into the house and save the wooden structure from being damaged by moisture from snow.

Although *yukigakoi* is one of the traditional systems against snow, its use has been decreasing in the Hokuriku area. The decrease may be due to the absence of *yukigakoi* in both factory-made housing and housing magazines that are published in Tokyo. This influence is causing people in Hokuriku to forget the *yukigakoi*.

Yet, we can still apply the scheme of *yukigakoi* to a modern house, e.g. sun-room, sun-terrace, *kazeyokeshitsu* (wind avoiding room), and utility space. These facilities can give us more comfort in a snowy winter.



ph. 2. *Yukigakoi* with straw.

ph. 1. *Yukigakoi* with wooden boards.

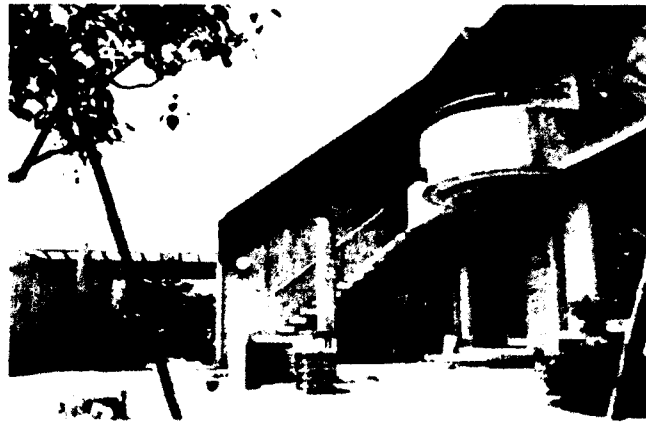


ph. 3. Inside of *yukigakoi*.





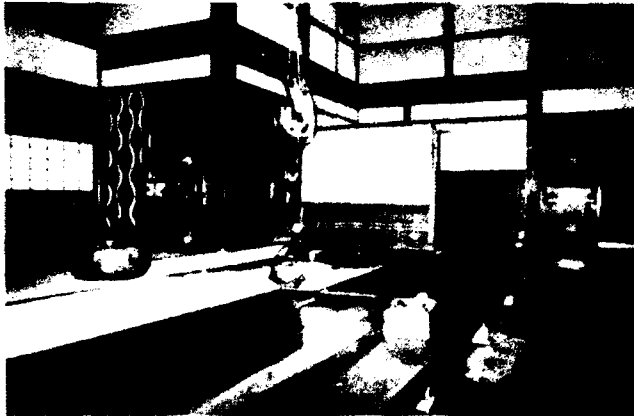
ph. 4. House in Nonoichi.



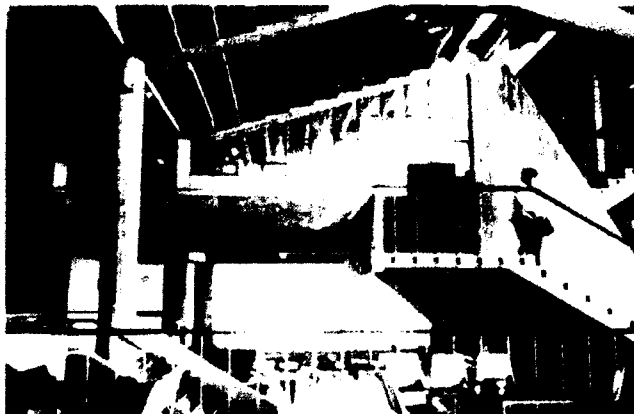
ph. 5. House in Terajishin.

(2) Doma

Many old houses in Hokuriku have an earth-floored room called a *doma*. It is the indoor space which is brought in from the outside, and it takes up the function of the snow-covered garden. This area has been used as a work space or for commercial purposes or for communication among people. The *doma* is one of the schemes that can offer people the same quality of life in winter as that in other seasons.



ph. 6. *Doma* in the Kita family House.
(This house is designated a National Treasure.)



ph. 7. The Main Building Lounge
at Kanazawa Institute of Technology.
(designed by Sachio Ohtani)

(3) Doen

Doen is an outside space with deep eaves between a house and a garden. *Doen* is always included in the traditional Japanese architecture. In the winter time, people stand glass doors against the edge of roofs to create an inside space, and use it as a garden. When the snow is gone, they remove the glass doors, and the garden and the inside space are united again. This new open space offers them various atmospheres through day and night.



ph. 8. *Doen*.

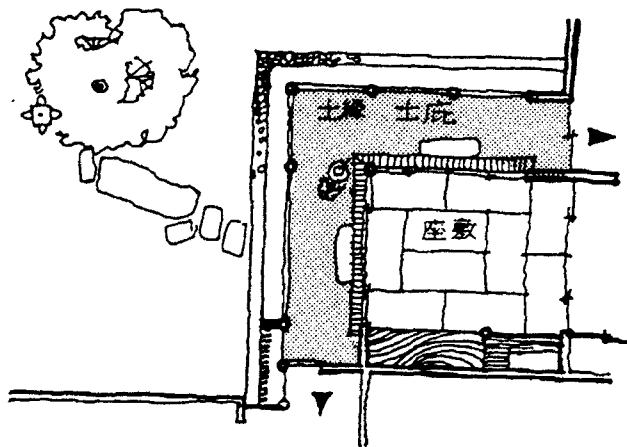
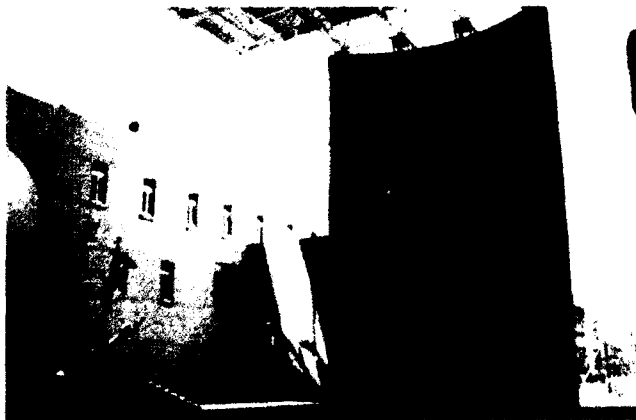


Fig. 1. *Doen*.



ph. 9. The semi-outdoor space
at Kanazawa Technical College.

(4) Gangi

Gangi is seen on a shopping street in the deep snow country. Each store building is backed away from the street, and the open space is roofed. When each of the roofed spaces along the street are linked together, it becomes a colonnade. Although the arcade in shopping areas, which are very popular in Japan, is similar to *gangi*, it is basically different because the *gangi* is created on a private lot by each store owner. Similar types of structures can be found around the world---the portico in Italy, the wooden terrace as shown in American western movies.

Gangi is very useful in the snow country, and its concept can be applied not only in shopping areas but also on university campuses or in a city center zone. This kind of application can contribute to produce a different city outlook in the snow country from the one where it does not snow.



ph. 10. *Gangi* in Nagaoka.



ph. 11. The colonnade at Kanazawa Institute of Technology.

(5) The Rule of Hirairi

A traditional Japanese house is a wooden building with a sloped roof. There has been a rule to decide which way the slope of the roof is directed: in the cities, the roof ridge is constructed at a right angle to the street, and this is called the rule of *tsumairi*; in the snow country it is in parallel with the facing street, this is the rule of *hirairi*. The *hirairi* roof guarantees that snow on your roof falls onto the street and to your garden, but never onto your neighbor's property so that you can avoid unnecessary arguments. The rule of *hirairi* has been violated in the snow country these days, and many *tsumairi* roofed houses have appeared in the suburbs in Hokuriku. This change has become the cause of many troubles among neighbors whenever it snows heavily.

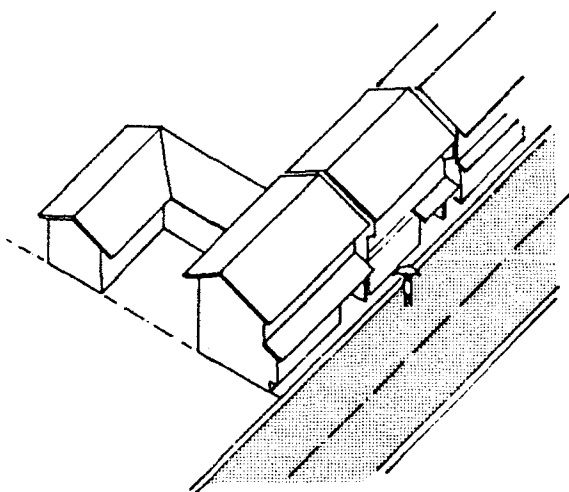


Fig. 2. *Hirairi*.



Fig. 3. *Tsumairi*.

(6) Ryusetsuko

In the past, irrigation canals, streams and rivers in both cities and rural areas served as the places where people could dump snow. These water flow systems are called *ryusetsuko*. Along with the mechanization of snow removing work, people started dumping greater amounts of snow in the water. This resulted in frequent flooding, and snow dumping in rivers was eventually banned. In addition, more conduits, to which people could not dump snow, were built because of the increase of automobiles on the street.

Recently people have again looked at the *ryusetsuko* system utilizing the natural river water energy. Now some devices are available to prevent flooding due to snow dumping: a grating is attached to a river bank which break mass snow into small chunks while snow falls down to the water, and a net is spread on the river bed to reserve water flow.

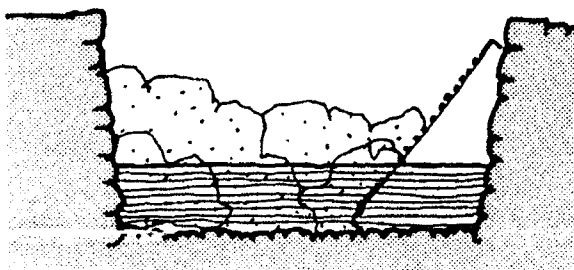


Fig. 4. A side grating.

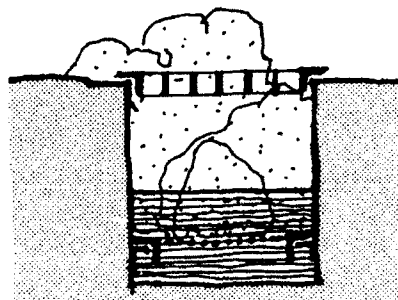


Fig. 5. Top and bottom gratings.

IV. CONCLUSION

Yukigakoi, *doma* and *doen* produce a middle space between the inside and the outside. This third space guarantees the same size of living space and contributes to comfort even in spring, summer and autumn. *Gangi*, the rule of *hirairi* and *ryusetsuko* are the wise schemes with which we can continue to have the same quality of city life even in a snowy winter.

My next research plan is to study similar mechanisms against snow around the world and publish them in a book. I believe that we should reconsider the usefulness of these schemes and apply them in the modern day life.

REFERENCES

Research Report

Mizuno, Ichiro (1988) "Ideas against snow for housing in Kanazawa," in *Kenchiku Kenkyu Shiryo*, No. 63, August 1988: *Techniques Against Snow for Housing and Residential Area Planning*, 329-354, published by Building Research Institute, Ministry of Construct, Tokyo.

Re-application Work Reports

Mizuno, Ichiro (1981) "House in Nonoichi---Yukigakoi," *Kenchiku Bunka*, Vol. 36(412), 107-114, 1981.

----- (1983) "Torigoe Village Bekku Miyanomori Housing," *Kenchiku Bunka*, Vol. 38(443), 137-143, 1983.

----- (1986) "House in Terajishin," *The Japan Architect*, Vol. 008, 103-109, December 1986.

----- (1990) "Technical Training Center For Basic Engineering at Kanazawa Institute of Technology," *The Japan Architect 1990*, 275-281, December 1990.

----- (1992) "Kanazawa Technical College," *Shinkenchiku 1992*, 242-249, February 1992.

Design Review for Snow Country

Jonathan C. Paine, P. Eng.

Snow Country Consultants, Ltd.
Whistler, British Columbia, Canada

ABSTRACT:

Designing buildings for the rigours of Snow Country has many challenges not experienced in other climates. There are several approaches to meeting the challenge. Many building designers do not fully appreciate the aspects of Snow Country which are different from coastal or arid climates. Once the snow flies, many designers are left wondering whether they have a project they can be proud of, or whether they must keep a low profile and avoid the owners. A professional's worst nightmare is being called by a disgruntled owner with a legitimate complaint, threatening a lawsuit.

By understanding the implications of snow and cold, many of the problems can be avoided. At the time of the initial concept, a careful review of the proposed design will identify potential problems that can then be mitigated.

This paper will outline a logical approach to reviewing a design for the rigours of Snow Country.

INTRODUCTION

Often when I am designing or reviewing a proposed building, a warm summer breeze is blowing, and it is far too easy to forget about the implications of snow. The other temptation is to simply ignore snow and ice as a design consideration.

All buildings have several factors which ultimately determine the shape, size, character, materials, and success of the finished project. Just as the client's and end user's needs must be kept in mind throughout the entire design process, a consideration and understanding of the implications of snow must be present.

Often the review of a project for snow starts when detailed design work is well underway. Designers often believe that snow problems can be solved by adding a few snow retainers, or ignoring the potential for leaks.

Before attempting a review of the project for snow, a project strategy is required which leads from general design concepts through to a finished building. By using this strategy, the implications of snow form one of the design parameters from the start, and hopefully leading to more successful buildings.

DISASTER STRIKES !!

In the spring of 1982 the ground snow pack in Whistler was as much as 1.8 meters deep with a density nearing 35% (350 kg/cubic meter). A pedestrian walking by the Whistler Conference Center noticed the sound of crackling wood. Upon further investigation, the large laminated wood fascia beams of the buildings roof could be seen shearing and deflecting as the roof snow pack crept down the slope. The hidden gutter and fascia detail was trying to hold back a slab of snow 1.5 meters deep, 60 meters long and 18 meters from the gutter to the ridge. A snow mass of nearly 600 tonnes! The engineers feared that if the snow suddenly avalanched, the impact could break through the adjacent precast concrete parking structure.

The placement of shoring under the slab was just being completed when the entire north facing slope avalanched off the building.

Fortunately, no one was hurt in this incident, although the repair bill and lawsuits could easily ruin a professional's career.

This is just one of several examples of buildings which fail to meet the expectations of the owners.

PROJECT STRATEGY:

The following is an outline of a project strategy which works for most buildings and the general principles can be applied to almost any project.

Objectives:

Clearly define the goals and objectives of the project. Is it a commercial venture with an anticipated return on investment, institutional or residential project? Will the present and future uses be different? This stage may include a study of the target user group, market analyses, and current occupancy levels.

Data:

Collect all the available data necessary for the site and building design. This will include site information such as soils and slope investigation, environmental impact studies, existing site servicing and access road locations. Availability of materials and trades may influence the design concept and should be researched. A copy of any local codes and bylaws should be obtained to avoid future surprises. One of the most important areas of information that is often considered too late, is the climatic data including rain, wind, solar exposure, and SNOW. The information on snow should include anticipated volumes, possibility of drifting, average densities, typical storm patterns, and design snow loads. Any information on average winter temperatures may help in assessing ice formation frequency and magnitude.

Analyses:

By analysing the collected data the design implications will start to appear, and design priorities can be identified. The analyses process may involve several consultants, all coordinated through a prime consultant.

Concept:

A preliminary design concept for the building can now be tested against the above objectives and data analyses. It is at this stage that a snow analyses can be performed to identify any potential problem areas. Since the design is still in the conceptual stage, changes or improvements can easily be made.

Design:

After signing off on the conceptual design, work on the details of design can start. If snow has been carefully considered in the conceptual stages, many of the problems associated with snow will be avoided. Careful detailing to allow for snow, ice, and melt water, at the detailed design stage, will pay off in long term benefits to the project.

Approvals:

The approval process includes client review as well as local building authorities. This is often an ongoing process starting at the conceptual design.

Construction:

Heavy snow fall can create havoc with site access, scheduling of work, availability of labour, and the length of the construction season.

CONCEPTUAL DESIGN REVIEW:

By following a project strategy, many of the problems associated with snow will be apparent at an early stage. The time to do a thorough review for the implications of snow is at the conceptual design stage. The following outlines some of the major points to look for when reviewing a proposed design, both for the building design, and the site design:

Building Design Considerations:

- a) General building shape: simple shapes generally have simple problems, more complex shapes may have multiple areas of concern, i.e., simple sloping roofs versus multiple dormer roofs.
- b) Snow accumulation: look at the wind exposure, solar exposure, effects of dormers and valleys, all in relation to anticipated snow volumes on the building.
- c) Snow Shedding: This is probably the most common problem in heavy snow areas. The analyses to determine the probability of snow sliding from a

roof should include a review of the roof angle, roofing materials, roof shape, and roof obstructions. Pedestrian and vehicle danger zones should be identified, and snow deposition areas considered. Snow trajectories from high roofs should be calculated (Paine, 1988).

- d) **Icicle formation:** Meltwater refreezing at a cold edge may occur on a daily basis, or in some climates, icicles grow for several months. Icicles often occur at the edges of roofs and at the bottom ends of valleys. Roof shape, materials, and orientation all have an effect. Downspouts and gutters often make the condition worse.
- e) **Access Points:** All points of entry to a building for both vehicles and pedestrians must be protected from snow and ice shedding from upper roofs. Either avoid the problem by relocating the access points, or protect with canopies or some other design feature. This also applies to stairs and ramps leading to the building.
- f) **Snow Management:** Some roofs, decks, canopies, and snow dump areas may require clearing of snow several times a winter. Wear surfaces should be tough enough to avoid damage from snow clearing equipment, and a method of removing the snow should be considered. ie. hand shovels, snow blowers, etc.

Site Design Considerations:

- a) **Slope:** Steep slopes may lead to snow creeping or avalanching, causing damage to the structure. If snow from a roof can shed into an area which is uphill of the building, the additional snow may wedge between the slope and the building, causing lateral pressure on the building.
Cuts in steep slopes often have large volumes of water during melting of the snowpack. A thorough geotechnical investigation will identify a potential problem.
- b) **Site Orientation:** Solar and wind exposure can be used to help keep roads and building access points clear of snow and ice. If snow drifting is a problem in the region, a drift analysis should be carried out.
- c) **Snow Accumulation:** Snow deposition areas from the upper roofs should be identified. Short and long term site snow storage should be considered,

as well as methods of clearing in unusually heavy snow seasons.

Access points, fire lanes, and utilities should all avoid areas where snow is to be stored. Site fixtures such as light standards, fire hydrants, and signs should be located to minimize damage from snow clearing equipment.

- d) Snow Removal: A general plan of snow removal should be considered for both the building and the site. The method of snow removal will have impacts on the site design. Heavy equipment may require a large working space. If not enough snow storage can be found on site, a plan for trucking excess snow away must be in place before the snow flies.

The roof plan and sections on the following pages indicates some of the above points. These drawings combined with a report can help form guidelines to aid in refining the conceptual design.

CONCLUSION:

Snow and ice can be major design factors for both building and site design. By considering snow from the first conceptual design stages, many of the problems associated with snow can be avoided. A thorough review of the proposed design at the early stages is essential.

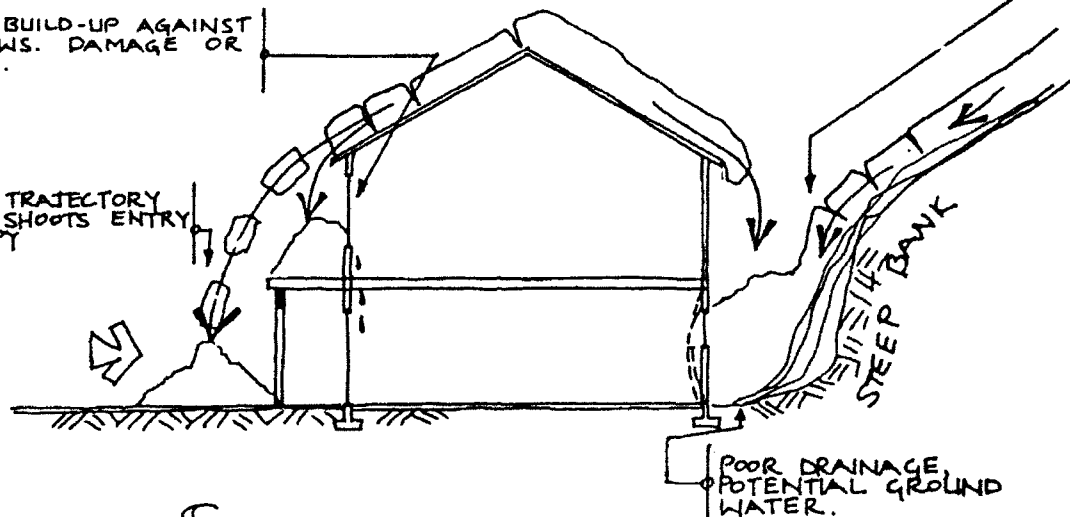
REFERENCES

Paine, J. C., (1988) "Building Design for Heavy Snow Areas," First International Conference on Snow Engineering, Santa Barbara, California.

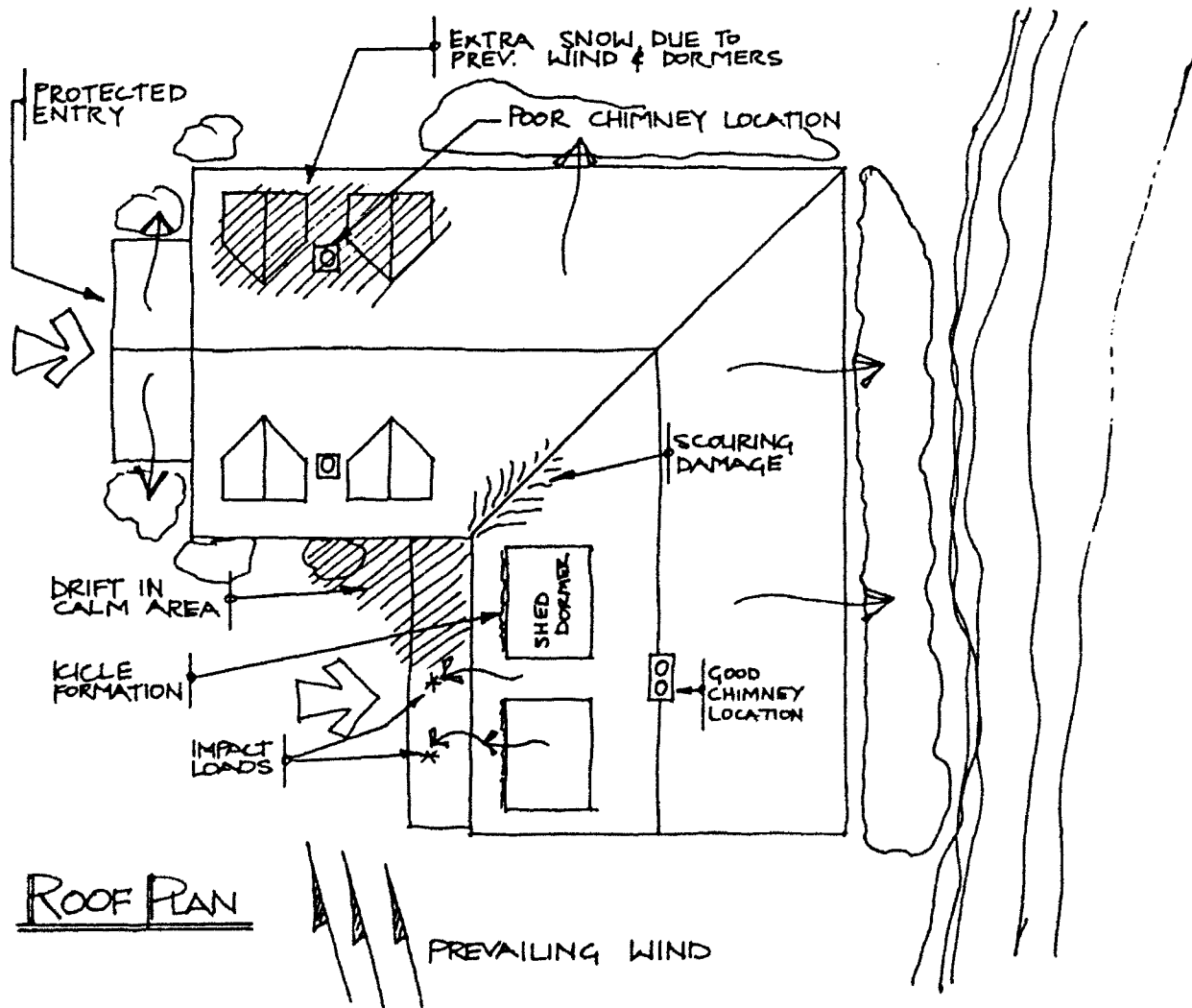
SNOW BUILD-UP AGAINST WINDOWS. DAMAGE OR LEAKS.

SNOW TRAJECTORY OVER SHOOTS ENTRY CANOPY

LATERAL PRESSURE FROM ROOF DUMPING AND POTENTIAL SNOW CREEP.



SECTION



ROOF PLAN

PREVAILING WIND

ASCE Standard 7 Snow Loads

Ronald L. Sack* and Ashvin Shah†

*Director/Professor, School of Civil Engineering and Environmental Science
University of Oklahoma, Norman, Oklahoma, U.S.A.

†Manager, Codes and Standards, American Society of Civil Engineers
New York, New York, U.S.A.

ABSTRACT

Historical information, research results, and previous codes and standards provide the basis for the 1988 edition of the ASCE standard for loads. Ground snow loads are prescribed using the National Weather Service data base. These meteorological records are used to provide loads with a 50-year mean recurrence interval; the station-specific loads are spatially extrapolated to yield the U.S. map. Some areas could not be mapped because of extreme local variations in snow loads. Previous Canadian studies, plus a nation-wide U.S. field investigation were used to obtain the effects on roof snow accumulations of roof exposure to wind and sun, roof geometry, roof cladding, and building thermal losses. Snow sliding coefficients were developed using Canadian results in conjunction with a 6-year U.S. field study. An extensive statistical evaluation of insurance failure records yielded the drift load provisions. Current efforts by the ASCE Snow Load Subcommittee should produce improvements in 17 areas of the 1995 edition of ASCE7. ASCE is working to have the three U.S. model codes adopt ASCE7-88 by reference and thus obtain uniformity of the U.S. building codes.

INTRODUCTION

The ASCE Standard, Minimum Design Loads for Buildings and Other Structures, (ASCE7-88, 1988) is a U.S.A. consensus document that addresses: dead loads; live loads; soil and hydrostatic pressure; wind loads; snow loads; earthquake loads; and load combinations. The seminal work was done under the auspices of the American National Standards, Inst. and originally published in 1972 (ANSI72). For the 1982 edition (ANSIA58.1), the National Bureau of Standards, serving as the secretariat, coordinated the efforts of 23 organizational representatives, 16 individual members and 6 subcommittees. The 1982 edition contained numerous and substantive changes from the 1972 edition. The standard was submitted to review and ballot by a broad cross section of the profession. In 1988 the American Society of Civil Engineering (ASCE) assumed the functions of secretariat and published the current document (ASCE7-88). Minor changes in the ANSI82 ground snow loads, plus new roof sliding relationships were used to produce ASCE7-88 snow loads; the latter document was also approved by a consensus procedure. Currently, the ASCE Snow Load Subcommittee membership is made up of 2 from government agencies, 7 from academia, 1 practicing architect, and 1 practicing engineer; the four corresponding members are from the insurance industry, structural engineering practice, the building industry, and meteorology consultancy. Work is now in progress to produce another edition of Standard 7 in 1995; seventeen specific issues are being investigated and updated for the new edition.

GROUND SNOW LOADS

Snow accumulation on a roof is influenced by the ground snow load. The Soil Conservation Service (SCS) and the National Weather Service (NWS) are the two principal agencies gathering ground snow data in the United States. The NWS makes daily snow load and depth measurements at 184 so-called first-order stations, and daily snow depths are recorded at approximately 9,000 additional locations. In the Western United States, the SCS makes monthly measurements of depth and water equivalent for the accumulated snow. The NWS stations are typically located adjacent to towns and cities; whereas, the SCS sites are in the remote high mountainous areas. The NWS stations are near the majority of the building activity; thus, the construction industry could potentially make use of these data, but snow depths alone do not yield design loads. In some of the western states the SCS stations vastly outnumber NWS sites.

We encounter a difference in the temporal content of the SCS and NWS data. The NWS daily measurements reveal small changes due to deposition and ablation (i.e., net volumetric decrease); whereas, the monthly SCS data do not reflect these changes. Typically, the NWS quantities peak during January and February; whereas, snow packs in mountainous areas, as characterized by the SCS data, maximize in March and April.

Annual maxima are typically extrapolated beyond the historical period of observation using the Frechet (type II), log Pearson type III, Gumbel (type I) or lognormal cumulative probability distribution function (cdf) as a model. The parameters describing the cdf are determined from the data at a given site. Since the cdf extrapolates extreme values from the historical data, it is imperative that the correct model be chosen by examining the data using measures such as the Chi-square test of fit, the Kolmogorov-Smirnov test, or probability plot correlation coefficients. For example, predicting the annual extreme water equivalents at first-order NWS sites from the Dakotas to the East coast requires both Gumbel and lognormal distributions (Ellingwood and Redfield, 1983). Europe and Canada use the Gumbel distribution (Newark 1984); whereas, in the United States, ANSI82 used the lognormal model. In the western United States, the log Pearson type III distribution is used in Idaho (Sack and Sheikh-Taheri, 1986), Montana (Stenberg and Videon, 1978), and the state of Washington (SEAW81). Annual probabilities of exceedance, ranging from 0.01 to 0.04, are used in the United States, but attempts are being made to standardize on 0.02. The American Society of Civil Engineering (ASCE7-88) prescribes a 50-year mean recurrence interval (mri), and the states of Idaho, Montana, and Washington have also adopted this value. The mri is the reciprocal of the annual probability of being exceeded (e.g., a 50-year mri corresponds to an annual probability of being exceeded of 0.02).

We must estimate the snow density to use the snow depths recorded at many stations; these sites are typically located near populous areas and constitute a potentially useful data base. ASCE7-88 for the United States involves plotting the 50-year mri ground depths against the 50-year mri ground loads for the 184 first-order NWS stations. The resulting nonlinear regression curve relating these extreme values was used to predict ground snow loads for the 9,000 NWS synoptic stations where only depths are measured. Another approach is reflected in the Colorado study (SEAC84); wherein, a power law regression was applied to the snow course data from 128 stations in the state to relate snow load and depth. A similar approach was used for the 1986 study of Idaho; the depth-snow load relation was obtained using bilinear regression and data from 3,000 western SCS stations with over five years of record (Sack and Sheikh-Taheri, 1986).

The country-wide ASCE7-88 ground snow load map displays zone intervals of 10 lb/sq ft. The zones represent 50-year mri values obtained using a lognormal distribution to model the loads from the 184 first-order NWS stations and depths from the 9,000 NWS synoptic stations. The latter were converted to loads using equivalent densities calculated from the 184 first-order stations. In certain areas, the snow loads shown are not appropriate for unusual locations such as high country, and some locales may have extreme variations in snow deposition. As a result, building associations, local jurisdictions, and entire state areas have initiated and published their own snow load studies (Brown, 1979; Meehan, 1979; Placer, 1985; Sack and Sheikh-Taheri,

1986; Stenberg and Videon, 1978; SEAA81; SEAONC64; SEAC84; SEAO71; SEAW81). These local studies are referenced in ASCE7-88, but not all use a 50-year mri. Also these analyses use various annual extremes and different extreme value statistical distributions.

FLAT ROOF SNOW LOADS

Exposure of the roof to wind and sun, thermal losses from the building, roof geometry, roof cladding, and obstructions on and around the roof significantly influence roof snow loads. The 1941 edition of the National Building Code of Canada (NBCC) mandated that the roof-to-ground snow load ratio depends upon roof environment and geometry. Canada initiated a country-wide survey of snow loads on roofs in 1956 (Peter et al, 1963) and found that the basic roof snow load for a flat roof in a location sheltered from the wind is typically 80% of the ground snow load; this information was incorporated into the 1960 NBCC. The survey also indicated that the basic snow load coefficient can be reduced by 25% where the roof is fully exposed to the wind (this reduction was introduced into the 1965 NBCC). The recommendations of ANSI A58.1-72 (ANSI72) were similar to those of the 1965 NBCC.

In 1978 ANSI established a snow load subcommittee to formulate revisions for the 1982 standard using the results of a country-wide program of snow measurements initiated by the Cold Regions Research Engineering Laboratory (CRREL). The subcommittee recommended the following for the contiguous United States and Alaska, respectively (O'Rourke et al, 1983):

$$p_f = 0.7 C_e C_t I p_g \quad (1a)$$

$$p_f = 0.6 C_e C_t I p_g \quad (1b)$$

in which p_f = the flat roof snow load; C_e = a dimensionless exposure factor (Table 1); C_t = a dimensionless thermal factor (Table 2); and I = a dimensionless importance factor that converts the ground snow load to a mri different from 50-year (Table 3). A study of 103 representative U.S. locations revealed that the ratio of the 25- and 50-year mri snow loads averaged 0.81 and the ratio of 100- and 50-year mri averaged 1.21. The coefficient of 0.7 and 0.6 in Eqs. 1a and 1b stem from the analysis of the CRREL data base. Using measured values for the roof load and the associated ground load, O'Rourke found that the expected value for the conversion factor p_f/p_g was $0.47 C_e C_t$. There was, however, a fair amount of scatter of data points about the expected value, which was modeled as an error term with a lognormal distribution. Considering the variability of both the annual maximum ground load and the conversion factor, O'Rourke and Stiefel (1983) determined that the 50-year mri roof load was equal to the 50-year mri ground load times $0.606 C_e C_t$. However, O'Rourke used values of C_e ranging from 1.32 (sheltered) to 0.95 (windswept), whereas, the corresponding factor for the contiguous U.S. (see Eq. (1a)) is a reasonably accurate simplification.

SLOPED ROOF SNOW LOADS

Using field observations (Lutes, 1971; Schriever, 1967), experience, and judgment, the distributions of snow on shed, gable, and arched roof shapes were obtained and included in Supplement Number 3 to the 1965 NBCC; the same results were incorporated into ANSI72. Canada made minor changes in their 1970 and 1975 code editions.

The 1941 NBCC allows a slope reduction factor (C_s) to be multiplied by the flat roof snow load. Roof slopes between 20° and 62.9° are reduced as shown by line C in Fig. 1, while slopes in excess of the upper limit are considered free of snow, and slopes less than 20° have the flat roof load. This slope reduction factor was changed in the 1960 edition of NBCC, with an upper limit of 70° and a snow-free angle of 30° (line D in Fig. 1).

Table 1. Exposure Factor, C_e

Nature of Site *	C_e
A. Windy area with roof exposed on all sides with no shelter ⁺ afforded by terrain, higher structures, or trees	0.8
B. Windy areas with little shelter ⁺ available	0.9
C. Locations in which snow removal by wind cannot be relied on to reduce roof loads because of terrain, higher structures, or several trees nearby	1.0
D. Areas that do not experience much wind and where terrain, higher structures, or several trees shelter ⁺ the roof	1.1
E. Densely forested areas that experience little wind, with roof located tight in among conifers	1.2

*The conditions discussed should be representative of those that are likely to exist during the life of the structure. Roofs that contain several large pieces of mechanical equipment or other obstructions do not qualify for siting category A.

⁺Obstructions within a distance of $10h_o$ provide "shelter" where h_o is the height of the obstruction above the roof level. If the obstruction is created by deciduous trees, which are leafless in winter, C_e may be reduced by 0.1.

Table 2. Thermal Factor C_t

Thermal condition*	C_t
Heated structure	1.0
Structure kept just above freezing	1.1
Unheated structure	1.2

*These conditions should be representative of those that are likely to exist during the life of the structure.

Table 3. Importance Factor, I

Nature of occupancy	I
All buildings and structures except those listed below	1.0
Buildings and structures where the primary occupancy is one in which more than 300 people congregate in one area	1.1
Buildings and structures designated as essential facilities	1.2
Buildings and structures that represent a low hazard to human life in the event of failure	0.8

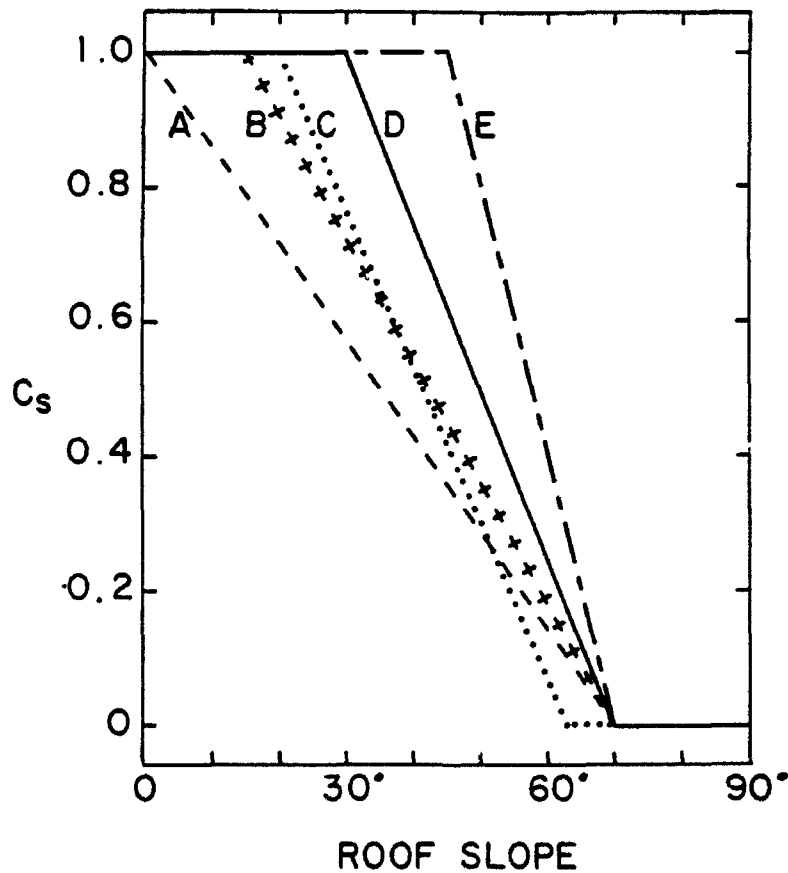


Figure 1. Slope Reduction Factors for NBCC41 (Line D), ANSI82 (Lines B, D, and E), and ASCE7-88 (Lines A, B, D, and E)

ASCE7-88 indicates that if the roof has a sufficient slope, the flat roof snow load may be reduced as follows:

$$p_s = C_s p_f \quad (2)$$

where p_s = the sloped roof snow load, and C_s = a dimensionless coefficient dependent upon roof slope, roofing materials, and thermal characteristics. Slope reduction factors for unobstructed roofs with sufficient room at the eave line to shed snow are shown in Fig. 1. Line A applies to warm ($C_t = 1.0$) slippery surfaces; line B for cold ($C_t > 1.0$) slippery surfaces; and for all other surfaces lines D and E for warm and cold roofs, respectively.

The C_s values were changed significantly for unobstructed slippery surfaces between ASCE7-88 and ANSI82 based upon research (Sack et al, 1987). In ANSI82 line B applied to warm ($C_t = 1.0$) slippery surfaces; line D for all other warm surfaces and cold ($C_t > 1.0$) slippery surfaces; and line E was used for all other cold surfaces.

Sliding snow will reduce the load on the roof of origin, but it can impose significant static and dynamic loads on a lower receiving roof. ASCE7-88 prescribes using all snow from the upper roof, but defines no distribution on the lower roof; this standard acknowledges that a portion of the upper roof load may slide clear of the lower roof.

NONUNIFORM SNOW LOADS

Snow deposition is affected by wind speed and direction, terrain relief upwind and around the structure, air temperature, humidity, snow deposition rate, and building geometry (Isyumov and Davenport, 1974). These effects influence the exposure factors in Eqs. 1a, 1b and 2, as well as the slope reduction factors.

Unbalanced Loads

Wind blowing normal to the ridge of a structure will create an area of aerodynamic shade on the leeward surface, yielding nonuniform snow deposition and transport of existing snow from the windward roof surface. Unbalanced roof snow loads may also result from sliding snow.

The initial data for unbalanced snow distributions came from the Canadian survey of roof snow loads of 1956 through 1967 (Lutes, 1971; Schriever, 1967). Additional work has been addressed to large multi-level roofs and curved roofs (Taylor, 1980). The design criteria resulting from the early Canadian case studies were introduced into the 1965 edition of NBCC; in general, for gable, arch, and curved roofs all snow is removed from one side with loading on the leeward side. Additional snow accumulations in valley areas of roofs are also prescribed. ANSI72 contained recommendations similar to NBCC, while ANSI82 and ASCE7-88 suggest a unique set of unbalanced loads.

Drifts on Lower Roofs and Adjacent Structures

Strong winds transport snow so that drifts form on roofs at abrupt changes in roof geometry and around obstructions. Drifts on multi-level roofs can constitute loads many times the ground snow load; they are cited as one of the primary causes of structural failure due to snow in the midwestern and eastern United States (O'Rourke et al, 1985).

ASCE7-88 incorporates new drift provisions based upon a recent study of approximately 350 drift snow load case histories gathered from the technical literature and insurance company failure investigations. Multiple regression analysis indicated that drift surcharge height is a function of: 1) length of the upper and lower roofs (i.e., the sources of snow); 2) the ground snow load (i.e., consistency of snow in the vicinity of the building); and 3) the difference in height

of the roofs (i.e., the space available for drift formation (O'Rourke, et al, 1985). The following drift design criteria emerged from that study (O'Rourke and Wood, 1986; O'Rourke, et al, 1986).

The triangular snow drift surcharge load (to be superimposed on the balanced roof snow load) has a maximum height h_d (ft), of

$$h_d = 0.43(L_u)^{1/3}(p_g + 10)^{1/4} - 1.5 \quad (3)$$

where L_u , the length of the upper roof, should be taken as not less than 25 ft nor greater than 600 ft. The density of the drift, D (lb/ft³), is

$$D = 0.13p_g + 14 \leq 35 \text{ lb/ft}^3 \quad (4)$$

The extra snow load at the top of the drift equals $h_d D$, and the total load there equals the drift load plus the balanced roof load (p_s). The maximum height of the drift must not exceed ($h_r - h_b$), where h_r is the difference in height of the two roofs and h_b is the depth of the uniform snow deposition. O'Rourke suggests that if p_g is less than 10 lb/ft² or if $(h_r - h_b)/h_b$ is less than 0.20, drift loads need not be considered. The drift surcharge load diminishes to zero at $4h_d$ from the change in roof elevation.

The drift load on a lower roof within 20 ft of a higher structure should be determined by the method described earlier, except that the maximum intensity of the drift load is to be reduced by the factor $(20 - s)/20$ to account for the horizontal separation, s (ft), between the buildings.

Drifts in areas adjacent to significant vertical roof obstructions (e.g., chimneys and parapet walls) must also be considered. ASCE7-88 proposes adaptations of Eqs. 3 and 4 with a drift length of $4h_d$.

PROPOSED CHANGES

In preparation for the 1995 edition of the standard, the ASCE Snow Load Subcommittee held its first meeting in early 1991; work is in progress to make significant improvements in a number of areas.

The meteorological data base is being updated with the 10 years of data since ANSI82 in order to improve the ground snow load maps. The 1995 edition will contain information in the appendix on conducting a site-specific snow load case study.

The next edition will contain improved drift load guidelines, with improved definitions of the length of lower upwind roofs. Consideration is being given to adjusting the 1:4 aspect ratio of drift geometry when the drift is limited by the difference in roof heights and to calculating drifts when the ground load is as low as 5 lb/ft².

Thermal factors are being rethought in light of the International Standards Organization's (ISO) publication on snow loads. The subcommittee is weighing all possibilities between the two extremes: a) designing all buildings as if they are unheated; and b) expanding the thermal factors.

Minimum loads are also being evaluated. That is, in locations where snow is a significant load, possibly the design roof live load should not be less than 20 lb/ft², provided the minimum roof slope is 0.25 in./ft.

The subcommittee is seeking improvements of unbalanced loads in light of work that has been done in Japan (Endo and Tomabechei, 1983). Also the subcommittee is considering increasing loads in valleys and seeking information on unbalanced loads toward the downwind end of large flat roofs due to channeling of snow. Load reductions with additional knowledge of prevailing wind and occurrence of blowing snow is being weighed.

Since temperature cycles can create meltwater that will freeze to sloping roof surfaces, improved information on sliding snow factors is being sought.

The exposure factors are being reexamined in light of the many suggestions that have been made. Some have suggested that existing values of C_e be used, while others prefer to use the

simplified value of 0.8 that originated in NBCC in 1960. Other questions associated with C_e is that it can change during the life of the structure; also large reductions in roof snow should probably not be allowed in areas where the ground snow load is low.

The next edition will probably contain guidance on wind tunnel and water flume studies for snow accumulations on complex structures.

The subcommittee will expand guidance on ice dams, since they can prevent snow from sliding off an otherwise unobstructed slippery surface. Ice dams are also the cause of ancillary damage such as water penetration and roofing distress.

Guidance will also be enhanced for accumulations on greenhouses, fabric structures and domes.

The ASCE Snow Load Subcommittee will meet at the Second International Conference on Snow Engineering on June 21-26, 1992 to chart progress on the proposed improvements discussed above. The first draft of the 1995 edition is scheduled to be submitted by the ASCE Standard 7 Technical Committee on August 15, 1993. The first letter ballot is scheduled to be issued on December 17, 1993, with balloting and resolution of negative votes completed by September 1995. The document is scheduled to be published in December 1995.

U.S. BUILDING STANDARDS AND CODES

Building construction in the United States of America is regulated through building codes. According to the U.S. Constitution, the federal government does not have authority to promulgate a national building code. The 10th Amendment to the United States Constitution gives states the right to legislate for the protection of public health, safety, and welfare. A state may choose to delegate a portion of its right of legislation and/or enforcement to the constituent local governmental units (e.g., cities) that are formed by the state legislature. Approximately one-half of the states have enacted a state-wide building code with some degree of scope and application.

The administration and enforcement of building codes has traditionally been a local government responsibility, even for states with a state-wide building code. Early in this century, code enforcement officials began regular national and regional meetings to discuss their common problems and concerns. These meetings produced three organizations of code enforcement officials: a) Building Officials and Code Administrators International, Inc. (BOCA), representing the code officials from the eastern and midwestern portions of the United States; b) the International Conference of Building Officials (ICBO), representing the code officials from the western United States; and c) the Southern Building Code Congress International, Inc. (SBCCI), representing the interests of the southern United States. Each of these three organizations eventually produced its own model code as a guide that legislative bodies could adopt as their own building code. While legislative bodies are not obligated to adopt a model code and may write their own code or portion of a code, recent studies have indicated that 97% of all United States cities have adopted one of the three model codes or are covered by a state-wide building code based on one of the model building codes. The three model codes are: the Basic/National Building Code of BOCA, the Uniform Building Code of ICBO, and the Standard Building Code of SBCCI.

Historically the three model codes have differed in their technical provisions, format and use of standards. Working through an ASCE Administrative Committee on Building Codes, the three model codes have committed to achieve uniformity in building codes. They support the ASCE Policy Statement 340, "Uniformity of Building Codes," that states:

"The American Society of Civil Engineers actively encourages the model building code groups and governmental agencies to develop uniformity among the codes in their technical provisions, format and use of standards as applied to the field of civil engineering. All governmental jurisdictions and agencies, federal, state and local, are encouraged to adopt one of the three model codes without alteration. The three model code groups are

encouraged to adopt by reference those standards developed and maintained through a nationally recognized consensus process such as ANSI and ASTM."

ASCE is a voluntary consensus standards organization accredited by the American National Standards Institute (ANSI). ASCE standards committees have balanced representation from three interest groups: a) producers; b) consumers; and c) general interest, including regulatory interests. The ASCE standards committee on Minimum Design Loads on Buildings and Other Structures currently has 97 members and is responsible for the ASCE7 standard.

The Standard Building Code adopted the snow load provisions of ASCE7-88 by reference in the fall of 1991. BOCA's code changes committee rejected the ASCE7-88 snow load provisions because they contain "non-mandatory, permissive and subjective" language, thus making them difficult to enforce by the code officials. All ASCE standards written for adoption by reference by model codes should be written in mandatory language and should be worded so that the reader can interpret where it has, or has not, been followed and the extent to which it has, or has not, been followed. BOCA officials identified about a dozen places where the language of the ASCE7-88 snow load provisions is non-mandatory, permissive and/or subjective. The ASCE7 standards committee will prepare the 1995 edition in mandatory language that is acceptable to model codes and can be adopted by reference.

SUMMARY AND CONCLUSIONS

The ASCE7-88 is a consensus standard containing the most advanced data, methodology and miscellaneous information on United States building snow loads as of 1988. The document is based upon information from earlier U.S. standards, information from the National Building Code of Canada, and research consisting of field and laboratory studies. The ground snow loads were prescribed using 10 years of additional meteorological data beyond the previous U.S. map in the ANSI72 standard. New statistical methods and spatial extrapolation methods were also used for ASCE7-88. The ground-to-roof relationships in the current standard are the result of a nation-wide field study of roofs with various regional characteristics, building sitings and roof constructions; thus, exposure and thermal factors are explicitly incorporated to reflect this knowledge base. ASCE7-88 also contains the latest information on sliding snow so that structures are not penalized if the roof surface will permit snow to slide. Drift provisions, obtained from extensive statistical analysis of extensive failure case histories, are also contained in ASCE7-88. Work is currently in progress by the ASCE Snow Load Subcommittee to upgrade the snow load provisions on 17 issues and incorporate them into the 1995 edition. Extensive liaison work is also underway by the ASCE Manager on Codes and Standards to persuade the three U.S. model building codes to unify the building codes by adopting by reference ASCE7-88 and subsequent editions.

REFERENCES

American National Standard - Minimum Design Loads for Buildings and Other Structures. (1982). A58.1-1982, American National Standards Inst., New York, N.Y.

American Society of Civil Engineers (1988). *Minimum Design Loads for Buildings and Other Structures.* A58.1-1982, American Society of Civil Engineers, New York, N.Y.

Boyd, D. W. (1961). "Maximum Snow Depths and Snow Loads on Roofs in Canada," *Proc. 29th Annual Meet. West. Snow Conf.*, Res. Pap. 142, Div. Build. Res. NRC 6312, NRCC, Ottawa, Ont., 6-16.

The BOCA Basic/National Building Code. (1990). Building Officials & Code Administrators International, Inc., Ninth Ed., Country Club Hills, Ill.

- Brown, J. W. (1979) "An Approach to Snow Load Evaluation," *Proc. 38th Annual Meet. West. Snow Conf.*, Sparks, Nev.
- Ellingwood, B., and R. Redfield (1983) "Ground Snow Loads for Structural Design," *J. Struct. Engrg.*, ASCE, 109(4), 950-964.
- Elliott, M. (1981) "Snow Load Data for Arizona," Structural Engineers Association of Arizona, Tucson, Ariz.
- Endo, A. and Tomabechi, T. (1983). "Wind Channel Experiment of the Forming Conditions of the Snow Deposition on Various Roofs With Model Snow," *Memoirs of the Hokkaido Institute of Technology*, No. 11, 163-178 (in Japanese).
- Isyumov, N., and A. G. Davenport (1974) "A Probabilistic Approach to the Prediction of Snow Loads," *Can. J. Civ. Engrg.*, 1, (Sept.) 28-49.
- Lutes, D. A., and W. R. Schriever (1971) "Snow Accumulations in Canada: Case Histories: II," *Tech. Paper 339*, Div. Build. Res., NRCC No. 11915, Nat. Res. Counc. Can., Ottawa, Ont., 1-17.
- Meehan, J. F. (1979) "Snow Loads and Roof Failures," *Proc. Struct. Engrg. Assn. Calif.*, 38th Ann. Conv., San Francisco, Calif.
- Newark, M.J. (1984). "A New Look at Ground Snow Loads in Canada," *Proc.*, 41st East. Snow Conf., New Carrollton, Md.
- O'Rourke, M. J., P. Koch, and R. Redfield (1983) "Analysis of Roof Snow Load Case Studies, Uniform Loads," CRREL Rept. 83-1, Hanover, N. H.
- O'Rourke, M. J., and U. Stiefel (1983) "Roof Snow Loads for Structural Design," *J. Struct. Engrg.*, 109(7), 1527-1537.
- O'Rourke, M. J., R. S. Speck, Jr., and U. Stiefel (1985) "Drift Snow Loads on Multilevel Roofs," *J. Struct. Engrg.*, ASCE, 111(2), 290-306.
- O'Rourke, M. J., and E. Wood (1986) "Improved Relationship for Drift Loads on Buildings," *Can. J. Civ. Engrg.*, 13(6), 647-652.
- O'Rourke, M. J., W. Tobiasson, and E. Wood (1986) "Proposed Code Provisions for Drifted Snow Loads," *J. Struct. Engrg.*, ASCE, 112(9), 2080-2108.
- Peter, B. B. W., W. A. Dalgliesh, and W. R. Schriever (1963) "Variation of Snow Loads on Roofs," *Trans. Engrg. Inst. Can.*, 6(A-1), 1-11.
- Placer County, Building Division (1985) *Placer County code*, Ch. 4, Sec. 4.20(v), "Snow Load Design," Auburn, Calif.
- Sack, R. L., and A. Sheikh-Taheri (1986) *Ground and Roof Snow Loads for Idaho*, Dept. of Civil Eng., Univ. of Idaho, Moscow, Idaho.
- Sack, R. L., D. Arnholtz, and J. S. Haldeman (1987) "Sloped Roof Snow Loads Using Simulation," *J. Struct. Engrg.*, ASCE, 113(8), 1820-1833.

Sack, R. L. (1988) "Snow Loads on Sloped Roofs," *J. Struct. Engrg.*, ASCE, 114(3), 501-517.

Schriever, W. R., Y. Faucher, and D. A. Lutes (1967) "Snow Accumulations in Canada: Case Histories: I," *Tech. Pap. 237*, Div. Build. Res. NRC No. 9287, NRCC, Ottawa, Ont., 1-29.

Standard Building Code (1991), Southern Building Code Congress International, Inc., Birmingham, Ala.

Stenberg, P. and F. Videon (1978) "Recommended Snow Loads for Montana Structures," Dept. of Civ. Eng./Eng. Mech., Montana State Univ., Bozeman, Mont.

Structural Engineers Association of Colorado (1984) "Snow Load Design Data for Colorado," Boulder, Colo.

Structural Engineers Association of Northern California (1964) "Snow Load Design Data for the Lake Tahoe Area," San Francisco, Calif.

Structural Engineers Association of Oregon (1971) "Snow Load Analysis for Oregon," Portland, Oreg.

Structural Engineers Association of Washington (1981) "Snow Load Analysis for Washington," Seattle, Wash.

Taylor, D. A. (1980) "Roof Snow Loads in Canada," *Can. J. Civ. Engrg.*, 7(1), 1-18.

The Uniform Building Code (1991), International Conference of Building Officials, Whittier, Calif.

An Overview of Snow Loads for Fairbanks, Alaska

Wayne Tobiasson and Alan Greatorex

U.S. Army Cold Regions Research and Engineering Laboratory
Hanover, New Hampshire, U.S.A.

ABSTRACT

In the 1970s design roof snow loads for Fairbanks, Alaska, ranged from 1.4 kPa (30 psf) to 3.1 kPa (65 psf) among the various "local experience" guidelines available. Three studies done between 1973 and 1978 each provided a statistical basis for new guidance. The range of values was less among these new guidelines but differences persisted. Heavy snows during the 1990–91 winter caused several roofs to collapse and existing snow load design criteria to be questioned.

Measurements were made of ground and roof snow loads during these record snows and meteorological information was updated and reanalyzed. The updated data base indicated that the 50-year *ground* snow load should be 2.9 kPa (60 psf). Observations and measurements of snow on the ground and on roofs indicated that the 0.6 factor in the equation used to convert ground loads to roof loads should be increased to 0.7 for roofs in the Fairbanks area. Winter winds in that area are quite low.

Because the design snowpack is quite deep, it is not considered necessary to add a rain-on-snow surcharge load to roof snow loads. Rain has already been included in the water equivalent measurements used to establish the 2.9-kPa (60-psf) ground snow load.

TWENTY YEARS AGO

In the early 1970s snow loads used in the design of roofs for Fairbanks, Alaska, varied considerably among the various guidelines available at that time as follows:

City of Fairbanks Building Code	1.9 kPa (40 psf)
Design data map of the Alaska District, Corps of Engineers	1.4 (30)
U.S. Army and Air Force Technical Manual TM 5-805-1	1.7 (35)
U.S. Navy Cold Regions Design Manual	3.1 (65)
ANSI Standard A58.1-1972	Nothing for Alaska

No information could be obtained on how each of the above loads was arrived at except that they were based largely on "local experience."

In an attempt to improve upon this situation and develop a systematic way of developing design snow loads, CRREL personnel studied Alaskan snow load data and summarized findings in "Alaskan Snow Loads" (Tobiasson and Redfield, 1973). That work introduced us to the difficulties of establishing design values from incomplete and imperfect measurements. We learned that the meteorological data base had the following limitations:

1. Essentially no long-term information is available on snow loads on roofs. Thus predicting long-term (e.g., 50-year mean recurrence interval) values for design must be based on measurements of snow on the ground.

2. The *depth* of snow on the ground is measured periodically at many stations in the USA but only a few stations measure the weight of that snow. In Alaska in the 1970s, the *depth* of snow on the ground was measured at 137 locations but the weight (i.e., water equivalent) of that snow was only measured at 25 of those locations.

3. Some other stations that report both depths and water equivalents base these water equivalents on the assumption that 10 in. of snow has a water equivalent of 1 in. In other words, the density of that snow is assumed to be only 100 kg/m^3 (6.2 pcf). That is too low a density for most snow on the ground in Alaska.

4. Some stations measure the water equivalent once in a while and then estimate the *increase* in water equivalent using the above "10 to 1 rule" until they measure the water equivalent again. Because the estimate is inaccurate, there is a jump in the water equivalent data series even though no new snow has fallen. Since measured and estimated values are not differentiated, it is then difficult to separate good information from bad information.

Unfortunately, these limitations continue at the present time.

In "Alaskan Snow Loads" log-normal extreme value statistics were used on the series of maximum snow depths for each season of record for each station to determine the depth of snow on the ground for return periods of 5, 10, 25, 30, 50 and 100 years. Thom (1966) had shown that climatological series

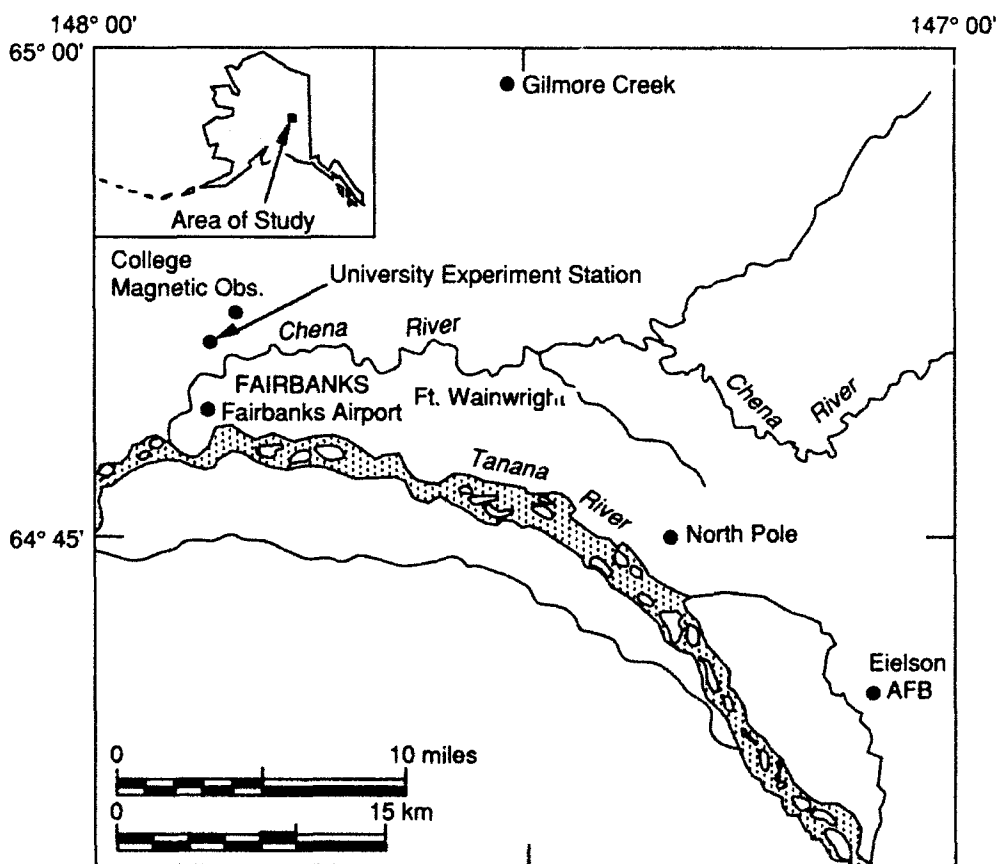


Figure 1. Stations in the Fairbanks, Alaska, area.

of annual maximum snow depths on the ground closely follow log-normal distributions. Figure 1 shows the location of several stations in the Fairbanks area and Table I lists the 25-year mean recurrence interval depth for some of those stations.

To determine the load of that snow, the concurrent records of snow depth and snow load were examined for each station where both depths and loads are measured. In Alaska there were only 25 such stations. For each year of record the maximum depth and maximum load were used to determine a "conversion density." By plotting that density against its maximum load, the trend in conversion density with large loads was established. The "conversion density—load" plot for Fairbanks is shown in Figure 2. The dashed line represents the general trend of increasing density with load and the number at its right end is the conversion density considered appropriate to use to represent a large, "design" snowpack.

Such conversion densities were developed for each of the 25 stations in Alaska and the results were used to develop regionalized conversion densities. Fairbanks fell within interior region "B" to which the conversion densities in Table II were assigned.

Table I. Twenty-five year mean recurrence interval ground snow depths for stations in the Fairbanks area (period of record ends in 1973).

Station m (in.)	Snow depth
Fairbanks AP	1.52 (60)
College Magnetic Obs.	1.42 (56)
University Experiment Station	1.32 (52)
Eielson AFB	1.70 (67)

Table II. Regionalized conversion densities used for the Fairbanks area in "Alaskan Snow Loads."

Elevation m (ft)	Conversion density kg/m ³ (pcf)
0-152 (0-500)	250 (15.6)
152-457 (500-1500)	300 (18.7)
Above 457 (above 1500)	350 (21.8)

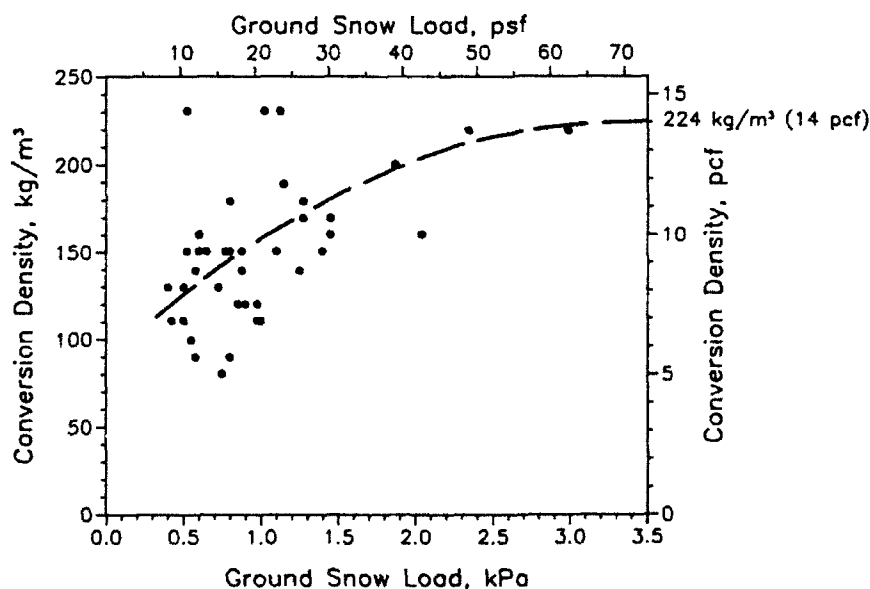


Figure 2. Conversion density vs ground snow load for the Fairbanks AP station (period of record ends in 1973).

Table III. Twenty-five year mean recurrence interval ground snow loads for stations in the Fairbanks area using the depths in Table I and the regionalized conversion densities in Table II (period of record ends in 1973).

Station	Ground snow load, kPa (psf)
Fairbanks AP	3.7 (78)
College Magnetic Obs.	4.2 (87)
University Experiment Station	3.3 (68)
Eielson AFB	5.0 (105)

Table IV. Design snow loads for low slope roofs for stations in the Fairbanks area using the information in "Alaskan Snow Loads."

Station	Range in design roof load kPa (psf)	Common value* kPa (psf)
Fairbanks AP	1.9-3.4 (39-71)	2.4 (51)
College Magnetic Obs.	2.1-3.8 (44-79)	2.7 (57)
University Experiment Station	1.6-3.0 (34-62)	2.2 (45)
Eielson AFB	2.5-4.6 (52-96)	3.3 (69)

* Where exposure factor equals 1.2 and thermal factor equals 1.1 in "Alaskan Snow Loads."

Comparison of Table II and Figure 2 shows that the regionalized conversion densities used for the Fairbanks area greatly exceed those obtained from measurements at the Fairbanks Airport (AP). Thus, it is likely that loads generated by applying these regional conversion densities to the 25-year depths in Table I would be too high. Those loads are presented in Table III.

In "Alaskan Snow Loads" a methodology was also developed to convert 25-year ground snow loads to design roof loads. This involved the use of a "regional ground-to-roof conversion factor," which, for the Fairbanks area, was 0.5; a "roof exposure factor," which varied from 1.0 for a windswept roof to 1.3 for a roof in among trees; and a "roof thermal factor," which varied from 1.0 for a heated building with an unventilated roof to 1.4 for an unheated building. When ground snow loads were multiplied by these factors, the roof design loads in Table IV were generated.

Over the years many Alaskan designers used the information in "Alaskan Snow Loads." Perhaps much of its wide use in Alaska can be ascribed to its use by the late Elbert ("Eb") Rice in his University of Alaska, Arctic Engineering courses that were often taken by engineers seeking to obtain their license to practice in Alaska.

NATIONWIDE SNOW LOADS

After completing "Alaskan Snow Loads" our interest in snow loads at CRREL expanded to include all of the United States. We funded others to obtain concurrent measurements of ground and roof loads and we used those findings to improve ground-to-roof conversion factors (O'Rourke et al., 1983). We also analyzed ground snow depths for over 9,000 stations across the USA and used log-normal extreme value statistics to generate a 50-year mean recurrence depth for each of these locations. We changed from a 25-year to a 50-year mean recurrence value to be consistent with design wind loads that were 50-year values.

The conversion density issue was handled differently than had been done for Alaska. The 50-year depth and load were determined at each of 184 stations across the USA where both depth and water equivalent measurements were taken. However, we did not include Alaskan stations in this study. The method of least squares was used to determine the best fit relationship between all the 50-year depths and 50-year loads. That generated the following equation:

$$L = 0.302 D^{1.33} \quad \text{English Units (1a)}$$

where L = 50-year ground snow load in psf
 D = 50-year ground snow depth in inches.

In the SI system with D in meters and L in kPa this equation is:

$$L = 1.91 D^{1.33} \quad \text{S.I. Units (1b)}$$

For much of the USA the ground snow loads thus generated were mapped. However, for Alaska, limited data and extreme local variations precluded meaningful mapping and site-specific values were determined for a number of population centers. These values were based on measured water equivalent information, where available, supplemented by depth information nearby. Eq. 1, while not developed from Alaskan data, was used to convert 50-year depths to loads when doing each site-specific case study, even those in Alaska. Table V shows the information used to establish the 50-year ground snow load of 2.6 kPa (55 psf) for Fairbanks in ANSI (1982), Dept. of Army (1986) and ASCE (1990).

The major discrepancy in Table V is between the one value based on measured loads (i.e., 2.2 kPa, 45 psf) and all the other, much higher values based on measured depths converted to loads using Eq. 1. Since the measured load value was based on a long period of record (26 years), with most of the data quite believable, we relied on it heavily. However, since the conversion density generated by dividing the 2.2 kPa (45 psf) "50-year" load by the 1.57 m (62 in.) "50-year" depth, produced a low conversion density of 144 kg/m³ (9 pcf) we had some reservations. From Figure 2 we had expected a conversion density closer to 208 kg/m³ (13 pcf). Using 208 kg/m³ (13 pcf) and the 1.57-m (62-in.) depth, the load would calculate to 3.2 kPa (67 psf). The 2.6 kPa (55 psf) value was selected as a compromise between what the two data sets were producing.

In ANSI (1982), Dept. of Army (1986) and ASCE (1990) ground loads in *Alaska* are converted to loads on low slope roofs using the following equation

$$P_f = 0.6 C_e C_t I P_g \quad (2)$$

where P_f = flat roof snow load (kPa or psf)

C_e = exposure factor which varies from 0.8 for exposed roofs in windy areas to 1.2 for roofs located tight in among conifers in areas that experience little wind

C_t = thermal factor which varies from 1.0 for roofs of heated structures to 1.2 for roofs of unheated structures

I = importance factor which varies from 0.8 for buildings that represent a low hazard to human life to 1.2 for essential facilities needed in emergencies

P_g = 50-year ground snow load (kPa or psf).

Using this equation and the 2.6-kPa (55-psf) ground load established for the Fairbanks area, design snow loads for most low slope roofs (i.e., those with an importance factor of 1.0) ranged from 1.2 to 2.3 kPa (26 to 48 psf) with most roofs at 1.6 kPa (33 psf.) To these values many designers added a 0.2-

Table V. Information in the Fairbanks area used to establish the 2.6 kPa (55 psf) ground snow load tabulated in ANSI (1982), Dept. of Army (1986) and ASCE (1990).

Station	Elevation m (ft)	Years of record	Ground snow load, kPa (psf)
Fairbanks AP (water equivalent)	134 (440)	26	2.2 (45)*
Fairbanks AP	134 (440)	26	3.5 (74)
College Magnetic Obs.	189 (620)	22	3.4 (72)
University Experiment Station	146 (480)	19	3.2 (67)
Eielson AFB	168 (550)	19	4.9 (103)

* This value is based on measured water equivalents not measured depths converted to loads using Eq. 1.

Table VI. Information in the Fairbanks area from the AEIDC study.

Station	Ground snow load, kPa (psf)	
	As published (Eq. 4)	Corrected value (Eq. 3)
Fairbanks AP	2.2 (45)*	2.2 (45)*
Fairbanks AP	3.4 (70)	4.4 (92)
College Magnetic Obs.	3.0 (63)	3.9 (82)
University Experiment Station	2.9 (61)	3.7 (78)
Eielson AFB	3.9 (82)	5.1 (106)
North Pole	3.4 (70)	4.3 (90)
Gilmore Creek	3.1 (64)	3.9 (82)

* This value is based on measured water equivalents and does not use either Eq. 3 or 4.

kPa (5-psf) rain-on-snow surcharge load if the slope was less than 1:24 (1/2 in./ft) in accordance with recommendations in the three references cited above. This increased the design value to 1.8 kPa (38 psf).

Comparing this information to that in Table IV, it is evident that our more recent work resulted in a reduction in design snow loads for the Fairbanks area. This seemed appropriate since the regionalized conversion densities used to establish the older design values (i.e., those in Table IV) were high for the Fairbanks area.

MORE RECENT ALASKAN GUIDANCE

In the mid-1980s CRREL helped fund the Arctic Environmental Information and Data Center (AEIDC) of the University of Alaska, to update snow load design guidance for Alaska. In 1987 the AEIDC report "Snow Loads in Alaska" was published (Leslie et al., 1987). The period of record was expanded beyond what we had analyzed for ANSI (1982) to include information collected from 1978 to 1987. A log-normal statistical analysis of the maximum annual water equivalents at the Fairbanks AP station once again generated a 50-year value of 2.2 kPa (45 psf).

An attempt was made to develop regionalized conversion densities as had been done in CRREL's "Alaskan Snow Loads" paper but, in the words of the first author, that attempt "met with failure."

Rather than use Eq. 1 to generate 50-year loads from maximum annual depths, the AEIDC authors developed an "Alaskan" version of that equation in much the same way Eq. 1 was developed except that only Alaskan stations having concurrent depth and water equivalent measurements were used. The total number of such stations was expanded by also including several locations where the Soil Conservation Service collects such information once or twice a month during the winter. The equation generated was as follows:

$$L = 0.44 D^{1.31} \quad \text{English Units (3a)}$$

where L = 50-year ground snow load in psf

D = 50-year ground snow depth in inches.

In the S.I. System with D in meters and L in kPa this equation is:

$$L = 2.59 D^{1.31} \quad \text{S.I. Units (3b)}$$

Unfortunately, this equation was incorrectly applied to the 50-year depths in the following form:

$$L = (0.44 D)^{1.31} \quad \text{English Units (4a)}$$

$$L = 2.01 D^{1.31} \quad \text{SI Units (4b)}$$

Table VI presents ground snow load information for the Fairbanks area from the AEIDC report "Snow Loads in Alaska" using Eqs. 3 and 4. The values generated by incorrect Equation 4 are about the same as the Table V values we generated with a somewhat shorter period of record and Eq. 1. The Eq. 3 values exceed all prior values. For the Fairbanks AP, Eq. 3 generates a conversion density of 300 kg/m³ (18.7 pcf) which, in light of the information in Figure 2, seems too high.

From this we expect that the correct application of the AEIDC method generates excessively high ground snow loads for stations in the Fairbanks area.

In 1990 the Structural Engineers Association of Alaska (SEAA) examined the tabulated Alaskan information in ANSI (1982) and that in the AEIDC report. In a memorandum to their members, SEAA recommended that the higher of the two values at any location be used for design in Alaska. For Fairbanks the ANSI and AEIDC values for ground snow load were 2.6 and 3.4 kPa (55 and 70 psf), respectively. Thus the 3.4-kPa (70-psf) value was to be used according to the SEAA recommendation. At the time of this recommendation neither AEIDC, CRREL nor SEAA were aware of the calculation error in the AEIDC report. Once this problem was uncovered, AEIDC alerted the Alaskan design profession. SEAA will provide further guidance to their members once more information becomes available.

THE WINTER OF 1990-91

The winter of 1990-91 brought record snows to Fairbanks, Alaska, and a number of roof collapses. The maximum water equivalent on the ground at the Fairbanks AP station was 0.3 m (12 in.) of water. In other words, the ground snow load was 3.0 kPa (62 psf). That stands as the largest value observed since such records began in 1952. The maximum depth of snow during the 1990-91 winter was 1.37 m (54 in.) and thus the conversion density for that record year was 222 kg/m^3 (13.9 pcf) which is close to the 208 kg/m^3 (13-pcf) value obtained from the 1952-1973 period of record as shown in Figure 2.



Figure 3. Troops clearing snow from a residential roof at Ft. Wainwright, January 1991. (U.S. Army photograph.)

During the 1990-91 winter, several buildings collapsed under heavy snow loads in Fairbanks. At nearby Ft. Wainwright on January 11 over 2000 troops and civilian employees began shoveling snow off roofs. The extent of that operation is shown in Figures 3 and 4. A lot of damage was done to these roofs by all this activity.

During that winter CRREL personnel from our office on Ft. Wainwright measured the depth and weight of snow on the ground and on some roofs at Ft. Wainwright. The measurements they obtained are presented in Figure 5. The maximum ground load of 3.0 kPa (62 psf) is the same as the maximum reported that winter at the Fairbanks AP several miles away. However, the maximum depth of 1.12 m (44 in.) at Ft. Wainwright was significantly less than the 1.37-m (54-in.) maximum at the Fairbanks AP. These measurements suggest a 1990-91 Ft. Wainwright conversion density of 270 kg/m^3 (17 pcf) which exceeds the 222 kg/m^3 (13.9 pcf) conversion density for the Fairbanks AP during that winter.

Measurements were also taken on low slope roofs on January 9, 1990 and March 26, 1991. Those measurements produced overall ground-to-roof conversion factors (i.e., ratios P_f to P_g) of 0.94 and 0.75 respectively. The 0.75 value is of most interest since it occurred later in the season



Figure 4. Troops clearing snow from a low slope roof at Ft. Wainwright, January 1991. (U.S. Army photograph.)

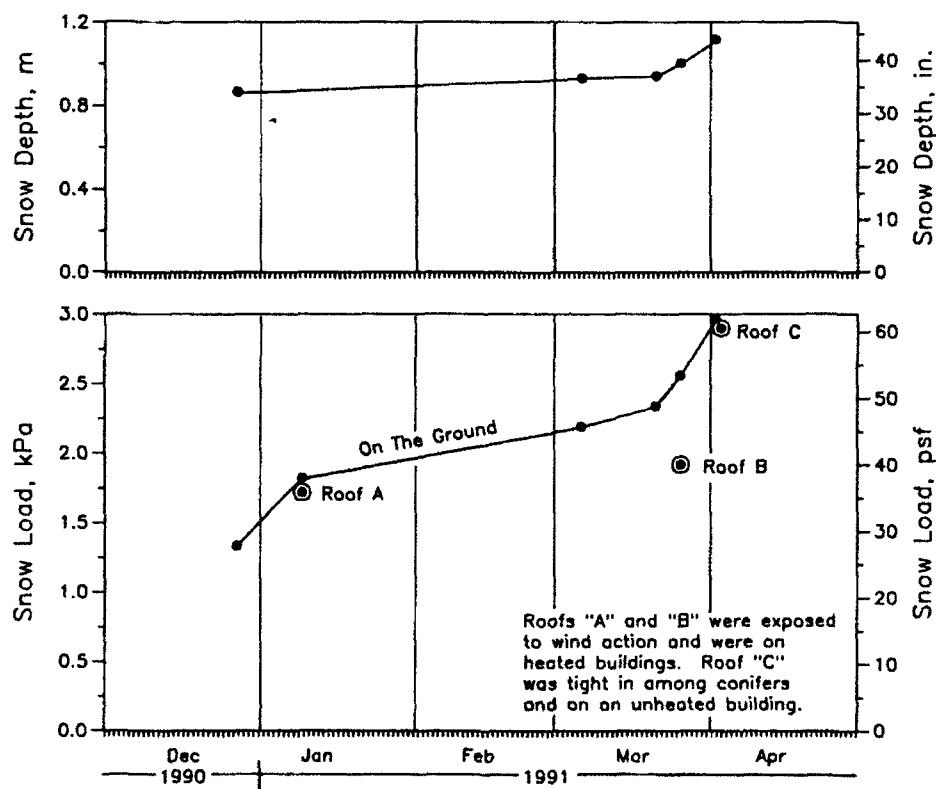


Figure 5. Snow depths and loads measured at Ft. Wainwright during the 1990-91 winter.

when higher ground loads were present. The 0.75 value is much greater than the 0.6 factor that would be used to calculate design loads for such roofs in the current national design load standard (ASCE, 1990) and somewhat above the 0.7 factor that would be used in the Uniform Building Code (1988) unless otherwise advised by "the building official."

On April 3, readings were taken on the Ft. Wainwright low slope roof of an unheated building surrounded by spruce trees. The overall ground-to-roof conversion factor for those readings was 0.98 which, again, was above the ASCE (1990) value of 0.86 and the Uniform Building Code (1988) value of 0.9 for that situation.

During this period of heavy snows, Charles Jeannet of the City of Fairbanks also made observations of ground and roof snow loads. He concluded that many roofs in the Fairbanks area had about 90% of the ground snow load on them (Jeannet, 1992).

Some individuals suggested that all prior snow load guidance was no longer appropriate since it did not include this record year. While we agreed that the statistics should be updated to include all records available through the 1990–91 winter, we expected that ground snow loads would not change much as a result.

Once we had the maximum values of ground snow load and ground snow depth for the 1990–91 winter we updated those statistics. The 50-year load at the Fairbanks AP increased to 2.4 kPa (49 psf). The new 50-year depth was 1.47 m (58 in.) which was less than the 1.50 m (59 in.) that AEIDC calculated using maximum depths through the 1986–87 winter and less than the 1.57 m (62 in.) used in our calculations, which were current only through the 1977–78 winter.

Using the CRREL equation (Eq. 1) and the 1.47 m (58 in.) depth, the 50-year load calculates to 3.2 kPa (67 psf) and the conversion density is 220 kg/m^3 (13.8 pcf) which is believable. Using the corrected AEIDC equation (Eq. 2) the 50-year load calculates to 4.3 kPa (90 psf) and the conversion density is 300 kg/m^3 (18.6 pcf) which seems high.

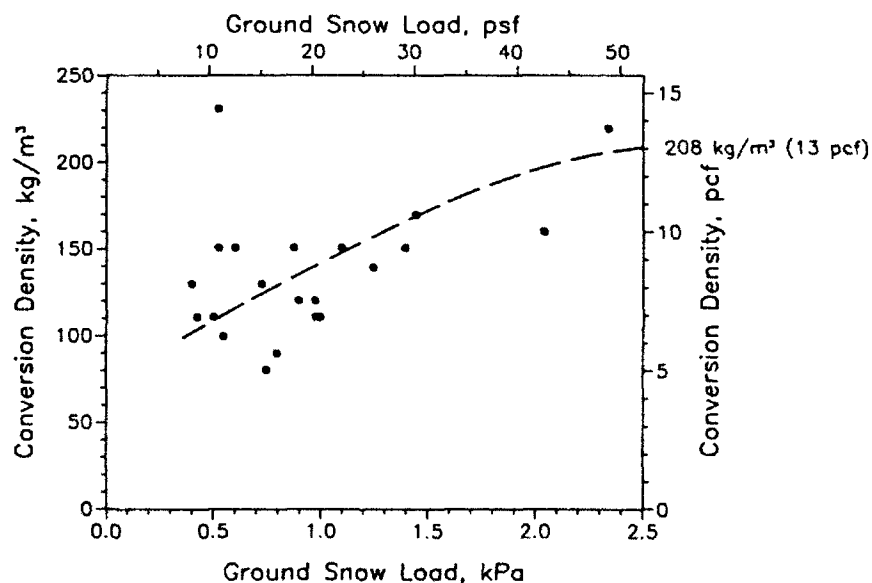


Figure 6. Conversion density vs ground snow load for the Fairbanks AP station (updated version of Figure 2 with data through the 1990–91 winter).

Figure 2, which proved to be valuable in the past, was updated to include data for all winters from 1952–53 through 1990–91. The update is presented in Figure 6. The conversion density for high values of ground snow loads has increased from 208 to about 224 kg/m³ (13 to about 14 pcf).

RECOMMENDATIONS

After examining all this information, we have developed the following recommendations:

1. In the Fairbanks area 2.9 kPa (60 psf) is a reasonable value to use as a 50-year ground snow load (i.e., P_g in Eq. 2).
2. In the Fairbanks area the 0.6 factor in the ground-to-roof equation (i.e., Eq. 2) should be increased to 0.7 and the Fairbanks area should be considered to be “an area that does not experience much wind” when establishing a value for C_e .
3. In the Fairbanks area it is not necessary to add a rain-on-snow surcharge load of 0.2 kPa (5 psf) to the roof snow load.
4. At Eielson AFB, which is about 37 km (23 miles) southeast of Fairbanks, 3.6 kPa (75 psf) is a reasonable value to use as a 50-year ground snow load.

These recommendations are based on the following:

1. Ground snow loads should be increased somewhat to include the effect of the heavy snows of the 1990–91 winter. When establishing a ground snow load, considerable emphasis should be given to the long record of *measured* water equivalents at the Fairbanks AP. However, long records of the depth of snow on the ground at other stations in the Fairbanks area are also of value and should be considered. When such depths are converted to loads by various methods, ground loads are generated that are consistently in excess of those obtained from the Fairbanks AP water equivalent measurements. To give this source of information some value, the recommended ground load has been increased above that indicated by the Fairbanks AP water equivalent measurements.
2. Low winds in the Fairbanks area during the winter result in higher overall ground-to-roof conversion factors there than in many other places in Alaska. Thus the “Alaska-wide” equation (Eq. 2) generates roof loads that are too low. That equation should be modified to produce higher roof loads for the Fairbanks area. By increasing the 0.6 in Eq. 2 to 0.7 and considering the Fairbanks area as “an area that does not experience much wind” when establishing C_e , design snow loads increase to values more in line with those observed during heavy snow years.
3. In the Fairbanks area during heavy snow years, loads often peak late in the season when rain-on-snow is likely. However, the snowpack is quite deep then, and rain is retained in it for some time. Therefore, rain has already been included in the water equivalent measurements used to establish the 2.9-kPa (60-psf) ground snow load.
4. Snow loads are greater at Eielson AFB. Ratios of the Eielson AFB and Fairbanks area information in Tables I, III, IV, V and VI range from 1.2 to 1.45. A reasonable value for the 50-year ground snow load for Eielson AFB is 3.6 kPa (75 psf) when used with an increased factor of 0.7 in Eq. 2.

ACKNOWLEDGMENTS

The willingness of Lynn Leslie of AEIDC, Charles Jeannet of the City of Fairbanks and Art Whitmer of SEAA to share information and ideas is much appreciated. The measurements on Ft. Wainwright during the 1990-91 winter were made by Charles Collins, Walter Olson and David Dillingham of CRREL's Ft. Wainwright Office.

REFERENCES

- American National Standards Institute (1972) *Building Code Requirements for Minimum Design Loads in Buildings and Other Structures*, ANSI Standard A58.1-1972, New York.
- American National Standards Institute (1982) *Minimum Design Loads for Buildings and Other Structures*, ANSI Standard A58.1-1982, New York.
- American Society of Civil Engineers (1990) *Minimum Design Loads for Buildings and Other Structures*, ASCE 7-88, New York.
- City of Fairbanks, Alaska (1971) *City of Fairbanks Building Code Ordinance No. 2070*, Fairbanks, Alaska.
- Corps of Engineers (1958) *Design Data for Military Construction in Alaska*, Map prepared by the Office of the District Engineer, Anchorage, Alaska.
- Department of the Army (1986) *Load Assumptions for Buildings*, Army Technical Manual TM 5-809-1, Washington, D.C.
- Department of the Navy, Naval Facilities Engineering Command (1967) *Design Manual, Cold Regions Engineering*, NAVFAC DM-9, Washington, D.C.
- Departments of the Army and Air Force (1966) *Load Assumption for Buildings*, Technical Manual TM-5-809-1, Washington, D.C.
- International Conference of Building Officials (1988) *Uniform Building Code*, 1988 Edition, Whittier, California.
- Jeannet, C. (1992) Personal communication.
- Leslie, L., J. Wise, and J. Fredston (1987) *Snow Loads in Alaska*, Arctic Environmental Information and Data Center (AEIDC), Technical Note No. 4, Anchorage, Alaska.
- O'Rourke, M., P. Koch and R. Redfield (1983) *Analysis of Roof Snow Load Case Studies: Uniform Loads*, CRREL Report 83-1, Hanover, New Hampshire.
- Thom, H.C.S. (1966) *Distribution of Maximum Annual Water Equivalent of Snow on the Ground*. Monthly Weather Review, Volume 94, No. 4, April 1966.
- Tobiasson, W. and R. Redfield (1973) *Alaskan Snow Loads*, Paper presented at the 24th Alaskan Science Conference, University of Alaska, August 1973. Copies available from CRREL, Hanover, New Hampshire.

Snow Recycling House in a Heavy Snowfall District

Toshiaki Higuchi

Tokamachi City Hall Construction Division
Tokamachi-shi, Niigata-ken, Japan

ABSTRACT

This research has been undertaken in Tokamachi City, Niigata, which has a population of 50,000 and an average January temperature of -0.6 C. With its maximum snow depth of 243.4 cm and a cumulative snowfall of 1197.5 cm per year, Tokamachi is considered to have the heaviest snowfall in the world for a city of its size. As a permanent resident of Tokamachi, I have learned that instead of battling the abundant snowfall, it is much easier to utilize it and live in harmony with it. In order to achieve this, I built my "Snow Recycling House" in Tokamachi in 1988. Combining traditional wisdom, existing technology and future-focused thought, I created what I call the "Higuchi Style" house. It utilizes snow to provide water and to reduce energy costs.

The following figures show the systems of the Snow Recycling House. First, the snow on the roof slides down into the snow pond (A in Figures 1 & 2) and rain is gathered in the water pond (B in Figures 1 & 2). Each pond is built above a separate well (C in Figure 2). The wells collect water from their respective ponds. Second, the water pump (D in Figure 2) draws the water from the wells into the house. The water is used for the bathroom, air conditioning systems, snow melting pipes and so forth. According to my four years of research, the annual water expenses were reduced by approximately one half, snow removal costs and air conditioning costs were less than in previous years, and the wells contained water all year by utilizing the stored snow.

My future vision is to establish a snow recycling model town by making use of the technology used in the snow recycling house. It can be used in a town hall, public buildings and so forth. The model town will be a big attraction on a local, national and global level. I believe snow utilization has a strong appeal in areas with great snowfall as a method for energy conservation. Consequently, it is an environmentally friendly way of living.

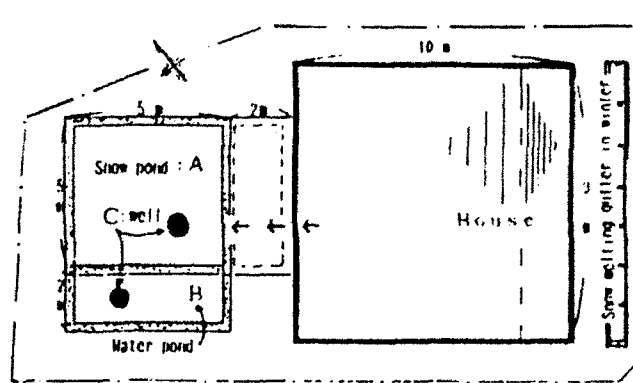


Figure 1. Plan view.

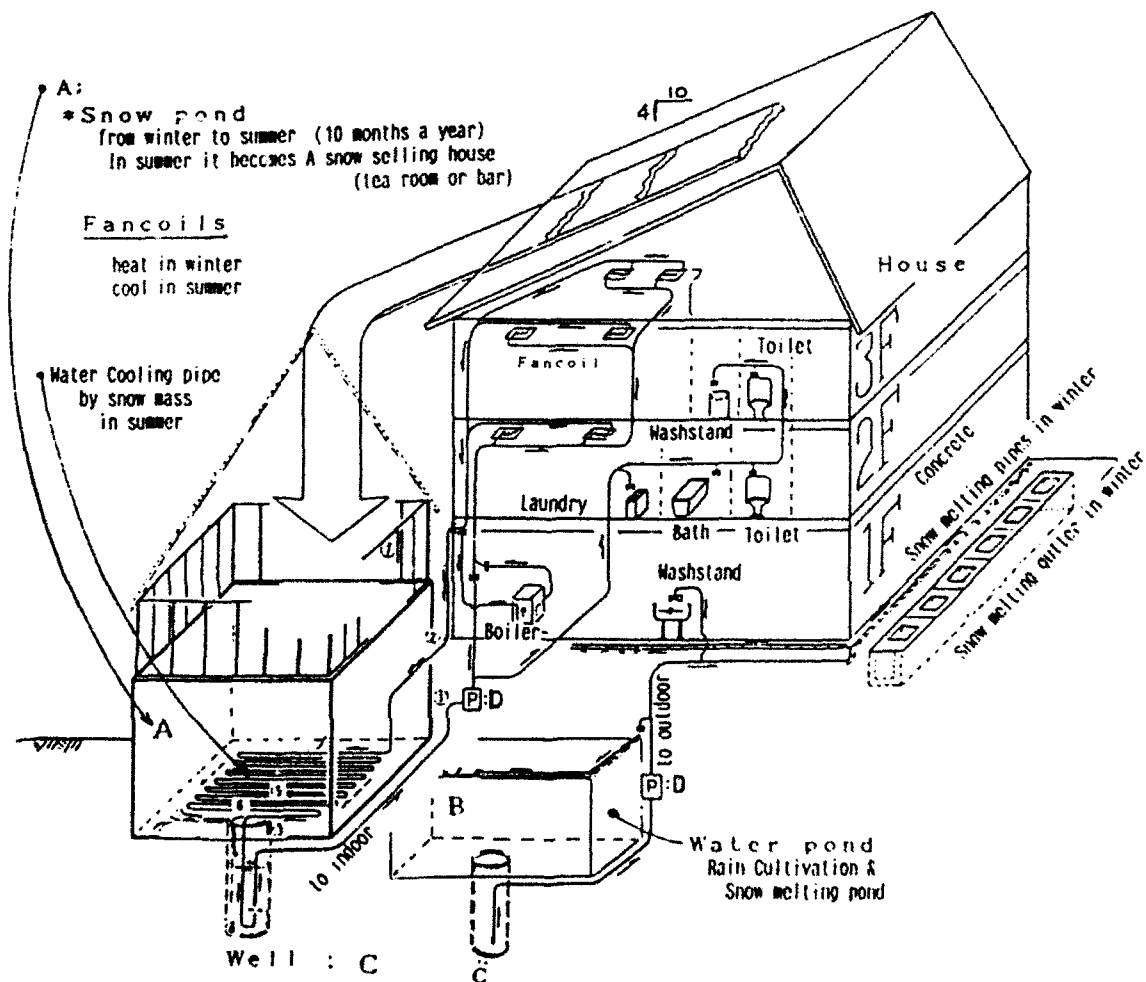


Figure 2. Side view.

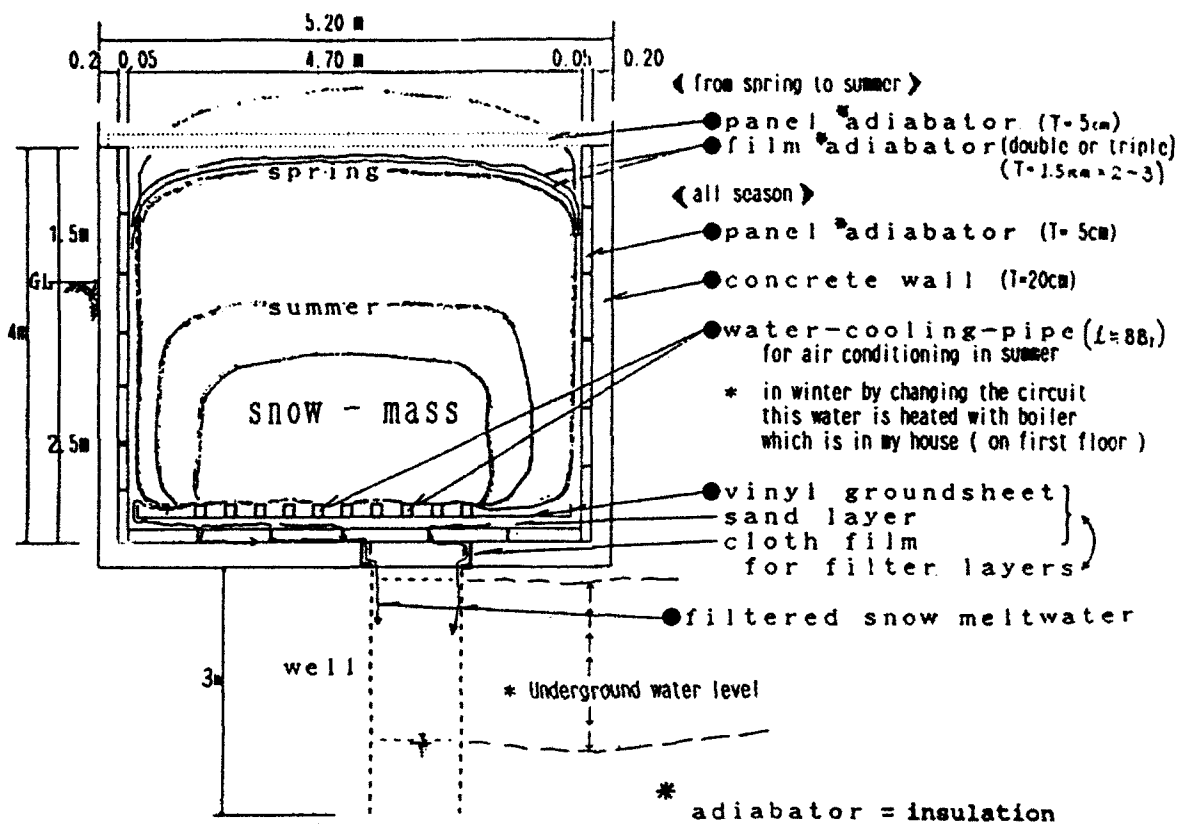


Figure 3. Snow pond.



Figure 4. Snow pond covered in February.



Figure 5. Snow pond covered in August.



Figure 6. July party on snow within the covered area.

8

Codes and Standards

Kristoffer Apeland, Chairman



Snow guards are used to hold snow on these metal roofs in Vermont, U.S.A. (Photograph by Wayne Tobiasson.)

Standardization of Snow Loads on Roofs

DIS 4355: Revision of ISO Standard 4355

Kristoffer Apeland

Oslo School of Architecture
Oslo, Norway

ABSTRACT

The revisional work on ISO Standard 4355, "Bases for design of structures - Determination of snow loads on roofs", which was reported in [1], has been completed. The DIS 4355 has been forwarded to ISO for combined voting among the member countries.

The Draft International Standard DIS 4355, [2], presents a more general format for the determination of snow loads on roofs, than did the existing ISO 4355. In principle, however, the format is based on the same assumption as earlier, i.e. that the snow load on a roof may be determined as a product of the characteristic snow load on the ground, s_0 , and a shape coefficient, μ , which depends on a number of parameters.

In this paper, a review of the snow load format is given. In particular, the effect of the exposure coefficient is discussed. Reduction due to melting on glass roofs is exemplified.

The basis for the presented specification of snow load on multilevel roofs is discussed, and illustrations of the consequences are presented.

The recommendations for snow load on curved roofs, and the effects of unbalanced loads on arches are discussed in some detail.

INTRODUCTION

The Working Group 1 under ISO/TC 98/SC 3 has been working on revision of ISO 4355 Snow loads for about eight years.

The first edition was based on knowledge available up to 1977.

Snow loads specified in the first edition were mainly based on a wide range of experience and National Standards. Consequently, the specified snow loads in some cases were rather high in order to be on the safe side. In the second edition, later investigations, e.g. field measurements, and physical-, theoretical- and statistical analyses have also been taken into account in order to improve the level of accuracy and to extend the domain of standardized specifications of snow loads.

Although the second edition has more detailed specifications, there is still a need for judgement by experts in practical snow load design as the data base is still very limited for many types of roofs.

The format for the snow load on roofs presented in the standard, contains a number of additional parameters as compared with the first edition, in which such additional parameters were discussed in the text, for the designer to decide upon. In essence, however, the general format has not been changed. The effect of exposure may, with the new format, be treated in a more elaborate way than earlier. A variation with the slope of the roof is introduced in order to improve the physical representation and to make the format easily applicable to computer interpretation.

For examining the effect of the wind on the distribution of snow loads on roofs of unusual shapes or shapes not dealt with in the International Standard or in national standards, suitable models; e.g. tests carried out in a wind tunnel, especially equipped for reproducing accumulation phenomena, may give significant results.

The annexes determining the characteristic snow load on the ground, exposure coefficient, thermal coefficient and loads on snow fences are made informative as a general consequence of the limited amount of documentation and available scientific results.

GENERAL FORMAT OF DIS 4355

The DIS 4355 defines the snow load on roofs by the following equation:

$$s = s_0 \mu (C_e, C_t, C_m, \mu_b, \mu_d, \mu_s) = s_0 \mu \quad \dots(1)$$

where:

s is the snow load on the roof

s_0 is the characteristic snow load on the ground

C_e is an exposure reduction coefficient, defining the balanced load on a flat horizontal roof of a cold building, as a fraction of the characteristic snow load on the ground. The exposure coefficient includes the effect of snow being removed from flat roofs by wind. This effect depends on the temperature and the corresponding wind of the region.

C_t is a thermal reduction coefficient, defining the reduction of the snow load on the roof as a function of the heat flux through the roof, causing snow melting

C_m is a surface material coefficient

μ_b is a slope reduction coefficient, defining the reduction of the snow load on the roof due to the slope of the roof, β , and the surface material coefficient

μ_d is a drift load coefficient, which multiplied by μ_b , defines the amount and distribution of additional load on a leeward side or part of a roof, depending on the exposure of the roof and geometrical configurations of the roof

μ_s is a slide load coefficient, defining amount and distribution of slide load on a lower part of a roof, or a lower level roof.

DIS 4355 defines the snow load on the roof as the sum of a balanced load, s_b , a drift load part, s_d , and a slide load part, s_s . Thus, for the most unfavourable condition (lower roof on leeward side):

$$s = s_b + s_d + s_s \quad \dots(2)$$

Effects of the various parameters are simplified by the introduction of product functions. Thus,

$$s_b = s_0 C_e C_t \mu_b \quad \dots(3.1)$$

$$s_d = s_0 C_e C_t \mu_b \mu_d \quad \dots(3.2)$$

$$s_s = s_0 C_e C_t \mu_s \quad \dots(3.3)$$

The balanced load, s_b , is uniformly distributed in all cases, except for curved roofs, where the distribution varies with the slope β .

In addition partial loading due to melting, sliding, snow redistribution and snow removal shall be considered by the designer. In particular, such considerations should be made for structures which are sensitive to the form of the load distribution, e.g. curved roofs, arches, domes etc.

EXPOSURE COEFFICIENTS

In DIS 4355 the exposure coefficient C_e is defined by the standardized values as given in Table 1.

The exposure coefficients are determined from a set of defined winter wind categories and a set of winter temperature categories.

Table 1 Exposure coefficient, C_e .

		Winter wind category		
		I	II	III
Winter temperature category	A	1,0	1,0	0,8
	B	1,0	0,8	0,6
	C	0,8	0,8	0,5

The determination of the exposure coefficient is given in an informative Annex B to DIS 4355, which for ready reference is included as Appendix 1 to this paper.

It should be noted that an exposure coefficient $C_e = 0,8$ makes the DIS 4355 correspond reasonably well with the existing ISO 4355. The value $C_e = 0,8$ is also recommended for use in cases where there is not sufficient winter climatological data available.

THERMAL COEFFICIENT

The thermal coefficient, C_t , is introduced to account for the reduction of snow load on roofs with high thermal transmittance, in particular glass covered roofs, from melting caused by heat loss through the roof. For such cases C_t may take values less than unity. For all other cases $C_t=1,0$ should be used.

Bases for the determination of C_t are the thermal transmittance of the roof, U , and the lowest temperature, θ , to be expected for the space under the roof, and the snow load on the ground, s_0 .

Methods for the determination of C_t for roofs with high thermal transmittance are described in annex D of DIS 4355, and is for ready reference included as Appendix 2 of this paper.

SURFACE MATERIAL COEFFICIENT

The amount of snow which slides off the roof will, to some extent, depend on the surface material of the roofing.

The surface material coefficient, C_m , defines a reduction of the snow load on roofs for surface materials with low surface roughness.

In DIS 4355 C_m is defined to vary between unity and 1,333, and takes the fixed values:

$C_m = 1.333$ for slippery, unobstructed surfaces, for which the thermal coefficient $C_t < 0.9$ (e.g. glass roofs)

$C_m = 1.2$ for slippery, unobstructed surfaces, for which the thermal coefficient $C_t > 0.9$ (e.g. glass roofs over partially climatic conditioned space, metal roofs etc.)

$C_m = 1,0$ for all other surfaces.

SLOPE REDUCTION COEFFICIENT

The reduction of the snow load on the roof due to the slope, β , of the roof, and the surface material coefficient, C_m , is defined by the shape coefficient, μ_b , which is given by the function:

$$\begin{aligned}\mu_b &= \sqrt{\cos (C_m 1.5 \beta)}; \text{ for } C_m 1.5 \beta < 90^\circ \\ \mu_b &= 0; \text{ for } C_m 1.5 \beta \geq 90^\circ\end{aligned}\quad \dots(4)$$

For roofs with snow rails or obstructions preventing the snow from sliding off; $\mu_b = 1.0$. For multiple pitched roofs and inner bays of multispans roofs, sliding may lead to redistribution of the snow load.

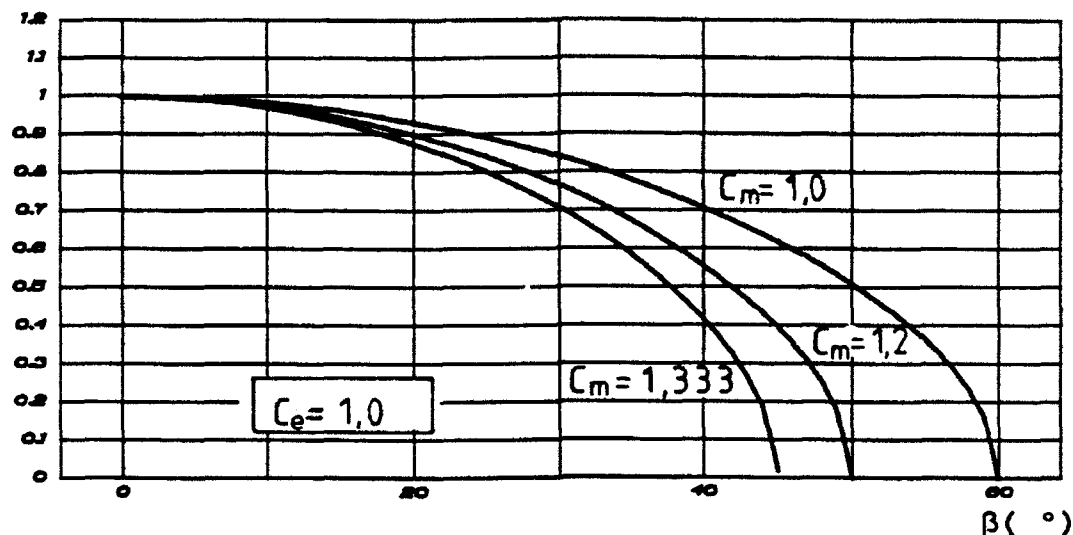


Figure 1 $C_e \mu_b$ for defined values of C_m .

Variation of $C_e \mu_b$ for $C_e = 1.0$ is shown in Fig. 1 for the three standardized values of C_m .

DRIFT LOAD COEFFICIENT

The geometrical influence of the shape on the drift load accumulating on the leeward side of a pitched roof is defined by the shape coefficient $\mu_b \mu_d$, which for a roof with roof angle β is defined by the function:

$$\begin{aligned} \mu_b \mu_d &= \mu_b (2.2 C_e - 2.1 C_e^2) \sin(3\beta) ; \text{ for } 0^\circ \leq \beta \leq 60^\circ \\ \mu_b \mu_d &= 0 ; \text{ for } \beta > 60^\circ \end{aligned} \quad \dots(5)$$

Eq. 5 includes effects of loss of snow being blown away from the roof by wind, and is scaled to yield total loads corresponding to measured loads on ordinary pitched roofs.

Note:

The form of the drift load coefficient ensures that a certain drift load part always must be checked even for regions with very calm weather; i.e. $C_e = 1.0$.

The shape coefficient $C_e(\mu_b + \mu_b \mu_d)$ for the total load on the leeward side of a pitched roof is shown in Fig. 2 for the three standardized values of C_m .

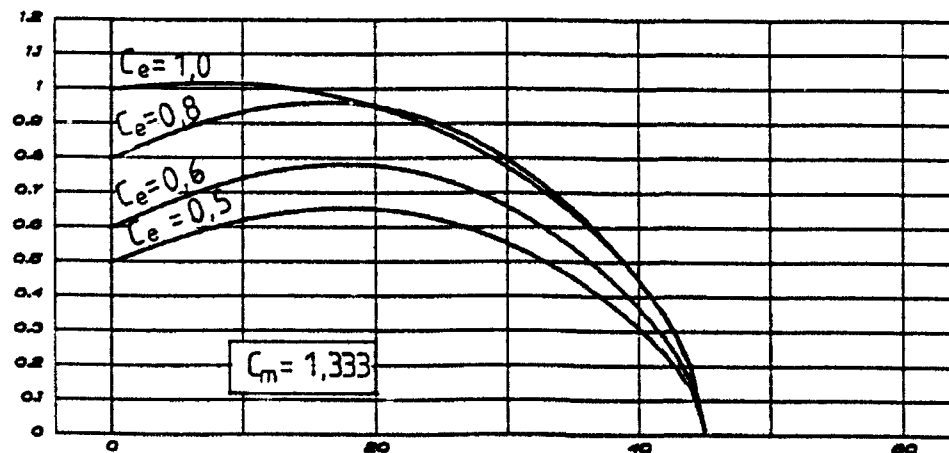
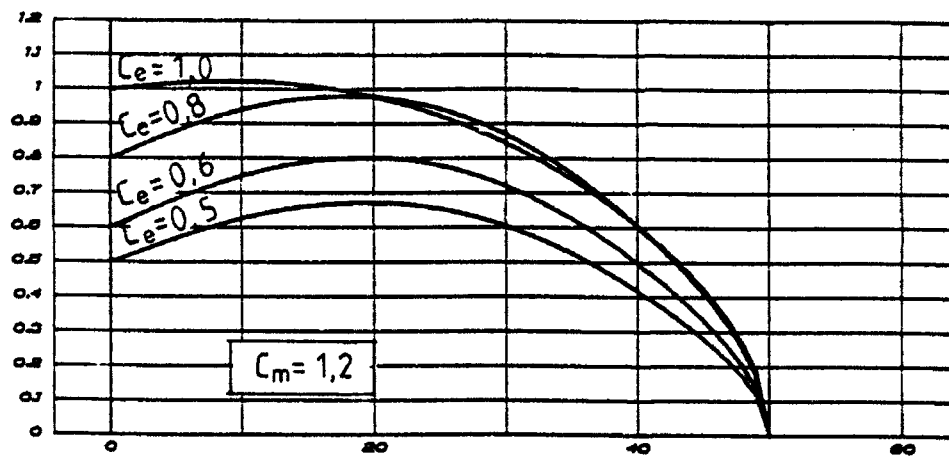
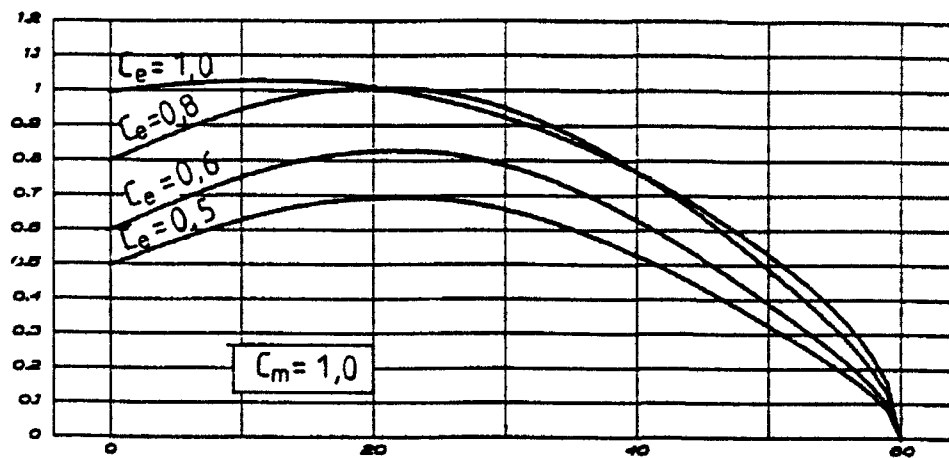


Figure 2 - $C_e(\mu_b + \mu_b \mu_d)$ for defined C_e -values.

MULTILEVEL ROOFS

The prescriptions of DIS 4355 for multilevel roofs are shown in Fig. 3. The formula for the drift load is given as

$$s_d = s_0 C_e C_t (\mu_b \mu_d) \quad \dots(6)$$

For $C_t = 1,0$, $\mu_b = 1,0$, which is the normal case, Eq. 6 yields

$$s_d = s_0 C_e \mu_d \quad \dots(7)$$

where s_d is the maximum intensity of the triangular drift load, and where

$$\mu_d = \sqrt{0,5(1-0,95C_e)(l_1 \rho g / s_0)} \quad \dots(8)$$

The formula is developed under the assumption that the snow that is removed from the upper roof of width l_1 , reduced with the exposure coefficient C_e , may accumulate as drift load, with a length of the triangle $l_d = 4(\mu_b \mu_d)(s_0 / \rho g)$.

Thus,

$$(1-0,95C_e)l_1 s_0 C_e = 0,5 s_d l_d = 0,5 s_0 C_e \mu_d 4 \mu_d (s_0 / \rho g)$$

which yields Eq. 8 for $\mu_b = 1,0$.

For $\rho g = 3,0 \text{ kNm}^{-3}$ the values of s_d are illustrated in Fig. 4 as a function of s_0 for various values of C_e .

The values lie somewhere between the values proposed by O'Rourke, [3], and the values which resulted from the prescriptions of the existing ISO 4355, which were larger, and were based on Soviet specifications.

Since it is well known that for roofs with wide lower roofs, a drifting may occur against the wall of the upper building, it is prescribed that when $l_2 > 2l_1$, l_1 should be replaced by $0,5l_2$.

Multilevel roofs (Lower roof with slope β_2)

	<p>"Windward side": $s=s_b$ Leeward side: $s=s_b+s_d$ Slide: $s=s_s$</p> <p>s_0 - see Clause 4 C_e - " " 5.1 C_t - " " 5.2 C_m - " " 5.3</p>
	<p>Balanced load part $s_b=s_0C_eC_t\mu_b$ ¹⁾</p> <p>$\mu_b=\sqrt{\cos(C_m1,5\beta_2)}$; for $0^\circ \leq C_m1,5\beta_2 \leq 90^\circ$, $\mu_b=1,0$; for $\beta_2 < 0^\circ$ ²⁾ $\mu_b=0$; for $C_m1,5\beta_2 > 90^\circ$</p>
	<p>Drifting load part $s_d=s_0C_eC_t(\mu_b\mu_d)$</p> <p>$\mu_d=\sqrt{0,5(1-0,95C_e)(l_1\rho g/s_0)}$ ³⁾</p> <p>If $l_1 < 10m$, $l_1=10m$ applies. If $l_1 < 0,5l_2$, l_1 shall be replaced by $0,5l_2$.</p> <p>$\mu_b\mu_d \leq (\rho g/C_eC_t s_0)h - \mu_b$; where l_1, h are in metres, s_0 is in kNm^{-2}, ρg is in kNm^{-3}, and may be set to $3,0 kNm^{-3}$. For $h < 3(s_0/C_eC_t\rho g)$: $\mu_b\mu_d=2,0$. $l_d=4/(\mu_b\mu_d)(s_0/\rho g)$ ⁴⁾ $l_d < 15m$</p>
	<p>Sliding load part $s_s=s_0C_eC_t\mu_b\mu_s$</p> <p>$\mu_s=(h_u/l_s \tan \beta_u)$ ⁵⁾ $\mu_s \leq (\rho g/C_eC_t s_0)h - \mu_b\mu_d$</p> <p>$l_s=2h_u \cos \beta_u \sqrt{(h/kh_u)(\sqrt{1+k}-1)}$ ⁶⁾ $k=h/[h_u(\sin \beta_u - \tan \beta_2 \cos \beta_u)^2]$ For $h < 3(s_0/\rho g)$: $\mu_s=1,0$.</p>
<p>1) For lower roofs with slopes normal to the cross section of the figure the basic load is determined from 5.4.5.1-5. 2) Sloping towards taller part of building. 3) The total drift load is equal to the load reduction on the upper roof due to exposure, i.e. $s_0(1-0,95C_e)l_1$. Alternative formulas for μ_d are described in annex C. 4) If $l_d > l_2$, the trapezoidal form of the diagram applies. 5) Impact effects shall be considered. 6) If $l_s > l_1$, the trapezoidal form of the diagram applies.</p>	

Fig. 3 DIS 4355 prescriptions for multilevel roofs

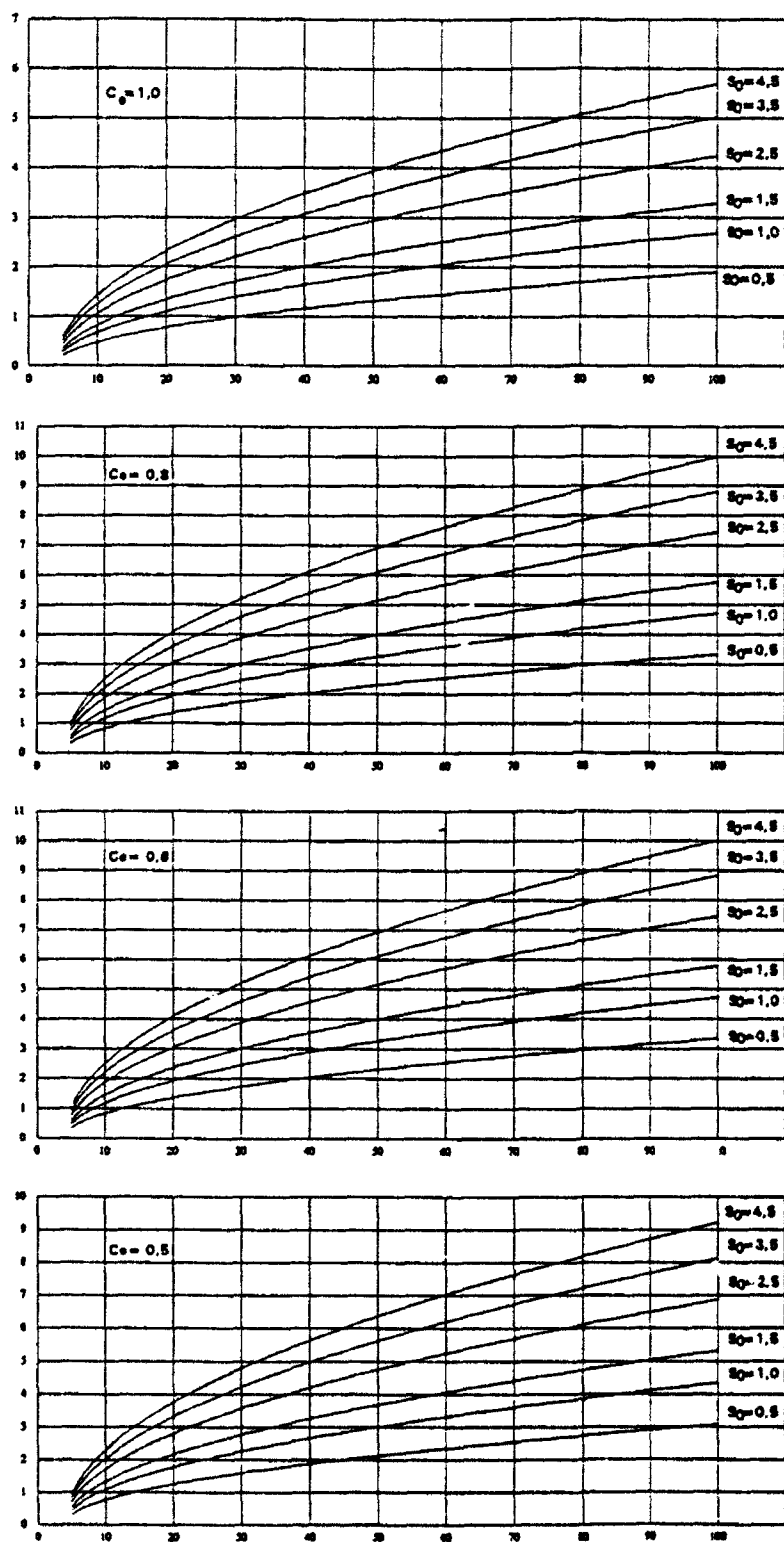


Fig. 4 Drifting load part, s_d , for multilevel roofs

CURVED ROOFS AND ARCHES

The prescriptions and recommendations of DIS 4355 for curved roofs are shown in Fig. 5.

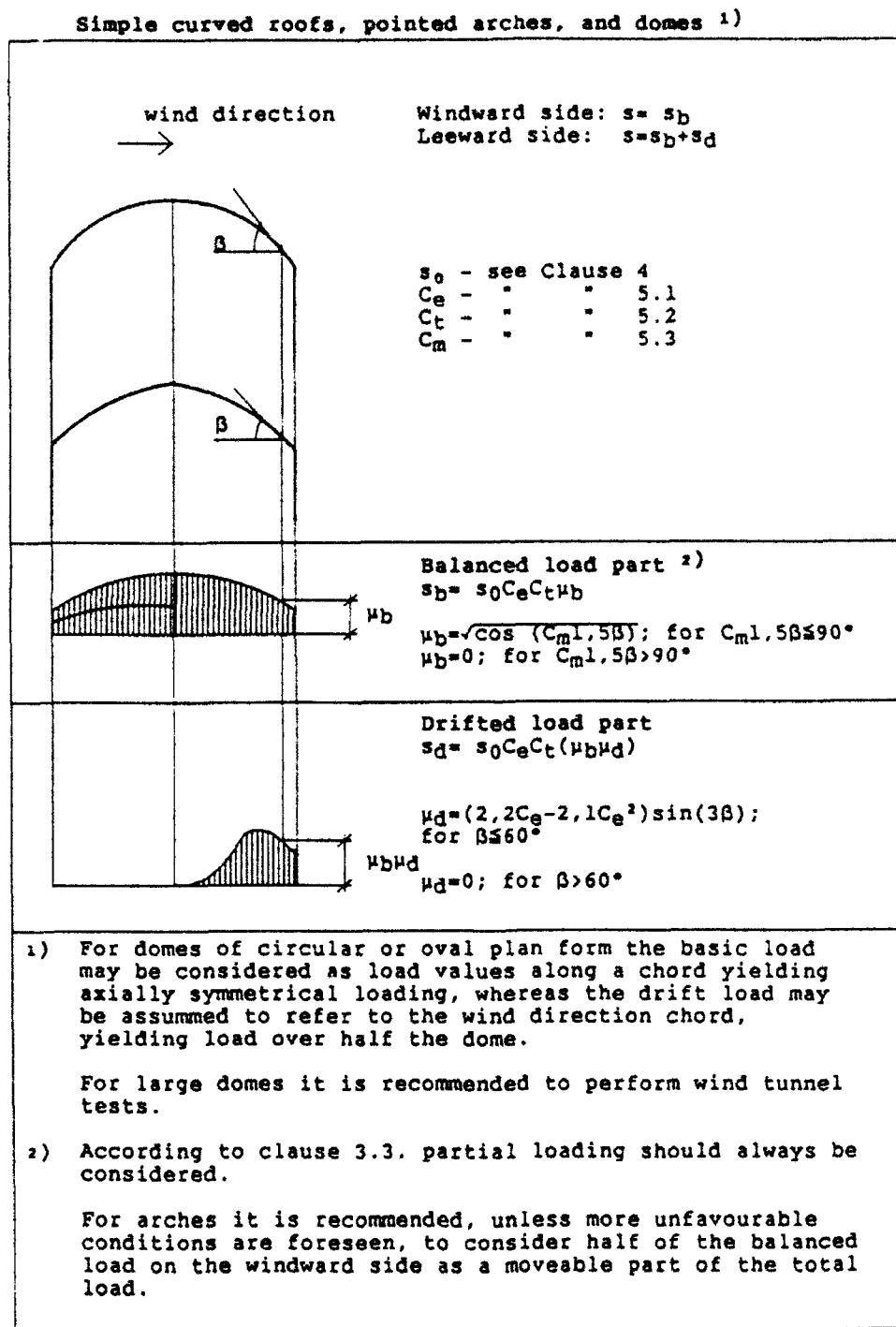


Fig. 5 DIS 4355 prescriptions for curved roofs

The recommendation given in footnote 2 of Fig. 5, is a result of the fact that experience has proven that a pure onesided load on an arch yields too conservative moment values, see Appendix 3 of this paper, which is a study made by Åkerlund for the Working Group of ISO in 1989.

Results of the present recommendation for an arch with $\beta_0 = 30$ degrees is shown in Fig. 6, which yields acceptable moments.

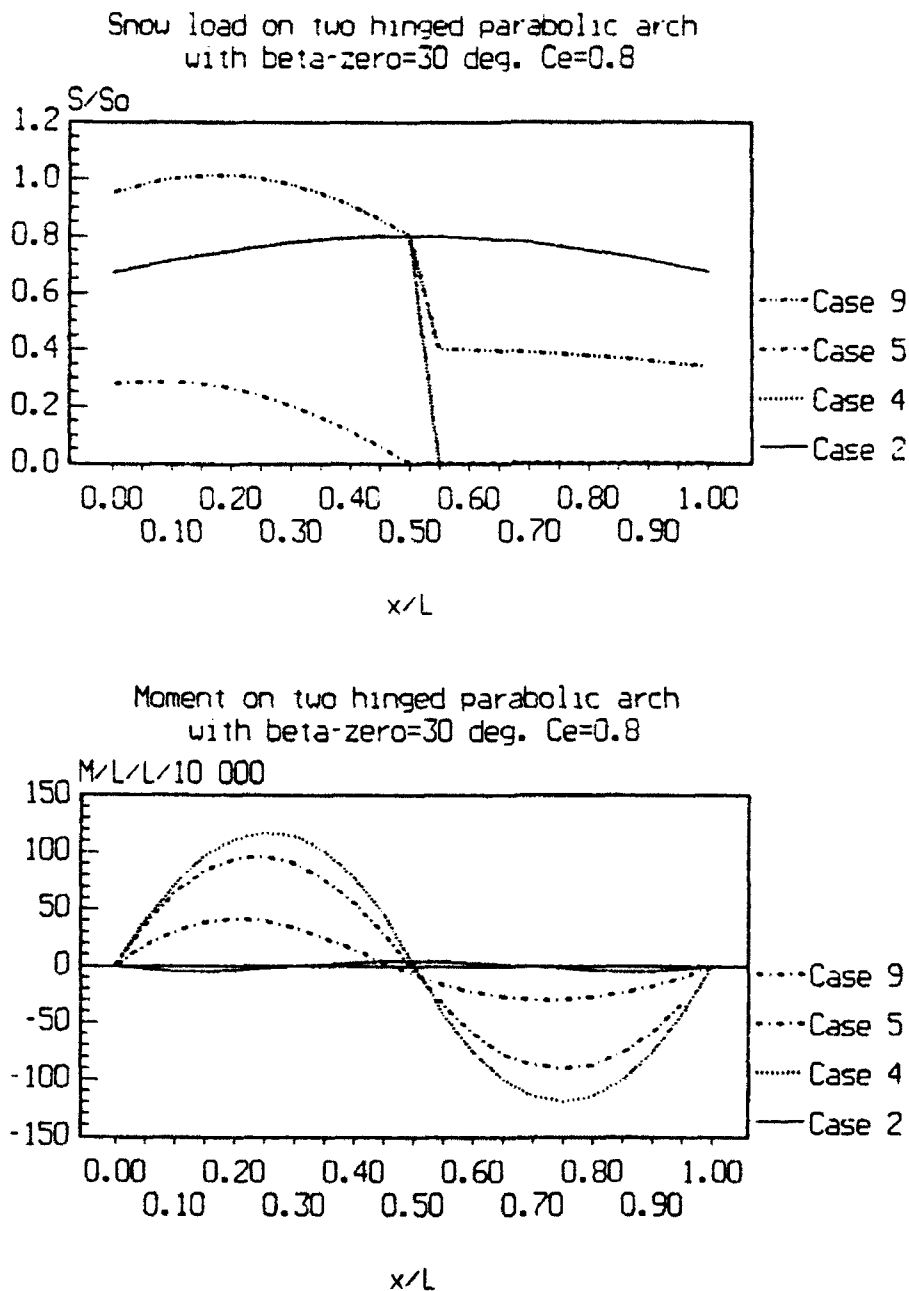


Fig. 6 Moments recommended in DIS 4355 - Case 9

CONCLUSIONS

The revised ISO standard for snow load on roofs, DIS 4355, presents a more general approach to snow load prescriptions, than does the existing ISO 4355. Hopefully, the new document will prove to be a useful tool for code-makers as well as designers throughout the world.

REFERENCES

- 1 Apeland, K.: "New development in Code Specifications and Standards for snow load". USA Cold Regions Research and Engineering Laboratory, Special Report 89-6. First International Conference on Snow Engineering, Santa Barbara, July 1988.
- 2 ISO/TC98/SC1: DIS 4355 "Bases for design of structures - Determination of snow loads on roofs", 1992.
- 3 O'Rourke, M. et al.: "Proposed Code Provisions for Drifted Snow Loads". Journal of Structural Engineering, ASCE, Vol. 112, No 9, 1986.

APPENDICES

- 1 DIS 4355 Annex B: "Determination of the exposure coefficient".
- 2 DIS 4355 Annex D: "Thermal coefficient".
- 3 Åkerlund, S.: "Bending moment in a twohinged parabolic arch due to snow load", 1989.

APPENDIX 1

Annex B (informative)

Determination of the exposure coefficient

B.1 General

The exposure coefficient, C_e , is a general coefficient reflecting the effect of snow removal at a roof location independent of the roof shape. The definition of C_e is given in the main text of the standard.

In this annex C_e is determined using section B.5, after the characteristics of the regional winter wind and temperature climates, have been considered. These characteristics are outlined under B.2 and B.4, respectively. The effect from local topography is determined from B.3.

Wind during a snow fall may cause a reduction in the uniformly distributed snow load on a roof as compared to the snow load on the ground. However, the local maximum of a non-uniform snow load caused by wind can be considerably higher than the ground load.

Strong wind, in the absence of snow fall, may also cause a uniform decrease or a redistribution of existing snow on the roof. This is highly dependent on the air temperature and the temperature history of the snow layer. Beneath a threshold windspeed no transport occurs. This threshold wind speed increases with the air temperature, as the cohesion forces between snow particles are observed to increase with the temperature.

The above described effects are well-known both from observations and analytical studies. Important physical studies in this field are described by Schmidt [1], and analysis of observation projects concerning snow loads on buildings have been carried out by several researchers, among which are Otstavnov [2], O'Rourke [3] and Taylor [4]. Water flume studies of drifting were conducted by Isyumov [5], and wind tunnel studies by Anno and Tomabechi [6], and Endo and Tomabechi [7].

Quantitative values of the main variables involved in drifting are not yet available to such an extent that it can provide a general basis for calculating the exposure coefficient by statistical methods. Therefore the values of C_e in this annex should be regarded as nominal. Although the range of C_e is 0,5 - 1,0, only $C_e = 1,0, 0,8, 0,6$ and 0,5 are used as a consequence of the limited accuracy in the practical determination of C_e .

B.2 Winter wind climate

The mean frequency of wind speed above a threshold value (10 m/s) is used rather than the monthly mean of wind speed as the main parameter for drifting. This is due to the fact that the effectiveness of drifting of both falling and old snow depends on the occurrence of relatively strong wind during snow falls, and snow falls are often accompanied by strong winds.

The following winter wind climates should be considered, normally by using the average value of the three coldest months of the year:

Average monthly number of days, N, with occurrence of 10 min. average wind speed exceeding 10 m/s	Winter wind category
$N < 1$	I
$1 \leq N \leq 10$	II
$N > 10$	III

The data on wind frequency is available for meteorological stations recording the wind speed in open terrain 10 m above ground level.

B.3 Local topography

If the local topography at a site indicates a significantly lower wind speed than that recorded by the most representative nearby meteorological station, a change in category under B.2 shall be considered as follows.

When the recorded wind frequency is within the lowest half of the interval defined by the range of Category II given from B.2, Category I applies. For frequencies between 10 and 15 for Category III, Category II applies.

B.4 Winter temperature climate

In regions with a relatively warm winter climate only drifting of falling snow is usually possible. In such regions snow falls are accompanied by the lowest temperatures of the winter. This is normally not the case in cold regions. A common variable reflecting the temperature during snow falls for different climates is therefore difficult to obtain. For practical reasons the parameter used in this annex is the lowest monthly mean temperature of the year. Note that this parameter has lower values than the winter mean temperature being referred to in B.6.

The following monthly mean temperatures, θ , for the coldest month of the year should be considered

Monthly mean temperature, θ , for the coldest month of the year (°C)	Winter temperature category
$\theta > 2,5$	A
$-2,5 \leq \theta \leq 2,5$	B
$\theta < -2,5$	C

B.5 Exposure coefficient

When the winter wind and temperature categories have been determined from B.2 and B.4 and adjusted due to local topography according to B.3, the exposure coefficient can be determined from Table 1.

Table 1 Exposure coefficient, C_e .

		Winter wind category		
		I	II	III
Winter tempera- ture category	A	1,0	1,0	0,8
	B	1,0	0,8	0,6
	C	0,8	0,8	0,5

The value $C_e = 0,5$ (i.e. Category C III) applies only to buildings in extremely exposed and open terrain in all directions.

B.6 Alternative determination of the exposure coefficient

In the Soviet Union [2] the following formula for the exposure coefficient has been derived for regions having mean winter temperature (average temperature for the three coldest month of the year) less than -5°C :

$$C_e = 1.0 \quad \text{for } v \leq 2 \text{ m/s}$$

$$C_e = 1.2 - 0.1v \quad \text{for } 2 < v < 8 \text{ m/s}$$

$$C_e = 0.4 \quad \text{for } v \geq 8 \text{ m/s}$$

where

v is the mean wind speed (m/s) at 10 m above ground level for the snow fall season.

For winter temperatures exceeding -5°C no drifting is considered.

B.7 Bibliography (Annex B)

- [1] Schmidt, RA. Threshold wind-speeds and elastic impact in snow transport, Journal of Glaciology, 1980, vol. 26, no. 94.
- [2] Otstavnov, VA., et al. 1969. Consideration of wind effect in standardization of snow load, CIB Committee W 23 in Basic Structural Engineering Requirements for Buildings.
- [3] O'Rourke, M., et al. 1983. Analysis of roof snow load case studies. Uniform loads., Cold Regions Research & Engineering Laboratory, CRREL Report 83-1.
- [4] Taylor, DA. A survey of snow loads on roofs of arena-type buildings in Canada. Canadian Journal of Civil Engineering., 1979, Vol 6., No. 1.
- [5] Isyumov, N. 1971. An approach to the prediction of snow loads, ph. d. thesis, University of Western Ontario, London, Canada.
- [6] Anno, Y. and Tomabechei, T. 1985. Development of a snowdrift wind tunnel, Cold Regions Science and Technology, 10.
- [7] Endo, A. and Tomabechei, T. 1983: Wind channel experiment of the forming conditions of snow depth on various roofs with model snow. Memoirs of the Hokkaido Institute of Technology, 1983, no. 11.

APPENDIX 2

Annex D (informative)

Thermal coefficient

Annex D specifies values of the thermal coefficient for reduction of snow load on glass²⁾ roofs caused by heat flow through the roof.

The thermal coefficient, C_t , reduces the snow load caused by melting and is given by a formula which was developed assuming $s_0 \geq 1,5 \text{ kN/m}^2$:

$$C_t = [1 - 0,054 \left(\frac{s_0^{0,25}}{3,5} \right) f(U_0, \theta)];$$

where

$$f(U_0, \theta) = \begin{cases} 0; & \dots\dots\dots U_0 < 1,0 \\ (\theta - 5) [\sin(0,4 U_0 - 0,1)]^{0,75}; & \dots\dots 1,0 \leq U_0 \leq 4,5 \text{ and } 5 \leq \theta \leq 18 \text{ } ^\circ \\ \theta - 5; & \dots\dots\dots U_0 > 4,5 \text{ and } 5 \leq \theta \leq 18 \text{ } ^\circ \end{cases}$$

U_0 is the thermal transmittance assuming the external thermal surface resistance is equal to zero. ($\text{W}/(\text{m}^2\text{K})$)
 β is the roof angle in degrees
 s_0 is the characteristic snow load on the ground ($s_0 \geq 1,5 \text{ kN/m}^2$)
 θ is the lowest expected internal temperature during the winter. ($^\circ\text{C}$)

For significantly lower values of s_0 , especially in combination with low roof angles, $C_t = 1,0$ should apply. The unit for the argument of the sine function is radians (If degrees are preferred, the argument should be multiplied by a constant, 57,3). The parameter, U_0 , is representing the glass covered²⁾ area only. If U is based on a different value of the external thermal surface resistance, $R_e > 0$, U is transformed to U_0 by the formula:

$$U_0 = \frac{U}{1 - UR_e}$$

where

R_e is the external thermal surface resistance for U ($\text{m}^2\text{K}/\text{W}$)

1) If $\theta < 5$; $\theta = 5$ applies. If $\theta > 18$; $\theta = 18$ applies in the formula.

2) This may also apply to other materials.

C_t is graphed in Figure 1, 2 and 3.

If a calculated C_t value is less than unity, a thorough check and eventual adjustments shall be undertaken according to the following specifications:

- if the monthly mean temperature for the coldest month of the year is below -8°C , C_t shall be increased by the factor 1,2, however, $C_t \leq 1,0$.
- if calculated additional local maximum load due to drifting exceeds 30% of mean snow load on the roof surface excluding drifting, the exceeding part of the load shall not be reduced by the thermal coefficient C_t .
- if sliding on to the roof surface is possible, C_t equal to unity applies.

A check that melting water can be drained from the roof surface without risk of icing, shall always be carried out.

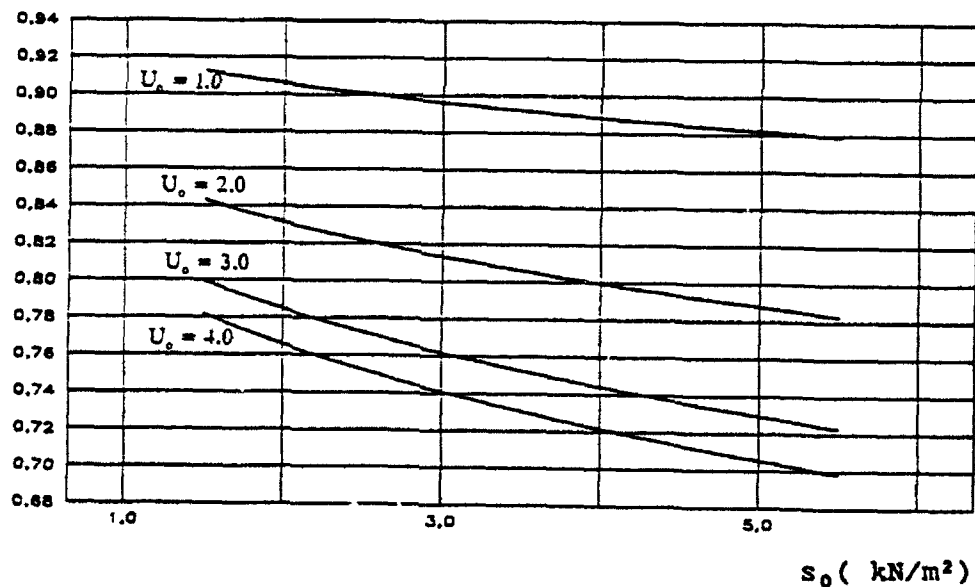


Figure 1 Thermal coefficient C_t for $\theta = 10^{\circ}\text{C}$

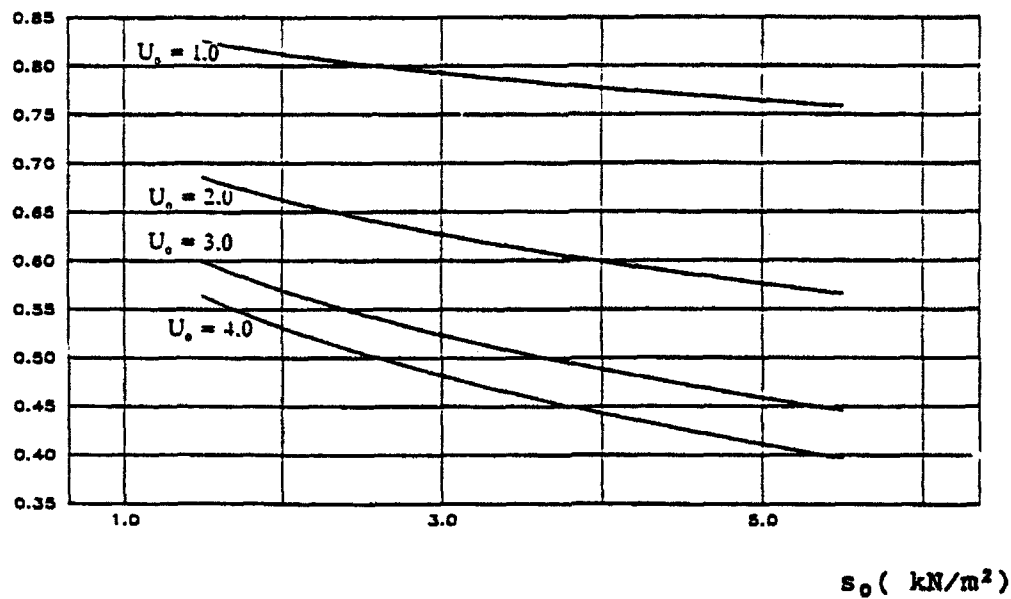


Figure 2 Thermal coefficient C_t for $\theta = 15^\circ\text{C}$

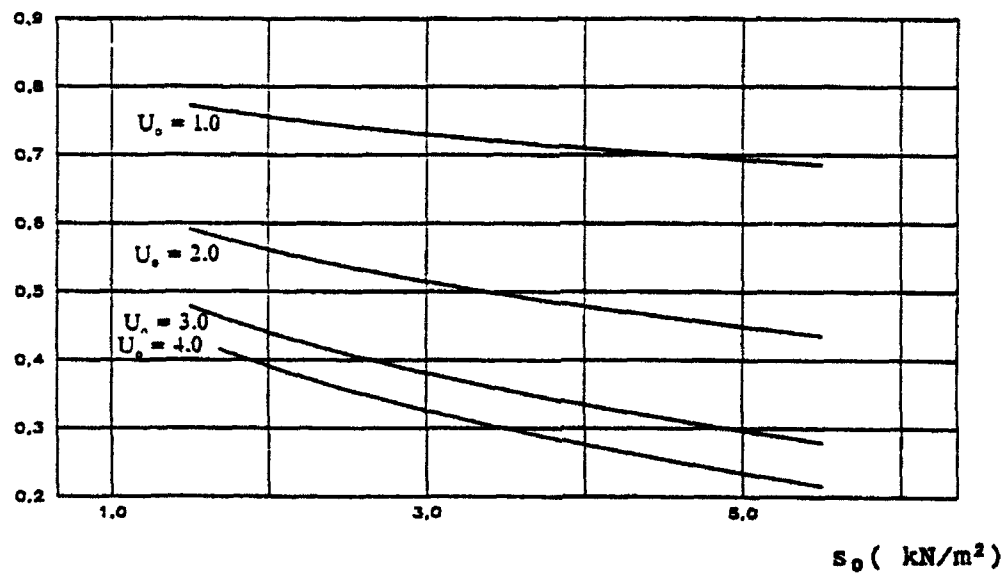


Figure 3 Thermal coefficient C_t for $\theta = 18^\circ\text{C}$

BENDING MOMENT IN A TWOHINGED PARABOLIC ARCH DUE TO SNOW LOAD

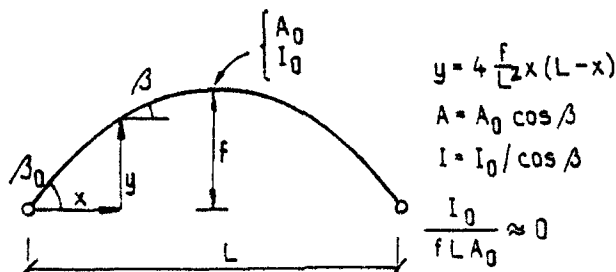
Load case

Case	Left half of the arch	Right half of the arch	Page
1	$\mu=0.8$	$\mu=0$	2,3
2	$\mu=0.8\cos(1.5\beta)$	$\mu=0.8\cos(1.5\beta)$	4,5
3	$\left\{ \begin{array}{l} \text{Triangular load with} \\ \mu_{\max}=\mu_0 \text{ at onset} \\ \mu_0=0.3+2.5\tan(\beta_0) \leq 1.75 \end{array} \right\}$	$\left\{ \begin{array}{l} \text{Triangular load with} \\ \mu_{\max}=\mu_0/2 \text{ at onset} \\ \mu_0=0.3+2.5\tan(\beta_0) \leq 1.75 \end{array} \right\}$	2,3
4	$\mu=0.8\cos(1.5\beta)$	$\mu=0$	2,3
5	$\mu=0.2\cos(1.5\beta)4(\sin(3\beta))^3$	$\mu=0$	4,5,6,7
6	Case 2 + Case 5	Case 2 + Case 5	4,5
7	$\left\{ \begin{array}{l} \text{Triangular load with} \\ \mu_{\max}=\mu_0 \text{ at onset} \\ \mu_0=0.3+2.5\tan(\beta_0) \leq 1.75 \end{array} \right\}$	$\mu=0$	4,5
8	Case 4 + Case 5	$\mu=0$	6,7

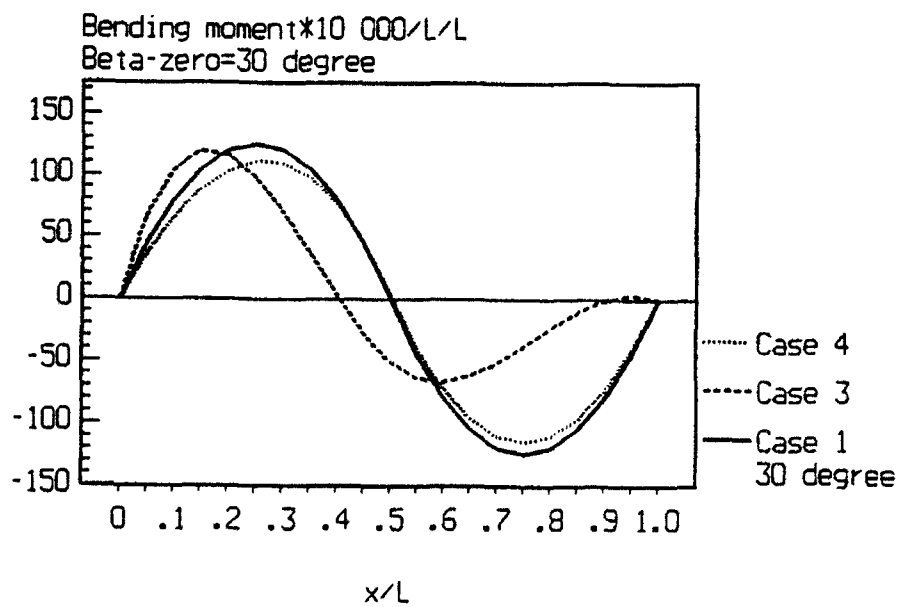
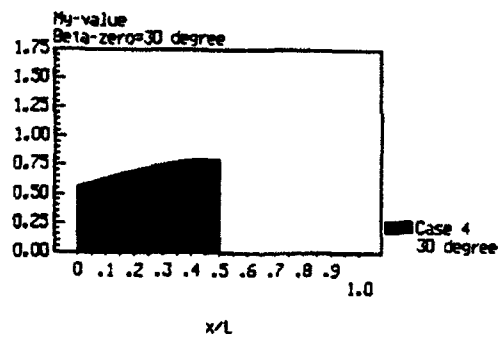
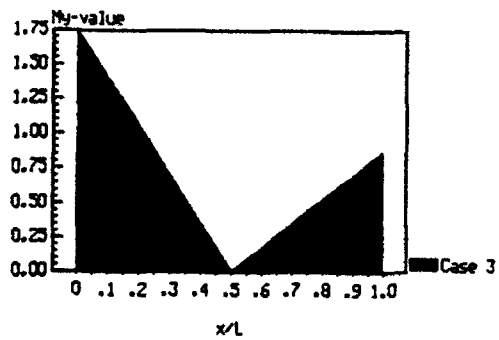
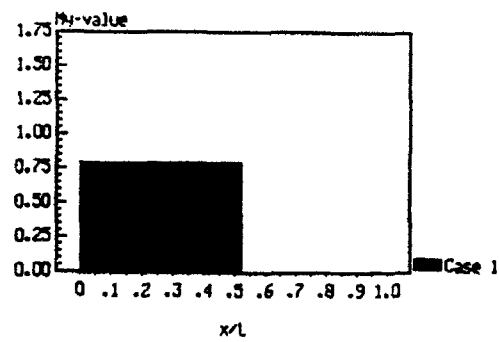
Maximum bending moment in a twohinged parabolic arch

Maximum bending moment = constant (in table below) * $L^2 \cdot 10^{-4}$, where L is the span.

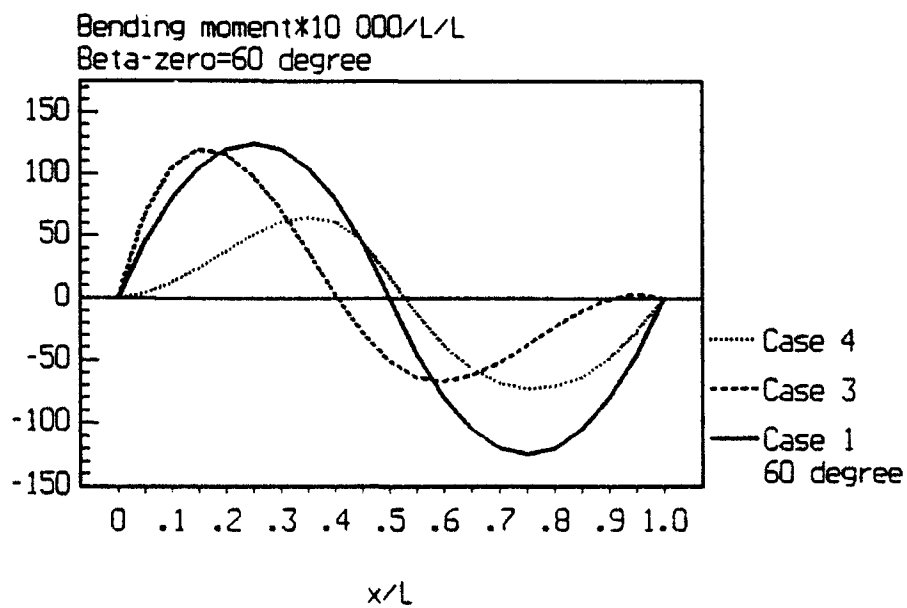
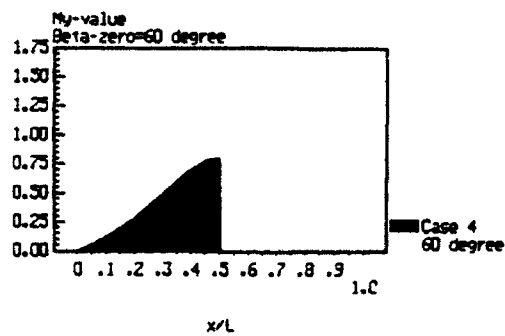
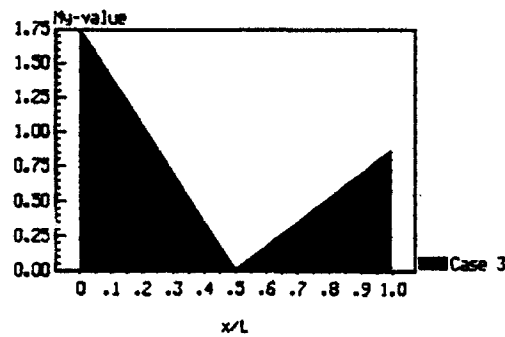
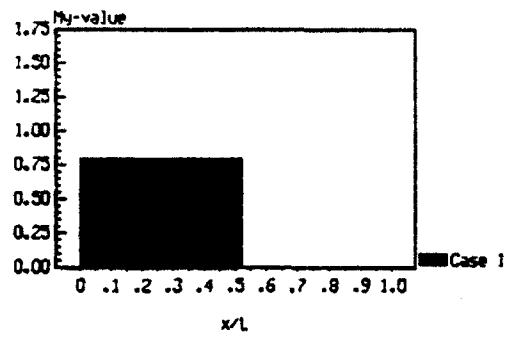
Slope at onset, β_0	S - N - O - W L - O - A - D C - A - S - E							
	1	2	3	4	5	6	7	8
10°	125	-1	51	124	5	4	72	127
20°	125	-4	82	-121	31	27	118	137
30°	125	-9	119	-115	65	57	117	167
40°	125	-17	119	-106	81	68	171	175
50°	125	-27	119	-93	68	-72	171	148
60°	125	-39	119	-73	49	-72	171	-112



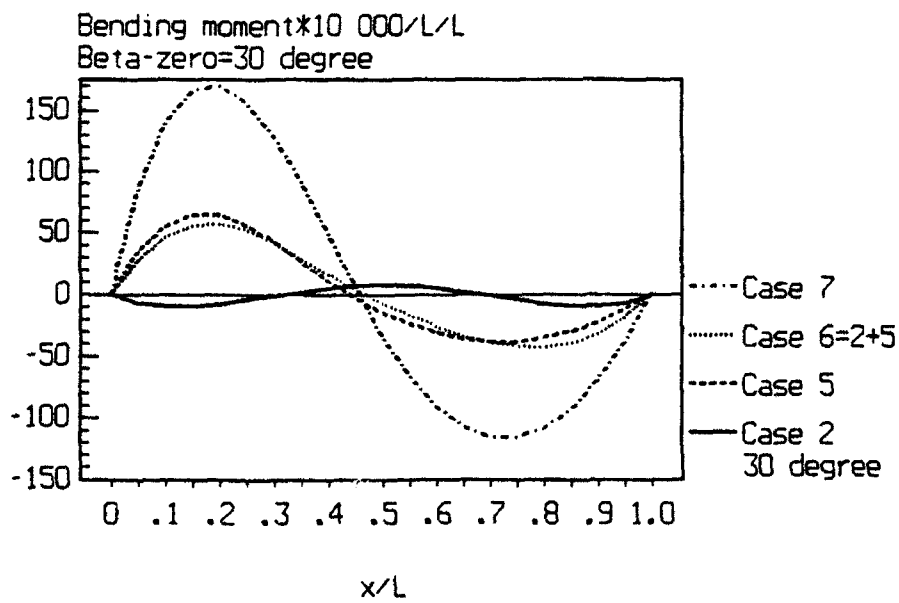
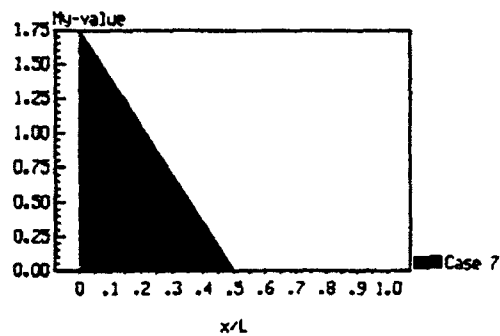
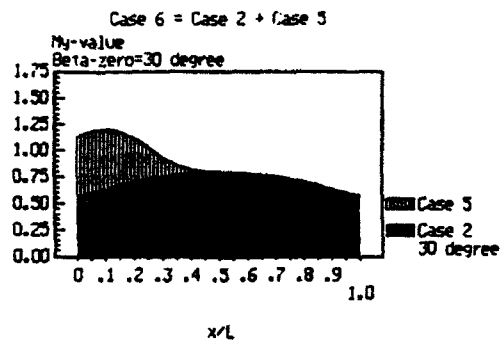
2(7)



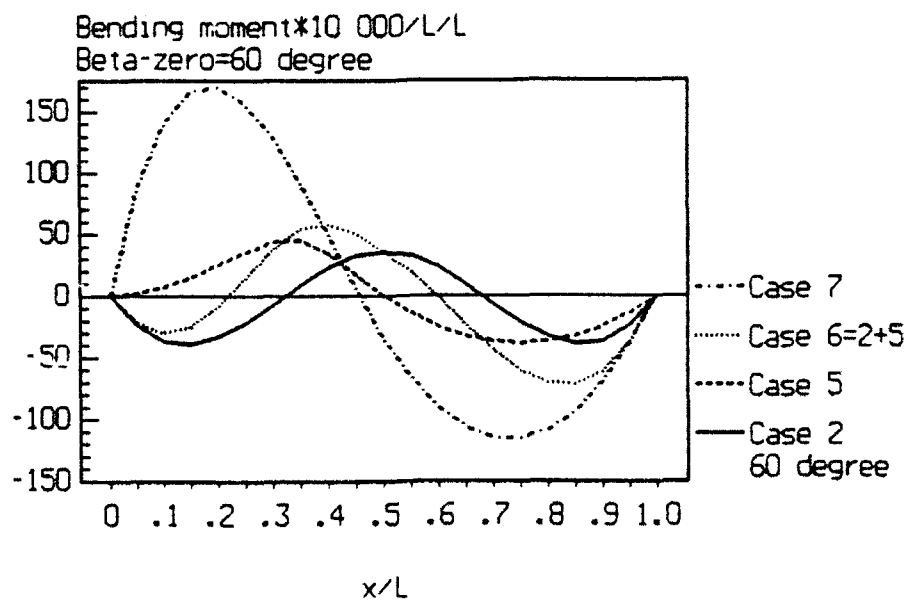
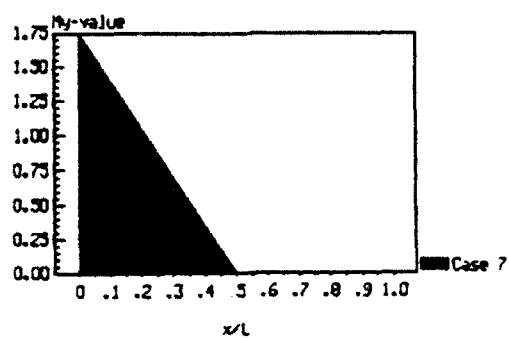
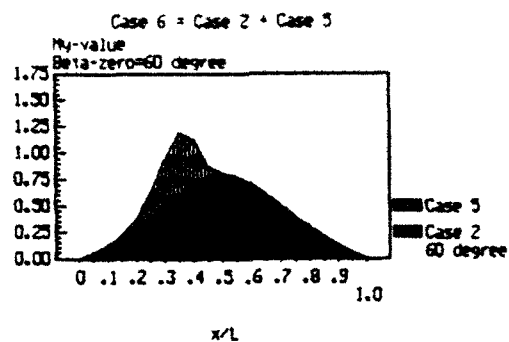
3(7)



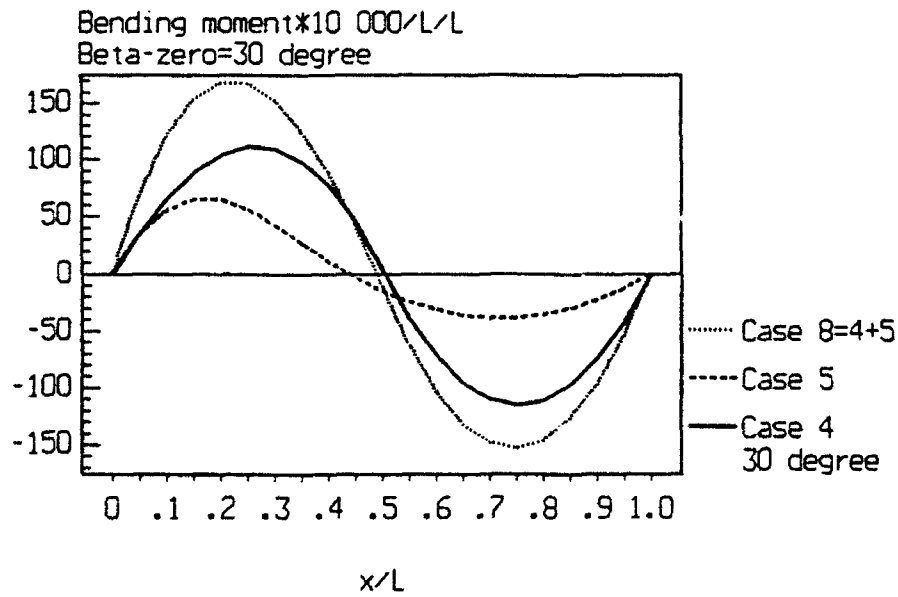
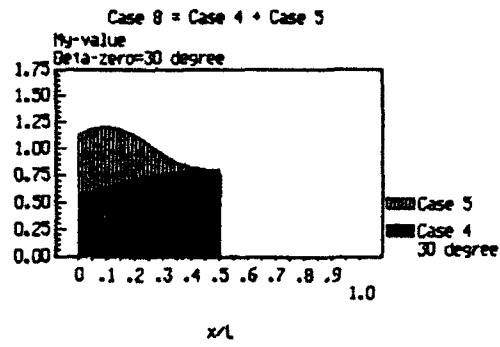
4(7)

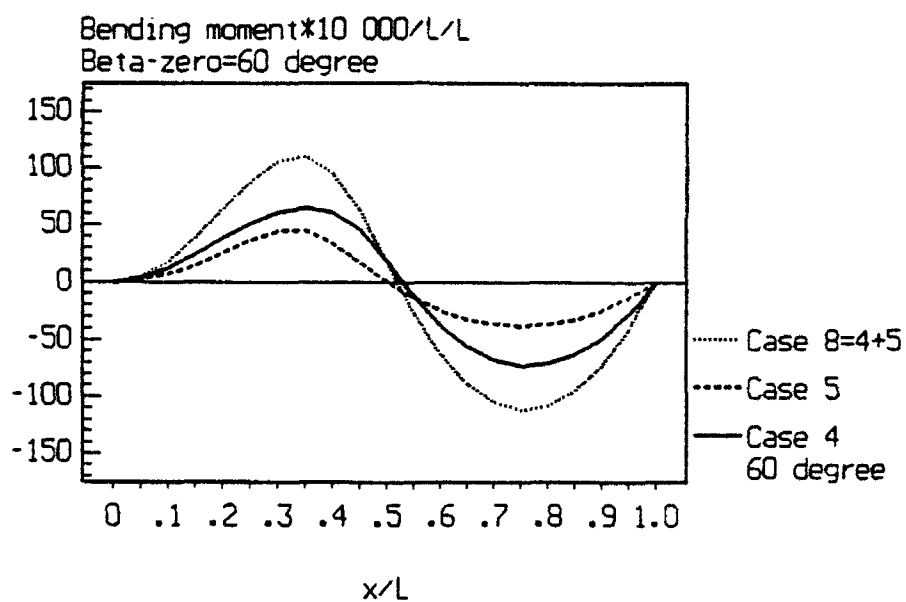
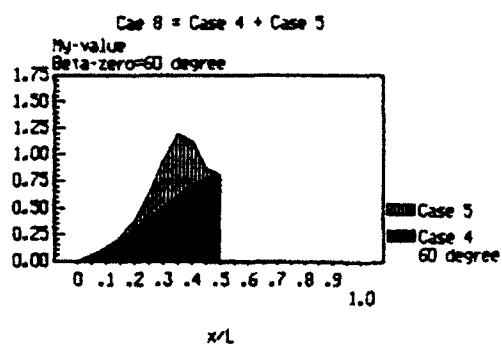


5(7)



6(7)





The Effectiveness of Code Provisions for Snow Accumulations on Stepped Roofs

D.J. Laurie Kennedy,* Nicholas Isyumov[†] and Michael Mikitiuk[†]

*Department of Civil Engineering, The University of Alberta
Edmonton, Alberta, Canada

[†]Boundary Layer Wind Tunnel, The University of Western Ontario
London, Ontario, Canada

ABSTRACT

In most building codes, snow loads on roofs are estimated by multiplying the ground snow load by coefficients to take drifting and sliding into account. These coefficients are generally given for relatively simple roof geometries and may vary from 0.6 to 3 or more. The drift that accumulates on a lower roof against a higher roof is considered, in the National Building Code of Canada (NBCC), to decrease linearly from the level of the high roof to the "normal" snow depth over a horizontal distance equal to twice the difference in elevation of the two roofs. The provisions for triangular drifts on stepped roofs in codes of Canada, ASCE, ANSI, ISO and the former USSR are discussed.

When the stepped roof has a large plan area and when wind velocities change while or after the snow falls, significantly different and potentially more severe drifts can accumulate. Tests reported here show that these drifts on lower roofs result not only from the transfer of snow from the higher to the lower roof but the drifting of the snow, as influenced by the roof geometry, on the low roof itself. While these drifts may not be deeper than the maximum code provisions for triangular drifts, they may extend significantly beyond the area given in the code.

The implications of such drifts on the design of the roof structure are examined.

INTRODUCTION

In most building codes, snow loads on roofs are estimated by multiplying the design ground snow load by appropriate snow load coefficients. These are generally given for relatively simple roof geometries and may vary from 0.6 to 3 or more. Apart from accumulations due to sliding snow, coefficients greater than one apply

to situations where drifts tend to occur as a result of wind action. A common situation included in most codes is the "triangular" drift that accumulates on a lower roof adjacent to a roof of higher elevation, considered to be due to the transfer of snow from the higher roof to the lower roof. In the NBCC and its supplement (Associate Committee on the National Building Code (ACNBC) 1990a, 1990b) this drift is considered to have a maximum depth, adjacent to the high roof, equal to the difference in roof elevation but not greater than that corresponding to three times the design ground snow load. (A uniformly distributed rain load is also added.) The drift is considered to extend from the high roof a distance equal to twice the difference in elevation of the two roofs but within the range of 3 to 9 m. At the toe of the drift, the roof snow load is the "normal" value.

Although this drift requirement may be quite sufficient in most cases, certain roof geometries and weather conditions can combine to produce significantly different and potentially more severe accumulations. These can arise when the roof area is large and when the wind velocities change while or after the snow falls.

The provisions of the National Building Code of Canada (ACNBC, 1990a, 1990b), American Society of Civil Engineers, ASCE 7-88 (ASCE, 1988), its precursor American National Standard A58.1 (ANSI, 1982), International Standards Organization DP4355 (1991), and Design Standards of the former USSR (USSR State Construction Department, 1980) for snow loads on stepped roofs are presented and compared. The results of a series of wind tunnel tests, modelling snow accumulations on a large stepped roof, with different wind speeds and directions are presented and discussed in relation to code provisions.

The implications of such drift accumulations on the design of the roof structure are examined.

CODE PROVISIONS

National Building Code of Canada (ACNBC 1990a, 1990b)

Putting aside the rain load, which simply adds a uniform charge to the snow, but considering drifts that can occur, the specified snow loading on a flat roof is given in the NBCC (ACNBC 1990a) as

$$S = S_g C_b C_a \quad (1)$$

where S_g is the ground snow load in kPa as is given in the supplement to the NBCC (ACNBC 1990b) for many locations in Canada, C_b is the basic snow load factor of 0.8 and C_a is the accumulation factor. For the ultimate limit state the specified snow load given by equation (1) is multiplied by a load factor of 1.50. Therefore, in the limit, if the accumulated snow load were to reach 1.5 times its specified value and if the minimum factored resistance were provided, a member designed for snow loads alone would be on the point of collapse.

Figure 1(a) shows an elevation of a building with a step of height h . The corresponding triangular drift load, presented in the NBCC, is given in Fig. 1(b). It extends the full width of the step. The drift has a maximum height equal to the step height h but the maximum load is not to exceed 3 times the ground snow load S_g . The drift extends a distance $2h$ from the step with the limit that $3\text{m} \leq 2h \leq 9\text{m}$.

Commentary H of the supplement (ACNBC 1990b) also states (Paragraph 34) that "drifts produced by snow blown from larger roofs (75 m long) may exceed the limits shown" on Fig. 1 (b). In addition Paragraph 38 of the same commentary states:

"In some cases, particularly roofs of unusual shapes, exceptionally large roofs, the prediction of snow loads is difficult. In such cases, the designer should calculate and plot the snow depths to scale applying a unit weight of 3.0 kN/m^3 (19.1 pcf) to judge whether the distributions look reasonable. In some circumstances wind tunnel or water flume tests might be used to assist in the evaluation."

The commentary to the code therefore at least recognizes that other drift patterns can develop but gives little guidance other than to suggest that model tests be conducted.

Taylor (1992) compares 33 roof-years of highest measured snow drift loads on five different roofs, four in Ottawa and one in Arvida, with the NBCC provisions (ACNBC 1990b). The upper roof fetches ranged from 31 to 71 m and therefore did not exceed the limit of 75 m in the note of paragraph 34 of ACNBC (1990b). Generally the drifts did not extend more than $2h$ from the step as given in ACNBC (1990b), except for the roof at Arvida where a value of $3h$ would appear more appropriate. In at least 5 instances the load profiles gave maximum loads significantly higher than the NBCC provisions. Taylor mentions another case where a building failed because of a large overload due to an excessively long drift. Although a histogram of 56 observations plotted by Taylor of the maximum drift load/1990 NBCC drift load indicates that only 5.4% exceeded a value of 1 and none reached the factored value of 1.5, concern exists as to whether the NBCC provisions are stringent enough. Buildings with small step heights, such as the unidentified one that collapsed and the Arvida building, appear to be more vulnerable.

American Society of Civil Engineers (ASCE, 1990)

Except for Alaska, the snow load on an unobstructed flat roof is given as

$$p_f = 0.7 C_e C_t I p_g \quad (2)$$

where p_g is the specified ground snow load at the building site and the designer uses judgement to select the exposure factor, C_e , the thermal factor, C_t , and the importance factor, I , from a range of specified values. Assuming the structure is heated and that the other factors are 1.0 gives

$$p_f = 0.7 p_g \quad (3)$$

By dividing the flat-roof snow load, p_f , in pounds per square foot by the snow density in pounds per cubic foot given by

$$\gamma = 0.13 p_g + 14, \text{ but not greater than } 35, \quad (4)$$

the "balanced" snow load height, h_b , is obtained.

The height of the drift surcharge in feet next to a high roof, is given as a function of the fetch length of the high roof and the ground snow load as

$$h_d = 0.43 \sqrt[3]{L_u} \sqrt[4]{p_g + 10} - 1.5 \quad (5)$$

and produces a maximum intensity of load of $\gamma(h_d + h_b)$ as shown in Fig. 1(c). Of course $h_d + h_b$ cannot exceed h . The drift extends for a length of $4h_d$ from the step.

The ASCE rules, with little extra computational effort, introduce several factors not considered in the NBCC: the effect of heating the structure, the importance of the structure (which is considered in Canada for both earthquake and wind loads), the variation of snow density with snow depth and the length of the high roof over which the wind blows.

In Figure 2, comparisons of the provisions in the two codes are given for 3 locations in Canada; Toronto, Ottawa and Goose Bay, for two different step heights of 2.5 m and 5.0 m and for two very different fetch lengths of 7.6 m and 228 m. (The NBCC suggests that it should not be used for fetches greater than 75 m). The fetch length has a marked effect on the ASCE provisions, increasing the surcharge load intensity and length of drift by about 3 and 5 times respectively in this range. The NBCC provisions, limited to a fetch of 75 m give intermediate values. The effect of different storey heights in both codes becomes more pronounced as the ground snow load increases. Figure 3 compares the NBCC provisions to those of the ASCE for a fetch of 75 m for the same 3 locations and a roof step height of 3.75 m. Here the comparisons are in reasonable agreement but the limitation of $3.0 S_g$ makes the NBCC requirement significantly less than the ASCE when the ground snow load is relatively small e.g. $S_g = 0.80$ for Toronto.

American National Standards Institute (1982)

This earlier version of ASCE (1990) takes into account the same factors as the ASCE provisions with the very important exception that the increase in the drift depth (and therefore, as well, the extent of the drift) due to the fetch length of the upper roof is not considered. The provisions of this standard are not discussed further here.

International Standards Organization (ISO) (1991)

As in other standards the roof snow load is considered to be proportional to the ground snow load and limiting the discussion to drift loads on stepped or multi-level flat roofs, ISO (1991) gives the roof snow load as

$$\begin{aligned} s &= s_b + s_d \\ &= s_o C_e C_t \mu_b + s_o C_e C_t \mu_b \mu_d \end{aligned} \quad (6)$$

where s_o is the characteristic ground snow load, s_b is the balanced snow load and s_d is the drift snow load. C_e is a exposure reduction coefficient which may be set at 0.8. C_t is a thermal reduction coefficient which may be less than 1.0 where melting occurs due to heat loss through the roof, μ_b is slope reduction coefficient = 1.0 for a flat roof and μ_d is the drift load coefficient. With $C_e = 0.8$, $C_t = 1.0$ and $\mu_b = 1.0$ the roof load from Eq. 6 is

$$s = 0.80 s_o + 0.80 s_o \mu_d \quad (7)$$

which is similar to the Canadian and ASCE provisions,

The drift load factor, describing the maximum value of the triangular drift load at the step is given by

$$\mu_d = \sqrt{0.5(1-0.95 C_e) L_u \rho g / s_o} \quad (8)$$

where L_u is the fetch of the upper roof. With $C_e = 0.8$ and $\rho g = 3.0 \text{ kN/m}^3$ this becomes

$$\mu_d = 0.60 \sqrt{L_u / s_o} \quad (9)$$

Incorporating this in Eq. 7 gives a maximum total load of

$$s = 0.80 s_o + 0.48 \sqrt{L_u / s_o} \quad (10)$$

This is quite similar to the ASCE (1990) expression (in different units) of

$$p = 0.70 p_g + (0.43 \sqrt[3]{L_u / s_o} \sqrt[4]{p_g + 10} - 1.5) (0.13 p_g + 14) \quad (11)$$

Both provisions take into account the fetch of the upper roof (L_u) and the ground snow load, s_o or p_g .

ISO (1991) places an upper limit on the value of the μ_d , which limits the total maximum load to a drift equal to the step height h with a weight density of 3.0

kN/m³ (19.1 pcf). This is the same limit as the Canadian code. The length of the triangular drift is given as

$$l_d = 4\mu_d s_o / \rho g = 4\mu_d s_o / 3 \quad (12)$$

with an upper limit of 15 m.

This is similar to the ASCE provisions where the drift length is related to the drift height while the Canadian provisions relate the length to the step height.

Figure 4 compares the ISO provisions to those of the ASCE for the three locations in Canada used previously. The ISO provisions are generally more stringent than those of the ASCE but both show, as would be expected, significant increases in drift loads with the upper level fetch. For Goose Bay, at a fetch of 228 m, the ISO provisions are limited for a step height of 5.0 m while those of the ASCE are not. For the same fetch and a step height of 2.5 m, both are curtailed, the ISO more so than the ASCE.

USSR State Construction Department (1980)

The standard roof load is given by

$$p_{st} = c p_o \quad (13)$$

where c is the transfer coefficient and p_o is the ground snow load varying from 0.49 to 2.45 kN/m² except that in certain areas it is to be established meteorologically.

For two-level flat roofs the value of c is taken as

$$c_o = 1 + 0.5 (L_u + L_L') / h \quad (14)$$

where L_u is the length of the upper roof, $L_L' = L_L - 2h$, in which L_L is the length of the lower roof, h is the height of the roof step and L_L' is not less than zero.

Limits are imposed on the value of c_o , it cannot exceed 6 or $1.96h/p_o$ when h is expressed in metres and p_o in kN/m². Because the roof load is $c p_o$ the latter limit gives

$$p_{st} = \frac{1.96h}{p_o} \cdot p_o = 1.96h \quad (15)$$

which is only 2/3 of the value given in the National Building Code of Canada of $3h$. This limit comes into play when either the fetch L_u is long or the ground snow load is large.

The length of the drift S is defined as

for $c_o \leq \frac{1.96h}{p_o}$, $S = 2h \nless 15 \text{ m}$

$c_o > \frac{1.96h}{p_o}$, $S = \frac{c_o - 1}{\frac{1.96h}{p_o} - 1} \cdot 2h$ but $\nless 5h$, $\nless 15 \text{ m}$

Figure 5 compares the drift loads (all for a roof step of 5 m and assuming that for the USSR provisions that $L_L' = 0.5 L_u$) of the ASCE and the USSR for the 3 Canadian locations. For relatively small ground snow loads (Toronto) the provisions of the two codes are in reasonable agreement but it is noted that the drift length by the USSR tends to be much larger resulting in a greater total weight of the drift. At an intermediate ground snow load these conditions are again true. For large ground snow loads the USSR limiting provision of a load of $1.96 h$ is even more restrictive than the Canadian limit of $3h$, resulting in a maximum intensity of load of only 55% of the ASCE value.

Summary of Code Provisions

From Figure 1 all the codes attempt to define a triangular drift load on the lower portion of a stepped roof by stipulating the maximum load at the step and the extent of the drift. One could say the similarity ends there.

As yet the NBCC does not account for the upper roof fetch length as the other codes do, although the need is recognized in the commentary (ACNBC 1990b). At a fetch of 75 m the NBCC provisions agree well with the ASCE, below this fetch they would be relatively conservative and above this the reverse is true. The ISO and ASCE provisions, for the most part, are similar.

The USSR provisions tend to be less demanding in terms of maximum drift load than those of the ASCE but generally require longer drifts.

For long fetches and heavy snow loads, the ASCE provisions are the most demanding. Here limits on maximum loads of both Canada and the USSR gave substantially smaller values.

WIND TUNNEL TESTS

Procedures

Figure 6 shows the plan and elevation of a building with a stepped roof for which snow transfer from one portion of the roof to another and drifting were simulated in the Boundary Layer Wind Tunnel of the University of Western Ontario. The scales used were: length, 1/100; velocity, 1/1; and therefore time, 1/400. The fetch of the high roof is 228 m for which the low roof drift provisions of the ASCE, ISO and USSR have been compared previously. The skylight shown dashed in Figure 6 was added for tests 7 and 8 only. In all tests, bran, used to simulate snow,

(Isyumov and Mikitiuk, 1989) was sifted uniformly on the entire roof surface to a depth of 1.5 to 3 mm, equivalent to 0.6 to 1.2 metres of snow on the prototype. In each test the wind was brought up to the required wind speed and then maintained at that speed for 6 minutes, equivalent to 40 hours prototype, before being shut off. Test details and results are given in Table 1. Wind speeds at roof level, V_H , are reported absolutely and also normalized by dividing by V_{Ht} (3.48 m/s), the wind speed, measured at 0.5 m full scale from the ground, at which sustained particle motion by drifting occurs on the ground. Table 1 also gives the maximum longitudinal extent of snow cover, d , in metres, on the lower roof at the end of the test measured parallel to the longitudinal axis of the building from the step in the roof to the toe of the snow drift. The extent of cover is also normalized by dividing by the height of the roof step, h , (8.9 m). In test 8, essentially a continuation of test 7, the normalized wind speed was increased to $V_H/V_{Ht} = 2.19$ just at the end of the test.

TABLE 1
Test details and results

Test	1	2	3	4	5	6	7	8
Wind angle θ°	0	0	45	45	180	0	-30	-30
V_H , m/s	4.52	4.66	4.7	5.57	5.57	5.60	5.60	7.62
V_H/V_{Ht}	1.30	1.34	1.35	1.60	1.61	1.61	1.61	2.19
Extent of cover, d,m	105	100	102	99	84	78	99	58
d/h	11.8	11.2	11.5	11.1	9.4	8.8	11.1	6.5

The total flux of material removed (Isyumov and Mikitiuk 1989) was found to increase considerably more rapidly than the velocities raised to the one-third power, which would be typical of transport in saltation. This increased rate is attributed largely to the wind turbulence, as the increase is greater for rougher urban terrain than for smoother open terrain.

Spatial Distributions

Only those drift patterns or spatial distributions most pertinent to drifts on lower roofs are discussed here. In Figures 7a, 7b and 7c are sketched the areas where snow remained at the end of three pairs of tests; tests 2 and 6, 3 and 4, and 7 and 8 respectively. Each figure allows a comparison to be made of the extent of snow cover when the wind direction is kept constant but the wind speed is increased. The line with hatching in each figure is the boundary of the snow cover corresponding

to the lower normalized wind velocity and the stippled area is the area where snow remained at the higher wind velocity.

In Figure 7a the increase in normalized velocity from 1.34 to 1.61 resulted in virtually all the upper roof being scoured clean. On the lower roof, the scoured area has not increased nearly as much and indeed in one area there is more snow on the lower roof at the higher velocity.

Figure 7b compares the areas where snow remained after tests 3 and 4, with the wind at 45° , and normalized velocities of 1.35 and 1.60 respectively. Again the increase in the normalized velocity essentially cleared the upper roof while the drift pattern on the lower roof has changed less substantially.

In Figure 7(c) the skylight added on the high roof acts as a keel or sail in directing the flow of the wind, and a drift formed at the end of the skylight with a prototype depth of about 4.8 m in test 8. The snow drift pattern on the lower roof was also influenced by the skylight and a relatively narrow but long drift in the form of a "spike" of snow formed on the lower roof downwind from the skylight. (A spike of snow extending over most of the lower roof length also formed in test 3 and became more evident in test 4. Even in tests 2 and 6, with the wind acting symmetrically at 0° , the snow distribution in the lower roof is non-uniform.)

These tests show that drift patterns can be substantially different from typical code values in the presence of strong winds, unsymmetric or quartering wind directions and roof geometries which can accentuate local drift transport. The skylight shown in Figure 7(c) is an example of a geometry where a wall or vertical element acts as a deflector which locally organizes and speeds up the flow over the roof surfaces. For quartering winds, the corner vortices, formed downstream of main building corners create elongated drifts as shown in Figures 7(b) and 7(c). These "spike" or "quartering" drifts can result in loads which are substantially different from the triangular drift loads included in most building codes.

From table 1 it is seen that the maximum lateral longitudinal extent of snow cover on the lower roof at the end of the test, measured from the roof step, after 40 hours duration of wind, extends from 6.5 to 11 times the roof step height. This is consistent with the extent of the aerodynamic cavity found behind bluff objects in turbulent boundary layer flow.

A Snow Profile on the Lower Roof

By careful examination of the photographs after test 8 it was possible to estimate with reasonable accuracy the depth of the snow spike on the lower roof downwind from the skylight near the step of the roof. This depth was about 3.2 m or 0.36 of the step height of 8.9 m. The spike, with a convex upward shape, extended to a point 58 m from the step as shown in Figure 8. While the depth is not excessive, what becomes apparent, when the code drifts are plotted, is the total volume and hence weight of snow in the spike. In comparison with the code drifts

it has been assumed that the upper limit of 1.2 m of snow deposited initially on the roof represented the basic roof snow load for all codes. This, of course, is conservative and, if the lower limit in the depth of 0.6 m had been used, the normal roof load would have been halved. This comparison of the experimental data with code values is clearly approximate, but does give a valuable indication of the relative importance of the "spike" or "quartering" drifts. Unless otherwise calculated, as for the ASCE provisions, the unit weight of the snow was taken as 3.0 kN/m³.

Figure 8 shows that the "spike" of snow causes excessive loading. Spikes existed for other tests as well and appear to develop most when the wind attack angle is oblique. The spikes are relatively narrow but long drifts. They can extend many times the triangular drift patterns given in the codes for low roofs. What is important for the spikes is both the maximum snow load and the length of the spike.

IMPLICATIONS ON STRUCTURAL DESIGN

It appears quite possible that a "spike" drift could form a line load in excess of the factored snow load on the roof as given in current codes. Consider two roof framing systems: the first with a series of secondary framing members, such as open web steel joists, oriented perpendicular to the roof step and thus more or less parallel to the spike, and the second with the joists parallel to the roof step and perpendicular to the spike. In the second case, although joists near the roof would have to be designed for the relevant and more usual "triangular" load intensities, joists further from the roof would be designed for the "normal" roof load over most of their length and the spike intensity over a portion of the length. To account for the variability in the position of the spike, its greater load intensity could be positioned in the most unfavourable position. The supporting beam perpendicular to the roof could, of course, have the spike sitting directly above it. However, it is designed for a larger tributary area and the spike overload is only part of its total load. The likelihood of the beam being grossly overloaded is reduced because of its greater tributary area.

In the first case, with the joists perpendicular to the roof step, the spike is much more likely to act as a line load on the top of a few joists overloading however many are under its foot print. The joists are not part of a load sharing system and, with sufficient overload, collapse. The collapse is likely to cover several bays as bridging attachments pull down adjacent joists and beams are twisted by falling joists. The impact of the collapsing system can carry lower floors to the ground. Therefore, if the spike axis can be established as being perpendicular to the roof step, the preferred orientation of the secondary roof members (the OWSJs) is parallel to the roof step.

From the point of view of snow drifting it is essential to establish whether or not such spike or quartering drifts can form. Conditions favourable for their formation include:

- (i) a long fetch of the upper roof,
- (ii) sails or keels that deflect the wind flow when it strikes at an oblique angle,
- (iii) relatively heavy snowfalls to deposit considerable amounts of snow (on the upper roof). This deposition is enhanced under calm conditions but may be exacerbated if the wind speeds are somewhat above the threshold value to form drifts which can later be redeposited,
- (iv) wind directions moving around the compass, playfully forming drifts, but leaving much snow on the roof,
- (v) a final strong wind, with or without snow, striking at an oblique angle and capable of significant flux.

CONCLUSIONS

1. Considerable differences exist in the code provisions for the formation of "triangular" snow drifts on lower roofs at changes in the roof elevation. These all seem to address the issue of the more or less uniform drift extending across the width of the roof.
2. The fetch of the high roof should be considered in establishing drift loads. Currently ASCE, ISO and the USSR treat this in some manner.
3. Limitations on the maximum intensity of drift load other than that of a drift to the top of the step may be appropriate.
4. Code provisions on the drift length may be inadequate.
5. Relatively narrow spike or quartering drifts, extending many times the code triangular distance from the step and therefore of a load magnitude in this extended area in excess of the factored snow load, can form under certain geometric and weather conditions. When these conditions prevail, the formation of such unusual drifts should be investigated.
6. A partial design strategy against collapse due to spike or quartering drifts is to orient the secondary members, if possible, more or less perpendicular to the spike so that each such member carries only a portion of the spike load. Primary members parallel to the spikes, with larger tributary areas, would tend to be overloaded proportionately less due to the spikes than the secondary (OWSJ) members.

7. Code writing bodies may wish to define a "quartering" or "spike" drift load in addition to the existing triangular drift loads.

REFERENCES

American National Standards Institute (ANSI) (1982) Minimum design loads for buildings and other structures. ANSI A58.1-1982. American National Standards Institute, Inc. Washington, D.C.

American Society of Civil Engineers, ASCE (1990). Minimum design loads for buildings and other structures. ASCE 7-88, Revision of ANSI A58-1-1982, American Society of Civil Engineers, New York, NY.

Associate Committee on the National Building Code, (1990a). National Building Code of Canada, National Research Council Canada, Ottawa, Ontario.

Associate Committee on the National Building Code, (1990b). Supplement to the National Building Code of Canada, National Research Council of Canada, Ottawa, Ontario.

International Standards Organization (1991) Bases for design of structures - determination of snow loads on roofs. ISO DP 4355-2.

Isyumov, N. and Mikitiuk, M. (1989) Wind tunnel model tests of snow drifting on a two-level flat roof. Sixth National Conference on Wind Engineering, Houston, TX, March.

Taylor, D.A. (1992) Snow on two-level flat roofs - measured vs 1990 NBC loads. Canadian Journal of Civil Engineering Vol. 19, No. 1, pp. 59-67.

USSR State Construction Department, (1980). Building standards and regulations, Part II: Design Standards, Chapter 6: Loads and Effects. Draft Translation 736, United States Army Corps of Engineers, CRREL, Hanover, NH.

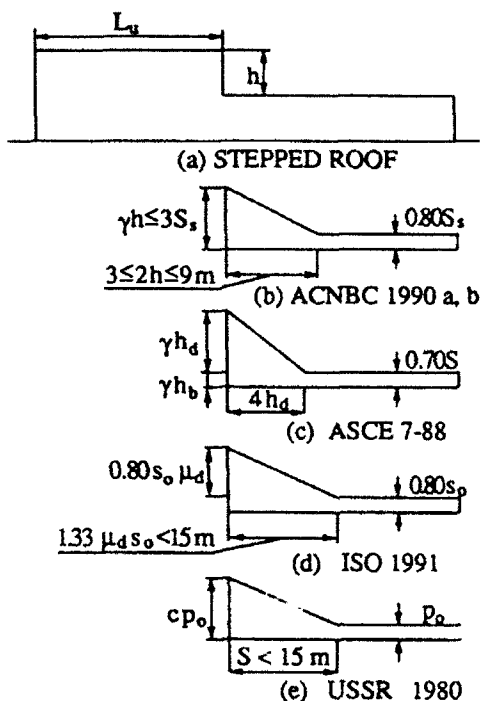


Figure 1 Stepped roof and code provisions

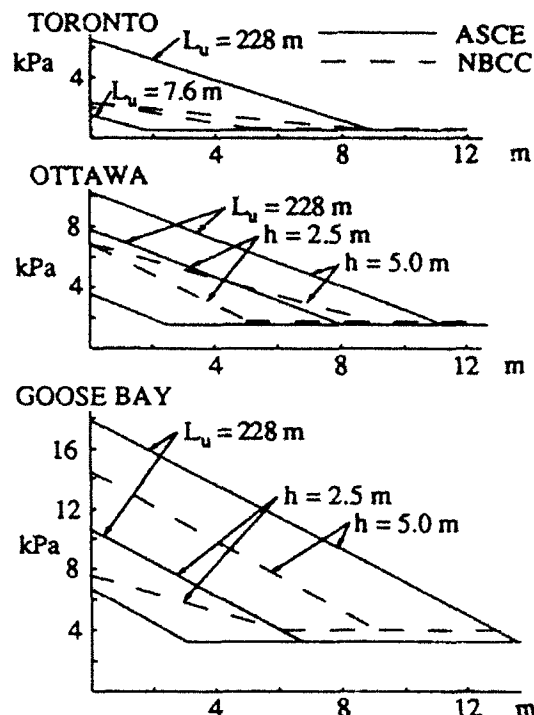


Figure 2 Comparison of drift loads by NBCC and ASCE

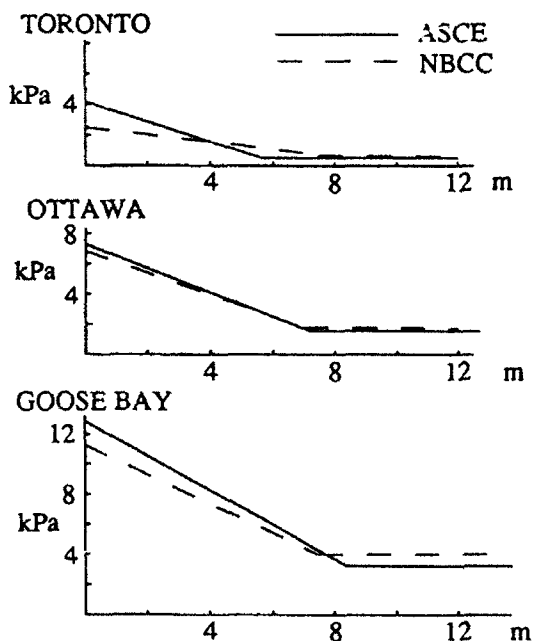


Figure 3 Comparison of drift loads by NBCC and ASCE for $L_u = 75m$

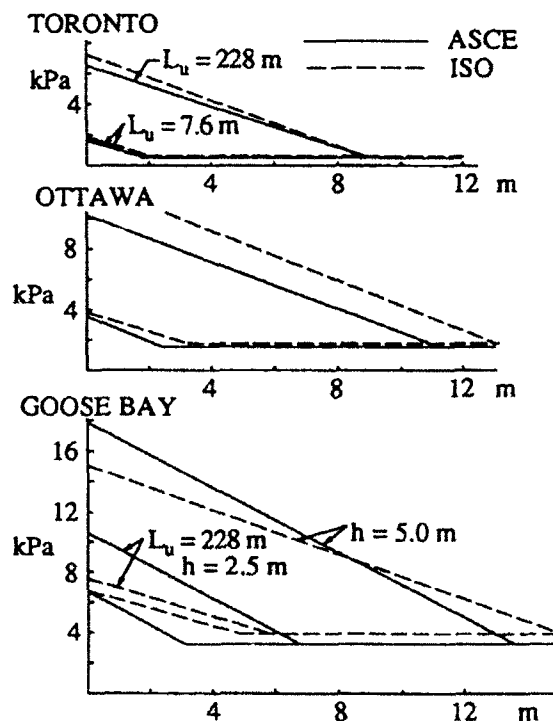


Figure 4 Comparison of drift loads by ASCE and ISO

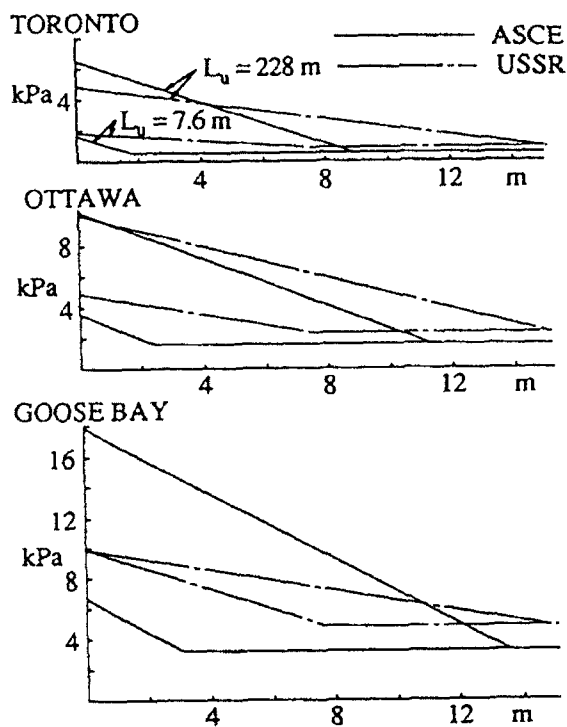


Figure 5 Comparison of drift loads by ASCE and USSR

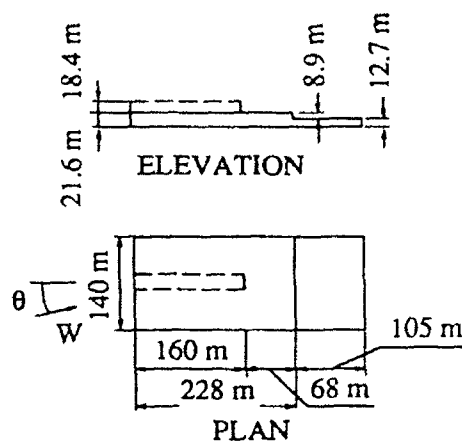


Figure 6 Plan and Elevation of test building

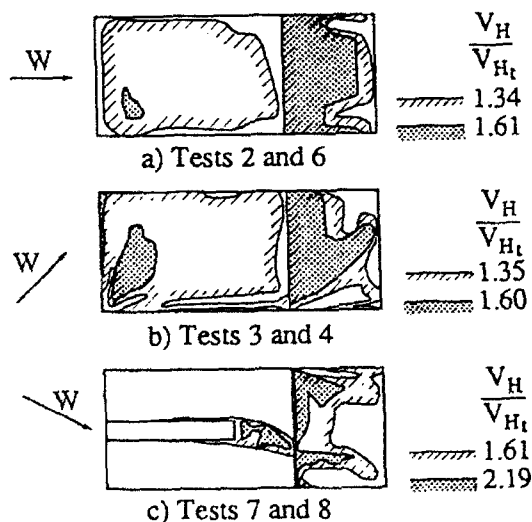


Figure 7 Spatial distribution of snow at end of tests

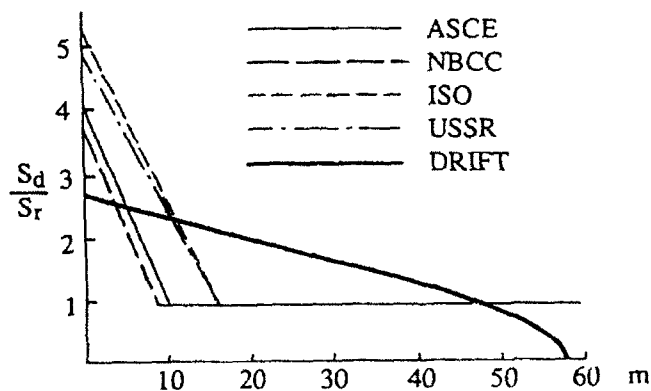


Figure 8 Spike drift of test 8 and code provisions

The Codification of European Snow Loading

John R. Tory

Building Research Establishment
Watford, United Kingdom

ABSTRACT

The work on the drafting of the structural Eurocode for actions on structures has moved from the Commission of the European Communities to a Project Team selected by the European Committee for Standardisation, Technical Committee 250, Subcommittee 1 (CEN/TC 250/SC 1). This change in the Standard's administration authority, which has increased from 12 to 18 the number of countries to be covered by the Eurocode, has had significant implications for that part of the Code concerned with snow loading. The additional countries to be considered all have snow loading codes which differ from those of the countries of the ECE: their inclusion also significantly increases the geographical and climatic coverage required of the Code.

This paper details some of the difficulties involved in the production of a harmonized code, particularly with regard to the enhanced geographical scope. It reports the progress of the CEN Project Team in the further development of a draft; considers the problems that have been identified and how they are to be resolved within the CEN timetable requirements. The paper also presents a view on the further developments of the Code that are likely in the longer term.

BACKGROUND

Preparation of Structural Eurocodes for the countries of the Common Market was originally initiated in 1976, and in 1979 the Commission of the European Communities (CEC) entrusted the task of drawing up the series of codes to several teams of experts. Since the first draft Eurocode 1 was produced in 1984 the title and content have changed to encompass both the design rules and loading, and work has also progressed on the other Eurocodes. Also, since the priority parts of the loading code were listed in a paper to the First International Conference on Snow Engineering by Judge (1988) they too have changed in form and content.

At one time the loading code was titled EC A and limited in scope to design loads. More recently it has become integrated into a new EC 1 which combines both loads and the rules for design. Judge listed Parts of the code, which then changed to Chapters and have now reverted to Parts. And within those Parts there have been, and continue to be, other less significant changes to content and format. Until final publication as an ENV (voluntary Euronorm) the format and content of the code might therefore be considered somewhat fluid and perhaps, at times, somewhat confusing. However, for reference, the present titles of all the Eurocodes and

all the Parts of Eurocode 1 are given in Annex A. Snow loads will form EC 1, Part 2.5.

Some of the background to the development of the structural design codes has previously been described by Judge(1988). He also described the work on snow loads then being carried out within a CEC Task Group and detailed some of the content of the existing national snow loading codes of Common Market members. This paper describes the more recent developments of that Part of EC1 which concerns snow loading, including the extension of the work to cover the CEN member states.

THE DRAFTING OF EC 1, PART 2.5

To advance the work on Eurocode 1 CEN have appointed small teams of experts for each section or Part of the Code. The function of the experts, who operate without national allegiance, is to produce and submit to CEN by January 1993, draft codes or provisional 'pre-standards' that will be acceptable to all the CEN member states. The convenor of the team concerned with snow loading, Project Team 4, is Professor Sanpaolesi of Universita di Pisa, Italy. Other members of the Team are drawn from France, Germany, Norway, Switzerland and the United Kingdom.

It is the intention of the Project Team for snow loads to draft a code that in the first instance should not be too dissimilar from present national codes. This is necessary, first to be readily usable by, and gain the acceptance of, designers within each CEN country. Secondly, because within the timetable imposed by CEN for the production of working documents it is unlikely to be possible to produce a fully integrated standard with uniform derivations and procedures that would receive the approval of the member states. Indeed the achievement of a truly harmonized approach must be many years away since it perhaps depends on consistent collection and analysis of basic meteorological data and that will take many years to achieve.

The current work on snow loads is therefore seen by the Project Team as a first phase of work towards a more justifiable and integrated Code.

THE SCOPE

Geographical scope

In 1990 the responsibility for all the structural Eurocodes was transferred from the Commission of the European Community (CEC) to the European Committee for Standardisation (CEN). This transfer was particularly important for snow loading codification because it introduced not only the problem of consideration of more national codes but also of extended climatic diversity.

Between the 12 countries¹ of the ECE there is a fair degree of climatic variability, but the introduction of the six countries of the European Free Trade Association (EFTA) countries - Austria, Finland, Iceland, Norway, Sweden and Switzerland - added another dimension to that problem for the standardisation of snow loads. From being limited to the western and southern countries of Europe, the transfer to CEN extended the geographical scope of the code to an area

¹ Belgium, Denmark, France, Germany, Greece, Ireland, Italy, The Netherlands, Luxembourg, Portugal, Spain, United Kingdom.

greater than that of the United States, extending further North than Point Barrow in Alaska.

Towards the northern extremities, in Norway, snow loads are particularly significant. Loads as high as 6.5kN/m^2 are possible and in addition to being very deep, the snow in many parts of that country is also present for much of the year.

At lower altitudes in the south (southern Spain, Italy and Greece) snow loads are perhaps less significant than in the north but nevertheless are still an important consideration for building design.

Technical scope

Part 2.5 gives guidance on loads due to snow which has fallen in either calm air or in windy conditions, for the loads imposed by snow sliding down a pitched roof to a fence or other obstruction, and for the loads due to snow overhanging the cantilevered edge of a roof.

Such is the climatic variability across Europe that for some areas it is appropriate to consider the snow loading having been created by an accumulation of snow from several weather systems, and in other areas to be due to loading from a single system. For example; Ireland and the United Kingdom have maritime climates influenced by the Gulf Stream, with relatively high winds. The snow that falls is considered to be associated with single weather systems which may have durations of perhaps three or four days. Between one weather system and the next there is a reasonable expectation that the snow deposited on roofs will thaw. The UK loading code therefore only requires consideration of either a uniform load or a drift load: the two are not expected to occur together. The German standard, DIN 1055: Part 5 (1975), adopts a similar principle where, for simple pitched roofs a reduced load on one half of the roof is assumed to occur without a load on the other half. And for north lights DIN 1055 requires consideration of a redistribution of the snow that would be present in the uniform load case, not a combination of drift and uniform load cases.

In much of continental Europe and Scandinavia the fallen snow is generally more persistent than in the UK. Snow falling in calm conditions may well be followed by further snow, carried by another weather system and perhaps driven by wind; and there may be several repetitions of these events before there is significant thawing. An accumulation of snow composed of simultaneous uniform and drift components is therefore a likely occurrence and should be allowed for in design.

In earlier drafts of Part 2.5 the two eventualities described above were termed single snow events and multiple snow events. Although these terms are no longer used the distinction between them is retained and separate provision is made for each. In the present draft, multiple snow events are dealt with in the body of the code; single snow events are in an annex. Because the provisions for each have been extracted from different sources the forms of presentation are also quite different at this stage of the drafting.

The code is notionally limited in its application to sites at altitudes up to 1500m. In practice, and as explained later in this paper, it is further limited in respect of altitude by the national data available. For example, although there are many parts of Germany at higher altitudes, the snow data available for everyday design in that country does not extend beyond 1000m.

In common with most other codes, further limitations of this Part of the Code are that it does not give guidance for -

- (i) impact snow loads resulting from snow sliding off or falling from a higher roof;

- (ii) loads which could occur after thawing if snow and ice have blocked gutters;
- (iii) the change in wind loads which could result from changes in the shape or size of the building structure due to the presence of snow or the accretion of ice (nor is this covered by EC 1 Part 2.7 'Wind Loads');
- (iv) loads in areas where snow is present all the year;
- (v) ice loading (which will form Part 2.6 "Ice Loads");
- (vi) lateral loading due to snow (eg lateral loads exerted by drifts).

The code also reminds users that there are a number of other imposed roof loads given in other Parts of EC 1 which should also be considered in design.

Field of application

The code will apply primarily to new buildings and structures and significant alterations to existing buildings and structures. Some guidance may also be provided for snow loading on bridges and silos although this is unlikely to be very detailed. Similarly, some guidance will be provided for temporary structures.

DEFINITIONS AND SYMBOLS

The definitions given in the Part 2.5 are, to all intents and purposes, self-explanatory and should present no difficulty for anyone likely to have use for the Eurocode. But the use of the term 'characteristic value of snow load on the ground' perhaps warrants comment.

The definition given in Part 2.5 is -

"characteristic value of snow load on ground. The load intensity of undrifted snow at ground level, at the altitude of the site, with an estimated probability of being exceeded of 0.02 in any one year."

But a characteristic value has been defined in Eurocode parlance as - "..... that value which has a prescribed probability of not being attained in a hypothetical ... series (corresponding to a fractile in the distribution of the ... parameter)".

There is clearly a difference here. The Part 2.5 value relates to a return period of 50 years whereas a 95% probability of occurrence of the maximum load might correspond to, say, a two thousand year return period (the 95th fractile being the one used for load definition in the Eurocodes). A decision has yet to be taken on how this problem might be resolved. One possibility might be to apply the existing definition to the term 'representative load'.

The symbols used in Part 2.5 are in accordance with ISO 3898 (1987). This International Standard is widely accepted in Europe and even though it is different in some respects to some current national practice its formal use in the Eurocodes is not expected to present difficulty.

SNOW LOAD ON THE GROUND

Within the countries of CEN there are at present several different methods of defining ground snow loads. Even adjoining countries that would appear to have many climatic and

geographical similarities have quite different approaches to this basic meteorological criterion. Some countries choose to define one snow load for the whole country, others divide the country into zones on the basis of either snow load classes or administrative regions, others give equations to calculate load from altitude and some provide detailed snow load maps. In his paper Judge also drew attention to the widely disparate views within the ECE countries on how ground snow loads were related to altitude.

The Project Team is agreed that Part 2.5 should follow the guidelines provided by the International Standard on snow loading, ISO 4355 (1981), in that where more precise data are not available, a map of ground snow loads should be provided. Such a map should necessarily cover nearly all of the CEN countries, with the ground snow loads defined and derived in the same way for each, from the analysis of consistent meteorological data. This is of course a prerequisite for the final objective of a fully harmonized code with a sound scientific base. However, it will not be possible to achieve that objective in the immediate future because first, the meteorological data is not sufficiently detailed for all countries; and secondly, it will not be possible to reanalyse the available data within the timescale imposed by the CEN EC 1 subcommittee.

In Norway with its high snow loads, the snow loads on the ground are defined individually for each local municipality. The Project Team have not looked too closely at how this data might be fitted into any pattern established for the other countries. Even in the long term, it may be necessary to accept that the data is more detailed than could be provided by a map and that special provision should be made. Certainly the possibility of integration into a fully harmonized approach is likely to be extremely difficult to achieve.

A European snow map

The need for a European map of ground snow loads becomes evident if the patterns of the ground snow loads given in current codes throughout continental Europe are studied. There is a lack of continuity across political frontiers; anomalies having arisen because each country has quite naturally derived its ground snow loads from its own data, to fulfil its own needs, with no reason to refer to its neighbours. Within their borders each country has defined its snow loads to produce satisfactory design solutions (although the design solutions are also functions of snow load shape coefficients too). In the region of the Austrian/French/German/Swiss borders, where there is appreciable snow fall almost every year, there are particularly noticeable discrepancies.

Already two attempts have been made to establish a coordinated European snow map. The first, by Gränzer (1989), considered all the available basic meteorological data for the ECE countries. It foundered because of the difficulty of establishing a satisfactory common curvilinear statistical relation between snow load and altitude for even a limited number of countries; because there was insufficient consistent data for many of the countries; and also because of the difficulty of extending the methodology to the EFTA countries within the time available.

Another snow map has been produced by Del Corso (1992) and is at present being discussed within the Project Team. Six climatic regions are defined, each being divided into snow load zones based on current national code values of ground snow load corrected to a common return period and reference altitude. It is too early to say how this map will be received: it does not pretend to fulfil all the requirements of a harmonized code, nor does it attempt to accommodate the Norwegian practice of defining individual loads for each municipality; but it does offer a compromise solution to the cross-frontier problem.

An interim solution

Unless there is agreement on acceptance of the Del Corso map, Part 2.5 will, at least for the immediate future, have to rely on present national data extracted almost directly from the national snow loading codes and therefore presented in a variety of different formats. Few other steps towards uniformity will be possible.

Most countries define their ground snow loads on the basis of a return period of 50 years. Exceptions are Germany (20 years) and Norway (5 years). The codes of Denmark, Iceland and Spain do not relate their loads to a probability of exceedance and there is some uncertainty about Switzerland, although it is thought to be about 50 years. With the adjustment of some data it is therefore unlikely to be difficult to standardise on a definition of ground snow load related to a return period of 50 years. Already Germany has provided the necessary adjustment factors for its data. However, it will be difficult to accommodate current Norwegian data and practice and perhaps an exception will have to be made.

For particular purposes, such as the design of temporary structures or structures where greater than normal safety is required, a formula has been included in an annex of Part 2.5 to permit adjustment of the characteristic snow load to return periods other than 50 years. The formula is not applicable for return periods of less than 5 years.

The reference altitudes for ground snow load and the maximum altitudes for which the national code data are applicable also vary throughout the member states. Standardisation on these points is not possible because it would require the Project Team to extrapolate from the most reliable sources of information. However, a limiting maximum altitude of 1500 metres has been introduced.

SNOW LOAD ON THE ROOF

For the calculation of roof snow loads, most of the CEN countries follow the method outlined in International Standard ISO 4355 (1981) and calculate the load as the product of the snow load on the ground and a non-dimensional snow load shape coefficient. This basic procedure has also been adopted by Part 2.5. However, Part 2.5 also makes provision for further modification of the roof snow load by the introduction of other coefficients to allow for heat loss through the roof and for abnormal exposure to the elements. The provision of these other two roof snow load coefficients is in line with a proposed amendment of ISO 4355 (ISO DP 4355 (1992)) but for the Eurocode they have not been quantified for other than 'normal' use and conditions, when they have a value 1.0. National regulatory authorities have the discretion to approve the use of smaller values of these coefficients.

Load duration

The duration for which loads are applied is an important consideration for several structural materials but few if any national loading codes provide guidance on it. At a national level it has generally been considered sufficient to leave the definition of load durations to the materials design codes that required them (notably timber). Within CEN/TC 250/SC 1 it is considered more appropriate that the full and proper description of loads be accepted as a responsibility of EC 1; not of the materials Eurocodes EC 2 to EC 9.

It is evident that snow laying on roofs will be much more persistent in some areas of Europe than in others. However, because the Project Team have been unable to establish a consistent approach to the definition of load duration because of the lack of suitable data, all roof snow loads are assumed to be of medium term duration (1 week to 6 months) unless ruled otherwise by the national regulatory authorities. The UK and Ireland have taken advantage of this provision to specify that the uniform snow distributions from their 'single snow events' should be considered medium term whilst the alternative drift loads will be short term (less than 1 week). It is expected that other countries will also wish to qualify the duration of the snow loading for some or all of their regions.

The coefficients to be related to each of the load duration classes are not defined in EC 1. They will be dependent on material characteristics and behaviour and are therefore the responsibility of the materials codes EC 2 to EC 9.

Snow load shape coefficients

Throughout Europe there are quite significant differences in the snow load shape coefficients assigned to particular roof configurations; even taking account of the different methods of defining snow loads. There are also differences in the numbers of roof shapes for which shape coefficients are provided.

The present draft Part 2.5 gives shape coefficients for monopitch, duo-pitched and multi-pitch roofs in addition to coefficients for drifting at abrupt changes in roof height and at obstructions on roofs. It is possible that in a later draft guidance will also be provided for arched roofs. As mentioned previously, the Code will cater for both single and multiple snow events.

For single snow events the snow load shape coefficients are at present identical to those provided in British Standard BS 6399: Part 3 (1988), although fewer in number. Drift lengths and shape coefficients are determined by reference to flow diagrams but an attempt is to be made to simplify the presentation to bring it into line with that for multiple snow events. In the annex in which the coefficients are given it states that - "The most unfavourable of the loading cases arising from either a uniformly distributed layer of snow over the complete roof or the drift loads shall be used for design."

The coefficients for multiple snow events are taken directly from the current International Standard ISO 4355 except that for duo-pitched roofs Part 2.5 specifically requires consideration of a loading case with no load on one side of the roof. The coefficients are given in diagrammatical form. It is clear that they cover the combination of uniform and drift loads together.

Figure 1 shows some of the extreme values of shape coefficients for simple pitched roofs at present given in current national codes and provides a comparison with the provisions of the draft Part 2.5 for multiple snow event coefficients. Also included in Figure 1 are curves based on ISO DP 4355 (1992). Although providing a comparison between the ISO proposals and the others, of the order of the shape coefficients, it should be borne in mind that exposure, thermal and roofing surface coefficients are expected to be applied to calculate the ISO roof loads but do not usually apply in the other cases.

FUTURE DEVELOPMENT OF PART 2.5

The CEN contract for the drafting of EC 1, Part 2.5 requires Project Team 4 to submit a 'final' draft document as a prENV (a draft European pre-standard) by 31 January 1993; for formal voting on publication as an ENV (a voluntary European pre-standard, numbered ENV 1991). CEN/TC 250/SC 1 aims to agree the suitability of the draft at its meeting on 21/22 April 1993. If approved then, subsequent editorial treatment within CEN should lead to its release early in 1994.

At that time the relevant parts of EC 1 should be published by member standard bodies for provisional application, initially for 3 years. It will be for member states of ECE and EFTA to determine the arrangements for use in relation to their national requirements. After 2 years the members of CEN will be invited to submit their comments on the Code, particularly on the question of whether the ENV can be converted into a European Standard (EN).

The exact arrangements for the conversion to a fully agreed EN and the period of coexistence of the European Standard for design with the corresponding national standards have yet to be agreed.

As has been pointed out in this paper, there are still numerous inconsistencies in Part 2.5 and even by the contract completion date the Project Team is unlikely to consider the production of this part of the Eurocode for actions to be complete. Like all design codes it must continue to develop to cover the requirements of the designers and to present them with information based on the latest results of research. There must also be further movement towards a more consistent definition of snow loads.

The two areas in which one might reasonably expect amendment of the code between the prENV and EN stages are in reappraisal of ground snow loads and reconsideration of the roof snow load shape coefficients.

Future work on the ground snow loads will almost inevitably centre on the production of a coordinated European snow map. In the short term some progress will be made by the CEN Project Team but a technically credible map on which building designs may be confidently based, must in the end depend on cooperation with, and input from, the meteorologists and climatologists. At present much of their attention is focused on providing data for other purposes such as tourism and transport: it remains to be seen whether they also have adequate data, with a sufficiently long history, to fully cope with the needs of building and construction.

It is admitted by most countries that their snow load shape coefficients are largely empirical, owing more to crude approximations of a very few observations than to scientific derivation and justification. And there have been numerous instances of roof failures attributable to the inadequate modelling of the snow loads that have occurred in practice. Already ISO DP 4355 (1992) is introducing new ideas on the description of shape coefficients, breaking the snow loads down into components attributable to uniform deposition, drifts and sliding. If that Draft International Standard receives approval the new concepts and flexibility of application that it seeks to introduce will almost certainly be adopted by Eurocode 1. But more research is required in this field, to cover a wider range of standard roof configurations and to enable calibration of computer models that can be applied to almost any roof configuration.

CONCLUSIONS

This paper has drawn attention to some of the difficulties faced by the CEN Project Team charged with producing a harmonized snow loading code for the 18 member states. It has pointed out the problems associated with the wide geographical diversity and varied current code requirements.

Although it has not been difficult to agree the general structure and methodology to be adopted by the Code there is considerable difficulty reconciling the existing snow loads of the member states with those required for a truly consistent approach. As an interim solution it is to be proposed that member states should continue to use their existing ground snow data, with some amendment for a minority of countries. However, the Code will present a limited range of standardised snow load shape coefficients for use with those ground snow loads.

In the medium term it is expected that the Code will eventually adopt the methodology of ISO DP 4355 (1992) for the derivation of snow load shape coefficients.

The longer term aim of establishing a European snow map has been explained as a way of achieving full harmonisation. A particular difficulty will be the assimilation of the more detailed data related to Norway.

ACKNOWLEDGEMENT

This paper is contributed by courtesy of the Chief Executive, Building Research Establishment, United Kingdom and reproduced by permission of the Controller of Her Majesty's Stationery Office.

REFERENCES

British Standard BS 6399: Part 3 (1988). "Code of Practice for Imposed Roof Loads". British Standards Institution, London.

Del Corso R. (1992) "European snow load map: 1st phase". Università di Pisa.

Deutsche Normen DIN 1055: Part 5 (1975) "Design Loads for Buildings. Live Loads. Snow Load and Ice Load" Detches Institut für Normung, Berlin.

Gränzer M. (1989) "Schneelasten für EC 'Lasten'". Landesstelle für Baustatik, Tübingen.

International Standard ISO 3898 (1987) "Bases for Design of structures - Notations - General Symbols". International Organization for Standardization.

International Standard ISO 4355 (1981) "Bases for design of structures - Determination of snow loads on roofs". International Organization for Standardization.

International Standard ISO DP 4355 (1992) "Bases for design of structures - Determination of snow loads on roofs". International Organization for Standardization, Technical Committee TC/98.

Judge C J (1988). "Developing the Eurocode." First International Conference on Snow Engineering, Santa Barbara.

Report EUR 8847 DE, EN, FR. "Eurocode No 1: Common unified rules for different types of construction and material." Commission of the European Communities, 1984.

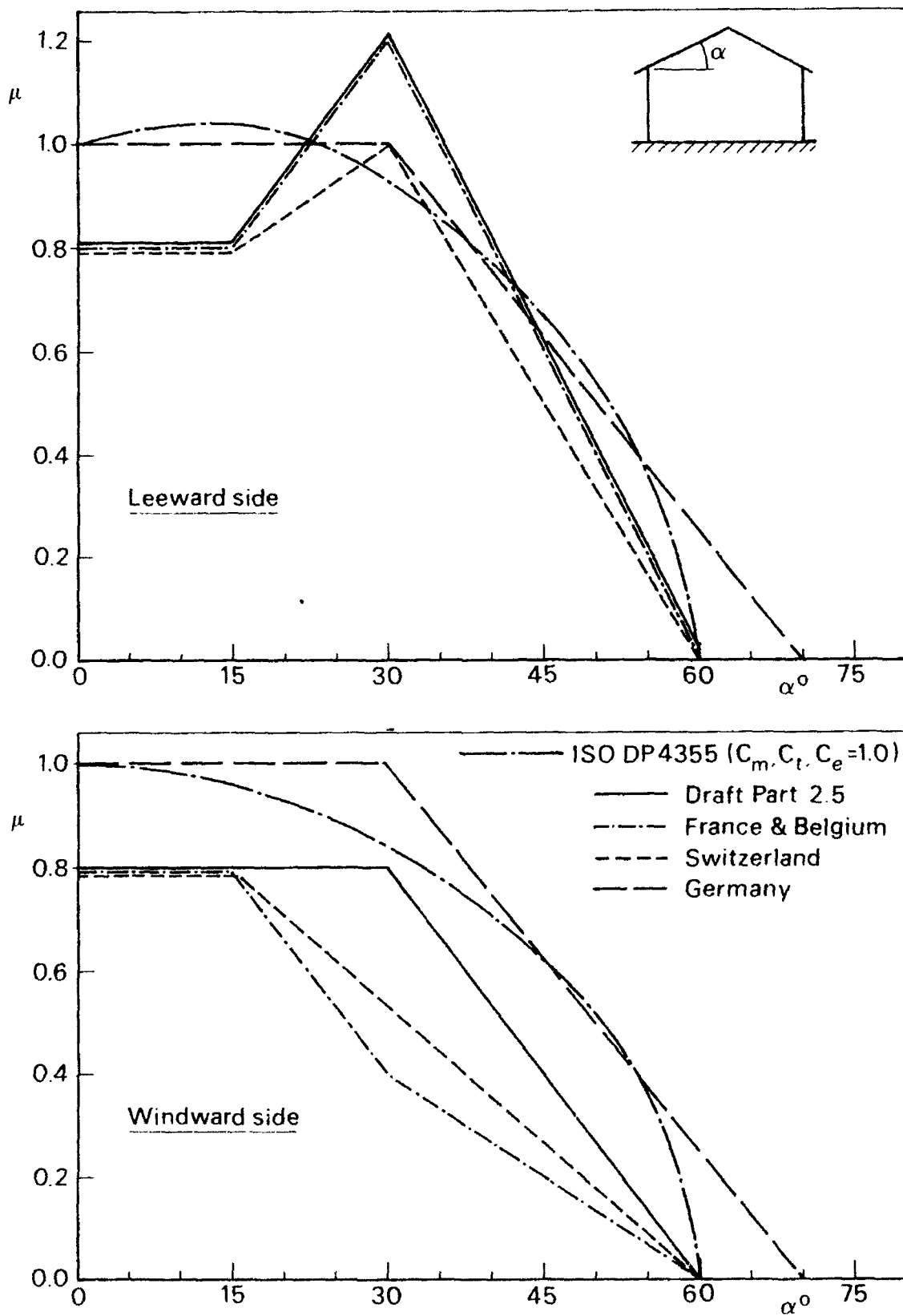


Figure 1 Snow load shape coefficients for simple pitched roof

Annex A : The European Loading Code within the framework of the Structural Eurocodes

This annex shows in table 1 how EC 1 will be accommodated within the present framework of the structural Eurocodes. The constituent Parts of EC 1 are detailed in table 2.

Table 1: Eurocodes for structural design

Number	Title
1	Basis of Design and Actions on Structures
2	Design of Concrete Structures
3	Design of Steel Structures
4	Design of Composite Steel and Concrete Structures
5	Design of Timber Structures
6	Design of Masonry Structures
7	Geotechnical Design
8	Design of Structures for Earthquake Resistance
9	Design of Aluminium Structures

Table 2 : Eurocode 1: Basis of Design and Actions on Structures

- Part 1 : Basis of Design
- Part 2 : Gravity, Imposed, Accidental and Environmental Actions and Actions Arising during Execution
 - 2.1 General
 - 2.2 Gravity Loads and Densities of Building and Stored Materials
 - 2.3 ?
 - 2.4 Imposed Loads
 - 2.5 Snow Loads
 - 2.6 Ice Loads
 - 2.7 Wind Loads (static and dynamic)
 - 2.8 Thermal Actions
 - 2.9 Loads and Deformations Imposed During Execution
 - 2.10 Accidental Actions
 - 2.11 Actions from Currents and Waves
 - 2.12 Soil and Water Pressure
- Part 3 : Traffic Loads on Bridges
 - 3.1 General
 - 3.2 Road Traffic Loads
 - 3.3 Loads due to Pedestrians and Cyclists
 - 3.4 Rail Traffic Loads
- Part 4 : Actions in Silos and Tanks
 - 4.1 General
 - 4.2 Actions in Silos and Tanks
- Part 5 : Actions induced by Cranes and Machinery
 - 5.1 General
 - 5.2 Actions induced by Cranes
 - 5.3 Actions induced by Machinery
- Part X : Accidental Actions from Fire
 - X.1 General
 - Z.2 Actions on Structures exposed to Fire

9

Perspectives

Ronald Sack, Chairman



Perspective Ground Snow

Hirozo Mihashi

Department of Architecture, Tohoku University
Sendai 989, Japan

INTRODUCTION

Measurements of snow loads on the ground are the principal data for the determination of design snow loads, since snow loads on roofs are greatly influenced by various factors, are difficult to collect and are limited in number. When the available field data of snow loads on the ground have been accumulated in a meteorological data base, a statistical analysis is performed to determine a value for a certain return period for use in design. In many places, however, the measured data are not the water equivalent of the snow cover but only the snow depths on the ground. Hence it is interesting to examine the relation of statistical properties of snow loads and those of snow depths. Moreover functions to convert snow depths to snow loads need to be found.

Since the number of observations is still limited, some estimation procedures are necessary to determine the snow load on the construction site where no available measured data exist, or to draw regional maps. Recently various kinds of automatic measurement have been developed, which make possible the collection of data on denser measuring points.

When snow cover on the roof can be often removed or melted, it may be more rational to reduce the design snow load. In such cases, the rate of snowfall is more important than the annual maximum snow load.

Presented papers and discussions in this session at this conference on the ground snow are subdivided into four categories: statistical analyses of snow loads and snow depths, estimation of snow depth at unobserved points, development of instruments and methods to measure snow load and snow depth, and snowfall intensity.

STATISTICAL ANALYSES OF SNOW LOADS AND SNOW DEPTHS

Since the design snow load is usually based on an extreme value, statistical analyses of the maximum annual ground snow depths or loads have been performed by many researchers. While the main point to be discussed has been which distribution provides the best fit, it is important to note the following two points: 1) the fitness of a distribution function is not usually dominated by the extreme values but by rather frequent ones; 2) it is assumed that all data belong to the same population, i.e., the annual maximum values occur in the same meteorological condition.

Joh showed that a unique distribution could not fit sufficiently the annual maximum ground snow loads and snow depths in Japan. He concluded that the probability distribution functions were identical for both the annual maximum snow load and the snow depth in the same spot. Moreover he found an obvious linear relation between the extreme snow depths and the extreme snow loads for return periods of 10, 30, 50 and 100 years. On the basis of this linear relation, he proposed the conversion coefficient from the snow depth to the snow load to be 350 kg/m^3 as a practical value in Japan.

ESTIMATION OF SNOW LOAD AT UNOBSERVED POINTS

In many previous studies, ground snow load has been related to altitude. The ground snow load maps for the National Building Code of Canada were revised in 1990, taking into consideration snow load variations with altitude. Draft Eurocode 1 is currently under discussion. In it, it is assumed that ground snow load varies with altitude.

Sandvik analyzed the variation of characteristic snow load on the ground in different parts of Norway. He finally concluded that relating snow load to altitude, is very complex and not as simple as is presented in Eurocode 1. Takahashi carried out multiple regression analyses to estimate the ground snow depth in all of Japan except Hokkaido island using topographic factors which were latitude, longitude, altitude, sea area ratio, inclination of the land, and land closing ratio. Altitude was generally the most dominant factor but not the single regression variable. The sea area ratio was also influential near the coast. It is important to note that the mechanism of snowfall and the influence of wind on ground snow should also be taken into account when subdividing regions for analysis.

INSTRUMENTS AND METHODS TO MEASURE GROUND SNOW

Powell described instruments and methods to measure ground snow including a traditional snow sampler, snow sensors, telecommunication measuring systems, and measurement by flying. Tamura developed a new instrument to continuously measure snowfall. That instrument is compact, light weight and simple.

SNOWFALL INTENSITY

Takahashi related differences in the snowfall mechanism to cause the extreme value of snowfall intensity and the annual maximum snow depth. He also pointed out that high rates of snowfall were the main cause of damage to buildings during the heavy snow disasters in 1963 and 1981 in Japan. Further studies of snowfall intensity are needed for the safety of buildings.

In the final session, Powell promoted use of the Soil Conservation Service data base since it gives both depth and water equivalent information. In the USA there are 1,500 sites with such data. Up to 60-years of data are available at some stations. Snow sensor data can give snowfall information. Looking at the maximum storm intensity was also suggested.

CONCLUSION

The collection of data is obviously an important part of snow load studies. Even if development of automatic measurement systems provides denser networks of data, an estimation procedure on the basis of regional topographic factors needs to be developed. It is important to consider the snowfall mechanism and the influence of wind. Snow intensity should be further studied to prevent building damages in heavy snow disasters.

Perspective Structural Case Histories

Michael O'Rourke
Rensselaer Polytechnic Institute
Troy, New York, U.S.A.

INTRODUCTION

Case histories of snow loads on structures are the backbone of building code and load standard provisions for snow loading. During the session of Structural Case Histories a total of five papers were presented. One discussed an automated data gathering technique for roof snow depth information using aerial photogrammetry. Two of the papers were on detailed case histories, one in a combination with wind tunnel testing. Another paper presented a statistical analysis of roof and ground snow depth data from an extensive collection of case histories. Finally, a computer-based analytical method, the finite area element method, was discussed.

During the Structural Case Histories portion of the Perspectives session, an attempt was made to generate comments on and questions about the papers as opposed to simply reviewing the papers themselves. Presented below is a synopsis of that discussion.

DATA GATHERING

The paper by Sakurai et al. on aerial photogrammetry generated questions on the possible application of the method to determine ground snow depths. Sakurai noted that measuring ground snow photogrammetrically poses problems because of the presence of obstructions. Photo targets could be installed to obviate some of these problems.

Another question concerned snow density since the paper dealt only with depth measurement. Powell noted that the U.S. National Weather Service's Office in Minneapolis, MN, obtains water equivalent data by flying, suggesting that information on loads is possible.

MacKinlay noted that the photogrammetric method of measuring roof snow loads requires advanced planning (e.g., targets placed and calibrated in the summer). Finally, Sandvik suggested that multiple pitch and curved roofs should be monitored to obtain roof load distributions.

DETAILED CASE HISTORIES

The paper by Nakamura et al. resulted in a question on the measured values of ground-to-roof conversion factor. Specifically, what is the physical reason for the conversion factor for moderate conditions being less than that for both light and heavy conditions. In addition, Isyumov suggested that possibly we should try determining structural loads by measuring structural response as done by Nakamura.

The paper by Suzuya et al. on correlation of full-scale snow case histories with wind tunnel tests resulted in a question on the proper wind profile coefficient α . Noting that the value $\alpha = 0.2$ in the wind tunnel resulted in a good comparison with field results for roof snow, the question is whether $\alpha = 0.2$ actually matched the velocity profile coefficient in the field. That is, what value of α should be used in wind tunnel simulations for a new structure?

ANALYTICAL METHODS

In discussing the finite area element (FAE) method described in the paper by Irwin et al., O'Rourke noted that the FAE method would probably prove most useful as a tool for one-of-a-kind structures and somewhat unusual structures (e.g., very long upper level roofs) for which case histories are not available. Also there is a need for better understanding of some modeling parameters as well as benchmark comparisons with established case histories. Irwin agreed that case histories are valuable. We should attempt to measure snow patterns over time. Also it would be helpful to: a) devise full-scale measurements to obtain short-term changes and b) follow the roof load distributions for a single storm. Such measurements could be used to validate analytical methods.

Perspective Analytical Modeling

Peter A. Irwin

Rowan, Williams, Davies and Irwin, Inc.
Guelph, Ontario, Canada

INTRODUCTION

Analytical methods in snow engineering cover a broad range of topics. In the session on this topic the first paper, by Brandstatter, Weiser and Schaffhauser from Austria, described the use of Computational Fluid Dynamics to predict avalanche forces. This was followed by a paper, by Williams, Gamble and Retzlaff from Canada, describing the application of the Finite Area Element method (first introduced at the preceding conference 4 years ago) to predict snow loading on two contrasting roofs, one a very heavily loaded roof in a deep snow area in Chile, and the other a glass roof in an area of lighter loading in Canada. The paper by Ito from Japan was concerned with statistics, using past data to develop an index of severity of snow problems. The paper by Kamimura and Umemura, from Japan, was also primarily concerned with statistics, in this case the objective being to develop a method of predicting the buildup of snow mass on a roof using meteorological data and thus indicating when snow clearing should be initiated. The last paper, by Yamada and Ikarashi, described the interpretation of data from an automated meteorological data acquisition system.

PERSPECTIVES

The topics of these papers, although wide ranging, did not cover the full range of analytical methods used in snow engineering applications. In the previous conference, for example some papers applied analytical methods to snow sliding problems, a topic that did not receive so much attention at this conference. Analysis of snow infiltration was another problem not discussed much at the present gathering but which is probably a promising area. During the discussions Ian Mackinlay described how important a design problem snow infiltration can be and Wayne Tobiasson related some practical experiences in controlling infiltration in the Arctic and Antarctic.

It was of interest to see the use of Computational Fluid Dynamics (CFD) in a snow engineering application at this conference. There appear to be a number of snow related problems where CFD methods will be a powerful tool in gaining a better understanding. The problem of how falling snow accumulates on a roof in the presence of wind is one interesting one. Another is the capture efficiency of a backwards facing step on a roof, i.e. determining how much of the snow drifting over the edge of the step lands in it and how much is carried onwards by the wind. One can also envisage the use of CFD methods combined with the FAE method, in this case CFD being used to replace the wind tunnel as a means of determining the wind velocity distribution on the roof.

The FAE method first introduced at the preceding conference has been further developed since then and been applied, together with physical model tests, on a number of large roofs. This method can be expected in the future to be used to explore several interesting problems, e.g. how to combine wind loads with snow loads. For some roofs, especially those adjacent to higher buildings, this is important because downwards wind forces can occur, thus adding to the snow loads. Another promising area for the FAE approach is the study of snow load durations, which can be important for wooden structures for example.

The statistical papers indicated some of the future trends that can be expected in statistical analysis. Clearly, modern computing power allows us to look at much more data and many more variables than before. Also improved methods for automatically recording important meteorological variables are going to greatly increase the quantity and coverage of the available data. It will still be a challenge to identify which are the most important variables that influence snow accumulations.

CONCLUSIONS

What are the best uses of analytical methods? For large one of a kind construction projects, sensitive to snow loading, it becomes worthwhile to use all available tools to establish the design snow or avalanche loads as accurately as possible and to try to foresee likely snow problems. The primary tools are analytical methods in judicious combination with scale model tests in wind tunnels and waterflumes. The strength of analytical methods is their ability to deal with cumulative effects, e.g. the buildup of snow and its drifting over a sequence of storms. The scale model tests provide important input data for the analytical methods and can provide valuable physical insights into drifting, but tend to be limited in their ability to go beyond anything but a single event, i.e. drifting from a single predominant direction in one storm.

Another useful application of analytical methods is the study of snow loading trends to assist in the development of building codes. Several of the papers at this conference, not necessarily in the Analytical Methods session, were on this theme. The analytical methods provide useful ways of extrapolating and interpolating from a limited number of field data points.

Finally it has to be emphasized how important it is to use every opportunity to compare the results of analytical predictions with field data so as to ensure that the methods reflect the real world as faithfully as possible.

Perspective Experimental Modeling

N. Isyumov

OVERVIEW

A substantial emphasis has been given during this Conference to physical model studies of snow drifting and accumulation. This included four papers in Session T2; two papers in Session M2, dealing with structural case histories, one paper in Session T1, dealing with analytical modelling; and one paper in Session R2, dealing with Codes and Standards. In total, experimental modelling of the transport and deposition of snow on and around buildings was directly or indirectly addressed in 8 of the approximately 40 papers, presented at this Conference. While experimental modelling played a significant role in the other papers, I would like to limit my overview to the four papers presented in Session T2 on Experimental Modelling.

- i) The paper by Isyumov and Mikitiuk reviewed Canadian experience at The University of Western Ontario. It included an overview of the similarity requirements for such studies and stressed that it is difficult to make progress without some approximations of the modelling laws. The experimental procedures developed appear to be in reasonable agreement with full-scale data for dry snow. On the other hand, wet snow conditions are almost impossible to simulate at a reduced scale. A dominant similarity requirement in such studies is the modelling of the mean and turbulent characteristics of natural wind. The methodology which has been developed appears to provide good estimates of the overall or "bulk" characteristics of snow load formation, as long as the snow can be assumed to remain "dry" and driftable. It is more difficult to model detailed features such as cornices, etc.
- ii) The paper by O'Rourke described modelling studies carried out in a water flume to provide data to assist in developing improved procedures for estimating the drift snow loads which occur on lower levels of multi-level roofs. The model snow material used in this study was crushed walnut shells. This relatively new research programme is intended to improve our understanding of how triangular drift loads may depend on wind speed and wind direction, and the plan dimensions and changes in elevation of the roof. These studies are judged to be extremely important, as approximately 75% of all snow-related failures tend to be due to drifts on multi-level roofs.

- iii) The paper by Toyoda and Tomabechi described the development of a special wind tunnel facility to study snow drifting. This wind tunnel is located at the Cold Regions Technical Center of the Hokkaido Institute of Technology. Activated clay particles are used to simulate natural snow. Laser displacement sensors are used to describe three-dimensional drift geometries. The paper describes the wind tunnel apparatus, data acquisition procedures and the results of model studies of snow drifting and accumulation at snow fences and around simple building shapes.
- iv) The paper by Wiannecki and Chevallier described a wind tunnel study of snow accumulation on a roof with and without parapets. The tests were made in a specially designed wind tunnel referred to as the SANEV Wind Tunnel, which has been constructed at the CEBTP. Specially cut and sorted pine sawdust was used as the model snow material. The similarity requirements stress the modelling of natural wind and scale the snow particle using procedures first developed by Mateescu in Romania. In addition to snow loads on a flat roof with and without parapets, the paper presented information on snow loads on a stadium roof.

STATE OF THE ART

Experimental or "physical" models of snow drifting and/or snow accumulations around and on buildings are used:

- i) to gain or improve the understanding of the snow transport and accumulation process,
- ii) to provide empirical data to support analytical and numerical methods, and
- iii) to deal with situations for which there is no previous experience.

Physical models, such as described in papers presented in Session T2, can be effective to estimate the drifting and deposition of dry or "driftable" snow. There are clear difficulties with "wet" snow or with situations where cohesion and adhesion forces become significant. As indicated in the papers presented, such studies can be carried out in wind tunnels or in water flumes. A brief summary of some of the procedures reported in the literature is given in the following table.

SOME APPROACHES

Flow Modelling	"Model Snow"	Experimenters
Wind Tunnel (Air)	• activated clay	• Toyoda & Tomabechi • Anno (Japan & at CRREL) • CRREL
	• Pine sawdust	• Wianecki & Chevallier (C.E.B.T.P.)
	• Bran (finely ground wheat)	• Isyumov, Mikitiuk, Kennedy (BLWTL, UWO)
	• Cracked Wheat	• Suzuya, Uematsu, Mozawa
	• Glass Beads	• Cermak, Petersen, Peterka • Iversen • CRREL
	• Sand	• Kind • Isyumov & Mikitiuk
	• Sodium Bi-Carbonate	• Srivastava • Kwok, Kim (Univ. Sydney)
Water Flume (Water)	• Ground Walnut Shells	• O'Rourke
	• Sand	• Irwin, Williams,...RWDI • Theakston • Isyumov • CRREL

All reduced scale model studies of snow transport and deposition include some approximations or "relaxations" of strict similarity requirements. Invariably, some compromise is needed to achieve a realizable experiment. It is generally possible to achieve overall or "bulk" similarity of snow depositions but it is extremely difficult to simulate details such as cornices, the adhesion of snow to vertical walls, effects relating to evaporation, melting and refreezing, etc. Also it is extremely difficult to achieve proper Froude number similarity of the model snow particles. Based on the papers presented at this Conference, it appears that good progress can be made with approximate rather than precise Froude number scaling. On the other hand, a proper modelling of the mean and turbulent characteristics of the wind is important, particularly in studies of roof snow loads. In such studies the building aerodynamics play a dominant role in determining the magnitudes of snow accumulations, as well as their locations.

WISH LIST

Comparisons with full-scale observations are essential, in order to demonstrate the validity of experimental models. While some full-scale data are available, there is a real need for full-scale observations which are more completely documented. In addition to knowing the geometry, immediate siting and

surrounding terrain of the roof, full-scale experimenters should try to quantify the wind speed and wind direction, duration of the snowfall and the depth and distribution of snow drifts formed during particular time segments of the snow storm. It would be very valuable to obtain snow drift flux measurements over roofs to allow in-depth evaluations of modelling techniques.

Experimental techniques have tended to examine the effects of single snow storms or drifting conditions. Properties of a storm are seldom constant and it is common to find substantial changes in wind speed and wind direction, as well as a variation of the snowfall rate over the course of the storm. Essentially, this requires the capability to superimpose the consequences of multiple weather events. There are indications that experimental models can be effectively used to study a series of snowfall and drifting episodes, as long as the full-scale snow can be considered to remain driftable. In other words, as long as no rain occurs and the temperatures remain below freezing. Clearly, analytical or numerical methods like the FAE, discussed in Session T1, have a role to play in such simulations. In fact, the prediction of extreme snow loads may be best achieved with hybrid methods which use both experimental and numerical modelling techniques.

Perspective Snow Control

Colin Williams

Rowan, Williams, Davies and Irwin, Inc.
Guelph, Ontario, Canada

The papers presented in the Snow Control section covered by specific areas of snow management. These were:

- Removal of snow from roofs by promoting sliding using heated roof surfaces.
- Power consumption considerations for systems which completely melt accumulated snow.
- Relocation of snow from within a builtup area using pneumatic or hydraulic transmission lines.

Comments/further research/potential applications arising from these presentations and the ensuing discussions are:

The measurement of the static friction of ice masses on various roofing materials (Watanabe & Hirai) could be extended to give information on the dynamic coefficient of friction. This information would be useful for calculating the trajectory of snow masses which have been released from various types of roofs. An estimate of the dynamic coefficient of friction as being 10–20% of the static coefficient was provided during the question period by one of the paper's authors.

An understanding of local meteorological data can reduce installation costs, power requirements and the predictability of snow melting systems (Fyall & Hart). The FAE simulation method (described by Irwin and Williams in other sessions) uses detailed computations of historical meteorological data to produce time histories of snow accumulations, and this could be used to further refine the energy requirements of snow melting systems.

Snow removal from roofs using only sufficient heat transfer through the roof to initiate sliding is a technique which will use only a fraction of the energy for complete melting (Higashiyama et al. and Otsuka et al.). However, a large enough storage area for the snow to slide must be provided or manual removal of the snow after the slide has taken place must be undertaken. This is particularly true in heavy snowfall areas.

Details of the lower roof edge are important to ensure that sliding will occur on systems which rely on sliding to remove snow from roofs. Research on the effects of typical roof shapes at the lower edges of steel roofs and membrane structures is required.

The effect of artificial surface roughness on roofs, i.e., snow arresters such as tabs and snow barriers or fences, is not well understood. The effectiveness of snow arresters; the advisability of using them in low, moderate and high snowfall zones; and the optimum spacing and height should be researched.

Relocation of snow using pneumatic or hydraulic conveyors can be an attractive alternative to trucking snow away from an area (Kobayashi and Kamagai; Umemura). Snow removal from large roofs is a labour intensive exercise as a result of carrying snow to the edge of the roof. Could the pneumatic device be applied to this problem?

In the Arctic and Antarctic, removal of large snowdrifts by trucks is a large consumer of expensive energy. Would the hard packed drifted snow of these regions be amenable to pneumatic relocation?

No papers were presented on other aspects of snow control such as: snow fences, highway design, building details and design (this was covered in Session R1 – Building Design). These are all known to be active areas of research and application and, in future conferences, papers on these subjects will be welcome. Possible topics are:

- Geographical differences in snow fence applications
- Large arctic snow fences
- Design methods for optimizing snow fence installations
- Details of snow fence installations
- Mechanical snow removal methods from roofs

During the discussion Ian Mackinlay stated that:

More needs to be known about snow arresters (e.g., tabs and barriers) and that a session in a future conference would be useful.

For snow barriers at the eave, we should design for ground snow load.

Snow barrier design is analogous to avalanche prevention fence design.

Jon Paine stated his experience with snow stops or tabs is that they work well for roofs with slopes of 20° to 30° but not very well for steeper roofs.

Perspective Mechanical Properties and Behavior

Wayne Tobiasson
US Army Cold Regions Research and Engineering Laboratory
Hanover, New Hampshire, USA

The mechanical properties of dry snow are quite different from those of wet snow. Changes in behavior with snow type and temperature are appreciated but quantitative values for a range of conditions are not known with much confidence.

Static and quasi-static properties are of interest in the design of roofs and avalanche defenses when snow movement is to be prevented or only allowed to occur slowly by creep, glide or densification. As an example, snow guards on roofs are commonly designed to hold the snow on the roof but not resist the dynamic forces of sliding snow.

Use of Swiss guidelines for the design of avalanche defense structures in Japan has resulted in failures. The Japanese snow was quite dense and it subjected defense structures to heavier loads than in the guidelines. Design procedures have been modified accordingly.

Tapping tests and uniaxial compression tests have been developed to study the metamorphosis of snow and its relationship to wet snow avalanches on mountains and on roofs. Those tests show the dramatic influence of water content on behavior. The snow behaves viscoelastically when it is not saturated and plastically at saturation.

The behavior of snow subjected to dynamic loads is of interest relative to movement of wheels, tracks, skids and skis on snow. The behavior of snow in motion is an important issue relative to the design of avalanche defenses once an avalanche is triggered and to the design of roofs to cope with snow that does slide. A dramatic videotape shown by Karl Wieser of Austria illustrated strides made to simulate the motion of powder avalanches and the effectiveness of various defense structures in redirecting avalanches.

A significant amount of attention at this conference was devoted to snow drifting. Much of that was directed at the use of other materials in wind tunnels and flumes to simulate the behavior of snow in air and in water. Snow modeling materials range from sand in water to sawdust, activated clay, and bran in air. Analytical modeling is being used in Canada by Rowan, Williams, Davies and Irwin Inc. to complement their wind tunnel and flume studies.

In Japan several large cities are located in areas of very heavy snowfall. Ways of removing that snow include use of snow-air and snow-water mixtures. Studies of movement of snow-air mixtures through tubes have used polystyrene to simulate snow. To reduce the energy needed to transport snow long distances, an innovative system has been devised that makes snowballs (perhaps "ice balls" is a better way to describe them) and then transports them pneumatically in pipes of about their diameter.

In some Japanese cities, snow is transported in water-filled pipes and troughs. Clogging of those conduits is a problem that is being studied in flumes using water and sand mixtures to examine

particle segregation. Other flume studies are aimed at determining energy losses at various concentrations and velocities.

While the thermomechanical properties of snow continue to be of interest, few specific studies focused in that area were presented at this conference. Determining the energy required to melt snow or cause snow to slide on various surfaces is an example of an application where thermomechanical properties are needed.

By savvy application of snow engineering technology, winter snow has been used for summer refrigeration. The snow has been stockpiled in winter; thermally protected with reflective coatings, polystyrene foam and rice hulls; and then used to refrigerate goods and a dwelling in Japan. Meltwater produced has been used for irrigation purposes. This demonstration illustrates how a better understanding of the properties of snow, through the high technology now available, can permit back-to-basics approaches that are sensitive to resource limitations and concerns for our environment.

Perspective Building Design

Ian Mackinlay (FAIA) and Richard S. Flood (AIA/CSI)

Ian Mackinlay Architecture, Inc.
San Francisco, California, U.S.A.

Papers presented discussed unique snow country problems and ways to utilize the snow for the benefit of the building.

1. In Japan, a residence is using collected winter snow and ice to provide summer air conditioning. A large pit was dug adjacent to the house and an entire winter's snow is collected and compacted in the pit. This large "ice" cube melts slowly enough that it can provide an entire summer's worth of natural cooling for the house as well as a natural refrigerator for the storage of perishable items. Meltwater is used to supplement irrigation.
2. In the United States, a Visitor Center is being designed for the deep snow mountain country. The design is taking into account that the building will only be open during the summer and it will be totally closed and unmaintained during the winter. The building will have to "hibernate" until spring and emerge virtually undamaged from the winter environment and any seismic events.
3. In the United States, the phenomenon of ice dams at the eaves of sloped roofs is a common occurrence. In the deep snow country of the Sierra Nevada, these ice dams can get quite large, especially on north-facing roofs. Current code design allows for roof snow load reductions. It is believed that this reduction should not be permitted due to the ice dam phenomenon. Consequently, a testing program is proposed to be undertaken in the Lake Tahoe area to measure the relative snow loads between site ground snow load and the north-facing roofs of both heated and unheated structures. Results of this test program could lead to revised structural code requirements.
4. In Japan, the modernization of the country has made regional cultures more homogeneous in nature. This blending has introduced architectural styles used in temperate climates into cities with heavy snowfall. This has caused many sociopolitical and economic problems in these heavy snowfall cities. This study looks at the use of some traditional Japanese design elements and their appreciation in contemporary architecture to alleviate these problems. These are:

- a) Yukigakoi - a covering to enclose the exterior side of a roofed overhang. It creates an open air but snow-free exterior space alongside a house. In summer, the covering is removed and stored.
- b) Doma - an earth floored room. This is indoor space brought in from the outdoors. In winter, it takes the place of an unusable snow-covered garden.
- c) Doen - an outside space under a wide roof overhang between a house and the garden. This space can be closed using "yukigakoi."
- d) Gangi - a covered walkway on a shopping street. Similar to an arcade but each section of the "gangi" is on private land.
- e) Hirairi - a rule in which the eave line is parallel to the street, ensuring snowfall off the roof will be into the street and into the rear garden, not into a neighbor's yard.
- f) Ryusetsuko - water flow systems such as irrigation canals, streams and rivers. In the past, "ryusetsuko" were used to dump snow. This resulted in frequent flooding and were banned from this use. Now they are being reconsidered as snow dumps. Grating or nets are being utilized to ensure water flow is not dammed up by the snow dumping.

5. In Western Canada, deep heavy snow is predominant during the winter. The paper presented was a guideline for design review of projects in deep snow. The basic outline is in three sections. The first section is "Project Strategy" where objectives and goals are defined, and all physical and environmental data are collected (with particular emphasis on snow/storm conditions). These data are analyzed in conjunction with the project goals and tested against conceptual design solutions.

The second section is "Conceptual Design Review." This includes general building shape and geometry (the simpler the better); snow accumulation (effects of valleys and dormers, solar exposure, etc.); snow shedding (roof pitch and covering, dump zones, trajectories, etc.); pedestrian and vehicular ingress and egress protection from snow shedding, drifting, etc.; icicle formation, roof water removal, etc.; and roof snow management. (Does snow remain; is it shoveled; maintenance costs; etc.).

The third section is "Safe Design Considerations." This includes site slope consideration (snow avalanche, creep, meltwater drainage, additional sidewall lateral pressure); site orientation (solar and wind exposure, snow drifting, etc.); snow accumulation (roof dump areas, long and short-term storage locations, etc.); snow removal (methodology, frequency, costs, equipment, etc.).

By thoroughly understanding the implications of snow and cold, many design problems can be avoided or substantially mitigated. A careful initial snow country design review is the best insurance against unforeseen ice/snow damage to the completed project.

6. In Fairbanks, Alaska, design roof loads in the early 1970s were based upon "local experience" guidelines. No foundational information could be found to support the guideline load data. This paper describes the work done 20 years ago to provide a more definitive snow load basis and how current Alaska snow load data for Fairbanks (ANSI 1982, Dept of Army 1986, ASCE 1990) came into being. Furthermore, this paper describes the updating of loads published in the 1987 AEIDC report "Snow Loads in Alaska," the mathematical error discovered in the report, and how the report methodology appears to be inappropriate for the Fairbanks vicinity. Lastly, the paper describes the record snowfall of 1991 in Fairbanks, the data taken, its effect on the previous data base and the recommendations for revising the Fairbanks area snow load values.

In conclusion, the session chairman summarized the importance of the work presented:

- a) The collection and storage of snow/cold natural forces to provide summer energy sources.
- b) Design of projects that will withstand the effects of "hibernation."
- c) Investigating the ice dam loading effects.
- d) Utilization of traditional architectural snow country concepts in contemporary structures and city planning.
- f) The importance of snow country design review in the architectural design process.

One must remember that the end user of all the work presented at this conference and in the future will be the building designer. To this end the architect must assimilate, digest, interpret and implement the knowledge regarding snow and cold. This information must be broadly disseminated in easily understandable formats. In the past, building codes spoke very little about snow problems. Only in the past few years have these codes recognized the complex snow influence on building design. This has primarily been in regard to structural design loads. Although ASCE Standard 7 is the best snow load document currently published, much more research work and data need to be done to update it and to regionalize and localize the variable data needed to implement it.

Architects must set their minds to provide design solutions in three distinct realms. The first is the "very large" realm, the snow/cold implications of city and regional planning. This includes how to minimize the snow/cold impact on transportation/communication systems, utility and drainage infrastructure and budget expenditures.

The second realm is the "large" one. This has to do with a building's geometry: site-specific features such as elevation, topography, solar orientation, access means, vegetation, and local climatological data. These parameters need to be utilized to minimize the snow/cold impact on the building form and site constraints.

The third and last realm includes the "small" conditions. The details of the building can make or break (quite literary) the project. Leaks, impact damage, roof snow avalanches, blocked exits, and frozen pipes are some architectural implications. Structural overloading due to ice dams and drifting snow are common. Destroyed chimneys, vents and gutters are frequent results of snow creep or roof snow avalanche.

Most of the problems encountered are interactive and compound one another. The architectural and engineering communities must seek out innovative methods to harness the forces of snow and cold and utilize their attributes in building design.

Perspective Codes and Standards

Kristoffer Apeland

Oslo School of Architecture
Oslo, Norway

Session R2 gave a good review of the state-of-the-art for international and regional work in the field of codes and standards.

K. Apeland presented the ISO Draft International Standard DIS 4355 Snow Loads, which was approved by the ISO Technical Committee TC 98 on March 5, 1992. The DIS 4355, which takes into account new international findings in the field of snow engineering, is a general document which is primarily meant for code writers. However, it is developed in such a way that it may be used as a code by the designers.

J.R. Tory presented the work on codification of European Snow Loading. The European Committee for Standardization, CEN, has taken over the work on the number of "regional" countries from the 12 ECE countries to 18, which makes harmonization of snow load codes more difficult than for the ECE countries alone. Great efforts have been made to produce a European snow map. For snow load on the roof the existing ISO 4355 will be the primary basis for the work

R.L. Sack and A. Shah presented the ASCE work on Standard 7 Snow Loads, 1988. Substantial changes are made in ground snow load specifications and in drift load provisions. For the ASCE 7-95 edition improvements are planned in 17 areas. ASCE is working to have the three U.S. model codes adopt the ASCE 7-88 by reference and thus obtain uniformity of the U.S. building codes.

D.J. Laurie Kennedy, N. Isyumov and M. Mikituik reported on the effectiveness of code provisions for snow accumulations on stepped roofs. Comparisons of provisions for rift load on multilevel roofs were presented, and results of wind tunnel tests were reported. A spike load on the lower roof may yield the most severe load condition. Such an effect is not included in any code provisions.

During the discussion on perspectives, T. Nakamura raised the question whether a unified standard (e.g., ISO) is necessary. Unification could pose problems when applied to areas of dissimilar snow such as Niigata, Sapporo and Sendai in Japan.

K. Apeland pointed out that the main objective of national and international uniformity of building regulations is to minimize trade hindrances. Additionally, it is of importance for the exchange of general knowledge.

P. Irwin pointed out the importance of snow load duration by material design. J.R. Tory informed that CEN probably will apply medium-term uniform loads and short-term drift loads.

K. Apeland explained that the general philosophy of the ISO TC 98-committee is that the loading documents should only give the load duration for the purpose of characterizing the load. The problem of how to apply the load duration in design should be left to the design documents.

N. Isyumov proposed to look beyond using a statistically derived maximum ground snow load as the basis for roof snow loads. For example, the maximum single snowfall or the seven-day maximum may be better design values in some locations.

I. Mackinlay gave some comfort to those of us who feel that codes change too slowly. Progress is being made. It is important for groups such as ours to make suggestions for improvements.